

Examining the Functional Role of Transporters in Modulating Drug Absorption across Lung Epithelium.

A thesis submitted in accordance with the conditions
governing candidates for the degree of
Philosophiae Doctor in Cardiff University



June 2011

Danielle Francombe

B.Sc. (Hons)

*Welsh School of Pharmacy
Cardiff University*

DECLARATION

This work has not previously been accepted in substance for any degree and is not concurrently submitted in candidature for any degree.

Signed..... Phancourh.....(candidate) Date 24/01/2012

STATEMENT 1

This thesis is being submitted in partial fulfilment of the requirements for the degree of PhD

Signed..... Phancourh.....(candidate) Date 24/01/2012

STATEMENT 2

This thesis is the result of my own independent work/investigation, except where otherwise stated.

Other sources are acknowledged by explicit references.

Signed..... Phancourh.....(candidate) Date 24/01/2012.

STATEMENT 3:

I hereby give consent for my thesis, if accepted, to be available for photocopying and for inter-library loan, and for the title and summary to be made available to outside organisations.

Signed..... Phancourh.....(candidate) Date 24/01/2012

Acknowledgements

I would firstly like to express my gratitude to my supervisors; Dr. Mark Gumbleton, Dr. Glyn Taylor, and Chris Edwards, for their support and guidance throughout my PhD. I would also like to offer sincere thanks to all members of the Gumbleton lab, especially Mat, Marc, Andrew, Ghaith and Lee who have all helped to make my PhD a thoroughly unforgettable experience.

Special thanks to my friends, who without their unwavering support, I would have failed long before this goal had been reached. A special thanks to Jess who, through the chaos, has always held my hand.

Finally, this thesis is dedicated to my family. To Jill, Darren, Charlie, Ross and Adam, Jen, Terry and Lee, Glenys and Colin. A huge thank you to you all, for supporting me all the way, never faltering in your encouragement and for not disowning me when things got ugly. Without such support none of this would have been possible.

Ad astra per aspera

Student ID Number:	0207367
<p><u>Summary of Thesis:</u></p> <p>P-glycoprotein (P-gp – MDR-1), a 170 kDa glycosylated membrane bound protein, is a member of the ATP-binding cassette transporter family. The potential for P-gp to reduce drug absorption across lung epithelia is of significant interest; this is particularly so, given P-gp's broad substrate specificity mediating efflux transport of a range of structurally unrelated substrates. Within lung, P-gp expression is evident in bronchial and alveolar epithelia with functional characterisation of P-gp transport capacity within lung epithelial cells currently restricted to respective in-vitro cell culture models.</p> <p>The aims of this project were to establish the relative mRNA expression of several <u>A</u>TP <u>B</u>inding <u>C</u>assette (ABC), <u>S</u>olute <u>C</u>arrier (SLC) and <u>S</u>olute <u>C</u>arrier <u>O</u>rganic Anion (SLCO) drug transporters within rat lung samples through use of RT-PCR; expression suggesting the potential to serve as targets for pulmonary drug delivery. Further, validation of an Isolated Perfused Rat Lung preparation for use in assessment of drug transport across the lung was conducted. In order to assess the functional significance of the ABC drug transporter, P-glycoprotein, on drugs instilled intra-tracheally to the IPRL set-up, use of the P-gp substrates; Rhodamine 123 (Rh123), digoxin, and flunisolide and the P-gp inhibitor, GF120918 was employed. Further, use of kinetic modelling was employed to establish pharmacokinetic parameters involved.</p> <p>Using the IPRL, the P-gp dependent pulmonary absorption of the P-gp substrate, Rh123, was demonstrated. Dose-dependent absorption, consistent with a saturable component in the molecule's pulmonary absorption, was demonstrated. Further, the absorption of low dose Rh123 was promoted by the presence of the highly selective P-gp inhibitor GF120918, consistent with a functional role of P-gp mediated efflux within an intact lung; an efflux process which may limit the pulmonary absorption of a lung administered molecule. Further studies using this system and extending the range of molecules studied will provide greater understanding of the quantitative significance of P-gp in limiting pulmonary absorption across lung epithelium.</p>	

Table of Contents

DECLARATION	i
Acknowledgements	ii
Summary of Thesis	iv
Table of Contents	v
List of Tables	ix
List of abbreviations	xvii
CHAPTER 1	1
GENERAL INTRODUCTION	1
1. Introduction	2
1.1. Structure and function of the lung: barriers to drug absorption	2
1.2. Advantages and disadvantages of pulmonary drug delivery.....	5
1.3. Techniques for pulmonary drug delivery	7
1.4. Examples of pulmonary drug delivery for both local and systemic action	9
1.5. Mechanisms of drug transport and absorption across the lung	10
1.6. Drug transporter proteins	12
1.7. Drug transporter proteins of interest to drug discovery	17
1.8. Experimental models to assess pulmonary drug transport.....	21
1.9. Isolated Perfused Rat Lung (IPRL).....	24
1.10. Thesis aims and objectives	28
CHAPTER 2.....	29
RT-PCR DERIVED ANALYSIS OF DRUG TRANSPORTER EXPRESSION	29
IN CELL MODELS AND WHOLE LUNG	29
2.1. Introduction	30
2.2. Materials and Methods	37
2.2.1. Rat whole lung tissue harvest for RNA isolation.....	37
2.2.2. Isolation and primary cell culture of rat alveolar epithelial cells.....	37
2.2.3 SPOC1 Cell culture.....	46
2.2.4. Isolation and quantitation of total RNA from animal cells and animal tissue	47
2.2.5. Primer design	49
2.2.6. Digestion of potential DNA contamination.....	53
2.2.7. Reverse transcriptase – polymerase chain reaction (RT-PCR)	54
2.2.8. Polymerase chain reaction (PCR)	56
2.2.9. PCR optimisation.....	58
2.2.10. Agarose gel electrophoresis.....	58

2.3. Results and Discussion.....	60
2.3.1. Expression analysis of ATP Binding Cassette transporters	60
2.3.2. Expression analysis of Amino Acid transporters.....	69
2.3.3. Expression analysis of Glucose transporters	75
2.3.4. Expression analysis of Monocarboxylate transporters	79
2.3.5. Expression analysis of Nucleoside transporters	82
2.3.6. Expression analysis of Peptide transporters.....	85
2.6.7. Expression analysis of Organic cation transporters	89
2.3.8. Expression analysis of organic anion transporting polypeptides.....	93
CHAPTER 3.....	99
DEVELOPMENT AND VALIDATION OF AN ISOLATED PERFUSED RAT LUNG MODEL FOR PULMONARY DELIVERY	99
3.1. Introduction	100
3.2. Materials and Methods	106
3.2.1. Validation of IPRL perfusate - extent to which Bovine Serum Albumin contributes to perfusate background fluorescence	106
3.2.2. Isolated Perfused Rat Lung	108
3.2.3. Validation of IPRL dosing equipment.....	115
3.2.4. Validation of the forced solution instillation technique for IPRL dosing	116
3.2.5. Validation of the IPRL – transport of a molecular weight range of fluorescent probes... 117	
3.2.6. Validation of the IPRL – gel filtration analysis of FITC-dextran	118
3.2.7. Validation of the IPRL – determining IPRL viability by wet: dry weight.....	119
3.3. Results	120
3.3.1 Bovine Serum Albumin contribution to perfusate background fluorescence	120
3.3.2. Validation of IPRL dosing equipment.....	121
3.3.3. Validation of the forced solution instillation technique for IPRL dosing	123
3.3.4. Validation of the IPRL – transport of a molecular weight range of fluorescent probes... 125	
3.3.5. Validation of the IPRL – gel filtration of FITC-dextran.....	127
3.3.6. Validation of the IPRL – determining IPRL viability by wet: dry weight.....	128
3.3.7. Relationship between absorption rate and molecular weight across the IPRL	130
3.4. Discussion	131
CHAPTER 4.....	137
FUNCTIONAL SIGNIFICANCE OF AN ACTIVE DRUG TRANSPORTER (P-GP) UPON THE SUBSTRATES DELIVERED TO THE ISOLATED PERFUSED RAT LUNG	137
4.1. Introduction	138
4.2. Materials and Methods	144
4.2.1. Materials	144

4.2.2. HPLC analysis: Rh123/F-Na analytical method development.....	145
4.2.3. Rh123 protein and tubing binding	148
4.2.4. Rh123 absorption from airways: Dose-ranging studies.....	150
4.2.5. Rh123 absorption from airways: Effect of GF120918.....	151
4.2.6. Digoxin absorption from airways: Effect of GF120918 co-instilled and in IPRL perfusate.....	156
4.2.7. Flunisolide absorption from airways: Effect of GF120918 co-instilled and in IPRL perfusate	157
4.3. Results	162
4.3.1. Rh123 analytical validation: Precision and accuracy	162
4.3.2. Rh123 protein and tubing binding	163
4.3.3. Rh123 absorption from airways: Dose ranging studies	165
4.3.4. Rh123 absorption from airways: Effect of GF120918 co-instilled and in IPRL perfusate	167
4.3.5. Rh123 absorption from airways: Effect of GF120918 co-instilled with Rh123.....	169
4.3.6. Pharmacokinetic modelling: Rh123 absorption from the IPRL in presence and absence of GF120918.....	171
4.3.7. Digoxin absorption from airways: Effect of GF120918 co-instilled and in IPRL perfusate	176
4.3.8. Flunisolide absorption from airways: Effect of GF120918 co-instilled and in IPRL perfusate	177
4.4. Discussion	180
CHAPTER 5.....	192
EFFLUX FUNCTIONALITY AT THE PULMONARY ENDOTHELIUM: LIMITING DRUG TRANSPORT FROM VASCULATURE TO LUNG.....	192
5.1. Introduction	193
5.2. Materials and Methods	196
5.2.1. Isolated Perfused Rat Lung (IPRL)	196
5.2.3. Rh123 accumulation in lung (perfusate to lung): Effect of GF120918.....	197
5.2.4. Data Analysis.....	198
5.3. Results	199
5.3.1. Rh123 accumulation in lung (perfusate to lung): Effect of GF120918.....	199
5.4. Discussion	203
CHAPTER 6.....	208
INVESTIGATING THE IMPACT OF PULMONARY P-GP UPON AIRWAY INSTILLED SUBSTRATES WITHIN AN INDUSTRIAL SETTING; USE OF AN <i>IN SITU</i> IPRL MODEL	208
6.1. Introduction	209
6.2. Materials and Methods	214
6.2.1. Single-pass perfusion Isolated Perfused Rat Lung model	214

6.2.2. Evans blue lobar deposition	218
6.2.3. Rh123 absorption in the single-pass perfusion model	218
6.2.4. Perfusate plasma Sample and Dose Solution Preparation for Analysis (automated)	219
6.2.5. Flunisolide absorption in the single-pass perfusion model	222
6.2.6. Perfusate plasma Sample and Dose Solution Preparation for Analysis (automated).....	223
6.2.7. Mass balance studies	226
6.2.8. Data Analysis	228
6.3. Results	230
6.3.1. Evans blue distribution following intra-tracheal instillation.....	230
6.3.2. Rh123 absorption in the single-pass perfusion model	230
6.3.3. Flunisolide absorption in the single-pass perfusion model: Influence of GF120918.....	232
6.3.4. Power Analysis	234
6.4. Discussion	238
CHAPTER 7	248
GENERAL DISCUSSION	248
7.0. General Discussion.....	249
Appendix i	280
Transporter expression intensities - raw data	280
Appendix ii	284
Chapter 4: Rh123 analytical validation: Precision and accuracy	284
Precision and accuracy calibration curves	284
Individual calibration plots used to assess F-Na HPLC assay precision.....	284
Chapter 4: Functional significance of a drug transporter on instilled substrates to the IPRL	284
Appendix iii	296
Chapter 6: Functional significance of drug transporters in a first-pass IPRL	296

List of Tables

Table Number	Title	Page
1.1	SLC transporters of clinical significance	19
1.2	ABC transporters of clinical significance	20
1.3	Advantages and disadvantages of techniques used to examine drug transporters in the lung	23
2.1	Studies examining pulmonary expression of ABC transporters in human tissues and cell culture	33
2.2	Advantages and disadvantages of experimental techniques used to identify presence of drug transporters	35
2.3	Forward and reverse primer sequences for ABC transporters to be studied	50
2.4	Forward and reverse primer sequences for amino acid transporters to be studied	51
2.5	Forward and reverse primer sequences for glucose transporters to be studied	51
2.6	Forward and reverse primer sequences for nucleotide transporters to be studied	52
2.7	Forward and reverse primer sequences for monocarboxylate transporters to be studied	52
2.8	Forward and reverse primer sequences for peptide transporters to be studied	52
2.9	Forward and reverse primer sequences for organic cation transporters to be studied	53
2.10	Forward and reverse primer sequences for organic anion transporters to be studied	53
2.11	RT-PCR expression profiles of ABC transporters in various lung samples	61
2.12	RT-PCR expression profiles of amino acid transporters in various lung samples	69
2.13	RT-PCR expression profiles of glucose transporters in various lung samples	76
2.14	RT-PCR expression profiles of monocarboxylate transporters in various lung samples	79

2.15	RT-PCR expression profiles of nucleoside transporters in various lung samples	82
2.16	RT-PCR expression profiles of peptide transporters in various lung samples	86
2.17	RT-PCR expression profiles of organic cation transporters in various lung samples	90
2.18	RT-PCR expression profiles of organic anion transporters in various lung samples	94
3.1	Background fluorescence of perfusate samples containing bovine serum albumin	121
3.2	Dose retention in custom dosing equipment	122
3.3	Evans Blue deposition pattern in the isolated perfused rat lung	124
3.4	Sodium Fluorescein deposition in the isolated perfused rat lung	124
3.5	Sodium Fluorescein transport across the isolated perfused rat lung	125
3.6	FITC-labelled dextran transport across the isolated perfused rat lung	127
3.7	Wet: dry lung weight ratio after a dosing procedure in the isolated perfused rat lung	129
4.1	Clinically relevant substrates of ABCB transporters	140
4.2	P-glycoprotein specific transport modulators	141
4.3	Efficacious concentrations of GF120918 for the inhibition of P-glycoprotein	153-154
4.4A	Rhodamine 123 and sodium fluorescein assay coefficient of variation (determined across a concentration range)	162
4.4B	Rhodamine 123 and sodium fluorescein assay accuracy	163
4.5	Percentage Rhodamine 123 recovered from perfusate containing bovine serum albumin	164
4.6	Percentage Rhodamine 123 recovered from perfusate in isolated perfused rat lung model tubing	165
4.7	Transport of Rhodamine 123 and sodium fluorescein across the isolated perfused rat lung	166
4.8	Effect of GF120918 upon Rhodamine 123/sodium fluorescein transport across the isolated perfused rat lung	169
4.9	Effect of GF120918 co-instilled with dose upon Rhodamine 123	171

	transport	
4.10	Pharmacokinetic parameters associated with substrate transport across the isolated perfused rat lung. Parameters generated by WinNonlin	175
4.11	Effect of GF120918 upon Digoxin transport across the isolated perfused rat lung	177
4.12	Effect of GF120918 upon Flunisolide transport across the isolated perfused rat lung	178
4.13	Comparison of percentage Flunisolide dose transported at various sample time points	179
5.1	Effect of GF120918 upon the lung accumulation of Rhodamine 123	201
5.2	Effect of GF120918 upon parameters reflecting Rhodamine 123 loss from pulmonary perfusate	202
6.1	Preparation of calibrations for LC/MS/MS analysis	227
6.2	Dose escalation of Rhodamine 123 and the effect of GF120918 upon transport across the single-pass isolated perfused rat lung	232
6.3	Dose escalation of Flunisolide and the effect of GF120918 upon transport across the single-pass isolated perfused rat lung	234
6.4	Area under the curve data for all single-pass Rhodamine 123 experiments	235
6.5	Calculated area under the curve data and summary statistics for Rhodamine 123 transport data generated using the Cardiff isolated perfused rat lung model	236
6.6	Cellular localisation of P-glycoprotein in lung-specific cells: summary of recent literature	238
6.7	Comparison of Cardiff and GSK isolated perfused rat lung models	245
6.8	Summary of power analysis studies performed upon substrate transport data	246

List of Figures

Figure Number	Title	Page
1.1	Diagram of human respiratory system	3
1.2	Mechanisms of drug transport across lung epithelia	10
1.3	Types of drug transporter present within a eukaryotic cell.	12
1.4	Mechanism of action of Na^+/H^+ exchanger protein	14
1.5A	Sequence organisation of the Nucleotide Binding Domain of ATP transporter	16
1.5B	Secondary structure of an ABC transporter	16
1.6	Examples of human drug transporters in tissues with a barrier function	18
2.1	Gauze-syringe filter unit used to retrieve crude alveolar suspension	45
2.2	Percoll™ discontinuous gradient centrifugation - setup	45
2.3	RTPCR studies - typical signal intensities and the corresponding expression index assigned	60
2.4	Representative gel electrophoresis images illustrating selected ABC transporter mRNA expression	61-63
2.5	Representative gel electrophoresis images illustrating selected amino acid transporter mRNA expression	70-71
2.6	Representative gel electrophoresis images illustrating selected glucose acid transporter mRNA expression	77
2.7	Representative gel electrophoresis images illustrating selected monocarboxylate acid transporter mRNA expression	80
2.8	Representative gel electrophoresis images illustrating selected nucleoside acid transporter mRNA expression	84
2.9	Representative gel electrophoresis images illustrating selected peptide acid transporter mRNA expression	87
2.10	Representative gel electrophoresis images illustrating selected organic cation acid transporter mRNA expression	90-91
2.11	Representative gel electrophoresis images illustrating selected organic anion acid transporter mRNA expression	94-95
3.1	Isolated perfused rat lung setup established by Byron <i>et al.</i>	103

3.2A	Custom-made dosing equipment of the Cardiff University Isolated perfused rat lung	111
3.2B	Custom-made oesophageal hanging rod of the Cardiff University isolated perfused rat lung	111
3.3	Schematic of isolated perfused rat lung setup at Cardiff University	112
3.4	Diagram illustrating the tying off of the pulmonary artery catheter	115
3.5	Calibration curve representing sodium fluorescein in each of the three different perfusate samples	120
3.6	Mean amount of dose remaining, as a percentage, in custom dosing equipment after deployment of a test dose to the isolated perfused rat lung	122
3.7	Deposition pattern of Evans Blue dye dosed to the isolated perfused rat lung via a forced solution instillation technique	123
3.8	Cumulative percentage of deposited dose of sodium fluorescein absorbed with time across the isolated perfused rat lung	125
3.9	Cumulative percentage of deposited dose of FITC-labelled dextrans absorbed with time across the isolated perfused rat lung	126
3.10	Gel filtration chromatography of FITC-dextrans; pre and post transport through the isolated perfused rat lung	127-128
3.11	Relationship between initial transport rate (k_{in}) and Stokes' diameter of four fluorescent probes	130
4.1	Excitation and emission spectra for Rhodamine 123 in mobile phase	146
4.2	Example of a HPLC chromatogram produced by a sample of Rhodamine 123	147
4.3	2D chemical structure of Rhodamine 132 at neutral pH	149
4.4	Example of a HPLC chromatogram produced by a sample of Rhodamine 123 and spiked with GF120918	152
4.5A	Cumulative percentage of deposited Rhodamine 123 absorbed with time	166
4.5B	Cumulative percentage of deposited sodium fluorescein absorbed with time	166
4.6A	Effect of GF120918 at concentrations of 150 nM and 500 nM upon cumulative percentage of deposited Rhodamine 123 absorbed with time	168
4.6B	Effect of GF120918 at concentrations of 150 nM and 500 nM upon cumulative percentage of deposited sodium fluorescein absorbed	168

	with time	
4.7A	Effect of GF120918 at a concentration of 500 nM co-administered with dose upon the cumulative percentage of deposited Rhodamine 123 absorbed with time	170
4.7B	Effect of GF120918 at a concentration of 500 nM co-administered with dose upon the cumulative percentage of deposited sodium fluorescein absorbed with time	170
4.8	Example plots generated by fitting a WinNonlin model to Rhodamine 123/sodium fluorescein dose ranging data	172
4.9	Example plots generated by fitting a WinNonlin model to Rhodamine 123 +/- GF120918 data where the P-gp inhibitor was both co-instilled with Rh123 dose and present in the IPRL perfusate	173
4.10	Example plots generated by fitting a WinNonlin model to sodium fluorescein +/- GF120918 data where the P-gp inhibitor was both co-instilled with F-Na dose and present in the IPRL perfusate	173
4.11	Example plots generated by fitting a WinNonlin model to Rhodamine 123/sodium fluorescein +/- GF120918 data where the P-gp inhibitor was present only in co-instilled Rh123/F-Na dose	174
4.12A	Effect of GF120918 at a concentration of 500 nM upon cumulative percentage of deposited Digoxin absorbed with time	176
4.12B	Effect of GF120918 at a concentration of 500 nM upon cumulative percentage of deposited Mannitol absorbed with time	176
4.13A	Effect of GF120918 at a concentration of 500 nM upon cumulative percentage of deposited Flunisolide absorbed with time.	177
4.13B	Effect of GF120918 at a concentration of 500 nM upon cumulative percentage of deposited sodium fluorescein absorbed with time	177
4.14	Example of plots generated by nonlinear regression performed upon Flunisolide transport data	179
4.15	Diagram illustrating pharmacokinetic models describing F-Na and Rh123 transport across the IPRL.	184
5.1A	Key upper thoracic arteries of the rat, not including pulmonary vasculature	193
5.1B	Main upper thoracic veins of the rat, pulmonary vasculature not detailed	193
5.1C	Diagram of the rodent heart (distal view)	193
5.1D	Deposition pattern of Evans Blue dye dosed to the IPRL via a forced solution instillation technique (Chapter 3; Figure 3.7)	193

5.2	Monoexponential model applied to all Rhodamine 123 perfusate loss data	198
5.3A	Rhodamine 123 (0.025 µg/mL) loss from pulmonary perfusate in the isolated perfused rat lung	199
5.3B	Rhodamine 123 (0.01 µg/mL) loss from pulmonary perfusate in the isolated perfused rat lung	199
5.4	Loss of sodium fluorescein from pulmonary perfusate over time	200
5.5A	Nonlinear regression of data representing Rhodamine 123 loss from perfusate (1 µg nominal dose) in the presence of 0.1 % DMSO	202
5.5B	Nonlinear regression of data representing Rhodamine 123 loss from perfusate (1 µg nominal dose) in the presence of 500 nM GF120918	202
5.5C	Nonlinear regression of data representing Rhodamine 123 loss from perfusate (2.5 µg nominal dose) in the presence of 0.1 % DMSO	202
5.5D	Nonlinear regression of data representing Rhodamine 123 loss from perfusate (2.5 µg nominal dose) in the presence of 500 nM GF120918	202
5.6	Proposed transport of Rh123 and Flunisolid within the isolated perfused rat lung, mediated by P-glycoprotein	206
6.1A	Percentage of UK/EU & USA trademark drugs produced by GSK targeting specific disease/condition areas	210
6.1B	Generic composition of pulmonary targeted drugs presented as percentage of total trademark pulmonary drugs produced by GSK	210
6.1C	Specific pulmonary-associated diseases and conditions treatable via trademark GSK 'pulmonary drugs'.	210
6.2	Image representing the in situ isolated perfused rat lung setup employed at GSK.	212
6.3	Diagrammatic representation of single-pass isolated perfused rat lung preparation	216
6.4	Example molecular ion peaks for substrates dosed to the single-pass isolated perfused rat lung (Analysed by LC/MS/MS).	229
6.5	Lobar distribution of Evans Blue dye in isolated lungs of the single-pass isolated perfused rat lung following intra-tracheal instillation with a Hamilton syringe	230
6.6	Cumulative increase in percentage deposited Rhodamine 123 dose transported to pulmonary perfusate of the single-pass isolated perfused rat lung	231
6.7	Effect of dose escalation and addition of GF120918 (500 nM), in perfusate and instillate, upon cumulative percentage of deposited	233

	Flunisolide dose in the single-pass isolated perfused rat lung	
6.8	Power curves modelled from mean and S.D AUC data	236
6.9	Generated power curves comparing individual dose treatments of the Cardiff dose-ranging study	237
6.10	Comparison of initial transport profile of Rhodamine 123 delivered to the WSOP isolated perfused rat lung and the GSK single-pass isolated perfused rat lung	242
7.1	Graphical presentation of drug transporter expression in the rat lung	251
7.2	Transport profiles of two P-glycoprotein substrates, Rhodamine 123 and Flunisolide, after dosing to the isolated perfused rat lung	253
7.3	Transport profiles of three P-glycoprotein substrates across the isolated perfused rat lung in the presence of GF120918	254
7.4	Mean transport profiles of Rh123 and Flunisolide across the single-pass isolated perfused rat lung	255

List of abbreviations

Mucociliary clearance (MCC)	<i>Staphylococcus aureus</i> (S. aureus)	Cystic fibrosis conductance regulator protein (CFTR)
Surfactant-specific proteins (SP)	Normal human bronchial epithelial cells (NHBE cells)	Cystic fibrosis (CF)
Alveolar epithelial type I cells (AEI)	Isolated perfused rat lung (IPRL)	Non-small cell lung cancer (NSCLC)
Alveolar epithelial type II cells (AEII)	Isolated perfused lung (IPL)	Human immunodeficiency virus (HIV)
Alveolar epithelia (AE)	Ex-situ isolated perfused rat lung at GlaxoSmithKline (IPRLu)	Acquired immune deficiency syndrome (AIDS)
Chronic obstructive pulmonary disease (COPD)	Reverse transcription polymerase chain reaction (RT-PCR)	<i>Pneumocystis carinii</i> (P. carinii)
Pressurised metered-dose inhalers (pMDI)	Approximately (~)	<i>Pseudomonas aeruginosa</i> (Ps. aeruginosa)
Dry powder inhaler (DPI)	Multidrug-resistance protein (MRP)	Antimicrobial peptide (AMP)
P-glycoprotein (P-gp) [also known as MDR1/ABCB1]	Blood-brain barrier (BBB)	Absorption, Distribution, Metabolism, Elimination (ADME)
Adenosine triphosphate (ATP)	Organic cation transporter (OCT)	Dosing rod (DR)
ATP-binding cassette transporter (ABC)	Organic anion transporter (OAT)	Dosing port (DP)
Solute carrier transporter (SLC)	Organic anion polypeptide transporter (OATP)	Tracheal cannula (TC)
Organic solute carrier transporter (SLCO)	Central nervous system (CNS)	Artificial glass thorax (AGT)
Transmembrane domain (TMD)	Transepithelial electrical resistance (TEER)	Hanging rod (HR)
Nucleotide-binding domains (NBD)	Red blood cells (RBC)	Pulmonary artery catheter (PAC)
Breast cancer resistance protein (BCRP)	Macrophage (Mφ)	Ultraviolet/visible (UV/VIS)
Transmembrane (TM)	Forward (F)	Analysis of variance (ANOVA)
	Reverse (R)	FITC-labelled dextran (FD)
		High Performance Liquid Chromatography (HPLC)

Lower limit of detection (LLD)	Tuberculosis/tubercule bacillus (TB)	Minute (min)
Lower limit of quantitation (LLQ)	Kilogram (kg)	Seconds (s)
Counts per minute (CPM)	Gram (g)	Unit (U)
Decompositions per minute (DPM)	Milligram (mg)	Gauge (G)
Mass Spectrometry (MS)	Microgram (µg)	Revolutions per minute (rpm)
Liquid chromatography mass spectrometry (LC/MS)	Nanogram (ng)	Times gravity (x g)
Liquid chromatography tandem mass spectrometry (LC/MS/MS)	Metre (m)	Base pairs (bp)
Internal Standard (IS)	Centimetre (cm)	Excitation wavelength (λ_{ex})
Declustering Potential (DP)	Millimetre (mm)	Emission wavelength (λ_{em})
Cell entrance potential (CEP)	Micrometre (µm)	Cubic centimetre (cc)
Cell exit potential (CXP)	Nanometre (nm)	Grams/mole (g.mol)
Standard deviation (StDev)	Kilodalton (kDa)	Weight for volume (w/v)
Welsh School of Pharmacy (WSOP)	Greater than (>)	Volume for volume (v/v)
Multidrug resistance (MDR)	Less than (<)	Coefficient of variation (Cv)
Centre of Excellence for Drug Discovery (CEDD)	Greater than or equal to (≥)	Chlorofluorocarbon (CFC)
GlaxoSmithKline (GSK)	Percent/age (%)	Hydrofluoroalkane (HFA)
Sprague Dawley (CD)	Litre (Lr)	Human Growth Hormone (hGH)
Versus (vs.)	Millilitre (mL)	Somatropin inhalation powder (SIP)
Intravenous (iv)	Microlitre (µL)	Amine (NH₂)
<i>Candida albicans</i> (C. albicans)	Molecular weight (MW)	Carboxylic acid (COOH)
Intraperitoneal (IP)	Molar (M)	Sodium ion (Na⁺)
	Millimolar (mM)	Hydrogen ion (H⁺)
	Micromolar (µM)	Potassium ion (K⁺)
	Picomole (pmol)	Dihydroxyphenylalanine- phenylalanine (DOPA-Phe)
	Degrees centigrade (°C)	
	Hour (h)	

Oxygen (O₂)	Calcium chloride dehydrate (CaCl₂.2H₂O)	Deoxyribonucleotide triphosphate (dNTP)
Carbon dioxide (CO₂)		
Nitrogen dioxide (NO₂)	Magnesium sulphate heptahydrate (MgSO₄.7H₂O)	Dithiothreitol (DTT)
Adenosine diphosphate (ADP)	di-Sodium hydrogen orthophosphate dehydrate (Na₂HPO₄.2H₂O)	Moloney Murine Leukemia Virus Reverse Transcriptase (M-MLV RT)
Phosphate (Pi)		Magnesium chloride (MgCl₂)
Drug-drug interaction (DDI)	Sodium dihydrogen orthophosphate dehydrate (NaH₂PO₄.2H₂O)	Tris (hydroxymethyl) aminomethane (Tris)
Drug metabolising enzyme (DME)		
γ-aminobutyric acid (GABA)	Sodium Bicarbonate (NaHCO₃)	Disodium ethylenediaminetetraacetic acid (Na₂EDTA.2H₂O)
Cis-3-aminocyclohexane carboxylic acid (ACHC)	Potassium dihydrogen phosphate (KH₂PO₄)	Ethidium bromine (EtBr)
L-2, 4-diamino-N-butyric acid (DABA)	N-2- Hydroxyethylpiperazine-N'- 2-ethanesulfonic acid (HEPES)	Reverse transcriptase (RT)
Ribonucleic acid (RNA)		Glutathione (GSH)
Deoxyribonucleic acid (DNA)	D-Glucose anhydrous (C₆H₁₂O₆)	Nitric oxide synthase (iNOS)
Messenger ribonucleic acid (mRNA)	Foetal bovine serum albumin (FBS)	Uridine triphosphate (UTP)
Small interfering RNA (siRNA)	Dulbecco's Modified Eagle's Medium (DMEM)	Benzo (a) pyrene (BaP)
Copy Deoxyribonucleic acid (cDNA)	Sodium hydroxide (NaOH)	Sodium fluorescein (F-Na)
Long chain fatty acid (LCFA)	Epidermal growth factor (EGF)	Distilled water (dH₂O)
Coenzyme-A (CoA)	Bovine pituitary extract (BPE)	Phosphate buffered saline (PBS)
3-hydroxy-3-methylglutaryl- coenzyme A (HMG-CoA)	Bovine serum albumin (BSA)	Rhodamine (Rh123)
Sodium chloride (NaCl)		Sodium fluorescein (F-Na)
Ethanol (EtOH)	Nutrient mixture F12 (F12)	Dimethyl sulfoxide (DMSO)
Potassium chloride (KCl)	β-mercaptoethanol (β-ME)	Acetonitrile (ACN/MeCN)
		Polyethylene glycol (PEG)
		Hydroxypropyl Methylcellulose (HPMC)

Water for injection (**WFI**)

GF120918 (**GF**)

Neonatal Fc Receptor
(**FcRn**)

Rhodamine 6G (R6G)

Pharmacokinetic/s (**PK**)

Pharmacodynamic/s (**PD**)

Substrate concentration at
which V is 50% of V_{\max} (**K_M**)

Rate constant describing
input into the perfusate;
determined by linear
regression (**k_{in}**)

Rate constant describing
input into the perfusate;
determined by nonlinear
regression (**k_a/k_{01}**)

Rate constant describing
loss from the perfusate;
determined by nonlinear
regression (**k_{10}**)

Pharmacokinetic lag time
(**t_{lag}**)

Pharmacokinetic half-life
(**$t_{1/2}$**)

Rate constant describing
loss of Rh123 from
perfusate; determined by
linear regression (**k_{perf}**)

Rate constant describing
disappearance of Rh123
from perfusate, determined
by nonlinear regression
(**k_{NL}**)

Pharmacokinetic clearance
(**CL/F**)

Area under curve (**AUC**)

Chapter 1

General Introduction

1. Introduction

1.1. Structure and function of the lung: barriers to drug absorption

The primary role of the respiratory system is gaseous exchange, providing a continuous supply of oxygen for cellular respiration and allowing removal of the waste product carbon dioxide. In consequence of this essential function, pulmonary morphology allows airflow from the oropharynx through the conducting airways to the deeps lungs where the lung epithelial surfaces are in close proximity to the pulmonary circulation. These features also afford the lungs to represent a route for the delivery of drugs for both local or indeed systemic actions [1]. Drugs delivered to the lungs are in the form of an aerosol; be this a solution aerosol or dry powder. However, the branching architecture of the lung airways and an individual's breathing pattern leads to significant technical demands on inhaler device design and aerosol production. For example, with aerosol inhalation via the mouth in humans, particles of $\geq 10\ \mu\text{m}$ diameter will encounter impaction upon the trachea and upper airway divisions. Generally, particle sizes of 5-10 μm in diameter are then removed by mucociliary clearance, with particles 2-5 μm in diameter having the most potential to reach the deeper parts of the lung, including the alveolar airspace [2]. Figure 1.1 illustrates the lung's branching architecture and highlights the multifaceted surfaces available for drug delivery. Nevertheless, as a drug delivery route, the lung presents an extensive, somewhat potentially more permeable absorptive surface with a reduced metabolic barrier in comparison to the gastrointestinal tract and first-pass through the liver [3].

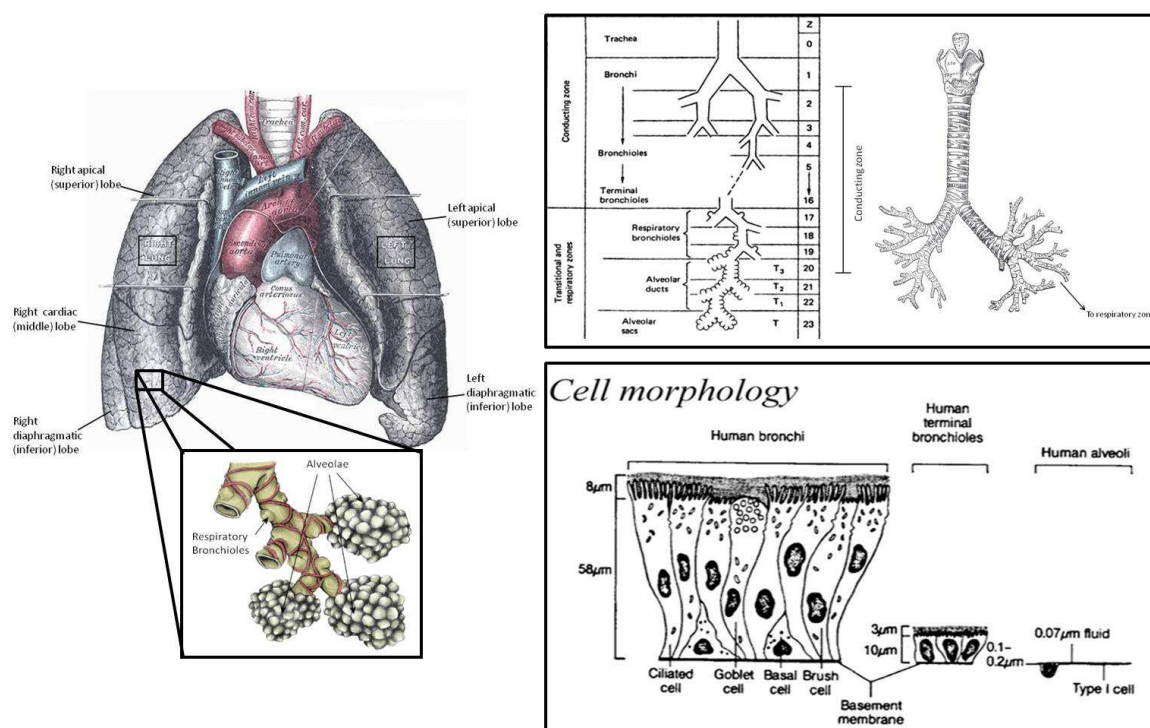


Figure 1.1 Diagrammatic representation of the human respiratory system. Shown, is a simplified model of the branching architecture of the lungs. Further, cell morphology and depth of the epithelial cell barrier to drug delivery decreases as the number of bronchial bifurcations increases and decreases even further with increased depth into the respiratory zone. Taken from [4-6].

The human lung has a large surface area available for drug delivery. Studies have estimated the surface area of the alveolar region alone to be approximately 100 m² which would represent more than half of the surface area of a singles tennis court [7]. To function optimally the respiratory system, and in particular the mucosal barrier, is comprised of many morphologically different and specialised cells; to serve not only respiratory requirements but also to act as a defence against inhaled foreign particles [1]. In order for the successful delivery of a drug to the submucosal regions and beyond to blood, the compound in question has to pass through a number of barriers. These would include; the airway luminal cells, the mucus barrier covering the epithelium lining the airways, and the lung epithelium itself, which is represented by many different histological cell types from the trachea, through the bronchi to the bronchioles, and the alveolar air sacs themselves. This varied lung epithelial cell barrier decreases in thickness with increasing depth into the lung; from an epithelial layer of approximately 50-60 μm at the trachea, to only a single-celled barrier of less than 0.5 micron in the deep lung, all of which may present this region to be a more favourable target for systemic drug delivery [1, 8].

The physical organisation of the respiratory system alone provides a number of barriers to drug delivery and molecule absorption:

Trachea The trachea itself is a significant component of the respiratory system being approximately 11 cm long with a diameter of 2-2.5 cm [4]. The trachea branches to two main bronchi which subdivide for 23 generations [1, 6].

Generation 1–4	Bronchi (cartilaginous airway)	} Conducting airway – no gas exchange
Generation 5-16	Non-respiratory bronchioles that conclude as terminal bronchi	
Generation 17-22	Respiratory bronchioles	} Alveoli – gas exchange
Generation 23	Alveolar ducts	

The airways of the trachea-to-bronchi, of approximately 2 mm diameter, are cartilaginous airways and are comprised of incomplete cartilage rings and smooth muscle. Bronchi of approximately 2 mm to 0.6 mm are deficient in cartilage; generations 13-17, (cartilage ends at generation 12) but do have smooth muscle and it is the smooth muscle contraction that increases rigidity and regulates the airways during respiration [1].

Mucosal barrier The process of mucociliary clearance (MCC), which represents a substantial barrier, accounts for the removal of particulate matter through the sweeping action of ciliated cells moving particles ‘trapped’ within mucus upward toward the oropharynx. Mucus itself is a hydrated mucosal layer which, in mammals, is mainly comprised of mucin glycoproteins secreted, in part, by goblet cells [9]. The pseudostratified, ciliated columnar epithelial cells of the larger airways gradually transform to a single layer of cuboidal ciliated cells at the terminal bronchioles. With mucociliary clearance only involving ciliated cells, which decrease in number toward the terminal bronchioles, the impact of mucociliary clearance lessens, i.e., the rate of MCC is reduced the narrower the airways become, i.e., in the higher airway generations [10].

Surfactant Airway surfactant is composed of approximately 90 % lipids; namely the phospholipids phosphatidylcholine and phosphatidylglycerol, with smaller quantities of phosphatidylethanolamine, phosphatidylinositol and phosphatidylserine. The remaining 10 % is comprised of surfactant-specific proteins (SP) -A, -B, -C and -D. These proteins are divided to two subgroups; hydrophilic SP-A and SP-D, and hydrophobic SP-B and SP-C [11, 12] and function in pulmonary host defence. As a whole surfactant act to reduce lung surface tension and decrease the

possibility of alveolar collapse and have a role in pulmonary host defence systems. Lung surfactant has also been suggested to aid mucociliary clearance via interactions with inhaled particles [13].

Cells There are over 40 different cell types within the lung, presenting a substantially varied barrier for any molecule. The upper airway is mainly comprised of 3 cell types; basal cells; which are thought to possess an ability to differentiate, goblet cells; which secrete mucus and ciliated cells; which specialise in ciliary action [14]. While perhaps the more extensive barrier, the alveolar region, contains 2 major cells types(not including macrophage); alveolar epithelial type I (AEI) cells and the type II (AEII) cells [7]. AEI cells are squamous in appearance, constitute approximately 95 % of the alveolar epithelial surface area and yet only approximately 30 % of the total alveolar epithelia (AE) cell population. These squamous pneumocytes in their more peripheral attenuated regions form a cellular barrier of only 0.1 – 0.3 μm in thickness; this thin cell phenotype is considered important in to gaseous exchange. The AEII cells are cuboidal in shape and although are more numerous (approximately 66 % total AE cell population), account for only approximately 5 % of the alveolar surface area [14]. These granular pneumocytes possess microvilli and lamellar inclusion bodies involved in surfactant production, surfactant protein secretion and recycling [13].

Interstitium The interstitium is regarded as the extracellular and extravascular space between cells and is mainly comprised of collagen fibres, fibroblasts and basement membrane or extracellular fibres. This barrier acts as both a tough fibrous filter and an extracellular matrix for the attachment of cells [7]. Despite the interstitium presenting an obvious physical barrier, studies have suggested that it does not contribute considerably as an obstacle to absorption. For example, Schneeberger-Keeley and co-workers have demonstrated, by ultrastructural cytochemistry, the ability of horseradish peroxidase (40 kDa) to readily traverse the basement membrane [15] from the vasculature, i.e. the limiting barrier from airspace to blood is the lung epithelium.

1.2. Advantages and disadvantages of pulmonary drug delivery

Regardless of the obvious anatomical barriers to inhaled particles, the lung is an important drug delivery route for the local treatment of pulmonary diseases such as asthma and chronic obstructive pulmonary disease (COPD), and with certain examples as a route for the systemic delivery of drugs [8]. This delivery route was first exploited in 1925 by Gänsslen who delivered insulin via a number of inhalation devices (Stäubli-Inhaler, Riviera-AA-inhaler) to five diabetic subjects and in turn noted a decrease in blood glucose level [16]. Therapeutic molecules delivered via this route generally show more extensive absorption than by other routes of administration and permeation enhancers; such

as sodium deoxycholate or sodium lauryl sulphate, are not generally a feature of a pulmonary formulation [7, 17]. Advances in aerosol science have allowed for more efficient and reproducible delivery of particles to the lung and improved penetration to the deep lung, where clearance of particles is slower [18]. For local lung disease, administration by the pulmonary route provides for higher concentration of drug at the target site, permitting rapid onset of action and lower systemic exposure, with reduced potential of systemically-mediated side effects [19].

As mentioned above, the lungs provide a relatively large area for drug absorption, with the potential for aerosolised drug to almost simultaneously reach a significant proportion of this surface. The lungs receive full cardiac output from the right-hand side of the heart and in the alveolar region, the blood flowing through the pulmonary vasculature is separated from the luminal epithelial surface by only a short distance (less than 1 μm); comprising the thin attenuated regions of the AEI and pulmonary microvascular cells. This extremely well vascularised, thin air-blood barrier provides great capacity for rapid absorption of dissolved molecules. Further, the lung has a comparatively low metabolising enzyme activity when compared to the liver (i.e. liver is of influence when delivering drugs via the [very common] oral route). Analysis of phase I and II metabolising enzymes in lung parenchymal cells and hepatocytes by Somers and colleagues indicated phase I activity to be < 10 % of that in hepatocytes when comparing rates of probe substrate metabolism ($\text{mL/min}/10^6$ cells) in freshly isolated parenchymal cells to hepatocytes; negligible expression of CYP3A4 in parenchymal cells was also reported [3]. In summary it is clear why the lungs are an important route for the delivery of locally acting drugs in pulmonary disease, and why this route has also attracted significant attention in terms of the systemic delivery of drugs, particularly biologics such as antibodies (e.g. monoclonal antibodies that target bacterial antigens such as those of *Yersinia pestis* have been investigated) [7, 20, 21].

However, despite the lungs representing a very attractive means of non-invasive delivery, it is by no means without issue. There are several anatomical, technical, and lung defence factors that need to be considered. As mentioned previously, there is a marked difference in cell morphology, i.e. cell barrier, from the upper lung airspace to deep lung. This not only provides an array of barriers to traverse in terms of systemic delivery but also raises the issue of different permeability profiles down the respiratory tract. Clearly, for local drug delivery, there will likely be the need to target specific regions of the airways for optimum local action, the same is true when systemic delivery is the aim, where more preferential deposition in the deeper lungs will be important [22].

The delivery of drugs to the lung is technically challenging, requiring the reproducible generation of an aerosol particle population emitted from an inhalational device that displays appropriate particle size and population size distribution; hygroscopic aerosol particles sizes can change significantly upon exposure to humid conditions. The drug formulated into the inhaler device must be stable for prolonged periods of storage as a dry powder, in organic propellant or in solution. How the device is used by patient and the patient's breathing pattern can all influence the deposition pattern of the aerosol within the respiratory tract. Particle deposition within the conducting airways involves susceptibility to clearance by the mucociliary escalator. Particle deposition beyond the conducting airways is subject to macrophage engulfment within the alveolar sacs. Due to the virtual lack of fluid movement in the alveoli, sequestration in lining fluid, and the delicate nature of the epithelium, drug retention and possible onset of toxic effects or immune/phagocyte induction/activation within the alveoli cannot be overlooked [8, 22, 23].

1.3. Techniques for pulmonary drug delivery

Aerosol devices to enable the delivery of drugs to the lung have been in existence since the 1900's, however, these early devices were inefficient and impractical [18]. In order to fully utilise the pulmonary system as a delivery route, new more efficient devices were required. This necessity for development is, and remains, not without issue [22].

Continued improvements in aerosol device and particle technology have allowed production of stable formulations and accurate delivery methods (over 25 inhalation drugs on the market for lung diseases by development peak of 2004; by 2010, 27 breath-activated and metered-dose products exist for the treatment of asthma and COPD alone) [20, 24]. Drug aerosols with optimum aerodynamic characteristics can be delivered to the lung with efficiencies as high as 90 %, however, this is highly dependable upon patient compliance. Several different devices have been developed. These include pressurised metered-dose inhalers (pMDI), dry powder inhalers and nebulisers; each one of which has undergone significant technical development to ensure 'fit-for-purpose' functionality. These devices allow controlled dose metering, producing delivery of a single dose of drug with a specific formulation which has been developed to meet the requirements of pulmonary delivery. However, as with any patient-controlled dosing device, issues of education and compliance arise. Incorrect usage having the potential to impact upon release of drug from a device and drug deposition/sedimentation within the lung [25].

Pressurised metered-dose inhalers (pMDI)

Development of pMDI's has allowed delivery of aerosol particles at high velocity, which can increase lung penetration but also lead to significant impaction on the oropharynx [22]. Such devices are highly desirable as they are portable, easy to use, tamper proof and allow accurate multi-dosing [25]. Initially however, many pMDI devices utilised chlorofluorocarbons (CFC's) to provide the pressure needed for drug delivery. In 1991, under the Montreal protocol [26], these propellants were withdrawn from use in all technology due to the threat they posed on the environment. At this time pharmaceutical companies began researching alternative propellants and began using hydrofluoroalkanes (HFA's) while simultaneously focussing further upon delivery methods such as dry powder inhalers and liquid aerosol nebulisers for the pulmonary delivery of therapeutic drugs [18].

Dry powder inhalers (DPI)

Many therapeutic molecules are not readily formulated into pMDI but nevertheless require to be formulated in a way that enables efficient delivery of drug to the lung surfaces and provide protection of the drug against chemical degradation. The use of dry powder formulation devices represents an alternative aerosol device technology which can afford a reproducible and convenient inhalation method [27]. Dry powder preparations provide pre-metered drug packed in 'blisters', producing a metered dose that can be accurately assessed. However, dry powder inhalers only deliver drugs when a patient inhales, thus raising patient technique compliance issues. Further, both pMDI and dry powder devices suffer from dose retention within the device and dose deposition in the oropharynx region therefore influencing dose deposition in the lung and drug bioavailability [25].

Nebulisers

The nebulisation of liquids to generate aerosols is an efficient means of pulmonary delivery. Drugs in a nebulised solution allow deposition of larger drug doses (which are sometimes seen as more 'respirable' by patients) to the deep lung.

There are two main types of nebuliser device, the air-jet nebuliser and ultrasonic nebuliser. These devices create highly respirable drug aerosol droplets of optimum aerodynamic parameters for effective pulmonary delivery. However these systems require reasonable aqueous drug solubility and are often not very portable, negatively impacting as a delivery device in this way [25]. Further, drug stability issues in the nebulisation process itself and dose retention in the nebuliser are considerations.

1.4. Examples of pulmonary drug delivery for both local and systemic action

The delivery of drugs to the pulmonary system is well established for the treatment of respiratory diseases such as asthma, COPD, cystic fibrosis and pulmonary infections and so the delivery of drugs such as bronchodilators and anti-inflammatory steroids is well recognised. Increasingly, the lungs have been utilised for the delivery of a variety of molecules including peptides, proteins and antibiotics with the delivery of the first nebulised protein, DNase, for cystic fibrosis in 1994 and nebulised antibiotic, tobramycin, in 1998 [22].

Perhaps the most publicised protein to be delivered to the lung is insulin for the treatment of diabetes. The work of Gänsslen gave the first example of the efficacy of insulin after pulmonary administration in 1925; however, studies then lay dormant for many years. Several animal studies sought to demonstrate the potential of inhaled insulin and gave direct evidence of the absorption and efficacy of insulin following administration by aerosol [16, 28]. Work progressed to human proof-of-concept with Skyler *et al.* demonstrating the capability of inhaled insulin to treat type I diabetes in 2001 [29]. Inhaled insulin in the DPI product Exubera (Pfizer) was approved in 2005 in both Europe and America for the treatment of adults with diabetes [22] but it was approved for use only in limited indications which resulted in Pfizer eventually withdrawing the product from the market.

Despite the withdrawal of inhaled insulin, predominantly on commercial grounds, it is this work together with the very early groundbreaking work of Gänsslen [16] that has served as proof-of-concept for the delivery of peptides and proteins to the systemic circulation via the lung. While there are few licensed inhaled drugs for systemic action, this area of pulmonary delivery has produced a number of preclinical and clinical development examples for the delivery of peptides, proteins and other small molecules to the systemic circulation. For example, the work of Dershwitz and co-workers found that administering inhaled morphine to human lung produced a bioavailability of 59 % absorption displaying similar kinetics to that of intravenous bolus administration. Rapid absorption would provide swift onset of drug action (pain relief) whilst avoiding problems of slow absorption and metabolism associated with oral administration [30]. Another successful example is that of inhaled human growth hormone (hGH). Together with improvements in aerosol technology, inhaled hGH; termed somatropin inhalation powder (SIP) has been successfully introduced via the pulmonary system and has recently undergone extensive toxicology, pharmacokinetic (PK) and pharmacodynamic (PD) studies in primates and adult human males and has proved to be safe and tolerable as a treatment regimen [31, 32]. Other examples of treatments being investigated for

systemic delivery via the pulmonary system include; Interferon β for multiple sclerosis, leuprolide acetate to treat prostate cancer, calcitonin and parathyroid hormone to treat osteoporosis, heparin to prevent thrombosis, and dihydroergotamine for treatment of migraine [18].

1.5. Mechanisms of drug transport and absorption across the lung

The precise mechanism(s) of drug absorption from the lung, especially for large macromolecules remain relatively unknown. Further, for small molecules the role of active transport processes as a component of the drug absorption process remains unquantified; indeed for some molecules the overall penetration across lung epithelium will reflect a combination of different processes. The majority of drugs and solutes are probably absorbed from the airspace by two general transport mechanisms; transcellular passive diffusion and paracellular passive diffusion (Figure 1.2). Clearly active transport will also be important for some drugs. In particular, higher molecular weight biologic-based drugs, such as proteins, will also have a component of their transport that is managed by an endocytic vesicular-mediated process such as clathrin-mediated uptake. There will also be some low molecular weight drugs whose transport is determined by active or facilitated carriers [7].

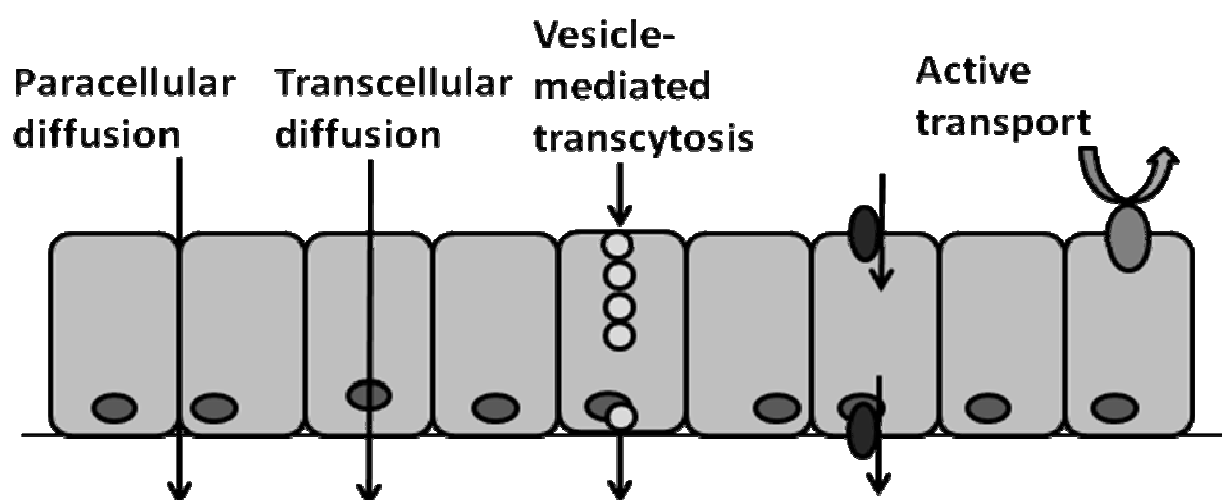


Figure 1.2 Mechanisms of drug transport across lung epithelia. Adapted from [33].

Paracellular transport Major mechanism by which hydrophilic molecules pass across an epithelial barrier through the fibrillar network of intercellular tight junctional proteins which circumvent the apical border of each epithelial cell forming the epithelial barrier layer [8].

Transcellular transport Mechanism by which hydrophobic molecules possessing the physico-chemical properties that afford membrane partitioning can enter the epithelial cell and diffuse from the apical membrane through to the basal—lateral membrane to access the sub-epithelial layers [8].

During the 1970's and 80's the body of work of Shanker and co-workers, examining the disappearance from the intact lung of a diverse range of compounds following intratracheal and aerosol administration, illustrated that most compounds are absorbed and transported via passive diffusional pathways [34, 35]. From this data, it was predicted that macromolecules with a molecular weight under 40 kDa and hydrophilic molecules will traverse cell membrane barriers via tight junctions while lipophilic compounds will permeate predominantly via transcellular diffusion; n.b., these lipophilic compounds will also access the paracellular route, albeit with the paracellular route contributing, to a minor extent, to overall lipophilic drug absorption [7, 36]. The density of membrane vesicles within the alveolar region also provides the opportunity for vesicle-mediated transcytosis as a transport mechanism in the lungs. Many of these vesicles are morphologically recognised as caveolae and are involved in the active vesicular transcytosis of macromolecules across endothelial cells [37]. The transport of proteins, such as albumin, in rat pulmonary endothelial cells has been shown to be mediated by caveolae, suggesting vesicle-mediated transport to contribute to the mechanism of protein transport at the air-blood barrier [38].

Active transport Molecule transport that is energy-dependent and can be inhibited by other molecules that can compete for common or alternative binding sites on membrane carrier proteins. There are a variety of mechanisms by which membrane carrier proteins can transport a drug across the biological membrane.

The presence and contribution of carrier-mediated active transport in the lung is relatively poorly defined. Influx transporters such as the peptide transporter PEPT2 have been localised to several lung regions and cell types [39]. The efflux transporter P-gp/MDR1 and many other ATP-binding cassette (ABC) transporters have also been localised to the lung epithelial cells [40]. While there is increasing evidence as to the presence of active transporters in the lung, the data accumulated by Schanker and colleagues between the 1970s and 80s, suggest that molecules that are substrates for active transporters do not significantly deviate in their absorption profile from other molecules of similar molecular weight or lipophilicity [20]. Schanker *et al.* studied tens of lipid insoluble substrates, with molecular weights ranging from 60 - 70,000 kDa and reported that; overall, absorption within the lung was inversely related to molecular weight. For example, guanidine (59 M_w) displayed an absorption half-life of 6.3 ± 0.2 min., mannitol (130 M_w), a half-life of 60 ± 6 min

and dextran (20,000 M_w) a half-life of 688 ± 51 min in adult rat lung, highlighting a relationship that is dependent upon properties such as molecular weight and lipid-solubility regardless of any active transport mechanisms that may be present [34, 41].

1.6. Drug transporter proteins

There are many examples of drug permeability at epithelial and endothelial membranes that is influenced by membrane transporter proteins that recognise drug substrates and facilitate or indeed limit their transport across these barriers [42]. Drug transporters have been broadly classified into either uptake or efflux proteins (Figure 1.3) [43].

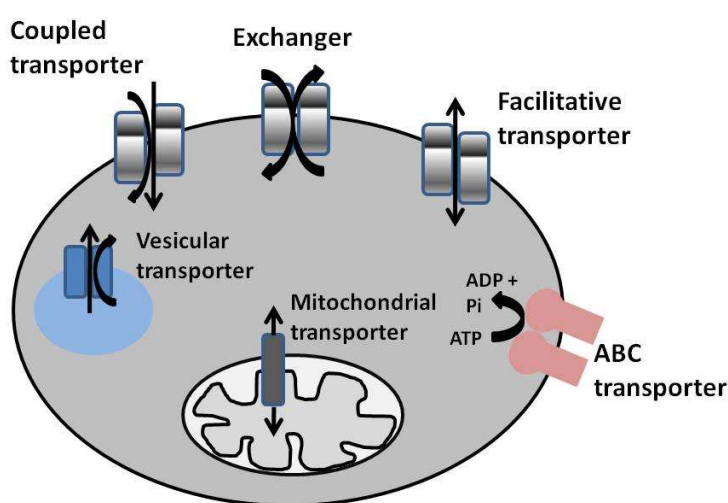


Figure 1.3 Diagrammatic representation of the types of solute carrier transporter; SLC, and ABC transporters present within a cell. Adapted from Hediger *et al.*, 2004 [44].

A large number of genes encoding membrane transporters have been identified in both eukaryotic and prokaryotic genomes. However, not all of these membrane transporters act as functional drug transporters, many have constrained substrate specificity and only a small percentage are associated with the disposition of compounds involved in drug discovery and clinical use [45].

Drug transporters are characterised into two main families; the solute carrier family or SLC transporters and the ATP-binding cassette family, or ABC transporters.

Solute Carrier (SLC) Transporters

The SLC transporter family is comprised of 43 families containing some 298 members. Members of this super-family are assigned based on amino acid sequence identity; family members share 20-25

% sequence identity while subfamily members share at least 40 % sequence identity. It is generally thought that >2000 (5 %) of all human genes are transporter-related, with the SLC family holding a significant number of these genes (currently ~300 SLCs identified) illustrating deep ancestry and affirming the significance of transporter proteins in maintaining cell homeostasis [44]. In order to identify members of each transporter family and subfamily, each gene is labelled using a root symbol, i.e., SLC or ABC. SLC members are identified with a numeral to indicate family; SLC1, followed by a letter divider; SLC1A, and finally a number to identify an individual gene; SLC1A1. While this system of nomenclature easily and accurately identifies the majority of SLC family members by gene (note - a selection of transporters can be identified by more than one protein name), the SLC21 family required modification of the classification system. Originally SLC21, the family number and letter divider were replaced with the letter 'O' representing 'organic transporter'. This alteration occurred in order to accommodate species-independent identification of transporter isoforms that arose due to rapid family evolution [44, 46].

In comparison to ABC transporters, SLC transporters are a very diverse family and contain genes that are known to encode facilitative transporters, ion-coupled transporters and exchangers [44]. Despite this diversity, SLC transporters share the same basic structure as their ABC counterparts, comprising transmembrane domains (TMD) for anchoring and some form of functional domain(s) to facilitate transport of specific substrates. For example, the passive urea transporter UT-B1 is comprised of 10 TMD and 1 glycosylated extracellular loop, while the ion-coupled transporter SLC14A1 is comprised of 12 TMD which are flanked by hydrophobic NH₂ and COOH- terminal domains with an extracellular loop at TMD 7-8 [47, 48]. Because SLC transporters do not utilise ATP, the secondary topology of these transporters appears much simpler than transporters of the ABC family, however, their diverse nature and expansive substrate specificity suggest them to be more complex than they initially appear.

In contrast to ABC transporters, many SLC transporters do not achieve the driving force for substrate transport from ATP hydrolysis but rather from the electrochemical gradient of their substrates and are therefore termed secondary active transporters [49]. While drug transporter secondary topology is comparable between SLC transporter families, their mechanism of action varies from simplistic to complex. For example, mammalian sodium-proton exchanger transporters have a simple 1:1 exchange mechanism where 1 Na⁺ and 1 H⁺ traverse the membrane down electrochemical gradients (Figure 1.4) [49]. In comparison, long chain fatty acid (LCFA) transporters of the SLC27 family are proposed to have a more complex mechanism of action where extracellular

LCFA bind directly to fatty acid transporter complexes to be transported into cells and then couple to intracellular coenzyme-A (CoA) via long chain fatty acid acyl-CoA synthetase, to prevent LCFA efflux [50]. Unlike many other SLC family transporters, fatty acid transporters require ATP binding to facilitate LCFA transport [50].

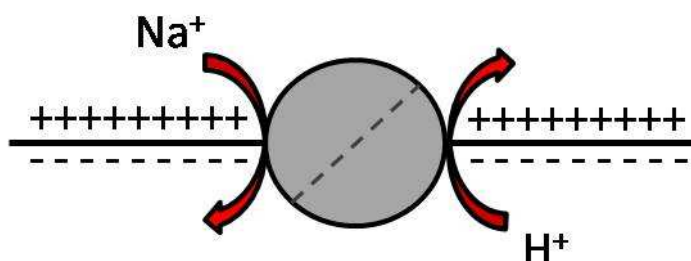


Figure 1.4 Diagram illustrating the mechanism of action of simple Na^+/H^+ exchanger proteins (SLC9 family) present in mammalian cells. Adapted from Orłowski *et al.*, 2004 [49].

ATP Binding Cassette (ABC) transporters

Examples of ABC family transporters are found in eukaryotes and prokaryotes and evidence of prokaryotic and eukaryotic ancestry suggest that many subfamily members began to specialise early in the ancestry of these proteins, perhaps highlighting significant physiological roles for these proteins. Paralleling SLC transporters, ABC family members are also assigned based on amino acid sequence identity, which is influenced by ABC family divergence from a common ancestor into 7 subfamilies denoted with a letter; ABCA - ABCG. To allow individual identification of ABC transporters, a letter corresponding to the subfamily; ABCA and a number to identify an individual member; ABCA1 are added [51, 52].

Transporters of the ABC family can be divided into two groups based on the direction of substrate transport; (1) ABC importers which are present only in prokaryotes, and (2) ABC exporters. All ABC exporters share a basic structure of transmembrane domains (TMD), which provides passage for substrates; and at least one nucleotide-binding domains (NBD), which binds and hydrolyses ATP [53].

Nucleotide-binding domains (NBD) These structures act as the motor unit of ABC transporters and consist of RecA-like and helical sub-domains. Within each NBD there are conserved sequence motifs that are involved in either ATP binding and hydrolysis or in aiding interface formation in the assembled protein. A comprehensive review by Hollenstein *et al.* describes these conserved sequences, briefly motifs include: Walker-A domain or P-loop, which binds the nucleotide; LSGGQ

motif which contacts the nucleotide in an ATP bound state; Walker-B domain which provides a conserved glutamate residue that coordinates nucleophilic attack on ATP via a water molecule; Q-loop which is thought to sense the γ -phosphate moiety and aid in interfacial contact with the TMD; D-loop which is involved in formation of a contact loop between the two NBD; A-loop which provides an aromatic side residue that stacks against the adenine moiety of the bound nucleotide, and finally the Switch motif that is thought to contribute a histidine side chain to the catalytic reaction [53]. In the case of full ABC transporters bearing two nucleotide-binding domains, these NBD domains arrange themselves in a 'head-to-tail' conformation creating two ATP binding sites between a Walker-A domain of one NBD and a LSGGQ motif of the other. Transporters do exist and function with only one NBD, for example, the half-transporter BCRP bears only a single NBD and then creates a homodimer with another BCRP protein to create a functional transporter. Figure 1.5A illustrates the arrangement of these conserved motifs in each NBD [53-56].

Transmembrane domains (TMD) These domains are membrane-spanning and are highly variable in primary sequence, length, architecture and number of helices. As can be seen in figure 1.5A, ABC export proteins generally consist of 12 transmembrane (TM) helices although BCRP is an example of a half-transporter with 6 TMDs and MRPs-1,-2,-3 each have 17 TMDs. These helices form a channel within the membrane for substrate passage and protrude into the cytoplasm, splitting into two distinct arrangements, sometimes referred to as 'wings', towards the extracellular side of the membrane [53, 57, 58].

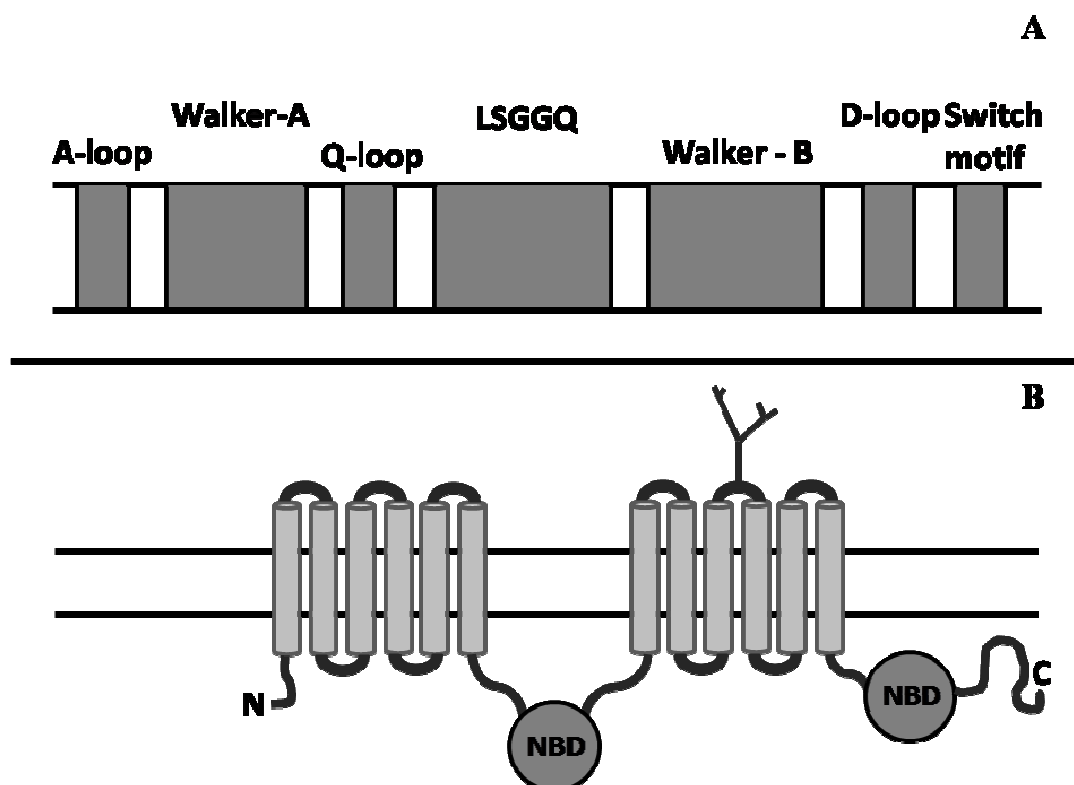


Figure 1.5 (A) Diagram illustrating the organization of conserved sequence motifs in the nucleotide-binding domain of ATP transporter proteins. (B) Example of the predicted secondary structure of an ABC transporter. Structural information is assumed from the homologous Sav1886 *S. aureus* transporter protein, for which the structure has been determined [53, 59, 60].

The binding and hydrolysis of ATP to drive drug transport by ABC transporters creates a complex mechanism of action. Structural data obtained for the ABC drug transporter ABCB1/P-gp/MDR1 combined with data obtained from the homologous Sav1886 transporter of *S. aureus* have given rise to the ATP switch model. This model is the most widely accepted model to explain the mechanism of ABC drug transport, the driving force for transport being a switch between two conformations of the NBD dimer [59].

While there is only moderate information available regarding ABC drug transporter structure especially when substrate-bound, more information [57, 58, 61-67] is available on the mechanism of action of ABC substrate transport, essentially:

Two TMB form a chamber in the membrane which they 'capture' substrate molecules from the inner leaflet of the lipid bilayer. Two NBD then form a 'head-to-tail' sandwich dimer so that each NBD contacts both TMB. Two ATP binding pockets are then formed at the NBD dimer interface and ATP binding causes a rigid rotation of the domains within each NBD creating a closed dimer with 2 ATP molecules sandwiched at the interface. ATP hydrolysis and ADP + Pi release return the dimer to an

open configuration. The ATP-binding at the NBD and the formation of a closed dimer induce conformational changes in the TMDs which aids substrate translocation, causing a reduction in drug-binding affinity and reorientation of the drug binding site to expose it to the extracellular membrane face for release [57, 58, 61-67].

1.7. Drug transporter proteins of interest to drug discovery

For many drugs and clinically relevant compounds, there are a number of significant determinants of PK profile and elicited therapeutic response and there are often contributions from passive diffusion, metabolising enzymes and active transporter processes. In order to minimise, or indeed utilise such contributions, preclinical drug evaluation has focussed on examining the contribution of drug-drug interactions (DDI) and drug metabolising enzymes (DME) to the safety and efficacy of drugs in development. The role and influence of drug transporters has been increasingly recognised as of importance to *in vivo* drug absorption and disposition, efficacy and adverse reactions [68].

In 2007 a group of scientists formed the International Transporter Consortium to identify transporters of interest, discuss techniques to differentiate drug transporter interactions and recommend guidelines for drug transporter scientists working in the preclinical and clinical studies arena. In 2010, the consortium published a set of decision trees to support those involved in clinical studies and advised upon investigations. Decision trees posed questions regarding assay flux ratios and the effect of inhibitors on transport assays. The full publication can be reviewed in a publication by Giacomini *et al.* [68].

Relative to the total number of recognised drug transporter proteins, only a small number of families are currently thought to impact significantly upon the absorption or disposition of therapeutic compounds. Variation in the function and expression of drug transporter proteins has the potential to produce unexpected and variable pharmacokinetic profiles *in vivo* and the distribution or entry of compounds to specific organs or tissues can often be positively or negatively influenced by uptake and efflux transporters. Understanding the importance of drug transporters and transporter-dependent pathways may aid in the drug discovery process by allowing transporters to be used for target site entry or to avoid developing drug candidates whose pharmacokinetics are negatively affected by transporters [45].

For drug discovery and development, transporters that are expressed in the liver, kidney and intestine, and the endothelium of the blood brain barrier are of particular focus, figure 1.6 represents the membrane localisation of a number of these transporters in organs of interest.

Traditionally these transporters function to uptake vital endogenous substrates or protectively function to eliminate harmful or toxic compounds from the body and it is these physiological functions and expression profiles that have highlighted the transporters of these organs as worthy of investigation in the field of pharmaceuticals [45, 68]. These sites also represent the major tissues or barriers known to affect drug pharmacokinetics, be that from oral absorption and first-pass, through both metabolic and excretory elimination pathways to accessing the brain across a most distinctive barrier.

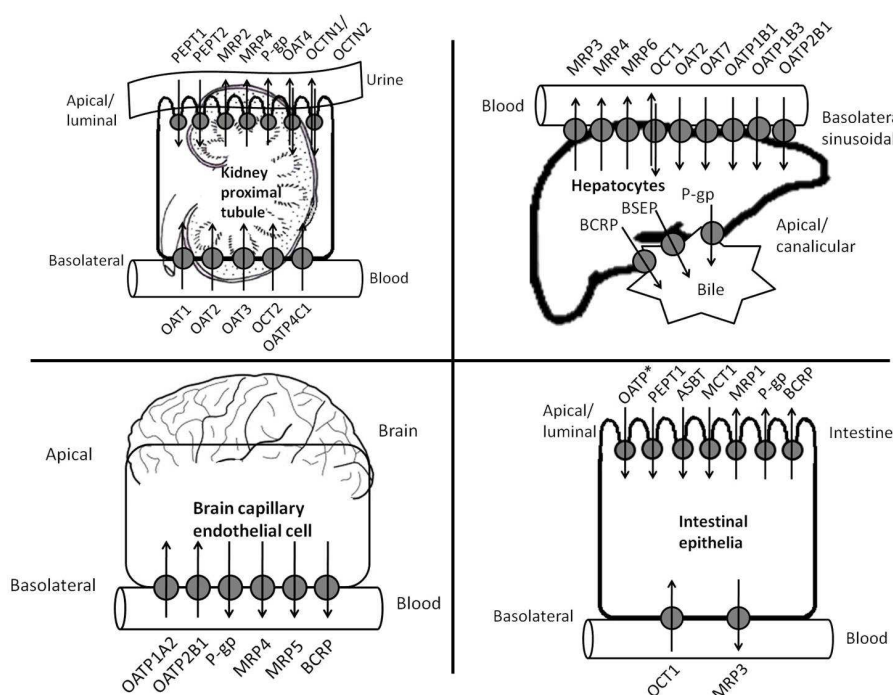


Figure 1.6 Examples of human drug transporter with the ability to transport a number of clinically relevant drugs and endogenous substrates. Transporter proteins of the kidney, liver, brain and intestines are displayed. Adapted from [68].

Drug transporters can either function as targets for drugs, or indeed as processes which can either positively or negatively affect a drug's pharmacokinetics. Of the 400+ identified human 'drug transporter' proteins, many *could* be considered for their influence in drug disposition and therapeutic response. For example, glucose transporters of the SLC5 family have been targeted to treat glucose malabsorption, neurotransmitter transporters of the SLC6 family have been targeted with antidepressants and antiepileptics for the treatment of epilepsy, depression and schizophrenia, and peptide transporters of the SLC15 family have been targeted with drug analogues, such as DOPA-Phe, and nucleoside based antivirals to improve bioavailability via PEPT1 [44]. Other sub-

families of interest include; SLC16, SLC17, SLC22, SLC29 and SLCO [69]. Highlighted in table 1.1 is a selection of SLC drug transporters of particular interest to drug discovery and development.

Transporter Family	Substrates (S)/ Inhibitors (I)	Expression	Disease association	Therapeutic implications	Ref.
SLCO1 OATP1B1 (SLCO1B1) OATP-B (SLCO2B1)	S: Bile acids, Bilirubin, Oestrone-3-sulphate, Statins, Fexofenadine I: Saquinavir, Rifampicin, Cyclosporine	Hepatocytes, Endothelia	Link of polymorphisms with hepatotoxicity	<ul style="list-style-type: none"> • Influence upon drug disposition and elimination • DDI • Clinically relevant polymorphisms 	[68]
SLC7 CAT-1 (SLC7A1)	S: Cationic L-amino acids I: Many substrates act as competitive inhibitors	Ubiquitous - except human adult liver	Link to retroviral infection susceptibility	<ul style="list-style-type: none"> • Influence upon drug disposition and elimination • DDI 	[68]
SLC22 OAT1 (SLC22A6) OCT1 (SLC22A1) OCTN1 (SLC22A4)	S: Methotrexate, Zalcitabine, Metformin, Tetraethylammonium I: Novobiocin, Probenecid, Quinidine	Kidney proximal tubule, Placenta, Hepatocytes, Intestinal enterocytes, Skeletal muscle	Gene mutations of OAT1 result in gyrate atrophy	<ul style="list-style-type: none"> • Influence upon drug disposition and elimination • DDI • Clinically relevant polymorphisms/mutations 	[68]
SLC5 SGLT1 (SLC5A1) SLGT2 (SLC5A2) NIS (SLC5A5)	S: Glucose, Galactose, Biotin, Iodine I: Phlorizin	Small intestine, Kidney, Heart, Lung, Skeletal muscle, Thyroid, Placenta	Gene defects can result in Familial renal glycosuria, Glucose and galactose malabsorption and Thyroid hormonogenesis	<ul style="list-style-type: none"> • SGLT1 cytoprotective function has potential to be exploited during chemotherapeutic treatment with cisplatin • Increased transporter expression can aid in overcoming Insulin resistance. 	[68]
SLC6 GAT1 (SLC6A1) GAT3 (SLC6A11) DAT (SLC6A3)	S: GABA, Norepinephrine, Dopamine, Serotonin, Glycine, Creatine I: ACHC, DABA, Cocaine, Benztrrophine, Many antidepressants	GABAergic neurons, Adrenal gland, Placenta, Dopaminergic neurons, Spinal cord.	Gene defects can result in Epilepsy, Schizophrenia, Anorexia nervosa, Parkinsonism, Tourette syndrome, Cardio-myopathy	<ul style="list-style-type: none"> • GABA transporters targets for anti-epileptic drugs • DAT transporter target for blocking dopamine uptake in Parkinson's disease 	[68]
SLC16 MCT1 (SLC16a1)	S: Lactate, Pyruvate I: Quercetin, Phloretin	Ubiquitous	Link to muscle weakness associated with exercise	<ul style="list-style-type: none"> • Influence upon substrate ADME 	[68]
SLC15 PEPT1 (SLC15A1) PEPT2 (SLC15A2)	S: Di- and Tri-peptides, Glycylsarcosine, Cephalexin, Cefadroxil I: Glycyl-proline, Zofenopril, Fosinopril	Intestine, Kidney, Lung, Brain	Suggested link with Crohn's disease and Ulcerative colitis	<ul style="list-style-type: none"> • Influence upon drug disposition and elimination • DDI • Numerous splice variants – may have relevance in future drug discovery • Potential target for treatment of IBD 	[68]

Table 1.1 SLC transporters of clinical significance. Each transporter has the capacity to in some way influence a drugs' pharmacokinetic profile *in vivo*. The selected transporters below represent the transporter families of interest; other family members may also be of clinical significance. Note that only examples of transporter substrates and inhibitors are included and that listed diseases do not necessarily correlate to specific members mentioned here. (GABA) γ -aminobutyric acid, (DDI) drug-drug interaction, (ACHC) cis-3-aminocyclohexane carboxylic acid, (DABA) 1-2, 4-diamino-N-butyric acid [68, 70-75].

Active transporters of the ABC family are extremely influential upon the behaviour of many clinically relevant drugs. In terms of drug discovery, ABC transporters that have been of particular focus are members of the ABCB, ABCC and ABCG families [60]. For example, P-gp/MDR1 (ABCB1) was the first cloned and characterised human ABC transporter and was discovered through its ability to confer drug resistance in tumour cells [70]. It has been reported that three genes; P-gp (ABCB1), MRP1 (ABCC1), and BCRP (ABCG2) are responsible for the majority of all transporter-related multidrug resistance observed in both human and rat tumours [71]. Those members of the ABC superfamily that are influential to drug discovery are mainly expressed in the same tissues mentioned for the SLCs, namely liver, kidney and intestine, and the endothelium of the blood brain barrier. ABC efflux transporters function to remove toxic metabolites protecting cells from chemical toxicity and oxidative stress [72]. Table 1.2 highlights a selection of ABC transporters that have evidential influence upon the transport and action of a large number therapeutic compounds and thus are very significant to the drug discovery process.

Transporter Family	Substrates(S)/Inhibitors(I)	Expression	Disease/condition association	General therapeutic implications
ABCB P-gp/MDR1 (ABCB1)	S: Many hydrophobic substrates, lipids, Steroids, Xenobiotics, peptides, Drugs e.g. Fexofenadine, Vinblastine, Digoxin. I: Verapamil, Cyclosporin, Elacridar (GF120918) [70-75].	Mainly secretory cells such as those of the Kidney, Liver, Intestine, and adrenal gland. Brain endothelia, Pulmonary epithelia [70-75].	Immune deficiency, Ivermectin susceptibility [70-75].	<ul style="list-style-type: none"> • Influence upon drug absorption, disposition and elimination • DDI • Influence upon drug bioavailability • Influence on brain entry of drugs (barrier) • Influence on multidrug resistance • Clinically relevant polymorphisms <p>[68, 70-75]</p>
ABCC MRP1 (ABCC1) MRP2 (ABCC2) MRP3 (ABCC3) MRP4 (ABCC4)	S: Diverse range of endogenous substrates and xenobiotics including glutathione, Glucuronide conjugates, Methotrexate, Etoposide, Mitoxantrone, Valsartan, Olmesartan. I: Cyclosporin, Emtricitabine, Delaviridine, Efavirenz [70-75].	Kidney proximal tubule, choroid plexus, hepatocytes, intestinal enterocytes [70-75].	Cystic Fibrosis, Dubin-Johnson syndrome, Pseudoxanthoma elasticum, CBAVD, FPHH [71].	
ABCG BCRP (ABCG2)	S: Mitoxantrone, Methotrexate, Topotecan, Imatinib, Irinotecan. I: Fumitremorgin C, Elacridar (GF120918), Oestrone [70-75].	Placenta, BBB, mammary glands, Kidney proximal tubule, Intestinal enterocytes, Hepatocytes [70-75].	Sitosterolemia [71].	

Table 1.2 ABC transporters of clinical significance. Each transporter has the capacity to in some way influence a drug's pharmacokinetic profile *in vivo*. The selected individual transporters included represent the transporter family of interest; other family members may also be of clinical significance. Note that only examples of transporter substrates and inhibitors are included and that listed diseases do not necessarily correlate to specific members mentioned here. (DDI), drug-drug interaction, (CBAVD), congenital bilateral absence of the vas deferens, (FPHH) familial persistent hyperinsulinemic hypoglycaemia of infancy. [68, 71-74].

The interplay between drug transporters present in the lung and drugs targeted to this region will influence greatly drug discovery processes involving the pulmonary system. Combined with the need for a comprehensive review of drug transporters expressed in the lung, it is important to exploit a model that accurately represents the morphological environment and transport processes present in this region.

1.8. Experimental models to assess pulmonary drug transport

In order to reproduce conditions within the lung, and specifically at epithelial barriers which are regarded as a prominent obstacle to drug absorption, four main model types are employed. These are; cell culture models, *in vivo* whole animal models, *ex vivo* isolated perfused lung organ models and tissue explants [23, 75].

Cell culture models The use of cell culture models is now widely accepted within the pharmaceutical industry and is promoted by some as having predictive ability (this is particularly so in the intestinal oral absorption field) and certainly provide high throughput. In the lung discipline, *in vitro* model systems are particularly used for mechanistic investigation. The use of *in vitro* models to study permeability and relate this to *in vivo* lung absorption is, for the most part, poorly developed; mainly limited to academic laboratories. It should be of note that the use of *in vitro* models for the intestine gained acceptance only after many years of experimentation and thousands of compounds addressing *in vitro* to *in vivo* relationships. Almost every pharmaceutical company had an interest in oral drug delivery and contributed to the knowledge base; this is not the case for pulmonary delivery which represents a more limited commercial market.

Both models of the alveolar epithelium and also of the bronchial epithelium are used in studies of lung transport [76]. Alveolar models are used as this epithelium represents the largest epithelial surface area in the lung; however model systems most often involve the isolation of primary AEL from human [77], rat [78] or other species, e.g. pig [79]. These cells undergo a phenotypic change in primary culture moving from a type II phenotype at isolation and initial culture to more of a type I-like phenotype by day 6 to 8 post-seeding. These type I-like cells can form (depending upon the

enzymes used to isolate the type II cells) a highly restrictive monolayer with functional tight junctional complexes. Bronchial models of the conducting airways are more readily available for study and include normal human bronchial epithelial cells (NHBE cells) that can be purchased as low passage cell lines through to a range of transformed continuous bronchial cell lines of human origin; 16HBE14o-, Calu-3, BEAS-2B cell lines. In terms of drug delivery, cell culture models allow examination of drug permeability, absorption mechanisms, drug metabolism and toxicology and also some correlation to the *in vivo* state [76].

Rapidly developing methods of cell culture and cell-lines, along with a plethora of drug permeability data in prevalent cell-lines, together with a cost-effective, high throughput nature, may mean lung cell culture models could serve as a possible alternative to more costly, time-consuming *in vivo* or *ex vivo* models. *In vitro* models will certainly allow an opportunity for simpler experimental design to address aspects of mechanism of transport in the lung [75]. However, as noted in comments above, so little has been done with *in vitro* to *in vivo* correlations that this ideal is a long way off. Further, the absorptive surface in the lung will be complex comprising a range of different epithelial cell types very much dependent upon the deposition pattern of the inhaled aerosol.

In vivo whole animal models The area of *in vivo* animal testing to evaluate drug permeability was pioneered by the works of Schanker and colleagues in the 70's and 80's (for a comprehensive review see reference [23]). *In vivo* experimentation provides an opportunity to examine drug absorption, disposition and candidate pharmacokinetics within a fully intact organ. Many laboratories use small animal models such as mouse or rat, at least initially in early drug discovery. These models afford the use of smaller amounts of candidate compound. The ability to catheterise these animals for serial blood sampling affords *in vivo* animal experimentation real value in the study of drug candidate fate in the lung [23]. However, there are significant issues for *in vivo* experimentation including ethical considerations and correlation to the human patient. More technical issues include: conscious versus anaesthetised animals, use and variations in anaesthetic, delivery device used and the posture of the animal during delivery. Development of more accurate dosing techniques for small animals is essential.

Ex vivo isolated perfused lung organ models Isolated perfused lung models act as an intermediate between *in vivo* and *in vitro* models. While they are quite complicated in nature, they provide an excellent representation of the *in vivo* state whilst allowing division and study of the many mechanisms involved in drug delivery to the lung [75]. The isolated perfused lung (IPL) maintains *in vivo* architecture while separating the lung from whole body complications of tissue

distribution and clearance and as such the model can be used to define closely the pulmonary transport of drugs. However, such a technique is technically demanding and time-consuming and unlike cell culture models could not be used as a screening process for drug discovery [23].

Table 1.3 summarises the advantages and disadvantages of each model type and highlights model applicability when examining the effect of drug transporter proteins upon drug delivery to the lung.

	Advantages	Disadvantages	Ref
<i>In vitro</i> cell culture models	<ul style="list-style-type: none"> • High-throughput • Simple methodology • Reasonable amount of permeability data from multiple labs can be readily obtained • Cost-effective • Transformed cells – of known origin • Primary cells – closer representation of <i>in vivo</i> state 	<ul style="list-style-type: none"> • Only represent single cell-line • May not accurately represent <i>in vivo</i> metabolising enzyme activity • Primary cells – limited number of cells and lifespan • Tight junctions and cell cycles are less representative of <i>in vivo</i> state • Drug transporter activity highly culture dependent 	[23] [75] [76] [80]
<i>In vivo</i> whole animal models	<ul style="list-style-type: none"> • Many methodologies available • Number of animal models available • More representative data • Allows species comparison • Blood sampling allows examination of serum/plasma interactions 	<ul style="list-style-type: none"> • Costly • Not high throughput • High inter-laboratory variation • Difficult to determine individual processes • Challenges in dosing 	[23]
<i>Ex vivo</i> isolated perfused organ models	<ul style="list-style-type: none"> • Very close representation of <i>in vivo</i> state • Removes whole body complications • Maintains architecture and functionality of organ • Intact drug transporter activity 	<ul style="list-style-type: none"> • Limited lifespan • Complex methodology • Not high throughput • Costly • Both <i>in vivo</i> and <i>ex vivo</i> models represent but are not identical to human lung structure. i.e. human lung structure dichotomous and symmetrical, rat lung more monopodial – impact on extrapolation of particle deposition data 	[23]

Table 1.3 Advantages and disadvantages of 3 main techniques employed to examine drug transport in the lung. The *Ex vivo* isolated perfused organ model marries the advantages of both *in vivo* and *in vitro* techniques providing an excellent model to examine drug delivery to the lung. [23, 75, 76, 80, 81].

The selection of a model type should meet the requirements of each experimental design together with being as efficient and accurate as possible. While there are many advantages and

disadvantages for each experimental model, the use of an *ex vivo* Isolated perfused lung marries the advantages from other main techniques while overcoming the disadvantages they produce.

1.9. Isolated Perfused Rat Lung (IPRL)

Isolated organ preparations have been exploited since the mid 19th century and while the lung was initially utilised for blood oxygenation in organ preparations, as interest increased, refinement of the isolated perfused lung (IPL) allowed the creation of an excellent model for the examination of non-respiratory lung processes [82-84].

Examples of IPL use flourished in the 1960s and 70s and allowed development of isolation techniques for somewhat routine application of the IPL to examine lung processes and mechanisms. Such applications included examination of lung circulatory and ventilatory mechanisms, gaseous exchange and oedema formation, pulmonary glycolytic activity and drug metabolism [85-91].

A range of IPL techniques now exist, allowing method variation and preparation adaptations to suit experimental needs. One major variable is animal selection, decisions being based upon the nature of the experiment, cost, availability and animal maintenance and requirement for specific genetic characteristics. Of the range of suitable animal models, rat and rabbit preparations prove most popular [84]. Here, the isolated perfused rat lung will be considered.

Table 1.3 highlighted the advantages and disadvantages of isolated organ preparations, the IPRL shares many of these and provides many advantages over other lung model techniques:

- Isolation of the organ avoids limitations imposed by *in vivo* models while allowing access to deliver compounds of interest via physiological routes [83]
- The model provides structural and functional lung integrity, maintaining membrane barriers and cell-cell interactions thus accurately mimicking *in vivo* state [83, 84]
- *Ex situ* lung isolation provides many IPRL uses and applications such as toxological, metabolism and drug delivery studies [84]
- IPRL methodology allows control over important experimental parameters such as ventilation and perfusion [83, 84]
- Perfusate reservoirs provide the possibility to take multiple samples and organ isolation allows mass balance of compounds administered to the lung to be established [84]
- Assessment of biochemical and physiological processes following toxic exposure is possible [84]

- IPRL provides opportunity to assess the lungs role in drug disposition [83, 84]

However, disadvantages that are associated with IPRL preparations must also be taken into consideration:

- A major limitation of the IPRL is the relatively short period of preparation stability and integrity [83]
- The complex methodology involved requires extensive operator training and renders the IPRL as a less time-efficient model to set-up than other preparations [92]
- There is potential for the recognised cellular heterogeneity of the lung may negatively impact data interpretation and results, i.e. which specific cell surfaces are accountable for observed results; this is avoided with *in vitro* models. [92]
- IPRL perfusion rate is generally only $\sim \frac{1}{2}$ that of physiologic rate [83, 84]

The inherent nature of the IPRL produces a complex methodology with many factors contributing to a successful preparation. Aspects for consideration include; surgery, ventilation, perfusion and apparatus.

Surgery The increase in use of the isolated perfused lung as an individual technique in the 1960s and 70s led to a generalised surgical protocol for the isolation of the lungs. In essence, the animal is anaesthetised with an agent such as pentobarbital sodium, gaseous agents having the potential to adversely affect the organ and subsequent results. A tracheotomy is performed to allow ventilation and access for dosing and the lungs are exposed via the diaphragm. The pulmonary circulation is then perfused and the lungs isolated. Distinction in methodology typically arises from a variety of factors associated with ventilation, perfusion and apparatus [93].

Ventilation Generally, within IPRL methodology the lungs are ventilated as soon as access is established. This is to mimic, as well as possible, physiological conditions and to minimise damage to the lungs [93]. In terms of ventilation of the lung, volume and pressure are the two main issues to be considered. To allow inspiration and expiration of lungs in an IPRL setup, either positive pressure ventilation or negative pressure ventilation is employed; however, both methods are essentially equal within the setup as they are both required to establish a pressure gradient to facilitate ventilation. To achieve perfusate oxygenation and to avoid injury, lung tidal volume is also important. Optimum tidal volume will allow even and rhythmical lung ventilation and aid in maintaining the IPRL preparation. Generally, a small animal ventilator is used to achieve ventilation

with parameters of 60 cycles/min and a volume of 2 mL/cycle reasonable for an IPRL preparation [83]. A further important consideration of IPRL ventilation is ventilation gas. Of main physiological concern are O₂ and CO₂ which are required to be present at optimum levels to maintain normal metabolic processes and to control perfusate and intracellular pH. A typical gas mix for IPRL is 95 % O₂ 5 % CO₂, especially if a bicarbonate buffer system is being used, where this gas mix will aid in maintaining perfusate pH [83].

Perfusion The perfusion of an IPRL preparation is largely determined by two main factors; perfusion method and perfusate type. Each main factor is dependent on a number of choices and issues that are interlinked between perfusion method and perfusion media. IPRL perfusion is either 'single-pass' or 'recirculating' and each has a number of important advantages and disadvantages. A recirculating method of IPRL perfusion allows for a small volume of perfusate to be used (especially important if using whole blood perfusate) and is an important method for facilitating assessment of slowly metabolised drug candidates. In contrast, single-pass perfusion produces a simpler IPRL system but does involve a larger volume of perfusate media [94]. Both perfusion methods require a pump to perfuse the IPRL preparation and perfusion is controlled by flow rate which, in an IPRL preparation, is typically set at half the physiological resting cardiac output (e.g. 15 mL/min for a 250 g rat). Many IPRL preparations also include a bubble trap within their perfusion circuit to avoid air bubble facilitated oedema formation [83].

The second major consideration of IPRL perfusion is the perfusion media itself; either natural or artificial perfusate. Again, each perfusate type offers advantages and disadvantages. Natural, whole blood perfusate mimics the *in vivo* state, delays oedema formation and allows examination of serum and plasma drug binding. However, the volumes of perfusate required result in large numbers of animal sacrifice, the blood perfusate requires addition of an anticoagulant, and using whole blood creates sourcing and storage issues. Artificial perfusate media, while not identically reproducing the *in vivo* state, allows control over constituents and properties such as ionic composition, osmolality and pH, requires less animal sacrifice, is easier to store and source and produces fewer problems of binding and metabolising toxins and xenobiotics [83, 94].

Apparatus The choice of apparatus for an IPRL is largely dependent on experimental parameters such as choice of pressure ventilation, perfusion technique and dosing mechanism. For example, if positive pressure ventilation is employed then lungs can remain *in situ*, however, if negative pressure ventilation is employed then an artificial, air tight, thorax is required. To create an easily accessible dosage point, lungs can remain horizontal (a means of 'hanging' the lungs is

required). To maintain the lungs and perfusate at a representative temperature, a form of temperature control is also required. This commonly takes the form of a water-jacketed setup thus creating the need for water-jacketed apparatus of an inert material and a heated water pump, producing a large IPRL setup.

Viability/metabolic function One major disadvantage of the IPRL preparation is its viability; however, experimental parameters can be optimised and monitored in order to prolong model life-span. For example, inclusion of albumin in artificial perfusion media and running perfusate flow rate at half the physiological rate both aid to reduce oedema formation [83]. Further, the monitoring of parameters such as lung weight, ventilation, pressure and lung appearance allow visual determination of lung viability and may provide confidence on result interpretation [84].

The correlation of the IPRL to *in vivo* state is very important and allows use of the model in a number of experimental situations. It is essential to establish the extent of 'normal' activity within the IPRL to allow correct model use and data interpretation. Issues such as extent of tissue perfusion and metabolic activity are of importance. During lung isolation the bronchial circulation is severed therefore it is only the pulmonary circulation that is intact and is used to perfuse the lung. While this could influence experimental uses, studies have illustrated the necessity for only intact pulmonary circulation for successful lung perfusion and preparation viability [83]. The extent of metabolic activity within the IPRL is also of importance. Many studies of isolated perfused lung preparations have shown that these models are under normal metabolic control and exhibit normal metabolic activity with the inclusion of glucose in perfusion media, providing confidence when using an IPRL for metabolic studies [92].

Applications The variety of IPRL methodology available allows this model to be utilised for a number of applications. Use of the IPRL has flourished since the mid 20th century when interest in the lung and non-respiratory processes increased [85, 88, 91]. In recent times, significant uses of the IPRL have included research in to pulmonary drug deposition and metabolic processes. The work of Byron *et al.* during the 1980s examined closely the fate of aerosolised drugs delivered to the lung and provided excellent reference data regarding the absorption of a range of molecular weight markers across the IPRL [95]. These works led to the development of the IPRL as a screen for aerosol formulations and provided data to allow improvement of aerosolised drug dissolution and release [96]. Other major uses of the IPRL include the examination of xenobiotic metabolism in the lung and the damage to the lung caused by agents such as cigarette smoke and NO₂ [92].

The isolated perfused lung is an excellent lung model with extensive uses within pulmonary research. The large number of experimental variables and flexible methodology creates excellent opportunity to optimise the IPRL for individual experimental needs. The maintenance of structural and functional integrity, ability to dose via a number of techniques and the ability to investigate lung specific pharmacokinetics provides the IPRL as a particularly advantageous model for the investigation of specific pulmonary mechanisms involved in the delivery of drugs to the lung. Previous application of this model to investigate drug dissolution and absorption mechanisms, drug disposition and metabolism provides evidential support and reference points for future IPRL use in biopharmaceutical research [42, 97-102].

1.10. Thesis aims and objectives

- To establish the relative mRNA expression of several ABC, SLC and SLCO drug transporters within the rat lung through use of reverse transcription polymerase chain reaction (RT-PCR)
- To set-up and fully validate an isolated perfused rat lung preparation for use in assessment of drug transport across the lung
- To assess the functional significance of the ABC drug transporter P-glycoprotein on drugs intra-tracheally instilled to an *ex vivo* IPRL set-up.
 - Use of the P-gp substrates; Rhodamine 123, digoxin, and flunisolide and the P-gp inhibitor, GF120918 will be employed.
 - Use of kinetic modelling to establish pharmacokinetic parameters
- To examine whether any effects in substrate transport can be conclusively attributed to P-gp.
 - Consider contribution from other drug transporters, substrate lipophilicity, cell membrane fluidity and permeability.
- To assess the functional significance of the ABC drug transporter P-glycoprotein on drugs delivered to the perfusate of an *ex situ* IPRL model. i.e. possible insight into significance of P-gp on drugs delivered to the systemic circulation.
 - Use of P-gp substrates; Rhodamine 123 and flunisolide and the P-gp inhibitor GF120918
- To establish comparability between two IPRL setups (*ex situ* and *in situ*).

CHAPTER 2

RT-PCR derived analysis of drug transporter expression in cell models and whole lung

2.1. Introduction

Drug transporter genes code for a wide number of proteins that belong to transporter superfamilies, (e.g. ABC or SLC/SLCO superfamilies), these drug transporters are further defined based upon amino-acid sequence identity, into smaller families, subfamilies and eventually individual protein isoforms. Drug transporters have the ability to recognise and transport a diverse range of endogenous substrates, xenobiotics and pharmaceutically relevant drugs. Through the interaction of these proteins with structurally differing compounds, drug transporters have the potential to critically alter the systemic exposure and bioavailability of drug substrates and therefore influence the fields of drug discovery and development. Such proteins are increasingly recognised as important factors in determining drug absorption and disposition and affecting drug concentrations in target or non-target tissues. This has implications not only in terms of the therapeutic management of patients but also in terms of identifying new chemical entities during the drug discovery process which may be subject to active transport.

Many drug transporter proteins have been discovered and initially investigated through their mediation of multidrug resistance to chemotherapy agents, e.g. transporters P-gp, BCRP, MRPs. However, despite the potential for a large number of drug transporters to have impact upon the absorption and disposition of drugs, only a few transporters have to date been shown to have a significant influence. It is fair to say that the most widely studied is the adenosine triphosphate (ATP)-dependent binding cassette (ABC) efflux transporter, P-glycoprotein, which is a clinically significant cause of multidrug resistance. Further, P-gp has a clinically important role in limiting absorption from the intestine and limiting transport across the blood-brain barrier (BBB). A number of other transporters are also recognised to affect drug absorption and disposition, including members of the ABC-C family, i.e. MRPs, the ABCG2 protein, i.e. BCRP, as well as members of the SLC/SLCO superfamily; including polypeptide transporters (PEPT1/PEPT2), organic cation transporters (OCT/OCTN) and organic anion transporters (OAT) and organic anion polypeptide transporters (OATP) [45].

Pharmaceutical companies provide major investment into assessing the *in vivo* distribution of any drug candidate. For example, metabolic stability assays are utilised to design and optimise drugs to avoid various undesirable metabolic pathways such as first-pass metabolism and P450 metabolism. However, in-depth knowledge of drug transporter contribution is minimal in comparison. A deeper understanding could give further insight to variable factors such as efficacy and bioavailability, with continued exploitation allowing either targeting of specific organs (through small changes to drug

molecular structure to induce specificity to organ-specific transporters) or avoidance of such transporters that would limit entry to desired site of action [45]. A number of pharmaceutical drugs have been developed through exploiting attributes of a drug transporter. The HMG-CoA reductase inhibitor pravastatin, for example, achieves liver-selective distribution through interaction with the organ specific uptake transporter OATP1B1, thus prolonging exposure to the target and aiding in reducing adverse effects in non-target organs. Furthermore, knowledge of transporter activity in the blood-brain barrier has aided development of the newer generations of H1-antagonists, such as fexofenadine and cetirizine. These drugs are called 'non-sedating' as they do not penetrate the BBB line of defence, thus resulting in a reduction of CNS mediated side effects. Continued application of such knowledge would also allow assessment of both organ toxicity and drug-drug interactions and give rise to more efficient drug discovery, drug targeting and lead optimization strategies [103].

In contrast to the knowledge gained of drug transporter expression and functionality in a number of tissues and organs important to drug absorption and disposition i.e. intestine, liver, kidney and increasingly the BBB [103], there exists a very poor knowledge on the potential impact of active efflux and uptake transporters upon the absorption and disposition of drug molecules delivered to the lung, or indeed of uptake of molecules from the blood into the lung. Such active transporters may have the capacity to influence not only the bio-distribution of inhaled therapeutic compounds but also any foreign molecules and toxins that enter the lung leading to issues of toxicity [104] and can lead to accumulation of drugs in the lung that have been administered or gained entry into the body from other routes.

As stated above, the biological transporters that appear relevant to xenobiotic transport fall into a number of distinct superfamilies; (i) ABC transporters, (ii) the SLC and the recently reclassified SLCO transporters. Not all family members/isoforms of the above superfamilies serve as functional transporters for drugs and many have constrained substrate selectivity. It is mainly the members with the capacity to transport relevant (or specific) compounds that have been the focus of research [105].

Solute carrier transporters represent the largest of the three families. Initially the SLC super-family was sub-divided to 47 subfamilies with a total of 300 members. Both uptake and efflux SLC's have the ability to alter a drugs absorption, disposition and function and subgroups of interest include amongst others the; amino acid transporters, organic cation transporters and organic anion transporters [71]. In 2004, Hagenbuch and co-workers reclassified the OATP subfamily to SLCO using an open-ended nomenclature system that was species independent [46]. The newly classified SLCO

family contains several organic anion transporters and is comprised of 37 family members to date [104]. Of interest to drug discovery and development are OATP1B1, OATP1A2 and OATP1B3 [106].

The ABC transporters comprise a family of approximately 50 members classified into 7 subfamilies; ABCA-G. Many members, for example P-glycoprotein (ABCB1), MRP1 (ABCC1) and BCRP (ABCG2), are widely recognised for their ability to transport a wide variety of structurally diverse substrates and for their diverse expression profiles, thus underlining the considerable role of these transporters within the body and the, as yet, reasonably unappreciated significance in drug discovery and development [71].

The expression of several of these transporters has been investigated within the human lung, with implications made relevant to inhaled drug discovery. As an illustration, table 2.1 gives examples of the techniques used to investigate the expression of ABC transporters of interest in various lung samples.

Transporter (Protein name)		Reference
P-gp	Intact Lung Tissue RT-PCR (+) Immuno-histochemistry (+) Primary Peripheral Lung Cells RT-PCR (+) Immuno-histochemistry (+) Primary Bronchial Epithelial Cells RT-PCR (+) Immuno-histochemistry (+) Primary Alveolar Epithelial Cells RT-PCR (+) Immuno-histochemistry (+) Western blot (+)	[107] [108], [109], [110], [43] [111] [111] [104, 111, 112] [111] [112] [113], [104] [16] [113]
MRP1	Intact Lung Tissue RNA Microarray (+) Primary Peripheral Lung Cells RT-PCR (+) Immuno-histochemistry (+) Primary Bronchial Epithelial Cells RT-PCR (+) Immuno-histochemistry (+) Primary Alveolar Epithelial Cells RT-PCR (+)	[69] [14] [111, 114] [104, 111, 115] [43, 111, 114, 115] [104]
BCRP	Intact Lung Tissue RT-PCR (+) Immuno-histochemistry (+) Flow cytometry (+) RNA Microarray (+) Primary Bronchial Epithelial Cells RT-PCR (+) Primary Alveolar Epithelial Cells RT-PCR (+)	[40] [43] [116] [69] [104] [104]

Table 2.1 Studies examining the expression of three ABC transporters of interest to drug discovery in human lung cell tissue and primary cell culture. (+) signifies reported presence within a sample. Primary peripheral cells were cultured from human distal bronchial tree samples. Adapted from Gumbleton *et al.*, 2010 [117].

There exists growing evidence of active transporter expression within the human lung; however, the significance of transporters is essentially unknown. Even in animal models the role of drug transporters in pulmonary absorption and disposition is very poorly defined. Techniques used to investigate drug transporter expression within the lung include microarray technologies, Western blotting, RT-PCR and immunohistochemistry. In particular, the recent microarray studies completed by Bleasby *et al.* are of note. Here the mRNA expression of 50 clinically relevant drug transporters was examined and translated to comprehensive quantitative expression profiles representative of 40 human and pre-clinical animal tissues. The expression profiles generated allow both comparison of

inter-individual variation between human tissue samples and data extrapolation from pre-clinical to human tissues [69]. Table 2.1 illustrates immunohistochemistry is a well utilised tool for examining transporter expression and protein localisation, the technique is generally undertaken using a low throughput approach with a single tissue sample on a glass slide but can be adapted for much higher sample processing using tissue microarray technologies. The other techniques listed provide no indication of the localisation of transporter within a tissue/organ. For the lung, the spatial expression of a transporter is vital as the lung contains greater than forty different cell types.

Reverse-transcriptase polymerase chain reaction allows recognition of individual transporter genes through uniquely designed transporter primer sequences and provides a more high-throughput system for examining transporter expression in a variety of tissues. However this technique is semi-quantitative at best, only indicating transporter mRNA presence or absence in a specific sample and requires the assumption that gene presence will result in the presence and functional activity of an active protein. Individual experimental techniques exhibit specific advantages and disadvantages and choice of technique should reflect the nature of the study. For example, if an investigator wishes to examine the localisation of a specific drug transporter then immunohistochemistry is applicable; however, if a broader study wanting to assess the number of drug transporter genes present in a tissue or cell culture sample is required, then a technique with ease-of-use and high data yield is perhaps more relevant. Table 2.2 outlines the advantages and disadvantages of a number of frequently used techniques, as can be seen; RT-PCR stands out as a rapid, efficient and simple methodology which provides a high yield of data. For the purposes of this chapter, RT-PCR was identified as the technique of choice.

Technique	Advantages	Disadvantages
RT-PCR	<ul style="list-style-type: none"> • No critical sample size • Tolerates partially degraded sample material • Excellent limit of detection • Efficient • Rapid • Very sensitive • Simple methodology 	<ul style="list-style-type: none"> • High level of optimization required • Unable to localise mRNA expression within cells or tissues • Unable to detect alternatively spliced transcripts • Only shows presence of mRNA
Immunohistochemistry	<ul style="list-style-type: none"> • Very sensitive • Able to localise specific component within cell or tissue • Can illustrate presence of protein 	<ul style="list-style-type: none"> • Time consuming • Labour intensive • Expensive • Can require optimization
Western blotting	<ul style="list-style-type: none"> • Relatively rapid technique • Sensitive • Allows localisation of target to specific tissue or cell • Number of detection methods possible 	<ul style="list-style-type: none"> • Labour intensive • Limited flexibility in choice of primary antibody (for less well-known transporters) • Non-specific staining is possible
Northern blotting	<ul style="list-style-type: none"> • Widely accepted technique • Simple methodology • Versatile protocol 	<ul style="list-style-type: none"> • Often radioactivity is used – disposal issues • Time consuming • Does not tolerate degraded sample material • Not as sensitive as other techniques
DNA Microarray	<ul style="list-style-type: none"> • High throughput • Only small sample size required • Easily automated • Good limit of detection 	<ul style="list-style-type: none"> • Only evaluates expression at transcriptional level • Time consuming and labour intensive • Expensive
Flow cytometry	<ul style="list-style-type: none"> • Rapid, quantitative and detailed • Low error rate • Guaranteed to reveal non-uniformity in cell population 	<ul style="list-style-type: none"> • Other methods are more rapid and less expensive • Can overwhelm with detailed data

Table 2.2 Overview of the advantages and disadvantages of several experimental techniques with the capacity to identify the presence of specific drug transporter mRNA/gene/protein target within an experimental sample [118-124].

In order to examine the presence of drug transporter genes within the lung, a comprehensive range of lung cell models are available. The use of primary cell culture is highly advantageous with protocols for isolation in existence since the 1970s. Isolation of primary cells provides a well-differentiated monolayer with a diverse phenotype which can be more closely physiologically

representative of the *in vivo* state thus rendering results obtained from such culture systems more comparable to *in vivo* whole organ experiments [125]. The use of immortalised or cancer cell line models has also been well documented. Such cell lines models bear many advantageous features, such as ease of use, low cost and reproducibility. These models also allow swift setup of the culture system and therefore afford a rapid turnover of results [75].

Aims and Objectives

In this chapter, the following will be sought:

- Examine the expression at mRNA level of selected ABC, SLC and SLCO transporters in rat lung tissue and cell samples.
- Identify transporters of interest based upon reported evidence of it influencing drug disposition in other tissues of the body at least.
- Develop an expression profile for each transporter - Each expression profile illustrating not only a transporter's presence within the rat lung, but also to some degree, presence within specific regions of the lung, i.e. primary alveolar epithelial cell versus a primary bronchial epithelial cells.
- Utilise primary alveolar epithelial cell culture to provide a physiological representation of active transporter expression at the alveolar epithelial surface.
- Utilise SPOC1, a rat tracheal goblet cell line with the potential to differentiate to both secretory and squamous cells in culture [126], to provide evidence of transporter presence in this area of the lung.
- Utilise whole rat lung tissue to give an overall picture of active transporter expression within the whole rat lung.

Overall Aim of Chapter:

It is hypothesised that development of such a transporter expression profile will give insight into a specific transporter's presence within rat lung and will support some of the later studies conducted in this thesis involving the use of intact rat lung. It is also hoped that, once developed, an expression profile will provide useful species specific information for research in drug discovery particularly, but not exclusively, those involved in inhalational drug delivery.

2.2. Materials and Methods

2.2.1. Rat whole lung tissue harvest for RNA isolation

Materials

Animals

Male-specified pathogen-free Sprague-Dawley rats (Harlan UK Limited, Bicester, UK) were used throughout and housed in rooms controlled between 19 °C – 21 °C and 40-60 % humidity with dark-light cycling every 12 h. The animals had free access to food and water and were acclimatised for at least 2 days prior to experimentation. All animal experiments adhered to the Animal (Scientific Procedures) Act 1986, UK and were approved by Cardiff University.

Consumables

0.9 % Sodium chloride solution; NaCl, (Fisher Scientific, Loughborough, UK, Cat: S/3105/63). NaCl solution was prepared by dissolving 0.9 g NaCl in 100 mL distilled water and autoclaving at 121 °C

70 % Ethanol; EtOH, (Fisher Scientific, Loughborough, UK, Cat: E/0551DF/17)

Method

Surgery

Animals (Male-CD, 300-350 g) were terminated using schedule 1 technique (The Animals (Scientific Procedures) Act 1986). The abdomen was liberally covered with 70 % EtOH and an arc dissection made to expose the diaphragm. The diaphragm was dissected and ribs cut to expose the lungs. Care was taken to avoid damage to the lung tissue. The trachea was exposed and taking hold of this, the lungs were cut free. Tissue was placed in 0.9 % NaCl in a Petri dish before RNA isolation.

2.2.2. Isolation and primary cell culture of rat alveolar epithelial cells

Materials

Animals

Male-specified pathogen-free Sprague-Dawley rats, 120-180 g body weight (Harlan UK Limited, Bicester, UK) were used for cell isolation and were housed as described previously.

Consumables

Beakers (Sterile covered with foil; 250 mL), (Fisher Scientific, Loughborough, UK, Cat: FB33112)

Centrifuge tubes (Sterile; 50 mL and 15 mL), (Fisher Scientific. Loughborough, UK, Cat: FB55956 & FB55951)

Syringes (Sterile; 10 mL), (Fisher Scientific, Loughborough, UK, Cat: SZR-150-041H)

Syringe filters (Sterile; 0.2 μm pore, 25 mm), (Fisher Scientific, Loughborough, UK, FDR-050-071N)

Filter syringe units (Sterile; 20 mL), (Beckton Dickenson, Oxford, UK)

Filter membranes, attached to filter syringe units:

(a) Gauze (NHS Quality)

(b) Nylon mesh (150 μm and 30 μm mesh), (Lockertex Warrington, Cheshire, UK)

Intravenous catheter without injection port; Tro-venocath 20G, (Troge, Hamburg, Germany)

Cell scraper, (Fisher Scientific, Loughborough, UK, FB55199)

Chemicals and Enzymes

Sodium chloride; NaCl, (Fisher Scientific, Loughborough, UK, Cat: S/3105/63)

Potassium chloride; KCl, (Fisher Scientific, Loughborough, UK, Cat: P/4280/53)

Calcium chloride dihydrate; $\text{CaCl}_2 \cdot 2\text{H}_2\text{O}$, (Fisher Scientific, Loughborough, UK, Cat: C/1500/50)

Magnesium sulphate heptahydrate; $\text{MgSO}_4 \cdot 7\text{H}_2\text{O}$, (Acros Organics, Belgium, Cat: 124900010)

di-Sodium hydrogen orthophosphate dehydrate; $\text{Na}_2\text{HPO}_4 \cdot 2\text{H}_2\text{O}$ (Fisher Scientific, Loughborough, UK, Cat: S/4450/53)

Sodium dihydrogen orthophosphate dehydrate; $\text{NaH}_2\text{PO}_4 \cdot 2\text{H}_2\text{O}$ (Fisher Scientific, Loughborough, UK, Cat: S/3760/53)

N-2-Hydroxyethylpiperazine-N'-2-ethanesulfonic acid; HEPES (Fisher Scientific, Loughborough, UK, Cat: BPE310-100)

D-Glucose anhydrous; $\text{C}_6\text{H}_{12}\text{O}_6$, (Fisher Scientific, Loughborough, UK, G/0450/60)

Percoll™ (Sterile), (GE Healthcare, Buckinghamshire, UK, Cat: 17-0891-01)

Foetal Bovine Serum; FBS, (Invitrogen Corporation (Gibco), Renfrew, UK, Cat: 10108-16)

Dulbecco's Modified Eagle's Medium; DMEM; with 25 mM HEPES, (Invitrogen Corporation (Gibco), Renfrew, UK, Cat: 42430-025)

Penicillin G, (Sigma-Aldrich, Dorset, UK, Cat: P7794)

Gentamicin; (10 mg/mL), Invitrogen Corporation (Gibco), Renfrew, UK, Cat: 15710-031)

Dexamethasone, (Sigma-Aldrich, Dorset, UK, Cat: D4902)

Phenol red, (Fisons, Ipswich, UK, Cat: P/2420/44)

Sodium hydroxide; NaOH Solution; (5 M), (Fisher Scientific, Loughborough, UK, Cat: S/3105/63)

Saline intravenous bag, (500 mL), Baxter, Berkshire, UK, Cat: FE1306)

Pentobarbital sodium; (200 mg/mL); Euthatal, (Vericore Ltd, Dundee, UK)

70% Ethanol; EtOH, (Fisher Scientific, Loughborough, UK, Cat: E/0551DF/17)

Stock solutions: to be prepared 24 h before cell isolation

The following solutions were prepared one day prior to cell isolation and stored under appropriate conditions. Glassware was washed and dried thoroughly before use with solutions being filter sterilised and aliquoted in a laminar flow cabinet.

10X solution: 500 mL, for approximately 20 rats, stable up to 3 months at 4 °C.

Chemicals listed below were dissolved in distilled water (\approx 400 mL) and the volume adjusted to 500 mL. Solution pH (\sim pH 6.5) was adjusted to pH 7.4 with 5 M NaOH and the solution filter-sterilised and aliquoted to 50 mL centrifuge tubes for storage in the dark at 4-8 °C.

Chemical	Molecular Weight	g / 500 mL
NaCl	58.44	38.86
KCl	74.55	1.94
Na ₂ HPO ₄ ·2H ₂ O	177.99	1.42
NaH ₂ PO ₄ ·2H ₂ O	156.01	0.78
HEPES	238.30	11.92
Glucose	180.20	5.00

100X CaCl₂ and 100X MgSO₄: 100 mL, for approximately 40 rats, stable up to 6 months at 4 °C.

Chemicals listed below were dissolved in distilled water (\approx 90 mL) and the volume adjusted to 100 mL. Each solution was filter-sterilised and stored in the dark at 4-8 °C.

Chemical	Molecular Weight	g / 500 mL
CaCl ₂ ·2H ₂ O	147.00	2.77
MgSO ₄ ·7H ₂ O	246.40	3.18

Dexamethasone: 20 μ M

Dexamethasone, (7.85 mg), was dissolved in 5 mL EtOH and mixed with 995 mL of distilled water. This yielded a 20 μ M solution which was filter-sterilised and stored at -20 °C.

Penicillin and gentamicin

Penicillin G, (126.6 mg, 1580 U/mg), was dissolved in 10 mL gentamicin solution (10 mg/mL). This solution was filter-sterilised, aliquoted into 300 mL volumes and stored at -20 °C

0.9% sterile saline: (1 x 100 mL/rat)

NaCl (0.9 g) was dissolved in 100 mL distilled water and autoclaved at 121 °C

Double-distilled water; sterile (3 x 100 mL/rat)

Double-distilled water was prepared by aliquoting 3 x 100 mL in suitable bottles and autoclaving at 121 °C.

Phenol red-coloured double-distilled water; sterile (100 mL)

A trace amount of phenol red was dissolved in 100 mL distilled water and autoclaved at 121 °C.

Filter syringe unit preparation: to be sterilised overnight before cell isolation

Gauze webbing or nylon mesh cloth (150 µm or 30 µm) were cut into square pieces and fixed over filter syringes to create 3 separate filter syringe units of decreasing mesh size. Each unit was first soaked in distilled water and then 70 % EtOH for 10 minutes to remove particulate matter and sterilize. Syringes were then stored under UV light overnight for further sterilization.

Preparation of solutions immediately before cell isolation

The following solutions were prepared immediately before cell isolation in a laminar flow cabinet.

Buffer A (1 bottle/rat)

10X solution (11 mL) was added to 100 mL bottle of sterile water = **1 bottle**

Buffer B (2 bottles/rat)

The below listed solutions were added to 100 mL bottle of sterile water. Two bottles were prepared.

Solution	Volume (mL)
10X solution	11.0
100X CaCl ₂	1.1
100X MgSO ₄	1.1

Buffer B (2 x 40 mL) from one bottle was placed in 2 x 50 mL centrifuge tubes for elastase suspension preparation. The remaining 160 mL of Buffer B was placed in a 250 mL beaker, covered with foil and stored in a water bath at 37 °C

Heavy and light Percoll™ gradient solutions

Two of each of the following solutions were prepared in separate 50 mL centrifuge tubes and stored on ice

Heavy Percoll™ solution	Light Percoll™ solution
6.49 mL of Percoll™	2.72 mL of Percoll™
50 µL of FBS	50 µL of FBS
2.51 mL of distilled water	6.28 mL of phenol red-coloured water
1 mL of 10X solution	1 mL of 10X solution

DNase I solution

To 11 mL of Buffer A, 8500 U of DNase I was added in a 15 mL centrifuge tube. The solution was shaken vigorously and filter-sterilised.

Low concentration DNase: 4.5 mL of the above solution was placed in a 50 mL centrifuge tube and the volume adjusted to 35 mL with Buffer A solution.

High concentration DNase: 6.5 mL of the above solution was placed in a 15 mL centrifuge tube and the volume adjusted to 10 mL with Buffer A solution.

Both DNase solutions were stored on ice.

Cell culture medium; stored for use in 37 °C water bath.

Solution	Volume (mL)
DMEM	45.0
FBS	5
Dexamethasone, 20 µM	0.25
Penicillin/gentamicin	0.25

Prior to lung isolation:

In a 37 °C water bath:

- 1 bottle of NaCL for lung lavage
- 160 mL of Buffer B in 250 mL beaker covered with foil
- 40 mL of Buffer B in a 50 mL centrifuge tube for elastase suspension
- 5 mL FBS for terminating elastase digestion
- 50 mL cell culture medium.

On ice:

- Heavy Percoll™
- Light Percoll™
- High concentration DNase
- Low concentration DNase

Method (adapted from laboratory protocol)**Surgery & lung isolation**

The surgical procedure requires two operators and was conducted in the surgery room of Joint Services. Prior to surgery, all surfaces and kit were wiped with 70 % EtOH and dried thoroughly.

A Male CD rat was anaesthetised with 0.2 mL Euthatal via intraperitoneal injection. Sufficient anaesthesia was checked by tail or paw pinch.

The rat was placed on its back on a surgical mat and its neck and abdomen liberally covered with 70 % EtOH. A midline incision (1-2 cm) was made in the neck and the trachea exposed by careful dissection through the salivary glands and muscle layers. The trachea was cannulated between the 2nd and 3rd cartilage rings using a 20G intravenous catheter. The catheter was tied securely using linen thread.

The abdomen was exposed in an arc dissection and the diaphragm revealed. The diaphragm was then dissected away using Spencer Wells forceps to hold the xiphisternum, and the lungs visualised. The ribs were then carefully cut towards the sternum with blunt scissors. To allow access to the thorax, the xiphisternum was clamped with Spencer Wells forceps and the cut chest wall turned over. The weight of the clamp was used to maintain this access. The thymus, now visible, was removed using two pairs of forceps.

Flow was released from an intravenous saline bag. Immediately following this, an incision was made in the left atrium to allow saline/blood drainage. Next, the pulmonary artery was located through slight displacement of the heart to the left. A small incision was then made in the right ventricle. Once an incision was made, the saline catheter was inserted through the right ventricle and its tip visualised in the pulmonary artery. With the catheter maintained in the pulmonary artery, the lungs were manually inflated with 4-6 mL of air using a 10 mL syringe attached to the tracheal cannula. Air

was released by removal of the syringe and this was repeated 5-6 times or until the lungs appeared clear of blood. Saline perfusion was then stopped.

The lungs were removed from the thorax by holding the trachea and pulling gently in a downwards direction. At the same time, the connective tissue between the lungs and the abdomen was cut away. Care was taken not to touch the lung tissue. Once removed, lungs were washed with normal saline and placed in a Petri dish of the same solution.

The procedure was then repeated with a second animal.

Lung Lavage

This procedure was performed on the bench top

The plunger was removed from a 10 mL syringe and the remaining barrel clamped in a retort stand. The tracheal cannula (in the trachea of the isolated lungs) was firmly attached to the syringe. The lungs, via the attached syringe, were filled slowly with 6-8 mL of warm saline. Simultaneously, 2 x 80 U of elastase was added to 40 mL of Buffer B and stored in a 50 mL centrifuge tube in a 37 °C water bath.

Once the lungs had fully inflated (no more saline was able to enter the tissue), the tracheal cannula was disconnected from the syringe and the lungs inverted to allow drainage of lavage fluid. Initially lavage fluid was white in colour due to the presence of alveolar macrophage. Lavage was repeated until fluid appeared clear.

Enzymatic digestion of lung tissue

This procedure was performed in the 37 °C water bath

Lung tissue was submerged in 160 mL of warm Buffer B. Warm elastase, in 5 mL volumes, was then slowly added via the 10 mL syringe. Drainage of the elastase solution was slow, requiring approximately 15-20 minutes for 40 mL of solution.

Isolation and purification of alveolar type II epithelial cells

This procedure was carried out in a laminar flow cabinet.

High concentration DNase solution was placed in 37 °C water bath. Lung tissue (glassy in appearance and soft in texture) was placed in a sterile Petri dish (1 pair of lungs/Petri dish) in a laminar flow cabinet. The trachea and bronchi were carefully cut free then lung tissue was finely chopped (~1-2 mm² pieces) using sharp scissors.

Once lung tissue was sufficiently dissected, 5 mL of warm FBS was added to each Petri dish to terminate elastase action. 10 mL of warm high concentration DNase was then added to prevent cell clumping. Using a cell scraper, both tissue suspensions were added to one 50 mL centrifuge tube.

Cell suspension was then slowly added to the widest gauze syringe filter, with the resulting filtrate solution being collected in a fresh 50 mL centrifuge tube. The filtrate was then added to the 150 μm filter unit, filtrate collected and finally added to the 30 μm filter unit. The filtrate from the 30 μm was the crude alveolar cell suspension. (Figure 2.1)

The crude alveolar cell suspension was stored in the 37 °C water bath until the Percoll™ discontinuous centrifugation gradients were prepared.

Two Percoll™ gradients were prepared using a Power Pipetter on the lowest power setting to very carefully layer the light Percoll™ solution (10 mL) onto the heavy Percoll™ solution (10 mL). Once finished, the first Percoll™ gradient was stored on ice, this helping the interfaces to settle, until the second gradient was prepared.

Very slowly and carefully, half of the crude cell suspension was added to the top of each Percoll™ gradient, figure 2.2. Each gradient was then centrifuged at 250 x g at 6 °C for 20 minutes (1050 rpm on Allerga 6 KR Centrifuge, Beckman Coulter and 1100 rpm on Avanti J-25 centrifuge, Beckman Coulter). Centrifuge buckets were pre-cooled. Maximum acceleration and no brake were employed.

After centrifugation, cell debris and the majority of the light Percoll™ layer (Figure 2.2) was discarded. AEII cells were contained in the opaque band between the two Percoll™ solutions.

The opaque band and the Percoll™ solutions interface was removed (25 % of the light layer and 50 % of the heavy layer i.e. ~7.5 – 12.5 mL on the centrifuge tube volume markings) and placed in 35 mL low concentration DNase solution. This was then repeated for the second Percoll™ gradient.

Low concentration DNase/cell suspension was centrifuged as previously described, using both maximum acceleration and deceleration. The resulting supernatant was removed and the cell pellets re-suspended in 10 mL warm cell culture media. This cell suspension was then transferred to a sterile Petri dish and placed for 1 h in the CO₂ incubator to allow removal of contaminating macrophage. After 1 h the AEII cells remained free from the Petri dish while macrophage had attached to the plastic, appearing as large granular cells. The cell suspension was transferred to a sterile 50 mL centrifuge tube, 100 μL sample removed for cell counting, fluid volume recorded, and centrifuged at 250 x g at 6 °C for 10 minutes. 50 μL cell suspension was added to an equal volume of Trypan blue solution and left for 10 minutes at room temperature. The percentage of viable cells was then calculated using a haemocytometer and the centrifuged cell pellet re-suspended in the correct volume of media to allow a seeding density of $0.9 - 1.2 \times 10^6$ cells/cm².

Primary cell culture

Successfully isolated alveolar epithelial cells were maintained in a culture flask in a humidified incubator (37 °C; 95 % air; 5 % CO₂). To induce differentiation of type II alveolar epithelial cells to type I-like cells, 0.1 μM dexamethasone was added to culture medium. Spent culture medium was replaced every 48 h. Cells seeded to Transwell™ plates were pre-washed with warm PBS to remove debris prior to culture medium replacement. In order to monitor monolayer confluence,

Transepithelial electrical resistance (TEER) was measured from day 4 of cell culture, with cells typically reaching confluence on day 8 of culture.

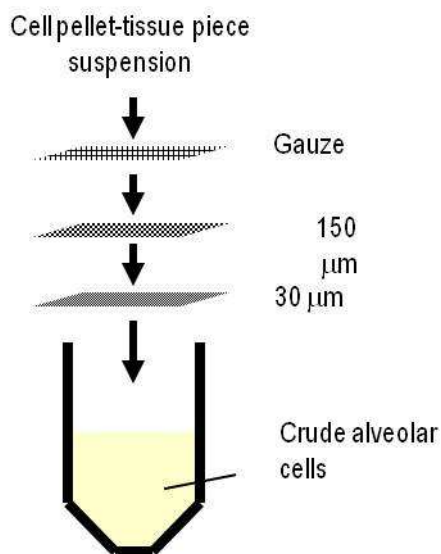


Figure 2.1 Gauze-syringe filter unit used to retrieve crude alveolar suspension

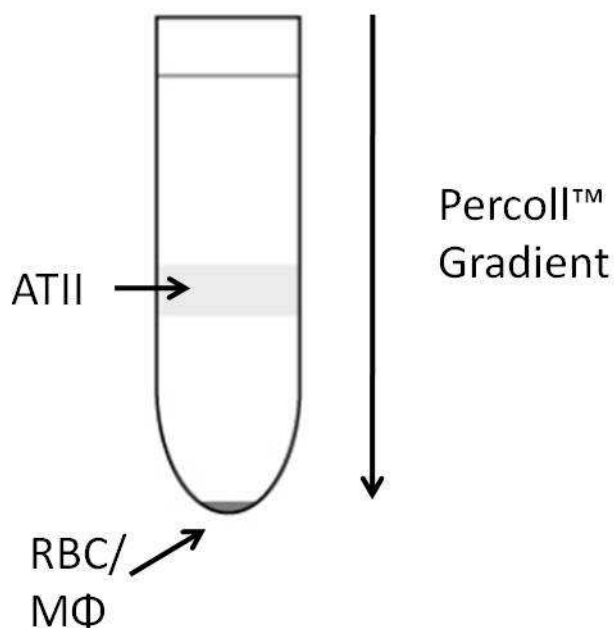


Figure 2.2 Percoll™ discontinuous gradient centrifugation of crude alveolar cell suspension to allow isolation of alveolar epithelial Type II cells. Adapted from laboratory protocol.

2.2.3 SPOC1 Cell culture

Materials

Cell line

SPOC1 cells were a kind gift from Professor Davis, Cystic Fibrosis/Pulmonary research & treatment centre, University of North Carolina.

Consumables

Dulbecco's Modified Eagle's Medium: Nutrient mixture F12; DMEM/F12, (Invitrogen, Renfrew, UK, Cat: 11039-021)

Insulin, (Sigma-Aldrich, Dorset, UK, Cat: I1882)

Hydrocortisone, (Sigma-Aldrich, Dorset, UK, Cat: H6909)

Cholera toxin, (Sigma-Aldrich, Dorset, UK, Cat: C3012)

Transferrin, (Invitrogen, Renfrew, UK, Cat: 11108-016)

Phosphoethanolamine, (Sigma-Aldrich, Dorset, UK, Cat: P0503)

Ethanolamine, (Sigma-Aldrich, Dorset, UK, Cat: E0135)

Epidermal growth factor; EGF, (Collaborative Research, Waltham, MA, USA, Cat: 40001)

Bovine pituitary extract; BPE, (Invitrogen, Renfrew, UK, Cat: 13028014)

N-2-Hydroxyethylpiperazine-N'-2-ethanesulfonic acid; HEPES (Fisher Scientific, Loughborough, UK, Cat: BPE310-100)

Bovine serum albumin; BSA, fraction V, very low endotoxin, (Serologicals, Livingston, UK, Cat: 81-068-2)

Trypsin, (Invitrogen, Renfrew, UK, Cat: 15400-054)

Tissue culture flasks, (Fisher Scientific, Loughborough, UK, Cat: TKT-130-150L)

Method

SPOC1 cells, passage 9, were seeded at a density of $9-10 \times 10^3$ cells per cm^2 in a 25 cm^2 tissue culture flask in 6 mL of culture medium. Culture flasks were housed in an incubator (37°C ; 5 % CO_2 ; 95 % air) and culture medium changed every 48 h. Culture medium consisted of a base medium of DMEM/F12 (50 mL) to which, the following additives were supplemented.

Additive	Stock concentration	Volume added to 50 mL DMEM/F12	Final concentration
Insulin	10 mg/mL	50 µL	10 µg/mL
Hydrocortisone	50 µg/mL	100 µL	0.1 µg/mL
Cholera toxin	0.1 mg/mL	50 µL	0.1 µg/mL
Transferrin	5 mg/mL	50 µL	5 µg/mL
Phosphoethanolamine	50 mM	50 µL	50 µM
Ethanolamine	80 mM	50 µL	80 µM
EGF	25 µg/mL	50 µL	25 ng/mL
BPE	15 mg/mL	333 µL	0.1 mg/mL
HEPES	0.5 M	3 mL	30 mM
BSA (low protein concentration)	150 mg/mL	167 µL	0.5 mg/mL

Once confluent, cells were sub-cultured to further tissue culture flasks. To subculture, spent media was removed and cells washed with 3 mL sterile PBS. To dislodge cells, 3 mL trypsin was added to the cell monolayer and the culture flask incubated at 37 °C for 10 minutes or until cells were observed to be dissociating from the culture flask. Trypsin activity was neutralized by the addition of 5 mL fresh culture medium. Cells were counted, diluted appropriately and seeded at a density of 9×10^3 cells per cm^2 .

2.2.4. Isolation and quantitation of total RNA from animal cells and animal tissue

Materials

Consumables

β-mercaptoethanol; β-ME, molecular biology, ≥98 % (GC/titration), (Sigma-Aldrich, Dorset, UK, Cat: M3148-25ml)

70% Ethanol; EtOH, (Fisher Scientific, Loughborough, UK, Cat: E/0551DF/17)

RNeasy® Mini Kit, (Qiagen, Crawley, UK, Cat: 74104)

Method

Isolation of total RNA from cultured cells

The cell samples included SPOC1 cells, AEII freshly isolated cells, AEII cells cultured for 2 days, and AEI-like cells cultured for 8 days. All cells were grown in monolayers. Total RNA was isolated from all cell samples through use of an RNeasy® Mini Kit. RNeasy® Mini Kit third edition protocol was followed. Before use, 10 µL of β-ME was added to 1 mL of Buffer RLT in a fume hood. Cell culture medium was completely aspirated from the culture flask and 350 µL Buffer RLT was added. Buffer volume is dependent upon culture vessel size, with vessel size governing cell number and therefore volume of Buffer RLT to be added, p18 of RNeasy® Mini Handbook. Cell monolayers were disrupted through use of Buffer RLT and a cell scraper. Cell lysate was then collected using a pipette and added to a 1.5 mL microcentrifuge tube which was vortexed to mix the cell sample.

Each cell sample was homogenised by passing the lysate through a 20G needle attached to an RNase-free syringe (BD Plastipak. Cat: 300185). This was repeated 5 times to ensure complete disruption of the cell sample. A volume of 70 % EtOH equal to the volume of Buffer RLT (350 µL) was then added and mixed well by pipette.

Each sample (700 µL) was then added to an RNeasy® mini column which was placed in a 2 mL collection tube and centrifuged at 10,000 rpm for 15 s at 20 °C. The through-flow was discarded and 700 µL Buffer RW1 added to the same RNeasy® mini column. Again this was centrifuged at 10,000 rpm for 15 s at 20 °C. (Eppendorf Centrifuge 5417R). The through-flow and collection tube were then discarded and the RNeasy® mini column placed in a new collection tube. To this, 500 µL Buffer RPE added and each sample was centrifuged at 10,000 rpm for 15 s at 20 °C. Before use, Buffer BPE was reconstituted with 4 volumes of 100 % EtOH to obtain a working solution. The through-flow was discarded and a second volume (500 µL) of Buffer RPE was added to the RNeasy® mini column. This was then centrifuged at 10,000 rpm for 2 min at 20 °C in order to dry the RNeasy® silica-gel membrane to avoid any residual ethanol affecting further reactions.

Finally, each RNeasy® mini column was then placed in a 1.5 mL microcentrifuge tube and 30 µL RNase-free water was added directly to the RNeasy® silica-gel membrane. Samples were then centrifuged at 10,000 rpm for 1 min at 20 °C to allow elution of the total RNA sample. Samples were stored at 4 °C for use in RT-PCR reactions or at -20 °C for prolonged storage.

Isolation of total RNA from animal tissue

Total RNA was isolated from rat whole lung samples through use of an RNeasy® Mini Kit. RNeasy® Mini Kit, third edition protocol was followed.

Whole lung tissue was placed in a mortar and a small volume (approx. 3 mL) of liquid nitrogen added. The tissue was then homogenized and added to 1.5 mL microcentrifuge tubes where 600 µL Buffer RLT+β-ME was added before the tissue could thaw. Each sample was then further homogenised through use of a 20G needle attached to an RNase-free syringe (BD Plastipak. Cat:

300185). The crude lysate was centrifuged at maximum speed (14,000 rpm) for 3 min and the resulting supernatant transferred to a new 1.5 mL microcentrifuge tube. A volume of 70 % EtOH equal to the volume of Buffer RLT (600 µL) was then added and mixed well by pipette.

The procedure then continued in the same manner as total RNA isolation from cell samples.

Each sample (700 µL) was then added to an RNeasy® mini column which was placed in a 2 mL collection tube and centrifuged at 10,000 rpm for 15 s at 20 °C. The through-flow was discarded and 700 µL Buffer RW1 added to the same RNeasy® mini column. Again this was centrifuged at 10,000 rpm for 15 s at 20 °C. (Eppendorf Centrifuge 5417R). The through-flow and collection tube were then discarded and the RNeasy® mini column placed in a new collection tube. To this, 500 µL Buffer RPE added and each sample was centrifuged at 10,000 rpm for 15 s at 20 °C. Before use, Buffer BPE was reconstituted with 4 volumes of 100 % EtOH to obtain a working solution. The through-flow was discarded and a second volume (500 µL) of Buffer RPE was added to the RNeasy® mini column. This was then centrifuged at 10,000 rpm for 2 min at 20 °C in order to dry the RNeasy® silica-gel membrane to avoid any residual ethanol affecting further reactions.

Finally, each RNeasy® mini column was then placed in a 1.5 mL microcentrifuge tube and 30 µL RNase-free water was added directly to the RNeasy® silica-gel membrane. Samples were then centrifuged at 10,000 rpm for 1 min at 20 °C to allow elution of the total RNA sample. Samples were stored at 4 °C for use in RT-PCR reactions or at -20 °C for prolonged storage.

Total RNA was spectrophotometrically analysed to measure the concentration and purity of each sample. Using a Genequant DNA/RNA calculator, (Pharmacia Biotech, St Albans, UK), the UV absorbance ratio at 260 nm/280 nm was established to show purity of sample, a ratio of 1.8-2.0 indicating high purity. The concentration (ng/mL) of each sample was also given. Samples were measured against DNPC treated water as a blank using a path length of 0.5 mm. All other parameters remained as standard.

2.2.5. Primer design

Method

Specific DNA primers were designed against drug transporters of interest in order to determine DNA fragments for amplification and thus establish presence of those drug transporters in rat lung cells and tissue. Final primer sequences for each drug transporter of interest can be viewed in tables 2.1-2.8 below.

Drug transporter gene sequences were searched using the *National Center for Biotechnology Information* 'ENTREZ' database, <http://www.ncbi.nlm.nih.gov/entrez/query.fcgi?db=gene>. Both mRNA and nucleotide sequences were visualised and compared using 'BLAST' (Basic Local Alignment Search Tool), <http://www.ncbi.nlm.nih.gov/BLAST/>, to locate a universal sequence from which to design the primer for a specific gene. Results from this were then copied to Primer3, an internet based program for the design of DNA primers

(http://frodo.wi.mit.edu/cgi-bin/primer3/primer3_www.cgi), where primers were automatically picked. Primers for use were then chosen based on Guanine Cytosine percentage (45-60 %), optimum annealing temperature (2-4 °C lower than melting temperature), and predicted product size (150-300 bp). Chosen primer sequences were then entered into a BLAST search in order to ensure the results, i.e. primer sequences, were only present in the gene of interest. BLAST results showing sequences from clones and other species were ignored as these are unlikely to be present in the reaction mixture; sequences from human genes were taken into consideration as there is possibility for these to be present due to contamination.

Once chosen, primers were manufactured at Invitrogen, stock lyophilized powder diluted to 10 pmol/mL in STERILE water.

NOTE: ALL TRANSPORTER NAMES AND GENE DESIGNATIONS ARE DENOTED AS REPRESENTED EXACTLY IN BLAST RESULTS. Transporter names/gene names have remained consistent throughout this thesis. When referring to a human transporter that is traditionally denoted by the transporter name used here (including notations involving letter case), a reference has been made in the text to differentiate between human and rat gene.

Transporter name	Gene	Primer pair 5' to 3'	Product size (bp)	Gen Bank Accession No.
mdr1a	ABCB1a	F: 5'-CATCCAGAACGCAGACTTGA-3' R: 5'-CTCGCATGGTCACAGTTCAT-3'	152	NM_133401
mdr1b	ABCB1b	F: 5'-ACCATCCAGAACGCAGACTT-3' R: 5'-ACCTCAAATACTCCAGCTCA-3'	150	NM_012623
mrp1	ABCC1	F: 5'-GCGATCACCCATGAGTTTCT-3' R: 5'-GGATGATGATGACAGCTCCA-3'	155	NM_022281
mrp 2	ABCC2	F: 5'-GACGGTTGGATTCTGTCACC-3' R: 5'-CACCTGTTGGAGGTAATCCAG-3'	172	NM_012833
mrp 3	ABCC3	F: 5'-CGCCTCAGTCCTTCTTTGAC-3' R: 5'-CTGCACGAAGCCATAGAACA-3'	215	NM_080581
mrp 4	ABCC4	F: 5'-GAGGTCTGGCCTCTTCCTG-3' R: 5'-GTGCGACGTTGAGAGAATCA-3'	194	NM_133411
mrp 5	ABCC5	F: 5'-CTTCTCCAGCTGGTCGTTTC-3' R: 5'-TGAGAAATTCACGGTGCTCTG-3'	157	NM_053924
mrp 6	ABCC6	F: 5'-CTGAGGATGGCCTTGAACAT-3' R: 5'-GCCAGTTTGAGCAAGAGACC-3'	215	NM_031013
mrp 8	ABCC7	F: 5'-CGTCAATAGTGACAACGCAAT-3' R: 5'-TGACGACTTTATTCTGTAGACATATCC-3'	150	NM_013039
CFTR	ABCC8	F: 5'-CCTGGTACTGACCCTGCTGT-3' R: 5'-AAAGCGTGACAGCCAACTCT-3'	238	NM_031506
White1	ABCG1	F: 5'-AGACTCTCCCAACCCAACCT-3' R: 5'-GTGTGTCCTAGACCCCTGGA-3'	231	NM_053502
BCRP	ABCG2	F: 5'-CTTGATAAATCAGGGCATCG-3' R: 5'-CAATAGTCCTTTCAAGGGGAAA-3'	152	NM_181381
β-actin	ACTB	F: 5'-AGCCATGTACGTAGCCATCC-3' R: 5'-CTCTCAGCTGTGGTGGTGAA-3'	228	NM_031144

Table 2.3 Forward (F) and reverse (R) primer sequences designed for each individual rat ABC transporter to be studied.

Transporter name	Gene	Primer pair 5' to 3'	Product size (bp)	Gen Bank Accession No.
Eaac1	Slc1a1	F: 5'-AAGCTACAGCCTGACCCTCA-3' R: 5'-GATGACCCAGTGAACCTCGT-3'	208	NM_013032
ASCT2	Slc1a5	F: 5'-CCTGCTCTTTTCTGCTGCA-3' R: 5'-AGGAAGGAATCCAGCACCTC-3'	159	NM_175758
rBAT	Slc3a1	F: 5'-ATACCCATGCCGTTTCTCTG-3' R: 3'-TACAGAGCTGCCTAGCACGA-3'	169	NC_005105
GLYT2	Slc6a5	F: 5'-ACCAACATCTTGGAGGCAAC-3' R: 5'-CATCCGCAGACTGGAAAGTT-3'	166	NM_203334
Cat-1	Slc7a1	F: 5'-GGCTGCAAAAACCTGTTGAG-3' R: 5'-AGCGATCAGGAAGGAGATGA-3'	216	NM_013111
Cat-3	Slc7a3	F: 5'-ATGCCTGAGCACTCTCGACT-3' R: 5'-CAGCCAACACAGAGGACAGA-3'	152	NM_017217
Asc-1	Slc7a10	F: 5'-GGACAAGCCCTTGAAGACAC-3' R: 5'-GAGAAGCTAGCAGGGCATTG-3'	214	NM_053726
PHT1	Slc15a4	F: 5'-TCTTCATGGGCCTCACCTAC-3' R: 5'-GATCCCCGAGAGAAAAGAG-3'	168	NM_144758
Lyaat1	Slc36a1	F: 5'-TATGGGTGTGCTCCCTTAC-3' R: 5'-TGTAGCCCAGGTTACCCAAG-3'	151	NM_130415
SNAT1	Slc38a1	F: 5'-TCAGCATCCCCCTAGTCATC-3' R: 5'-TGAGTCTCTGTGTCGCAACC-3'	194	NM_138832
SNAT3	Slc38a3	F: 5'-CCAAGGACAAAAGGAAGCTC-3' R: 5'-CTGCTTCGTGGGGTATGAGT-3'	157	NC_005107
β -actin	ACTB	F: 5'-AGCCATGTACGTAGCCATCC-3' R: 5'-CTCTCAGCTGTGGTGGTGAA-3'	228	NM_031144

Table 2.4 Forward (F) and reverse (R) primer sequences designed for each individual rat amino acid transporter to be studied.

Transporter name	Gene	Primer pair 5' to 3'	Product size (bp)	Gen Bank Accession No.
Glut1	Slc2a1	F: 5'-GCCTGAGACCAGTTGAAAGC-3' R: 5'-GAGTGTCCGTGTCTTCAGCA-3'	154	NM_138827
Glut2	Slc2a2	F: 5'-TCCTGGTCTTCACCTGTTC-3' R: 5'-ACCTGGTCCCTTCTGGTCT-3'	204	NM_012879
Glut4	Slc2a4	F: 5'-AATGACTGAGGGGCAAAATG-3' R: 5'-GGGAGAAAAGCCCATCTAGG-3'	235	NM_012751
Glut5	Slc2a5	F: 5'-ACTCAGTGGGGCACCTGAC-3' F: 5'-AGGACCCTCACGTCTTGTCT-3'	226	NM_031741
Glt-1	Slc5a1	F: 5'-GTCAGGGCTGGATGCTAAAG-3' R: 5'-CACCTCGTCGTTCTTCTCC-3'	172	NC_005113
β -actin	ACTB	F: 5'-AGCCATGTACGTAGCCATCC-3' R: 5'-CTCTCAGCTGTGGTGGTGAA-3'	228	NM_031144

Table 2.5 Forward (F) and reverse (R) primer sequences designed for each individual rat glutamine transporter to be studied.

Transporter name	Gene	Primer pair 5' to 3'	Product size (bp)	Gen Bank Accession No.
Cnt1	Slc28a1	F: 5'-GGGACTCGTCACTACCTCCA-3' R: 5'-AGGTTCCCAAGGAAAGAGGA-3'	162	NM_053863
rENT1	Slc29a1	F: 5'-CTTCCTGCTCACTTCCTTCG-3' R: 5'-CAGTCAGCCATCTGTCTCCA-3'	243	NM_031684
Ent2	Slc29a2	F: 5'-CCCTCATGACCTTCTTCCTG-3' R: 5'-CCAAGAGACCCGGTATAGCA-3'	166	NM_031738
Ent3	Slc29a3	F: 5'-ACTACATGAGGCCGGTTGTC-3' R: 5'-GAAGATAAGGGCGGTGATGA-3'	194	NM_181639
β -actin	ACTB	F: 5'-AGCCATGTACGTAGCCATCC-3' R: 5'-CTCTCAGCTGTGGTGGTGAA-3'	228	NM_031144

Table 2.6 Forward (F) and reverse (R) primer sequences designed for each individual rat nucleoside transporter to be studied.

Transporter name	Gene	Primer pair 5' to 3'	Product size (bp)	Gen Bank Accession No.
MCT	Slc16a2	F: 5'-ATTCGCCTTTCAACCATCAC-3' R: 5'-GCCAGCTTGATTCTGTCTCC-3'	150	NM_147216
MCT1	Slc16a1	F: 5'-CCCTGGAGTCCTCTAGTCC-3' R: 5'-GCGGGAGGTGGGTACTTACT-3'	239	NM_012716
Mct7B	Slc16a6	F: 5'-CGCTGCATTCTTACTGTCCA-3' R: 5'-AAGGTGAAGGCGAACAGAGA-3'	150	NM_198760
β -actin	ACTB	F: 5'-AGCCATGTACGTAGCCATCC-3' R: 5'-CTCTCAGCTGTGGTGGTGAA-3'	228	NM_031144

Table 2.7 Forward (F) and reverse (R) primer sequences designed for each individual rat monocarboxylate transporter to be studied.

Transporter name	Gene	Primer pair 5' to 3'	Product size (bp)	Gen Bank Accession No.
Pept1	Slc15a1	F: 5'-CCAGCTGACAAGCATAAACG-3' R: 5'-CCCACACTAGAAGGGTGTGC-3'	101	NM_057121
Pept2	Slc15a2	F: 5'-CGGGTCTGCTAAGTTTGAGG-3' R: 5'-CAAGCTAGCCTCTGGATTGG-3'	181	NM_031672
β -actin	ACTB	F: 5'-AGCCATGTACGTAGCCATCC-3' R: 5'-CTCTCAGCTGTGGTGGTGAA-3'	228	NM_031144

Table 2.8 Forward (F) and reverse (R) primer sequences designed for each individual rat peptide transporter to be studied.

Transporter name	Gene	Primer pair 5' to 3'	Product size (bp)	Gen Bank Accession No.
Oct1	Slc22a1	F: 5'-CTCCCATCTATGTGGGCATC-3' R: 5'-CTGGTCCAGTCCACCTCAT-3'	197	NM_012697
rOCT2	Slc22a2	F: 5'-ATCTACGTGGGCATCGTTT-3' R: 5'-ACAGTGGGTCCACACAGTCA-3'	220	NM_031584
OCTN2	Slc22a5	F: 5'-ACTCAGGCTGCCAGACACTT-3' R: 5'-ATATTGGCAACTGCACACCA-3'	197	NM_019269
β -actin	ACTB	F: 5'-AGCCATGTACGTAGCCATCC-3' R: 5'-CTCTCAGCTGTGGTGGTGAA-3'	228	NM_031144

Table 2.9 Forward (F) and reverse (R) primer sequences designed for each individual rat organic cation transporter to be studied.

Transporter name	Gene	Primer pair 5' to 3'	Product size (bp)	Gen Bank Accession No.
oatp1	Slco1a1	F: 5'-ATCAGTTTCATCTACTCACTTACAGCC-3' R: 5'-AGAAACAGGAAATGACACAGGAGTGAG-3'	162	NM_017111
oatp2	Slco1a4	F: 5'-CTCATATTCAGGGGGCTTCA-3' R: 5'-GTTCGGTGGCAAACAGTTCT-3'	151	NM_131906
oatp3a1	Slco3a1	F: 5'-GGCACTGCCTGAATTCCTTA-3' R: 5'-CACGTGGTAGTACCTGTAGG-3'	250	NM_177481
oatp-H	Slco4c1	F: 5'-CAGGTGGAGGTCTGCTGT-3' R: 5'-CCTCAAGCTCGCTTAGCTGT-3'	157	NM_001002024
oatp-E	Slco4a1	F: 5'-CTGGGACGTGCCTGACTAAT-3' R: 5'-GGCGAATAGCTCGACTTGAC-3'	175	NM_133608
moat1	Slco2b1	F: 5'-TTTCCATCACAGCCTCCTT-3' R: 5'-AAGAGCGGCAAGCTGAGTAG-3'	178	NM_080786
β -actin	ACTB	F: 5'-AGCCATGTACGTAGCCATCC-3' R: 5'-CTCTCAGCTGTGGTGGTGAA-3'	228	NM_031144

Table 2.10 Forward (F) and reverse (R) primer sequences designed for each individual rat organic anion transporter to be studied.

2.2.6. Digestion of potential DNA contamination

Materials

Consumables

TURBO DNase Buffer, (Ambion, Huntingdon, UK, Cat: 8176G)

TURBO DNase, (Ambion, Huntingdon, UK, Cat: 2238G)

DNase inactivation reagent, (Ambion, Huntingdon, UK, Cat: 8174G)

Sterile water for RNA work, (Fisher Scientific, Loughborough, UK, Cat: BPE561-1)

Method

Removal of contaminating DNA from RNA samples was essential to avoid false positive results. A TURBO DNA-free™ kit which itself is RNase free, was used for DNA removal, this avoided damage to the RNA sample. All kit reagents were stored at -20 °C.

All RNA samples were diluted to 200 µg/mL with sterile water before DNA contamination; samples of a lower initial concentration were not diluted.

To a sterile PCR tube:

Ingredient	Volume added (µL)
RNA sample (200 µg/mL or less)	40
10 x TURBO DNase Buffer	5
TURBO DNase (2 U/µL).	1

Samples were incubated at 37 °C for 30 min on a PCR block (Peltier thermal cycler, PTC-200, MJ research) after which 5 µL of DNase Inactivation Reagent was added. Samples were then incubated for a further 2 min at room temperature.

After incubation, samples were centrifuged in a PCR micro-centrifuge (Technico Mini centrifuge, Fisher Scientific) for 2 min and supernatants transferred to a new sterile PCR tube and stored at -20 °C.

2.2.7. Reverse transcriptase – polymerase chain reaction (RT-PCR)**Overview**

RT-PCR is a variant of PCR in which isolated messenger RNA (mRNA) is reverse transcribed to complementary DNA (cDNA) using a reverse transcriptase enzyme; Moloney Murine Leukemia Virus Reverse Transcriptase in this instance.

A tradition polymerase chain reaction technique is then employed to amplify the cDNA produced. Use of RT-PCR is preferred as mRNA contains only genetic information transcribed from DNA, i.e. the mRNA does not contain spurious information and is considered a 'purer' information form.

Materials*Consumables*

5x first strand buffer; [250 mM Tris-HCl (pH 8.3), 375 mM KCl, 15 mM MgCl₂], (Invitrogen, Renfrew, UK, (Included with MMLV-RT, Cat: 28025-013))

dNTP mix; 2.5 mM, (Bioline, London, UK, Cat: BIO-39044)

Dithiothreitol; DTT; 0.1 M, (Invitrogen, Renfrew, UK, (Included with MMLV-RT, Cat: 28025-013))

pd(N)₆; 50 ng/mL, (Ambion, Huntingdon, UK, Cat: 313453)

RNasin; 40 U/μL, (Promega, Southampton, UK, Cat: N211A)

Moloney Murine Leukemia Virus Reverse Transcriptase; M-MLV RT; 200 U/μL, (Invitrogen, Renfrew, UK, Cat: 28025-013)

Sterile water for RNA work, (Fisher Scientific, Loughborough, UK, Cat: BPE561-1)

Method

All reagents and RNA samples were stored at -20 °C or were kept on ice when in use for RT-PCR reactions. DNase/RNase free PCR tubes and sterile tips were used for all reactions to avoid cross-contamination.

To a sterile PCR tube:

Ingredient	Volume added (μL)
H ₂ O	3.5
5x first strand buffer	4
dNTP mix (2.5 mM)	2
DTT (0.1 M)	2
pd(N) ₆ (50 ng/μL)	2
RNA sample (≤ 164 ng/μL)	5

Sample Concentrations; If RNA sample concentration was 200 μg/ml before DNase treatment, the concentration will be 164 μg/ml after treatment. It is not essential to achieve this concentration as experience has shown that DNase treatment of less concentrated samples (≥ 180 μg/ml) does not affect RT-PCR reagent volumes used.

Samples were incubated at 80-95 °C for 4-5 min to denature the RNA strands then quenched on ice for a further 2 min Both RNasin and M-MLV RT were then added to each sample, changing tips between each addition. A control sample excluding RNasin and M-MLV RT was also prepared to ensure the integrity of the RT-PCR reaction.

Samples were then placed on a PCR thermocycler under the following conditions:

Thermocycling procedure	Reaction conditions
Step 1; Annealing of primers	25 °C for 10 min.
Step 2; Amplification of cDNA	42 °C for 42 min.
Step 3; Termination of reaction	95 °C for 5 min.
Step 4; Cooling	4 °C for 10 min.

Samples were removed from thermocycler and stored on ice for PCR or stored at -20 °C.

2.2.8. Polymerase chain reaction (PCR)

Materials

Consumables

Custom designed primers; diluted to 10 pmol/mL with RNase-free water

dNTP mix; 2.5 mM, (Bioline, London, UK, Cat: BIO-39044)

RT-PCR grade water, (Ambion, Huntingdon, UK, Cat: AM9935)

MgCl₂; 25 mM, (Bioline, London, UK, Cat: BIO-37026)

10x ThermoPol reaction buffer, (New England Biolabs, Hitchin, UK, (Included with Taq Polymerase, Cat: M0267S)

Taq polymerase, (New England Biolabs, Hitchin, UK, Cat: M0267S)

Method

To a sterile PCR tube:

Ingredient	Volume added (μL)
H ₂ O	6.4
MgCl ₂ (1.5 mmol)	0.75
dNTP mix (2.5 mM)	1
cDNA sample (from RT-PCR)	1
Custom primer, forward (10 pmol/μL)	1
Custom primer, reverse (10 pmol/μL)	1
10x Taq buffer	1.25
Taq polymerase	0.1

The above PCR mix was prepared for each custom primer and run using cDNA samples from whole lung tissue, SPOC1 cells, AEII – freshly isolated cells, AEII - day 2 of culture cells and also AEI-like cells. A control sample excluding cDNA was also prepared to ensure integrity of the reaction.

Samples were placed on a PCR thermocycler under the following conditions:

Thermocycling procedure	Reaction conditions
Step 1; Initial denaturation of cDNA	94 °C for 5 min.
Step 2; Denaturation	94 °C for 30 s
Step 3; Annealing of primers	60 °C for 45 s
Step 4; Extension of new DNA strand	72 °C for 45 s
Step 5; Repeat cycle, multiplying product	Repeat stages 2-4 34 times
Step 6; Final extension	72 °C for 10 min.
Step 7; Cooling of reaction	4 °C for 1 h

Samples were removed from thermocycler and stored on ice for PCR or stored at -20 °C.

2.2.9. PCR optimisation

Method

PCR was optimised to yield one product band for each custom primer, i.e. drug transporter under investigation. Optimisation was achieved using a range of primer annealing temperatures, increasing volume of cDNA sample and addition of dimethyl sulfoxide; DMSO (0.25 µL). For all ABC transporter and PEPT transporter primers, the annealing temperature was increased to 61 °C. Addition of DMSO was included for OAT transporter primer PCR reactions and the volume of cDNA was increased by 1 µL for Amino acid transporter primer reactions.

2.2.10. Agarose gel electrophoresis

Overview

Agarose gel electrophoresis works on the principle of protein charge or size. Nucleic acid molecules are separated by applying an electric field to move the negatively charged molecules through an agarose matrix. Shorter molecules move faster and migrate farther than longer ones because shorter molecules migrate more easily through the pores of the gel. This phenomenon is called sieving. Proteins are separated by charge in agarose because the pores of the gel are too large to sieve proteins.

Gel electrophoresis uses the gel as an anticonvective medium and/or sieving medium during electrophoresis. The gel suppresses the thermal convection caused by application of an electric field retarding the passage of molecules [127].

Materials

Consumables

Agarose, (Bioline, London, UK, Cat: bio-41025)

Tris (hydroxymethyl) aminomethane; Tris, (Fisher scientific, Loughborough, UK, Cat: T/P630/60)

Boric acid, (Fisher scientific, Loughborough, UK, Cat: B/3750/60)

Disodium ethylenediaminetetraacetic acid; Na₂EDTA.2H₂O, (Fisher scientific, Loughborough, UK, Cat: D/0700/53)

Ethidium bromine; EtBr, (Pharmacia biotech, Buckinghamshire, UK, Cat: 17-1328-01)

Bromophenol blue, (Pharmacia biotech, Buckinghamshire, UK, Cat: 17-1329-01)

Hyperladder V, (Bioline, London, UK, Cat: BIO-33031)

Method

PCR products were run on a 2% agarose gel to visualize product bands. Correct products were identified by band size.

Stock Tris boric acid EDTA (TBE) buffer was prepared by adding the following to 1 L dH₂O:

54 g Tris

27.5 g boric acid

3.72 g Na₂EDTA.2H₂O

This was diluted 1:10 to give 0.5x buffer concentration.

To 100 mL 0.5x TBE buffer, 2 g agarose was added. This solution was heated to dissolve the agarose and then left to cool. While cooling, a gel tank was prepared by taping the ends to create a mold.

Once the gel solution was cool, 1 µL EtBr was added to allow visualization of the cDNA products by UV light. The gel was poured into the tank mold and a comb added to create lanes for the addition of PCR product.

The gel was then left to set while 0.5x TBE running buffer was prepared through addition of 50 mL 5x TBE stock to 450 mL dH₂O.

Once the gel was set it was immersed in running buffer and 10 µL volumes of cDNA samples were loaded. Before sample loading, each cDNA sample was mixed with a trace of bromophenol blue which allowed ease of loading and allowed each sample to sink into a gel lane. A molecular weight marker was also loaded for reference.

Gels were then run by applying 90 V to each electrophoresis tank for 45 min or until bromophenol blue could be seen at a point approximately two thirds through the length of the gel.

Final cDNA sample visualization was undertaken under UV light through use of a Bio Rad Geldoc 1000 and products identified through band size by comparison to a molecular weight marker.

2.3. Results and Discussion

Below are the results and discussion of RT-PCR expression-based analysis of drug transporter proteins in rat lung cell models and whole lung tissue.

Through use of RT-PCR and agarose gel electrophoresis, the semi-quantitative expression of 46 drug transporter proteins, spanning 8 families, was examined in rat lung samples. The highly conserved cytoskeletal protein β -actin was used as a positive control for each set of PCR experiments with cDNA and RT-negative reactions serving as negative controls. Gel electrophoresis signal intensities were interpreted in a semi-quantitative manner with a weak signal intensity indicating low expression and a strong signal intensity indicating high expression. Figure 2.3 illustrates typical signal intensities and the corresponding expression index assigned, i.e., (-) no expression, (+) low expression, (++) moderate expression, and (+++) high expression. The derived mean mRNA expression profiles for each drug transporter family are shown in tables 2.11 to 2.18; individual expression profiles can be seen in appendix i.



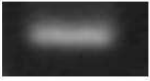

Sample Band	Level of Expression
	No expression -
	Low expression +
	Moderate expression ++
	High expression +++

Figure 2.3 Typical signal intensities and the corresponding expression index assigned i.e. (-) no expression, (+) low expression, (++) moderate expression, and (+++) high expression. The mRNA signal intensity for each drug transporter was examined and assigned an expression index in order to allow semi-quantitative analysis, a weak signal intensity indicating low expression and a strong signal intensity indicating high expression within the rat lung.

2.3.1. Expression analysis of ATP Binding Cassette transporters

The ATP Binding Cassette (ABC) transporter superfamily is comprised of approximately 50 members classified into 7 subfamilies; Families are constructed based upon amino acid structure and domain

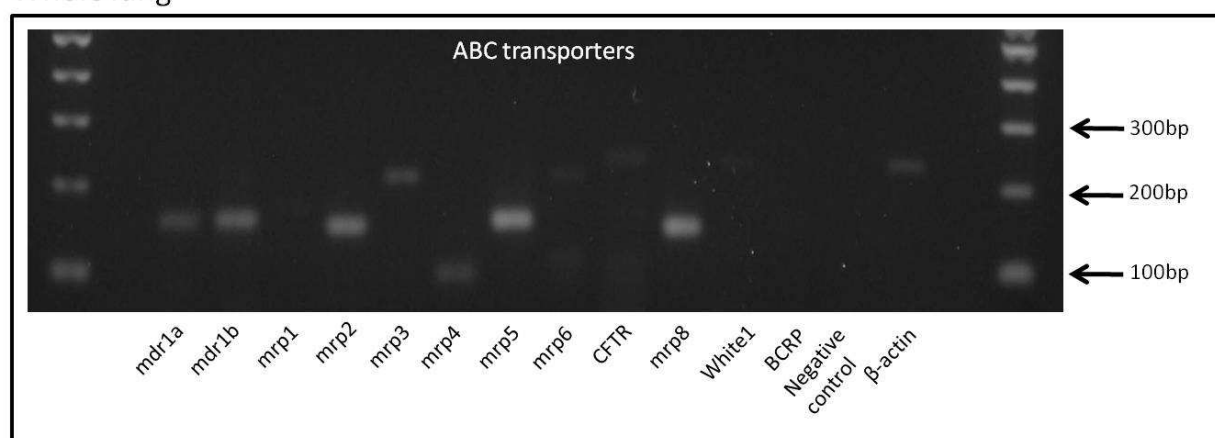
organization with relatively modest similarity in domain organization between family groups [52]. Table 2.11 summarises the mRNA expression profile of 12 key ABC transporter members in whole rat lung sample, the rat SPOC1 cells, rat AEII – freshly isolated cells, rat AEII – cells at day 2 of culture, and rat AEI-‘like’ cells (day 8).

Transporter	Gene	Whole Lung	SPOC-1	AEII – Freshly Isolated	AEII – Day 2 of Culture	AEI-‘like’ Day 8 of Culture
mdr1a	ABCB1a	++	+	+	+	+
mdr1b	ABCB1b	++	+	+	++	++
mrp1	ABCC1	++	++	+	+++	++
mrp2	ABCC2	-	-	+	+	-
mrp3	ABCC3	+	++	++	++	+
mrp4	ABCC4	+	-	-	-	-
mrp5	ABCC5	+++	+	+	++	+++
mrp6	ABCC6	++	-	+	-/+	+
CFTR	ABCC7	-/+	+	+	+	+
mrp8	ABCC8	+++	+	+	-	++
White1	ABCG1	++	++	++	+++	+++
BCRP	ABCG2	+	-	+	+	++
β -actin	ACTB	+++	+	++	++	+++

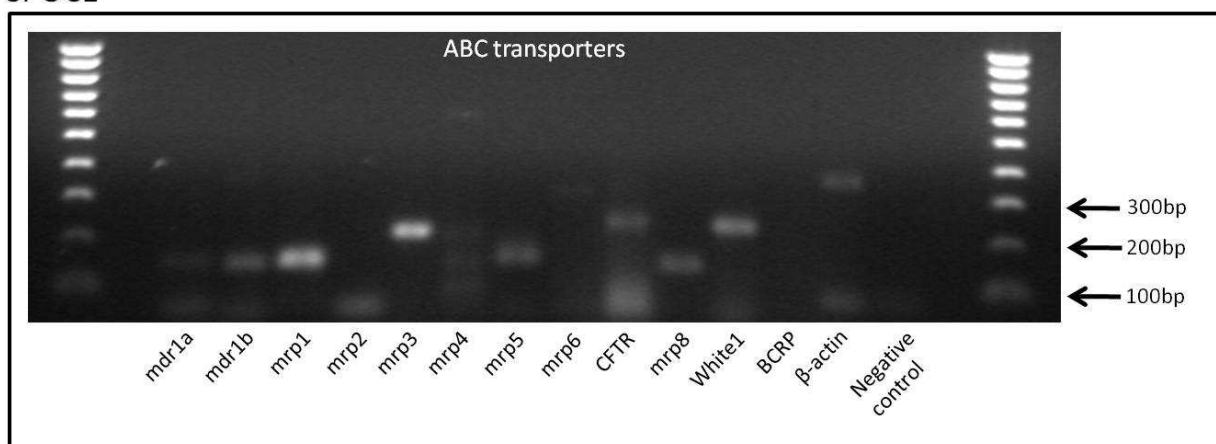
Table 2.11 Expression profile of 12 ATP Binding Cassette transporter family members, profile was determined from RT-PCR analysis in pulmonary cell samples. Transporter expression was ‘quantitated’ by signal intensity and assigning of an expression index. Mean data are shown, n=3.

The corresponding RT-PCR samples visualised by gel electrophoresis can be seen in figure 2.4 and illustrate variation in intensity of transporter mRNA expression within the rat lung cell samples studied.

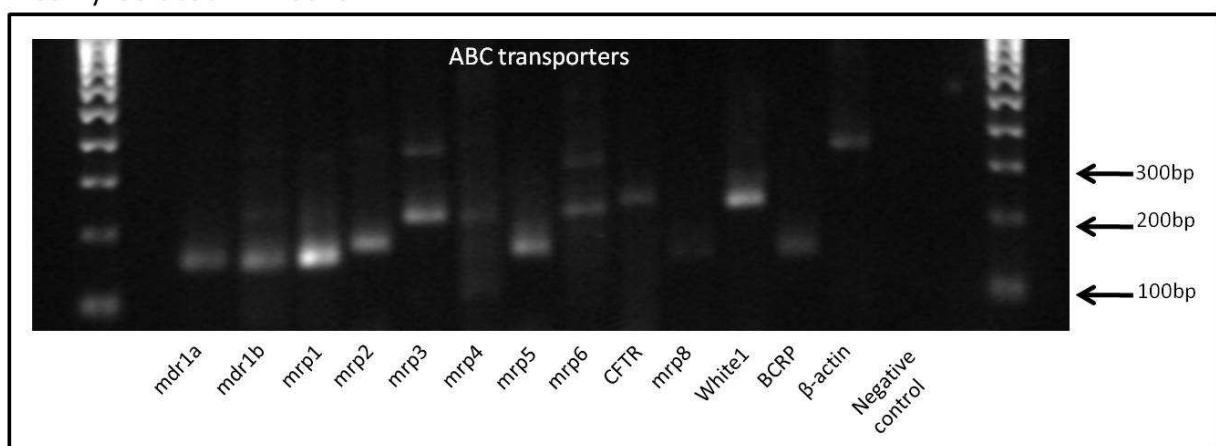
Whole lung



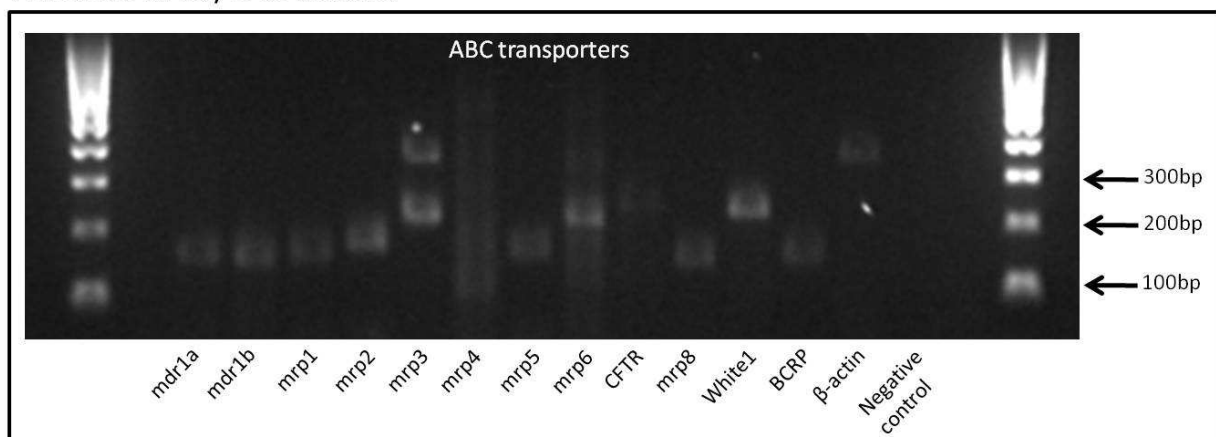
SPOC1



Freshly isolated AEII cells



AEII cells at day 2 of culture



AEI-'like' cells

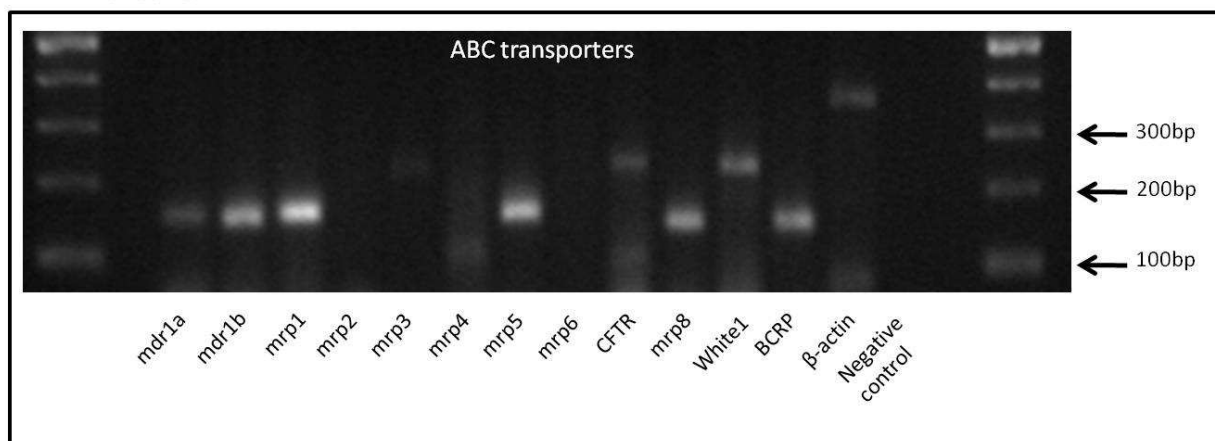


Figure 2.4 Representative gel electrophoresis images illustrating selected ABC transporter mRNA expression in 5 rat lung cell samples. Each set of RT-PCR reactions included a β -actin positive control and an RT-negative negative control to ensure result integrity.

The present study concentrated on ABC transporters that exhibited potential roles in drug absorption and disposition. Within the ABC-B sub-family, ABCB1/MDR1/P-glycoprotein (P-gp) was the only member to be studied. P-gp was first documented through its over-expression in mutant Chinese hamster ovary cells that exhibited resistance to a number of amphiphilic drugs [70]. P-gp has an extensive array of transportable substrates which include anti-cancer drugs, antibiotics, cardiac drugs, immunosuppressants and steroids and transport these by binding them in the cytosolic lipid leaflet of the plasma membrane [128, 129]. P-glycoprotein is expressed in a number of biological barriers and organs involved with absorption and disposition such as the blood-brain barrier, where P-gp is highly expressed, the intestine, the liver and kidney. For example, strong expression in the liver and kidney is indicative of P-glycoprotein involvement in the removal of toxic compounds from cells into the bile or urine [40, 130, 131].

P-glycoprotein is encoded by two isoforms of the *mdr1* gene in rats. Within the results of this chapter, the *mdr1a* isoform exhibited low expression (all semi-quantitative expression discussed here was approximated based upon typical expression intensities displayed in figure 2.3) in all cell culture samples and showed moderate expression in whole lung. In contrast, the *mdr1b* isoform showed low expression in SPOC1 culture and freshly isolated AEII cells but increased in expression intensity with time to show moderate expression in both AEII cells at day 2 of culture and AEI-'like' cells. Moderate expression was also seen in whole lung (Figure 2.4).

There exists some literature documenting the expression of P-glycoprotein in the lung. At both the mRNA and protein level, P-gp has been identified in human and rat lung tissue, including crude

alveolar tissue, bronchial tissue and nasal mucosa [43, 107-110, 113, 131-133]. The transporter has been immunohistochemically localised to both the apical and basolateral membranes of epithelial cells of the human lung and has exhibited a similar pattern of localisation in rat lung tissue [58, 134-136]. Specifically P-gp has been localised to the apical membrane of human ciliated epithelial cells, the apical and basolateral membrane of serous cells and the membranes of AEII and AEI-‘like’ cells [112, 113]. Within the rat lung, P-gp has also been localised to AEII cells whose phenotype was maintained to day 8 of culture and in AEI-‘like’ cells, but interestingly *mdr1a* and *mdr1b* isoforms have been reported to be absent in freshly isolated AEII samples examined by RT-PCR [113, 137].

Overall, the data presented here agrees with current literature evidence; Endter and co-workers have also reported P-gp mRNA to be expressed, on average, at low levels in a primary human lung cells and a number continuous cell models [104]. This trait was also observed by Bleasby and co-workers who reported the mRNA of human P-glycoprotein gene, MDR1, to be expressed at a low level in lung tissue, the rat isoform *mdr1a* was, however, found to be expressed at a relatively higher level in rat lung samples [69]. The moderate mRNA expression of *mdr1b* in whole lung has been reported by Brady, who examined expression via a DNA assay [138].

The ABCC subfamily is one of the larger transporter subfamilies and contains 12 full transporters. The most studied transporters of this family are the nine MRP transporters, while other family members include the sulfonylurea transporters, SUR1 & 2, and the cystic fibrosis related protein, CFTR. Within this study, the mRNA expression of the MRP transporters *mrp 1-7*, *mrp8* and the CFTR (ABCC7) ‘transporter’ were studied.

Of the ABCC family members, *mrp1* exhibited relatively moderate expression in the majority of samples (Figure 2.7). However, in a similar manner to *mdr1b*, expression intensity of *mrp1* increased from low expression in AEII freshly isolated cells to a high level of expression in AEII cells at day 2 of culture. MRP1 expression within the lung is well recognised and the transporter is thought to play a role in protecting lung tissue from inhaled xenobiotics [43, 114, 139]. There is less literature evidence to support the presence of many other MRP transporters within the lung, however, Endter and co-workers have shown all 9 MRP transporters to be present at mRNA level in human bronchial epithelial cells and human alveolar epithelial cells (AEII and AEI-‘like’) [104]. Similarly, the work of Bleasby and co-workers has produced an mRNA expression profile which demonstrates the various levels of expression of eight of the MRP transporters in both human and rat lung [69]. However, the remaining MRP transporters are thought to have a much more restricted expression profile.

Rodent mrp2 was barely detectable (present at only low levels) in both freshly isolated AEII cells and AEII cells at day 2 of culture. Human MRP2 is primarily expressed in the apical membranes of the kidney and liver where it effluxes a large number of endogenous compounds and xenobiotics to the bile and urine [139, 140]. Within the lung, there is conflicting evidence of MRP2 expression. Positive antibody staining for MRP2 on the apical side of human bronchial epithelium has been reported and transporter presence in several lung cell lines including PLC and NHBEC lines has been indicated though immunohistochemistry [114, 141]. The work of Endter *et al.*, shows human MRP2 expression at moderate levels in the vast majority of lung samples examined including both freshly isolated cells and continuously grown cell lines. The absence of mrp2 from whole lung tissue and the SPOC1 cell culture line is puzzling, however, the expression of several MRP transporters has been reported in primary lung cells and yet the same transporters have been absent in cell culture models [104]. Further, MRP2 was the only MRP transporter reported to be absent in human lung through the Bleasby *et al.*, expression profiling study [69]. The apparent restricted expression of mrp2 within the rat lung could represent a specific role for the transporter within this region. Rat mrp2 could function at apical cell membranes as an efflux transporter to extrude inhaled xenobiotics to the airspace, in a similar manner to its proposed function within the kidney and intestine. The low level of expression observed could represent its functional significance behind transporters such as MDR1 and MRP1.

Paralleling the observed results of mrp1, the mrp3 product also showed a moderate level of expression in the majority of lung cell samples. Interestingly, as AEII cell sample time in culture progressed from freshly isolated through to day 2 and then day 8 of culture, the expression level of mrp3 appeared to decrease visually, from a moderate to a low level. MRP3 has been localised to the basolateral membrane of the human intestine and has also been localised to hepatocytes where the transporter is thought to have a protective role [138, 139, 142]. There are conflicting results in the literature as to the presence of MRP3 in the human lung. Low levels of MRP3 have been reported in total lung RNA and the transporter has been localised to human primary bronchial and peripheral epithelial cells [114, 143-145]. In contrast to this, Scheffer and co-workers have reported the absence of MRP3 RNA in bronchial epithelial cells creating confusion over the presence of this transporter in the lung [43, 133, 135]. In the liver and kidney MRP3 participates in defence by eliminating a multiplicity of toxic organic anions and other compounds and could perform the same function in the lung. Recent works have reported MRP3 mRNA expression in a number of cells within the lung and Bleasby and co-workers also report moderate expression of mrp3 in rat lung samples [69, 104]. Literature evidence in combination with the results of this chapter suggests mrp3

to have a wide expression profile within the rat lung where mrp3 could be performing a defensive role.

The mrp4 drug transporter was absent in all lung cell samples examined in this study with the exception of whole lung tissue where a low level of expression was seen. Human MRP4 is predominantly expressed in the prostate, effluxing prostaglandins and in the kidney, effluxing drugs such as AZT [139, 146, 147]. The transporter is thought to be basolaterally expressed within the lung, with van der Deen reporting the presence of MRP4 mRNA in whole lung tissue and bronchial epithelia [141]. Chen & Klaassen have also reported presence of this transporter in whole rat lung through the use of PCR and oligonucleotide probes [141, 148]. With this current work, mrp4 was only present in whole lung samples. Since the major bronchi were not afforded individual sample status within this study, expression in 'whole lung' samples could represent expression within bronchial epithelia, particularly when combined with reported evidence of human MRP4 bronchial expression [141]. This specific lung expression is in contrast to the work of Endter and co-workers who reported clear MRP4 expression in human lung bronchial and alveolar epithelial cell samples [104]. These conflicting reports could indicate a differing species-specific expression profile for MRP4.

The fifth member of the ABCC family, mrp5, was expressed at a low level in SPOC1 cells and AEII freshly isolated cells with expression in the AE cells increasing in intensity with time in culture to a high level by day 8, i.e. AEI-'like' cells. This increase in expression intensity over time could be explained by the need for a cell isolated from the lung to establish itself in *in vitro* culture before being fully able to function with regard to transcriptional capability; a decrease in expression intensity i.e. mrp1, mrp3, could also be reasoned by the need for cell DNA transcriptional capacity to become established. Further, this result could also mean that a regulatory stimulus is missing in culture. Ideally, if one wished to study the effect of alveolar cell phenotype upon expression then the primary AEII cell phenotype should be retained in culture over the same time frame used to study the AEI-'like' cell phenotype. This strategy was used by Campbell *et al.*, whilst examining the phenotypic dependence upon caveolin-1 expression in alveolar epithelial cells [149]. A high level of mrp5 expression was also seen in whole lung samples. The transporter mrp6 was found to have negligible expression in all samples excluding the whole lung, where a moderate level of expression was seen. Similarly, CFTR was also expressed at a low level in all samples including whole lung tissue. The cystic fibrosis conductance regulator protein (CFTR) was also studied here and is unique among all ABC transporters as it functions as a chloride ion channel. Mutations in CFTR form the

genetic basis of the pulmonary disease cystic fibrosis (CF), with the $\Delta F508$ mutation (deletion of the phenylalanine codon at position 508) attributed to 50-80 % of CF cases in the Caucasian population [71]. CFTR has been localised to the apical surface of pulmonary epithelial cells such as ciliated cells, Clara cells and AEI cells. Expression has also been reported in AEII cells and nasal mucosa [150-154]. The results of this chapter show CFTR to be expressed at low levels in all rat lung cells examined suggesting the protein to function as a chloride channel in a number of regions throughout the lung.

The remaining ABC subfamily investigated was ABCG; specifically ABCG1 and ABCG2 isoforms were examined. The ABCG family is comprised of half-transporters that dimerise to form functional transporter proteins. White1 (ABCG1) was found to be expressed at a moderate level in whole lung tissue, SPOC1 cells and freshly isolated AEII cells. The expression level increased in intensity in the alveolar cells with time in culture, where a high level of expression was seen in both AEII cells at day 2 of culture and AEI-‘like’ cells (day 8 of culture). The breast cancer resistance protein (BCRP/ABCG2) was expressed at low levels in whole lung tissue and both freshly isolated and ‘day 2’ AEII cells. The level of expression increased in intensity where BCRP was found to be moderately expressed in AEI-‘like’ cells; again the requirement for stability in transcriptional capacity could be attributed to observed results. BCRP was absent in SPOC1 cells. ABCG1/White1 is reported to be expressed at high levels in tissues such as the thymus, spleen, lungs and brain [155, 156]. ABCG1 has been identified in human and rodent lung at RNA and protein level and is important in cholesterol efflux and maintaining pulmonary lipid homeostasis [40, 157]. The moderate-to-high levels of ABCG1/White1 expression observed in the rat lung cells studied show this transporter to have a stable expression profile across the rat lung. The second ABCG transporter, BCRP, typically shows strong expression in the mammary gland, brain and placenta and has also been localised to the apical membrane of the liver, kidney and intestine. Within the lung, BCRP expression has been shown to be present in human whole lung tissue, bronchial and alveolar epithelial cells, bronchial smooth muscle cells [40, 43, 116]. The results generated here show BCRP to be expressed at mainly low levels in all studied lung cells with the exception of SPOC1 cells where the transporter was absent. Within the lung BCRP expression could be restricted to more distal regions and would be absent from a tracheal cell line such as SPOC1.

Overall, the mRNA transcript for each ABCC transporter studied exhibited some degree of expression within the rat lung. Notable exceptions include mrp2 and mrp4, which were absent in many of the samples examined; the presence of both positive and negative reaction controls served to validate the results. Generally, these results are consistent with the existing literature where transporters

MRP1, MRP5, MRP6, and MRP8 are known to be ubiquitously expressed within the body of a number of species therefore reasoning the presence of such ABC transporters in the lung [40, 123, 139, 158-160].

ATP binding cassette transporters can have a crucial influence upon drugs delivered to the body. For example, transporters ABCB1 (P-gp), ABCC2 (MRP2) and ABCG2 (BCRP), all limit exogenous substances and xenobiotics entering the GI tract through the intestine while ABCB1, ABCC1, ABCC2, ABCC4, ABCC5 and ABCG2 all act at the blood-brain barrier to protect the central nervous system [161]. The influence of transporters upon drug substrates has been exploited in many instances to enhance therapeutic action or avoid toxic side-effects. For example, studies have shown that co-administration of the P-gp modulator elacridar with the anti-cancer drug doxorubicin can reduce doxorubicin-induced concentration dependent drug resistance [161].

The presence of drug transporters, including many ABC transporters, within the lung is becoming increasingly realised. ABC transporters that are expressed in the lung may have marked effects on drugs delivered to this region. It is notable that many ABC transporters are known to have a very broad substrate specificity able to mediate the transport of a range of diverse chemistries. P-glycoprotein for instance is known to transport hundreds of substrates including; anti-cancer drugs, antibiotics, antiemetics, cardiac drugs, Ca^{2+} blockers, β -blockers, CNS drugs, antihistamines, HIV protease inhibitors, immunosuppressants and steroids [103, 162]. Extensive knowledge of the expression and localisation of drug transporters within the lung will aid in drug design where transporter presence can be factored in to the design process. In this way, the effects of drug transporters upon therapeutic substrates can either be exploited or avoided and a maximal therapeutic effect can be achieved.

The results of this chapter have generated an expression profile of several ABC transporters in the rat lung. Overall, each transporter examined exhibited some level of mRNA expression in the rat cell samples. Extending and confirming the expression profile of important ABC transporters in a pre-clinical model such as the rat will help to advance knowledge of the effects such transporters have on drug disposition, drug excretion, drug toxicity and therapeutic effect. Knowledge of differences within pre-clinical models will aid in the extrapolation of data to humans.

2.3.2. Expression analysis of Amino Acid transporters

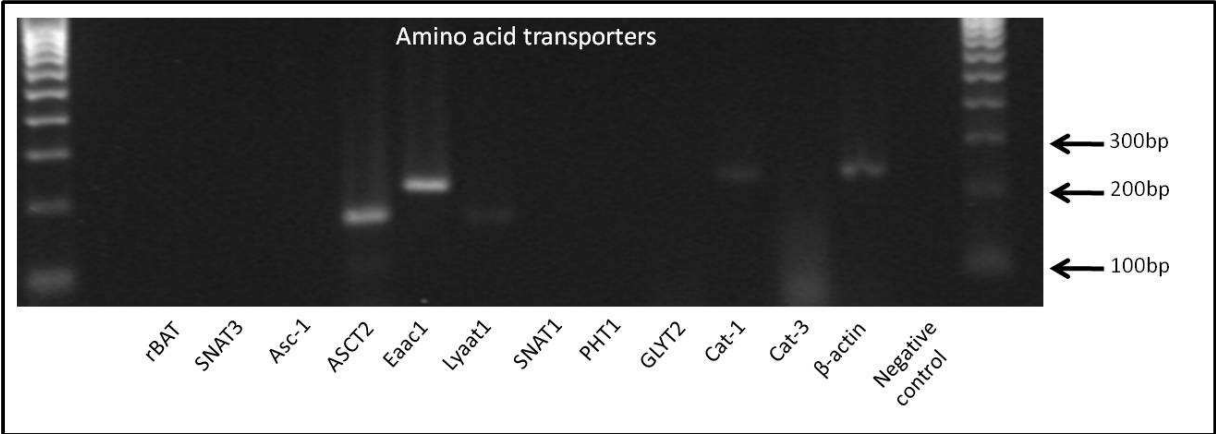
The Solute carriers comprise 43 families containing approximately 300 members [44]. The amino acid transporters are not restricted to one family group but instead span several transporter families. Within this study, members of the SLC1, SLC3, SLC6, SLC7, SLC15, SLC36 and SLC38 families were examined. Table 2.12 summarises the expression of 11 amino acid transporter members from the above seven families.

Transporter	Gene	Whole Lung	SPOC-1	AEII – Freshly Isolated	AEII – Day 2 of Culture	AEI-‘like’ Day 8 of Culture
rBAT	Slc3a1	-	-/+	+	-/+	-
SNAT3	Slc38a3	-	++	++	++	++
Asc-1	Slc7a10	-	-	-	-	-
ASCT2	Slc1a5	++	+	+	+	++
Eaac1	Slc1a1	+++	-	++	+++	++
Lyaat1	Slc36a1	-/+	-	+	++	+
SNAT1	Slc38a1	-	-	-	++	+
PHT1	Slc15a4	-	-	-	-/+	-
GLYT2	Slc6a5	-	-	-	+	-/+
Cat-1	Slc7a1	+	++	+	++	+
Cat-3	Slc7a3	-	-	-	-/+	-
β-actin	ACTB	++	++	++	++	+++

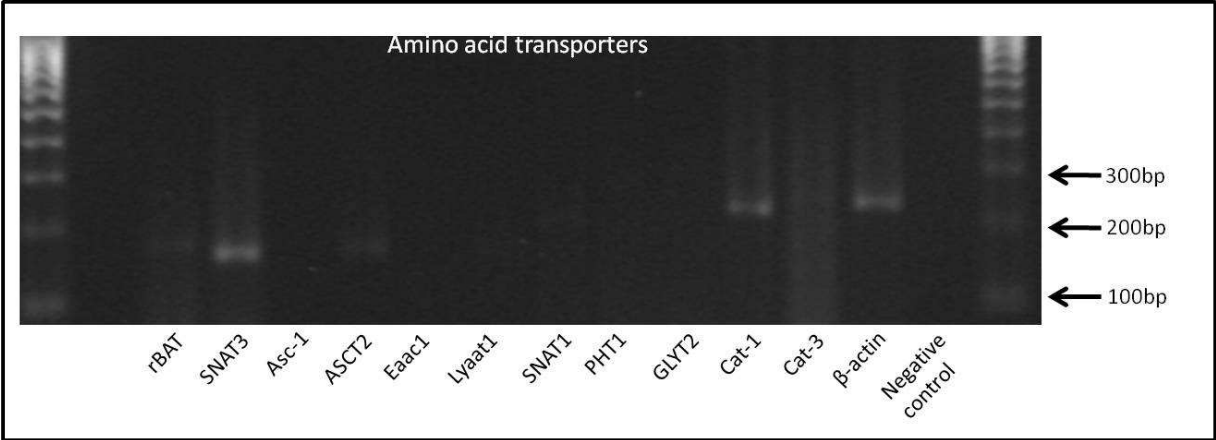
Table 2.12 Expression profile of 12 amino acid transporter family members, profile was determined from RT-PCR analysis in pulmonary cell samples. Semi-quantitative analysis of transporter expression was undertaken by examining signal intensity and assigning an appropriate expression index. Mean data are shown, n=3.

The SLC1 transporter family is comprised of five high affinity glutamate transporters and two neutral amino acid transporters [163]. Within this study, the mRNA expression of two family members; Eaac1 and ASCT2, was examined in rat lung cell samples. Figure 2.5 represents the corresponding gel electrophoresis images obtained.

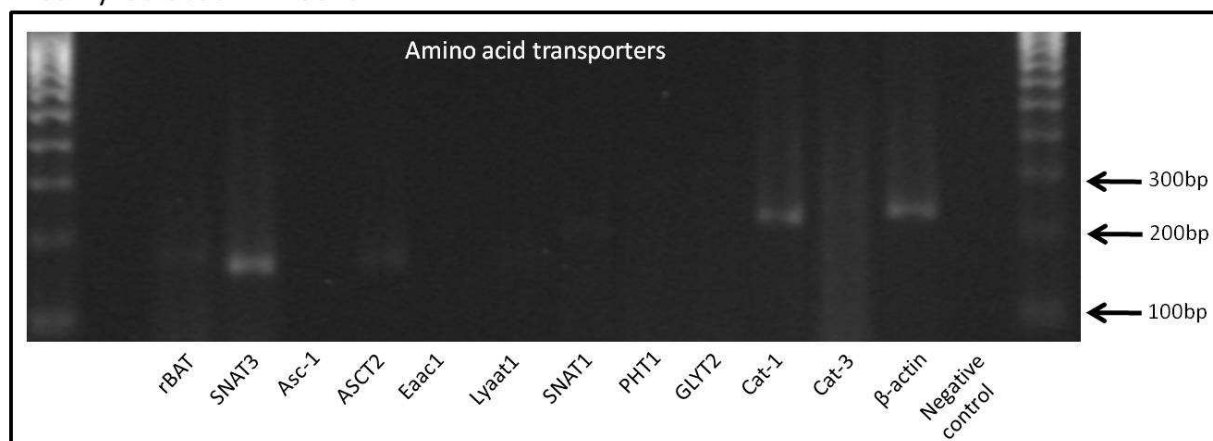
Whole lung



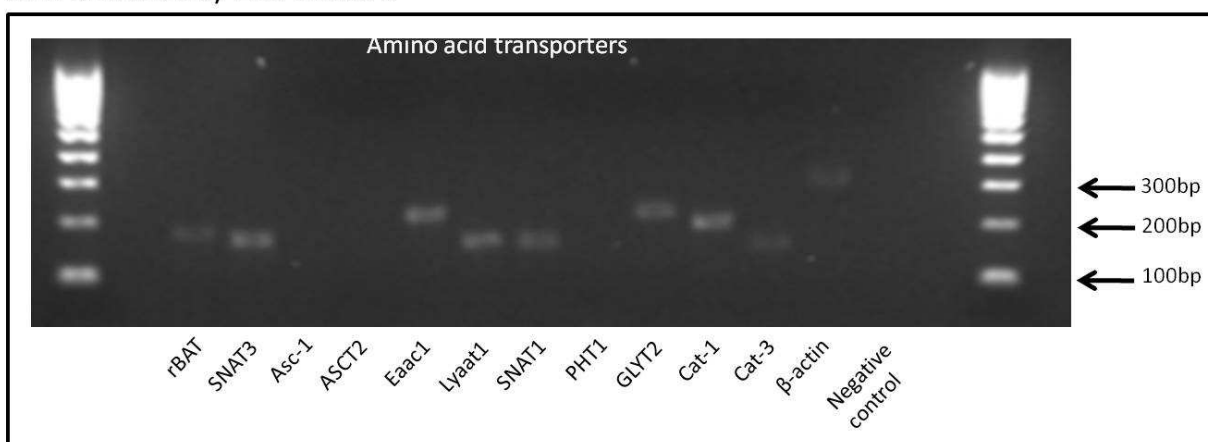
SPOC1



Freshly isolated AEII cells



AEII cells at day 2 of culture



AEI-'like' cells

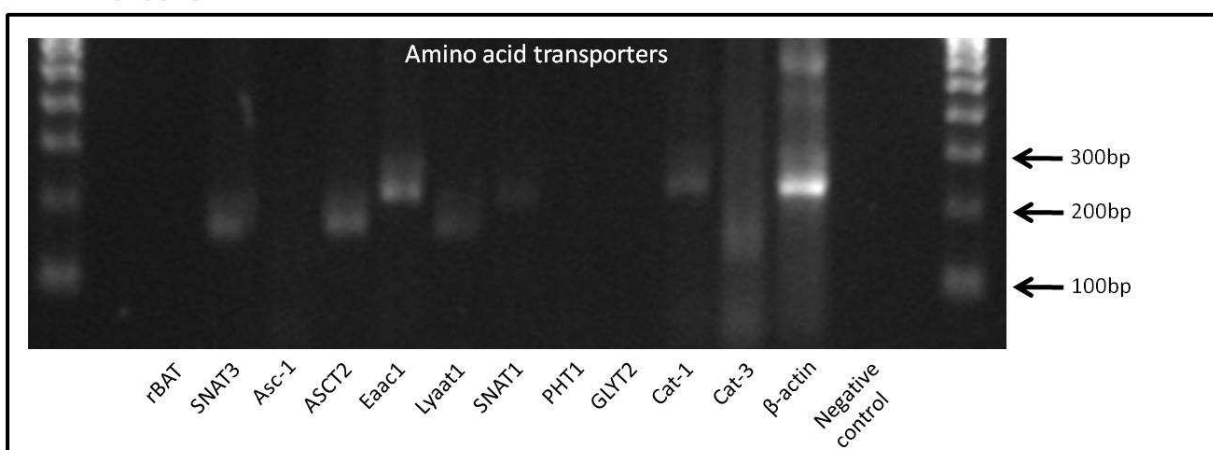


Figure 2.5 Representative gel electrophoresis images illustrating selected amino acid transporter mRNA expression in rat lung cell samples. Each set of RT-PCR reactions included a β -actin positive control and an RT-negative negative control to ensure result integrity.

Eaac1/SLC1A1 functions as a high affinity glutamate transporter and transports substrates, namely L-glutamate and D- and L-aspartate, by coupling to the electrochemical gradients of Na^+ , H^+ and K^+

[164]. Eaac1/SLC1A1 has been localised to the neurons of the hippocampus, cerebral cortex, olfactory bulb, striatum, superior colliculus and thalamus and also to the apical membrane of proximal tubules of the kidney [165-168]. Within the rat lung samples studied, Eaac1/SLC1A1 displayed moderate levels of expression in freshly isolated AEII cells and AEI-‘like’ cells. High expression levels were observed in AEII cells at day 2 of culture and whole lung tissue while Eaac1/SLC1A1 was found to be absent in SPOC1 cells. Within the literature, Northern blot analysis has shown Eaac1/SLC1A1 presence in rat and human lung supporting the evidence obtained through mRNA expression in this chapter [169, 170]. Absence of Eaac1/SLC1A1 in the SPOC1 sample suggests expression to be restricted to more peripheral regions of the lungs however, a lack in localisation data within the literature does not allow confirmation of this.

The SLC1 transporter ASCT2 exhibits a wider substrate range than its family member Eaac1/SLC1A1 and has been localised to the intestine and kidney where it functions as a neutral amino acid transporter [163, 171]. Examining mRNA expression in rat lung cell samples revealed ASCT2 to be present at low levels in SPOC1 cells, freshly isolated AEII cells and AEII cells at day 2 of culture. Expression intensity increased with time and ASCT2 exhibited moderate expression in AEI-‘like’ cells. A moderate level of expression was also seen in whole lung tissue. ASCT2 cDNA was first isolated from mouse testis and was first confirmed in the lung of this animal [172]. Both Northern and Western blot techniques have also illustrated ASCT2 expression in rat and mouse lung [173, 174].

The SLC3 family consists of only two proteins; rBAT and 4F2hc, neither of which functions as an amino acid transporter in their own right; only rBAT was studied. The rBAT protein functions as the heavy subunit of a heteromeric amino acid transporter and was first identified through expression cloning in *Xenopus* oocytes [175]. Predominantly functioning with characteristics representative of the amino acid transport system $b^{0,+}$, (mediated by heteromeric amino acid transporters), rBAT has been localised to the apical plasma membrane of epithelial cells of the intestinal mucosa and renal proximal tubule and has also been reported in the brain, pancreas and liver [150, 154, 164, 176-182]. Investigation of the mRNA expression of rBAT in rat lung cells revealed negligible expression levels in all samples, except freshly isolated AEII cells where rBAT was expressed at a low level. Through the formation of a heterodimer with $b^{0,+}$ AT (SLC7A9), rBAT functions as the primary re-absorption system for cystine in the kidney and has been localised to microvilli of the straight and convoluted proximal tubule of human, mouse and rat [175, 177, 183]. Literature evidence documenting rBAT expression in the lung is scarce. While there is little direct evidence available, a splice variant of rBAT has been reported to be absent from the human lung [184]. Within the rat lung, rBAT was

positively expressed at a low level in only freshly isolated AEII cells which could suggest a very narrow expression range for this transporter protein. The rBAT protein, in heterodimeric form, is recognised as being responsible for cystine re-absorption, suggesting this to be the transporter's function. Within the lung, several mechanisms for cystine transport have been identified, including system X_{AG} and system X_C . It is thought that, in a Na^+ independent manner, cystine transport occurs by system X_C or system $b^{0,+}$ (of which rBAT is involved); rat $b^{0,+}$ mRNA has been reported to be absent from rat lung by Northern blotting [176, 185]. The rBAT protein could be present at minimal levels within the rat lung and not function as a cystine transporter due to the absence of $b^{0,+}$ AT. Further, the association of the rBAT protein with cystine transport could provide an explanation for the presence of rBAT in freshly isolated AEII cells. The type I alveolar epithelia of the lung are particularly vulnerable to hyperoxic damage and are replaced by the more rapidly proliferating AEII cells that then differentiate to AEI cells. The presence and continual synthesis of the antioxidant glutathione (GSH) within the AEII cells is very important to avoid hyperoxia-related lung damage, however, in order to maintain GSH levels, the lung is dependent on an extracellular supply of cysteine [186]. The availability of cysteine is the rate-limiting step in GSH synthesis [187] and because cysteine is readily oxidised to cystine, the transport of cystine is fundamental in the maintenance of cellular GSH levels and the avoidance of lung damage [185]. While it is unlikely that rBAT is responsible for cystine transport within alveolar epithelia (due to the absence of rat $b^{0,+}$), the protein could simply be present because it was once part of a functioning system $b^{0,+}$ transport system within the lung. With no literature evidence to support these assumptions, together with the absence of rBAT in all other rat lung samples, they remain purely speculation.

The SLC7 family transporter, Asc-1, was absent from all studied rat lung cell samples. Typically, Asc-1 is expressed in the brain, lungs, small intestine and placenta and functions as a transporter of small neutral amino acids such as L-alanine, L-serine and L-cystine, [188]. Expression of Asc-1 at an mRNA level has been reported in mouse and human lung rendering the observations of this study a surprising result [188-190]. Each PCR reaction included both a positive and negative control suggesting the absence of Asc-1 in rat lung to be a true observation rather than an artifact of poor PCR. Due to the existence of many different amino acid transporters, it could be possible that the role of Asc-1 in this rat species is taken over by another protein which could explain absence of Asc-1 in the samples studied.

Many of the other amino acid transporters also exhibited negligible expression levels or were found to be absent in the majority of samples. The neuronal glycine transporter GLYT2, which functions to

control the accessibility of the neurotransmitter to glycinergic synapses, the peptide/histidine transporter, PHT1 and Cat-3, which functions to transport cationic amino acids independent of sodium [191], were absent in all lung samples with the exception of AEII cells at day 2 of culture. Additionally, both Lyaat1 (lysosomal amino acid transporter) and SNAT1 (sodium-coupled neutral amino acid transporter) displayed a pattern where expression was not observed or observed at low levels in all other cell samples and yet displayed moderate levels in 'day 2' and 'day 8' samples of alveolar epithelia. This observation of predominant expression in either the AEII cells at day 2 of culture or AEI-'like' cells could be the result of a burst of mRNA expression; either in preparation for or as a result of cell differentiation. Both GLYT2 and Cat-3 are reported to be restricted to the CNS of adult human or adult mouse and rat. Both transporters, however, are known to be widely expressed during embryonic development and therefore could be functionally active during the differentiation of AEII cells to AEI-'like' cells [120, 192, 193]. The transporters PHT1, Lyaat1 and SNAT1 have all been reported to be present in the lung of either human, rat or mouse. Expression limited to alveolar epithelium could represent a restricted expression profile for these transporters within the rat [190, 194-196].

The remaining amino acid transporter proteins studied in this section exhibited, overall, modest expression profiles. The SLC7 family transporter, Cat-1 showed low levels of expression in whole lung and freshly isolated AEII cells with expression increasing with time to a moderate level in AEII cells at day 2 of culture. Expression levels decreased to a low level with continuing time in culture i.e. as the AE II cell took on the characteristics of AEI-'like' cells. A moderate Cat-1 expression level was seen in SPOC1 cells. Cat-1 acts as a major system γ^+ transporter in most cells and is thought to be ubiquitously expressed; system γ^+ is a sodium-independent, basic amino acid transport system which favours amino acids such as lysine, arginine and ornithine [188, 197, 198]. Within the lung, Cat-1 has been localised to human and rodent lung in RT-PCR and Western blot studies [199]. Cat-1 has also been found in human and rodent alveolar macrophage and is involved in the production of nitric oxide through system γ^+ stimulation [200]. The final transporter SNAT3 was found to be expressed at a moderate level in all studied lung samples with the exception of whole lung where the transporter was found to be absent. Traditionally SNAT3 functions as a sodium-coupled neutral amino acid transporter and is known to be expressed in brain astrocytes, adipose tissue, skeletal muscle tissue, and within the liver, kidney and heart [122, 201-203]. Within the lung, SNAT3 has been shown to display a low mRNA signal in human lung, supporting results observed in the rat lung cell samples studied here [190].

Overall, each of the amino acid transporters studied exhibited an observable level of expression within the rat lung. Given the critical importance of amino acids, expression within the lung of at least one of the studied transporters is not surprising. The generated mRNA expression profile indicates few of the transporters to have comparatively strong expression in the lung areas studied, nevertheless, a discernable pattern of mRNA expression within alveolar epithelium was noted allowing these transporters to represent either a viable target or obstacle for pulmonary drugs systemic delivery; note - many drugs delivered via inhalation are for local targets, i.e. treatment of asthma, COPD, and therefore would target submucosal tissues of the conducting airways and not the alveolar epithelium. Several amino acid transporters have already presented themselves as therapeutic targets. For example, cationic amino acid transporters, such as Cat-1, which was observed at moderate levels in the rat lung, are capable of transporting nitric oxide synthase (iNOS) inhibitors [188]. In situations such as chronic inflammation, where iNOS activity could be detrimental, transporters such as Cat-1 present themselves as a potential drug target [188]. The lysosomal amino acid transporter, Lyaat1, is responsible for the intestinal absorption of orally administered D-serine and D-cycloserine which are used for treatment of affective disorders, such as bipolar disorder and schizophrenia [204, 205]. Lyaat1 has a known tissue distribution in the lung and was expressed at low-to-moderate levels in the rat lung samples, therefore, delivery of Lyaat1 substrates of potential therapeutic interest to the lungs could be an attractive target and provide improved bioavailability and therapeutic action for novel drugs [206].

The lack of strong lung expression from any of the amino acid transporters studied creates uncertainty surrounding the impact of the examined transporters on drug discovery and delivery to the lung, however, this family of transporters provide obvious potential within the field of drug discovery and should be factored in to a drug design rationale when targeting the pulmonary system for delivery.

2.3.3. Expression analysis of Glucose transporters

Research into the glucose transporter family began in the mid 1980's, prompted by investigations into the facilitated diffusion of glucose across plasma membranes, which began more than a decade before [207, 208]. Glucose transporters belong to the SLC2 transporter family and account for 12 of the 13 family members. Each transporter consists of a 12 transmembrane domain structure which has the capacity to transport glucose and other hexoses across the plasma membrane in a direction imposed by the electrochemical gradient of the substrate [209]. The first glucose transporter to be discovered, GLUT1, was cloned from a human hepatoma cell line and is the most intensely studied

family member, it is thought to act as the primary glucose transporter in a large number of cells [210]. The second family member, GLUT2, was first described through cloning from a human liver cDNA library using a GLUT1 probe. GLUT2 functions as a high affinity glucosamine transporter but also has the capacity to transport glucose, galactose, mannose and fructose [209]. Other transporters considered in this study include the rat orthologs of GLUT4, which has been cloned from human, rat and mouse tissues, and is a transporter of both glucose and glucosamine, GLUT5, which was isolated from human, rat and rabbit intestinal tissue, and functions as a fructose transporter and finally GLT-1, which belongs to the Slc5 family and is a sodium-dependent glucose cotransporter [209, 211].

Table 2.13 displays typical expression signals for each glucose transporter in 5 rat lung cell samples.

Transporter	Gene	Whole Lung	SPOC-1	AEII – Freshly Isolated	AEII – Day 2 of Culture	AEI-‘like’ Day 8 of Culture
Glut1	Slc2a1	-	+	+	+	+
Glut2	Slc2a2	-	++	-	-	-
Glut4	Slc2a4	-	-/+	-	-	-
Glt-1	Slc5a1	-	-/+	-	-	-
Glut5	Slc2a5	-	-/+	-	-	-
β-actin	ACTB	++	+++	++	+++	+++

Table 2.13 Expression profile of 5 glucose transporter members; expression profile was determined from RT-PCR analysis in pulmonary cell samples. Semi-quantitative analysis of transporter expression was undertaken by examining signal intensity and assigning an appropriate expression index. Mean data are shown, n=3.

Each of the glucose transporter family members exhibited poor/insufficient expression in all lung cell samples. Illustrated in figure 2.6 are the gel electrophoresis images obtained which proved to be difficult to document and ‘quantify’ in relation to an expression index.

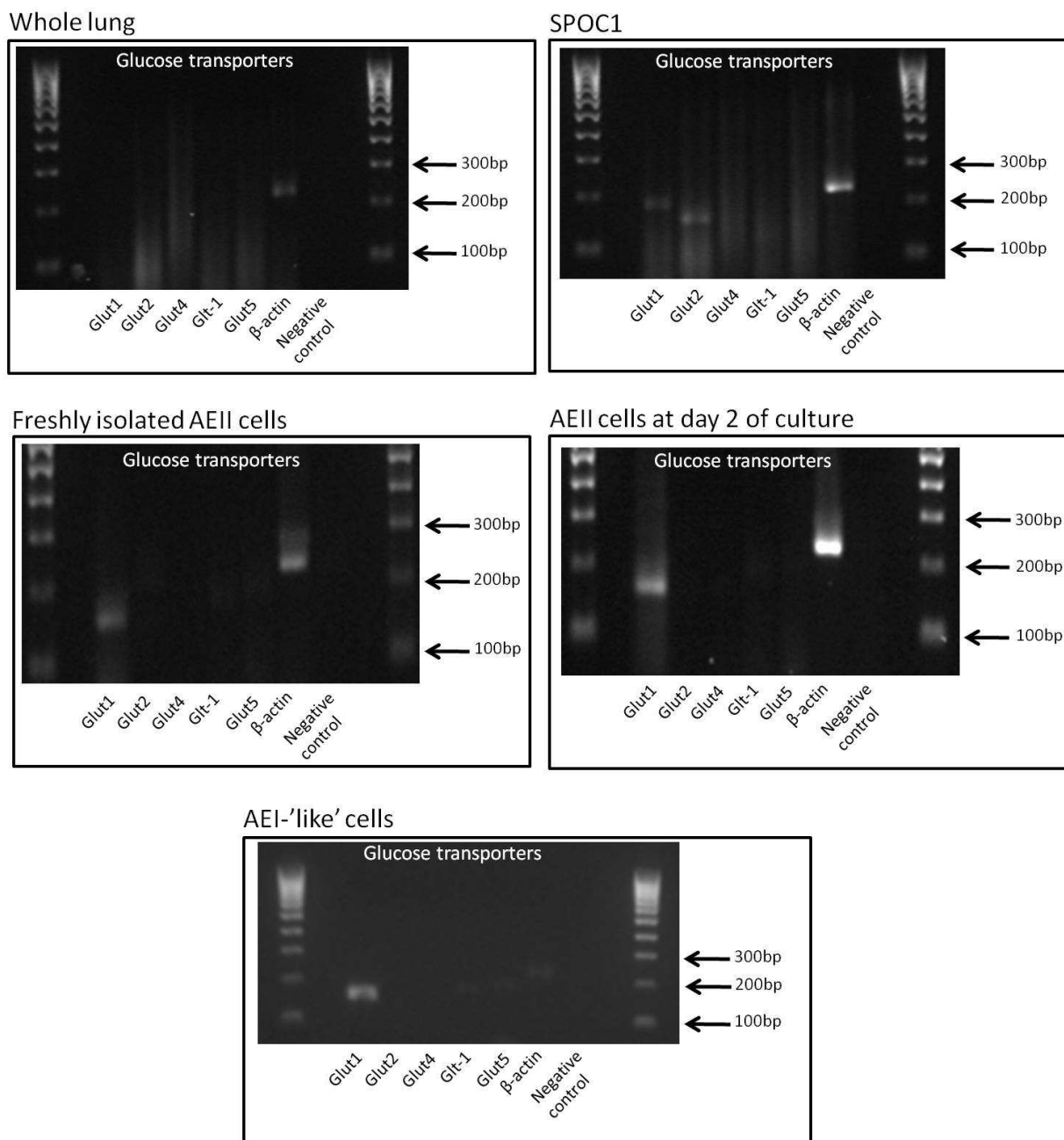


Figure 2.6 Representative gel electrophoresis images illustrating mRNA expression of selected Glucose transporters in 5 rat lung cell samples. Each set of RT-PCR reactions included a β -actin positive control and an RT-negative negative control to ensure RT-PCR reaction/result integrity.

Noteworthy is the presence of Glut1 in all samples at an expression index of low; except in whole lung samples where this transporter was absent. Glut1 is thought to have ubiquitous expression, transporting glucose to provide metabolic energy, and has been shown to be highly expressed in the blood-brain barrier [209, 212, 213]. Within the lung, glucose transporters function to maintain a low glucose concentration in airway surface liquid, contributing to pulmonary host defences [214]. Glut1 has been reported in human lung tissues by use of Western blotting, immunohistochemistry and RT-

PCR [215-217] and in freshly isolated rat AEII cells through RT-PCR [218]. The results obtained within this chapter are comparable to those reported in the literature; however, this study indicates an absence of Glut1 in rat whole lung samples. Given the positive results obtained for Glut1 in all other lung samples and the evidence of Glut1 lung expression in the literature, experimental error could explain the transporter's absence seen here. It is possible that such a result could be explained by the very high number of cell types within whole lung tissue not all of which will express a particular transporter. All other results indicate transporter absence, with negligible expression in few cases. The positive control β -actin showed good expression in all samples suggesting that the lack of transporter expression was not an artifact of poor PCR.

Unlike Glut1, the second glucose transporter, Glut2, has a more specific profile and is known to be expressed in the basolateral membrane of both intestine and kidney epithelial cells [219]. Glut2 expression has also been noted in human airway and pulmonary epithelial cells through RT-PCR and mRNA expression [214, 217]. This chapter's results illustrate the presence of Glut2 in the SPOC1 cell model while the transporter was found to be absent from all other lung cell samples. The SPOC1 cell line is derived from rat tracheal goblet cells and acts as a mucus secreting cell model [75]. Mucin, of which glucosamine is a known precursor [220], would be present in this cell line. Glut2 functions as a high affinity glucosamine transporter and could therefore be present in the tracheal airway region to function as a glucosamine transporter and facilitate mucin production. Due to this functional activity, it is likely that Glut2 mRNA be expressed at a detectable level in SPOC1 cell samples and yet be absent from all other lung samples. As a consequence of the suggested specific localisation of Glut2 within the lung, overall mRNA expression for this transporter within a whole lung sample would attribute to a very small percentage of the total mRNA present resulting in an insufficient concentration of specific template mRNA for PCR amplification.

Of the remaining glucose transporters studied here, Glut4 has been localised to both brown and white adipose tissue, skeletal and cardiac muscle and is the major transporter of glucose in these regions [209]. Glut5 is thought to be expressed mainly in the jejunal region of the small intestine, low mRNA levels have also been detected in kidney, skeletal muscle and blood-brain barrier [209, 221]. Finally, GLT-1 has been localised to the proximal tubule of nephrons, acting as a sodium-glucose symporter in this region [211]. There exists conflicting evidence regarding the expression of these transporters within the lung. Mamchaoui and co-workers have reported detection of Glut4, Glut5 and GLT-1 in freshly isolated rat AEII cells through RT-PCR, while these same transporters were not detected in other studies through Western blotting and immunohistochemistry in human, rat

and rabbit lung [215, 218]. Given the conflicting results within the literature it is difficult to interpret the results seen here, however; known presence of Glut1 and Glut2 in the lung and the documented specificity of Glut4, Glut5 and GLT-1 in other regions suggest the results obtained for these transporters to be true observations.

The presence of glucose transporters in the lung opens up possibilities for targeting these transporters and thus maintaining blood-glucose levels via the inhalation route, however, with regards to the impact of such transporters upon drug discovery it seems unlikely that there would be major therapeutic implications given the specific substrate nature of these transporters and the apparent absence of expression in the lung of a number of glucose transporters.

2.3.4. Expression analysis of Monocarboxylate transporters

Investigations into the existence of monocarboxylate transporters first began in the early 1990's soon after the discovery that the transport of lactate and pyruvate could be inhibited. To date there are 14 family members who each share a common 12 transmembrane domain structure and have a unique tissue distribution [222]. Monocarboxylate transporters play an essential role in cellular metabolism through rapid transport of substrates, such as lactate, in association with the transport of a proton [223]. Of the transporters studied here, MCT1 has been most extensively researched. MCT1 can transport a number of substrates such as pyruvate and ketone bodies, but most importantly, lactate. The transport of lactate by this transporter is essential and prevents both the decrease of cytosolic pH and the inhibition of glycolysis [224]. Of the remaining monocarboxylate transporters studied here MCT, which is also known as MCT8 in humans, is thought to be linked to the transport of the thyroid hormones thyroxine and triiodothyronine, while Mct7B or MCT7 in humans is a known orphan transporter, that is, a transporter that has no defined substrates or functions to date [224].

Table 2.14 summarises the expression of each of the three monocarboxylate transporter members in the lung cell samples examined.

Transporter	Gene	Whole Lung	SPOC-1	AEII – Freshly Isolated	AEII – Day 2 of Culture	AEI-‘like’ Day 8 of Culture
MCT	Slc16a2	+	++	+++	++	++
MCT1	Slc16a1	++	++	+++	+++	+++
Mct7B	Slc16a6	+	+	+++	++	++
β-actin	ACTB	+	+++	+++	++	+++

Table 2.14 Expression profile of 5 Monocarboxylate transporter family members, profile determined from RT-PCR analysis in 5 pulmonary cell samples. Transporter expression was determined by signal intensity and assigning of an expression index. Mean data are shown, n=3.

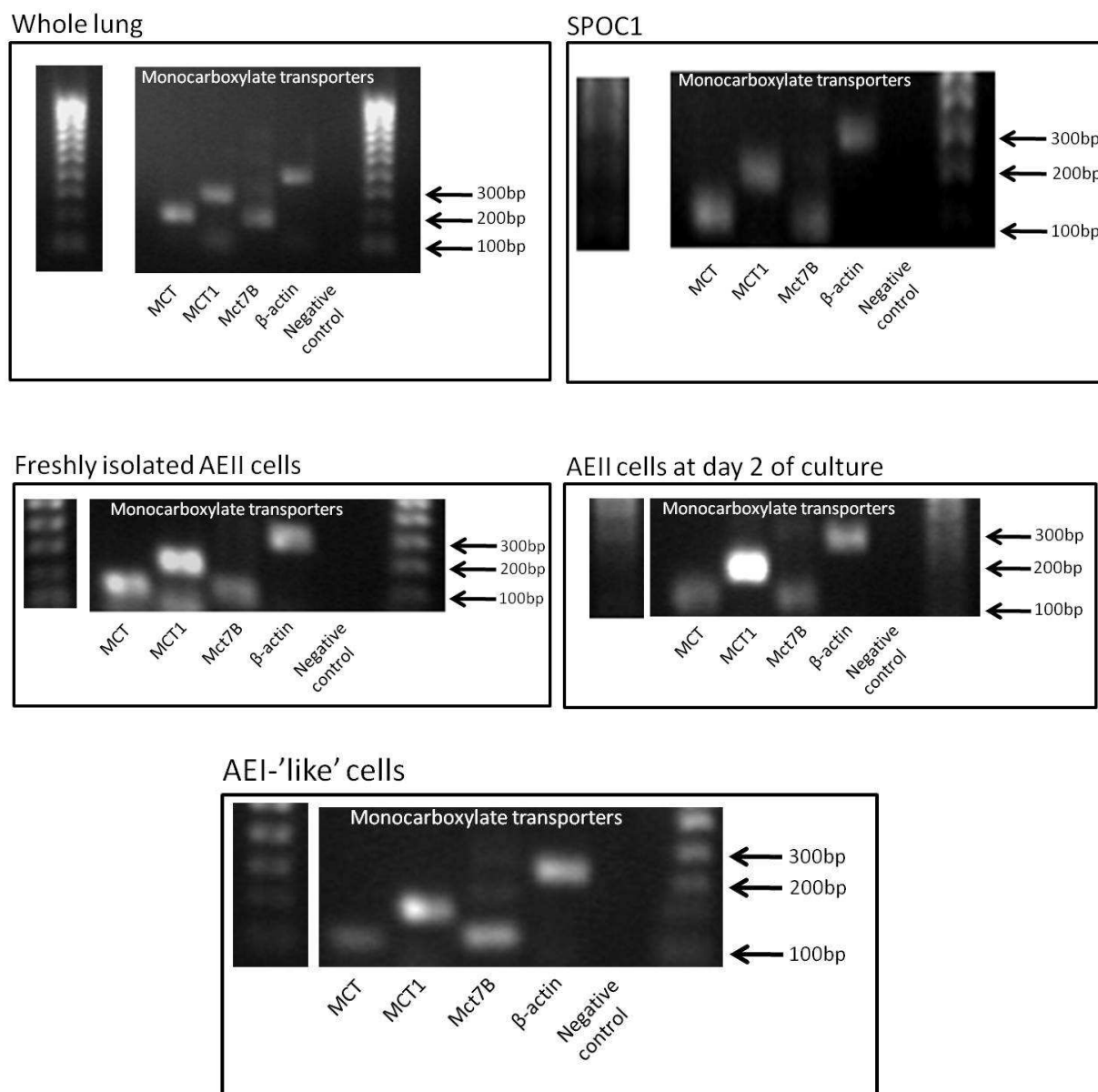


Figure 2.7 Representative gel electrophoresis images illustrating selected MCT transporter mRNA expression in 5 rat lung cell samples. Each set of RT-PCR reactions included a β -actin positive control and an RT-negative negative control to ensure result integrity.

As can be seen in figure 2.7, MCT exhibited relatively high expression levels in freshly isolated AEII cells. A decrease to a moderate level of expression intensity was observed with continued culture time. MCT also exhibited a moderate level of expression in SPOC1 cell culture, while only low levels were observed in whole rat lung samples. MCT1 displayed a relatively similar expression pattern to MCT (Figure 2.10); however, MCT1 was expressed at a high level in all primary AEII samples. The

final transporter to be studied in this group was the transporter Mct7B. This transporter exhibited an almost identical expression to the MCT transporter (Figure 2.10), with the exception of its relatively low expression index level in SPOC1 cell culture compared to a moderate level observed for MCT. Within the restrictions of this semi-quantitative approach, the primary cell culture samples displayed the highest expression levels for all 3 monocarboxylate transporters. Conversely, crude whole lung samples and the immortalised cell culture model SPOC1 produced only moderate or low expression levels for all transporters studied.

All three studied monocarboxylate transporters were expressed to some degree in each of the regions of rat lung examined. These results are perhaps none too surprising given the knowledge of MCT1 involvement in cellular metabolism. Through Northern and Western blotting, MCT1 has been found to be expressed in many human tissues, with expression levels varying in accordance with mitochondrial content [222]. The transporter has also been localised to the apical surfaces of many tissue in other species including both chicken and rat [198, 222, 225]. Within the lung, this chapter's findings are very comparable to those in the literature. MCT1 has been reported in hamster lung through Northern blotting, immunoblotting and immunofluorescence microscopy [181, 226, 227] and in mouse lung through RT-PCR and Western blotting [228].

Both MCT and Mct7B have been much less extensively researched and there exists little published data on these monocarboxylate isoforms. Within human tissues, MCT8 (rat MCT) is widely expressed, with high levels detected in liver and heart, while MCT7 (rat Mct7B) has been found in human brain, pancreas and muscle tissue and has given a very faint Northern blot result in human lung [229]. While it is very difficult to assume the presence of these MCT transporters in rat lung, the suggested ubiquitous expression of MCT8 in humans and the single report of MCT7 expression in the lung suggest the results obtained here through RT-PCR to be representative. Further, several other MCT family members have been localised to human lung lending further reasonable support to the current findings [230, 231]. Very little is known about these latter transporters and their family relation to MCT1 *could* hint at important cellular functions hence a somewhat ubiquitous expression.

Several monocarboxylate transporters are known to play a role in the transport of relevant drugs such as atorvastatin, salicylate and valproic acid [232]. The potential for such transporters to interfere with drug discovery through drug substrate interactions does exist. While there is real potential to inhibit the action of monocarboxylate transporters, currently, such inhibitors exert major effects on non-intended cellular targets and create devastating effects for cellular and whole

organ well being [223]. At present, it appears that the most effective strategy for evading negative interactions with monocarboxylate transporters and thus avoiding drug discovery issues would be to induce conformational changes in potential transporter substrates and thus prevent an interaction with these monocarboxylate transporters.

2.3.5. Expression analysis of Nucleoside transporters

Nucleosides, the primary substrate of nucleoside transporters, have a role in a number of biological functions including; catalysis, transfer of energy, coenzyme function, blood pressure control, regulatory function and mediation of hormone signals [233]. Both purine and pyrimidine nucleosides are involved in many cellular processes and some synthetic analogues are known to have activity against bacteria, fungi, viruses, yeast and neoplastic tissues [233]. The majority of mammalian cells display some level of nucleoside transport and therefore possess one or more known nucleoside transporter proteins, all of which possess ability to transport adenosine but differ in their ability to transport other nucleosides and nucleobases (nitrogenous base alone) [234].

Table 2.15 illustrates the nucleoside transporters studied here and summarises their semi-quantitative expression as determined by RT-PCR.

Transporter	Gene	Whole Lung	SPOC-1	AEII – Freshly Isolated	AEII – Day 2 of Culture	AEI-‘like’ Day 8 of Culture
rENT1	Slc29a1	+	+	-/+	+	+
Cnt1	Slc28a1	-	-	-/+	-/+	-/+
Ent2	Slc29a2	-	-	-/+	+	-/+
Ent3	Slc29a3	+	-/+	+	++	++
β-actin	ACTB	+++	+++	+++	+++	+++

Table 2.15 Expression profile of 4 Nucleoside transporter family members; transporter expression profile was determined from RT-PCR analysis in 5 pulmonary cell samples. Expression was semi-quantitated assigning an expression index to signal intensity. Mean data are shown, n=3.

Nucleoside transporters belong to two SLC families; SLC28 and SLC29. The SLC28 family has 3 members, each of which acts as a sodium-dependent concentrative transporter. These proteins are membrane bound and actively transport natural and synthetic nucleosides into cells along a sodium gradient. Cnt1, the only concentrative nucleoside transporter studied here, is the first member of the SLC28 family and acts primarily as a pyrimidine transporter, having a higher affinity for these nucleosides. Cnt1 also has a number of pharmaceutically relevant substrates including AZT, zalcitabine, cytarabine and gemcitabine thus playing an important role in the treatment of leukaemia,

HIV and several tumours [235]. Cnt1 has been shown to be expressed in rat intestine and kidney through Northern blot analysis with RT-PCR also displaying Cnt1 expression in the brain [236, 237]. Within the rat lung Cnt1 was absent or negligibly expressed in the majority of samples (Table 2.15/Figure 2.8).

The SLC29 family contains 4 members, all functioning in the facilitated diffusion of nucleosides, 3 members are considered here. ENT1 (rENT1 in rats) was the first identified equilibrative nucleoside transporter and is known to be crucial in nucleotide synthesis. This transporter has a broad substrate range, capable of transporting a number of purine and pyrimidine nucleosides [234]. Within the rat lung cell samples studied, rENT1 displayed negligible or low expression with the exception of AEII cells in culture, with expression level increasing with time (Figure 2.8). The remaining proteins studied here, rat orthologs of transporters ENT2 and ENT3, display many similarities to ENT1. Each transporter has comparable substrate specificity to ENT1 mediating, to a lower affinity, a wide variety of both natural and synthetic nucleosides and nucleobases [234]. Mean expression of these transporters, as determined by assignation of an expression index, can be seen in table 2.15. From this and figure 2.8, it can be seen that Ent2 was absent or negligibly expressed in the majority samples, however, did display a low level of expression in primary AEII cells at day 2 of culture. Ent3 exhibited an increase in expression level with time in culture in the primary AEII samples but displayed only negligible or low expression in all other samples examined.

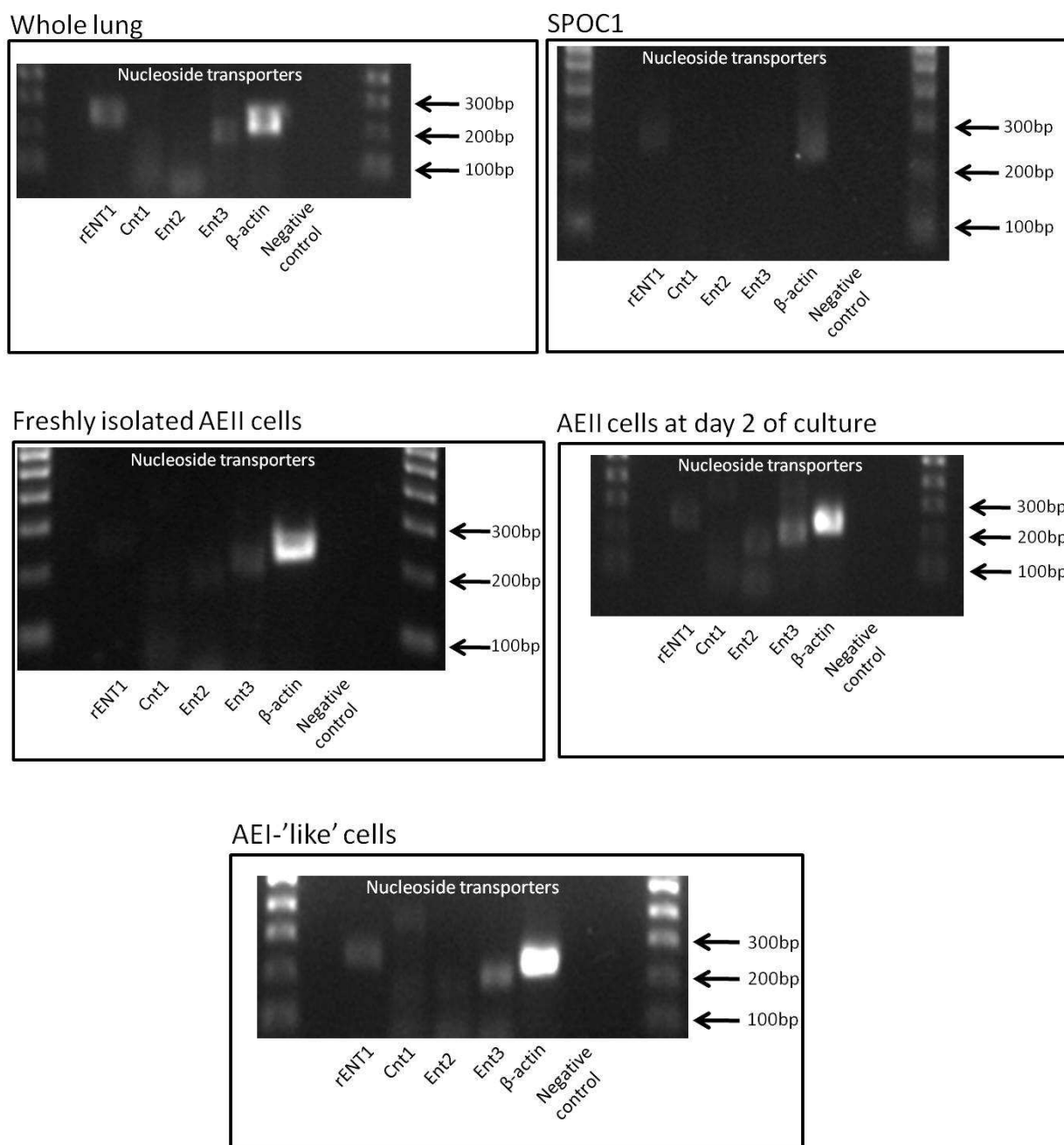


Figure 2.8 Representative gel electrophoresis images illustrating selected Nucleoside transporter mRNA expression in 5 rat lung cell samples. Each set of RT-PCR reactions included a β -actin positive control and an RT-negative negative control to ensure result integrity.

Nucleosides themselves are responsible for a number of actions within the pulmonary system including; stimulation of mucus and surfactant secretion and ciliary beating action, contraction and relaxation of airway smooth muscles and the modulation of inflammatory cells involved in lung disease [238]. Human equivalents of transporters studied here have been localised to a number of organ or tissue systems. For example, mRNA and protein levels of ENT2 have been found in human heart, brain, placenta, kidney, pancreas, thymus and skeletal muscle [239-241]. Similarly, ENT3 has

been localised to human placenta while ENT1 has been found to be ubiquitously expressed in both human and rat with expression levels varying between tissues [240-244].

Few reports have discussed nucleoside transporter expression within the lung, however, given the recognised functions of nucleosides within the lung and the lungs role in removing adenosine from the circulation, the presence of more than one such transporter within this organ system is predicted [245]. In the early 1980's Shi and co-workers illustrated the presence of 'nucleoside transporters' in both rat and guinea-pig lung through high-affinity binding of a transport inhibitor. ENT1 expression has been noted in human lung through Northern blot analysis and has been immunohistochemically stained in a number of non-small cell lung cancer (NSCLC) biopsies that responded to gemcitabine chemotherapy [246-248]. The results of this chapter illustrate selected nucleoside transporter expression to exist at low levels within the rat lung.

Development of an expression profile of nucleoside transporters has the potential to improve the efficacy of a number of nucleoside analog drug therapies. There are a number of therapeutic nucleoside analogs in existence for the treatment of conditions such as HIV, AIDS and AIDS related infections, a number of cancers and diseases caused by various infectious agents [249]. The presence of nucleoside transporters within the lung gives rise to the potential for inhaled therapeutic treatments. As a comparable example, pentamidine, a known nucleotide transporter substrate (nucleotide is nucleoside + 1-3 phosphate groups) has been trialed as an inhaled therapy in the treatment of *P. carinii* pneumonia in patients with AIDS. The nucleoside adenosine is known to indirectly provoke bronchoconstriction in asthma patients. Inhibition of nucleoside transporters would minimise adenosine transport and reduce bronchoconstriction in these patients. Finally, stimulation of calcium channels by inhaled ATP and uridine triphosphate (UTP) could help in hydrating the hypophase of CF patients [250].

The presence of nucleoside transporters within the lung opens up many therapeutic possibilities however; to fully exploit this, transporter activity within the lung should be further examined. Only low levels of nucleoside transporter expression were observed in this study, suggesting perhaps nominal impact of these nucleoside transporters on drug discovery of inhaled nucleoside drugs therapies.

2.3.6. Expression analysis of Peptide transporters

The proton-coupled oligopeptide transporter family contains 4 peptide transporter genes designated SLC15A1 to SLC15A4. Of the corresponding proteins, members PEPT1 (Pept1 in rat) and PEPT2

(Pept2 in rat) have been thoroughly investigated while the remaining members are relatively unknown. Both PEPT1 and PEPT2 act as integral membrane proteins capable of transporting a large number of short chain peptides along a proton gradient [251]. PEPT1, characterised as the intestinal isoform, is a low affinity, high capacity transporter, absorbing peptide fragments created by food digestion. PEPT2 acts as a renal isoform, and has a higher affinity yet lower capacity for its substrates. This isoform (PEPT2) has major importance in the reabsorption and renal handling of peptide substrates and peptide-mimetic drugs [252]. Due to their promiscuous nature, both isoforms have the potential to transport every di- and tri- peptide, resulting in a potentially large number of therapeutic compounds acting as substrates for these transporters. Such drug substrates include; β -lactam antibiotics (e.g. cyclacillin), cephalosporins (e.g. cefibuten), angiotensin-converting enzyme inhibitors (e.g. captopril), peptidase inhibitors (e.g. bestatin), receptor antagonists (e.g. sulpiride), novel prodrugs (e.g. enalapril) and other peptide-mimetic drugs (e.g. valacyclovir), suggesting peptide transporters to be very important in drug discovery [251, 253].

In this study the pulmonary expression of the two major rat peptide transporter orthologs was examined in 5 lung cell samples. Table 2.16 summarises the expression of these transporters in whole lung, SPOC1 cells, AEII – freshly isolated cells, AEII – cells at day 2 of culture, and the AEI-‘like’ cells.

Transporter	Gene	Whole Lung	SPOC-1	AEII – Freshly Isolated	AEII – Day 2 of Culture	AEI-‘like’ Day 8 of Culture
Pept1	Slc15a1	-	-	-	-	-
Pept2	Slc15a2	++	++	++	++	++
β -actin	ACTB	+++	+++	+++	+++	++

Table 2.16 Expression profile of 2 Peptide transporter family members; transporter expression profile was determined from RT-PCR analysis in 5 pulmonary cell samples. Expression was semi-quantitated assigning an expression index to signal intensity. Mean data are shown, n=3.

The transporter Pept1 was found to be absent in all studied samples (Figure 2.9). The positive control, β -actin, was present at a high level in all samples except the AEI-‘like’ sample where the positive control gene was moderately expressed. The second transporter studied, Pept2, was expressed at a moderate level in all samples, again figure 2.9 demonstrates this observed expression profile.

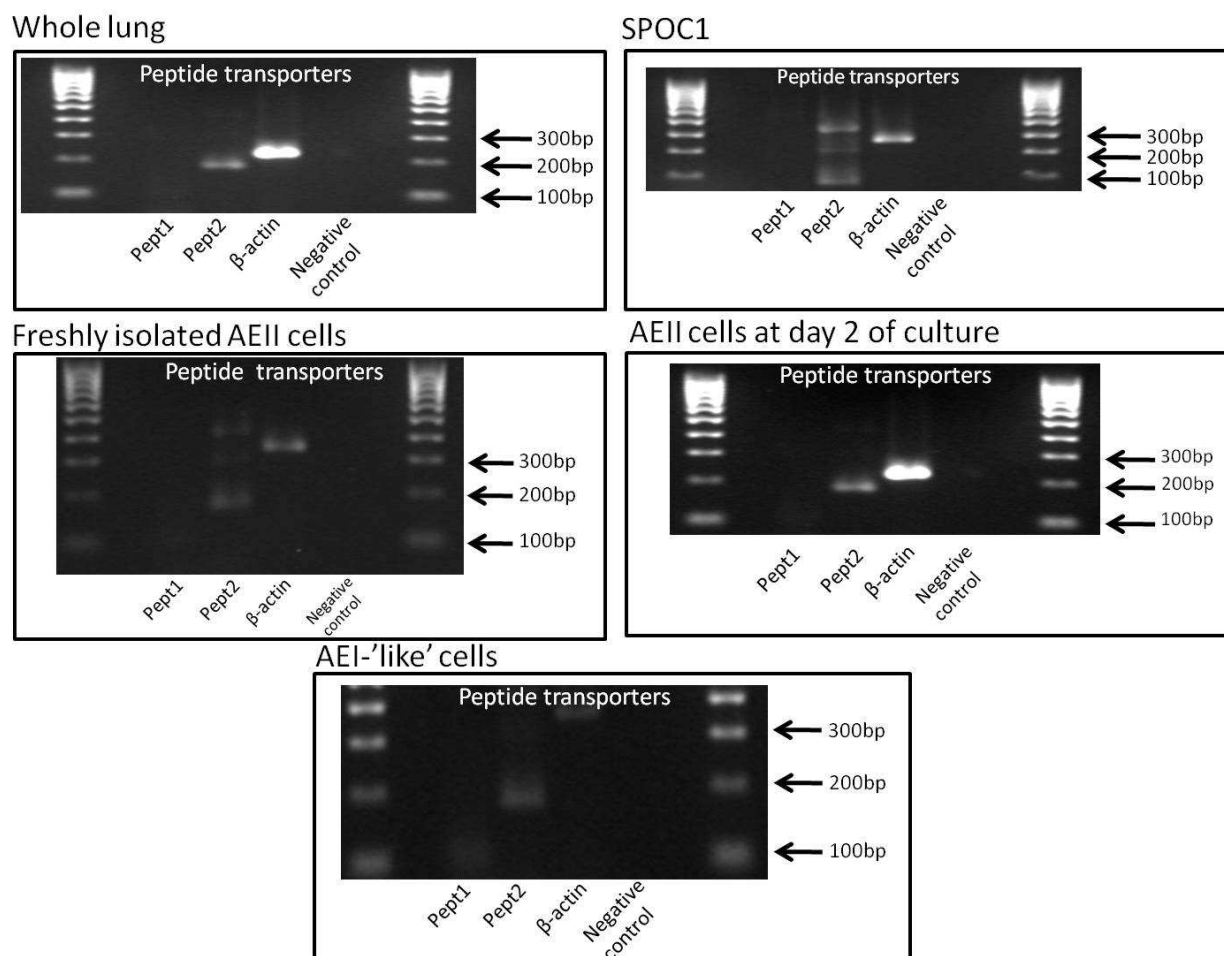


Figure 2.9 Representative gel electrophoresis images illustrating selected Peptide transporter mRNA expression in 5 rat lung cell samples. Each set of RT-PCR reactions included a β -actin positive control and an RT-negative negative control to ensure result integrity.

The expression profile of both PEPT1 and PEPT2 is well documented, with the observations of this study mirroring those reported in the literature, supporting the documented expression profile of peptide transporters within the lung and adding knowledge to help combat the potential problems facing drug discovery in this area. PEPT1 is known to possess a narrow expression profile, mainly localising to the apical plasma membrane of enterocytes in the small intestine [254]. The transporter has also been localised in the liver, kidney and pancreas of humans and a number of small mammals [121, 255, 256]. The localisation of PEPT1 in the small intestine renders this transporter the primary mechanism for transport of peptides and peptide-mimetic drugs that are delivered orally. While this has the potential to be advantageous to drug discovery, providing a target with the capacity to alter an 'oral' drug's systemic exposure, the transporter also has the capability to negatively influence a drug's absorption profile and create toxicity issues [253].

Both PEPT1 and PEPT2 transporters have significant pharmacological relevance; they are able to transport a wide variety of compounds and therapeutic agents to treat a number of conditions such as AIDS (saquinavir), hypertension (captopril) and cancer (bestatin) [257]. The rational design of compounds that possess improved oral bioavailability through utilising, for example, PEPT1 as an absorption mechanism could well improve many therapeutic treatments. PEPT1 represents an excellent target for enhancing absorption, not only due to its location but also by its potential substrates. Rational design of nucleoside analog antivirals to target CNT/ENT drug transporters and thus increase cellular uptake have already yielded successful antiviral drugs via this rationale [249]. With advances in combinatorial peptide libraries, peptide synthesis strategies and peptidomimetic drug design, there is excellent potential for this route to contribute to ever-improving therapeutic treatments [257].

In contrast to PEPT1, PEPT2 holds a more diverse expression profile, being found in kidney tubular cells, brain astrocytes, mammary glands, both bronchial and type II alveolar epithelial cells and the epithelial cells of the choroid plexus [39, 222, 258]. Within the lung, there is considerable evidence supporting the expression of PEPT2. Groneberg and co-workers have illustrated PEPT2 expression in AEII cells, bronchial epithelial cells and the endothelial cells of small vessels through RT-PCR, Northern blotting and immunohistochemistry [259]. RT-PCR has also been used to show PEPT2, but not PEPT1 expression in human lung tissues, while Bhahadduri *et al.*, have used the technique along with Western blotting to illustrate presence of functional PEPT2 in primary human lung cultures [260-262].

PEPT2 also has the potential to influence a therapeutic agent's absorption and distribution. For example, presence of this transporter in the choroid plexus results in transport of substrates (e.g. leptin, growth hormone) from plasma to cerebral spinal fluid [263] affecting regional pharmacokinetics [252].

Due to its low proteolytic activity and ability to bypass hepatic metabolism, the lung represents a very attractive route of delivery for therapeutic peptides and peptide-mimetic drugs. For example, the presence of PEPT2 in the lung signifies this transporter as a novel target for delivery of antibiotics to the lumen, such as cefadroxil, to treat Gram positive and Gram negative pulmonary infections [259]. Further, the work of Groneberg *et al.*, illustrated a similar pattern of PEPT2 expression in both normal and cystic fibrosis lung [39]. Up to 90 % of lung infections in CF are caused by the bacteria *Ps. aeruginosa*. This bacterium is very difficult to treat traditionally due to high intrinsic antibiotic resistance. Antimicrobial peptides (AMP) represent an extremely attractive

therapy to treat this and other infections as they are fast acting, bactericidal and active against multi-drug resistant bacteria. Theoretically, delivery of AMPs to the lung would allow treatment of pulmonary infections without the use of resistance causing antibiotics and allow avoidance of hepatic metabolism, thus creating a highly bioavailable therapy delivered directly to the target site [264].

Pulmonary localisation of PEPT2 combined with available literature evidence suggests the peptide transporter to be an excellent therapeutic target within the lung. Developments of rationally designed substrates to target this transporter have the potential to yield excellent drug therapies for both local and systemic action. However, due to this transporter's highly promiscuous substrate profile and widespread expression, altered drug exposure and toxicity issues should also be examined.

2.6.7. Expression analysis of Organic cation transporters

Organic cation transporters (OCT) are members of the SLC22 family, belonging to a major facilitator superfamily which is comprised of uniporters, symporters and antiporters. Members of this family act as polyspecific transporters capable of transporting charged monoamines, small organic cations and weak bases. Many organic cation transporters contain overlapping binding sites allowing access to a number of substrates from both sides of the plasma membrane. OCT1-3 mainly act as transporters of organic cations and weak bases, transporting these substrates in a reversible manner independent of Na^+ , while OCTN1-3 have a more ambiguous substrate specificity and function as zwitterions/cation co-transporters [265-267].

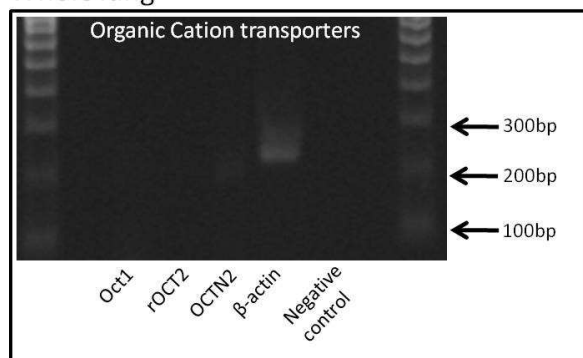
The first identified transporter of the SLC22 family was cloned from rat in 1994 [268]. Since then OCT1 has also been isolated from mouse, rabbit and human [268-271] and acts as a transporter of organic cations and weak bases. Transporter substrates include many drugs, such as acyclovir and metformin and also endogenous substrates, such as serotonin and prostaglandins [267]. The second member of this subgroup, OCT2, was identified in 1998 [272] and has been successfully cloned from rat, human, mouse, rabbit and pig [269, 270, 272]. OCT2 has very similar substrate selectivity to OCT1 and shares 70% sequence similarity with this protein. The final transporter to be studied in this current work acts as a Na^+ -carnitine co-transporter and was cloned in 1998 [273]. OCTN2 has a high affinity for carnitine and is responsible for its absorption from the kidney proximal tubule. OCTN2 can also transport a number of substrates independently from Na^+ including verapamil, choline and quinidine [274, 275].

Transporter	Gene	Whole Lung	SPOC-1	AEII – Freshly Isolated	AEII – Day 2 of Culture	AEI-‘like’ Day 8 of Culture
Oct1	Slc22a1	-/+	-	+	+	-/+
rOCT2	Slc22a2	-	-	-	-	-
OCTN2	Slc22a5	+	++	+	++	++
β-actin	ACTB	++	+++	+++	+++	+++

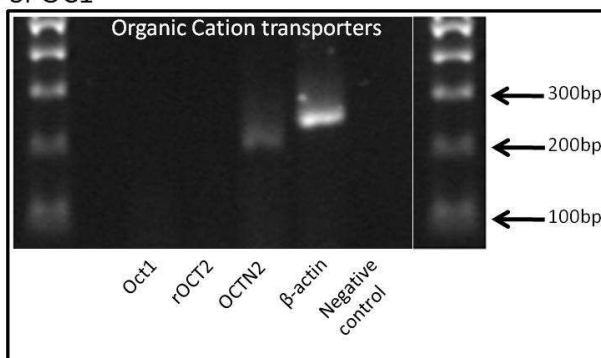
Table 2.17 Expression profile of 3 organic cation transporter family members where expression profile was determined from RT-PCR analysis in 5 pulmonary cell samples. Expression was ‘quantified’ by signal intensity and assigning of an expression index. Mean data are shown, n=3.

Table 2.17 summarises the expression of the 3 organic cation transporters; Oct1 (OCT1 in human), rOCT2 (OCT2 in human) and OCTN2; transporter expression was examined in 5 different lung cell samples. OCTN2 displayed a relatively low level of expression in freshly isolated AEII cells, which increased to a moderate level over time. This moderate level of expression was noted in both AEII cell samples at day 2 of culture and AEI-‘like’ cells at day 8 of culture (Figure 2.10), rOCT2 was absent or expressed at a negligible level in all lung samples studied while OCT1 was clearly expressed, although at only a low level in all samples.

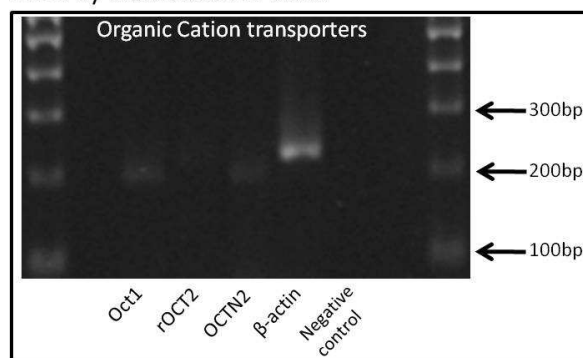
Whole lung



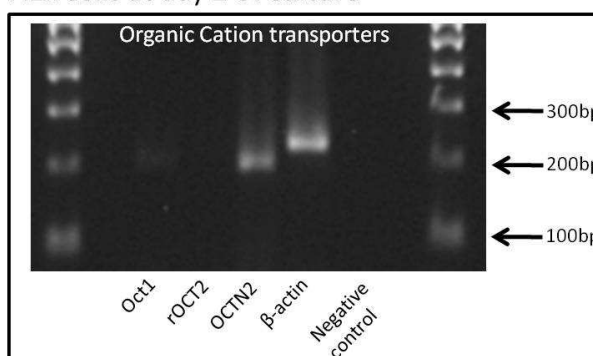
SPOC1



Freshly isolated AEII cells



AEII cells at day 2 of culture



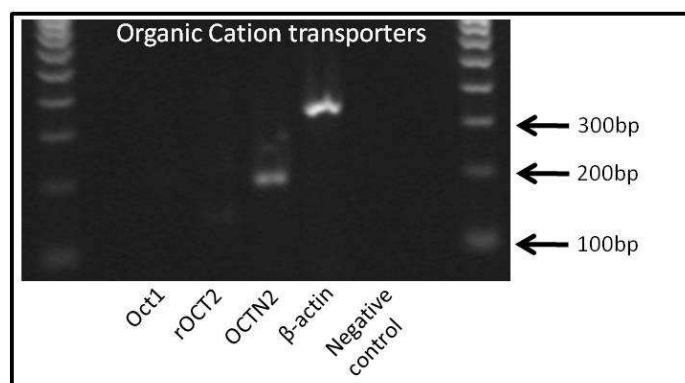


Figure 2.10 Example gel electrophoresis images illustrating chosen OCT transporter mRNA expression in 5 rat lung cell samples. Each set of RT-PCR reactions included a β -actin positive control and an RT-negative negative control to ensure result integrity.

As can be seen from figure 2.10, both Oct1 and OCTN2 were visualised in the lung samples studied while rOCT2 was consistently absent. Traditionally, OCT1 expression has been observed in liver, kidney, small intestine, colon and spleen [270]. More specifically, the transporter has been localised to the submucosal and myenteric plexuses of mouse intestine through RT-PCR and immunohistochemistry [276], to the basolateral membrane of rat kidney proximal tubules by use of *in situ* hybridisation [277] and immunohistochemistry and by RT-PCR to both human and rat primary hepatocytes [278]. There exists conflicting results with regards to OCT1 expression within the lung. Both Pavlova and co-workers and Zhang and co-workers have conducted Northern blot analysis of human lung tissue and have noted the absence of OCT1 [271, 279]. However, several studies have also illustrated this transporter to be present within the lung. The OCT1 transporter has exhibited a low level of lung expression through RT-PCR, Northern blotting and immunohistochemistry [119, 280] and has been successfully localised to the apical membrane of ciliated epithelium in mice [280, 281], [282] and to the airway epithelium and alveolar macrophage of mouse and rat [282, 283]. This current work showed consistent Oct1 expression, albeit at a low level, in AEII – freshly isolated and day 2 AEII cells. Documented localisation of this transporter to ciliated cells and alveolar macrophage coupled with reported absence in other studies suggests OCT1 to have a restricted localisation within the lung. Concurrent with this suggested narrow expression profile, results here documenting absence in ‘whole lung’ samples could be the result of a low template concentration for PCR amplification. Variation (i.e. no consistency in harvesting of the trachea with lung tissue) in lung harvest procedures resulted in the absence of the trachea in some ‘whole lung’ samples and therefore could have given rise to a lower number of ciliated cells within ‘whole lung’ samples, thus providing less Oct1 RNA for extraction and amplification. If OCT1 truly does display this specific expression profile, then Oct1 absence in ‘SPOC1’ samples is not surprising. The SPOC1 cell model is

derived from a denuded rat trachea and does not display ciliated cell differentiation [126]. Presence of Oct1 in samples of alveolar epithelia could be as a result of contaminating alveolar macrophage, however, as the results obtained here are averaged from three separate isolations and cultures, it seems more likely that Oct1 is also expressed at a low level in these cells.

OCT2 has a similarly broad expression profile to OCT1 and is known to be expressed in kidney, placenta, thymus, choroid plexus and neurons of the central nervous system [267]. Immunohistochemistry, RT-PCR, Northern blotting and *in situ* hybridization have been used to localise this transporter to the neurons of the cerebral cortex [283], the apical membrane of kidney distal tubules [269, 272] and a number of subcortical nuclei [284]. There are conflicting reports as to OCT2 presence within the lung and the results of this chapter support the absence of rOCT2. Okuda and co-workers report absence of rOCT2 in rat lung through Northern blotting and RT-PCR [272], while Kummer *et al.* also report absence through immunohistochemistry in mouse lung samples [282]. Several techniques including Northern blotting, Western blotting, RT-PCR and immunohistochemistry have, however, detected OCT2 presence within the lung and localisation to ciliated cells of the bronchi and trachea has been reported [119, 279, 281]. In a similar manner to Oct1, expression of rOCT2 within a limited cell phenotype could explain absence in the 5 lung cell samples examined here.

The transporter OCTN2, has previously been found in skeletal muscle, heart, kidney and brain and has been localised to the brush-border of renal proximal tubules in rat [273, 285-288]. Within the lung, Horvath and co-workers have localised OCTN2 to the apical membrane of human epithelial cells through immunofluorescence and quantitative RT-PCR [289]. Other studies using RT-PCR have also illustrated the presence of this transporter in human and rat lung [280, 283]. The results of this chapter also show OCTN2 to be at least moderately expressed in the lung and it is thought that this transporter is involved in the absorption of several bronchodilators, such as ipratropium and tiotropium, delivered through inhalation [289].

In view of conflicting literature, it is difficult to definitively conclude the presence of these OCT transporters within the lung. Documented expression of OCT1 and OCT2 to ciliated cells of the airway coupled with the low or negligible expression observed in this study suggests these transporters to have a restricted expression profile within ciliated cells of the lung. Literature reports of OCTN2 expression within the lung is supported through the results of this chapter and within the scope of this study; it is OCTN2 that presents itself as a transporter that could act as a therapeutic target and influence drug discovery and delivery to the lung.

The role of organic cation transporters in other organs and tissues is well recognised. These transporters play a crucial part in regulating plasma concentration of organic cations and in excretion of organic cations classed as xenobiotic [290]. Both OCT1 and OCT2 are known to affect the pharmacokinetics of drug substrates. For example, variable inter-patient metformin response is thought to be linked to OCT1 and OCT2 polymorphisms while renal handling and toxicity of cisplatin is critically influenced by OCT2 [291, 292]. Confirmed OCTN2 expression in the lung presents this transporter as a rational target for OCT substrates delivered to the lung, there is already reported evidence of OCTN2 involvement in the pH dependent uptake of inhaled cationic bronchodilators [289]. Conflicting reports of OCT expression within the lung and lack of supporting evidence presently rule out OCT1 and OCT2 as targets for rational inhaled drug design. It seems unlikely that these transporters will have significant impact on the absorption of drug candidates delivered to the lung. Definitive expression profiling of OCT transporters within the lung is needed before such transporters should be taken into consideration as a rationale for the targeted design of novel drug therapies.

2.3.8. Expression analysis of organic anion transporting polypeptides

Organic anion transporting polypeptides comprise a sodium-independent transport family that facilitates the transmembrane transport of a large number of endogenous and exogenous substances. Many of these organic anions are toxic to the body and elimination is fundamentally important [293]. Such a vital physiological role has resulted in the rapid and independent identification of many organic anion transporter members leading to confusing gene and protein nomenclature where many transporters failed to conform to a continuous numbering system based upon consecutive protein identification [294]. Further, the traditional SLC classification did not allow species-independent identification of genes and gene products, creating additional confusion where a human ortholog to a mouse or rat OAT did not exist. As a result of this, the SLC21 family was reclassified, with the new SLCO family representing a phylogenetically based, species-independent and open-ended classification system [46].

Generally, organic anion transporting polypeptides function as active transporters through an electroneutral and pH dependent anion exchange transport mechanism. This means that the family can mediate bidirectional substrate transport, rendering substrate directionality dependent upon the local concentration gradient [295]. The need to remove harmful organic anions has resulted in organic anion transporters displaying broad substrate specificity, with most OATPs capable of

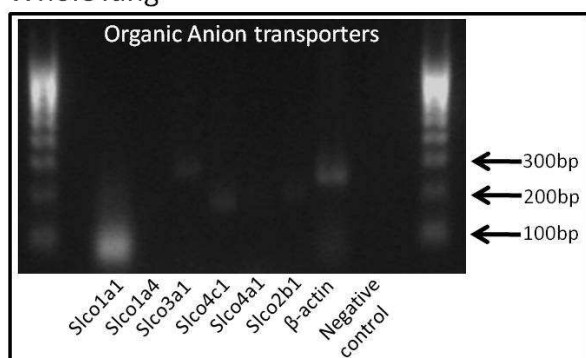
transporting endogenous compounds such as bile salts, organic dyes, steroid conjugates, thyroid hormones and anionic oligopeptides, as well as a number of xenobiotics and drugs [46, 293, 294].

A summary of the mRNA expression and generated expression profile of six OAT members in rat lung cell samples can be seen in table 2.18 and figure 2.11.

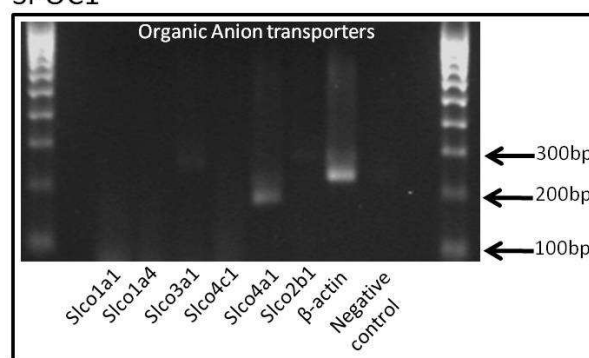
Transporter	Gene	Whole Lung	SPOC-1	AEII – Freshly Isolated	AEII – Day 2 of Culture	AEI-‘like’ Day 8 of Culture
Slco1a1/Oatp1	Slco1a1	-	-	-	-	-
Slco1a4/Oatp2	Slco1a4	-	-	-	-	-
Slco3a1/Oatp-D	Slco3a1	+	+	+	+	+
Slco4c1/Oatp-H	Slco4c1	+	-	+	+	+
Slco4a1/Oatp-E	Slco4a1	-	++	+	+	+
Slco2b1/Oatp-B	Slco2b1	-/+	+	+	-/+	+
β -actin	ACTB	++	+++	+++	++	+++

Table 2.18 Expression profile of 6 organic anion transporting polypeptides as determined by RT-PCR analysis in 5 pulmonary cell samples. Transporter expression was ‘quantified’ by signal intensity and assigning of an expression index. Mean data are shown, n=3.

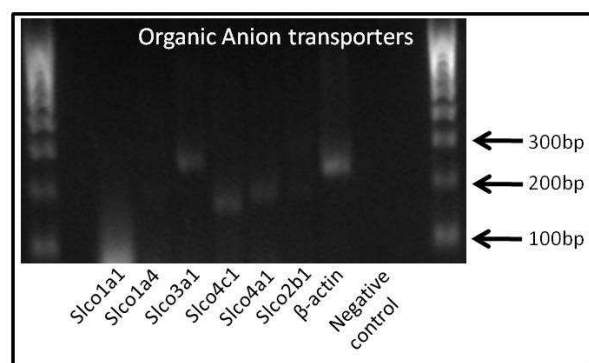
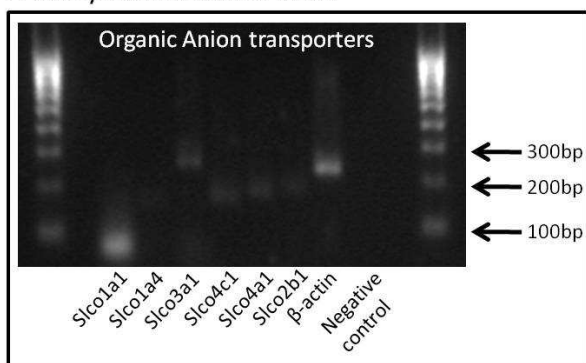
Whole lung



SPOC1



Freshly isolated AEII cells



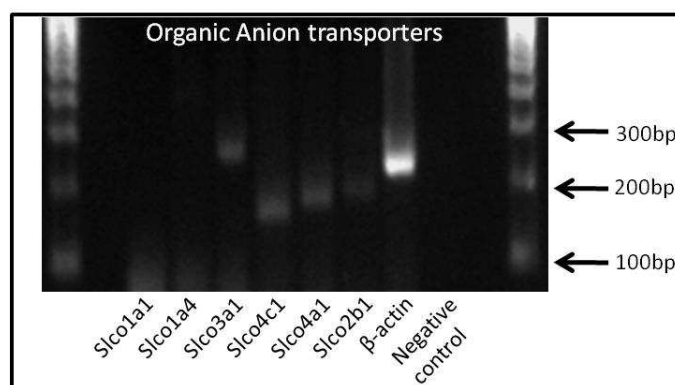


Figure 2.11 Example gel electrophoresis images illustrating selected OATP transporter mRNA expression in rat lung cell samples. Each set of RT-PCR reactions included a β -actin positive control and an RT-negative negative control to ensure result integrity.

Of the six OATP transporters studied, both Slco1a1 and Slco1a4 were absent from all lung cell samples. The transporters, Slco3a1 and Slco4c1, displayed a similar pattern of low expression in all samples, except for the SPOC1 cell sample, where Slco4c1 was absent. Again, the Slco4a1 transporter exhibited a relatively low mRNA level in the majority of samples, however, was found to be moderately expressed in SPOC1 cells but absent in whole lung samples. Finally, Slco2b1 also displayed a low level of expression in many of the studied lung cell samples with the exception of whole lung and AEII cells at day 2 of culture where only negligible expression levels were observed.

Many of the OAT transporters studied here displayed only low levels of expression in the selected lung cell samples. The majority of OATs have a wide expression profile, with documented expression in human blood-brain barrier, choroid plexus, heart, intestine, lung, kidney, placenta and testis [296]. The results observed in this chapter could represent a basal expression level of the selected organic anion transporters within the lung.

The first of the organic anion transporters studied here, Slco1a1 (previously Oatp1/Slc21a1), acts as a transporter of the largest number of amphipathic substrates and has been localised to the basolateral membrane of human hepatocytes, the apical membrane of kidney proximal tubules and the apical membrane of the choroid plexus [46, 295, 297]. Within the human lung, hOATP1 presence has been reported through use of Northern blotting [298]. The same technique aided by RT-PCR could not identify Slco1a1 in rat lung, instead illustrating specific expression within the kidney and choroid plexus [299, 300]. This discrepancy in reported Slco1a1 lung expression could illustrate a varying expression pattern between transporter orthologs. It is difficult to draw significant conclusions with regards to Slco1a1 expression profile as there is a lack of reported evidence to support either a presence or absence in rat lung.

The second transporter to be studied, Slco1a4 (Oatp2/Slc21a5), predominantly transports substrates such as thyroid hormones, cyclic peptides and steroid conjugates. The expression profile of a comparable human protein, OATP2/SLC21A6, is restricted to the basolateral plasma membrane of hepatocytes which could suggest the rat protein to also exhibit this specific expression profile [46, 295, 296, 301-303]. The results of this chapter report an absence of Slco1a4 in all lung cell samples studied. Together with the lack of reported evidence of Slco1a4 lung expression, the specific profile documented for OATP2/SLC21A6 seems also to be true for the rat protein.

The third transporter to be researched was Slco3a1/oatp3a1/Oatp-D. Based on a combination of RT-PCR experiments, human SLCO3A1/OATP3A1 is known to exhibit ubiquitous tissue expression. This protein displays 97 % sequence identity with both its rat and mouse orthologs. Together with wide tissue distribution, this highly conserved sequence could hint at an important physiological function [46, 295]. Within the lung, Northern blot analysis has shown SLCO3A1/OATP3A1 to be moderately expressed. Similarly, this same technique has also shown the rat ortholog Slco3a1 to be expressed at a moderate level within the rat lung [46]. The results of this chapter illustrate Slco3a1 to be expressed in all lung cell samples studied. These results complement the knowledge of this transporters ubiquitous tissue expression and could illustrate basal expression throughout the lung.

The fourth transporter to be examined was Slco4c1, also known as Oatp4C1/Oatp-H. The transporter forms part of a very small SLCO subfamily, little is known regarding specific substrates or physiological function, however, it has been reported that Oatp-H/SLCO4C1 shows tissue distribution within the human kidney [46, 295]. Within the lung cell samples studied in this chapter, Slco4c1 exhibited a low level of expression in all, with the exception of SPOC1 where no expression was noted. The rat transporter could have specific requirements to facilitate its expression which could be absent in the SPOC1 cell line, however, due to the distinct lack of literature evidence with regards to Slco4c1/Oatp-H expression, this cannot be confirmed. The results obtained here suggest Slco4c1 to be expressed within cells of rat lung parenchyma and not those of the trachea.

The fifth protein to be studied, transporter Slco4a1 (OATP-E/Oatp4a1), was originally isolated from both human brain and kidney but is known to be ubiquitously expressed in all human tissues. Human OATP-E/SLCO4A1 shows strongest expression in the liver, heart, placenta and pancreas [304] and is capable of transporting a number of important substrates such as taurocholate, thyroid hormones T3, T4 and rT3, a number of prostaglandins and steroid conjugates. The rat protein Slco4a1 shows 76 % sequence identity with its human ortholog, it is therefore possible that Slco4a1 also exhibits a ubiquitous expression pattern. Within the lung, human OATP-E/SLCO4A1 cDNA has

been cloned from adult lung and has also been detected in the lung through RT-PCR [296]. The suggested ubiquitous expression pattern of Slco4a1 combined with evidence of human OATP-E/SLCO4A1 expression within the lung could be reasoned to complement this chapter's results for the Slco4a1 transporter. Further, ability of Slco4a1 to transport thyroid hormones could add further evidence to its presence within the lung as thyroid hormone T3 and plays a role in late lung development [305].

The final transporter to be studied here was Slco2b1, human OATP-B/SLCO2B1. The human transporter is known to be ubiquitously expressed, displaying a decreasing level of expression from the liver to the spleen, placenta, lung, kidney, heart, ovary, small intestine and brain [296, 298, 306]. There is little literature evidence regarding the rat transporter Slco2b1, however, this transporter shares 77 % sequence identity to its human ortholog and is known to display similar functionality, therefore it seems plausible that Slco2b1 show a similar expression profile to OATP-B/SLCO2B1. Tamai and co-workers have illustrated human OATP-B/SLCO2B1 to be expressed at a low level in human lung through RT-PCR [296]. This same technique implemented in our study generated complementary results suggesting this transporter to be expressed at a low level within the lung.

Overall, the results of this chapter seem to illustrate a basal level of expression for several OATP transporters within the rat lung. In order to create a definitive expression profile for this family of transporters, extensive expression analysis would need to be completed.

Combining both the available literature evidence and this chapter's findings, transporters Slco4c1, Slco4a1, Slco3a1, and Slco2b1 have the potential to influence drug discovery directed to the lung. Organic anion transporters are capable of transporting several pharmacologically relevant drugs such as β -lactam antibiotics, non-steroidal anti-inflammatory drugs, antiviral drugs, several drugs that are toxic in overdose and neurotransmitter metabolites [297]. Due to the multispecific substrate nature of many OATs there is the potential for these transporters to interact with drugs delivered to the lung [293]. Drug transporter–drug interactions would affect a drugs pharmacokinetics, create potential toxicity and effect therapeutic response [297]. A broad transporter substrate spectrum also provides OATs with important roles in drug absorption, disposition and elimination [294]. Several OATs are known to influence both pharmacokinetic profiles of drugs and their pharmacological effects. For example, penicillin G displays an increased half life when simultaneously used with probenecid [293]. All OATs examined here were either absent or displayed, on average, a low level of expression in all lung samples studied. Many human OATs are known to display ubiquitous tissue expression suggesting the observed expression within

the rat lung to be true. Because of the multispecific substrate range of OATs and the expression of such transporters within a number of tissues important to drug pharmacokinetics, much OAT research has been focused here. It is difficult to estimate the impact of OATs on drugs delivered to the lung, but it seems likely that transporters of this family present within the lung would interact to drugs delivered via both inhalation and instillation.

Improving knowledge of the potential impact of organic anion transporters on drug discovery and drug ADME would have an ever-increasing effect upon the ability to improve medical treatment through reducing the risk of toxicity while maximising therapeutic effects. In an aid to achieve this, a comprehensive expression profile of all OATs, consolidating existing evidence is required.

In this study it was sought to examine the expression, at an mRNA level, of selected, pharmaceutically relevant ABC, SLC, and SLCO transporters in specified rat lung cell samples. The comprehensive mRNA expression profiles generated illustrate, to some degree, the localisation of these chosen drug transporters within specific regions of the lung. The development of the transporter expression profiles constructed here will give insight into the localisation of these proteins within the lung and, through this increased knowledge in transporter localisation, could benefit drug discovery research through exploitation of drug transporter functionality and improvement of candidate absorption, distribution and accumulation in both target and non-target organs.

CHAPTER 3

Development and validation of an Isolated Perfused Rat Lung model for pulmonary delivery

3.1. Introduction

The origin of the isolated perfused organ dates back to the 1800s while, during the development of pharmacological techniques, it was discovered that isolated organs and tissues were able to remain functionally intact for several hours in an aerated bath of physiological salt solution. Following this technical realisation, the concept of organ isolation for experimentation was applied to many organs and tissues of interest. Henrick Magnus first applied this technique to isolated strips of small intestine [307]. Claude Bernard followed with work on isolated nerve-muscle preparations in the 1850's [307] and in the early 1900's, Jean-François Heymans performed experiments with isolated mammalian hearts [308]. Early works with isolated organ preparations provided vital advances in the understanding of *in vivo* organ and tissue processes. For example, Claude Bernard made several important scientific breakthroughs with the aid of isolated organ preparations including; the role of the pancreas in digestion, understanding the glycogenic function of the liver, and discovering the vaso-motor system [309]. From this and other works, Claude Bernard went on to become regarded as 'one of the greatest men of all science', referred to as such by I. Bernard Cohen of Harvard University in the Foreword to the Dover edition (1957) of Bernard's book on scientific method, *An Introduction to the Study of Experimental Medicine*; highlighting the significance of works upon isolated organ preparations from the mid 1800's onwards [310].

Use of the lung in isolated organ preparations first emerged at approximately the same period as mammalian heart preparations, in the form of heart-lung models. Knowlton and Starling utilised the lungs as a 'respirator' in their model to research the heart [311] and adapted their protocol from other heart-lung preparations such as that reported by Newell Martin in 1883 [311, 312]. Developments such as these could be considered as the birth of isolated perfused lung methodology.

Refinement of the isolated perfused lung as a stand-alone model flourished in the 1950s and 1960s with Delaunois and King publishing 'improvements in an isolated perfused lung technique' in 1956, cementing use of such a model in modern pharmacological research [313]. Much initial work with isolated lungs utilised those of the rabbit, guinea-pig and dog, however, Davis and Levy in 1965 reported use of an isolated rat lung setup to examine removal of bacteria from the lung [314]. This published use of an isolated perfused rat lung setup (IPRL) represents one of the first documented uses of this model and in 1970, Leary and Smith went on to publish a comprehensive overview of their *in situ* isolated rat lung preparation, marking the beginnings of the use of the rat lung as an excellent standard for lung-specific experiments [315]. The Leary and Smith IPRL preparation

represented the early development of a 'standard' model and provided many techniques and measurements which continue to translate to current IPRL preparations. For example, their model consisted of a somewhat typical surgery technique, where the heart and lungs were exposed via the ribcage and the right and left ventricles of the heart cannulated. The preparation was perfused through the right heart at a rate of 6 mL/min and the venous affluent collected for sample analysis. Lungs were ventilated through a tracheotomy and perfusate was kept at 37 °C, pH 7.4 and aerated with 95% O₂ : 5% CO₂ [315]. The perfusion media utilised by Leary and Smith was first employed by Leary and Ledingham [316] and was developed by Hems *et al.*, [317] for use with isolated liver preparations. This medium consisted of physiological saline (Krebs and Henseleit, 1932 [318]), bovine serum albumin (fraction V) and washed human red blood cells and essentially represents the beginnings of what has now become a standard lung perfusion medium. To ensure the viability of the preparation, Leary and Smith examined the lungs after each experiment by electron microscopy to rule out gross lung damage and also examined angiotensin I conversion within the lung to provide evidence of the enzymatic competency of the IPRL [316, 319].

Development of initial preparations such as that of Leary and Smith have led to the emergence of a number of IPRL models and while there exists standard methodology for lung isolation and perfusion, there is great variation in a number of technical aspects of each preparation. There exists a large amount of literature describing the establishment and validation of IPRL preparations which has highlighted both inter-preparation variability and viability. Further, many reports of IPRL preparations include few parameters that are utilised to examine and evaluate lung viability. Generally, viability parameters studied are either morphological or biochemical, with morphological parameters including; monitoring wet organ weight, wet: dry ratio of lung weight and visual scoring for tissue oedema, and biochemical parameters including assay of the perfusate for; glucose, ATP, uric and lactic acid, serum proteins and cholesterol. Ideally, when validating an IPRL preparation, a variety of parameters should be monitored in order to produce an accurate picture of the performance of the preparation, however, monitoring biochemical parameters creates the need for sophisticated instruments and techniques and so more often monitoring relies on simple morphological factors. It is also important to avoid over-complicating an IPRL protocol and to avoid detracting from intended IPRL experimental purpose [320].

Many IPRL preparations continue to be exploited in a number of areas of scientific research and are now commonly employed in fields such as drug delivery, drug discovery and drug development. Recently, Ewing and co-workers have utilised an *ex vivo* IPRL to examine vasoconstriction after budesonide inhalation [321], highlighting not only the sustained applicability of the IPRL from its

initial use in the late 1800s but also the continued need for improved understanding of such issues as the influence of ADME parameters upon inhaled drugs and the real applicability of drugs delivered to the lung for systemic action [322]. The research of Ewing and co-workers also serves to highlight the diversity of model use; researchers sought to examine the absorption and metabolism of an inhaled model polycyclic aromatic hydrocarbon, (benzo(a)pyrene; BaP), within an IPRL. It was aimed to quantify the saturation of BaP in the IPRL and provide insight as to the reasoning behind carcinogenic activity of such compounds at the sight of entry. In order to achieve reliable results, this research group also monitored parameters such as tracheal airflow and thoracic pressure change in order to ensure only stable IPRL preparations were used [323]. Further, the IPRL setup of Niven, Byron and colleagues and its subsequent use represents a model that has been fully utilised within the realms of pharmaceutical research to examine issues such as drug delivery to the lung, drug deposition within the lung and drug absorption from the lung [95, 96, 324]. Niven and Byron initially used this preparation (Figure 3.1) to study the deposition and absorption of aerosolised drugs delivered to the IPRL. Their studies [95] established the use of the IPRL in examining the deposition and transport of inhaled drugs and represents the first documented use of the IPRL model for this purpose.

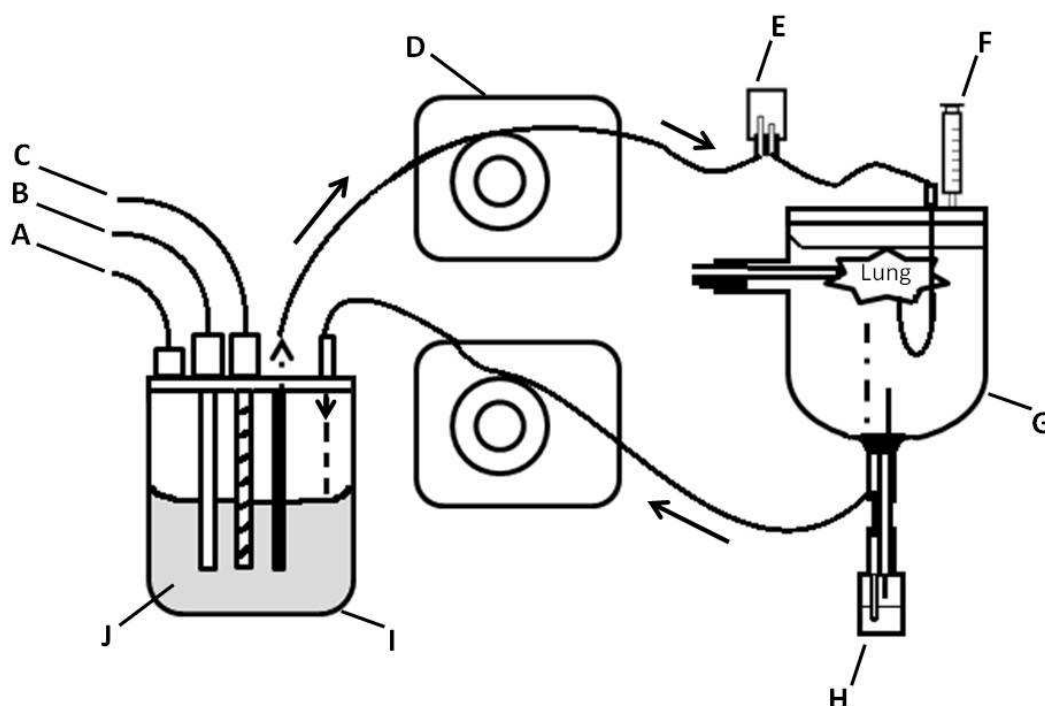


Figure 3.1 Byron *et al.* isolated perfused rat lung setup which was adapted for aerosol administration of substrates to the isolated lung. Key: (A) Carbogen supply, (B) pH electrode, (C) Temperature probe, (D) Peristaltic pump, (E) Bubble trap, (F) Syringe (20 ml), (G) Water-jacketed glass thorax, (H) Air removal trap, (I) Water-jacketed perfusate reservoir, (J) Perfusate. Diagram representing IPRL of Byron *et al.* [95].

Following the establishment of an isolated and perfused rat lung by Byron and colleagues, this research group began systematic use of this model, together with two delivery techniques; aerosol administration and forced-solution instillation, to examine solute absorption from the airways [324-327] and, in a similar manner to Schanker *et al.* [34, 35], began generating a body of disposition and absorption data. Niven and Byron, in 1988, initially began generating this data by examining the fate of aerosolised fluorescein dosed to the IPRL [324]. From this, a number of future studies extended including; examining the effect of surfactant upon fluorescein absorption, examining the absorption of a number of polypeptides dosed to the IPRL and examining the fate of insulin dosed to the lung; a study which highlighted the importance of reliable lung deposition and lung region-specific kinetics [101, 325-328]. Such research has given further insight to the deposition and transfer mechanisms of aerosolised drugs and has provided an excellent adaptation of an IPRL model to allow for target-relevant dosing systems.

Use of the IPRL model developed by Byron *et al.* for the study of drug delivery to the lung highlighted this specific model-type, i.e. ex situ lung and artificial thorax, as the basis for models for future use in this field. The use of a novel dosing method involving a pressurised metered dose

inhaler and a liquid dose 'packet' has also allowed this particular IPRL model to be employed in examining the airway-to-perfusate absorption kinetics of a number of liquid formulations [96]. Research conducted by Tronde *et al.* also employed a distinct dosing system with an IPRL model; delivering nebulised dose to vertically-hung lungs in an artificial glass thorax [102]. Utilising this isolated perfused rat lung setup, Tronde and co-workers sought to examine structure-absorption relationships of inhaled drugs such as budesonide, formoterol and propranolol and generated a significant body of work that provided comparison between drug pulmonary absorption and physicochemical properties [329, 330].

The success of the model developed and modified by Byron *et al.*, and its applicability to pulmonary drug discovery offered a very attractive model for use within this and subsequent chapters. There are many essential similarities between the model used here and that used by Byron *et al.* with exceptions mainly involving aspects of preparation monitoring. However, the availability of fluorescein absorption data performed in a very similar model to that of this chapter provides this as an internal standard for use in all IPRL experiments, thus providing parameters to employ to data and avoid wide data variability.

It has long been recognised that, compared with other mucosal barriers, the lung offers greater permeability to a wide molecular weight range of molecules which can display a fast rate and high extent of pulmonary absorption following airway administration [8].

Aims and Objectives

- The main objective of this chapter is to set up and fully validate an isolated perfused rat lung model for the study of pulmonary absorption processes in isolation from the rest of the body.
- 'Transfer' (in principal) the model developed by Niven and Byron [95] to Cardiff University from Virginia Commonwealth University
- Validate the IPRL in-house as a preparation for the study of pulmonary solute absorption through examining the reproducibility of the intra-tracheal dosing method and deposition pattern
- Validate drug deposition following airway administration using Evans blue and sodium fluorescein dyes delivered to the IPRL via the intra-tracheal dosing method and examining distribution within the lung

- Confirm the suitability of the IPRL for the study of pulmonary absorption by examining the rate, extent and reproducibility of fluorescent probe transport across the IPRL.
- Establish preparation viability by examining the wet: dry ratio of lung tissue post IPRL procedure and by noting presence or absence of pulmonary oedema.

3.2. Materials and Methods

3.2.1. Validation of IPRL perfusate - extent to which Bovine Serum Albumin contributes to perfusate background fluorescence

Materials

Consumables

Whatman Grade No. 91 filter papers, Fisher UK, (Cat No: FDH-200-169A)

Reagents

D-glucose anhydrous; $C_6H_{12}O_6$, (Fisher Scientific, Loughborough, UK, G/0450/60)

Potassium chloride; KCl, (Fisher Scientific, Loughborough, UK, Cat: P/4280/53)

Magnesium sulphate heptahydrate; $MgSO_4 \cdot 7H_2O$, (Fisher Scientific, Loughborough, UK, Cat: M/0600/53)

Sodium bicarbonate; $NaHCO_3$, (Fisher Scientific, Loughborough, UK, Cat: S/4200/60)

Calcium chloride dihydrate; $CaCl_2 \cdot 2H_2O$, (Fisher Scientific, Loughborough, UK, Cat: C/1500/50)

Sodium chloride; NaCl, (Fisher Scientific, Loughborough, UK, Cat: S/3105/63)

Potassium dihydrogen phosphate; KH_2PO_4 , (Fisher Scientific, Loughborough, UK, Cat: P/4800/53)

Bovine serum albumin; BSA, (Sigma-Aldrich, Dorset, UK, Cat: A7906-1kg)

Bovine serum albumin; BSA, (Biosera, East Sussex, UK, Cat: P6150)

Sodium fluorescein; F-Na, (Fluka, Sigma-Aldrich, Dorset, UK, Cat: 46960)

Method

Preparation of stock solutions

Chemical	g / L perfusate	g / 500 mL stock solution
KCl	0.35	0.035
$MgSO_4 \cdot 7H_2O$	0.29	0.029
$CaCl_2 \cdot 2H_2O$	0.37	0.037
KH_2PO_4	0.16	0.016

Chemicals listed above were dissolved in distilled water (~ 400 mL) and the volume adjusted to 500 mL.

Perfusate

To prepare 1 L

The below listed chemicals and solutions were added to distilled water (~ 300 mL) and the final volume adjusted to 1000 mL. Order of addition:

- 1) Glucose 2.0 g
- 2) KCl 0.35 g (10 mL of stock solution)
- 3) $\text{MgSO}_4 \cdot 7\text{H}_2\text{O}$ 0.29 g (10 mL of stock solution)
- 4) NaHCO_3 2.10 g
- 5) $\text{CaCl}_2 \cdot 2\text{H}_2\text{O}$ 0.37 g (10 mL of stock solution)
- 6) NaCl 6.92 g
- 7) KH_2PO_4 0.16 g (10 mL of stock solution)
- 8) BSA 40.0 g (either 'Biosera' or 'Sigma' product)

Order of addition of perfusate components is very important to ensure that the formation of precipitate; namely CaCO_3 , is avoided, isotonicity (300-320 mOsm/kg H_2O) and pH (pH 7.4) are critical.

Isotonicity was measured using an osmometer (Advanced® 3D3 Single-Sample Osmometer) and a perfusate sample volume of 200 μL .

Perfusate solution was prepared and filtered using Whatman filter paper with a 15 cm diameter or equivalent.

Preparation of F-Na calibration curve

Calibration curves for F-Na were prepared by serial dilution with; a) Biosera BSA perfusate, b) Sigma BSA perfusate and c) Perfusate minus BSA. A concentration range F-Na of 0.001 $\mu\text{g/mL}$ – 0.1 $\mu\text{g/mL}$ was prepared.

FLUOstar analysis: F-Na levels in IPRL perfusate

F-Na concentrations in perfusate were determined fluorometrically using a microplate fluorometer (FLUOstar, Optima, BMG). Perfusate samples (200 μL) containing F-Na calibration concentrations were analysed (λ_{ex} 485 nm, λ_{em} 520 nm) and calibration curves constructed, using perfusate made from: (a) Biosera BSA perfusate, (b) Sigma BSA perfusate and (c) Perfusate minus BSA. Perfusate samples without F-Na were also analysed for background fluorescence which was subtracted from all F-Na perfusate samples. The extent to which BSA contributes to background fluorescence and the most suitable BSA product in terms of background fluorescence and F-Na limit of quantitation were examined by use of each specific perfusate calibration curve.

3.2.2. Isolated Perfused Rat Lung

Materials

Animals

Male-specified pathogen-free Sprague-Dawley rats (Harlan UK Limited, Bicester, UK) were used throughout and housed in rooms controlled between 19 °C – 21 °C and 40-60 % humidity with dark-light cycling every 12 h. The animals had free access to food and water and were acclimatised for at least 2 days prior to experimentation. All animal experiments adhered to the Animal (Scientific Procedures) Act 1986, UK and were approved by Cardiff University.

Equipment list

Constant volume mechanical ventilator, (Harvard Apparatus Ltd, UK, Model No: 50-1718)

Artificial glass thorax, (Richmond Glassware, USA, Custom Made)

Condenser, (Richmond Glassware, USA, Custom Made)

Perfusate reservoir, (Richmond Glassware, USA, Custom Made)

95%/5% O₂/CO₂ (BOC, Manchester, UK)

Circular tripod, (Fisher Scientific, Loughborough, UK, Cat: STK-940-030W)

Custom made stainless steel dosing rod (DR), port (DP) and tracheal cannula (TC), (Harvard Apparatus Ltd, UK, Figure 3.2A)

Magnehelic® differential pressure gauge, measuring -5 to +5 cm H₂O, (Dwyer® Instruments, High Wycombe, Bucks, UK, Model: 2300-10cm)

Hanging rods (HR),(custom made, see Figure 3.2B)

Syringes (Sterile; 50 mL), (Fisher Scientific, Loughborough, UK, Cat: SZR-CSE-060U)

pH/ temperature meter (Hanna Piccolo®, Sigma-Aldrich, Dorset, UK, Cat: P9565, or equivalent)

Peristaltic pumps

Watson Marlow, (Falmouth, Cornwall, UK, Model: 505S)

Gilson, Inc., (Middleton, WI, USA, Model: Minipuls 3)

Tubing

Perfusate lines: Masterflex 96400-14 peroxide cured, (Fisher Scientific, Loughborough, UK, Cat: PMM-505-515G)

Water lines: Tygon R-3603, (Fisher Scientific, Loughborough, UK, Cat: TWT-700-150N)

Connectors

Perfusate line to condenser: Tubing connector Kartell unequal inlet and outlet, (Fisher Scientific, Loughborough, UK, Cat: ADF-610-030D)

T-piece tubing connectors, (Fisher Scientific, Loughborough, UK, Cat: ADF-715-030L)

Y-piece tubing connector for ventilator attachment, (Fisher Scientific, Loughborough, UK, Cat: ADF-690-010W)

Tubing clips

Tubing clips 14-19 mm, (Fisher Scientific, Loughborough, UK, Cat: CNK-641-040T)

Tubing clips 13-17 mm, (Fisher Scientific, Loughborough, UK, Cat: CNK-641-030W)

Tubing clips 22-30 mm, (Fisher Scientific, Loughborough, UK, Cat: CNK-600-050E)

Silicone bungs

Dosing port stopper, (Fisher Scientific, Loughborough, UK, Cat: FB55019)

Drain stopper, (Fisher Scientific, Loughborough, UK, Cat: FB55015, or equivalent)

Perfusate reagents

D-glucose anhydrous; $C_6H_{12}O_6$, (Fisher Scientific, Loughborough, UK, G/0450/60)

Potassium chloride; KCl, (Fisher Scientific, Loughborough, UK, Cat: P/4280/53)

Magnesium sulphate heptahydrate; $MgSO_4 \cdot 7H_2O$, (Fisher Scientific, Loughborough, UK, Cat: M/0600/53)

Sodium bicarbonate; $NaHCO_3$, (Fisher Scientific, Loughborough, UK, Cat: S/4200/60)

Calcium chloride dihydrate; $CaCl_2 \cdot 2H_2O$, (Fisher Scientific, Loughborough, UK, Cat: C/1500/50)

Sodium chloride; NaCl, (Fisher Scientific, Loughborough, UK, Cat: S/3105/63)

Potassium dihydrogen phosphate; KH_2PO_4 , (Fisher Scientific, Loughborough, UK, Cat: P/4800/53)

Bovine serum albumin; BSA, (Sigma-Aldrich, Dorset, UK, Cat: A7906-1kg)

Filter papers

Whatman Grade No. 91 filter papers, (Fisher Scientific, Loughborough, UK, Cat: FDH-200-169A)

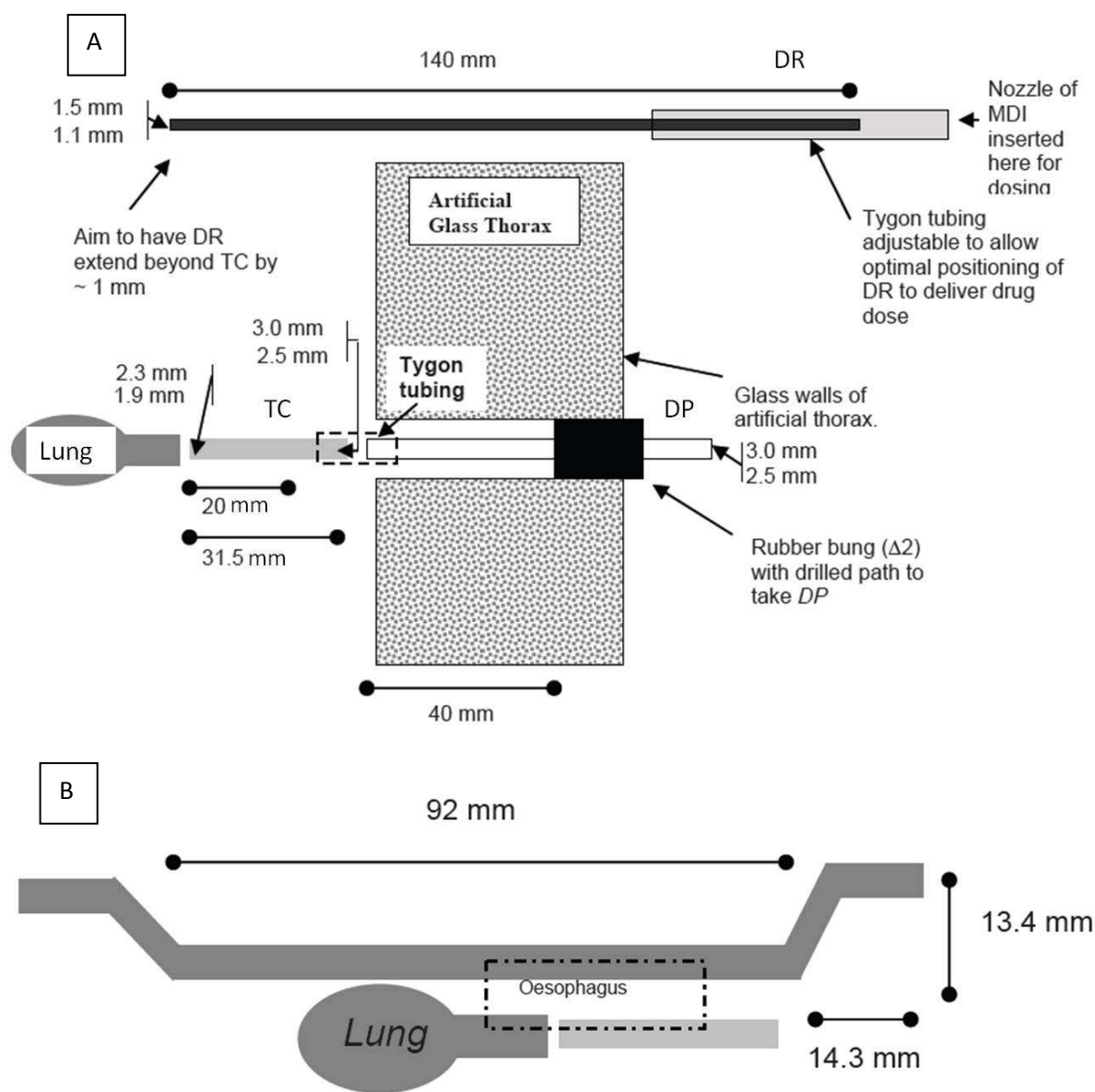
Surgery reagents

Euthatal, (Merial Animal Health Ltd., Harlow, UK)

Syringes (Sterile; 1 mL), (Fisher Scientific, Loughborough, UK, Cat: SZR-150-011Q)

Needles (Sterile; 25G x 5/8IN), (Fisher Scientific, Loughborough, UK, Cat: SZR-175-510A)

Heparin sodium (contains preservative) – previously known as Multiparin®, (1000 I.U. /ml), (Wockhardt UK, Wrexham, UK, Order No: FP1086)



*Hanging Rod (DR) 1.6 mm diameter
The profile of this depends on the individual AGT.
Lung hangs below rod and is attached via the oesophagus.*

Figure 3.2 Profile and measurements of equipment custom made for the IPRL. **Figure 3.2A** represents the Dosing Rod (DR), Dosing Port (DP), and Tracheal Cannula (TC) for use with IPRL. Each component was individually custom made/adapted for use with this specific IPRL model. Also depicted is the organisation of each component to allow dosing to the isolated lung via the DR. **Figure 3.2B** represents the specific measurements of the custom made hanging rod for use within an individual artificial glass thorax.

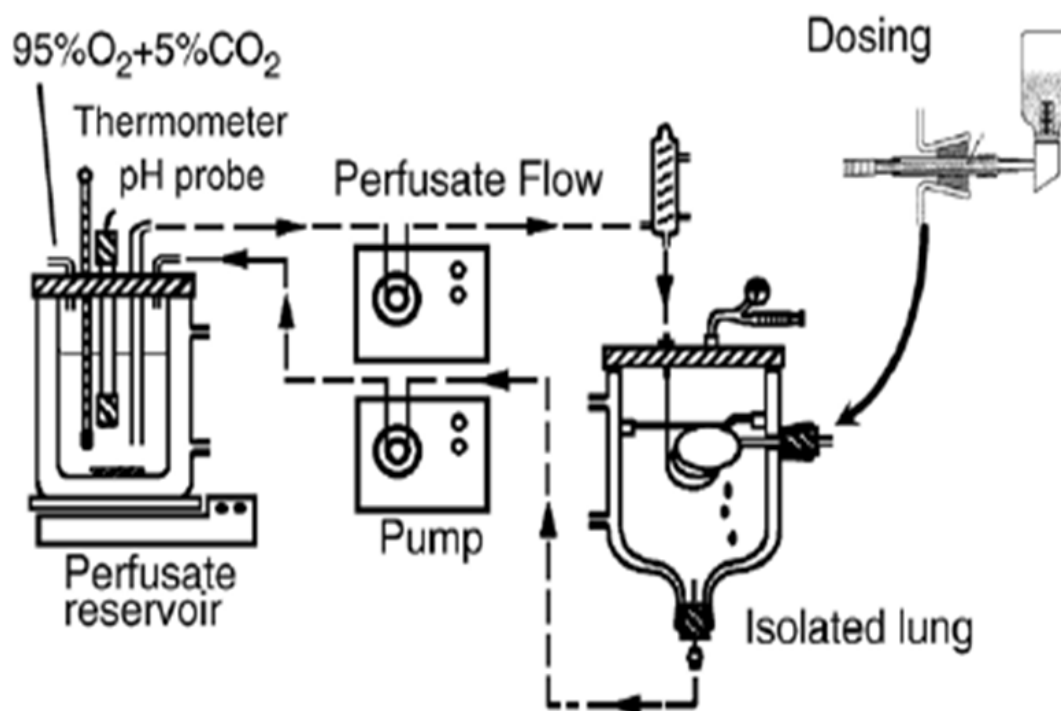


Figure 3.3 Schematic of IPRL equipment setup; kindly provided by Masahiro Sakagami. The setup is adapted from that first described by Byron and Niven. The isolated lung is situated within a water-jacketed artificial glass thorax and is dosed whilst ‘hanging’ inside. Perfusate is maintained at 37 °C and flow controlled by a peristaltic pump. In order to retain a recirculating setup, perfusate is returned to the reservoir post-circulation of the pulmonary vasculature. This recirculating setup also allows easy sampling from the reservoir and easy maintenance of perfusate volume.

Method

Perfusate solution was prepared with Sigma BSA and filtered using Whatman Grade No. 91 filter papers with a 15 cm diameter or equivalent. Each batch of perfusate was prepared between 16 h and 24 h before an IPRL experiment, importantly the solution containing BSA was left stirring for 16 h at 4 °C prior to use. Any perfusate batch not used within 48 h of preparation was discarded.

Pre-surgery

All glass vessels and perfusate were brought to temperature (37 °C) via the heated water pump. Once perfusate had reached temperature, the solution was circulated through the IPRL system and initially run to waste (~15 mL) before being set in ‘recirculating’ mode. All bubbles were removed from perfusate lining by flicking the tubing to dislodge. Surgical instruments, clamps, and cotton (for securing both tracheal cannula and pulmonary artery catheter) were ensured to be clean and available. Finally, a heparin dose (0.1 mL of a 1000 U/mL) and a Euthatal dose (50 mg/mL dose i.p. at 60 mg/kg) were prepared, each in a 1 mL syringe with sterile needle attached.

Surgery

A surgical incision was made in the neck to expose the trachea; from this point surgery was aimed to be completed in 10-12 min. Once the trachea was exposed, a cut was made between the 4th and 5th

cartilage rings. The cut were approximately half of the trachea circumference to allow insertion of the tracheal cannula. Positioning is important as the site of dissection and the length to which you insert the tracheal cannula into the trachea influence the deposition of any administered forced liquid instillation.

The tracheal cannula was then inserted into the trachea and secured with cotton and threads trimmed. Care was taken to tie cotton between cartilages rings as tying directly on cartilage may result in a loosely secured tracheal cannula. Note the presence of a tubing connector on the distal end of the cannula to allow manual ventilation. During the remainder of the surgery it was sought to avoid changes in the position of the animal that would restrict the airspace, e.g. doubling up of the head and neck. The animal was fixed to surgery tray using autoclave tape if necessary.

The abdominal cavity was opened in an arc dissection and the sternum clamped and lifted to expose the diaphragm and thoracic organs. Next the diaphragm was dissected around the margins of the ribcage to the inferior surface to expose the lungs. Great care was taken not to touch any lung tissue. Once the ribcage and lungs were exposed, the ribcage was dissected. The cut was made quite high to avoid injury to the lungs through contact with the cut ribcage. The clamped sternum was then lifted towards the head of the animal and the chest wall turned over to fully expose the heart and lungs.

Heparin sodium (0.1 mL of 1000 U/mL) was injected into the heart by firmly grasping the heart with forceps. The injection was aimed for the crinkled surface tissue of the right ventricle and position checked by visualising blood leaking back into the syringe neck. Before injection the pressure of the forceps was released but the heart held in place so that heparin was not forced back out through the puncture site, heparin was then slowly injected.

The thymus was removed via forceps to allow visualization of the pulmonary artery. Sufficient removal was ensured to aid both good visualisation of the pulmonary artery and removal of the lungs from the animal carcass.

The heart tissue was gently held to expose the site for incision of the pulmonary artery catheter (PAC). An incision was made at 90 ° to the path of the pulmonary artery for insertion of the PAC. Care was taken not to cut too high near the exposed vessel, as it is very difficult to insert PAC from here, or too low into the heart tissue as the PAC will have to be forced through tough heart tissue. Further, the cut was ensured not to be too shallow as this would likely still be within cardiac tissue. Instead the cut was deep enough to access the lumen of the ventricle leading to the pulmonary artery. Next the perfusate line was transferred to the surgical tray and the left and right atrium cut to allow free flow of perfusate. The PAC was then inserted into the pulmonary artery, the way in which the forceps were held is critical at this point. Firstly the heart was held firmly for insertion of the PAC, then the catheter held in place between the operators 1st finger and thumb of the left hand. The forceps were then held between the operators 2nd finger and thumb to allow for placement of the artery clamp using the freed right hand (Figure 3.4). The artery clamp was placed at a sufficient distance from the PAC tip to allow for tying of the PAC within the heart tissue.

A 5 mL syringe was next attached to the tracheal cannula tubing connector for manual ventilation of the lungs. Lungs were ventilated with a tidal volume of approx. 4.5-5 mL for at least 5 repetitions or until the lungs appeared clear. The heart was then cut to allow further escape of perfusate and redundant heart tissue was removed as much as possible to avoid interfering with the hanging position of the lungs in the artificial glass thorax (AGT).

Next the lungs were gently lifted via the tracheal cannula and all thoracic connections cut away. Care was taken not to damage the oesophagus as this was needed to hang the lungs in the AGT. Once free, the hanging rod was inserted along the length of the oesophagus and the lungs mounted in the AGT. The tracheal cannula was connected to the dosing port (DP) and the position of the tracheal cannula within the trachea checked. The tip of the tracheal cannula was positioned just proximal to the 1st bifurcation.

The lungs were then gently washed with warmed perfusate and all tubing checked to be correctly positioned within the AGT. The angle of the pulmonary catheter entering the tissue was vital – care was taken to ensure that it was free flowing.

Initial perfusate flowing from the lung was run to waste to remove blood not wanted in the reservoir; the perfusate line was then placed in the reservoir to complete the circuit. Perfusate volume within the reservoir was checked and made up to a fixed volume with fresh warmed perfusate.

The interface between the AGT and plastic lid was sealed with perfusate to create a seal and the lid fixed in place with parafilm. Next, negative pressure of approx. 1-2 inches (2-5 cc water) was generated to help minimize formation of pulmonary oedema. Finally, the gas line (95% O₂/5% CO₂) was inserted to the airspace of the perfusate reservoir such that the perfusate bubbled gently and the ventilator was attached to the dosing port (DP) with lungs being ventilated with a tidal volume of 2.5 cm³ and a rate of 20 breaths/min

Dosing

As accurately as possible, 100 µL sample dose was inserted to the dosing rod (DR). The DR was held in a horizontal position and the dose inserted slowly to the distal end. The ventilator was then removed from the DP and the DR carefully inserted through to the tracheal cannula. At this point, the tip of the dosing rod could sometimes be seen (through the tracheal tissue) protruding from the end of the TC. A pMDI canister (5.5 mL CFC 11/12, 40:60 %) with a 25 µL valve (Bespak) was primed and the actuator placed into Tygon tubing at the proximal end of the dosing rod. In one quick movement, the pMDI actuator was depressed and the lungs observed for expansion, the pMDI and DR were immediately removed. This point was regarded as the start of drug dosing and a stop watch used to allow timing of sample removal.

The DR was immediately placed in dH₂O to wash any non-administered dose and at the end of the experiment, the tracheal cannula and dosing port were also washed to allow calculation of total dose administered. Total perfusate volume was also measured at the end of the experiment by running all remaining perfusate to the reservoir and transferring to a measuring cylinder.

All samples were centrifuged for 10 min at 18,000 x g to remove contaminating red blood cells and the supernatant stored for analysis.

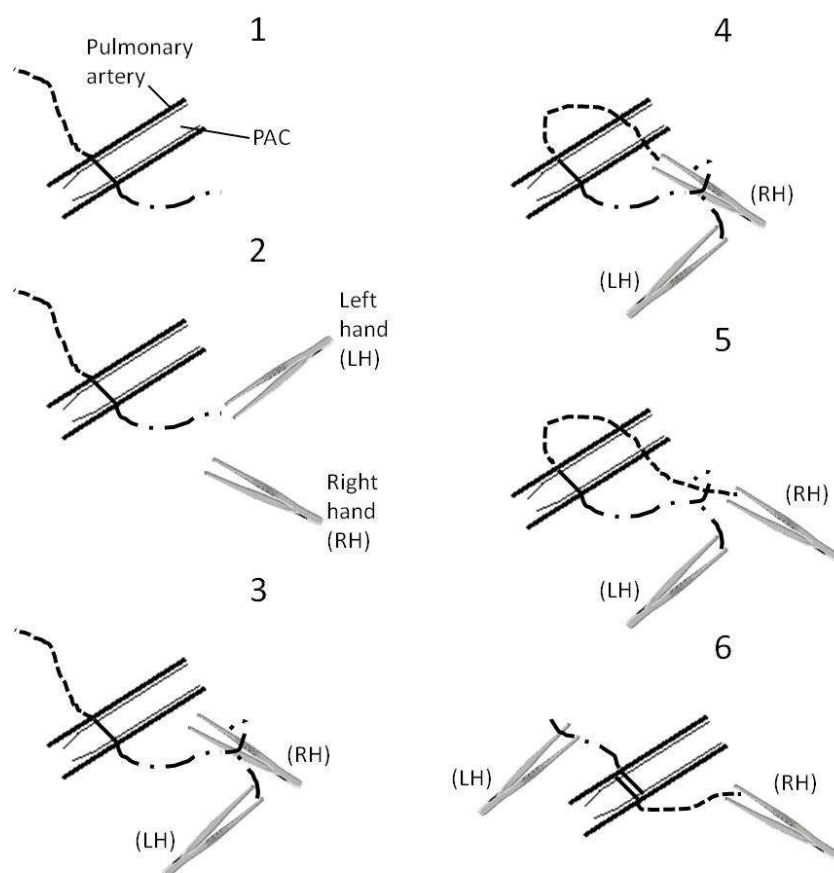


Figure 3.4 Diagram illustrating the tying off of the pulmonary artery catheter (PAC) after positioning in the pulmonary artery.

3.2.3. Validation of IPRL dosing equipment

Materials

Consumables

Sodium fluorescein; F-Na, (Fluka, Sigma-Aldrich, Dorset, UK, Cat: 46960)

Method

An IPRL preparation was conducted as described above. The lungs were dosed with F-Na (100 μ L of a 400 μ g/mL solution) and the experiment immediately stopped. All custom dosing equipment; i.e. dosing rod, dosing port and tracheal cannula, were collected and thoroughly washed in dH₂O. This 'dH₂O wash' was then stored for fluorometric analysis.

FLUOstar analysis: F-Na levels in dosing equipment

The level of F-Na remaining in IPRL custom dosing equipment after a single actuation of a propellant-only pMDI was determined fluorometrically using microplate fluorometry (FLUOstar, Optima, BMG). Dosing equipment wash samples (200 μ L) were analysed (λ_{ex} 485 nm, λ_{em} 520 nm) and concentration determined using a suitable calibration curve constructed in dH₂O. Samples of dH₂O without F-Na were also analysed for background fluorescence which was subtracted from F-Na dosing wash samples. The amount of F-Na remaining in dosing equipment after dosing was corrected for total wash volume and calculated as a percentage of the actual dose.

3.2.4. Validation of the forced solution instillation technique for IPRL dosing

Materials

Consumables

Sodium fluorescein; F-Na, (Fluka, Sigma-Aldrich, Dorset, UK, Cat: 46960)

Evans blue, (Fluka, Sigma-Aldrich, Dorset, UK, Cat: 46160-5G-F)

Phosphate buffered saline; PBS, (0.1 M, pH 7.2), (Fisher Scientific, Loughborough, UK)

Formamide, (Fisher Scientific, Loughborough, UK, Cat: BPE227-100)

Method

Preparation of PBS

Chemical	g / 1000 mL dH ₂ O
Na ₂ HPO ₄	10.9
NaH ₂ PO ₄	3.2
NaCl	90

Chemicals listed above were dissolved in ~ 800 mL dH₂O and the volume adjusted to 1000 mL, pH was adjusted to 7.4. PBS was stored at room temperature and diluted 1:10 for use. All chemicals were of the highest available quality from Fisher Scientific.

Evans Blue lobar deposition

In order to assess dose deposition reproducibility across the lung, Evans blue (3 mg/mL in dH₂O, filter sterilized) was instilled to the IPRL using the forced solution instillation technique. Immediately after dosing, the experiment was terminated and the lung tissue removed and dissected into individual lobes. Each lung lobe was transferred to formamide (1 mL) with the exception of the left lung lobe which was placed in 2 mL formamide. After 1 h samples were centrifuged (18,000 g, 10 min.) and the resulting supernatant (~1 mL) analysed via UV/VIS spectroscopy (Evans blue absorbance at 620 nm). The Evans Blue content of each lobe supernatant was determined using an

Evans blue calibration curve constructed in lung tissue supernatant (plus formamide 1 mL) from mock IPRL experiments where no dose was instilled into the lung.

Sodium fluorescein lobar distribution

Due to poor dye extraction, Evans blue experiments yielded excellent visualization but poor quantification of dose deposition pattern within the IPRL. As Na-F is much more water soluble, this was instilled (400 µg/mL in dH₂O, filter sterilized) to the IPRL using the forced solution instillation technique. Immediately after dose instillation, the experiment was terminated and lung tissue dissected into individual lobes. Each section of lung i.e. lung lobes, trachea and major bronchi, was homogenized in PBS (2 x 5 mL, PowerGen 125 homogeniser, Fisher Scientific, Loughbrough) and then centrifuged (18,000 x g, 10 min.) to yield a tissue supernatant. The F-Na content of each supernatant was fluorometrically determined (λ_{ex} 485 nm, λ_{em} 520 nm) using microplate fluorometry (FLUOstar, Optima, BMG), supernatant samples (200 µL) and an appropriate F-Na calibration curve constructed in control lung tissue homogenate where F-Na was not instilled to the IPRL were examined and a dose disposition profile constructed.

3.2.5. Validation of the IPRL – transport of a molecular weight range of fluorescent probes

Materials

Consumables – absorption substrates

Sodium fluorescein; F-Na, (Fluka, Sigma-Aldrich, Dorset, UK, Cat: 46960)

FITC-dextrans (various M_w), (Fluka, Sigma-Aldrich, Dorset, UK):

(FD4, Cat: FD4-100)

(FD20, Cat: FD20-100)

(FD70, Cat: FD70-100s)

Sample time points

Na-F: 0, 1, 2, 3, 5, 7, 9, 12, 15, 20, 30, 40, 50, & 60 minutes

FD4&20: 0, 1, 2, 3, 5, 7, 9, 12, 15, 18, 20, 25, 30, 40, 50 and 60 minutes

FD70: 0, 5, 10, 15, 20, 25, 30, 35, 40, 45, 50, 55, 60, 70, 80 & 90 minutes

Method

An IPRL experiment was conducted as per protocol. The preparation was dosed with a molecular weight probe (dose 100 µL; F-Na, 400 µg/mL; FD4, 2000 µg/mL; FD20, 200 µg/mL, FD70, 2000 µg/mL) and maintained for 60 or 90 min depending on the probe of choice. Aliquots (1 mL) were sampled from the perfusate reservoir at pre-determined time points and replaced with an equal

volume of warmed perfusate. Perfusate samples were centrifuged (18,000 x g, 10 min., 4 °C) to remove trace blood cells and the supernatant stored at -80 °C for fluorometric analysis. At the end of the experiment, deposits of dosing solution within the IPRL dosing equipment were collected for quantification by washing each equipment part with 50 mL dH₂O to allow determination of actual dose deposited into the isolated lung. To determine the extent of probe transport across the IPRL, sample supernatant (200 µL) from each IPRL experiment was fluorometrically analysed (λ_{ex} 485 nm, λ_{em} 520 nm) using microplate fluorometry (FLUOstar, Optima, BMG) and concentration determined using an appropriate calibration curve constructed in recirculated perfusate. Perfusate samples without fluorescent probe were also analysed for background fluorescence which was subtracted from probe perfusate samples. Cumulative mass of molecular weight probe absorbed was calculated by correcting for total perfusate volume and mass removed during sampling.

Data Analysis

To determine the significance of dose escalation, both the percentage of deposited F-Na dose absorbed at 90 min and the k_{in} of each transport profile was analysed. A one way Analysis of Variance followed by a post-hoc Duncan's test was performed on each. A value of $p < 0.05$ was considered significant. Similarly, to determine the significance of M_w escalation of FITC-dextran, a one way analysis of variance followed by a post-hoc Duncan's test was performed upon the same criteria. Again, a value of $p < 0.05$ was considered significant.

3.2.6. Validation of the IPRL – gel filtration analysis of FITC-dextran

Overview

Gel filtration and gel permeation chromatography, also known as size exclusion chromatography, allows separation based on differences in the size and/or shape of analyte molecules - a characteristic which governs the analytes' access to the pore volume inside the column packing particles.

The PD-10 columns used here are made of chemically inert polypropylene material and filled with 8.5 mL of Sephadex-25 gel filtration material. The exclusion limit of the Sephadex-25 is 5000 for globular protein [331].

Materials

Consumables

FITC-dextran (various M_w), (Fluka, Sigma-Aldrich, Dorset, UK):

(FD4, Cat: FD4-100)

(FD20, Cat: FD20-100)

(FD70, Cat: FD70-100s)

PD10 column, Sephadex G-25, (Sigma-Aldrich, Dorset, UK, Cat: G-25-80)

Phosphate Buffered Saline; PBS, (0.1 M, pH 7.2), (Fisher Scientific, Loughborough, UK)

Method

To rule out FITC-dextran lung metabolism, (i.e. to ensure perfusate samples represented FITC-dextran and not FITC conjugate alone), dose solution and 90 min IPRL perfusate sample of FD4, FD20 and FD70 were filtered through a PD10 column and fractions eluted over time.

Each sample (FITC-dextran dose and perfusate) was made up to a 2.5 mL volume with dH₂O. Gel filtration columns were washed with PBS (~20 mL), the column cap replaced and a sample added (2.5 mL). The column cap was then removed and the sample allowed to run through the column. An aliquot of PBS (0.5 mL) was added to the column to elute FITC-dextran and the fraction collected. This was repeated with a total volume of 24 mL PBS (48 fractions in all).

Each fraction was analysed fluorometrically using microplate fluorometry (FLUOstar, Optima, BMG). Fraction samples (200 µL) were analysed (λ_{ex} 485 nm, λ_{em} 520 nm) and results plotted to determine absence of FITC-dextran metabolism through the presence of only 1 peak in gel filtration chromatography.

3.2.7. Validation of the IPRL – determining IPRL viability by wet: dry weight

Materials

Consumables

Centrifuge tubes (Sterile; 50 mL), (Fisher Scientific, Loughborough, UK, Cat: FB55956)

Liquid Nitrogen (BOC, Manchester, UK)

Method

IPRL viability was established by determining isolated lung wet: dry weight at the end of each IPRL experiment. Lung tissue was removed from the AGT and blotted dry then placed in a centrifuge tube (50 mL) and weighed to give wet weight; centrifuge tube weight was determined and subtracted. Lung samples were then snap-frozen in liquid nitrogen and lyophilised (Thermo Systems, UK) until constant weight was established (~48 h). Samples were then weighed for a second time to yield a dry weight.

3.3. Results

3.3.1 Bovine Serum Albumin contribution to perfusate background fluorescence

Each BSA product was analysed for its contribution to background fluorescence and the lower limit to which F-Na could accurately be detected in the perfusate. Figure 3.5 represents the calibration curve for each perfusate sample used, i.e. Biosera BSA, Sigma BSA, no BSA. The fluorescence reading for the lowest F-Na concentration detected was x3 background fluorescence in each perfusate sample and so was deemed acceptable as the lower limit of quantitation.

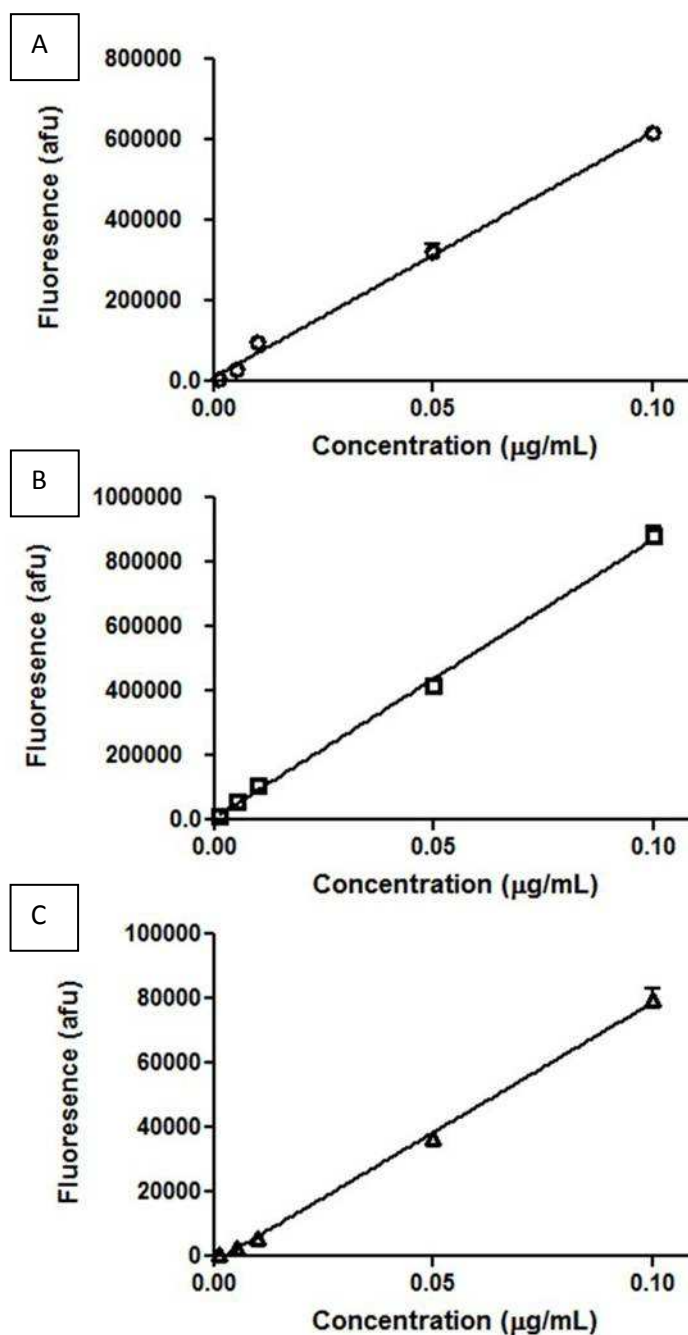


Figure 3.5 Calibration curve representing F-Na in each of the three different perfusate samples; Fig 3.5A - Sigma BSA, Fig 3.5B - Biosera BSA, Fig 3.5C - no BSA. Lower limit of detection was

deemed to be 1 ng/mL in each perfusate sample, i.e. F-Na fluorescence reading was three times that of background. Data shown are mean \pm S.D (n=6 for each treatment).

Table 3.1 shows the two BSA products tested, the Sigma product displayed a lower level of background fluorescence. Perfusate not containing BSA, i.e., 'no BSA', provided an extremely low background fluorescence, only some 1.9 –fold higher than that of dH₂O (background reading of 66 ± 4.0 afu.). The lowest concentration of F-Na to be examined in each BSA product was 1 ng/mL and could be detected in each of the perfusate samples.

BSA product	Background Fluorescence (afu)	Lowest F-Na Fluorescence (afu) [Lowest F-Na concentration detected]
'Biosera' (standard quality, lyophilised)	3717.5 ± 84.4	11178.0 ± 71.3 [1 ng/mL]
'Sigma' ($\geq 98\%$ (agarose gel electrophoresis), lyophilised)	1753.8 ± 92.2	5821.7 ± 55.1 [1 ng/mL]
No BSA	128.2 ± 31.9	520.0 ± 21.0 [1 ng/mL]

Table 3.1 Background fluorescence of three perfusate samples containing either no BSA or BSA from different sources. Data shown are mean \pm S.D (n=6 for each treatment). Fluorescence readings are measured in arbitrary fluorescence units (afu).

3.3.2. Validation of IPRL dosing equipment

In order to evaluate the fraction of dose remaining in the custom made IPRL dosing equipment following a forced instillation procedure, a number of test doses of F-Na were deployed from the equipment with each element of the dosing apparatus subsequently analysed. Experiments were performed in the presence and absence of lung tissue. Each of the test doses that were deployed in the absence of lung tissue displayed an average of 1.58 ± 0.09 % of the total dose retained in the dosing equipment (Table 3.2). The majority of the retained dose was found in the dosing rod. In the presence of lung tissue, the total percentage dose remaining in equipment increased to 5.74 ± 1.40 % (Figure 3.6). In the presence of lung the majority of retained dose was found in the tracheal cannula at 2.53 ± 1.52 % of the dose. The use of a duplicate pMDI (identical HFA composition) to deliver dose in the absence of lung tissue did not significantly alter ($p > 0.05$, one-way ANOVA, post hoc Duncan's test) the total percentage of dose remaining in equipment.

			Amount in eqpt. as % of actual dose (%)			Mean (%)
			#1	#2	#3	
In absence of lung	Operator 1	Dosing Rod	2.93	1.84	1.23	2.00 ± 0.86
		Tracheal Cannula	0.0	0.15	0.16	0.16 ± 0.52
		Dosing Port	0.0	0.05	0.05	0.05 ± 0.49
		Total				1.62 ± 0.37
	Operator 2	Dosing Rod	1.17	0.93	1.58	1.23 ± 0.33
		Tracheal Cannula	0.27	0.44	0.27	0.33 ± 0.09
		Dosing Port	0.05	0.07	0.12	0.08 ± 0.04
		Total				1.64 ± 0.29
	Operator 1, duplicate. pMDI	Dosing Rod	1.57	1.02	1.18	1.26 ± 0.28
		Tracheal Cannula	0.14	0.17	0.22	0.18 ± 0.04
		Dosing Port	0.05	0.05	0.05	0.05 ± 0.00
		Total				1.48 ± 0.26
In presence of lung	Operator 2	Dosing Rod	2.39	0.32	2.56	1.76 ± 1.25
		Tracheal Cannula	3.06	3.71	0.82	2.53 ± 1.52
		Dosing Port	1.76	1.57	1.04	1.46 ± 0.37
		Total				5.47 ± 1.40

Table 3.2 Amount of dose retained in the custom dosing equipment (expressed as a % of dose) after deployment of a test dose. Each constituent part was analysed separately. Data are expressed as percentage of dose retained in dosing equipment in comparison to actual dose instilled to the dosing equipment. Only dose instilled in the presence of lung showed statistical difference ($p < 0.05$) when compared to all other dose instillations, i.e. variation of operator and variation of individual pMDI. Data shown are mean \pm S.D (n=3 for each treatment).

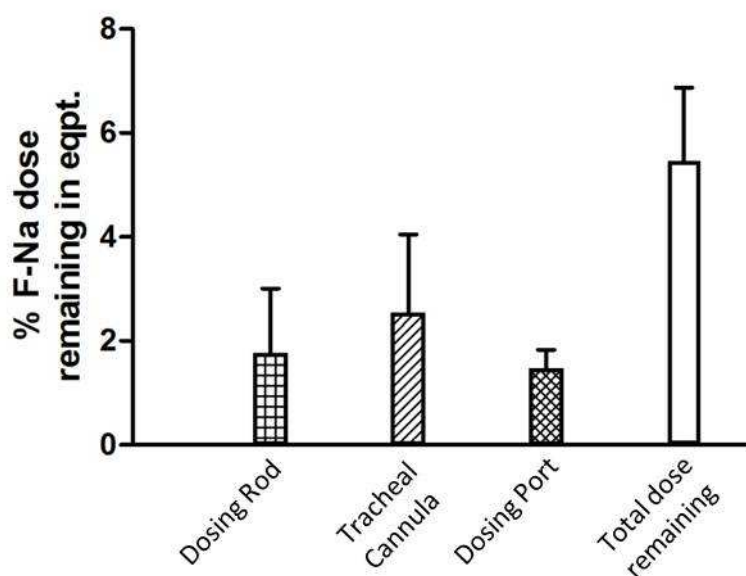


Figure 3.6 Mean amount of dose remaining, as %, in custom dosing equipment after deployment of a test dose to the IPRL in the presence of a lung. Overall, when dosing to the IPRL, the largest % of dose remaining in equipment was found in the tracheal cannula, the least in the dosing port. Data shown are mean \pm S.D. (n=3).

3.3.3. Validation of the forced solution instillation technique for IPRL dosing

To validate the deposition pattern of a dose instilled to the IPRL via the forced solution technique, Evans blue dye was instilled as a test dose. Figure 3.7 demonstrates the pattern of dye deposition within the lung, as can be seen dye is clearly deposited in the lung parenchyma.

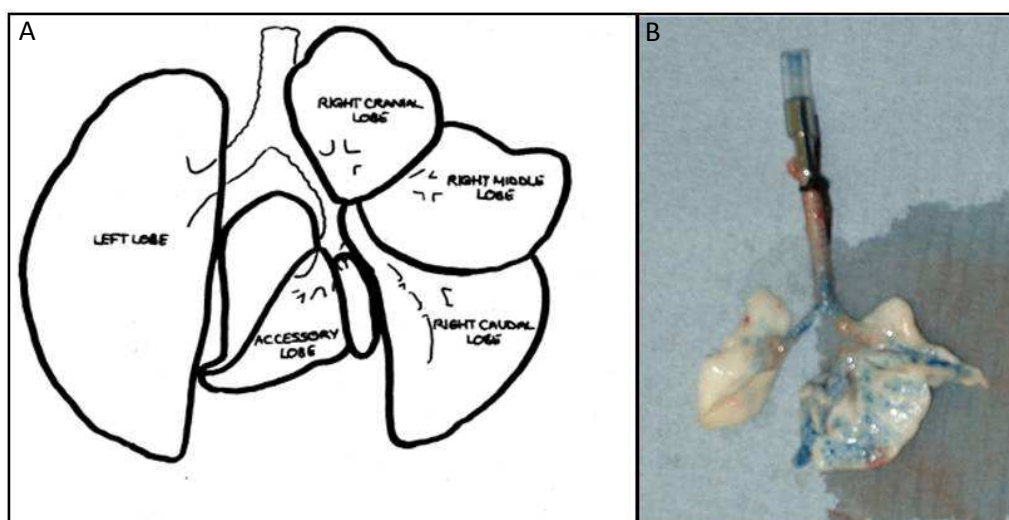


Figure 3.7 Deposition pattern of Evans blue dye dosed to the IPRL via a forced solution instillation technique. Figure 3.7A demonstrates rat lung lobe distribution, the same layout being mimicked in Figure 3.7B. The distribution of dye can be seen in lung parenchyma however, dye can also be visualised in the lower trachea and left major bronchi.

As can be seen in table 3.3, the largest percentage of dye recovered from any lobar region was from the left lobe, with 9.43 ± 5.92 % of actual dose delivered to the lung being recovered. The lowest percentage of dye recovered was from the trachea and major bronchi. Total recovery of Evans blue dye from lung tissue averaged 38.4 ± 12.5 % over three experiments, the resulting 61.6 % of dye not being extracted from the tissue. The observed large standard deviation associated with each mean percentage dose deposited illustrates poor reproducibility of dose deposition to a particular lobar region. For example, 1.83 % dye was deposited to the accessory lobe in experiment #1 and yet 9.70 % dose deposited to the same region in experiment #3 (Table 3.3). Despite this unpredictable pattern of distribution, the observed standard deviation of 0.23 % of dose delivered to the trachea and major bronchi is relatively small throughout suggesting reproducible deposition to this region.

	Amount deposited expressed as % of <i>Actual Dose</i> delivered to lung (%)			Mean \pm SD (%)
	#1	#2	#3	
Trachea & Major Bronchi	3.34	3.02	3.46	3.27 \pm 0.23
Left Lobe	14.08	2.77	11.45	9.43 \pm 5.92
Cranial Lobe	0.52	7.47	8.46	5.48 \pm 4.33
Middle Lobe	7.59	7.13	11.61	8.78 \pm 2.46
Caudal Lobe	5.43	8.87	7.95	7.42 \pm 1.78
Accessory Lobe	1.83	0.38	9.70	3.97 \pm 5.02
Total	32.79	29.64	52.63	38.35 \pm 12.46

Table 3.3 Deposition pattern of Evans blue dye to IPRL expressed as % deposited to each lobar region. Percentage deposition was calculated as a percent of the actual dose delivered to the lung, actual dose being corrected by subtracting the dose deposited in the dosing equipment. Data are expressed as mean \pm S.D, (n=3).

Due to poor Evans blue dye extraction, dose deposition pattern was also evaluated using F-Na. Table 3.4 highlights the deposition pattern of F-Na after forced solution instillation to the IPRL. In contrast to Evans blue, a considerably higher percentage of F-Na dose was recovered from lung tissue, i.e. 85.9 ± 10.5 % F-Na recovered. Overall, the forced solution instillation of F-Na dose resulted in 94.8 % of actual dose not being present in dose equipment, i.e. assumed to be delivered to the lung. When examining dose recovered from the lung, 81.4 ± 17.8 % was recovered from lobar regions of the lung. In a similar manner to Evans blue, deposited dose was not found to show a reproducible pattern within the lung lobes, however, the left lobe and right caudal lobe displayed a high percentage of deposited dose throughout.

	Amount deposited expressed as % of <i>Actual Dose</i> delivered to lung (%)			Mean (%)
	#1	#2	#3	
Trachea & Major Bronchi	1.79	5.01	6.62	4.47 \pm 2.46
Left Lobe	49.71	21.06	2.91	24.56 \pm 23.60
Cranial Lobe	1.32	5.40	4.21	3.64 \pm 2.10
Middle Lobe	2.35	19.96	0.92	7.74 \pm 10.60
Caudal Lobe	22.38	41.48	67.45	43.77 \pm 22.62
Accessory Lobe	0.20	4.86	0.03	1.70 \pm 2.74
Total	77.76	97.77	82.14	85.89 \pm 10.52

Table 3.4 Deposition pattern of F-Na delivered to the IPRL via intra-tracheal forced solution instillation. Percentage values represent calculated dye deposited to each lobar region expressed as a percentage of actual dose delivered to the lung. Data are expressed as mean \pm S.D, (n=3).

3.3.4. Validation of the IPRL – transport of a molecular weight range of fluorescent probes

In order to validate the suitability of the established IPRL setup for pulmonary transport studies, a molecular weight range of fluorescent probes were dosed to the IPRL. As can be seen in figure 3.8, the cumulative transport of F-Na across the IPRL initially displayed a more rapid rate of transport which began to decline to a slower rate at ~ 20 min onwards. Increasing nominal F-Na dose from 4 μg to 40 μg to 160 μg had no apparent effect upon F-Na transport, displaying no significant ($p>0.05$) increase in percentage deposited dose absorbed when increasing nominal F-Na dose.

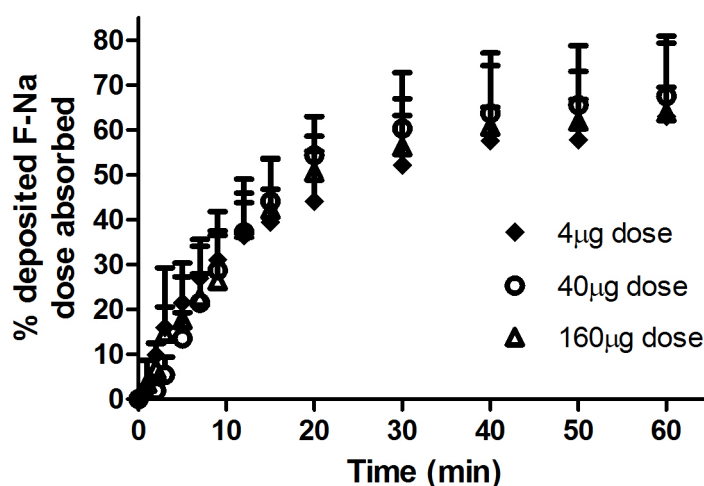


Figure 3.8 Cumulative % of deposited dose of F-Na absorbed with time across the IPRL. The transport of F-Na was not affected by dose escalation. Data shown are expressed as mean \pm S.D (n=3 for 4 μg dose, n=17 for 40 μg dose, n=3 for 160 μg dose).

From table 3.5, it can be seen that dose escalation of F-Na did not increase the percentage of deposited dose absorbed, and only increased cumulative mass absorbed in proportion to dose deposited. No significant ($p>0.05$) effect on initial k_{in} was observed.

Treatment (Nominal dose)	M_w (g.mol^{-1})	Stokes diameter (nm)	Cumulative mass of F-Na absorbed by 60 min(μg)	Percentage of deposited dose absorbed by 60 min(%)	k_{in} (min^{-1})
F-Na (4 μg)	396	1.5	1.56 ± 0.39	63.0 ± 16.4	0.027 ± 0.005
F-Na (40 μg)	396	1.5	26.44 ± 3.95	67.5 ± 13.4	0.037 ± 0.008
F-Na (160 μg)	396	1.5	103.86 ± 10.45	63.8 ± 5.7	0.040 ± 0.014

Table 3.5 Transport of airway administered F-Na dose across the IPRL. Increasing nominal dose of F-Na had no significant ($p>0.05$) effect on F-Na transport. Data are expressed as mean \pm S.D, (n=3 except F-Na 40 μg where n=17). k_{in} was determined from the initial linear portion of all absorption plots, all F-Na data in table 3.5 was determined by plate-reader assay.

Similarly, a molecular weight range of FITC-labelled dextran (FD) probes were also dosed to IPRL preparations. Figure 3.9 illustrates the cumulative transport of FD4, FD20 and FD70 over a 60 min period of time, in a contrasting manner to F-Na studies, M_w and not nominal dose was increased. Increasing the molecular weight of FITC-labelled dextran resulted in a disproportionate decrease in percentage probe absorbed.

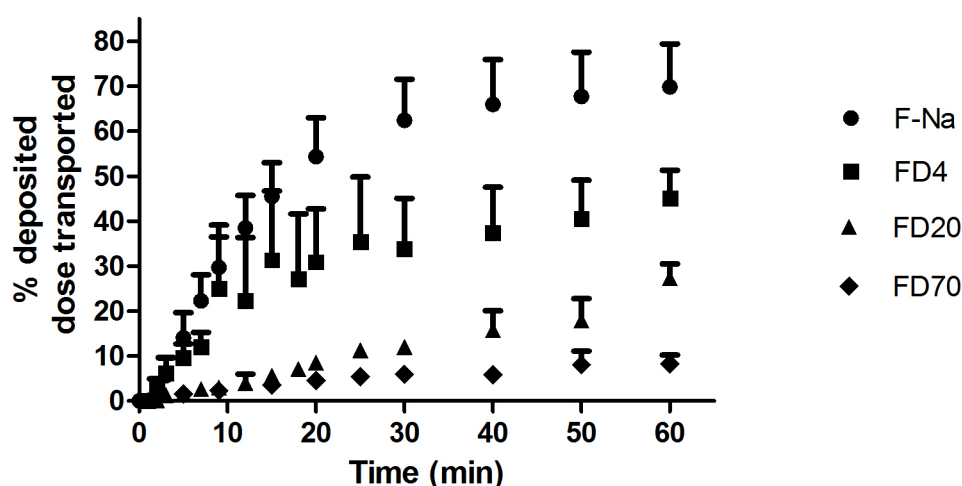


Figure 3.9 Cumulative % of deposited dose of FITC-labelled dextran absorbed with time across the IPRL. The transport of F-Na (40 μg) was included for reference. Data shown are expressed as mean \pm S.D (n=3, except n=17 for F-Na 40 μg dose).

Table 3. 6 illustrates that M_w escalation of FITC-labelled dextran affected the cumulative mass of FD absorbed, the percentage of FD absorbed and initial k_{in} . An increase in M_w from 3820 g.mol^{-1} to 20200 g.mol^{-1} (x5.29 increase) resulted in a x1.97 ($p < 0.05$) decrease in the percentage deposited dose absorbed by 60 min. An increase from 20200 g.mol^{-1} to 75090 g.mol^{-1} (x7.12 increase) in FD resulted in a x2.78 ($p < 0.05$) decrease in percentage deposited dose absorbed. Further, k_{in} for initial FD absorption also decreased with increasing M_w . However, only an increase in M_w from 3820 g.mol^{-1} to 20200 g.mol^{-1} , showed a significant ($p < 0.05$) decrease in initial k_{in} suggesting initial k_{in} to plateau with increasing M_w .

Treatment (Nominal dose)	M _w (g.mol ⁻¹)	Stokes diameter (nm)	Cumulative mass of FD absorbed by 60 min(μg)	Percentage of deposited dose absorbed by 60 min(%)	K _{in} (min ⁻¹)
FD4 (200 μg)	3820	2.8	95.01 ± 10.40	45.2 ± 6.2*	0.022 ± 0.013†
FD20 (200 μg)	20200	6.6	41.82 ± 7.20	23.1 ± 7.6*	0.004 ± 0.013
FD70 (200 μg)	75090	12	18.67 ± 6.27	8.3 ± 2.1*	0.002 ± 0.0002

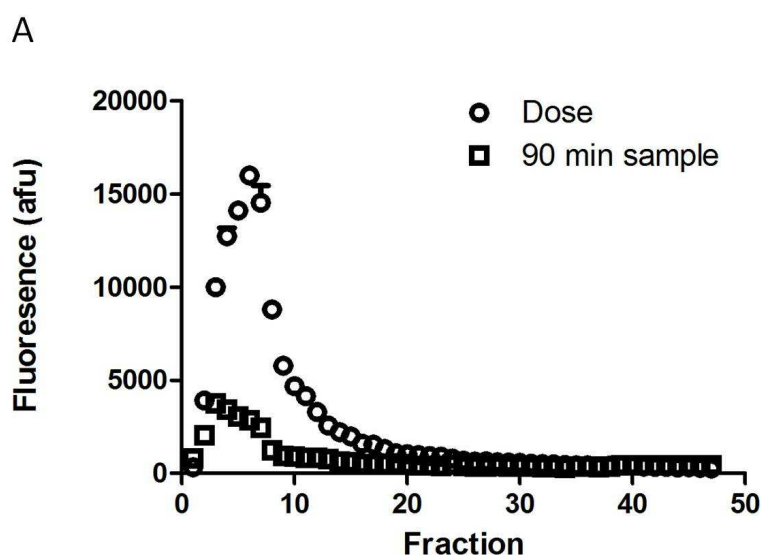
Table 3.6 Transport of airway administered FITC-labelled dextran across the IPRL. Data shown are expressed as mean ± S.D (n=3). K_{in} was determined from the initial linear portion of all absorption plots, all FD data in table 3.6 was determined by plate-reader assay.

*Percentage deposited dose significantly different (p<0.05) to all other FITC-labelled dextran probes in table 3.6

†K_{in} significantly different (p<0.05) to all other FITC-labelled dextran probes in table 3.6

3.3.5. Validation of the IPRL – gel filtration of FITC-dextrans

The potential metabolism of FITC-dextrans in the IPRL was investigated via gel filtration chromatography. Figure 3.10 A-C illustrate that, when transported through the IPRL and collected in perfusate, each FITC-dextrans probe only exhibited 1 peak when analysed fluorometrically. This suggests that it was the transport of FITC-dextrans as a whole that was being followed through the IPRL.



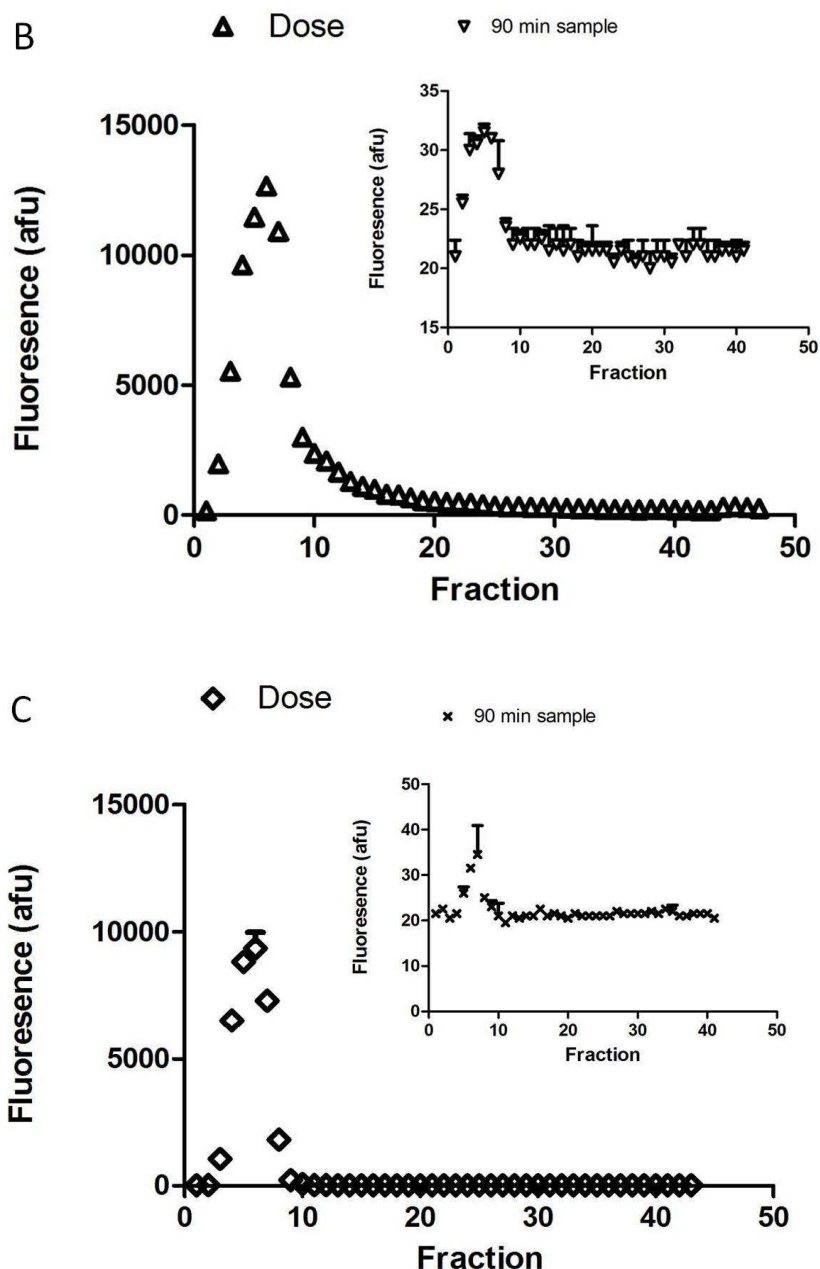


Figure 3.10 Gel filtration chromatography of FITC-dextran; pre IPRL dose solution and post IPRL 90 min perfusate sample. Figure 3.10A represents FD4 chromatography. Figure 3.10B represents FD20 and figure 3.10C represents FD70. A single peak can be observed for each sample. Data are expressed as mean \pm S.D. (n=3 for each sample).

3.3.6. Validation of the IPRL – determining IPRL viability by wet: dry weight

In order to assess the viability of the IPRL preparation following dosing by a forced solution instillation method, the lung wet: dry ratio of each IPRL performed was established. Table 3.7 illustrates the mean wet: dry ratio for each of the 'validation IPRLs' performed. A ratio of 4 and

below was considered to be normal i.e. no significant lung damage or oedema formation. Tissue water content was also established using the formula:

$$V_w (g / mL) = \frac{W_{wet} - W_{dry}}{W_{wet}}$$

Where:

Tissue water content (V_w); calculated assuming density of 1 g/mL

As can be seen in table 3.7, the value of wet: dry ratio and water content for each validation treatment does not vary significantly ($p > 0.05$) over the entire range of experiments performed, wet: dry ratio varying by 1.45 and tissue water content varying by 0.21 g/mL from lowest to highest data point, suggesting the IPRL to be reproducibly stable when meeting the wet: dry ratio criteria.

When examining the wet: dry ratio of failed experiments i.e. visual signs of lung damage/oedema formation, the mean ratio obtained was x3.39 higher than the mean ratio for successful experiments. As can be seen in table 3.7, both the lung wet: dry ratio and tissue water content of failed experiments was significantly different ($p < 0.05$) from all other experiments. Statistical difference was determined by a one-way ANOVA and post-hoc Duncan's test.

Treatment (Nominal dose)	Tissue wet weight (g)	Tissue dry weight (g)	Wet: Dry ratio	Tissue water content (g/mL)
F-Na (4 µg)	2.16 ± 0.93	0.64 ± 0.26	3.49 ± 1.00	0.70 ± 0.09
F-Na (40 µg)	2.38 ± 1.04	2.43 ± 3.12	2.96 ± 1.28	0.55 ± 0.29
F-Na (160 µg)	1.83 ± 0.58	0.49 ± 0.23	3.98 ± 0.62	0.74 ± 0.04
FD4 (200 µg)	3.37 ± 1.24	1.36 ± 0.13	2.51 ± 0.93	0.53 ± 0.25
FD20 (200 µg)	1.07 ± 0.48	0.31 ± 0.04	3.50 ± 1.56	0.65 ± 0.20
FD70 (200 µg)	1.73 ± 0.20	0.49 ± 0.12	3.59 ± 0.38	0.72 ± 0.03
Failed Experiment	2.39 ± 0.84	0.22 ± 0.10	11.32 ± 2.27*	0.91 ± 0.02†

Table 3.7 Calculated lung wet: dry ratio and water content of rat lung tissue determined by lyophilisation subsequent to an IPRL procedure. Data shown are expressed as mean ± S.D (n=3 for F-Na treatment except F-Na 40 µg where n=11, n=3 for FITC-labelled dextran treatment, n=4 for 'failed experiment').

*Wet: Dry ratio significantly different ($p < 0.05$) to all other fluorescent probes in table

†Tissue water content significantly different ($p < 0.05$) to all other fluorescent probes in table

3.3.7. Relationship between absorption rate and molecular weight across the IPRL

The principal aim of this chapter was to assess the suitability of the IPRL to the examination of pulmonary transport; therefore, the relationship between initial absorption and molecular weight of each probe dosed to the IPRL was examined. Figure 3.11 illustrates the relationship between initial transport rate (k_{in}) and the size related characteristic Stokes' diameter. The observed decrease in initial k_{in} with increasing Stokes' diameter demonstrating the molecular size dependent transport of the fluorescent probes examined.

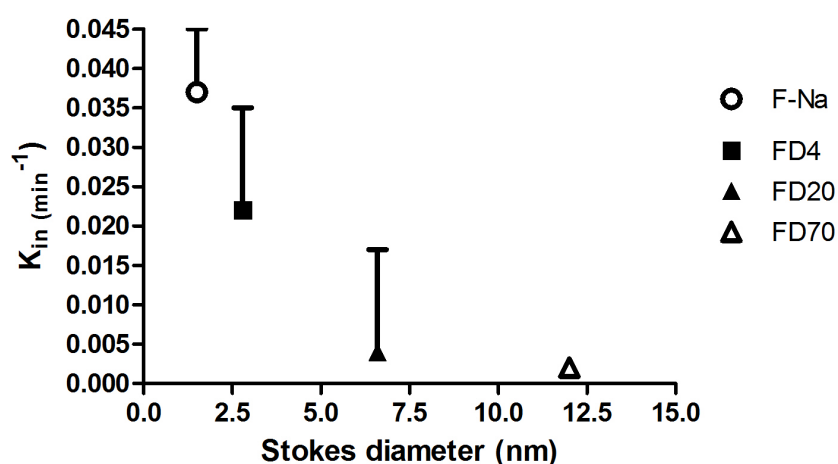


Figure 3.11 The relationship between initial transport rate (k_{in}) and Stokes' diameter of four fluorescent probes; illustrating the influence of M_w upon initial absorption across the IPRL. (F-Na - M_w 396, FD4 - M_w 3820, FD20 - M_w 20200, FD70 - M_w 75090). k_{in} was determined from the initial linear portion of each cumulative transport curve. All data are mean \pm S.D., (n=3 except F-Na where n=17).

3.4. Discussion

Investigation of the pulmonary route of administration as an alternative, non-parenteral route of delivery for macromolecules to the systemic circulation has advanced greatly in recent times and will likely break new ground in aiding the development of new non-invasive therapeutic treatments. Further, the pulmonary disposition for many low molecular weight drugs remains unknown but whose pharmacokinetics in the lung is important for local pulmonary pharmacology. From this perspective, the development of suitable models of the pulmonary system to examine drug transport is of great significance and has led to the development of an *ex vivo* isolated perfused lung model that accurately fulfils the required criteria [8, 22].

Primarily, this chapter focussed on the development and validation of an *ex vivo* isolated perfused rat lung model. The inherent nature of this isolated perfused rat lung model, developed from that of Byron *et al.* [95, 96], creates an accurate representation of the *in vivo* state while allowing full control of experimental parameters, maintenance of tissue architecture and importantly, affords sufficient determination of the pharmacokinetic parameters involved in pulmonary absorption.

In order to ensure the applicability of the IPRL to the study of drug transport across the lung, a number of experiments were conducted to allow full validation of this lung model. Validation included examination of the extent to which BSA contributes to background fluorescence in IPRL perfusate, determination of the reproducibility of the forced instillation dosing method; both in terms of dose deposition and amount of dose retained in equipment post-dosing, validation of the model as an instrument to examine pulmonary drug transport, i.e. through studying transport of a molecular weight range of fluorescent probes, and establishing the viability of each IPRL preparation post-dosing.

The addition of BSA to IPRL perfusate is regarded as a critical addition in order to protect the lung from the development of pulmonary oedema [83]. Fisher and colleagues illustrated a 2.47 to 5.25 – fold decrease in time to oedema formation with the addition of 3 % BSA to perfusate in their isolated rat lung preparation [332]. Further, the presence of albumin at the vascular lumen is well accepted to modulate protein permeability in pulmonary microvascular beds and Czartolomna and colleagues illustrated a >120 % increase in lung ‘permeability - surface area product’ (vasculature to lung) when replacing perfusate BSA with a synthetic alternative in perfused lungs; suggesting the importance of albumin inclusion in perfusate [333].

The illustrated importance of BSA inclusion in IPRL perfusate reflects the importance of its contribution to oncotic pressure and indeed contribution to drug transport/absorption where a drug

is influenced by albumin binding capacity. The perfusion media used in this chapter was prepared with 4 % BSA, in line with previous reports of perfusate BSA concentration by users of the 'Byron *et al.*' model [95, 334]. Whilst the inclusion of BSA to perfusate was unquestionable, it was sought to clarify the extent to which this inclusion contributed to background fluorescence and therefore limited the ability to detect fluorescence-emitting molecules using non-chromatographic methods. As can be seen in table 3.1, both the Biosera and Sigma BSA products displayed much higher background readings than perfusate minus BSA, demonstrating that the inclusion of any BSA will reduce the limit of quantitation by potentially masking compound fluorescence readings. Of the two products, it was the Sigma BSA that provided the lowest background fluorescence, with a reading 13.7-fold higher than perfusate not possessing BSA. The Biosera BSA provided background fluorescence x9.0-fold higher than perfusate not possessing BSA. This obvious difference in generated background fluorescence highlighted the Sigma BSA as product of choice for perfusate inclusion. Further, within the literature, this exact product has been previously included in IPRL perfusate [334]. Of the two BSA products, Sigma BSA is also of higher quality than Biosera BSA and has also been dialysed, reducing its fluorescence. These results confirmed the selection of the Sigma BSA for all subsequent IPRL experiments.

The novel dosing method employed in this and subsequent chapters has been utilised previously and was first exploited in the isolated lung preparation by Byron & Niven in 1988 [96]. During its establishment, this method was successfully validated and proved to give highly reproducible dosing in terms of both delivered dose and fraction of dose reaching the lobar lung [96]. This forced instillation technique has now been extensively utilised in published IPRL work addressing solute transport across the rodent lung; an excellent literature database is provided for reference and comparison when validating the dosing method used in the current work [324-327, 335, 336].

Validation of the forced solution instillation dosing method was undertaken to ensure the technique was complete and reproducible. Lung deposition pattern, together with reproducibility in amount of dose delivered, was examined whilst employing dosing method to 'test' IPRL procedures. The major constituent parts of the forced solution dosing method, i.e. a dosing cartridge extended to the rat trachea allowing expulsion of a dose via a propellant only pMDI, creates a proficient dosing method capable of efficient dosing to the deep lung. The custom made dosing rod aids in removing dosing inconsistencies by offering a set dose volume to the same position in subsequent preparations, further, the MDI actuator influences particle size and thus lung deposition via its nozzle diameter and the non-toxic MDI propellant aids in delivery by reproducibly inflating the lungs by a set volume

[337]. From this, the custom dosing system introduces a coarse spray with enough force to reach the deep lungs including reaching the extensive absorptive area offered by the alveolar region [337].

The technique also allows determination of the exact dose deposited by the collection of drug retained in the dosing rod and tracheal cannula. Through implementing a number of validation techniques, the results of this chapter found the forced solution instillation procedure delivered approximately 86 % of a nominal dose of test substrate to the tissue of the IPRL preparation. Such percentages of drug delivered mirror that of other data reported in the 'Byron IPRL', for example, Sakagami *et al.* reported delivery of 94.7 ± 1.7 % of a 0.02 mg F-Na dose introduced to the IPRL via the forced instillation procedure [101]. As can be seen in table 3.2, only 5.74 ± 1.40 % of a 40 μ g F-Na dose remained in dosing equipment after deployment of dose to the IPRL. Further, as is illustrated in figure 3.6, the majority of remaining dose was found in the tracheal cannula indicating that a small percentage (2.53 ± 1.52 %) of dose suffered impaction at the first bifurcation of the conducting airways with subsequent rebound into the tracheal cannula.

The distribution of expelled dose within the lung was examined by introduction of Evans blue and F-Na by the forced instillation method. While the dosing of Evans blue provided a visual distribution pattern to the lobar lung (Figure 3.7B) poor tissue extraction of the dye rendered the results unreliable. As can be seen in table 3.4, the distribution of F-Na dosed to the IPRL is constrained almost exclusively to the lobar region of the lung. The results illustrate poor reproducibility in terms of intra-lobular deposition in certain lung lobes; however, what is consistent is the percentage of dose delivered to the trachea and major bronchi suggesting similar consistency in delivery to the lobar lung as a whole. In a similar manner, Sakagami *et al.* also investigated the initial distribution of F-Na in an IPRL following forced solution instillation. While the presence of dose in specific lobar regions illustrated variability, again the percentage of dose deposited to the trachea was consistent. Further, when comparing *in vivo* and *ex vivo* (IPRL) dose distribution following forced solution instillation, Sakagami *et al.* reported little difference in the deposition patterns, highlighting that dose deposition in the IPRL can accurately represent deposition *in vivo* [101].

The findings of the dosing equipment validation experiments performed in this work gave assurance to the forced solution instillation dosing strategy. Further, in their validation of this dosing strategy, Byron and Niven reported no significant difference in F-Na absorption half-life determined with either forced instillation technique or instillation via syringe suggesting the forced instillation technique not to damage lung integrity and therefore influence substrate absorption. In addition to this, the establishment of accurate and reproducible dosing to the absorptive surfaces of the lobar

lung gives further confidence to the IPRL preparation as a whole in the examination of pulmonary drug absorption [96].

In order to provide support to accurate data interpretation, gravimetric analysis of IPRL tissue post-preparation was conducted. Together with the continuous monitoring for visual signs of pulmonary oedema, the analysis of tissue wet: dry weight has been extensively used to determine tissue viability [101, 338, 339]. Through ascertaining lung wet: dry weight post-IPRL and assuming that increase in tissue weight implied alterations in physiology such as oedema formation, each IPRL preparation was investigated to ensure that no significant tissue damage was induced by the forced instillation of any test substrate to the lung.

As is illustrated in table 3.7, the calculated wet: dry ratio of validation IPRL preparations deemed to be viable varied only between 2.51 ± 0.93 and 3.59 ± 0.38 while the mean wet: dry ratio of unviable preparations was 11.32 ± 2.27 , a statistically significant increase. A number of studies have established that average lung water content is ~80 % providing a wet: dry ratio of ~4 [338], a ratio beyond which no 'validation IPRL' exceeded. Further, when displaying wet: dry weight as lung water content, all 'validation IPRLs' displayed a water content of between 0.53 ± 0.25 g/mL and 0.74 ± 0.04 g/mL, a range comparable to that reported in the literature [339-342]. Performance criteria such as this gave assurance that pulmonary oedema did not alter tissue physiology or the absorption characteristics of the drugs.

The study of drug transport across the lung follows the complex processes of drug deposition, passive and active absorption, metabolism and tissue binding and the interplay of host defences. Because of such complex, region-specific processes, it is experimentally difficult to analyse the kinetic expressions associated. One of the more universal descriptors of pulmonary absorption is substrate absorption rate. Within this chapter, an IPRL lung permeability profile using a range of varying molecular size hydrophilic probes was constructed and the establishment of initial absorption rate, amongst other characteristics, determined. The choice of F-Na and FITC-labelled dextran probes for validation was based upon the properties of these solutes. Chosen probes were hydrophilic and known to be non-metabolised, -degraded, -tissue bound nor sequestered in the lung [325, 326, 335, 336, 343]. The probes F-Na and FD4 are also known to be passively transported across the lung *in vivo* and *in vitro* therefore signifying pulmonary region-specific absorption to be dose independent [344].

The cumulative percentage transport curves for F-Na across the IPRL, figure 3.7, illustrate no dose dependency in transport, indicating a passive absorption mechanism. Despite dose escalation, the

percentage deposited dose absorbed by 60 min was $\sim 64\%$ ($63.0 \pm 16.4 - 67.5 \pm 13.4$) across the dose range. Sakagami *et al.* also report dose independent transport of F-Na across their IPRL and witnessed a similar $\sim 60\%$ transport of deposited dose 60 min post-dosing [101]. The calculation of initial absorption rate (k_{in}) from the linear portion of cumulative transport curves show F-Na to demonstrate k_{in} of 0.027 ± 0.005 to $0.040 \pm 0.014 \text{ min}^{-1}$ across the IPRL, corresponding closely to those within the literature [95, 96, 101].

When examining the transport of FITC-labelled dextran across the IPRL, an inverse relationship with molecular weight was observed. As can be seen in figure 3.9, increasing molecular weight of probe administered to the IPRL whilst maintaining the same dose, resulted in a decrease in the percentage deposited dose absorbed by 60 min. There was also a general trend for the initial rate of transport, k_{in} , to decrease with increasing molecular weight of solute. Together, the transport data of F-Na and FD's across the IPRL, i.e. the smaller F-Na traversing faster than FD4 etc, suggest macromolecule absorption to be somewhat influenced by diffusion. The data is also consistent with the recognition that the lung generally shows higher permeability compared to other mucosal barriers [46]. Previous efforts have been made to consolidate lung permeability data and expose specific trends. Throughout the literature, there are many instances of molecular size influencing transport across the lung, [35, 101, 345-347]. In 1983, Effros and Mason compiled available data for solutes of ≤ 500 kDa and reported that permeability of the lung to a wide molecular weight range of solutes displayed a linear relationship between the absorption rate as a dependent variable (k_{in} in this chapter) and $\frac{1}{\sqrt{MW}}$ as an independent variable. Note that comparison of $\frac{1}{\sqrt{MW}}$ between each solute approximates to relative free diffusion coefficients as defined by Stokes' equation [36]. The F-Na and FD data in this chapter agree with this trend and figure 3.11 highlights that an increase in Stokes' diameter resulted in a decrease in initial absorption across the IPRL.

The permeability of the lung to such an extensive molecular weight range of hydrophilic solutes is widely regarded and the results of this chapter confirm and complement such findings. Within the IPRL, the absorption of test probes examined appears to conform to a first-order rate, as determined from cumulative absorption curves. This again conforms to the literature database where works such as that of Niven and Byron [96] report passive absorption from the airway to be a first-order process.

The agreement of data generated from this IPRL to that within the wider literature allow several assumptions to be made regarding this model. Firstly, together with advanced kinetic modelling, the IPRL can allow accurate and reliable examination of complex disposition mechanisms, clarifying the

contribution of each [23]. Secondly, the accurate control of experimental parameters and the confirmation that dosing method and dose distribution echo that of *in vivo* state give confidence to IPRL generated data and to data interpretation.

Overall, the principal aim of this chapter was to create a valid lung model for examining pulmonary delivery. The results of this chapter confirm the IPRL and its custom dosing method to fulfil this criterion allowing for research into the understanding of pulmonary absorption and examination of the processes involved.

Chapter 4

Functional significance of an active drug transporter (P-gp) upon the substrates delivered to the Isolated Perfused Rat Lung

4.1. Introduction

The applicability of the lung as a drug delivery route presents obvious advantages in providing local delivery for drugs acting in the lung; enabling reduced drug dosage to the patient, while maximising local beneficial effects and minimising systemic adverse effects. Further, it presents a non-invasive (i.e. avoiding injection) route of administration for the systemic delivery of drugs, and in doing so, bypasses hepatic first-pass metabolism, and provides for the potential for the rapid onset of drug action. The intrinsic biological properties of the lung, e.g. large epithelial surface area, together with the advances made in aerosol science and device technology continue to promote the lung as an important route of drug delivery [20, 22, 41, 348, 349].

The airways of the lung represent a series of bifurcations of decreasing luminal diameter, the epithelial surface of which undergoes marked morphological transition from the trachea and major bronchi through to the terminal bronchioles and into the gaseous exchange region of the alveoli. This complex branching system with the differing nature of the epithelial barrier means that the extent of lung epithelial transport for any given inhaled drug dose is highly dependent upon the variable patterns of inhaled aerosol deposition. Beyond this, a number of complex biological barriers protect the lung from the external environment. These include the secretion of mucus onto the epithelial surface within the conducting airways of the lung affording subsequent clearance of any deposited particles through the actions of the mucociliary escalator. Further, macrophages within the lung undertake phagocytosis to remove any inhaled particulates not cleared by the mucociliary barrier [18, 21, 22, 350].

Drug transporters expressed within the lung epithelial cells can clearly influence drug transport across the lung epithelium, with transported drug reaching the submucosal tissue for localised effects or progressing to the blood capillaries giving rise to systemic absorption. It is increasingly apparent that the expression of drug transporters within lung epithelium varies throughout the conducting and gaseous exchange regions of the lung [351]. It follows that the pattern of deposition of inhaled drug within the lung will influence the exposure of drugs to any particular transporter. For example, the neonatal transporter for IgG, i.e., FcRn, appears to be predominantly expressed within the epithelium of the larger airways, and as such, delivery of antibodies via the lung for the purposes of systemic absorption would benefit from targeting the larger proximal airways rather than the more peripheral distal airways. Indeed, Bitonti and Dumont have successfully shown proof of concept and have reported delivery of erythropoietin-Fc by inhalation via an immunoglobulin

transport pathway; they have also successfully experimented with other Fc-fusion proteins of therapeutic relevance [22, 352, 353].

For low molecular weight drugs inhaled into lungs for the purposes of local therapeutic benefit or for the purposes of achieving systemic absorption, it is the impact of drug transporters belonging to the ABC and SLC/SLCO superfamilies of membrane transporters that will be of potential importance. There exists increasing literature providing evidence localising several drug transporters to the lung. For instance, Bosquillon has reviewed the varying expression of a number of ABC, SLC and SLCO transporters in the human lung [354]. Endter *et al.* [104] have reported the presence of selected ABC, SLC and SLCO transporters in human lung epithelial cell models and Bleasby *et al.* [69] have investigated the presence of 50 known xenobiotic transporters in human tissues and reported 32 of the examined transporters to display > 25 % absolute intensity within the human lung as determined at the level of mRNA [69].

Amongst the number of documented drug transporters with a recognised presence within the lung, the ABCB drug transporter P-glycoprotein/MDR1 (P-gp) is perhaps the most researched. P-gp is 170 kDa glycosylated membrane bound protein and, in consensus with the majority of ABC transporters, is comprised of two homologous domains coupled together by a linker region [128].

P-glycoprotein is expressed in a variety of biological barriers, including most notably the liver and epithelial cells of kidney and intestine as well as the brain microvascular cells of the blood-brain barrier. It is apparent that this pattern of expression for P-gp can have a profound effect upon the absorption, distribution and elimination of drugs. P-gp is widely expressed within the body, for example, Bleasby *et al.* [69] reported the presence of P-gp at > 25 % absolute intensity in half of the 40 human tissues and organs examined. P-gp has attracted much attention as an efflux transporter due to its ability to efflux a plethora of structurally unrelated, clinically relevant substrates [69, 129, 352]. Table 4.1 illustrates a selection of these clinically relevant substrates, in turn highlighting the implicated importance of P-glycoprotein within the fields of drug discovery, drug delivery and pharmacokinetics.

	Anti-Cancer drugs	Antibiotics	Antiemetics	Cardiac Drugs	Ca²⁺ Blockers	β-Blockers	CNS Drugs
Substrate	Daunorubicin Irinotecan Paclitaxel Topotecan Doxorubicin Mitomycin C Tamoxifen Vinblastine Doxetaxel Mitoxantrone Tenoposide Vincristine	Cefazolin Cefoperazone Erythromycin Levofloxacin	Domperidone	Amiodarone Digitoxin Digoxin Propafenone Quinidine	Diltiazem Mibefradil Nicardipine Verapamil	Bunitrolol Celiprolol Talinolol	Perphenazine Phenoxazine Phenytoin
	Antihistamines	HIV Protease Inhibitors	Immuno-Suppressants	Lipid Lowering Drugs	Morphins	Steroids	
Substrate	Fexofenadine Terfenadine Cimetidine Ranitidine	Amprenavir Indinavir Nelfinavir Ritonavir	Cyclosporine Tacrolimus	Atorvastatin Lovastatin Simvastatin	Morphine Loperamide	Aldosterone Dexamethasone Hydrocortisone	

Table 4.1 Several clinically relevant examples of substrates of the ABCB family transporter P-gp. Substrates are structurally and functionally diverse highlighting of the importance of P-gp in pharmaceutical research. Adapted from [162, 355].

Although P-gp substrates represent a diverse range of therapeutic and chemical properties, the localisation of the substrate binding sites for P-gp to the interior of the plasma membrane results in P-gp substrates generally displaying hydrophobic properties. The molecular size of molecules does not appear to be highly influential as a limiting factor in P-gp transport and a size range of ~ 200 – 1900 Da is common [129]. The hydrophobic nature of P-gp substrates required to access P-gp binding sites from within the membrane bilayer also provides for a unique balance of factors that determine the impact of P-gp efflux upon overall epithelial or endothelial transport. The factors promoting P-gp efflux would include; a higher expression of P-gp in the biological membrane, a higher affinity of drug for P-gp, a drug displaying lower intrinsic passive membrane permeability, i.e., P-gp efflux is able overcome more readily the drug's passive membrane permeability. Conversely, factors diminishing the role of P-gp efflux would include; a lower expression of P-gp in the biological membrane, a lower affinity of drug for P-gp, a drug displaying higher intrinsic passive membrane

permeability, i.e., P-gp efflux is less able to overcome the drug's passive membrane permeability [129, 356]. A further consequence of the above is that the inhibition of P-gp will provide increased availability of a drug substrate to cross the biological barrier and reach its target site.

Initially, the development of modulators for P-gp was sparked by the desire to overcome P-gp associated multi-drug resistance in cancer cells [357, 358]; however, wider applicability soon became apparent. Early recognised inhibitors of P-gp, such as verapamil, served as poor substrates but nevertheless competitive inhibitors. However, such 1st generation P-gp inhibitors often exerted their own pharmacological effects upon the body, e.g., verapamil and cardio-toxicity, thus limiting their applicability as clinical P-gp inhibitors. Successive generations of P-gp modulators were then developed with the aim of optimising specificity and action [129]. Inhibitors of P-gp can be classified into one of three generations, First generation inhibitors - clinically active drugs with pharmaceutical roles other than the inhibition of P-gp but which are also known to exhibit P-gp inhibitory activity. Second generation inhibitors – where the off-target pharmacology of first-generation inhibitors was reduced as the molecules were engineered to display increased affinity for P-gp. Third generation inhibitors – novel P-gp modulators, manufactured with high P-gp specificity and low toxicity [357]. Table 4.2 lists examples of known P-gp inhibitors.

	P-gp modulators
1st Generation	Cyclosporine A Verapamil Quinidine Tamoxifen Toremifene Reserpine Yohimbine
2nd Generation	SDZ PSC833 (Valspodar) S9788 R-verapamil VX-710 VX-853 MS-209 PSC-833
3rd Generation	GF120918 (Elacridar) OC144-093 (Ontogen) XR9576 (Tariquidar) LY335979 (Zosuquidar)

Table 4.2 Selected P-gp specific transport modulators. Adapted from [358, 359].

The broad substrate specificity and diverse expression profile displayed by P-glycoprotein implies a role in defence through extrusion of xenobiotics. It therefore follows that P-glycoprotein present in the lung would also fulfil this implied protective role. P-glycoprotein expression throughout the respiratory system has become increasingly well documented. In the human lung alone, P-gp has been localised to a number of cells at an mRNA and protein level. For example, MDR1-P-gp has been localised to bronchial epithelial cells, bronchial capillary endothelial cells, alveolar epithelia and alveolar macrophage [43, 104, 108, 110, 112]. Further, the transporter has been immunohistochemically localised to both the apical and basolateral membrane of nasal ciliated epithelial cells [109], epithelial cells of the trachea and bronchi [108] and also epithelial cells of the distal lung. Campbell *et al.*, immunohistochemically displayed P-glycoprotein in human AEI cells but not AEII and also paralleled this work in rat alveolar epithelia [137]. Further, these authors demonstrated polarised P-gp function in the alveolar epithelial cells effluxing P-gp substrate into what would be the luminal or airway surface. Functional P-glycoprotein efflux has also been reported to be present in the intact rabbit lung through use of an isolated lung preparation. Here Roerig *et al.*, observed accumulation in the lung of the P-glycoprotein substrate, rhodamine 6G, as determined by monitoring the disappearance of rhodamine 6G from circulating perfusate. The accumulation in the lung was increased by the introduction of the P-glycoprotein inhibitor, GF120918, into the perfusate [355]. This data of Roerig *et al.* is indicative that there is an efflux mechanism that hinders transport of drug from blood into the lung. It is yet to be confirmed by other investigators in an intact isolated lung model, however, it is of note that there are conflicting results regarding studies conducted in *mdr1a/mdr1b* knockout mice, where following parenteral or oral administration, a range of P-gp substrates have shown a greater lung accumulation of these P-gp substrates over that in wild-type normal mice [360-362].

Demonstration that P-gp in the lung can affect lung epithelial transport would have significance for airway residence and systemic absorption of P-gp substrates administered by the inhaled route and also for the accumulation from the systemic circulation of P-gp substrates administered by non-pulmonary routes.

Aims and Objectives

In this chapter, it will be sought to:

- Investigate the functional expression of P-glycoprotein in the intact isolated perfused rat lung through examining the pulmonary absorption pharmacokinetics of a P-gp substrate and the impact of chemical modulation of P-gp activity.
- The use of an *ex vivo* isolated perfused rat lung model will be employed to achieve maintenance of tissue structure and function while excluding the whole body disposition issues that can complicate *in vivo* pharmacokinetic studies.
- It is hypothesised that the model will provide for a higher level of precision and will permit the use of a novel dosing mechanism to the lung, which has been validated and utilised in a previous chapter.
- In order to demonstrate the functional significance of P-glycoprotein, a number of P-glycoprotein substrates (rhodamine 123, digoxin, and flunisolide) will be instilled into the airways of the IPRL.
- Further, the known P-gp inhibitor GF120918 will be co-instilled in a parallel treatment arm to illustrate inhibition of an active efflux process.
- It will also be aimed to address the issue of P-gp upon lung accumulation; examined by investigating the perfusate to lung accumulation of rhodamine 123 and the subsequent affect of GF120918.

4.2. Materials and Methods

4.2.1. Materials

Consumables and reagents

Rhodamine 123; Rh123, >98 % electrophoresis grade, (Sigma-Aldrich, Dorset, UK, Cat: R-8004)

Sodium fluorescein; F-Na, (Fluka, Sigma-Aldrich, Dorset, UK, Cat: 46960)

Acetonitrile; ACN, 99.6+ %, HPLC grade, (Fisher Scientific, Loughborough, UK, Cat: A/0626/17)

Sodium acetate buffer, 20 mM, pH 3.6/pH 4.0, (Fisher Scientific, Loughborough, UK, Cat: BPE334- 500)

GF120918; obtained from GlaxoSmithKline, Stevenage, UK.

Flunisolide, (Sigma-Aldrich, Dorset, UK, Cat: F5021-100MG)

Formic acid, 98+ %, (Acros Organics, Fisher Scientific, Loughborough, UK, Cat: 14793-2500)

Dimethyl sulfoxide; DMSO, BioReagent, for molecular biology, ≥99.9 %, (Sigma-Aldrich, Dorset, UK, Cat: D8418-50ML)

HPLC grade H₂O, (Fisher Scientific, Loughborough, UK, Cat: W/0106/PB17)

IPRL perfusate incl. bovine serum albumin; BSA, (Sigma-Aldrich, Dorset, UK, Cat: A7906-1kg; See chapter 3)

HPLC System

Thermo Finnigan™ SpectraSYSTEM™ (Thermo Scientific, Loughborough, UK)

Solvent degasser - SCM1000

Injector - AS3000

Pump - P2000

UV - UV2000

FL - FL3000

HPLC Column

4 µm Genesis C18 column, (Grace, Illinois, USA).

IPRL equipment

Perfusate lines: Masterflex 96400-14 peroxide cured, (Fisher Scientific, Loughborough, UK, Cat: PMM-505-515G)

Peristaltic pump: Gilson, Inc., (Middleton, WI, USA, Model: Minipuls 3)

Radiochemicals and associated material

Digoxin, [$^3\text{H}(\text{G})$]-, 1 mCi/mL, specific activity 15-40 Ci/mmol, (PerkinElmer, USA, Cat: NET222250UC)

Mannitol, D-[1- ^{14}C]-, 0.5mCi/mL, specific activity 45-60 mCi/mmol, (PerkinElmer, USA, Cat: NEC314250UC)

Scintillation cocktail high performance ScintiSafe 3 (formally known as Optiphase Hi-safe 3) liquid scintillation counting, (Fisher Scientific, Loughborough, UK, Cat: SC/9205/21)

Scintillation vials, (Fisher scientific, Loughborough, UK, Cat: FB72435)

Animals – Cardiff University

Male-specified pathogen-free Sprague-Dawley rats (Harlan UK Limited, Bicester, UK) were used throughout and housed in rooms controlled between 19 °C – 21 °C and 40-60 % humidity with dark-light cycling every 12 h. The animals had free access to food and water and were acclimatised for at least 2 days prior to experimentation. All animal experiments adhered to the Animal (Scientific Procedures) Act 1986, UK and were approved by Cardiff University.

Animals – GSK

Male Sprague-Dawley rats were used throughout. All animals were housed in standard holding cages. Water and food were available *ad libitum* throughout the study. All animal experiments adhered to the Animal (Scientific Procedures) Act 1986, UK and were approved by GlaxoSmithKline R&D, Stevenage.

4.2.2. HPLC analysis: Rh123/F-Na analytical method development**Method**

In order to effectively analyse Rh123 and F-Na in perfusate samples post dosing to the IPRL, an analytical method utilizing High Performance Liquid Chromatography (HPLC) was developed. Further to this, method precision, accuracy and limit of substrate quantitation were assessed.

Method development

Substrate	Mobile Phase	Ratio (%)
Rh123	Acetonitrile	50
	dH ₂ O	30
	20 mM Sodium acetate buffer (pH 4.0)	20
F-Na	Acetonitrile	45
	dH ₂ O	45
	20 mM Sodium acetate buffer (pH 3.6)	10

Mobile phase developed from Iqbal *et al.*, 2005 [363]

In order to establish the correct wavelength for solute detection, Rh123 (1 µg) was spiked into the appropriate mobile phase and fluorometrically scanned using a spectrofluorometer (Aminco-Bowman; SQ-340). An excitation scan was performed with wavelength ranging 300 – 600 nm and an emission scan performed using a wavelength range of 450 – 650 nm. Figure 4.1 represents the resulting excitation and emission spectra obtained.

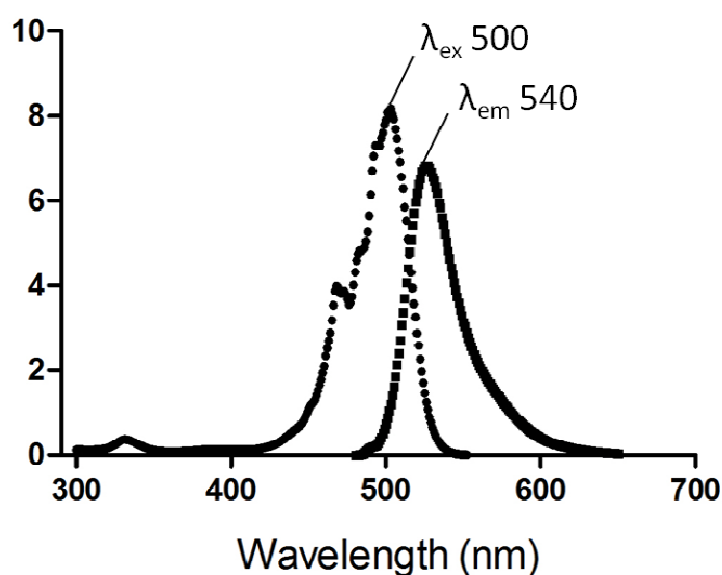


Figure 4.1 Excitation and Emission spectra for Rh123 in mobile phase. (● - Excitation spectrum, ■ - Emission spectrum).

From figure 4.2, subsequent solute concentrations were determined fluorometrically, Rh123 analysis undertaken at λ_{ex} 500 nm, λ_{em} 540 nm and F-Na analysis undertaken at λ_{ex} 485 nm, λ_{em} 520 nm (established from Chapter 3).

Rh123 and F-Na samples (0.1 mL) were separately injected onto a 4 μm Genesis C18 column (Grace, Illinois, USA) and mobile phase was pumped through the HPLC system at an isocratic flow rate of 1 mL/min with chromatic measurements being performed at room temperature. Run time for Rh123 and F-Na was 10 min Chromatogram peak asymmetry of $\sim 65 - 135\%$ was accepted and solute retention time was determined as ~ 2.5 min for Rh123 and ~ 3.5 min for F-Na. Figure 4.2 illustrates a typical Rh123 chromatogram.

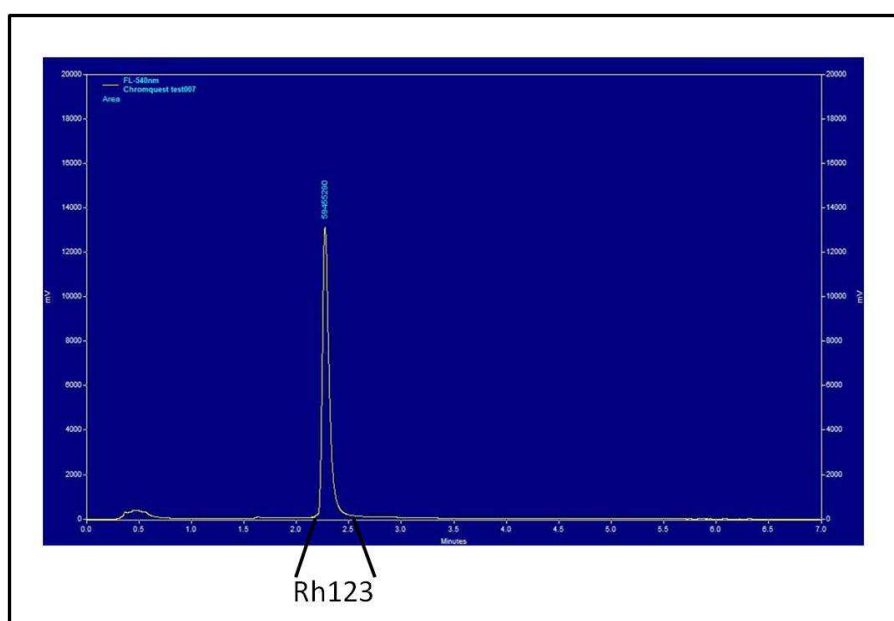


Figure 4.2 Example of a HPLC chromatogram produced by Rh123 sample.

HPLC chromatography of IPRL perfusate that had been circulated through rat lungs was compared to Rh123/F-Na chromatography to ensure no interference in solute chromatograms as a result of the perfusate recirculation.

Precision and accuracy

While assays were initially developed with solute dissolved in mobile phase, the assay required that solute be analysed from perfusate.

Deproteinisation was undertaken with the addition of acetonitrile (3:1 v/v Acetonitrile: Perfusate sample). Samples were then equilibrated for 1 h at 37 °C and kept in darkness to avoid sample bleaching. Each sample was subsequently centrifuged for 10 min at 18,000 g and the deproteinated sample supernatants (0.1 mL) were injected onto the HPLC column for quantitation.

Deproteinated perfusate including the presence of spiked Rh123 or F-Na was injected onto the HPLC according to the above assays and subsequent chromatograms were deemed acceptable. In order

to assess solute assay precision, Rh123 was spiked into three separate IPRL perfusate samples and a calibration curve prepared from the serial dilution of each. A concentration range of 0.025 µg/mL to 0.5 µg/mL Rh123 was prepared. Three separate F-Na calibration curves were prepared in a similar manner, concentration range 0.01 µg/mL to 1 µg/mL. Once sample concentrations were determined and individual calibration curves constructed, the coefficient of variation (C_v) for each triplicate concentration point was determined and represented as a %. A percentage of $\leq 15\%$ was deemed acceptable.

Together with assay precision, the accuracy of the assay was also determined. Three individual samples of Rh123 in IPRL perfusate were prepared at three varying concentrations. This was repeated for F-Na. Samples were prepared by spiking Rh123 or F-Na to perfusate and diluting to the concentrations; 0.25 µg/mL, 0.0625 µg/mL, 0.025 µg/mL. Each sample was deproteinated as above, and concentration determined fluorometrically by HPLC. Actual sample concentration (as determined by HPLC) was compared to theoretical (intended sample concentration) and accuracy determined. Accuracy of $\geq 80\% - 120\%$ (Theoretical/Actual * 100) was deemed acceptable [364].

Limit of detection

In order to establish assay lower limit of detection (LLD) and thus establish lower limit of quantitation (LLQ), a range of Rh123 concentrations were prepared by spiking Rh123 to IPRL perfusate and were deproteinated as above. Again, this was repeated for F-Na. Each set of samples was fluorometrically analysed via HPLC and the lowest detectable concentration determined. A peak AUC (Area Under Curve) x3 baseline was accepted. A concentration range of 0.00025 µg/mL (very low) to 1 µg/mL to was prepared to allow establishment of LLQ [364].

4.2.3. Rh123 protein and tubing binding

Method

Rh123 Protein binding

To assess an approximate extent and consistency of the fluorescent dye, Rh123 (Figure 4.3) binding to Bovine Serum Albumin, a range of Rh123 concentrations (0.0125 µg/mL to 5.0 µg/mL) were prepared by serial dilution in IPRL perfusate.

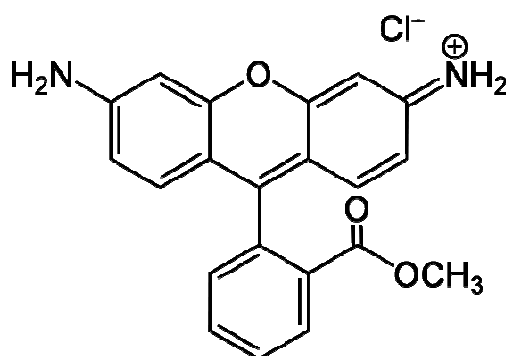


Figure 4.3 The 2D chemical structure of the fluorescent aromatic cation, rhodamine 123, at neutral pH [365].

Each individual concentration was prepared in triplicate and acetonitrile added to each at a ratio of 3:1 (ACN: Sample). Samples were equilibrated for 1 h in the dark and subsequently centrifuged for 10 min at 18,000 g. Sample supernatants were fluorometrically analysed using HPLC (as above).

To allow comparison, Rh123 samples of the same concentration were also prepared in perfusate without the BSA (i.e. Krebs-Henseleit buffer). These samples were exposed to the same 'deproteinisation' step as applied for full perfusate and subjected to fluorometric analysis. Studies were performed in triplicate samples.

Rh123 tubing binding

To assess the extent to which IPRL perfusate tubing influenced Rh123 levels in perfusate through nonspecific binding, a range of Rh123 concentrations in IPRL perfusate were prepared in triplicate by serial dilution (0.01 µg/mL to 1.0 µg/mL). Two conditions were assessed: (i) Pumping conditions - each perfusate sample (25 mL) was placed in a 50 mL glass beaker and passed through the tubing via the peristaltic pump in 'recirculating mode' for 1 hr. Perfusate flow rate was set to that of the IPRL system; (ii) Static conditions - the same concentration range of perfusate samples were prepared as above and introduced to IPRL tubing via a pipette. Again, samples were left for 1 hr.

All samples were deproteinated with ACN (3:1; ACN: Sample), centrifuged for 10 min at 18,000 g and fluorometrically analysed by HPLC to allow comparison.

To further establish the influence of the P-gp inhibitor, GF120918 upon Rh123 tubing binding, perfusate samples containing a concentration range of Rh123 (0.001 µg/mL to 0.5 µg/mL) were spiked with GF120918 (500 nM). Similarly, perfusate samples containing GF120918 (500 nM) were spiked with a concentration range of Rh123 (0.001 µg/mL to 0.5 µg/mL) to ensure order of addition had no influence upon Rh123 tubing binding. All samples were deproteinated with ACN (3:1; ACN: Sample), centrifuged for 10 min at 18,000 g and fluorometrically analysed by HPLC to allow comparison.

The P-gp inhibitor, GF120918, was shown to have no influence upon Rh123 HPLC chromatography: (See section 4.2.5 for GF120918 analytical method development).

4.2.4. Rh123 absorption from airways: Dose-ranging studies

Method

Assumptions and assay conditions for determining choice of initial low Rh123 dose to administer into the airways of the IPRL:

The LLQ for Rh123 HPLC is 0.25 ng/mL. For an IPRL perfusate volume of 50 mL this would mean a lower limit of detection for a mass of 0.0125 µg or 12.5 ng of absorbed Rh123 dose. If we assume a low extent of bioavailability for Rh123 and the need to be able to measure Rh123 concentrations absorbed into the perfusate throughout the experiment, a 2 µg dose of Rh123 was determined as satisfactory. That is, if 5 % of the Rh123 is absorbed there will be 100 ng of absorbed Rh123 dose. Further, the K_M of Rh123 for P-gp (at least in some *in-vitro* cell lines) has been reported to approximate 10 µM [366-368]. Next we should consider the lung epithelial fluid lining volume in the rat of between 0.35 and 0.5 mL, and add the additional 0.1 mL of dosing volume to give an initial volume in the lung of between 0.45 and 0.6 mL. With an instilled Rh123 dose of 2 µg (M_w is 380.82) or 5 nmoles into the IPRL; this will yield an initial concentration in the airway lining fluid of the IPRL of between 8 and 11 µM, i.e. approximating the K_M .

Dose-ranging studies

Rh123 in dH₂O (2 µg, 5 µg, 40 µg and 80 µg dose) was introduced to the IPRL via forced installation (As per chapter 3). Immediately before dosing a perfusate sample (1 mL) was removed from the reservoir as the 0 min sample. This initial sample volume was not replaced. Perfusate samples (1 mL) were removed at the following time points, 0, 1, 2, 3, 5, 10, 15, 20, 25, 30, 40, 50, 60, 70, 80, and 90 min and replaced with fresh perfusate (1 mL).

Again, Rh123 concentrations in pulmonary perfusate was determined by High Performance Liquid Chromatography coupled to a fluorometric detector as described above in 4.2.2

Data Analysis

To determine the significance of dose escalation, both the percentage of deposited Rh123 dose absorbed at 90 min and the k_{in} (from linear regression) of each transport profile was analysed. Subsequently, k_{01} , as determined by non-linear regression was also statistically analysed.

Pharmacokinetic modeling:

Background

Software - The Pharsight (Mountain View, USA) software product WinNonlin was used.

Intended use - to highlight similarity of Rh123/F-Na transport to that of a first order process*. Also used to establish pharmacokinetic parameters such as initial absorption rate and absorption half-life

*Substrate absorption being proportional to concentration.

Model use - Initial parameters are entered into the modelling software and a plot produced. This plot is then utilised by the software programme to establish associated pharmacokinetic parameters

Non-linear analysis was undertaken by WinNonlin (Pharsight, Mountain View, USA) with the following equation:

$$C_t = \frac{Dose}{V * (k_{01} - k_{10})} * (\exp^{-k_{10} * t} - \exp^{-k_{01} * t})$$

Where k_{01} is the rate constant describing input into the perfusate; k_{10} the rate constant describing loss from the perfusate; V is the volume of distribution/F; t is the actual time – lagtime for absorption. For Rh123 the initial estimates for the following parameters were set at: $k_{01} = 0.07 \text{ min}^{-1}$; $k_{10} = 0.000001 \text{ min}^{-1}$; $V = 2 \text{ l/kg}$; lagtime in absorption – 2 min A one way Analysis of Variance followed by a post-hoc Duncan's test was performed on each. A value of $p < 0.05$ was considered significant.

The analysis was repeated for F-Na data, however, the dose absorbed at 60 min was analysed.

4.2.5. Rh123 absorption from airways: Effect of GF120918

Method

Method development

To ensure the introduction of GF120918 (in 0.1 % DMSO v/v) to Rh123 samples did not adversely affect HPLC chromatography, GF120918 (500 nM) was spiked to a concentration range of Rh123 in IPRL perfusate, prepared by serial dilution. Samples were deproteinated and centrifuged as per preparation protocol, see above, and analysed fluorometrically by HPLC according to the above developed protocol described for Rh123.

No obvious significant alteration to the Rh123 chromatograms was observed by the addition of GF120918. When both Rh123 and GF120918 were co-injected into the HPLC a clearly separated peak for GF120918 could be clearly distinguished at 4.2 min which was baseline separated from the Rh123 peak at 2-2.5 min (Figure 4.4).

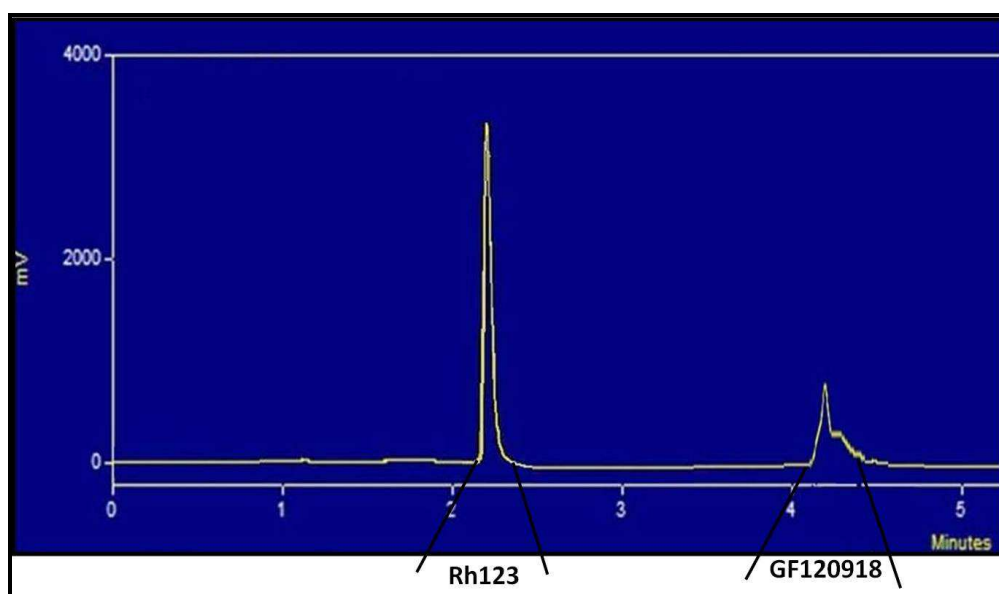


Figure 4.4 Example of a HPLC chromatogram produced by Rh123 sample spiked with GF120918 (500nM; 0.1% DMSO)

GF120918 Concentration	Cell Type	Substrate	Inhibitor Solvent	Notes	Reference
GF120918 M _w = 600.09; 10 µM = 6.0 µg in 1 mL					
2 µM, 10 µM, 20 µM, 70 µM	<i>In vivo</i> - Whole lung (Rabbit)	Rh123	DMSO	High Conc?	Roerig <i>et al.</i> , 2004 [17]
1 µM (no basis given for choice)	<i>In vitro</i> – HeLa cells	Rh123	N/A	Cells incubated in presence of inhibitor	Ejendal <i>et al.</i> , 2005 [7]
0.1-10mg/kg From Fig 4; Max Inhibitory conc. 2-3 mg/kg Mouse weight ~ 50-75 g. 2 mg/kg = 0.2 mg/100 g = 0.1 mg/mouse = 100 µL dose	<i>In vivo</i> - FVB/NTTafcbR Mice	Rh123	N/A	Dosed orally. Tariquidar IC ₅₀ = 38nM.	Choo <i>et al.</i> , 2006 [5]
0.5-2.0 µM	Primary Rat Hepatocytes	Rh123	N/A	Cells pre-incubated	Annaert <i>et al.</i> , 2001 [3]
100 nM	<i>In vitro</i> - EMT6/P H69/LX4	Rh213	PEG : 5 % Dextrose (3:2 v/v)	Cells incubated	Mistry <i>et al.</i> , 2001 [11]
100 mg/kg ~5 mg/mouse	<i>In vivo</i> - Whole Animal (Mice)	Saquinavir	N/A	Dosed orally 2.5 µL/g body weight. Very high conc. used.	Huisman <i>et al.</i> , 2003 [8]
500 mg/kg - Animal 0.5 µM – Cell culture	<i>In vivo</i> - Whole Animal (Rat BBB) <i>In vitro</i> – BBCEC	Rh123, Morphine	HPMC: Tween 80: H2O (0.5:1.0:98.5)	Dosed orally from 4 days before expt. Cited 20 nM effective <i>in-vitro</i>	Letrent <i>et al.</i> , 1999 [10]
25 mg/kg	<i>In vivo</i> - Whole Animal (Mice Brain)	Paclitaxel	WFI: 10 g/L HPMC & 2% Tween 80 (50:50)	Dosed p.o by gavage 2hr before paclitaxel	Kemper <i>et al.</i> , 2003 [9]

250 mg/kg – Animal 300 nM, 800 nM – Cell Culture	<i>In vivo</i> - Whole Animal (Mice) <i>In vitro</i> - KB 3-1 KB 8-5-11	Coelenterazine	0.5 % HPMC, 1 % Tween 80	Dosed orally 4 hr before imaging	Pichler <i>et al.</i> , 2004 [13]
0.001-10 μ M	<i>In vitro</i> – MDCKII	Calcein-AM, colchicine, digoxin, prazosin & vinblastine	1% DMSO in Transport Buffer	Cells incubated. IC ₅₀ 's cited from 20 nM – 100 nM	Rautio <i>et al.</i> , 2006 [16]
250 mg/kg – Animal 300 nM – Cell Culture	<i>In vivo</i> - Whole Animal (Rat Brain) <i>In vitro</i> - KB 8-5 NIH3TS	99mTc-sestamibi	0.5 % HPMC & 1 % Tween 80 in dH ₂ O	300 nM – max. inhibitory concentration	Rao <i>et al.</i> , 1999 [15]
0.5 μ M, 2 μ M, 10 μ M	<i>In vitro</i> - Caco-2	Fexofenadine	N/A	No change in P _{app} from 2-10 μ M suggesting complete inhibition of P-gp at 2 μ M?	Petri <i>et al.</i> , 2003 [12]
1 μ M	<i>In vitro</i> - MDCKII: WT, P-gp, MRP1 & MRP2	Saquinavir	DMSO	1 μ M – transport inhibition concentration	Williams <i>et al.</i> , 2002 [18]
250 mg/kg – Animal 500 nM – Cell Culture	<i>In vitro</i> - Caco-2	Amprenavir	0.5 % HPMC & 1 % Tween 80 in dH ₂ O	250 mg/kg to produce P-gp chemical knockout animal	Polli <i>et al.</i> , 1999 [14]
0.1, 0.3, 0.6, 1.0, 2.0 & 3.1 mg/kg/h	<i>In vivo</i> - Whole Animal (Rats & Mice)	Various P-gp substrates	2 % (v/v) 1,2 propanediol added to 5 % (w/v) glucose aq. containing 10 % (w/v) Kleptose HPB	2.5 mL/kg/h 24 hr infusion to produce P-gp chemical knockout animal	Cutler <i>et al.</i> , 2006 [6]

Effect of GF120918 co-instilled and in IPRL perfusate upon the pulmonary absorption of Rh123

Table 4.3 Efficacious concentrations of GF120918 utilised experimentally for the inhibition of P-gp. Key: PEG – Polyethylene glycol, HPMC – Hydroxypropyl methylcellulose, WFI – Water for injection, DMSO – Dimethyl sulfoxide.

Advice from GSK, together with data from table 4.3 resulted in initial use of 500 nM GF120918 concentration in the perfusate; a lower concentration of GF120918, 150 nM, was also used. GF120918 is soluble in DMSO at a concentration of 20 mg/mL. The solvent DMSO concentration in the perfusate was 0.1 % (v/v) upon the advice of GSK.

Chosen GF120918 concentration of 150 nM:

150 nM in terms of nmoles/doses. 15 pmoles administered to lung volume (300 μ L + 100 μ L of instillate) = GF120918 concentration in the lung of 40 nMolar, i.e. a dilution of 1 in 3.

Rh123 (2 μ g) was co-instilled into the airways of the IPRL (IPRL, see chapter 3) with either DMSO (0.1 % v/v) or GF120918 (150 nM and 500 nM) dissolved in DMSO. Maximum concentration of DMSO in instillate was 0.1 % v/v. In some experiments GF120918 (150 nM and 500 nM) was also present in the pulmonary perfusate and was perfused through the lungs for a 30 min period prior to lung dosing. Samples were taken from the perfusate reservoir (1 mL) and replaced with perfusate (1 mL) containing either GF120918 (150 nM and 500 nM) or DMSO (0.1 % v/v). Samples were removed at 0, 1, 2, 3, 5, 10, 15, 20, 25, 30, 40, 50, 60, 70, 80, and 90 min. Samples were deproteinated, centrifuged at 18,000 g for 10 min and the resulting supernatant was fluorometrically analysed by HPLC, as described above.

To allow comparison, the passive permeability probe, F-Na (40 μ g) was also co-instilled into the airways of the IPRL with either DMSO (0.1 % v/v) or GF120918 (150 nM and 500 nM) as a control. In some experiments, the IPRL perfusate also contained either DMSO (0.1 % v/v) or GF120918 (150 nM and 500 nM) and was recirculated through the IPRL system for 30 min prior to lung dosing. Samples were removed at 0, 1, 2, 3, 5, 7, 9, 12, 15, 20, 25, 30, 40, 50, 60, 70, 80, and 90 min, were deproteinated and were centrifuged at 18,000 g for 10 min. Resulting sample supernatant was fluorometrically analysed using HPLC as described above. Sample volumes were replaced with either GF120918 (150 nM and 500 nM) or DMSO (0.1 % v/v). HPLC analysis of F-Na was undertaken for these experiments as GF120918 is also fluorescent at similar wavelengths.

Data Analysis

To determine the significance of the addition of the GF120918 inhibitor, in instillate only and in both instillate and perfusate, a one way Analysis of Variance followed by a post-hoc Duncan's test was performed upon both the percentage of deposited Rh123 dose absorbed at 90 min, the k_{in} (linear regression) and the k_{01}/k_a (non-linear regression) of each transport profile. A value of $p < 0.05$ was considered significant. An independent samples t-test was performed on data sets with only two treatment groups i.e. F-Na data or Rh123 +/- GF co-instilled only data. Again, a value of $p < 0.05$ was

considered significant. For F-Na + 500 nM GF120918 co-instilled alone, percentage deposited dose absorbed at 60 not 90 min data was used.

GraphPad

Using GraphPad Prism 5 software, the nonlinear model:

$$Y = (K_a \cdot \text{Actual dose} / K_a) \cdot (1 - \exp(-K_a \cdot (x - t_{\text{lag}})))$$

was applied to the following data; F-Na 4 µg dose ranging data, F-Na 40 µg; instilled GF120918 only data and all flunisolide data.

Where k_a initial parameter was set at 0.001 to 0.01 min⁻¹ and T_{lag} was 5 min

4.2.6. Digoxin absorption from airways: Effect of GF120918 co-instilled and in IPRL perfusate

Method

Effect of GF120918 co-instilled and in IPRL perfusate upon the pulmonary absorption of digoxin

[³H] digoxin (0.25 pmol/animal containing 1 µCi of [³H] digoxin/animal) was co-instilled to the lungs (IPRL, see chapter 3) with either DMSO (0.1 % v/v) or GF120918 (500 nM). In a similar manner to 'Rh123' experiments, GF120918 (500 nM) or DMSO (0.1 % v/v) was also present in the pulmonary perfusate and passed through the lungs of the IPRL for a 30 min period prior to lung dosing. To allow comparison of digoxin absorption to a paracellular passive permeability probe, [¹⁴C] mannitol (8 pmol/animal) was also co-instilled with all digoxin administrations. Samples were taken from the perfusate reservoir (1 mL) and replaced with perfusate (1 mL) containing either GF120918 (500 nM) or DMSO (0.1 % v/v). Samples were removed at 0, 1, 2, 3, 5, 10, 15, 20, 30, 40, 50, and 60 min. Samples were immediately analysed by dual channel liquid scintillation counting.

Liquid scintillation analysis

Supernatant samples (200 µL) were added to translucent scintillation tubes, scintillation cocktail (3 mL) added and tubes sealed. To measure radioactivity, samples were placed in a Tri-Carb scintillation counter (Tricarb 2900TR, Perkin Elmer, USA) which was run on dual-counting mode, detecting emissions resulting from the decay of [³H] and [¹⁴C].

Scintillation counter output was given as 'counts per minute; CPM' from which corrected values of 'disintegrations per minute; DPM) were calculated and displayed.

Data analysis and pharmacokinetic modeling

To determine the significance of the addition of the GF120918 inhibitor upon the pulmonary absorption of [³H] digoxin across the IPRL, an independent samples t-test was performed upon the

percentage of deposited [^3H] digoxin dose absorbed at 60 min, the k_{in} (determined by linear regression of initial slope), and the calculated $t_{1/2}$ of each transport profile. A value of $p < 0.05$ was considered significant.

Further, use of a 1st order pharmacokinetic model was employed to all [^3H] digoxin data to accurately establish parameters involved in substrate absorption across the IPRL. This was also repeated for all [^{14}C] mannitol data. The model applied to digoxin/mannitol data was:

$$\%abs = F * dose * (1 - \exp^{-k_{01} * t})$$

(Where dose can be set to 100 %, F = fractional extent, k_{01} = absorption rate constant, t = time)

4.2.7. Flunisolide absorption from airways: Effect of GF120918 co-instilled and in IPRL perfusate

Method

Effect of GF120918 co-instilled and in IPRL perfusate upon the pulmonary absorption of flunisolide

As in the above IPRL studies, flunisolide (2 μg) was co-instilled to the lungs of the IPRL with either DMSO (0.1 % v/v) or GF120918 (500 nM). GF120918 (500 nM) or DMSO (0.1 % v/v) alone was also present in the pulmonary perfusate and passed through the lungs for a 30 min period prior to lung dosing. Samples were taken from the perfusate reservoir (1 mL) and replaced with perfusate (1 mL) containing either GF120918 (500 nM) or DMSO (0.1 % v/v). Samples were removed at 0, 1, 2, 3, 5, 7, 9, 12, 15, 20, 25, 30, 40, 50, 60, 75, and 90 min. Samples were stored at -80°C for shipping to GSK, Stevenage for analysis.

GSK: Sample analysis by LC/MS/MS (performed by Emma Sherrif at GSK)

Overview of analytical techniques

Mass Spectrometry (MS)

Mass spectrometry is an analytical technique that measures mass-to-charge ratio of charged particles and has a number of uses including; determining masses of particles, determining the elemental composition of a sample or molecule, and for elucidating the chemical structures of molecules.

In principle, compounds are ionised to generate a charged molecule and then measured according to their mass: charge ratio.

General procedure:

1. A sample is loaded onto the mass spectrometer and vaporised.

2. The components of the sample are ionized (by one of a variety of methods), resulting in the formation of ions.
3. The ions are separated according to their mass-to-charge ratio in an analyzer by electromagnetic fields
4. The ions are detected, usually by a quantitative method, and the signal is processed into mass spectra.

Traditionally MS instruments consist of three modules:

1. An ion source - converts gas phase sample molecules into ions.
2. A mass analyzer - sorts ions by their masses by applying electromagnetic fields
3. A detector - measures the value of an indicator quantity and provides data for calculating the abundances of each ion present.

Liquid Chromatography Mass Spectrometry

Definition: A method where a sample mixture is first separated by liquid chromatography before being ionised and characterised by mass-to-charge ratio and relative abundance using two mass spectrometers in series.

LC/MS is a technique similar to gas chromatography MS (GC/MS) in that compounds are separated chromatographically before they are introduced to the ion source and mass spectrometer. The technique differs in that the mobile phase is liquid, usually a mixture of water and organic solvents, instead of gas and the ions fragments cannot yield predictable patterns.

Liquid Chromatography Tandem Mass Spectrometry (LC/MS/MS)

LC/MS/MS is very similar to LC/MS but involves use of tandem mass analysers creating higher specificity than LC/MS as there is a second filtering process.

[369, 370]

Preparation of buffer calibration standards:

Two standard curves were prepared to cover the range 0.5 to 5000 ng/mL by serial dilution in control buffer (IPRL perfusate) using a TECAN robot, (Genesis, RSP 150). The TECAN also produced a carryover blank following the washes after the top standard was dispensed.

Preparation of buffer samples for analysis:

Flunisolide samples and standards were prepared by protein precipitation with acetonitrile containing 200 ng/mL of GSK977617B (internal standard, IS), followed by filtration using Whatman protein precipitation plates. Using a TECAN robot the samples and standards were extracted by protein precipitation. For extraction, 50 μ L of buffer from standards and samples was taken and 150 μ L of acetonitrile with internal standard was added.

The filtered extracts were collected into a 96 well plate and were blown down to dryness under a nitrogen stream at 40 °C. The dry extracts were reconstituted in 200 μ L of acetonitrile: water (10: 90 by volume).

The plate was then mixed on a plate shaker for at least 5 min before analysis by LC/MS/MS using an 18 μ L injection volume.

Re-injection of samples to check ion suppression:

The following samples were injected twice to allow assessment of the effect of ion suppression. The samples used were the 200 ng/mL calibration standard, the 5 min sample from animal 1 and 3 and the 15 min sample from animal 2 and 4. These samples were injected at a 6 μ L injection volume and then immediately re-injected at the 18 μ L injection volume used for the rest of the run.

LC-MS/MS analytical conditions

Analytical column:

Packing type	Luna C18
Particle size	5 μ M
Dimensions	50 x 2.1 mm
Injection volume	18 μ L (6 μ L for ion suppression check samples)

HPLC conditions:

Pump	Agilent 1100
Solvent A	0.1 % Formic acid in HPLC grade water
Solvent B	0.1 % Formic acid in acetonitrile
Flow rate	0.8 mL/min.
Initial divert to waste time	0.5 min.

Run time	3 min.
----------	--------

Gradient conditions:

Start Time (min.)	A (%)	B (%)
0	95	5
0.5	95	5
1.8	5	95
2.2	5	95
2.3	95	5
3.0	95	5

Detector conditions:

Detector	Applied Biosystems API4000 Mass Spectrometer
Mode	MSMS
Ion Source	TISP (turbo ion spray)
Ionisation	+ve
Source temperature	650 °C

MRM transitions:

Compound	Cassette	Q1 Mass	Q3 Mass	Declustering potential (V) (DP)	Cell entrance potential (V) (CE)	Cell exit potential (V) (CXP)
Flunisolide	1	345.101	285.151	66.0	57.0	18.0
GSK977617B (IS)	1	276.45	131.10	100	40	12

Data analysis and pharmacokinetic modeling

To determine the significance of the addition of the GF120918 inhibitor, in both instillate and perfusate, upon the pulmonary absorption of flunisolide across the IPRL, an independent samples t-test was performed upon the percentage of deposited flunisolide dose absorbed at 90 min, the k_{in} (linear regression), and the $t_{1/2}$ (nonlinear regression) of each transport profile. A value of $p < 0.05$ was considered significant.

Further, use of a 1st order pharmacokinetic model was employed to all flunisolide data to accurately establish parameters involved in substrate absorption across the IPRL.

4.3. Results

4.3.1. Rh123 analytical validation: Precision and accuracy

The precision of Rh123 and F-Na HPLC assays were illustrated by determining the coefficient of variation (% C_v) for triplicate samples across a concentration range. Table 4.4A displays the C_v as a percentage for each concentration point. As can be seen, calculated % C_v for both the Rh123 samples and F-Na samples were ≤ 15.0 % and deemed acceptable for precise quantitation [364].

Rh123	Mean ($\mu\text{g/mL}$)	Standard deviation	Coefficient of variation (% C_v)
0.025 $\mu\text{g/mL}$	0.022	0.003	11.60
0.0625 $\mu\text{g/mL}$	0.065	0.006	8.92
0.125 $\mu\text{g/mL}$	0.138	0.018	12.73
0.25 $\mu\text{g/mL}$	0.435	0.051	11.78
0.5 $\mu\text{g/mL}$	0.654	0.044	6.69
F-Na			
0.01 $\mu\text{g/mL}$	0.017	0.002	10.26
0.05 $\mu\text{g/mL}$	0.059	0.008	14.03
0.0125 $\mu\text{g/mL}$	0.113	0.012	10.59
0.25 $\mu\text{g/mL}$	0.243	0.023	9.46
1.0 $\mu\text{g/mL}$	0.982	0.119	12.12

Table 4.4A Calculated coefficient of variation (% C_v) for sample quantitation across a concentration range for the P-gp substrate, Rh123, and the paracellular probe, F-Na. (n=3 for each concentration point)

Table 4.4B displays the calculated accuracy of the same HPLC assays. Accuracy was calculated from three individual concentration samples of Rh123 or F-Na. An accuracy of within 80 – 120 % of the nominal concentration standard was deemed acceptable for accurate quantitation [364].

Rh123	Theoretical concentration ($\mu\text{g/mL}$)	Actual concentration ($\mu\text{g/mL}$)	Accuracy (%)	StDev
	0.025	0.023	108.70	1.05
	0.0625	0.058	108.23	2.34
	0.25	0.312	80.22	2.64
F-Na				
	0.025	0.022	116.06	2.30
	0.0625	0.060	103.93	1.70
	0.25	0.299	83.74	1.91

Table 4.4B Calculated accuracy, expressed as a % of measured concentration / theoretical or nominal standard concentration, across a concentration range for Rh123 and F-Na (n=3 for each concentration point)

4.3.2. Rh123 protein and tubing binding

Here the consistency of deproteination and recovery of Rh123 from the IPRL perfusate was examined across a range of Rh123 concentrations. A range of Rh123 concentrations were prepared in IPRL perfusate where BSA was either present or absent. The extent of Rh123 recovery from the perfusate after undertaking a 'deproteination' step was compared and expressed as % Rh123 concentration in 'protein samples' to 'protein-free' samples. Table 4.5 illustrates the mean % Rh123 recovered over a concentration range. As can be seen, no significant variation in recovered Rh123 was seen across the concentration range, suggesting that recovery was consistent irrespective of Rh123 concentration.

Rh123 ($\mu\text{g/mL}$)	Mean % Rh123 recovered
0.0125	79.61 ± 3.38
0.05	78.83 ± 2.50
0.1	78.06 ± 5.02
1.0	81.99 ± 1.44
5.0	80.14 ± 4.55

$p > 0.05$

Table 4.5 Mean % Rh123 recovered from Rh123 perfusate samples containing BSA compared to perfusate where BSA had not been included. Data are expressed as mean \pm S.D. (n=3 for each concentration point)

To determine the extent and consistency of Rh123 binding to IPRL perfusate tubing, the concentration of Rh123 samples recovered from tubing after 90 min was expressed as a percentage of Rh123 dose solution. Table 4.6 illustrates that recovery of Rh123 from the perfusate exposed to the tubing for 90 min did not vary significantly ($p > 0.05$) over a Rh123 concentration range. The presence or absence of GF120918 or whether the perfusate was pumped through the tubing or held static in the tubing had no influence over the non-specific binding of Rh123 to IPRL tubing.

Nominal concentration (µg/mL)	Rh123 alone	Rh123 spiked to GF120918	GF120918 spiked to Rh123
	Mean % Rh123 recovered after 90 min.		
0.001	84.06 ± 5.02	87.43 ± 2.50	89.43 ± 14.08
0.01	88.69 ± 5.30	83.70 ± 6.85	78.17 ± 12.77
0.1	93.68 ± 5.66	84.57 ± 8.10	89.90 ± 5.38
0.5	90.15 ± 4.90	89.84 ± 2.39	95.98 ± 3.01
		p>0.05	
	'Static'	'Pumped'	Combined
0.01	90.37 ± 8.86	85.40 ± 5.20	88.24 ± 7.44
0.1	83.13 ± 5.68	84.12 ± 12.23	83.67 ± 8.85
1.0	84.53 ± 5.53	78.13 ± 5.74	81.33 ± 6.24
		p>0.05	

Table 4.6 Mean % Rh123 recovered from perfusate placed in IPRL tubing. The effect of Rh123 concentration, presence or absence of GF120918 and the pumped or static nature of the perfusate conditions investigated. The order of addition of P-gp inhibitor GF120918 was also investigated. Data are expressed as mean ± S.D. (n=3 for each concentration point)

4.3.3. Rh123 absorption from airways: Dose ranging studies

As can be seen in figure 4.5A, increasing nominal Rh123 dose to lung from 2 µg to 5 µg resulted in a disproportionate increase in percentage deposited Rh123 dose absorbed. A similar nominal Rh123 dose increase from 5 µg to 40 µg also exhibited a disproportional relationship, but to a lesser extent. However, doubling nominal Rh123 dose from 40 µg to 80 µg did not show this increase in % dose absorbed. This data is consistent with overcoming a saturable barrier to absorption such as an efflux transporter restricting transport from the lung lumen into the pulmonary perfusate, i.e. equivalent to the blood compartment.

A similar pattern could not be observed for a comparable dose escalation strategy with F-Na (IPRL validation data). Figure 4.5B shows no significant (p>0.05) increase in percentage deposited dose

absorbed when increasing nominal F-Na dose from 4 μg to 40 μg , nor when increasing nominal F-Na dose from 40 μg to 160 μg .

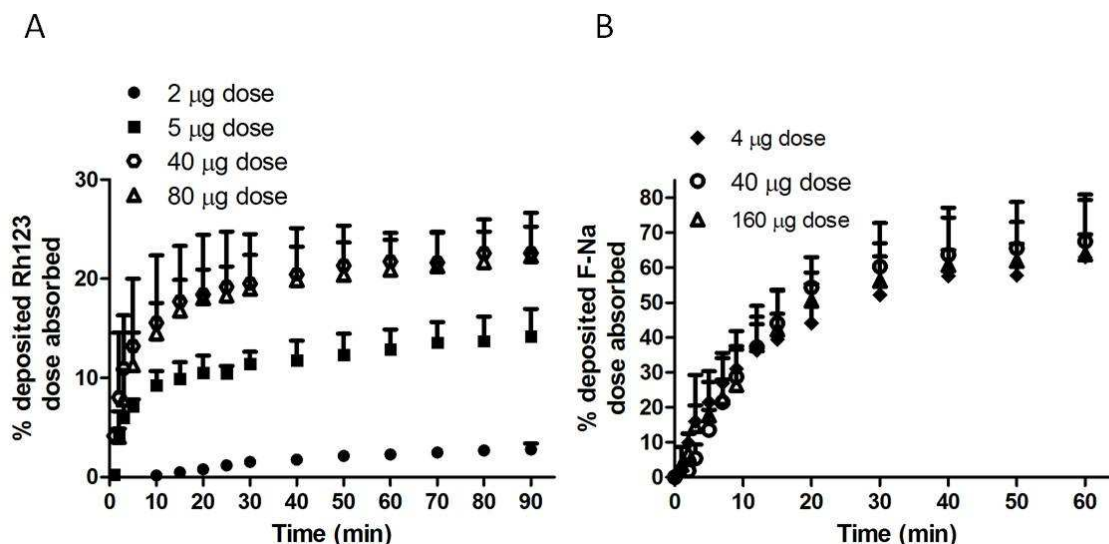


Figure 4.5 Dose-dependencies in cumulative % of lung deposited dose absorbed in the IPRL: **Figure 4.5A** – Cumulative % of deposited Rh123 dose absorbed with time. Data are expressed as mean \pm S.D (n=4 for each treatment); **Figure 4.5B** – Cumulative % of deposited dose of F-Na absorbed with time. The transport of F-Na is not affected by dose escalation. Data shown are expressed as mean \pm S.D (n=3 4 μg dose, n=17 40 μg dose, n=3 160 μg dose).

Treatment (Nominal Dose μg)	Deposited dose in lung (μg)	Cumulative mass of Rh123 absorbed by 90 min(μg)	Percentage of deposited Rh123 dose absorbed by 90 min (%)	K_{in} (min^{-1})
Rh123 (2 μg)	1.83 ± 0.30	0.05 ± 0.01	$2.79 \pm 0.58^*$	$0.0008 \pm 0.0001^\dagger$
Rh123 (5 μg)	4.22 ± 0.62	0.68 ± 0.15	$14.19 \pm 2.77^*$	$0.007 \pm 0.003^\dagger$
Rh123 (40 μg)	39.72 ± 6.76	9.05 ± 2.31	22.59 ± 2.68	0.028 ± 0.009
Rh123 (80 μg)	85.03 ± 2.75	19.04 ± 3.77	22.30 ± 4.38	0.027 ± 0.011
F-Na (4 μg)	2.48 ± 0.04	1.56 ± 0.39	63.02 ± 16.36	0.027 ± 0.005
F-Na (40 μg)	37.93 ± 6.75	22.44 ± 3.95	67.51 ± 13.38	0.037 ± 0.008
F-Na (160 μg)	162.78 ± 1.70	103.86 ± 10.45	63.76 ± 5.74	0.040 ± 0.014

Table 4.7 Transport of airway administered dose of Rh123 and F-Na across the IPRL: k_{in} was determined from the initial linear portion of the absorption plots. Data are expressed as mean \pm S.D with n=4 for each Rh123 treatment and n=3 for F-Na 4 μg dose, n=17 for F-Na 40 μg dose and n=3 for F-Na 160 μg dose. F-Na data in table 4.7 determined by plate-reader assay (Chapter 3), 'cumulative mass' and 'percentage' data are 60 min readings. * - Cumulative % of deposited Rh123 dose absorbed by 90 min is statistically different ($p < 0.05$) compared to all other Rh123 treatments. † - Rh123 k_{in} is statistically different ($p < 0.05$) compared to both 40 μg and 80 μg Rh123 nominal doses.

From table 4.7 it can be seen that dose escalation of Rh123 affected both the cumulative mass of Rh123 absorbed and initial k_{in} . Specifically, a 2.1-fold increase in deposited dose from 1.83 μg to 4.22 μg caused a 13.6-fold increase in cumulative mass absorbed by 90 min, while a similar 2.1-fold increase in deposited dose from 39.72 μg to 85.03 μg only yielded a 2.1-fold increase in cumulative mass transported, i.e. between the latter dose range, the % of dose absorbed remained the same at 22%. Further, k_{in} for initial Rh123 absorption followed a similar pattern. Dose escalation from 2 μg to 5 μg nominal Rh123 dose increased k_{in} 8.8-fold from 0.0008 min^{-1} to 0.007 min^{-1} . An increase in nominal Rh123 dose from 40 μg to 80 μg did not significantly ($p>0.05$) alter k_{in} .

Again, no comparable increase could be observed for F-Na. Dose escalation of F-Na did not significantly ($p>0.05$) increase the cumulative % dose absorbed nor alter initial k_{in} .

4.3.4. Rh123 absorption from airways: Effect of GF120918 co-instilled and in IPRL perfusate

Inclusion of the solvent vehicle alone DMSO (0.1 % v/v) in the pulmonary perfusate and co-administration in the airway instillate with a 2 μg nominal dose of Rh123 exhibited a similar transport profile to that of 2 μg Rh123 dosed alone (i.e. if data is compared from figure 4.5) indicating addition of 0.1 % DMSO had no significant effect upon substrate transport.

As illustrated in figure 4.6A, addition of GF120918 (150 nM) to both pulmonary perfusate and instillate resulted in a significant ($p<0.05$) increase in the % of the deposited Rh123 dose absorbed, illustrating an effect of the P-gp inhibitor on Rh123 transport. Addition of GF120918 (500 nM) also showed a significant ($p<0.05$) increase in the % of the deposited Rh123 dose absorbed compared to the 2 μg Rh123 + 0.1 % DMSO control. However, the increased concentration of GF120918 did not significantly ($p>0.05$) have any greater affect upon Rh123 above that of the 150 nM dose of GF120918.

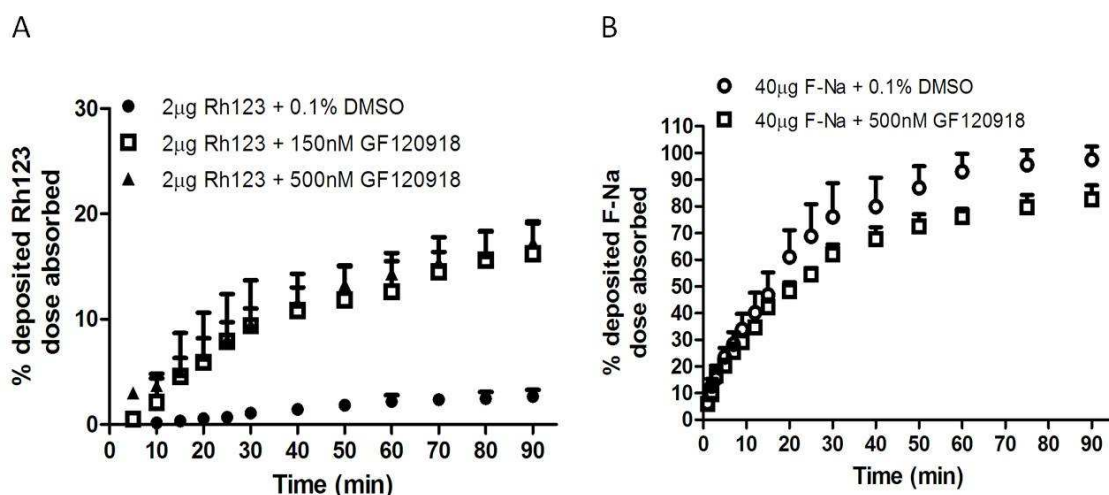


Figure 4.6 Effect of the P-gp inhibitor, GF120918 (in perfusate and airway instillate) upon cumulative % of lung deposited dose absorbed in the IPRL: **Figure 4.6A** – Effect of GF120918 at concentrations of 150 nM and 500 nM upon cumulative % of deposited Rh123 absorbed with time. The aqueous vehicle for GF120918 contained 0.1 % DMSO. The GF120918 was present in the pulmonary perfusate and co-instilled into the airways with Rh123. Data shown are expressed as mean \pm S.D (n=4 for each treatment). **Figure 4.6B** – Effect of GF120918 at a concentration of 500 nM upon cumulative % of deposited F-Na absorbed with time. Data shown are expressed as mean \pm S.D (n=4 for each treatment).

The inclusion of P-gp inhibitor resulted in Rh123 absorption kinetics showing similar profiles to high dose (40 μ g and 80 μ g) Rh123 absorption profiles. Table 4.8 illustrates that, with addition of GF120918 (150 nM), cumulative mass Rh123 absorbed by 90 min increases 6-fold in comparison to control. An increase can also be observed for initial k_{in} for each inhibitor treatment. Increase in GF120918 concentration from 150 nM to 500 nM did not significantly ($p>0.05$) increase any of the measured parameters.

Again, as with previous control experiments, no significant difference ($p>0.05$) in percentage deposited dose absorbed, or other measured parameters, could be observed between control F-Na (0.1 % DMSO) and GF120918 treatments.

Treatment (Nominal dose μg)	Deposited dose in lung (μg)	Cumulative mass Rh123 absorbed by 90 min(μg)	Percentage of deposited Rh123 dose absorbed by 90 min (%)	K_{in} (min^{-1})
Rh123 (2 μg) + 0.1 % DMSO	2.45 ± 0.26	0.06 ± 0.01	$2.67 \pm 0.62^*$	$0.0005 \pm 0.0001^\dagger$
Rh123 (2 μg) + 150 nM GF120918	2.22 ± 0.02	0.36 ± 0.06	16.20 ± 2.95	0.003 ± 0.001
Rh123 (2 μg) + 500 nM GF120918	2.25 ± 0.05	0.39 ± 0.04	17.33 ± 1.97	0.003 ± 0.0003
F-Na (40 μg) + 0.1 % DMSO	38.83 ± 2.22	35.62 ± 1.43	91.90 ± 5.95	0.022 ± 0.003
F-Na (40 μg) + 500 nM GF120918	40.08 ± 1.93	33.13 ± 3.12	82.55 ± 5.26	0.019 ± 0.002

Table 4.8 Effect of GF120918 upon the transport of Rh123 and F-Na in the IPRL. The P-gp inhibitor was present at 150 nM or 500 nM in the perfusate and in the co-instilled airway doses of either Rh123 or F-Na. Data shown are expressed as mean \pm S.D (n=4 for each treatment). F-Na data in table 4.8 determined by HPLC analysis. * - Cumulative % of deposited Rh123 dose absorbed by 90 min is statistically different ($p < 0.05$) compared to Rh123 + GF120918 treatments. † - Rh123 K_{in} is statistically different ($p < 0.05$) compared to Rh123 + GF120918 treatments.

4.3.5. Rh123 absorption from airways: Effect of GF120918 co-instilled with Rh123

Addition of GF120918 to only the instillate dose was used to explore the possibility of presence of spatial effects of P-gp inhibition upon Rh123 absorption. The airway instillate of GF120918 alone (i.e. in the absence of GF120918 in the perfusate) still resulted in a significant ($p < 0.05$) difference in the Rh123 absorption compared to control treatment (Figure 4.7).

With respect to F-Na administration, the co-instillation of GF120918 (500 nM) into the airways with F-Na did not have a significant ($p > 0.05$) effect upon F-Na absorption compared to control alone. Again, this corroborates a lack of effect of not only the GF120918 upon the general passive permeability properties of the pulmonary barrier but also the lack of effect of 0.1 % DMSO upon this barrier.

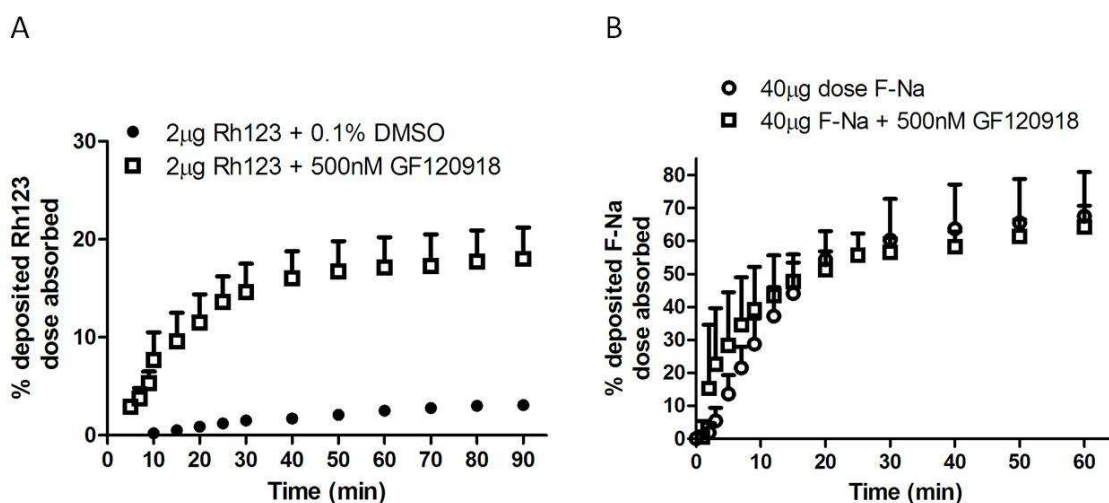


Figure 4.7 Effect of the P-gp inhibitor, GF120918 (in airway instillate only) upon cumulative % of lung deposited dose absorbed in the IPRL: **Figure 4.7A** - Effect of GF120918 at a concentration of 500 nM upon the cumulative % of deposited Rh123 absorbed with time. The aqueous vehicle for GF120918 contained 0.1 % DMSO. The GF120918 was present only in the co-instilled airway dose of Rh123. Data shown are expressed as mean \pm S.D (n=4 for each treatment). **Figure 4.7B** - Effect of GF120918 at a concentration of 500 nM upon cumulative % of deposited F-Na absorbed with time. Data shown are expressed as mean \pm S.D (n=4 for F-Na (40 µg) + GF120918 (500 nM), n=17 for F-Na (40 µg) *Dose ranging studies*.

Table 4.9 shows that inclusion of GF120918 with Rh123 in the airway co-instillate resulted in an increase ($p > 0.05$) in both % of the deposited dose absorbed and initial k_{in} . For example, a 5.8-fold increase in % of the deposited dose absorbed and 10-fold increase in initial k_{in} .

Treatment (Nominal dose μg)	Deposited dose in lung (μg)	Cumulative mass Rh123 absorbed by 90 min(μg)	Percentage of deposited Rh123 dose absorbed by 90 min (%)	$K_{in} (\text{min}^{-1})$
Rh123 (2 μg) + 0.1 % DMSO	1.93 ± 0.05	$0.06 \pm 0.01^*$	$3.10 \pm 0.36^*$	$0.0005 \pm 0.0001^*$
Rh123 (2 μg) + 500 nM GF120918	2.44 ± 0.03	0.44 ± 0.08	18.05 ± 3.19	0.005 ± 0.001
F-Na (40 μg) *Dose ranging data*	37.93 ± 6.75	22.44 ± 3.95	67.51 ± 13.38	0.037 ± 0.008
F-Na (40 μg) + 500nM GF120918	42.99 ± 1.68	27.57 ± 2.62	64.20 ± 6.53	0.032 ± 0.008

Table 4.9 Effect of GF120918 upon the lung accumulation of Rh123. The P-gp inhibitor was present at 500 nM in only the co-instilled airway doses of Rh123 or F-Na. Data shown are expressed as mean \pm S.D (n=4 for Rh123 treatment, n=4 for F-Na + 500 nM GF120918, n=17 for F-Na alone 'dose ranging data'). * - statistical difference ($p < 0.05$) compared to Rh123 + GF120918 treatments. F-Na (40 μg) 'dose ranging data' in table 4.9 determined by plate-reader assay (Chapter 3), all F-Na 'cumulative mass' and 'percentage' data are 60 min readings.

4.3.6. Pharmacokinetic modelling: Rh123 absorption from the IPRL in presence and absence of GF120918

A WinNonlin pharmacokinetic model was applied to all data, i.e. Rh123 treatments and F-Na control treatments, in order to accurately establish relevant parameters involved with substrate absorption across the IPRL. See Materials & Methods for details. Figures 4.8 – 4.11 illustrate examples of the plots generated by WinNonlin; all individual plots can be seen in appendix ii. Parameters such as k_{01} and $t_{1/2}$ were established from such plots.

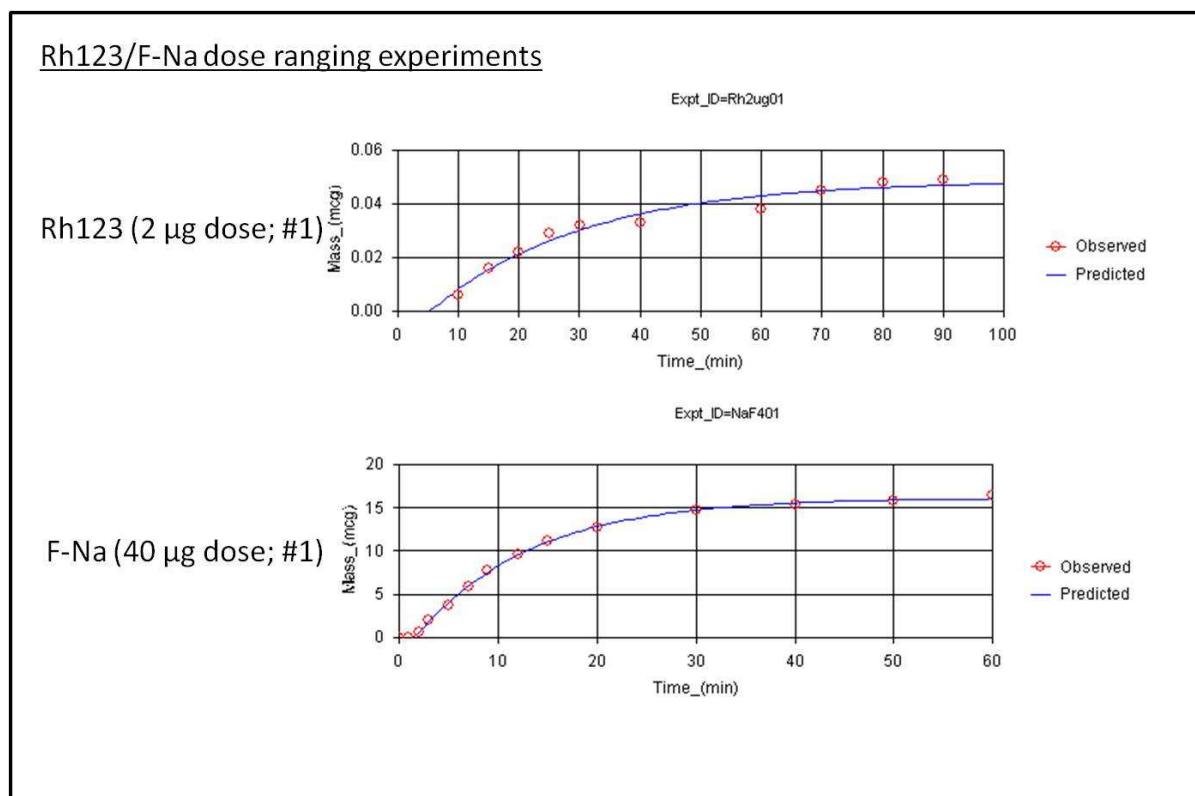


Figure 4.8 Example plots generated by fitting a WinNonlin model to Rh123/F-Na dose ranging data.

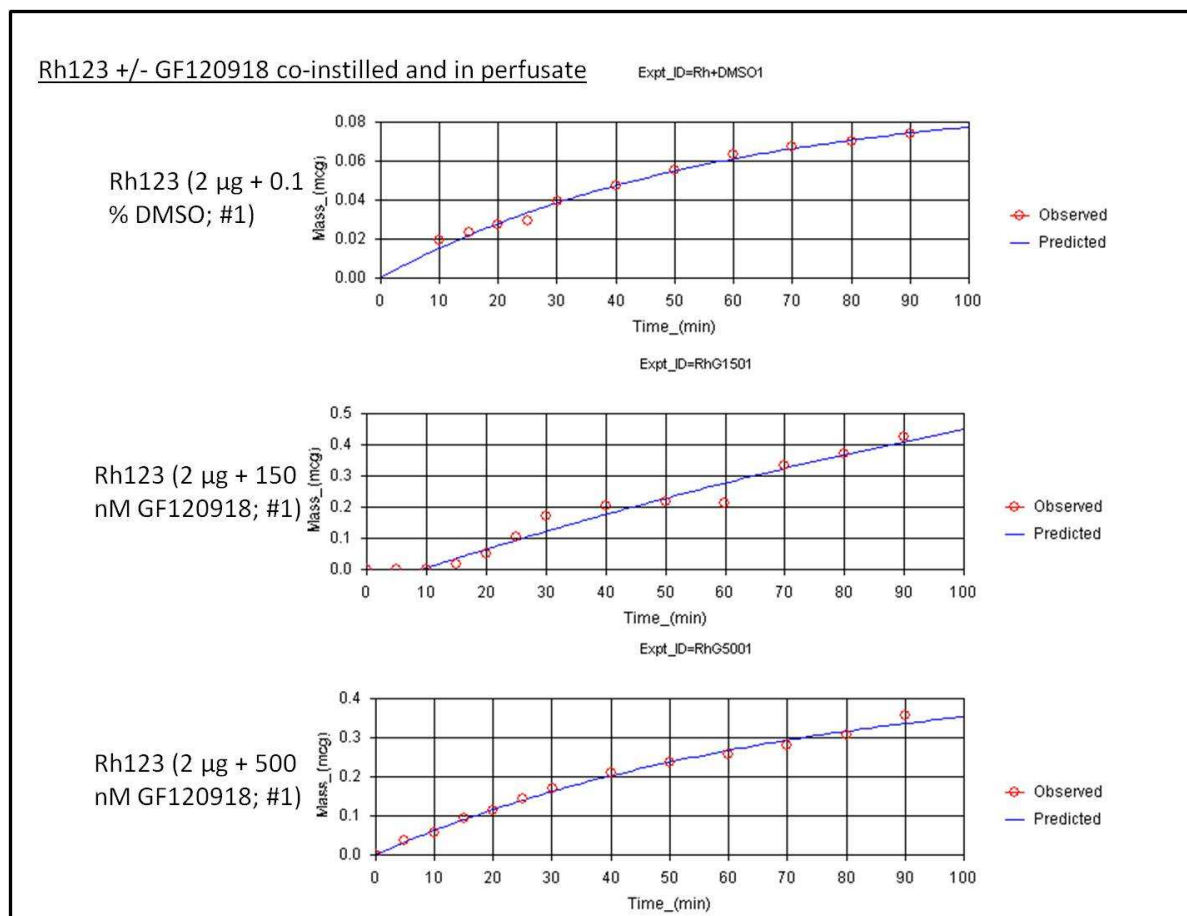


Figure 4.9 Example plots generated by fitting a WinNonlin model to Rh123 +/- GF120918 data where the P-gp inhibitor was both co-instilled with Rh123 dose and present in the IPRP perfusate.

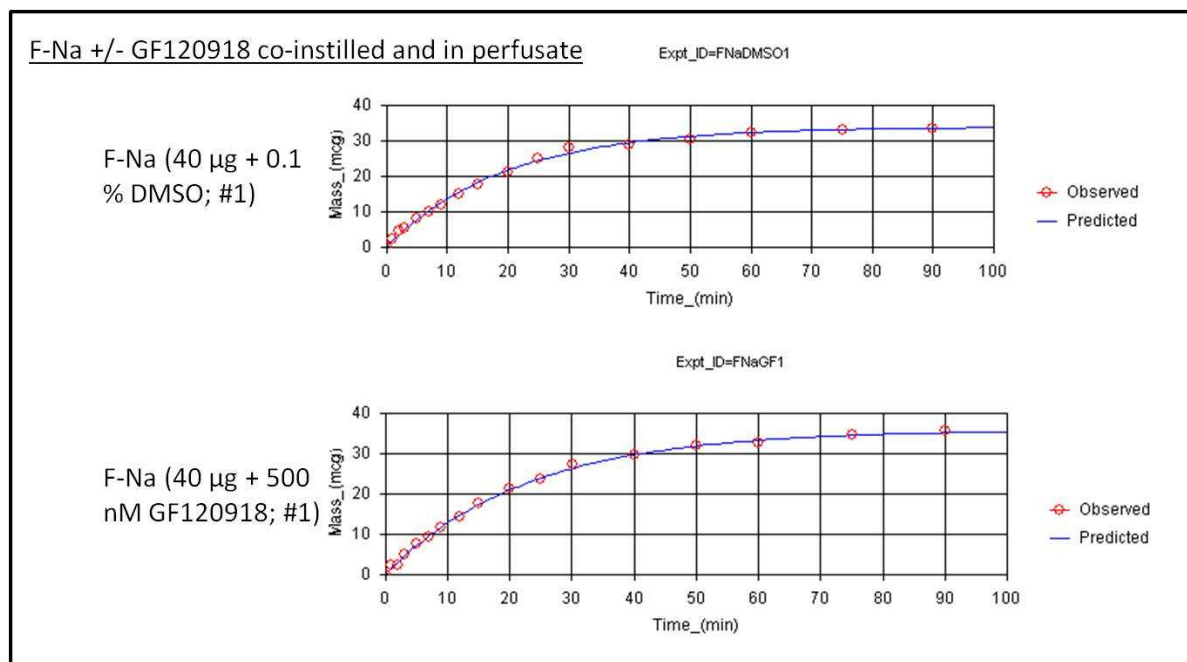


Figure 4.10 Example plots generated by fitting a WinNonlin model to F-Na +/- GF120918 data where the P-gp inhibitor was both co-instilled with F-Na dose and present in the IPRL perfusate.

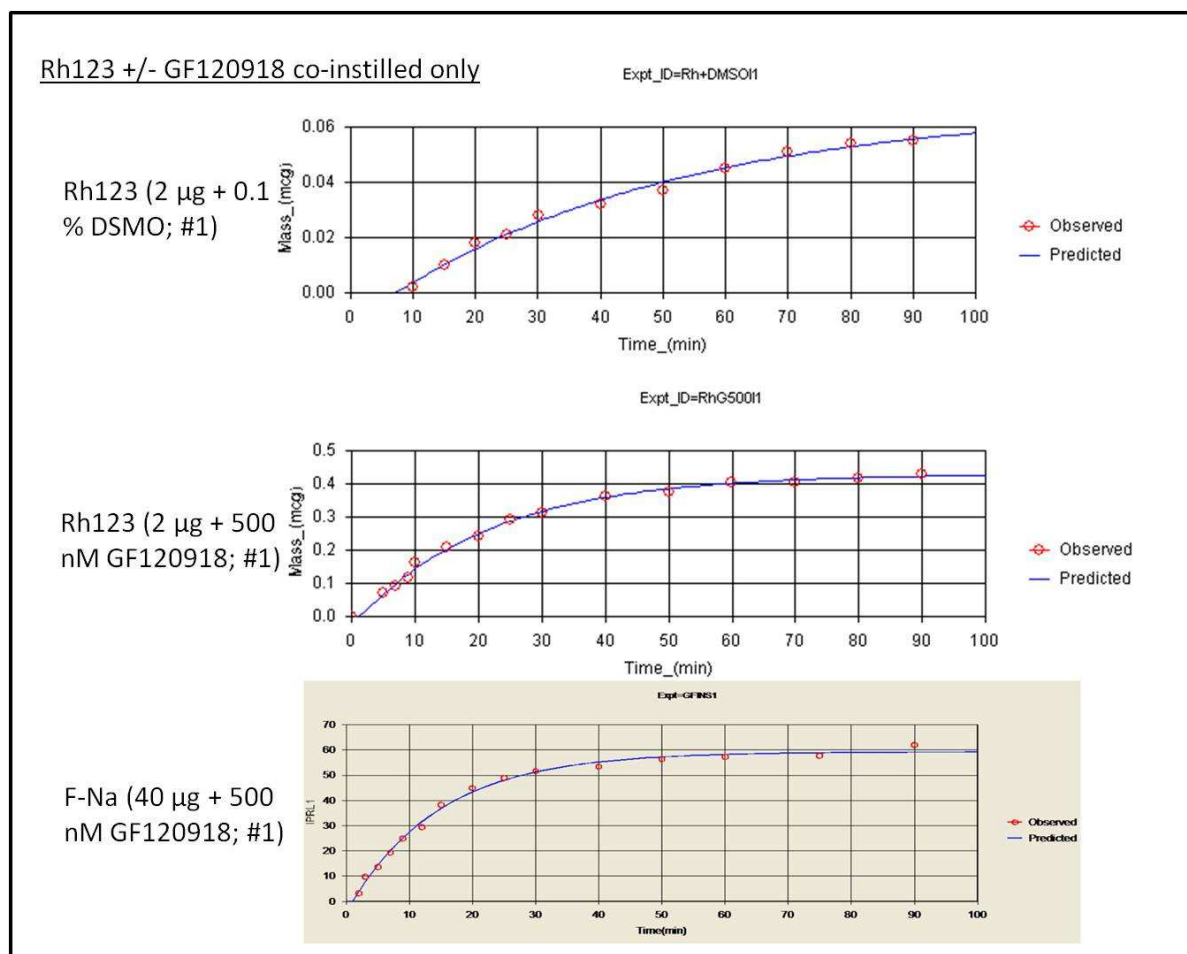


Figure 4.11 Example plots generated by fitting a WinNonlin model to Rh123/F-Na +/- GF120918 data where the P-gp inhibitor was present only in co-instilled Rh123/F-Na dose.

Model fitting to IPRL data generated individual k_{01} values, (comparable to k_{in} calculated by linear regression from cumulative absorption data), which were then used to calculate substrate absorption half-lives ($t_{1/2}$).

Table 4.10 shows the generated k_{01} and calculated $t_{1/2}$ for each treatment dosed to the IPRL. As can be seen, in contrast to k_{in} , which was determined from the initial linear portion of the absorption plots, calculated $t_{1/2}$ absorption does not highlight significant differences between the absorption of Rh123 in the presence or absence of GF120918. Only the calculated $t_{1/2}$ absorption of Rh123 2 µg dose (dose ranging studies) was found to be significantly ($p < 0.05$) different from all other dose ranging data absorption half-lives. Further, the calculated $t_{1/2}$ absorption of Rh123 2 µg dose, 24.83 ± 15.28 min, was found not to be significantly ($p > 0.05$) different when compared to 2 µg dose + 0.1 %

DMSO, 2 µg dose + 150 nM GF120918, 2 µg dose + 500 nM GF120918 and 2 µg dose + 0.1 % DMSO co-instilled only data.

Model fitting to F-Na data showed no significant ($p>0.05$) difference between any of the calculated $t_{1/2}$ absorption data regardless of treatment, i.e. presence or absence of GF120918 or DMSO solvent.

Treatment	K_{01} (min^{-1})	$t_{1/2}$ (min.) absorption
Rh123 dose ranging		
2 µg dose	0.034 ± 0.014	$24.83 \pm 15.28^*$
5 µg dose	0.163 ± 0.058	4.62 ± 1.39
40 µg dose	0.240 ± 0.197	6.09 ± 5.44
80 µg dose	0.148 ± 0.036	4.87 ± 1.05
F-Na dose ranging		
4 µg dose	0.078 ± 0.014	9.29 ± 1.79
40 µg dose	0.075 ± 0.016	9.63 ± 2.23
80 µg dose	0.080 ± 0.021	8.99 ± 2.01
Rh123 +/- GF120918		
2 µg dose + 0.1 % DMSO	0.019 ± 0.005	37.55 ± 10.28
2 µg dose + 150 nM GF120918	0.039 ± 0.003	51.01 ± 60.92
2 µg dose + 500 nM GF120918	0.022 ± 0.006	33.80 ± 10.33
F-Na +/- GF120918		
40 µg dose + 0.1 % DMSO	0.053 ± 0.002	13.18 ± 0.40
40 µg dose + 500 nM GF120918	0.049 ± 0.006	14.37 ± 1.72
Rh123 +/- GF120918 (co-instilled only)		
2 µg dose + 0.1 % DMSO	0.019 ± 0.004	38.47 ± 8.73
2 µg dose + 500 nM GF120918	0.062 ± 0.014	11.58 ± 2.68
F-Na +/- GF120918 (co-instilled only)		
40 µg dose *dose ranging data*	0.075 ± 0.016	9.63 ± 2.23
40 µg dose + 500 nM GF120918	0.086 ± 0.008	7.63 ± 3.96

Table 4.10 Pharmacokinetic parameters generated by fitting a WinNonlin model to Rh123/F-Na data in the presence and absence of the P-gp inhibitor GF120918. Absorption half-lives calculated as; $t_{1/2} = 0.693/K_{01}$. All data used in model fitting yielded from IPRL experiments (above results section). Data shown are expressed as mean \pm S.D. * - statistically different ($p<0.05$) $t_{1/2}$ compared to all other Rh123 dose ranging data.

Within generated data, k_{in} and k_{01} differ in the method by which they were calculated. k_{in} /initial slope data is limited as it is generated by analysis of a straight line, whereas k_{01} takes into account the full profile as it is calculated by non-linear regression. Calculation of k_{in} really is preliminary and only poorly represents the initial rate of absorption from the lung. Once acceptable and representative non-linear analysis has been achieved, k_{in} should not be focussed upon.

4.3.7. Digoxin absorption from airways: Effect of GF120918 co-instilled and in IPRL perfusate

As is illustrated in figure 4.12A, the inclusion of GF120918 (500 nM; 0.1 % v/v DMSO) in pulmonary perfusate and co-instilled into the airways along with 0.25 pmol nominal dose of digoxin did not affect significantly ($p>0.05$) the transport profile of digoxin when compared to digoxin control. The addition of GF120918 showed no significant ($p>0.05$) impact upon the % of deposited digoxin dose that was absorbed. Similarly, addition of the P-gp inhibitor did not significantly ($p>0.05$) influence mannitol transport across the IPRL (Figure 4.12B).

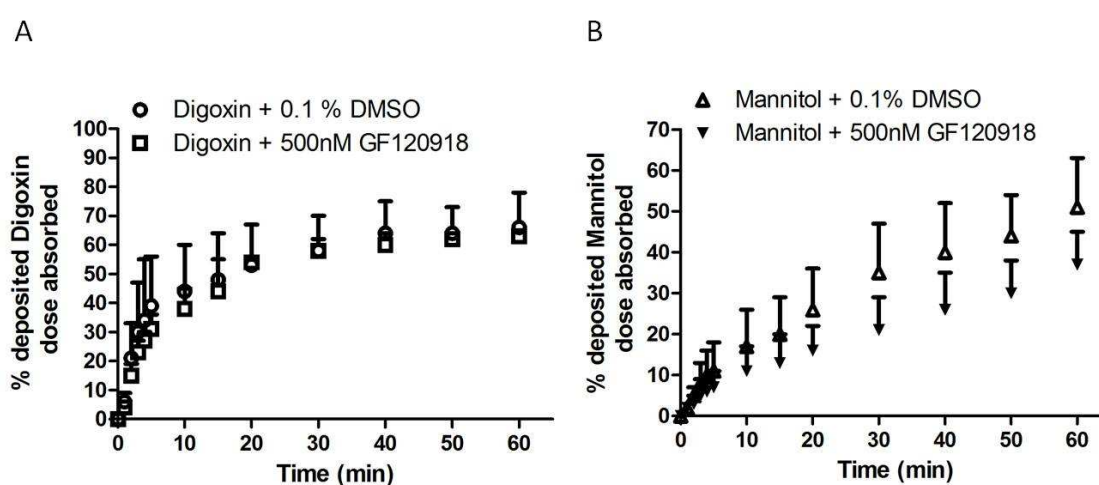


Figure 4.12 Effect of the P-gp inhibitor, GF120918 (in perfusate and airway instillate) upon cumulative % of lung deposited dose absorbed in the IPRL: **Figure 4.12A** – Effect of GF120918 at a concentration of 500 nM upon cumulative % of deposited digoxin absorbed with time. Data shown are expressed as mean \pm S.D (n=4 for each treatment). **Figure 4.12B** – Effect of GF120918 at a concentration of 500 nM upon cumulative % of deposited Mannitol absorbed with time. In this set of experiments, mannitol was co-administered along with digoxin dose. Data shown are expressed as mean \pm S.D (n=4 for each treatment).

As can be seen in table 4.11, the presence of the P-gp inhibitor, GF120918 (500 nM), in pulmonary perfusate and instilled dose had no significant effect ($p>0.05$) upon the percentage deposited dose absorbed by 60 min, the k_{in} (calculated from the initial linear portion of cumulative transport curves) nor the calculated $t_{1/2}$ (determined from nonlinear regression) of the P-gp substrate digoxin, when dosed to the IPRL. The inhibitor was also present in the IPRL perfusate 30 min prior to digoxin dosing.

Similarly, GF120918 (500 nM) had no significant effect ($p>0.05$) upon the absorption of mannitol in the IPRL. No significant difference could be observed for any of the measured parameters, suggesting the epithelial barrier to remain intact.

Treatment	Deposited dose in lung (DPM)	Cumulative mass of Digoxin absorbed by 60 min(DPM)	Percentage of deposited Digoxin dose absorbed by 60 min (%)	K_a (min^{-1})
Digoxin + 0.1 % DMSO	1867344 ± 636794	1240401 ± 410213	68.13 ± 12.03	0.262 ± 0.172
Digoxin + 500 nM GF120918	1955306 ± 923943	1259509 ± 570797	65.59 ± 4.05	0.126 ± 0.036

Table 4.11 Effect of GF120918 upon the transport of digoxin. The P-gp inhibitor was present at 500 nM in the perfusate and in the co-instilled airway doses of digoxin. k_a was calculated by linear regression. Data shown are expressed as mean ± S.D (n=4 for each treatment).

4.3.8. Flunisolide absorption from airways: Effect of GF120918 co-instilled and in IPRL perfusate

As can be seen in figure 4.13A, the addition of GF120918 (500 nM) co-instilled with a dose of flunisolide (2 µg) into IPRL perfusate had an apparent opposing effect to that seen with Rh123, in that, with flunisolide, the presence of GF120918 resulted in a decrease in the extent of absorption of flunisolide. Figure 4.13B acts as comparison; duplicate of figure 4.6B.

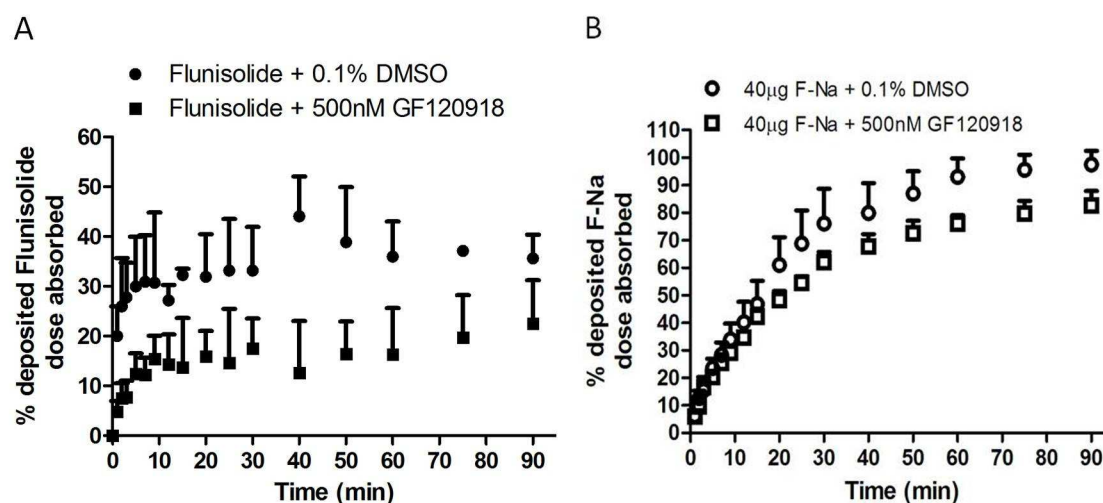


Figure 4.13 Effect of the P-gp inhibitor, GF120918 (in perfusate and airway instillate) upon cumulative % of lung deposited dose of flunisolide absorbed in the IPRL: **Figure 4.13A** – Effect of GF120918 at a concentration of 500 nM upon cumulative % of deposited flunisolide absorbed with time. Data shown are expressed as mean ± S.D (n=4 flunisolide + 0.1 % DMSO, n=5 for flunisolide + GF120918). **Figure 4.13B** – Effect of GF120918 at a concentration of 500 nM upon cumulative % of deposited F-Na absorbed with time. Data are of that shown in figure 4.6B and are expressed as mean ± S.D (n=4 for each treatment).

Table 4.12 illustrates that, with addition of GF120918 (500 nM), cumulative mass of flunisolide absorbed by 90 min decreased, by 1.45-fold in comparison to control. A decrease can also be observed for initial k_{in} (linear regression), when inhibitor is present. However, while the initial k_{in} of flunisolide absorption in presence of inhibitor is significantly different ($p<0.05$) from that of control, the percentage of deposited flunisolide dose absorbed by 90 min does not show a statistically significant ($p>0.05$) difference when comparing control data to inhibitor inclusion data.

Treatment (Nominal dose μg)	Deposited dose in lung (μg)	Cumulative mass Flunisolide absorbed by 90 min (μg)	Percentage of deposited Flunisolide dose absorbed by 90 min (%)	k_{in} (min^{-1})	$t_{1/2}$ (min.)
Flunisolide (2 μg) + 0.1 % DMSO	1.79 ± 0.66	0.625 ± 0.101	35.62 ± 4.74	$0.047 \pm 0.021^*$	$0.669 \pm 0.355^\dagger$
Flunisolide (2 μg) + 500 nM GF120918	1.92 ± 0.01	0.432 ± 0.170	22.49 ± 8.71	0.015 ± 0.005	0.246 ± 0.064
F-Na (40 μg) + 0.1 % DMSO	38.83 ± 2.22	35.62 ± 1.43	91.90 ± 5.95	0.022 ± 0.003	13.18 ± 0.40
F-Na (40 μg) + 500 nM GF120918	40.08 ± 1.93	33.13 ± 3.12	82.55 ± 5.26	0.019 ± 0.002	14.37 ± 1.72

Table 4.12 Effect of GF120918 upon the transport of flunisolide in the IPRL. The P-gp inhibitor was present at 500 nM in the perfusate and in the co-instilled airway doses of flunisolide. * - statistically different ($p<0.01$) k_{in} when compared to flunisolide + GF120918 data. † - statistically different ($p<0.01$) $t_{1/2}$ when compared to flunisolide + GF120918 data. Data shown are expressed as mean \pm S.D (n=4 for flunisolide (2 μg) + 0.1 % DMSO, n=5 for flunisolide (2 μg) + 500 nM GF120918). F-Na data are of that displayed in table 4.8 (n=4 for each treatment).

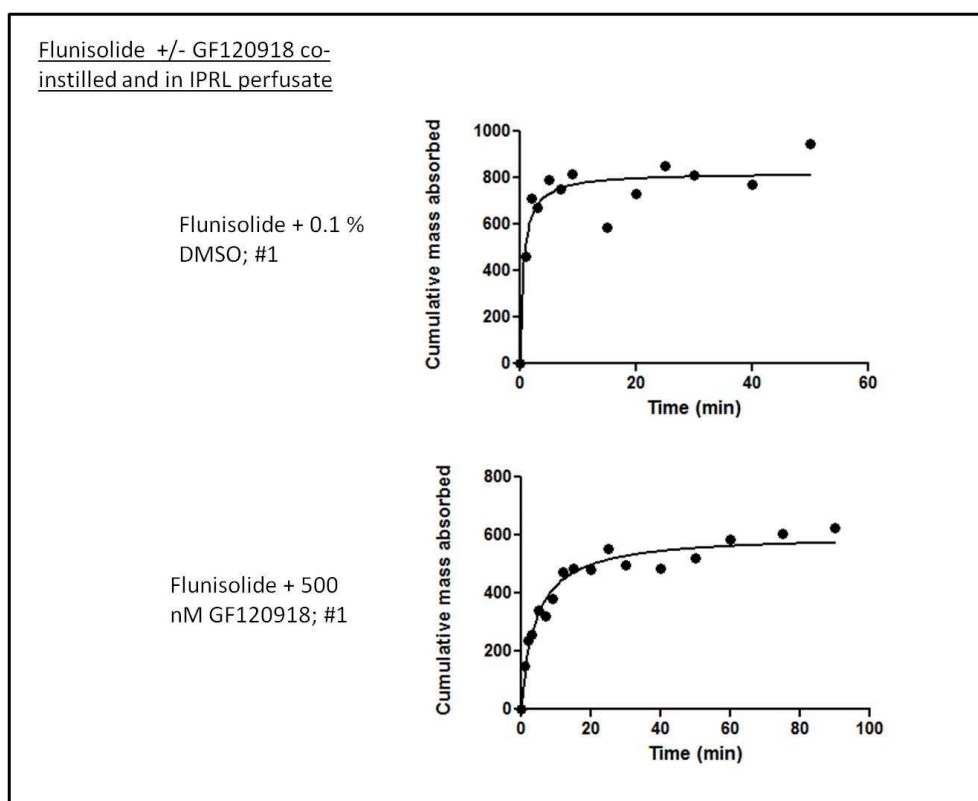
Despite the lack of significant difference between percentage of deposited flunisolide dose absorbed by 90 min(%) in the presence and absence of inhibitor, when comparing the same parameter at a number of different timepoints, a consistent significant ($p<0.05$) difference could be observed, table 4.13.

Treatment (Nominal dose μg)	Percentage of deposited Flunisolide dose absorbed by 20 min (%)	Percentage of deposited Flunisolide dose absorbed by 40 min (%)	Percentage of deposited Flunisolide dose absorbed by 60 min (%)	Percentage of deposited Flunisolide dose absorbed by 90 min (%)
Flunisolide (2 μg) + 0.1 % DMSO	31.92 \pm 8.56*	44.09 \pm 8.00*	35.96 \pm 7.05*	35.62 \pm 4.74
Flunisolide (2 μg) + 500 nM GF120918	15.91 \pm 5.11	12.61 \pm 10.41	16.34 \pm 9.28	22.49 \pm 8.71

p>0.05

Table 4.13 Comparison of the percentage deposited flunisolide dose in the presence and absence of P-gp inhibitor over a range of time points. Data shown are expressed as mean \pm S.D (n=4 for flunisolide (2 μg) + 0.1 % DMSO, n=5 for flunisolide (2 μg) + 500 nM GF120918). * - significantly different (p<0.05) when compared to corresponding timepoint data where GF120918 was present in instillate dose and IPRL perfusate at a concentration of 500 nM.

Figure 4.14 illustrates the nonlinear regression plots generated when fitting a Michaelis-Menton type equation to substrate absorption data. The model used was analogous to that used previously (detailed in materials and methods section).



Figures 4.14 Example of plots generated by nonlinear regression. Data shown are expressed as mean \pm S.D (n=4 for flunisolide (2 μg) + 0.1 % DMSO, n=5 for flunisolide (2 μg) + 500 nM GF120918).

4.4. Discussion

Since the discovery of P-glycoprotein by Juliano & Ling in 1976, [70], functional roles and expression patterns for this well studied ABC transporter have been hypothesised and investigated. The expression of P-glycoprotein within the respiratory system as a whole, and more specifically, within lung parenchyma, is generally accepted. Indeed, illustrated expression of this protein to particular cell types within parenchymal tissue has been achieved. Through use of immunohistochemistry in normal human lung samples, P-glycoprotein has been localised to both apical and basolateral epithelial cell membranes [43]. Further, localisation to alveolar epithelial cells has also been demonstrated by Campbell *et al.*, who established expression of P-glycoprotein in both human and rat type I alveolar epithelia [137].

In addition to localisation to several specific lung cell types, P-glycoprotein functionality has been illustrated. In both human and rat cell samples, active P-glycoprotein mediated efflux of a number of known substrates has been shown. Additionally, subsequent inhibition of such transport has also been illustrated, confirming P-glycoprotein as an active efflux transporter [113, 137].

The use of the flurophore dye, rhodamine 123 (Rh123) which is a known P-glycoprotein substrate, was chosen to illustrate functional activity of P-gp in the isolated perfused rat lung system. Of the rhodamine analogues, Rh123 is an attractive substrate of choice as it has been widely used as a P-glycoprotein substrate throughout the literature and in comparison to rhodamine 6G, has a lower passive permeability rate constant [367] therefore active efflux should be more pronounced. Rhodamine 123 has also previously been used to demonstrate efflux functionality of P-glycoprotein. In the human leukaemia cell line, K562, accumulation of the dye into both P-glycoprotein expressing and non-P-glycoprotein expressing cells was measured to allow characterisation of drug pumping action [371].

To further demonstrate the functionality of P-glycoprotein in the IPRL system, inclusion of the acridine derivative GF120918 (N-(4-[2-(1,2,3,4-tetrahydro-6,7-dimethoxy-2-isoquinolinyl)ethyl]-phenyl)-9,10-dihydro-5-methoxy-9-oxo-4-acridine carboxamide), which is a recognised P-glycoprotein inhibitor, was studied. For example, pre-treatment with GF120918 has been shown to increase concentrations of morphine, which is generally thought to be a P-glycoprotein substrate, in a rat cerebral microdialysis model; the blood brain barrier displays a particularly high expression of P-gp, limiting access of a wide range of xenobiotics to the CNS. Presence of the GF120918 increased morphine concentrations in the brain by 3-fold [372]. Moreover, Annaert *et al.*, demonstrated

reduced biliary excretion of Rh123 in sandwich-cultured rat hepatocytes in the presence of GF120918 [366]. GF120918, like many other 3rd generation P-glycoprotein inhibitors, was designed according to chemical structure-activity relationships in order to avoid limitations of previous generations of inhibitors such as toxicity and interaction with cytochrome P450 [373]. It is generally believed that GF120918 non-competitively inhibits P-glycoprotein through the inhibition of ATPase activity rather than competing as a substrate for the transporter [374].

In order to ensure the binding of Rh123 to BSA within the IPRL perfusate or indeed Rh123 binding to the plastic IPRL tubing did not detrimentally affect the analysis of Rh123 absorption across the IPRL, a number of validation experiments were conducted. Table 4.5 illustrated that, although there is a loss of approximately 20 % Rh123 in the post-deproteination supernatant, this loss is not concentration-dependent. Furthermore, this loss is accounted for during construction of the calibration curves that involve the same deproteination step. The 20 % loss suggests that some of the Rh123 remains bound to the precipitated and denatured protein. Moreover, Kajikawa *et al.*, reported Rh123 plasma protein binding at ~76 % [375]. Further, Rh123 recovery from IPRL tubing is also consistent independent of Rh123 concentration, with neither the presence nor action of a peristaltic pump, nor the addition of GF120918 influencing binding.

The dose escalation of Rh123 (Figure 4.5A) from a nominal dose of 2 µg to 80 µg showed Rh123 absorption to involve a saturable barrier to absorption, with saturation occurring within the range of 40 µg and 80 µg Rh123 instilled dose. Conversely, dose escalation of the paracellular transport probe, sodium fluorescein (Figure 4.5B), did not exhibit any dose-dependency in the % of deposited F-Na dose absorbed. This lack of effect of dose upon F-Na absorption supports the lack of any non-specific events that may have resulted in the observed Rh123 absorption data. The role of P-gp in the saturable barrier to Rh123 absorption within the IPRL was suggested by the experiments co-administering the P-gp inhibitor GF120918; either in the airway instillate alone or in both the airway instillate and the recirculating pulmonary perfusate. With GF120918 addition to the IPRL, significant increases in the amount of Rh123 absorbed were observed (Figure 4.6A). Increasing the concentration of GF120918 from 150 nM to 500 nM did not produce any enhancement in Rh123 absorption, suggesting a concentration of GF120918 of 150 nM to be sufficient in inhibiting P-gp-mediated reductions in pulmonary Rh123 absorption. Within the materials and method section of this chapter, an appropriate inhibitor concentration was considered with reference to the literature (Table 4.3). The current finding that inhibition of P-gp could not be improved at a GF120918 concentration above 150 nM is not inconsistent with the literature where similar concentrations

have been employed in order to achieve P-gp inhibition; and suggests P-gp functionality in the lung may be comparable to other experimental models [376-378]. As can be seen in figure 4.6B, P-gp inhibition had no effect upon F-Na absorption, substantiating that GF120918 has no capacity to increase the passive paracellular permeability of the pulmonary barrier. It is of note that inclusion of the P-gp inhibitor co-instilled into the airways with Rh123 or F-Na, i.e. not in the perfusate, resulted in a similar increase in Rh123 absorption to a situation where the inhibitor was present in both the airway instillate and in the perfusate (Figure 4.7A-B). This indicates that there is no requirement for pre-dosing of the inhibitor and that significant equilibration between perfusate and lung is not important in terms of GF120918 bringing about its actions upon P-gp, at least in the IPRL model used in these experiments.

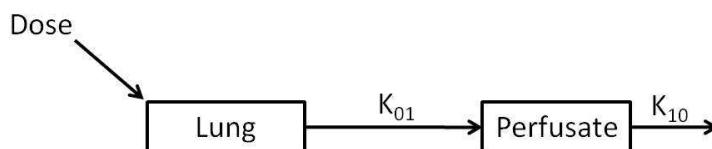
The saturation of P-glycoprotein in the Rh123 dose ranging studies reported here is consistent with Cisternino *et al.*, who demonstrated saturation of P-gp at the rodent blood-brain barrier with respect to the antitumor agent, TXD258. On increasing drug dose from 15 to 90 mg m⁻², a greater than proportional increase in concentration of TXD258 within brain extract was observed [379]. Further, saturation of P-gp with a rhodamine analogue, rhodamine-6G (R6G) has been observed in an isolated lung system by Roerig *et al.*, [21]. However, the work of Roerig *et al.*, suggested that a saturable barrier was present in the lung, limiting transport of R6G into the lung from the perfusate, i.e. from the 'blood'-to-lung direction. Further, Roerig *et al.*, also reported a ~20 % increase in the uptake of the rhodamine analogue, R6G, from perfusate to lung in an isolated perfused rabbit lung with the addition of 20 µM GF120918. The authors concluded that P-gp in the lung is saturable, in the blood-to-lung direction and can be modulated by drug substrates and chemical inhibitors [355]. No other laboratory has yet confirmed a P-gp mediated efflux mechanism limiting access of drug from blood to lung in a whole lung i.e. isolated organ preparation. Indeed systemic pharmacokinetic studies in *mdr1* knockout mice do not show a differential equilibrium partition between blood and lung when comparisons are made between the *mdr1* knockout mice and wild-type mice. If the Roerig data was applied to these knockout mice then we would expect to see reduced equilibrium partitioning in the lung in the *mdr1* (-/-) mice which is not what is observed [362, 380-383].

Nonlinear modelling of substrate transport data obtained from IPRL experiments was undertaken in order to further understand mechanisms involved in absorption in an isolated lung. Pharmacokinetic parameters including, k_{01} (rate of substrate transport from lung to perfusate) and absorption half-life ($t_{1/2}$) were determined. The initial absorption rate (k_{in}) of Rh123/F-Na across the IPRL, reported in Tables 4.7 – 4.9, was calculated from the initial linear portion of cumulative

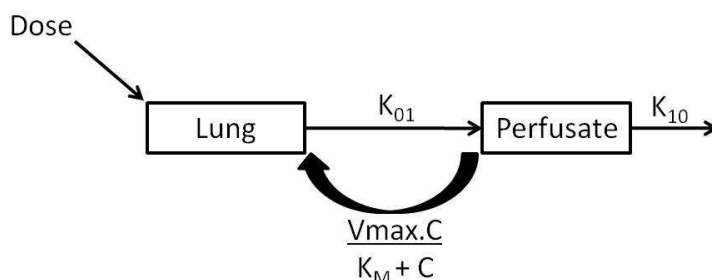
transport curves and the equation $y=mx+c$, i.e. k_{in} calculated as $k_{in} = m/\text{actual dose to lung}$. However, as the equation of a straight line does not accurately represent substrate absorption by the lung, a more descriptive model was applied to all data. Further, within the literature, many reports of substrate pulmonary transport are described via the application of kinetic modelling [328, 334, 344]. The pharmacokinetic software WinNonlin (Pharsight, Mountain View, USA) was employed to all data obtained from IPRL experiments and pharmacokinetic parameters were calculated by compartmental analysis. WinNonlin has been previously utilised by members of the Welsh School of Pharmacy [384] and in the wider literature to determine kinetic parameters associated with P-gp function [385].

Pharmacokinetic modelling of data obtained from Rh123/F-Na IPRL experiments (Table 4.10) demonstrated that calculated $t_{1/2}$ from all F-Na data showed no significant difference between treatments dosed to the IPRL. Such findings mirror the pattern of calculated k_{in} displayed in tables 4.7 – 4.9. The calculated $t_{1/2}$ (from nonlinear regression) of Rh123 treatments dosed to the IPRL does not mirror the pattern displayed by k_{in} (tables 4.7 – 4.9). Determination of pharmacokinetic parameters, by WinNonlin, associated with Rh123 absorption across the IPRL show no significant difference for the k_{01} (or the absorption rate constant) parameter between the dose treatments, with the exception of 2 μg Rh123 data from the dose-ranging study. There were large standard deviations associated with each calculated k_{01} and $t_{1/2}$ highlighting variability within the data set but also potential imprecision in the model. The pharmacokinetic model (see materials and methods) applied to all data was described by a first-order one compartment model with an elimination rate constant from the perfusate that was constrained to be essentially negligible. Figure 4.15 represents the model applied to IPRL data, both Rh123 and F-Na (top panel), and illustrates a potential model (bottom panel) that may improve the accuracy of parameter estimation for the Rh123 data, i.e. it provides the potential for a saturable mechanism in the uptake from perfusate to lung.

Model for F-Na transport



Model for Rh123 transport (P-gp substrate)



	Rhodamine 123	Digoxin	Flunisolide
K_M for P-glycoprotein (μM)	13.5	59	---
M_w ($\text{g}\cdot\text{mol}^{-1}$)	380.82	780.93	434.49
LogD	0.53	1.7	1.92

Figure 4.15 Diagram illustrating pharmacokinetic model describing F-Na and Rh123 transport across the IPRL. The chart illustrates parameters that might affect substrate transport by P-glycoprotein.

Despite the seemingly unsuitable nature of the employed pharmacokinetic model to Rh123 data, its application to this data has highlighted the more complex nature of Rh123 pulmonary absorption in comparison to F-Na absorption (i.e. involvement of P-gp), further confirming the functional significance of P-gp upon absorption of a substrate delivered to the lung.

The cardiac glycoside and well-recognised P-gp substrate digoxin was chosen to dose to the IPRL in the presence and absence of GF120918 with the aim of affirming the functional significance of P-gp upon substrates delivered into the airways. While the affinity of digoxin for P-gp appears to be lower than other P-gp substrates (Figure 4.15) [386], there is very compelling evidence that the cardiac drug is a substrate of this drug transporter [360]. P-glycoprotein mediated efflux of digoxin is well established, for example, Djuv and Nilsen reported significant basal – to – apical (B-A) transport of digoxin (30 nM) in the Caco-2 cell line which was decreased by 61 % with the introduction of the P-gp inhibitor verapamil (100 μM) [387]. In both the wild type MDCK cell line

and the MDCK-hMDR1 cell line that over-expresses human P-gp, verapamil has again been shown to decrease the efflux ratio (basal – to – apical/apical – to – basal) of digoxin. In MDCK-WT cells (which nevertheless contain canine P-gp), the efflux ratio of digoxin transport was reduced from 5.2 to 2.0 with the addition of 200 μ M verapamil. This decrease was more significant in MDCK-hMDR1 where the efflux transport ratio was reduced from 25.5 to 1.3 with the addition of the P-gp inhibitor [388]. Within the lung, tissue accumulation of digoxin in *mdr1a*⁻ mice is approximately twice that of *mdr1a*⁺ mice suggesting an apparent role of *mdr1a* in effluxing digoxin from the lung [360].

Within the isolated perfused rat lung utilised here, it was hypothesised that the inclusion of GF120918 co-instilled into the airways and present in IPRL perfusate would increase the percentage of deposited digoxin dose absorbed. As can be seen in figure 4.12, digoxin transport across the IPRL was not affected by the presence of GF120918. The mean percentage deposited dose of digoxin transported reached ~45 % by 10 min, in comparison, the maximum percentage deposited dose of Rh123 (all treatments) transported by 90 min was ~20 % and the passive permeability probe F-Na only reached ~30 % deposited dose transported by 10 min (Figure 4.5B). When comparing pharmacokinetic parameters, the initial k_{01} of digoxin absorption did not alter significantly ($p > 0.05$) with the addition of GF120918 (Table 4.11). Indeed, comparison of calculated $t_{1/2}$ for digoxin and the passive permeability probe mannitol revealed mannitol to have a longer absorption half-life in the IPRL than digoxin (data not shown). These results show digoxin to exhibit a more rapid absorption profile across the lung suggesting simple diffusion as a transport mechanism.

The apparent lack of significance of P-gp upon digoxin transport across the IPRL was initially surprising given the clear evidence for P-gp influence over Rh123 transport. Within the literature, Manford *et al.*, also examined the influence of P-gp upon the pulmonary absorption of digoxin. Here digoxin (3.5 mg/kg) was instilled to the lungs of CF-1 mice (which displays an *mdr1a*^{-/-}, *mdr1b*^{+/+} phenotype) and the absorption profiles compared to that of digoxin instilled into the lungs of wild-type mice (*mdr1a*^{+/+} and *mdr1b*^{+/+} phenotype). No significant difference in the 'lung concentration vs. time' or 'plasma-concentration' profiles of digoxin absorption were observed between the two strains. The ratio of digoxin: mannitol concentrations within the lung of both strains over 90 min was shown to be consistent suggesting lack of an active digoxin absorption mechanism [361].

The use of CF-1 mice does not take into consideration the contribution of the *mdr1b* gene isoform to digoxin transport within the lung, a tissue within which *mdr1b* has been shown to be more highly

expressed (rat lung) than the *mdr1a* gene [389, 390]. The apparent lack of P-gp effect upon digoxin transport across the lung could be interpreted as the significant influence of the *mdr1b* isoform upon this substrate, effluxing digoxin to the airspace of the lung for the duration of the experiment. The concordance of the results of this chapter to those of Manford *et al.*, somewhat reduce the likelihood of overlooked *mdr1b* involvement. Further, Lanman *et al.*, report similar rapid absorption of digoxin from the rat respiratory tract and constant extent of absorption over a concentration range, indicating the mechanism of transport to be unsaturable. These works also interestingly noted a relationship between a molecule's chloroform/water partition coefficient and its absorption rate from the lung, i.e., the higher the partition coefficient, the more rapid the absorption rate [391].

The association of passive permeability with drug transporter absorption kinetics has been increasingly investigated. The role of passive permeability in influencing a compound's absorption rate is well understood, the interplay with active transport less so. The promiscuous substrate specificity of P-gp only reveals certain substrate physico-chemical properties, such as a degree of hydrophobicity, planar structure and for some substrates a slight but depolarised positive charge to be of importance. It is now well recognised that P-gp binds substrates from the lipid phase of the plasma membrane before they reach the cytosol, therefore, highlighting relative partitioning into the membrane to be of importance [392]. Lentz and co-workers examined the relationship between passive permeability and P-gp absorption kinetics and illustrated that, within Caco-2 and MDCK-hMDR1 cell lines, the transport of both high and low permeability P-gp substrates was not affected by the introduction of GF120918 to culture medium. They postulated that substrates with a high passive permeability would dominate over the efflux action of P-gp, while low passive permeability substrates would be presented to P-gp only at low concentrations, presenting a negligible drug load to P-gp and hence resulting in low impact of this transporter. Both vinblastine and cimetidine are moderately permeable substrates and in the work of Lentz *et al.*, appeared to be affected by the presence of GF120918 [393]. Etyan *et al.*, reported that the inconsistent nature of P-gp substrate membrane permeability requires P-gp to overcome passive influx rate in order to be successful. They highlight that substrates such as gramicidin traverse the membrane in minutes and are therefore susceptible to P-gp involvement while substrates such as valinomycin traverse the membrane in microseconds, overcoming the efflux ability of the transporter [356]. To give further substance to the role of passive permeability within P-gp absorption kinetics, it has been observed that poor P-gp substrates commonly act as P-gp modulators possibly as a result of rapid inward

permeability, while slower inwardly permeable compounds are available at a rate where P-gp can efflux [392].

The importance of passive permeability upon P-gp absorption directly highlights the importance of factors that influence passive permeability. When comparing Rh123 and digoxin as P-gp substrates, Rh123 presents itself as the more attractive as it has a permanent positive charge and is relatively hydrophilic creating a more moderate rate of passive permeability, while digoxin has been found to have a much higher passive permeable potential that can prevail over P-gp action [367, 394]. The herein reported lack of influence of the P-gp inhibitor, GF120918, upon digoxin transport across the IPRL does not essentially eradicate the functional significance of P-gp within the lung, but instead highlights the intricate relationship between P-gp absorption and passive permeability.

Although not extensively recognised as a P-gp substrate, the synthetic, topically active corticosteroid, flunisolide, represents an appealing substrate for examining P-gp influence upon drugs delivered to the lung [395]. Traditionally employed in the treatment of persistent asthma, such synthetic corticosteroids were plagued with poor lung and high oropharyngeal deposition - post inhalation. However, in accordance with the Montreal protocol [26], the replacement of CFC content with HFA propellant in all MDI devices effectively reversed undesirable deposition problems, improving lung delivery and potentially enhancing therapeutic effect. Increased deposition to the lung however, has potential to create side effects such as toxicity and drug-transporter interactions [396]. Further, as an uncharged molecule with a moderate hydrophobicity value (ClogP), flunisolide presents itself as a candidate P-gp substrate with eligibility for investigation within the IPRL [397, 398].

Flunisolide was introduced to the IPRL in the presence and absence of GF120918. Since reported physico-chemical parameters strongly identify flunisolide as a P-gp substrate, it was hypothesised that addition of GF120918 to the IPRL would alter significantly the percentage of deposited flunisolide absorbed with time. As can be seen in table 4.12, the addition of GF120918 (500 nM) altered the percentage deposited flunisolide dose absorbed at 90 min by 1.45-fold. This change, however, was not statistically significant ($p > 0.05$) when compared to control (flunisolide + 0.1% DMSO). Tables 4.12 and 4.13 show that the addition of GF120918 to instillate and perfusate did however significantly alter ($p < 0.01$) the initial k_{in} , calculated $t_{1/2}$, and the percentage deposited flunisolide dose absorbed at 20, 40 and 60 min. Despite the non-significant ($p > 0.05$) decrease in percentage deposited flunisolide dose absorbed by 90 min, when examining the mean percentage of

deposited dose absorbed by 60 and 90 min, flunisolide + 0.1% DMSO control mean percentage remained relatively stable suggesting a plateau in absorption was reached pre-90 min time point.

As a substrate, flunisolide has previously been used in order to assess P-gp influence within the pulmonary system. Florea *et al.*, utilised flunisolide as an example of a synthetic corticosteroid and illustrated P-gp influence upon the transport of this drug within the Calu-3 cell line [398]. Within the Florea *et al.* study, clear polarised apical – to – basal transport was shown. Further, the influence of an ATP dependent process, and more specifically, involvement of P-gp was shown with use of specific inhibitors (verapamil, SDZ PSC 833 and LY335979) [398]. Florea and co-workers further illustrated involvement of P-gp upon flunisolide transport in MDR1-Pgp transfected, LLC-PK1 pig kidney epithelial cell lines, however, in this case polarized transport was observed in the basal – to – apical direction. The clear difference in the direction of polarized transport between the lung and kidney cell lines was rationalised by immunoblotting and confocal laser scanning microscopy; a 170 kDa P-gp band was observed in cell lysates from both Calu-3 and LLC-MDR1 cell lines [398]. Where P-gp was predominantly localised to the basolateral cell membrane in Calu-3 cells, localisation to the apical membrane in the LLC-MDR1 cell line was seen [398]. The findings of Florea and co-workers show disparity with the literature, within which P-gp is generally accepted to be apically expressed serving a barrier function, i.e., casting doubt over the involvement of P-gp in apical-to-basolateral polarised transport [362, 399]. However, Florea *et al.*, attribute the polarised transport of flunisolide to P-gp for a number of reasons; the clearly demonstrated involvement of an ATP-dependent process that was significantly reduced through the use of P-gp inhibitors, the amphipathic chemical structure of flunisolide lending itself to transport via P-gp and the recognised involvement of P-gp in the intracellular trafficking of cholesterol, to which flunisolide shares great structural semblance [397, 398, 400].

The preponderance of literature evidence reports P-gp to localise apically in a wide range of cells in a number of tissues. The use of various experimental techniques has localised P-gp to the apical membrane of; liver epithelia, small ductules of the pancreas, kidney proximal tubule epithelial cells, columnar epithelia of the colon and jejunum, and the apical surface of capillary endothelial cells of the blood-brain barrier [401, 402]. Within the deep lung, i.e. predominant deposition location of drugs dosed to the IPRL, P-gp has been localised to the apical membrane of type I alveolar epithelial cells of human and rat and has also been detected by Western blotting within type II alveolar epithelial cells [113, 137]. Cellular localisation of P-gp within the Calu-3 submucosal gland carcinoma cell line is less clear, Hamilton *et al.*, report P-gp functional activity consistent with an apical

localisation in Calu-3 cells and apical localisation of P-gp within similar cells of bovine olfactory and nasal respiratory mucosae have also been reported [403, 404]. However, in a similar vein, Uematsu *et al.* report localisation to the basolateral membrane of serous acinar cells of the salivary gland and P-gp mediated basolateral efflux of xenobiotics from interstitial fluid has been demonstrated, suggesting a similar mechanism in Calu-3 cells, which are derived from submucosal glands [398, 405].

The disparity in the localisation of P-gp within Calu-3 cells casts doubt over the subsequent efflux direction of substrates by this transporter. Indeed, in a contradictory manner, a 2001 study by Hamilton *et al.*, illustrated polarised basal – to – apical transport of Rh123 in Calu-3 cells thus supporting apical orientated P-gp effluxing to the lumen of the airways [403]. While a small number of studies share some concern over the possible involvement of other transporter proteins in the transport of Rh123 [385, 406], this substrate is widely utilised within the literature to examine the functional activity of P-gp [371, 375, 407, 408]. In a study with LLC-MDR1 cells, significant B-A transport of Rh123 by P-gp was demonstrated which was subsequently inhibited by Amyloid- β peptides. Further, P-gp was shown to be apically expressed within these cells by immunofluorescence and confocal laser scanning microscopy [409]. Additional examples of the use of Rh123 as a substrate for P-gp transport include, for example, *in vivo* rat intestines and Caco-2 cells, Chinese hamster fibroblasts, human leukaemia cell lines and transport to the aqueous humour of the rabbit eye [375, 407, 408, 410]. The abundance of available literature illustrating use of Rh123 as a P-gp substrate, combined with use of specific P-gp inhibitors in many studies suggests P-gp as the more likely mechanism for Rh123 transport. Further, as the results obtained for flunisolide transport in this chapter complement the data reported by Florea *et al.*, it is possible that a second mechanism of transport exists for the transport of flunisolide in Calu-3 cells and the IPRL rather than challenging the exactness of P-gp localisation within Calu-3. Indeed the possibility of a second mechanism; potential flunisolide transport by an OCT transporter, for flunisolide transport was considered by Florea and colleagues but not further explored. The involvement of OCT transporters OCT1 (SLC22a1) and OCT2 (SLC22a2) in the transport of other P-gp substrates has been illustrated within various kidney cell lines [385, 411], further both transporters have been suggested to be present in the lung; albeit with contradictory reports. Bleasby *et al.*, [69] reported moderate (25-50 % quartile) OCT2 expression and low (0-25 % quartile) OCT1 expression in human lung, Endter *et al.*, [104] report OCT1 expression at the mRNA level in a variety of lung cell culture models (they also report no OCT2 expression in the same samples). Within the results of this thesis, both OCT1 and

OCT2 mRNA was detected at some level in the rat lung cell samples studied. In addition, the contribution of passive permeability should be considered in the transport of flunisolide. The pharmacokinetics of flunisolide in humans displays a fast absorption phase with a short dwell time in pulmonary tissue. The literature reports of LogP or ClogP places flunisolide between Rh123 and digoxin in terms of their partition coefficient (Rh123 LogP = 1.06, flunisolide ClogP = 1.71, digoxin = LogP = 2.2) [398, 412, 413]. As discussed above passive permeability is likely to be somewhat inextricably involved in the susceptibility of molecules to efflux by P-gp. However, the alteration of flunisolide transport by P-gp inhibitors reported by Florea *et al.* and within this chapter presents the involvement of a second active transporter as a more likely mechanism of transport.

GF120918 is also known to be active upon the ABCG transporter BCRP [374]. Within the study conducted by Florea *et al.*, flunisolide transport is linked to ATPase activity and an additional number of 3rd generation P-gp inhibitors were used [398]. There exist a number of literature reports documenting the presence of a number of other drug transporters within the Calu-3 cell line. For example, Endter and co-workers report the presence of an additional 23 transporters from the ABC, SLC and SLCO families in Calu-3 cells in culture and drug transporters MRP1 and CFTR have been specifically localised within these cells [242, 414, 415]. From this, the involvement of an alternate drug transporter in the transport of flunisolide across Calu-3 cells and the IPRL could be feasible. In a recent literature review by Bosquillon, flunisolide was reported as a substrate of only P-gp [354], Florea *et al.*, also dismiss the involvement of alternative transporters, such as MRP1, as flunisolide was shown to be transported unmetabolised in the Calu-3 model [398]. However, the presence of other drug transporters in Calu-3 cells does enhance the possibility of alternate transporter involvement. The study by Florea and colleagues does itself compare the chemical structure of flunisolide to cholesterol, a substrate that is known to be transported by drug transporters of the ABCG family. Further, Endter *et al.*, report the presence of ABCG1 in Calu-3 cells and the results of Chapter 2 (RT-PCR studies) also confirm the presence of this transporter in the rat lung [113]. A study by Janvilisri has shown the transporter ABCG1 (White-1) to be involved in the transport of sterols, including cholesterol and estradiol and the *Drosophila* ABCG1 homolog *white* is known to act as an importer for eye pigment precursors [156, 416]. Whilst only supposition, it could therefore be deduced that flunisolide is a substrate of the ABCG1 transporter, providing polarised A-B transport, and that the addition of GF120918 (known inhibitor of the ABCG transporter BCRP) inhibits this ABCG transporter reducing the polarised transport observed in Calu-3 cells and within the IPRL.

In conclusion, through initial Rh123 studies performed with the IPRL, the functional expression of P-glycoprotein has been illustrated. The functional activity of P-gp shown within such a model as the IPRL is more likely to provide a truer representation of an *in vivo* state thus both illustrating the applicability of an *ex vivo* model to the investigation of drug transporter influence and also highlighting the issues created by the presence of such functional transporters within the lung. Further, the addition of additional P-gp substrates has emphasized the complexity of substrate absorption mechanisms across the lung highlighting the value in understanding the interplay of such mechanisms and the need for extensive further studies in this area of research.

Chapter 5

Efflux functionality at the pulmonary endothelium: limiting drug transport from vasculature to lung

5.1. Introduction

The laboratory rat is perhaps the most widely used and well recognised animal model employed in scientific research. Given the widespread role of this animal model in scientific advancement, it is sometimes easy to forget some of the underlying anatomy of this species [417].

This chapter focuses upon the potential for efflux at the pulmonary vascular barrier limiting drug uptake from the pulmonary circulation into the lung. The pulmonary circulation of the rodent is essentially similar to that of humans (Figure 5.1). Aside from the obvious physiological requirement of the lungs to receive the entire cardiac output for blood oxygenation, the lung tissue itself is perfused by both the bronchial and pulmonary circulations [418].

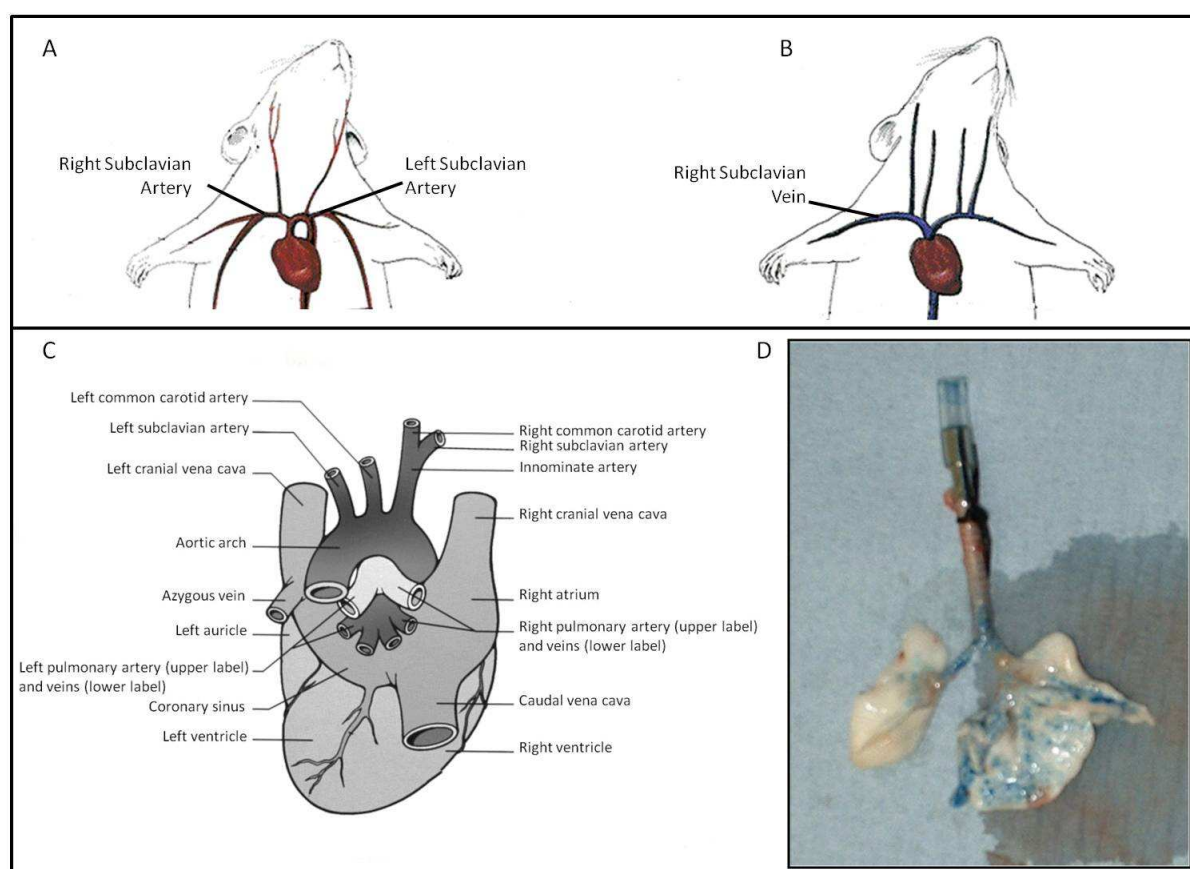


Figure 5.1 Major upper thoracic vasculature of the rat. A – Key upper thoracic arteries of the rat, not including pulmonary vasculature. B – Main upper thoracic veins of the rat, again, pulmonary vasculature is not detailed. C – Diagram of the rodent heart (distal view). The human heart is essentially comparable in architecture. D - Deposition pattern of Evans blue dye dosed to the IPRL via a forced solution instillation technique (Chapter 3; Figure 3.7) [419].

Perfusion of the lung parenchyma is derived from the pulmonary artery, branching to the right and left to perfuse both right and left lobar lung regions. Both the pulmonary artery and vein, and their respective subdivisions spread extensively throughout the lung lobar tissue. Previous experiments

earlier in this thesis have shown that perfusion of the IPRL via the pulmonary artery of Evans blue dye results in visible and extensive permeation of the dye throughout in lung parenchyma (Figure 5.1) demonstrating the overall importance of the pulmonary circulation to lung tissue perfusion. The bronchial circulation primarily provides perfusion to the trachea and major bronchi. In the rat, the bronchial arteries arise from the subclavian arteries (Figure 5.1) and are thought to be responsible for providing up to 90 % of tracheal blood supply [420, 421]. The above points are important when considering the IPRL setup, in that although the IPRL does quite precisely mimic the rodent pulmonary system *in vivo*, there are important differences in lung perfusion. The surgical technique for lung isolation employed within this thesis is relatively universal and whilst efficiently isolating the rodent lung, the technique does sever the bronchial circulation [328]. Since bronchial circulation perfuses the upper airways, an absence within the IPRL suggests that the trachea and major bronchi may be poorly, or indeed lack completely, any vascular perfusion [418, 420]. A study by Ferreira *et al.* has however highlighted that, in rats, anastomoses between the bronchial and pulmonary circulations frequently exist (50 % of animals examined and is also somewhat dependent upon strain) such that the supply to the trachea and major bronchi is in part from the pulmonary circulation [418, 420, 421]. Conversely, absorption of solutes across tracheal epithelium can, in part, drain through the pulmonary vein to be returned to the systemic circulation. Extending this point Sakagami *et al.* reported the presence of an intact mucociliary escalator within their IPRL model (note the exact same model as applied in this thesis) responsible for pulmonary – to – bronchial clearance; although they did report negligible tracheo-bronchial transport of a number of varying molecular weight compounds both *in vivo* and the *ex vivo* model [101]. They concluded that a viable mucociliary clearance mechanism is present in the IPRL and is responsible for the ‘pooling’ of substrates dosed to the lung within the negligibly functionally active tracheo-bronchial region [344].

Clearly the pulmonary vasculature and blood flow can impact upon both handling of locally and systemically acting drugs within the lung. For drugs which display perfusion-rate limited membrane permeation, changes in the blood flow to the lung parenchyma could enhance or reduce systemic bioavailability of pulmonary administered drugs, and/or alter the uptake of drug from the systemic circulation into the lung; potentially leading to toxicity issues and drug-drug interactions [422]. Beyond this, the vasculature itself can have a profound influence upon drug disposition. No better example of this is the presence of active transporters in endothelial cells; the best known example being P-gp expression in the vasculature of the blood-brain barrier (BBB) [423]. Within the brain, P-gp has been localised to capillaries of the BBB in a number of genus. For example, Schinkel *et al.*, reviewed a number of papers and reported immuno-localisation of P-gp to capillary cells in human,

rodent and bovine brain [424]. Further, P-gp at the blood-brain barrier is known to mediate the extrusion of a wide range of compounds, limiting transfer to the brain and acting in a protective manner [423-425].

From this, a number of companies have developed P-gp modulators whose clinical indications extend beyond overcoming multiple drug resistance in cancer cells but also include modulation of P-gp at absorption or dispositional barriers [426]. For example, Kaddoumi *et al.*, illustrated that, through inhibition of P-gp by zosuquidar at the BBB of primate brain, the distribution of the HIV-1 protease inhibitor, nelfinavir, to the brain increased by 146-fold [427]. Further, Syvänen *et al.*, reported that, in rats, a significant increase in the brain penetration of the P-gp substrate verapamil can be achieved through the inhibition of P-gp by cyclosporin A [428]. While these are just an insight in to the opportunity to improve brain and central nervous system pharmacotherapy, the modulation of P-gp at the BBB has obvious advantages. However, as with the control of any number of active processes, concern exists surrounding the potential to increase toxic side effects [381].

Within the lung, the presence of P-gp at the membrane of endothelial cells is poorly evidenced. Demeule *et al.* reported expression of P-gp in the endothelial cells of the rat lung [429] and Roerig *et al.* [355] undertook functional studies in an isolated perfused rabbit lung and presented data consistent with a P-gp efflux mechanism acting to limit movement of a P-gp substrate from the vasculature into the lung itself.

Aims and Objectives

In this chapter, it will be sought to:

- Investigate the influence of P-gp serving as an efflux mechanism limited drug uptake from the vasculature into the lung.
- It is hypothesised that if functional, this could reflect expression of an efflux transporter either at vascular endothelial cells or at the basal surfaces of lung epithelial cells.
- The p-gp substrate Rh123 will be dosed to pulmonary perfusate and disappearance noted. Rh123 disappearance will be recorded as a measure of the loss into the lung.
- The passive permeability marker sodium fluorescein will also be dosed to IPRL perfusate in a similar manner and again its disappearance recorded.

5.2. Materials and Methods

5.2.1. Isolated Perfused Rat Lung (IPRL)

Materials

Animals

Male-specified pathogen-free Sprague-Dawley rats (Harlan UK Limited, Bicester, UK)

Consumables & Reagents

IPRL perfusate, filter sterilised; see chapter 3

Method

The IPRL procedure and forced solution instillation technique have been extensively described in Chapter 3. Briefly, a rat trachea was cannulated between the 4th and 5th cartilage ring using a custom made tracheal cannula (Harvard Apparatus Limited, UK). On dissecting the diaphragm, lungs were perfused through the pulmonary artery and manually inflated 4-5 times with 5 mL air to remove blood. Lungs were then surgically removed from the animal, with careful attention paid to ensure lung integrity was not compromised. Once removed, lungs were hung horizontally in a humidified artificial glass thorax maintained at 37 °C and slight hypobaric pressure. IPRL perfusate consisted of Krebs-Henseleit buffer containing 4 % (w/v) BSA and was buffered to pH 7.4, filtered and stored at 4 °C. IPRL perfusate was re-circulated through the pulmonary circulation at a constant flow rate of 15 mL/min. Before dosing, lungs were equilibrated for 5 min and ventilated with a tidal volume of 2.5 cm³ at a rate of 20 breaths/min. Each IPRL was maintained for 90 min with perfusate samples being taken from the reservoir and replaced with an equivalent perfusate volume. IPRL viability was confirmed by determining lung wet: dry weight at the end of each experiment. F-Na was also used as a validation probe as a marker of pulmonary epithelial integrity.

5.2.2. HPLC analysis: Rh123/F-Na levels in perfusate

Materials

Consumables and reagents

Acetonitrile; ACN, 99.6+ %, HPLC grade, (Fisher Scientific, Loughborough, UK, Cat: A/0626/17)

Sodium acetate buffer, 20 mM, pH 3.6/pH 4.0, (Fisher Scientific, Loughborough, UK, Cat: BPE334-500)

HPLC grade H₂O, (Fisher Scientific, Loughborough, UK, Cat: W/0106/PB17)

HPLC Column

4 μ m Genesis C18 column, (Grace, Illinois, USA).

Method

Sample analysis was conducted as per Chapter 3. Briefly, perfusate samples were deproteinated with acetonitrile (3:1 v/v acetonitrile: perfusate sample) then centrifuged (18,000 g, 10 min.) to yield sample supernatant. Deproteinated samples (0.1 mL) were injected onto a HPLC column. Mobile phase consisted of acetonitrile, dH₂O and 20mM sodium acetate buffer (pH 4.0) at a ratio of 50:30:20 (v/v/v) for Rh123 analysis and acetonitrile: dH₂O (50:50) and 20mM sodium acetate buffer (pH 3.6) at a ratio of 90:10 (v/v) for F-Na analysis. Mobile phase was pumped through the HPLC system at a flow rate of 1 mL/min with chromatic measurements being performed at room temperature. The substrate content of each supernatant sample was determined using a suitable calibration curve constructed in re-circulated perfusate from control IPRL experiments where lungs were not instilled. Perfusate concentrations were determined fluorometrically, Rh123 analysis undertaken at λ_{ex} 500nm, λ_{em} 540nm and F-Na analysis undertaken at λ_{ex} 485nm, λ_{em} 520nm. Substrate accumulation in lung was calculated as disappearance from IPRL perfusate over time.

5.2.3. Rh123 accumulation in lung (perfusate to lung): Effect of GF120918

Materials

Consumables & Reagents

Rhodamine 123; Rh123, >98 % electrophoresis grade, (Sigma-Aldrich, Dorset, UK, Cat: R-8004)

Sodium fluorescein; F-Na, (Fluka, Sigma-Aldrich, Dorset, UK, Cat: 46960)

GF120918; obtained from GlaxoSmithKline, Stevenage, UK.

Dimethyl sulfoxide; DMSO, BioReagent, for molecular biology, ≥ 99.9 %, (Sigma-Aldrich, Dorset, UK, Cat: D8418-50ML)

Method

An IPRL surgery was performed as per protocol, Chapter 3; methods; 3.2.2. Lungs were perfused with either vehicle control, i.e. DMSO (0.1 % v/v) or GF120918 (500 nM) for 30 min After this, Rh123 was added as a bolus to achieve a final Rh123 concentration in the perfusate 0.01 μ g/mL or 0.025 μ g/mL; see dose ranging comments below. The Rh123 concentrations were chosen by analyzing the actual concentration (μ g/mL) in perfusate at 90 min after dosing of Rh123 (5 μ g nominal dose which was recognised from previous experiments not to cause saturation of efflux transport, at least from the airways). A perfusate sample (1 mL) was immediately taken to determine initial Rh123 perfusate concentration. Samples were removed from the reservoir at 0, 5, 10, 15, 20, 25, 30, 40, 50, 60, 70, 80, and 90 min and centrifuged at 18,000 g for 10 min Sample volumes were replaced with perfusate containing either DMSO (0.1 % v/v) or GF120918 (500 nM). Resulting supernatant was

fluorometrically analysed using HPLC and Rh123 accumulation in lung was determined by calculating Rh123 remaining in IPRL perfusate.

In a separate experiment, F-Na (0.1 µg/mL) was also dosed to IPRL perfusate and lung accumulation determined to act as a control.

5.2.4. Data Analysis

To determine the significance of GF120918 addition upon the loss of Rh123 from the perfusate: (1) Based upon the % of RH123 dose remaining in the perfusate compartment an initial rate of Rh123 disappearance was determined by linear regression to calculate (k_{perf}); (2) Based upon mass of Rh123 remaining in the perfusate compartment a disappearance rate constant (K_{NL}) was calculated by nonlinear regression.

Nonlinear regression analysis was undertaken using Graphpad software, the below equation was employed to model the mass of Rh123 remaining in the perfusate as a function of time.

$$M_t = M_0 * \exp^{-K_{\text{NL}} * t}$$

Where M_t is the mass of Rh123 at any time (t); M_0 is the mass of Rh123 in the perfusate immediately at the start of the experiment; K_{NL} is the first-order rate constant describing the loss of Rh123 from the perfusate. A $t_{1/2}$ can be calculated from the first-order rate constant as $0.693/K_{\text{NL}}$. The model is a monoexponential one and therefore represents the simplest approach.

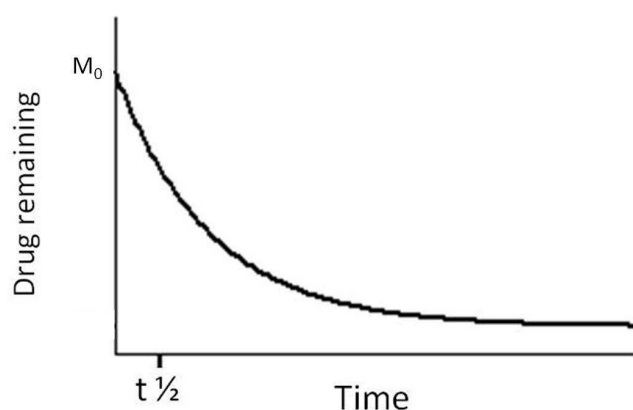


Figure 5.2 Monoexponential model applied to all Rh123 perfusate loss data

An independent samples t-test was performed on each criterion and a value of $p < 0.05$ was considered significant.

5.3. Results

5.3.1. Rh123 accumulation in lung (perfusate to lung): Effect of GF120918

Inclusion of Rh123 at 1 μg (to achieve an initial Rh123 concentration of 0.01 $\mu\text{g}/\text{mL}$) or at 2.5 μg (to achieve an initial Rh123 concentration of 0.025 $\mu\text{g}/\text{mL}$) nominal dose along with DMSO (0.1 % v/v) in the pulmonary perfusate reservoir resulted in Rh123 loss profiles that showed a more rapid decline in levels during the first 15-20 minutes and then plateaued off. As can be seen from figure 5.3A, the plateau achieved by 30 minutes of experimentation for 2.5 μg nominal dose, was not significantly ($p>0.05$) altered with the addition of GF120918 (500 nM). There is however, evidence that the addition of GF120918 (500 nM) significantly ($p<0.05$) altered the perfusate plateau level for Rh123 at the 1 μg nominal dose, (Figure 5.3B)

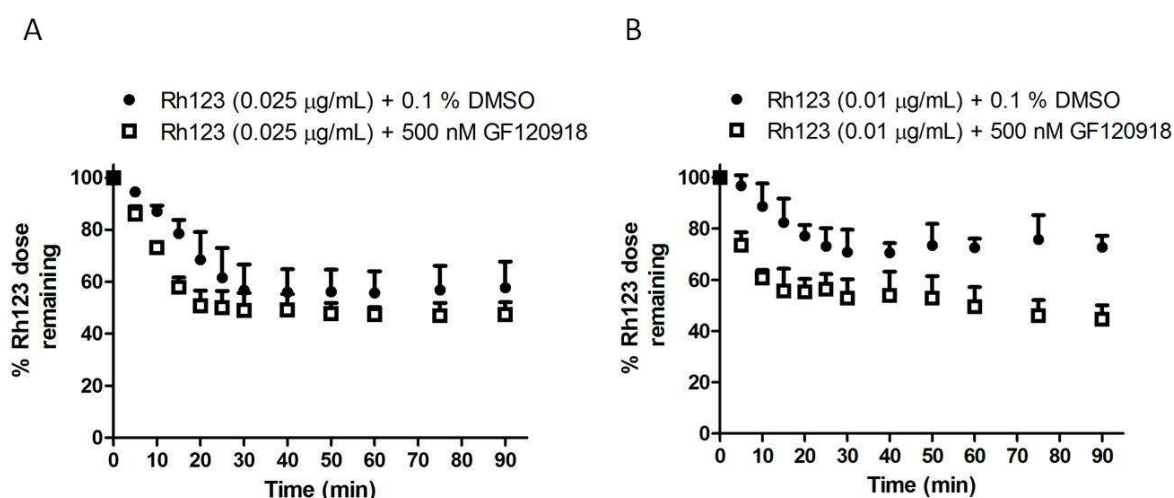


Figure 5.3 Effect of P-gp inhibitor, GF120918, upon the % Rh123 dose remaining in the pulmonary perfusate of the IPRL: **Fig 5.3A** - Rh123 dose (2.5 μg nominal dose) was added to the pulmonary perfusate (volume ~ 100 mL) to achieve an initial nominal concentration of 0.025 $\mu\text{g}/\text{mL}$. GF120918 (500 nM) in the IPRL perfusate did not significantly ($p>0.05$) modify plateau levels of Rh123 in IPRL perfusate. GF120918 did modify ($p<0.05$) the initial (times 0 to 20 min.) rate of loss of Rh123 from perfusate. Data shown are expressed as mean \pm S.D ($n=3$ for each treatment). **Fig 5.3B** - Rh123 dose (1 μg nominal dose) added to ~ 100 mL (as measured by marking 100 mL increment on perfusate reservoir) perfusate to achieve an initial nominal concentration of 0.01 $\mu\text{g}/\text{mL}$. Addition of GF120918 (500 nM) significantly ($p<0.05$) altered both perceived plateau of Rh123 levels and initial rate of Rh123 loss from the perfusate. Data shown are expressed as mean \pm S.D ($n=3$ for each treatment).

The paracellular probe, F-Na, was introduced to IPRL perfusate (10 μg nominal dose) to act as a comparison for Rh123 data. As can be seen in figure 5.4, no substantial loss of F-Na from pulmonary perfusate was observed over a 60 min experimental time period indicating minimal uptake into the lung of F-Na from pulmonary perfusate.

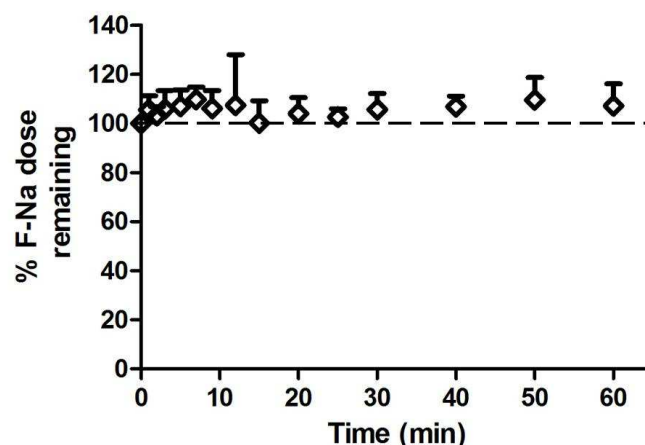


Figure 5.4 Loss of F-Na from pulmonary perfusate over time. The addition of GF120918 was not included as GF120918 nor its vehicle, DMSO, have previously been shown not to influence transport of F-Na. Data shown are expressed as mean \pm S.D (n=3).

Table 5.1 shows some of the key data for the Rh123 perfusate loss experiments:

At the nominal dose of 2.5 μg , the % of Rh123 dose remaining in the perfusate showed no significant ($p>0.05$) difference between control and inhibitor treatment, at both the 60 min and 90 min measurements. However at this dose of 2.5 μg , the initial rate of Rh123 disappearance (k_{perf}) as calculated by linear regression; was affected ($p<0.05$) by the inclusion of GF120918 (500 nM) with a greater (k_{perf}) determined, i.e. faster rate of loss, in GF120918 presence.

In contrast, at the nominal dose of 1 μg , the % of Rh123 dose remaining in the perfusate was significantly ($p<0.05$) lower in the inhibitor treatment experiment than in control, at both the 60 min and 90 min measurements. At this dose of 1 μg , the initial rate of Rh123 disappearance (k_{perf}) was similarly affected ($p<0.05$) by the inclusion of GF120918 (500 nM) with a significantly greater (k_{perf}) determined in inhibitor presence.

Of note is the % of Rh123 in the perfusate at plateau appearing markedly different even in the control treatments between the 2.5 μg and 1 μg doses (i.e., approximately 55 % and 72 % respectively).

	Rh123 (0.025 µg/mL)		Rh123 (0.01 µg/mL)	
	+ 0.1% DMSO	+ 500 nM GF120918	+ 0.1% DMSO	+ 500 nM GF120918
Percentage of initial Rh123 dose in IPRL perfusate at 60min(%)	55.6 ± 8.3	47.4 ± 2.9	72.6 ± 3.4	49.5 ± 7.7 [†]
Percentage of initial Rh123 dose in IPRL perfusate at 90min(%)	57.7 ± 10.0	47.5 ± 4.7	72.7 ± 4.5	44.6 ± 5.5 [†]
Initial rate of Rh123 loss from perfusate (k_{perf} ; min ⁻¹)	0.016 ± 0.005	0.025 ± 0.003*	0.035 ± 0.001	0.093 ± 0.002 [†]

Table 5.1. Effect of GF120918 upon the lung accumulation of Rh123. Rh123 dose (2.5µg or 1 µg nominal dose) was added to pulmonary perfusate (volume 100mL) and loss of Rh123 from perfusate monitored. The P-gp inhibitor GF120918 (500nM) was included in IPRL perfusate to assess the effect of P-gp upon Rh123 accumulation. *GF120918 treatment resulted in a statistically greater ($p<0.05$) initial rates of loss (k_{perf}) of Rh123 from perfusate compared to the respective control. [†] GF120918 treatment resulted in a statistically lower ($p<0.05$) Rh123 plateau levels when compared to the respective control. Data shown are expressed as mean ± S.D (n=3 for each treatment).

In order to explore more fully pharmacokinetic parameter for the loss of Rh123 from perfusate the data was also subjected to nonlinear regression analysis (as detailed in materials and methods section). Figure 5.5 highlights typical model fit to mean data.

As can be seen in table 5.2, the initial rate of loss of Rh123 (k_{NL}) from pulmonary perfusate calculated by nonlinear regression analysis varies in absolute magnitude from the calculated initial rate through linear regression (k_{perf}), although the pattern of change from control remains the same. Specifically the incorporation of GF120918 resulted in significantly ($p<0.05$) greater calculated k_{NL} values i.e. faster rates of proportional Rh123 loss from the perfusate, giving a shorter $t_{1/2}$ for both the 2.5 µg and 1 µg doses.

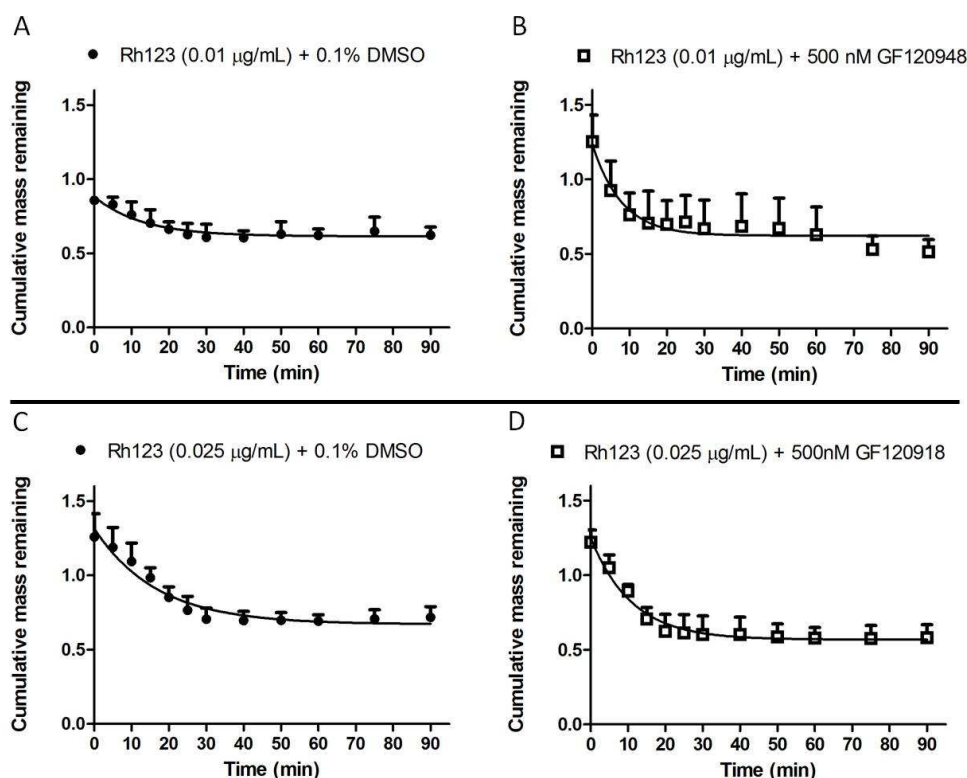


Figure 5.5 Non-linear regression modelling of Rh123 perfusate disappearance data. The model applied to all data was described in Chapter 5 Materials and Methods section. Figure 5.5A - Non-linear regression of data representing Rh123 loss from perfusate (1 µg nominal dose) in the presence of 0.1 % DMSO. Figure 5.5B - Non-linear regression of data representing Rh123 loss from perfusate (1 µg nominal dose) in the presence of 500 nM GF120918. Fig 5.5C - Non-linear regression of data representing Rh123 loss from perfusate (2.5 µg nominal dose) in the presence of 0.1 % DMSO. Figure 5.5D - Non-linear regression of data representing Rh123 loss from perfusate (2.5 µg nominal dose) in the presence of 500 nM GF120918. Data are expressed as mean \pm S.D. (n=3 for each treatment).

		$k_{\text{perf}} (\text{min}^{-1})$ [from table 5.1]	$k_{\text{NL}} (\text{min}^{-1})$	$t_{1/2} (\text{min.})$ from k_{NL}
Rh123 (0.01 µg/mL)	+ 0.1 % DMSO	0.035 ± 0.001	0.080 ± 0.020	9.05 ± 2.50
	+ 500 nM GF120918	$0.093 \pm 0.002^*$	$0.167 \pm 0.038^*$	$4.32 \pm 1.09^*$
Rh123 (0.025 µg/mL)	+ 0.1 % DMSO	0.016 ± 0.005	0.059 ± 0.005	11.83 ± 0.92
	+ 500 nM GF120918	$0.025 \pm 0.003^*$	$0.092 \pm 0.005^*$	$7.58 \pm 0.45^*$

Table 5.2. Effect of GF120918 upon parameters reflecting Rh123 loss from pulmonary perfusate. * The addition of GF120918 significantly altered ($p < 0.05$) the initial rate of loss of Rh123, calculated by both linear (k_{perf}) and nonlinear (k_{NL}) regression and the disappearance half-life ($t_{1/2}$) of Rh123 from pulmonary perfusate. Data shown are expressed as mean \pm S.D (n=3 for each treatment).

5.4. Discussion

To examine the relative influence of an efflux mechanism acting from lung to perfusate, the P-gp substrate Rh123 was introduced to the pulmonary perfusate of the IPRL and its disappearance recorded. To explore P-gp involvement in any such disappearance, the P-gp inhibitor GF120918 was also introduced to pulmonary perfusate and the effects monitored. This element of the work was part stimulated by the flunisolide results in the previous chapter of this thesis and the data of Florea *et al.* [398] which suggested flunisolide to be actively transported in the lung in an apical - to - basal direction, by P-gp. Furthermore the work of Roerig *et al.* [355] also has reported a lung to vasculature efflux mechanism in an isolated perfused rabbit lung model.

Within our IPRL system, Rh123 transport from pulmonary perfusate was monitored over a 90 min period. Employing an initial Rh123 concentration in perfusate of 0.025 µg/mL (2.5 µg dose), no significant difference between the plateau levels of Rh123 in the presence and absence of GF120918 (500 nM) could be observed. In contrast, when we utilised a lower perfusate concentration of 0.01 µg/mL (1 µg dose), the % of Rh123 dose remaining in the perfusate was significantly lowered by inhibitor treatment. Such plateau levels reflect the equilibrium achieved between perfusate and lung tissue (after 20-30 min of experimentation). The plateau level reflects the distribution volume for Rh123 for both perfusate and lung tissue combined, and accounts for the volume of the perfusate, the binding of Rh123 in the perfusate and the accumulation and binding of Rh123 within the lung. A lower plateau level (or % of Rh123 dose remaining) in the perfusate can be interpreted in the context of: (i) decreased specific binding within the perfusate (e.g. decreased protein binding) allowing more Rh123 to passively accumulate in the lung, (ii) an increase in the apparent volume of distribution of the lung toward Rh123; (iii) overcoming of a Rh123 transport barrier from perfusate to lung.

One possible explanation by which the 2.5 µg dose of Rh123 fails to show a difference between control and P-gp inhibitor treatments with respect to plateau levels while the 1 µg dose appears to show a difference, is one that relates to the 2.5 µg dose of Rh123 saturating any potential efflux mechanism from lung to perfusate. Thus suggesting that the 1 µg dose is still susceptible to efflux until co-administered with the P-gp inhibitor. Indeed the perfusate concentrations of Rh123 present at the end of the dose escalation Rh123 absorption experiments for either 40 µg or 80 µg Rh123 (Chapter 4) (doses which saturated the airway to perfusate efflux mechanism) are comparable to the plateau concentrations achieved here for the 2.5 µg dose of Rh123 directly administered into the perfusate.

However, the % of Rh123 in the perfusate at plateau was markedly different even in the control treatments between the 2.5 μg and 1 μg doses (i.e. approximately 55 % and 72 % respectively). This could imply a greater proportional loss of Rh123 from perfusate at the higher dose. This difference in % remaining at plateau between the control groups is not easily explained by a non-specific binding phenomenon (i.e. tubing) or by an increased capacity for specific binding within the lung tissue as both of these would have affected the lower dose Rh123 proportionally more. A closer inspection of the actual mass remaining data (Figure 5.3) however, reveals a marked difference between the time zero Rh123 mass remaining in the perfusate between the Rh123 control and GF120918 treatments for the 1 μg dose. This should not be the case and implies a lack of reliability in the % plateau calculation for the Rh123 1 μg dose, i.e. the 72 % of Rh123 remaining at plateau is likely to be an over-estimation. Indeed the actual plateau levels by mass between the control and GF120918 treatments for the 1 μg dose are very similar (Figure 5.3).

Nevertheless addition of GF120918 did significantly alter initial rate of Rh123 disappearance (k_{perf}) from perfusate and also the calculated rate constant for loss from non-linear regression (k_{NL}) (and disappearance half-life $t_{1/2}$) for both the 2.5 μg and 1 μg doses of Rh123. This could arise from protein binding displacement of Rh123 from the albumin in the perfusate allowing more Rh123 to more rapidly accumulate by passive mechanisms in the lung; both GF120918 and Rh123 are known to display high protein binding. Further, it could reflect functional inhibition, at least initially, of P-gp mediated efflux which would normally limit the rate of transport of Rh123 into the lung from perfusate. However, one may expect functional inhibition of a lung to perfusate – directed P-gp efflux to also alter equilibrium levels between lung and perfusate when comparing control of inhibitor experiments. Clearly this issue needs further research.

The passive permeability marker, F-Na, was introduced to pulmonary perfusate at a nominal concentration of 0.1 $\mu\text{g}/\text{mL}$ in order to examine the comparative apparent volume of distribution for F-Na and Rh123. Results demonstrated F-Na to predominantly remain within perfusate for the duration of the experiment, i.e. no significant F-Na disappearance from perfusate/lung accumulation was observed. This contrasts markedly to the lung accumulation of Rh123 where 30-50 % of Rh123 would appear to be lost to the lung from the perfusate. This is perhaps not surprising as F-Na is a polar but charged molecule not subject to significant protein binding. Indeed F-Na, when administered into the airways of the IPRL, displays extents of absorption of between 70-90 % within the initial 80 min. In the rat, the lung weight approximates to 0.6 % of total body weight such that for a 300 g rat the lung would weigh about 2 grams. With a density of 1 g/mL we would anticipate for a

drug not subject to binding within the lung to display an apparent volume of distribution for the lung itself of approximately 2 mL [417]. Against a perfusate volume of 100 mL such a volume would represent only a small proportion and certainly within the realms of experimental variance. Rh123 is a cationic molecule and positively charged molecules are known to accumulate in the lung and indeed the absorption of Rh123 from the airways is low [367].

Previously, Roerig *et al.* have sought to investigate P-gp activity within lung vasculature through use of an Isolated Perfused Rabbit Lung preparation. They used a rhodamine analogue, rhodamine 6G (R6G), and introduced this to perfusate in increasing concentrations from 1.25 μM to 12.6 μM . They showed disproportionate loss of R6G from the perfusate, i.e. greater loss as the concentrations in the perfusate increased. From this, they concluded that transport of R6G into the lung was a saturable process. Through the inclusion of GF120918 in perfusate, an approximate 21 % increase in R6G lung accumulation was observed compared to control. From this they concluded the involvement of P-gp [355].

The results of this chapter partly complement those of Roerig *et al.*, in that a P-gp inhibitor was observed to modulate the perfusate kinetics of Rh123 in a IPRL model. While Roerig demonstrated an increase in lung accumulation of a rhodamine dye with the inhibition of P-gp, the results of this current work remain equivocal as far as % accumulation data is concerned. Certainly, Roerig *et al.* reported a much higher percentage of R6G accumulation within the lung, which then increases further with the addition of GF120918, this second observation also true Rh123. For example after introducing a nominal concentration of 2.5 μM to perfusate, Roerig *et al.* report R6G lung accumulation of 66.6 ± 2.6 % (S.E), this increased to 87.5 ± 1.1 % (S.E) with the addition of GF120918 [355]. The analogue R6G is recognised to display a higher affinity for P-gp than Rh123 [356]. While Rh123 is also more highly protein bound than R6G and displays a lower passive permeability rate constant [367, 375]. Therefore, there may be a greater proportion of R6G 'free' in the isolated perfused rabbit lung system that also has a greater ability to passively diffuse across the endothelial barrier, thus displaying higher percentage transfers than Rh123.

As mentioned in the introduction to this chapter, 'endothelial P-gp' in the BBB is highly significant, influencing the brain penetration of such substrates as synthetic glucocorticoids, antihistamines, and a number of drugs with relevance to neurological disorders such as epilepsy, Alzheimer's disease, Parkinson's disease and brain cancer [430-434]. From this, the induction or modulation of P-gp at the BBB represents a real therapeutic target to enhance the treatment of a number of neurological-related health conditions [431].

The results of this chapter do not discount that P-gp within the pulmonary vasculature can display functionality. While we have focused the discussion so far on Rh123, there may also be merit in considering the influence of 'endothelial P-gp' upon results of the previous chapter concerning the transport of flunisolide within the IPRL. While it was hypothesised that an alternative drug transporter may be responsible for the observed polarised apical – to – basolateral transport of flunisolide, when comparing the relatively varied physico-chemical properties of other known P-gp substrates examined within this thesis and the integral relationship between passive diffusion rate and active transport mediated by P-gp, there is potential to relate the 'unconventional' directional transport of flunisolide to 'endothelially' expressed P-gp. Figure 5.6 diagrammatically represents the hypothesised transport of P-gp substrates, mediated by P-gp, in the isolated perfused rat lung.

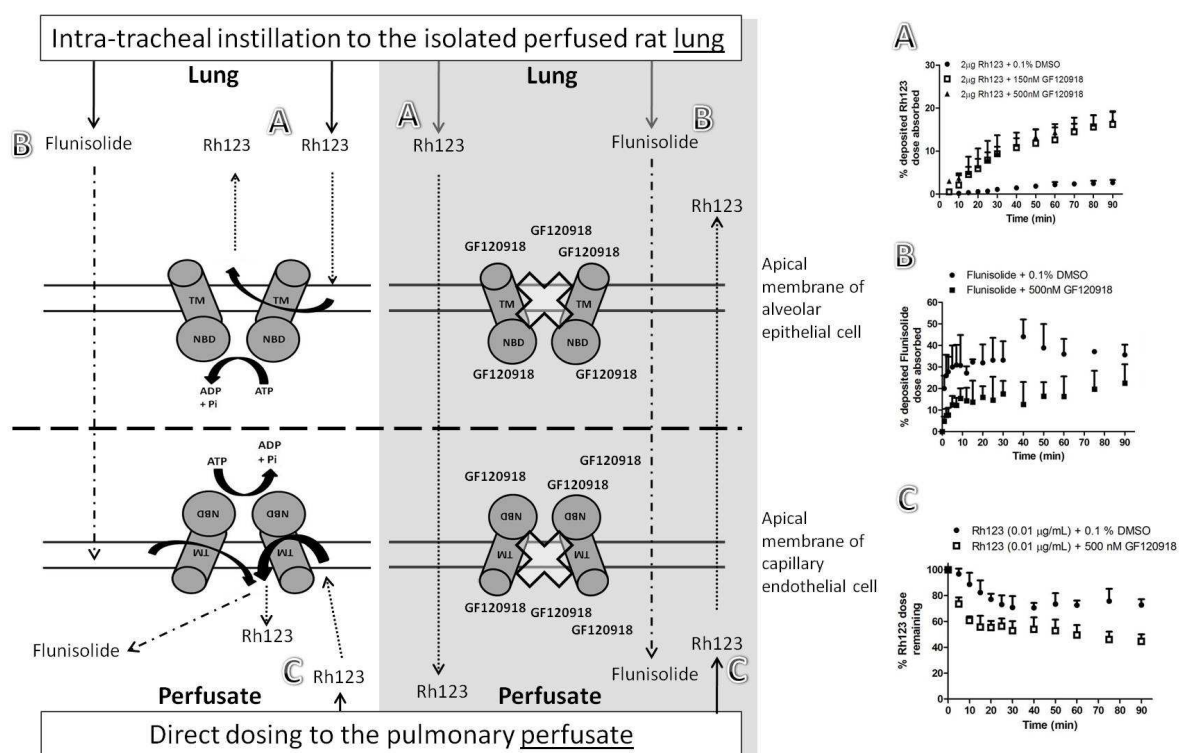


Figure 5.6 Proposed transport of Rh123 and flunisolide within the IPRL, mediated by P-gp. Letter 'A' relates to Rh123 transport within the IPRL after intra-tracheal instillation, i.e. transport from lung – to – perfusate. Letter 'B' relates to flunisolide transport within the IPRL, (lung – to – perfusate) post intra-tracheal instillation of dose. Letter 'C' relates to Rh123 transport, (perfusate – to – lung), after introduction of Rh123 dose to pulmonary perfusate. All variations of dashed arrows denote the predominant direction of substrate transport, 'white background' of diagram represents transport in the absence of GF120918, 'grey background' relates to transport in the presence of GF120918. Each cumulative transport plot, labelled A, B, or C, illustrates the % of substrate in perfusate over time and corresponds to respective letters relating to substrate transport within the IPRL (left panels of diagram).

As can be seen in figure 5.6;

- A. When considering Rh123 transport after intra-tracheal instillation, the presence of active P-gp would reduce perfusate concentrations of substrate by retaining Rh123 within the lung. A degree of abolition of P-gp action through addition of GF120918 would increase Rh123 perfusate concentrations by removing the limiting efflux activity of P-gp and therefore limiting active retention of Rh123 within the lung.
- B. Transport of flunisolide to perfusate in the presence of active P-gp *could* be enhanced by the action of P-gp present in endothelial cells propelling substrate to perfusate at a rate exceeding that of passive diffusion. Modulation of P-gp activity through introduction of the GF120918 inhibitor could thus reduce the rate of flunisolide transport over the experimental time period by eliminating the active propulsion of flunisolide from the cytosol of capillary endothelial cells to pulmonary perfusate.
- C. With similar focus, the transport of Rh123 dosed to pulmonary perfusate in the presence of functional P-gp could be constrained by active, 'endothelially' localised P-gp. Modulation of P-gp could therefore increase passage of Rh123 to the isolated lung by suppression of active efflux of Rh123 and retention of substrate within the pulmonary perfusate.

The results of this chapter and those of Roerig *et al.* [355] continue the intrigue over endothelial P-gp functionality within the complex mechanisms of absorption in the lung. However, it should not be forgotten that published investigations performed *in vivo* in *mdr1* (-/-) transgenic knockout mice can provide further insight. Specifically, the lung to blood distribution data generated in *mdr1a*(-/-) or *mdr1a/1b*(-/-) mice all indicate that for those P-gp substrates so far studied, the *mdr1*(-/-) knockout phenotype has little to no impact upon drug accumulation in the lung from the systemic circulation (reviewed in [117]). There is obvious scope for further study with regards to the influence of P-gp located in the lung. This would include: (i) electronic microscopy assessment of P-gp within the entire pulmonary tissue to localise with sufficient resolution P-gp to endothelial and epithelial membranes; (ii) uses of an isolated perfused mouse lung model with *mdr1a* and *mdr1b* knockout; and if (ii) is not possible then the conduct of quantitative kinetic studies within an IPRL using a range of substrates and inhibitors.

Chapter 6

**Investigating the impact of pulmonary P-gp upon airway
instilled substrates within an industrial setting; Use of an *in
situ* IPRL model**

6.1. Introduction

The history of P-glycoprotein, in terms of definitive literature references, dates back to its documentation within scientific literature by Juliano and Ling in 1976 [70]. By the mid-eighties, many literature reports were describing the drug resistance capacity of P-gp and by the later stages of the 80s, reports of P-gp inhibition were emerging [435, 436]. It is from this period onwards that industrial interest in the impact of P-gp upon drug absorption and disposition began and indeed the concept of developing chemical inhibitors of P-gp was formed. For example, In 1991 Fling and co-workers, based at Burroughs Wellcome in North Carolina, reported comparability between P-gp and a *C. albicans* gene conveying resistance to benomyl and methotrexate [437]. Following this, a team based at GLAXO in France documented the pharmacological activity of the inhibitor GF120918 upon P-gp and reported reversal of multidrug resistance both *in vitro* (CH^RC5 cells) and *in vivo* (mice) [373]. Industrial contributions to the literature have been significant, for example, the work of Joseph W. Polli [438]. To date, within the biomedical and life sciences literature archive PubMed Central, (<http://www.ncbi.nlm.nih.gov/pubmed>), Joseph W. Polli has authored or co-authored 24 articles relating to P-glycoprotein and continues to work at GSK [439].

This chapter describes studies undertaken at GSK within their respiratory Centre of Excellence for Drug Discovery (CEDD). The work was undertaken as part of as part of my studentship using GSK's own in-house developed *in situ* isolated perfused rat lung model; with the airway instillation of test compounds to determine the potential of P-glycoprotein to modulate pulmonary absorption. More specifically, experiments were conducted in order to consider the applicability and viability of such an isolated model within the pharmaceutical industry.

Of GSK's 101 trademarked prescription drugs currently available in the UK/EU and USA, 18 % are marketed for use in the treatment of pulmonary conditions (Figure 6.1 illustrates this [440]).

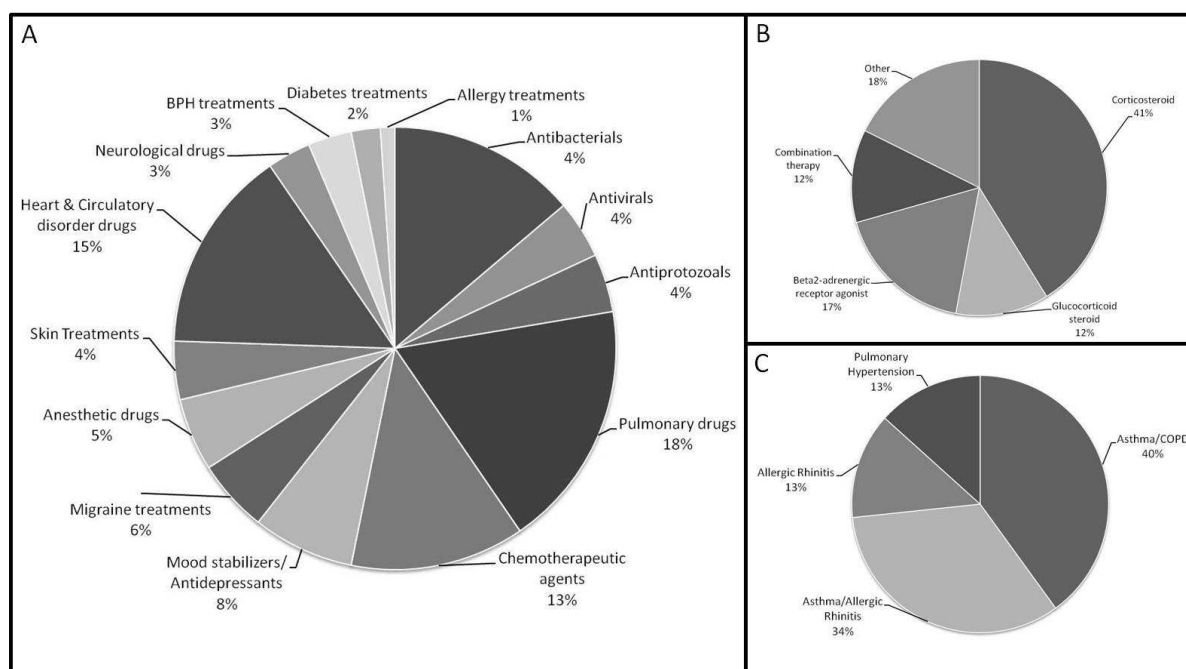


Figure 6.1. Graphical presentation of all (101 in UK/EU & USA) trademark products currently produced by GSK. Figure 6.1A – Percentage of drugs targeting specific disease/condition areas. Figure 6.1B – Generic composition of pulmonary targeted drugs presented as % of total trademark pulmonary drugs produced by GSK. Figure 6.1C – Specific pulmonary-associated diseases and conditions treatable via trademark GSK ‘pulmonary drugs’, expressed as % of total trademark pulmonary drugs produced by GSK [440].

Given the prevalence of ‘pulmonary drugs’ within the portfolio of GSK trademark products, it is very important that the numerous factors a target drug molecule is confronted with in the dynamic environment of the lungs are understood. Further, as it is common for 80-90 % of an inhaled dose to be swallowed, understanding the disposition of the remaining dose is vitally important and this can vary according to a number of factors (e.g. particle size, patient health). In order to achieve high-quality candidate inhaled medicines, proper pharmacokinetic profiles for each drug; poor oral absorption, short plasma half-life, high plasma clearance (reducing systemic exposure thus undesirable side effects), sustained lung retention and therefore pharmacologically active levels of candidate drug, is highly desirable and necessary for successful candidate selection [441]. To allow the appropriate selection and further development of such drug treatments for targeting specific diseases and conditions, the requirement for appropriate experimental models is essential. Within GSK an isolated perfused rat lung preparation (IPRLu) has been developed in order to generate biopharmaceutics information relevant to drug candidate selection for pulmonary disease.

For use as an experimental model to aid pulmonary drug discovery, an *in situ* IPRLu setup was constructed by GSK research and development scientists. The isolated perfused and respiring rat

lung (IPRLu) model is essentially desirable within the field of drug discovery because it allows deeper understanding of the transport of a drug molecule across the lung “*in situ*” via the inherent nature of the isolated model. By isolating the pulmonary blood system from that of the systemic circulation whilst maintaining perfusion and integrity of the vascular network surrounding the lung and manually ventilating the lungs, it is reasonable to assume that any compound dosed to the isolated lung via the trachea which is not present in the pulmonary vein must either be retained by the lung or metabolised/broken down in the lung tissue or mucus. From this, the IPRLu at GSK can be, and is, used as a ‘ranking tool’ i.e. a screen, to allow development of drug treatments for targeting specific pulmonary diseases and conditions, thus fulfilling the essential requirement for an appropriate experimental model [441].

Within the literature, *in situ* IPRL models are often employed in experiments with aims and objectives that are physiologically focussed. For example, Tschumperlin and co-workers exploited a similar model to that at GSK to examine alveolar surface area-volume relationships [442]. Within this research area, the main use of *in situ* IPRL models appears to be within the study of pulmonary ischaemia-reperfusion injury. Again, lung isolation protocol appears to be comparable to other studies; while retention of the lung within the thoracic cavity allows the maintenance of whole body integrity with relation to the pulmonary system and allows for permeations of injury cause and duration of ischaemic attack over the time course of the experiment [443, 444].

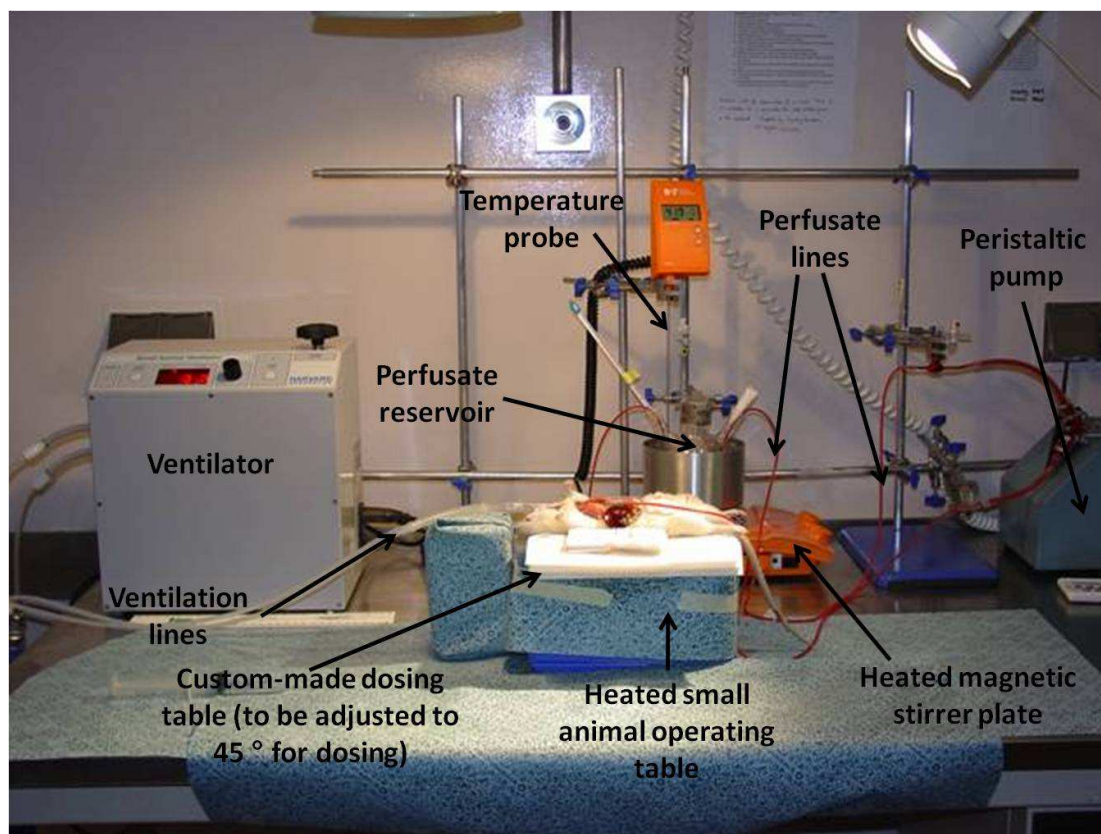


Figure 6.2 Image representing the *in situ* isolated perfused rat lung setup employed at GSK.

The *in situ* model employed by GSK functions as a single-pass model with ease of use ('single-pass' samples collected incrementally i.e. not 'pooled' in reservoir; easier sample analysis) in the examination of lung retention and metabolic activity upon candidate drug substrates. The model is however comparable to other published models in terms of its maintenance of tissue functionality and architecture and ability to assess post-deposition events and pharmacokinetics within the lung [23]. The image in figure 6.2 illustrates the setup established at GSK. As can be seen, overall, this model resembles that of the Cardiff IPRL with regards to equipment requirement and setup. Obvious differences include the lack of artificial thorax, the need for an angled dosing platform and the lack of water-jacketed glass equipment to maintain perfusate and preparation temperature. The lack of a recirculating perfusion system is also apparent, however, a single-pass perfusion method is employed at GSK as this allows for simple calculation of initial pharmacokinetic parameters.

Aims and Objectives

The studentship investigations using the GSK model included;

- Validation of dosing technique by introducing Evans blue dye to the IPRLu via the trachea.

- Examination of the functional significance of P-gp upon drugs instilled to the lung, substrates Rh123 (also tested in Cardiff) and flunisolide were dosed to the GSK IPRLu and dose escalation conducted to establish saturation of an active transporter
- Further, the P-gp inhibitor GF120918 will be introduced to IPRLu experiments to assess the effect of P-gp modulation upon instilled substrates.
- Examination of lung weight and dose mass balance will also be recorded to add to data analysis and data will be subjected to pharmacokinetic modelling in order to establish initial pharmacokinetic parameters in the presence and absence of an active efflux transporter.

6.2. Materials and Methods

6.2.1. Single-pass perfusion Isolated Perfused Rat Lung model

Materials

Animals

Species:	Rat
Strain:	Sprague Dawley (CD)
Sex & Number:	8 Male (2 for surgery, 5 for control blood, 1 spare)
Weight :	300-500 g. Animals were weighed prior to dosing
Husbandry:	Routine animal husbandry methods were applied. Animals were housed in standard holding cages. Water and food was available <i>ad libitum</i> throughout.

Consumables and reagents

Single animal, volume controlled ventilator, (Starling Ideal, Harvard Apparatus Ltd, UK, Cat: 401003)

Peristaltic pump, Harvard rodent blood pump/Model: 1407, (Harvard Apparatus Ltd, UK)

Round bottom, 3 neck flask, borosilicate, 50 mL, Quickfit, (Fisher Scientific, Loughborough, UK, Cat: QFM-230-W)

Magnetic stirrer hot plate with temperature probe, (Cole Palmer, UK)

Perfusate line; (Large: 0.187" ID x 0.063" WALL, type SFM1-4450, VWR code 228-0235)

(Medium : 0.104" ID x 0.044" WALL, type SFM1-3250, VWR code 228-0236)

(Small : 1.98mm ID x 3.17mm OD, VWR code 228-0239)

Syringes (Sterile; various volume capacities), (Fisher Scientific, Loughborough, UK)

Heparin Sodium (administered 0.5 mL of 100 u/mL i.v. via tail vein)

Ketamine, (100 mg/mL ketamine Hydrochloride), (Dodge Laboratories, Inc., Fort Dodge, Iowa, USA, Ref: 440728)

Dormitor®, (1 mg/mL medetomidine hydrochloride), Pfizer, UK)

Reagents (for buffer)

Potassium chloride; KCl, (Fisher Scientific, Loughborough, UK, Cat: P/4280/53)

Magnesium sulphate heptahydrate; $\text{MgSO}_4 \cdot 7\text{H}_2\text{O}$, (Fisher Scientific, Loughborough, UK, Cat: M/0600/53)

Sodium Bicarbonate; NaHCO_3 , (Fisher Scientific, Loughborough, UK, Cat: S/4200/60)

Calcium chloride dihydrate; $\text{CaCl}_2 \cdot 2\text{H}_2\text{O}$, (Fisher Scientific, Loughborough, UK, Cat: C/1500/50)

Sodium chloride; NaCl , (Fisher Scientific, Loughborough, UK, Cat: S/3105/63)

Potassium dihydrogen phosphate; KH_2PO_4 , (Fisher Scientific, Loughborough, UK, Cat: P/4800/53)

Bovine serum albumin; BSA, (Sigma-Aldrich, Dorset, UK, Cat: A7906-1kg)

Method

Preparation of Krebs-Ringer bicarbonate buffer

To prepare 1 L

The below listed chemicals and solutions were added to distilled water (~ 600 mL) and the final volume adjusted to 1000 mL. Order of addition:

1) KCl	0.35 g
2) $\text{MgSO}_4 \cdot 7\text{H}_2\text{O}$	0.29 g
3) NaHCO_3	2.10 g
4) $\text{CaCl}_2 \cdot 2\text{H}_2\text{O}$	0.37 g
5) NaCl	6.92 g
6) KH_2PO_4	0.16 g
7) BSA	30.0 g

Order of addition of buffer components is very important, isotonicity and pH are critical.

Buffer solution was prepared and adjusted to pH 7.4.

Preparation of diluted blood/buffer for single-pass perfusion

A total of 5 animals were exsanguinated under terminal anesthesia and control blood collected. Control blood was diluted with buffer (1:9; blood: buffer) and this diluted blood used for lung perfusion. Diluted blood was stored at 4 °C until required and a minimum of 200 mL was necessary for each single-pass perfusion preparation.

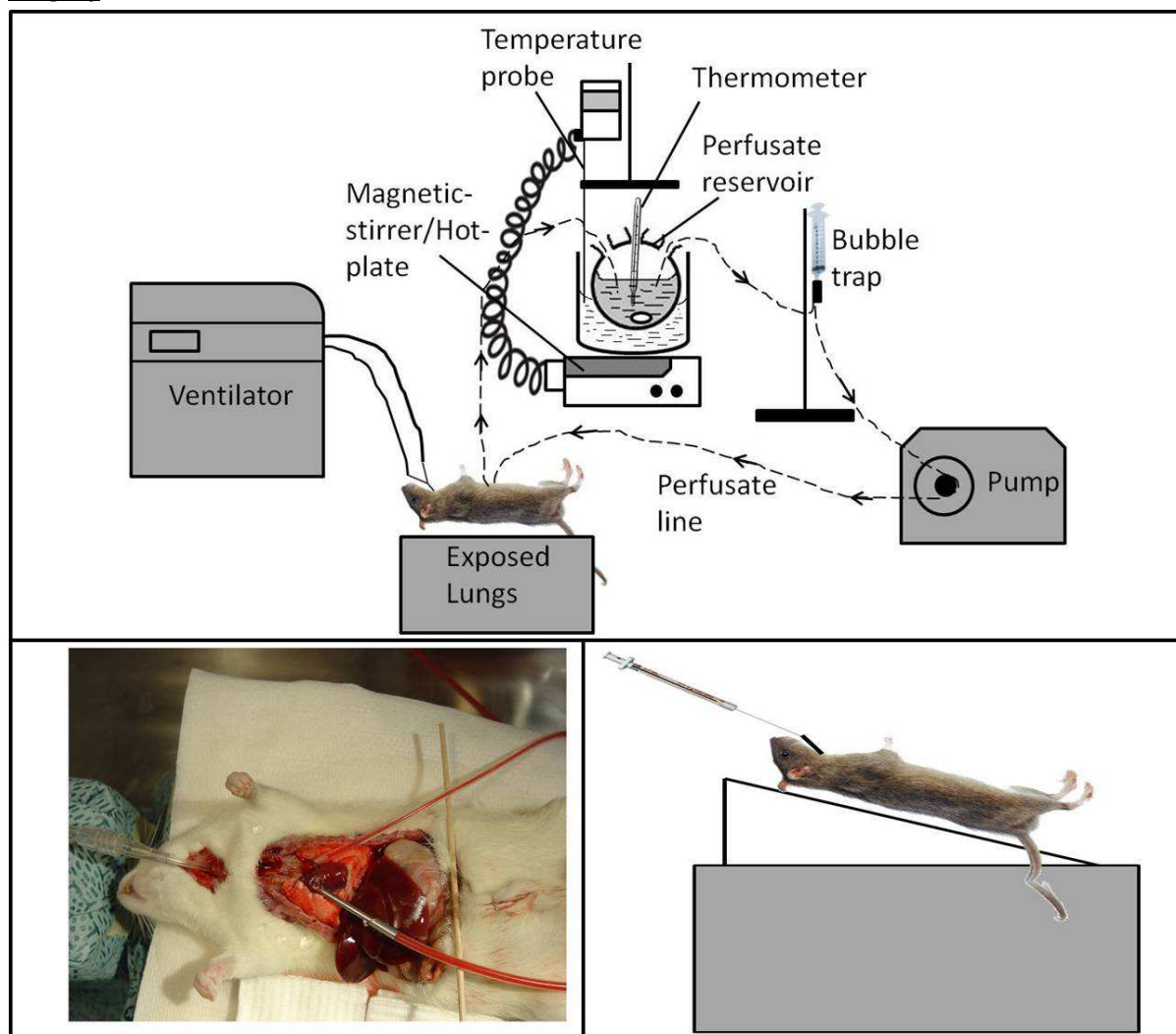
Surgery

Figure 6.3. Diagrammatic representation of single-pass IPRL preparation. Diagram also illustrates *in situ* cannulation of the heart to produce an isolated pulmonary perfusion system and position of animal and dosing method employed.

Following an IP injection (7.5 mL/kg ketamine & 0.5 mL/kg Dormitor) to provide terminal general anaesthesia, heparin was administered (0.5 mL of 100 U/mL) intravenously via a tail vein. The trachea was then cannulated and respiration transferred to the positive pressure ventilator and maintained at 40 breaths per min with a 1.8 mL tidal volume. (The ventilator was set at 4 mL volume to allow for dead space in the tubing). The rat was then exsanguinated via the abdominal aorta.

The pulmonary artery and vein were then cannulated through incisions in the left and right ventricles respectively (Figure 6.3). Following cannulation, the rat was raised and maintained at a fixed angle using the custom made elevating chamber (Figure 6.3).

Recirculating blood-based perfusate (10 % animal blood v/v; see perfusate preparation above) at 37 °C was then used to perfuse the lung preparation. The flow was gradually increased until a rate of 10 mL/min was achieved. This was measured by weighing the perfusate collected over a

30 second period. The predose flow rate was documented and the preparation left to equilibrate for 10 minutes. One spare animal was allocated for surgery, if not required this animal was returned to stock.

Dosing

Following equilibrium of the preparations and attainment of the required flow rate, 100 μ L of the cassette dose suspension/solution was administered to the trachea slightly above the bifurcation point by introducing a Hamilton syringe (50 mm needle) into the tracheal cannula followed by 3 x 1 mL syringe fulls of air. The trachea was then be immediately reattached to the ventilator.

Sampling

Immediately following dosing, the exit cannula (pulmonary vein cannula) from the lungs was removed from the reservoir and the perfusion was switched to single pass. The perfusate was then collected to universal tubes over a 1 min interval for 20 min (the total length of the experiment was 20 min).

Sample collection tubes (universal tube or equivalent) were weighed and recorded (to determine the sample volume collected). Tubes were weighed periodically (5, 10 & 15 min.) throughout the experiment to ensure collection volume and thus the perfusate flow rate was constant. Any deviations were rectified by altering the pumping capacity.

1 mL of perfusate was removed from each collection tube and placed in an eppendorf tube. This sample was centrifuged to yield perfusate plasma. The cell pellets were discarded and the plasma transferred into a second eppendorf tube and stored frozen until analysis. The bulk collected perfusate samples were discarded following weighing and preparation of a perfusate plasma sample.

At 20 min, the experiment was terminated.

The lungs were detached from the ventilator and the perfusion apparatus and excised from the thorax of the rat and retained. The trachea was removed and lungs and trachea separately stored frozen prior to analysis.

Plasma, lungs and residual dose were transferred to a -20 °C freezer as soon as possible following collection. Samples remained frozen until analysis.

Samples were subsequently analysed by LC/MS/MS after suitable preparation.

6.2.2. Evans blue lobar deposition

Materials

Consumables

Evans blue, (Fluka, Sigma-Aldrich, Dorset, UK, Cat: 46160-5G-F)

Method

In order to assess dose deposition pattern across the lung, Evans blue (3 mg/mL in dH₂O, filter sterilised) was instilled to the IPR using the Hamilton instillation technique. Immediately after dosing, the experiment was terminated and the lung tissue removed to allow visual assessment of deposition pattern.

6.2.3. Rh123 absorption in the single-pass perfusion model

Dose preparation

Consumables and reagents

Rhodamine 123; Rh123, >98 % electrophoresis grade, (Sigma-Aldrich, Dorset, UK, Cat: R-8004)

GF120918; obtained from GlaxoSmithKline, Stevenage, UK.

Dimethyl sulfoxide; DMSO, BioReagent, for molecular biology, ≥99.9 %, (Sigma-Aldrich, Dorset, UK, Cat: D8418-50ML)

Method

2 µg nominal dose airway administration of Rh123 (100 µL instilled dose volume)

- I. Rh123 was weighed out and dissolved in 10 mL H₂O and sonicated to achieve a homogeneous solution at 2.27 mg/mL
- II. This was diluted 1:100 with H₂O to produce a stock at 22.7 µg/mL
- III. To achieve 20 µg/mL, 0.12 mL H₂O was added to 0.88 mL '22.7 µg/mL stock solution'

40 µg nominal dose airway administration of Rh123 (100 µL instilled dose volume)

- I. Rh123 was weighed out and dissolved in 10 mL H₂O and sonicated to achieve a homogeneous solution at 2.27 mg/mL
- II. This was diluted 1:5 with H₂O to produce a stock at 454 µg/mL
- III. To achieve 400 µg/mL, 0.12 mL H₂O was added to 0.88 mL '454 µg/mL stock solution'

2 µg nominal dose airway administration of Rh123 co-administered with GF120918 (500 nM, 100 µL instilled dose volume)

GF120918: 500nM = 281.9 ng/mL (using 563.7 as M_w)

- I. GF120918 was weighed out and dissolved in 10 mL H_2O (containing 10 % DMSO) and sonicated to achieve a homogeneous solution at 28.19 $\mu\text{g/mL}$.
- II. 100 μL of this stock solution was spiked to 900 μL of a $\sim 20 \mu\text{g/mL}$ Rh123 solution in order to achieve a solution of $\sim 20 \mu\text{g/mL}$ Rh123, 500nM GF120918 as a dose.

GF120918 to be present in the perfusate at same concentration i.e 500 nM.

- I. GF120918 wanted at a concentration of 500 nM in IPRL perfusate; 500 nM = 5×10^{-7} M
- II. $5 \times 10^{-7} \times 563.7$ (GF120918 M_w) * 500 mL = 0.140925 g = 140.93 μg /500 mL perfusate

Rh123 transport in the single-pass IPRL

Single-pass isolated perfused rat lungs were prepared as per above protocol and equilibrated with diluted blood perfusate +/- GF120918 for 30 min. Following this, Rh123 (2 μg , 40 μg or 2 μg + GF120918 nominal dose) was introduced to individual IPRL preparations and each 1 min fraction collected via the single-pass setup.

6.2.4. Perfusate plasma Sample and Dose Solution Preparation for Analysis (automated)

Consumables

Rhodamine 123; Rh123, >98 % electrophoresis grade, (Sigma-Aldrich, Dorset, UK, Cat: R-8004)

Rolipram, (Sigma-Aldrich, Dorset, UK, Cat: R6520)

Acetonitrile; ACN, 99.6+ %, HPLC grade, (Fisher Scientific, Loughborough, UK, Cat: A/0626/17)

Control rat perfusate plasma and study samples were collected and stored frozen until analysis. On the day of analysis samples and control perfusate plasma were removed from the freezer and thawed.

Once defrosted all control perfusate plasma was vortexed and then centrifuged at 13000 rpm for 10 min to pellet down fibrin clots.

Preparation of perfusate plasma calibration standards:

A 1 mg/mL H_2O stock details:

Compound	OI	Mass (mg)	From 2.27 mg/mL stock	Date Prepared
Rh123	SC/159651	1.0	44 μL stock to 56 μL H_2O	25/09/2007

- B Dilute 10 μL of A (1 mg/mL) for each compound and 20 μL of B (0.5 mg/mL) into 450 μL acetonitrile: water (1:1) = 20 $\mu\text{g/mL}$.

A 200 ng/mL stock solution was prepared in control rat perfusate plasma.

Add 10 μL B (20 $\mu\text{g/mL}$) to 990 μL control rat perfusate plasma.

Control rat perfusate plasma was made up by adding 1 part of control rat plasma to 9 parts of Krebs-Ringer bicarbonate buffer, pH 7.4, containing 3 % BSA.

Standard curves were prepared, to cover the range 0.02 to 200 ng/mL, by serial dilution in centrifuged control rat perfusate plasma using the 0.2 $\mu\text{g/mL}$ perfusate plasma standards and a TECAN robot (Genesis RSP150). The TECAN also produced a carryover blank following the washes post-highest standard preparation.

Preparation of perfusate plasma samples for analysis:

The samples and standards were prepared by protein precipitation with acetonitrile containing 15 ng/mL of rolipram (internal standard). Followed by filtration using a TECAN robot the samples and standards were extracted by protein precipitation. For extraction, 100 μL of perfusate plasma from standards and samples was taken and 300 μL of acetonitrile with internal standard was added.

The filtered extracts were collected into a 96 well plate and were blown down to dryness under a nitrogen stream at 40 °C. The dry extracts were reconstituted in 150 μL of acetonitrile: water (25:75).

The plate was then mixed on a plate shaker for at least 5 min before analysis by LC/MS/MS.

Preparation of dose check samples:

Dose: Rh123 20 $\mu\text{g/mL}$

Dilute in triplicate to:

C 200 ng/mL: Take 10 μL dose and add to 990 μL H_2O .

D 20 ng/mL: Take 50 μL C and add to 450 μL H_2O .

E 2 ng/mL: Take 50 μL E and add to 450 μL H_2O .

Dose check samples were extracted and analysed following the same procedure used for study samples.

Re-injection of samples to check ion suppression:

The following samples were re-injected to allow assessment of the effect of ion suppression. The samples used were the 8 and 80 ng/mL calibration standard and 3-4 min and 15-16 min samples from rat #1. These samples were injected at a 10 µL injection volume and then immediately re-injected at the 30 µL injection volume used for the rest of the run.

LC-MS/MS analytical conditions

(Method development – Rh123 in dH₂O) sample was introduced to the LC/MS/MS via a pump and Hamilton syringe and the compound molecular weight used to set a MQ ion 'window' within which to scan via a manual tuning setting. Once complete a set of quantitation values were retrieved, from which optimum results were selected and inputted as MRM transitions to be used for sample analysis. See Figure 6.4 for example peaks obtained.)

Analytical Column:

Packing Type	Luna C18
Particle Size	5 µM
Dimensions	50 x 2.1 mm
Injection volume	30 µL (10 µL for ion suppression check samples)

HPLC Conditions:

Pump	Agilent 1100
Solvent A	0.1 % Formic acid in HPLC grade water
Solvent B	0.1 % Formic acid in Acetonitrile
Flow rate	0.8 mL/min.
Initial divert to waste time	0.5 min.
Run time	3 min.

Gradient conditions:

Start Time (min.)	A (%)	B (%)
0	95	5
0.5	95	5
1.8	5	95
2.2	5	95
2.3	95	5
3.0	95	5

Detector Conditions:

Detector	Applied Biosystems API4000 Mass Spectrometer
Mode	MSMS
Ion Source	TISP (turbo ion spray)
Ionisation	+ve
Source Temperature	650 °C

MRM Transitions:

Compound	Cassette	Q1 Mass	Q3 Mass	Declustering potential (V) (DP)	Cell entrance potential (V) (CE)	Cell exit potential (V) (CXP)
Rh123	1	345.101	285.151	66.0	57.0	18.0
Rolipram (IS)	1	276.45	131.10	100	40	12

6.2.5. Flunisolide absorption in the single-pass perfusion model**Dose preparation***Consumables and reagents*

Flunisolide, (Sigma-Aldrich, Dorset, UK, Cat: F5021-100MG)

GF120918; obtained from GlaxoSmithKline, Stevenage, UK.

Dimethyl sulfoxide; DMSO, BioReagent, for molecular biology, ≥99.9 %, (Sigma-Aldrich, Dorset, UK, Cat: D8418-50ML)

Method*2 µg nominal dose (100 µL instilled dose volume)*

- I. Flunisolide was weighed out to give 1.07 mg/mL flunisolide in H₂O inc. 10 % DMSO
- II. 1.07 mg/mL = 1070 µg/mL
- III. 1:10 dilution: (100 µL '1070 µg/mL solution' to 900 µL H₂O and vortexed to mix) = 107 µg/mL in H₂O inc. 1 % DMSO
- IV. 20 µg/mL / 107 µg/mL * 2 mL = 0.37 mL '107 µg/mL solution' up to 2 mL with H₂O

5 µg nominal dose (100 µL instilled dose volume)

- I. Flunisolide was weighed out to give 5.39 mg/mL flunisolide in H₂O inc. 10 % DMSO
- II. 5.39 mg/mL = 5390 µg/mL
- III. 1:100 dilution (10 µL '5390 µg/mL solution' to 990 µL H₂O and vortexed to mix) = 53.90 µg/mL in H₂O inc 0.1 % DMSO
- IV. 50 µg/mL / 53.90 µg/mL * 2 mL = 1.86 mL '53.90 µg/mL solution' up to 2 mL with H₂O

40 µg nominal dose (100 µL instilled dose volume)

- I. Flunisolide was weighed out to give 5.39 mg/mL flunisolide in H₂O inc. 10 % DMSO
- II. $5.39 \text{ mg/mL} = 5390 \text{ µg/mL}$
- III. 1:10 dilution: (100µL '5390 µg/mL solution' to 900 µL H₂O and vortexed to mix) = 539.0 µg/mL in H₂O inc. 1 % DMSO
- IV. $400 \text{ µg/mL} / 539.0 \text{ µg/mL} * 2 \text{ mL} = 1.48 \text{ mL '539.0 µg/mL solution' up to 2 mL with H}_2\text{O}$

80 nominal dose (100 µL instilled dose volume)

- I. Flunisolide was weighed out to give 5.39 mg/mL flunisolide in H₂O inc. 10 % DMSO
- II. $5.39 \text{ mg/mL} = 5390 \text{ µg/mL}$
- III. $800 \text{ µg/mL} / 5390 \text{ µg/mL} * 2 \text{ mL} = 0.29 \text{ mL '5390 µg/mL solution' up to 2 mL in H}_2\text{O}$

2 µg nominal dose of flunisolide inc. GF120918 (500 nM; 100 µL instilled dose volume)

- I. GF120918: $500 \text{ nM} = 281.9 \text{ ng/mL}$ (using 563.7 as M_w)
- II. GF120918 was weighed out and dissolved in 10 mL H₂O (containing 10 % DMSO) and sonicated to achieve a homogeneous solution @ 28.19 µg/mL.
- III. 100 µL of this stock solution was spiked to 900 µL of a ~20 µg/mL flunisolide solution in order to achieve a solution of ~ 20µg/mL flunisolide, 500nM GF120918 as a dose.

GF120918 to be present in the perfusate at same concentration i.e 500 nM.

- I. GF120918 wanted at a concentration of 500 nM in IPRL perfusate; $500 \text{ nM} = 5 \times 10^{-7} \text{ M}$
- II. $5 \times 10^{-7} * 563.7 \text{ (GF120918 M}_w\text{)} * 500 \text{ mL} = 0.140925 \text{ g} = 140.93 \text{ µg/500 mL perfusate}$

Flunisolide transport in the single-pass IPRL**Method**

Single-pass isolated perfused rat lungs were prepared as per above protocol and equilibrated with diluted blood perfusate +/- GF120918 for 30 minutes. Following this, flunisolide (2 µg, 5 µg 40 µg 80 µg or 2 µg + GF120918 nominal dose) was introduced to individual IPRL preparations and each 1 minute fraction collected via the single-pass setup.

6.2.6. Perfusate plasma Sample and Dose Solution Preparation for Analysis (automated)*Consumables*

Flunisolide, (Sigma-Aldrich, Dorset, UK, Cat: F5021-100MG)

Rolipram, (Sigma-Aldrich, Dorset, UK, Cat: R6520)

Acetonitrile; ACN, 99.6+ %, HPLC grade, (Fisher Scientific, Loughborough, UK, Cat: A/0626/17)

Sample preparation was conducted as per protocol for 'Rh123 samples and dose solutions'.

Preparation of perfusate plasma calibration standards:

A 1 mg/mL H₂O stock details:

Compound	OI	Mass (mg)	From 1.07 mg/mL stock	Date Prepared
CCI18772	SC/160270	1.0	470 µL stock up to 500 µL with H ₂ O	15/11/07

B Dilute 10 µL of A (1 mg/mL) into 990 µL acetonitrile: water (1:1) = 20 µg/mL.

A 200 ng/mL stock solution was prepared in control rat perfusate plasma.

Add 10 µL B (20 µg/mL) to 990 µL control rat perfusate plasma.

Similarly, perfusate plasma samples, dose check samples and ion suppression samples were prepared and analysed as per 'Rh123 protocol' above.

LC-MS/MS analytical conditions

(Method development – Flunisolide (in dH₂O) sample was introduced to the LC/MS/MS via a pump and Hamilton syringe and the compound molecular weight used to set a MQ ion 'window' within which to scan via a manual tuning setting. Once complete a set of quantitation values were retrieved, from which optimum results were selected and inputted as MRM transitions to be used for sample analysis. See Figure 6.4 for example peaks obtained.)

Analytical Column:

Packing Type	Luna C18
Particle Size	5 µM
Dimensions	50 x 2.1 mm
Injection volume	30 µL (10 µL for ion suppression check samples)

HPLC Conditions:

Pump	Agilent 1100
Solvent A	0.1 % Formic acid in HPLC grade water
Solvent B	0.1 % Formic acid in Acetonitrile
Flow rate	0.8 mL/min.
Initial divert to waste time	0.5 min.
Run time	3 min.

Gradient conditions:

Start Time (min.)	A (%)	B (%)
0	95	5
0.5	95	5
1.8	5	95
2.2	5	95
2.3	95	5
3.0	95	5

Detector Conditions:

Detector	Applied Biosystems API4000 Mass Spectrometer
Mode	MSMS
Ion Source	TISP (turbo ion spray)
Ionisation	+ve
Source Temperature	650 °C

MRM Transitions:

Compound	Cassette	Q1 Mass	Q3 Mass	Declustering potential (V) (DP)	Cell entrance potential (V) (CE)	Cell exit potential (V) (CXP)
Flunisolide (CCI18772)	1	435.175	320.95	41.0	21.0	18.0
Rolipram (IS)	1	276.45	131.10	100	40	12

6.2.7. Mass balance studies

Materials and Method

Consumables

Flunisolide, (Sigma-Aldrich, Dorset, UK, Cat: F5021-100MG)

Rhodamine 123; Rh123, >98 % electrophoresis grade, (Sigma-Aldrich, Dorset, UK, Cat: R-8004)

Acetonitrile; ACN, 99.6+ %, HPLC grade, (Fisher Scientific, Loughborough, UK, Cat: A/0626/17)

Lung Sample Preparation

‘Study lungs’ were from IPRLu preparations, ‘Control lungs’ from donor blood animals. All lung samples and control rat lungs were thawed.

Mean *empty tube weight* and *study lung plus tube weight* was determined.

Preparation of compound standards in lung homogenate:

A H₂O stock details:

Compound	Conc. mg/mL	Date prepared
Rh123/Flunisolide	1	25/09/07

B Dilute 50 µL of A in 450 µL MeCN:H₂O (1:1) = 100 µg/mL

C Dilute 40 µL of B in 360 µL MeCN:H₂O (1:1) = 10 µg/mL.

D Dilute 40 µL of C in 360 µL MeCN:H₂O (1:1) = 1 µg/mL.

Table 6.1. Each calibration line was prepared by spiking into control rat lung homogenate:

Concentration	Volume of Stock Solutions Required (µL)		
µg/lung (10 mL Homogenate)	1 µg/mL	10 µg/mL	100 µg/mL
0.0	-	-	-
0.01	10	-	-
0.05	50		
0.1	100	-	-
0.5	-	50	
1	-	100	-
5	-	-	50
10	-	-	100
20	-	-	200

(The calibration range was 0.01 - 20 µg/Lung and was calculated for lung homogenate. The stock solutions were spiked onto control rat lungs after homogenising with the acetonitrile solution).

Lung Sample extraction

- ◆ Acetonitrile:Water (90:10), 10 mL, was added to each sample and homogenised using a TOMTEC Autogiser or equivalent. The dispersion tool was washed between each sample with water or alternative solvent.
- ◆ Control homogenate (10 mL) was spiked with Rh123 or flunisolid according to table 6.1 and vortexed to mix thoroughly.
- ◆ Each homogenate solution ~250 µL was placed in an Eppendorf tube and centrifuged at 13000 rpm for 10 min
- ◆ The control lungs (2 used for dilutions if necessary) were centrifuged in falcon tubes at 3500 rpm for 10 min.
- ◆ Using the Tecan (Genesis RSP 150) 100 µL of the supernatant was transferred from each eppendorf and 100 µL of a 15 ng/mL rolipram solution (15 ng/mL rolipram in MeCN) as internal standard was introduced to a 96 well filter plate and filtered to a 96 well plate.
- ◆ H₂O (200 µL) was added to give final ratio of ~50:50 acetonitrile: water.
- ◆ 96 well plates were then shaken for 5 min before analysis by LC/MS/MS

The resulting lung samples were analysed by LC/MS/MS using a 30 µL injection volume according to protocols outlined above i.e. the LC/MS/MS protocol appropriate for dose substrate. Levels of Rh123/flunisolid in lung homogenate (ng) were adjusted for the individual lung sample weights to give results in ng/g.

6.2.8. Data Analysis

Noncompartmental analysis of Pharmacokinetic parameters

The pharmacokinetic modelling software PKTools was utilised in order to estimate pharmacokinetic parameters for all generated data. Input data existed in the form of 'concentration remaining vs. time' as a percentage of dose to lung. Other input parameters included the molecular weight of substrate and dosing method. Model fits were extrapolated from observed data and pharmacokinetic parameters such as AUC, $t_{1/2}$ and CL/F estimated. See appendix iii for PKTools output.

Statistical analysis

To determine the significance of dose escalation of Rh123 and the inclusion of GF120918 within the IPRL preparation, a one way Analysis of Variance followed by a post-hoc Duncan's test was performed upon both the percentage of deposited Rh123 dose absorbed at 20 min and the $t_{1/2}$ (as calculated by PKTools) of each transport profile. A value of $p < 0.05$ was considered significant.

Power Analysis

In order to calculate the appropriate number of subjects required for each study performed with the IPRL to have adequate power, AUC calculations summarising data over various time points were conducted.

AUC calculations:

Estimates of area under the curve were calculated using the trapezium rule, splitting up the curve into trapeziums and approximating the AUC by calculating the area of each trapezium.

Power curves

To assess the number of animals that were required to give the experiment adequate power, power curves were created. Ideally, ~ 80 % power was preferred. See appendix iii for full Power analysis output.

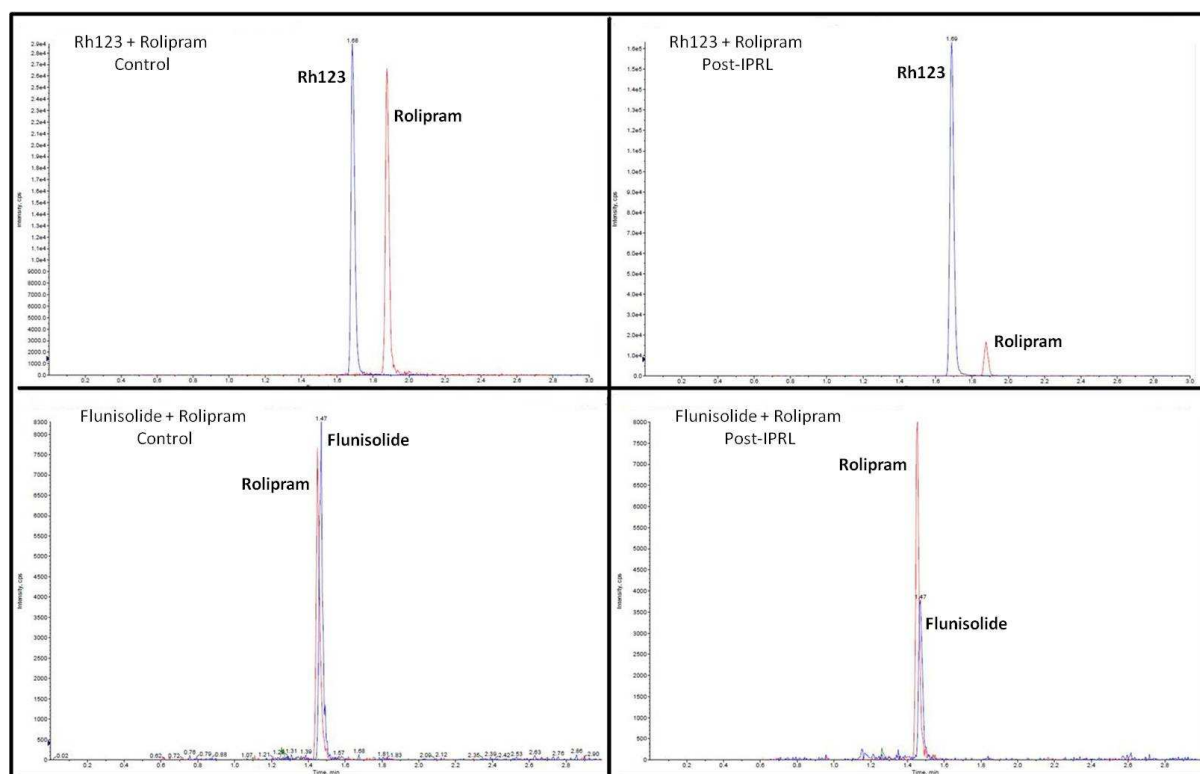


Figure 6.4 Example molecular ion peaks for substrates dosed to the single-pass IPRL (Analysed by LC/MS/MS).

6.3. Results

6.3.1. Evans blue distribution following intra-tracheal instillation

The instillation of Evans blue dye to the single-pass IPRL was conducted at GSK in order to establish the probable deposition pattern of substrates delivered via intra-tracheal instillation. Figure 6.5 clearly illustrates the distribution of Evans blue within much of the lung parenchyma; each individual lobe exhibiting a degree of colouration as a result of the dye.

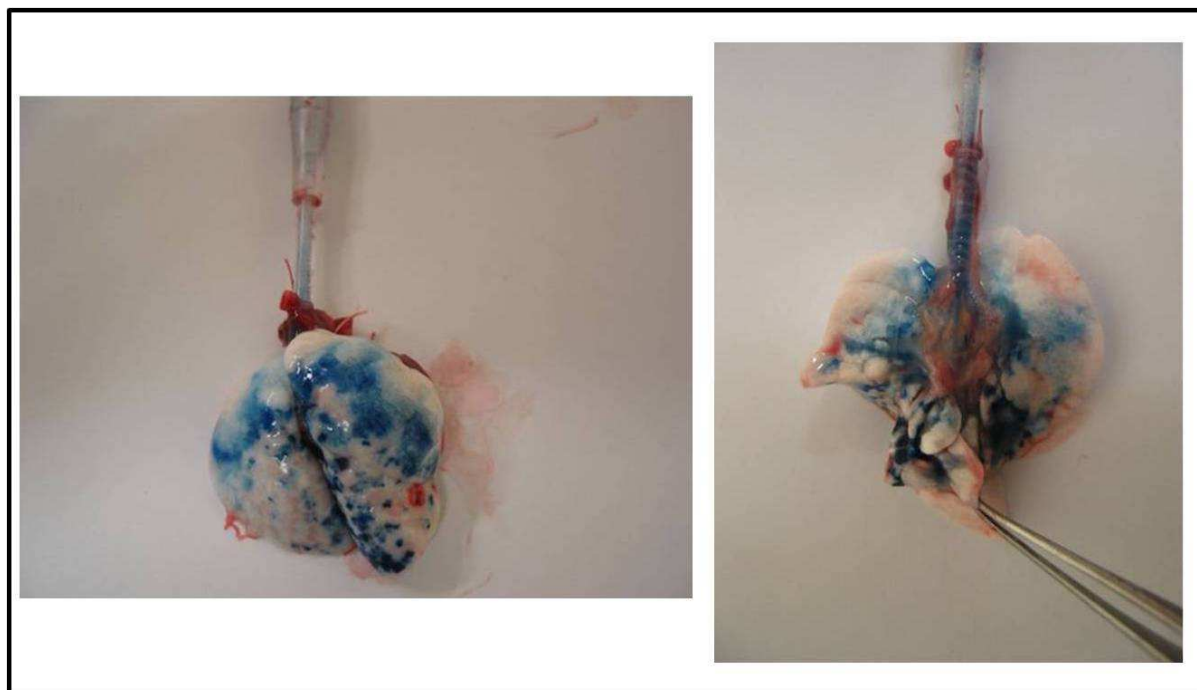


Figure 6.5 Lobar distribution of Evans blue dye in isolated lungs of the single-pass IPRL following intra-tracheal instillation with a Hamilton syringe. Left-hand panel shows anterior view of lung parenchyma. Right-hand panel shows posterior view of lung parenchyma.

When comparing the deposition of Evans blue within the tissue of the single-pass IPRL with that of the recirculating IPRL at Cardiff, (Figure 3.7, Chapter 3), a greater proportion of Evans blue was present in the trachea following ‘Hamilton instillation’ than following ‘forced solution instillation’. However, as is also the case with instillation of dye to the ‘Cardiff’ model, much of the Evans blue administered to each IPRL was found to be present within lobar regions of the isolated tissue.

6.3.2. Rh123 absorption in the single-pass perfusion model

From figure 6.6, it can be seen that increasing nominal Rh123 dose to lung from 2 μ g to 40 μ g resulted in a disproportionate increase in percentage deposited Rh123 dose transported to pulmonary perfusate. Further, addition of the P-gp inhibitor GF120918 (500 nM) to pulmonary perfusate and instilled dose of Rh123 (2 μ g) resulted in a similar disproportionate increase of

percentage deposited dose absorbed. From this it can be stated that inclusion of GF120918 in Rh123 dose and perfusate significantly ($p < 0.05$) altered the percentage of deposited Rh123 dose absorbed in the single-pass IPRL.

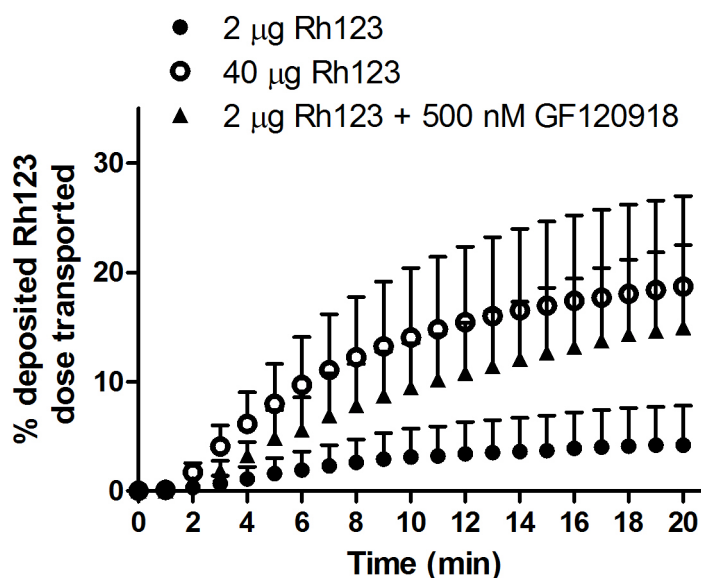


Figure 6.6 Cumulative increase in percentage deposited dose transported to pulmonary perfusate. The percentage of deposited dose is influenced by both nominal dose concentration and inclusion of GF120918 (in perfusate and airway instillate). Data shown are expressed as mean \pm S.D (n=4 for each treatment).

As can be seen in table 6.2, dose escalation of Rh123 from a nominal dose of 2 μg to 40 μg resulted in significant ($p < 0.05$) alteration of percentage deposited dose absorbed and calculated $t_{1/2}$. A 20-fold increase in nominal dose caused a 89.1-fold increase in cumulative mass absorbed from 0.084 μg to 7.482 μg . Further, calculated $t_{1/2}$ exhibited a comparative trend in that increase of nominal Rh123 dose resulted in a significant ($p < 0.05$) decrease in calculated $t_{1/2}$. The addition of GF120918 (500 nM) also resulted in significant alteration of documented parameters when comparison was made to the equivalent nominal Rh123 dose minus the inhibitor ('control'). Addition of GF120918 (500 nm) resulted in an almost 4-fold increase in percentage deposited Rh123 dose absorbed in comparison to control. Similarly, inclusion of GF120918 significantly ($p < 0.05$) decreased the calculated $t_{1/2}$ from 594.0 ± 482.1 min to 101.8 ± 58.8 min, a 5.8-fold decrease.

Further, as is illustrated in both figure 6.6 and table 6.2, comparison of the results of the higher dose Rh123 experiment (Rh123 40 μg) to the data obtained in the presence of the P-gp inhibitor (Rh123 (2 μg) + GF120918 (500 nM)) demonstrate that introduction of GF120918 to the IPRL resulted in a

lack of statistical significance ($p>0.05$) between these treatments in both the percentage deposited dose Rh123 absorbed and calculated $t_{1/2}$.

Treatment (Nominal Dose μg)	Cumulative mass of Rh123 absorbed by 20 min(μg)	Percentage of deposited Rh123 dose absorbed by 20 min (%)	$t_{1/2}$ (min)
Rh123 (2 μg)	0.084 ± 0.072	4.2 ± 3.6	594.0 ± 482.1
Rh123 (40 μg)	7.482 ± 3.311	18.7 ± 8.3	78.8 ± 43.8
Rh123 (2 μg) + 500 nM GF120918	0.239 ± 0.130	15.0 ± 7.5	101.8 ± 58.8

Table 6.2 Dose escalation of Rh123 and the effect of GF120918 upon the transport of Rh123 in the single-pass IPRL. The P-gp inhibitor was present at 500 nM in the perfusate and in the co-instilled airway doses of Rh123. Data shown are expressed as mean \pm S.D (n=4 for each treatment).

6.3.3. Flunisolide absorption in the single-pass perfusion model: Influence of GF120918

As can be seen in figure 6.7, the addition of GF120918 (500 nM) to flunisolide dose and pulmonary perfusate resulted in a decrease in the percentage deposited flunisolide dose absorbed with time, an opposing effect to that observed in conjunction with Rh123 dose. Further, dose escalation of flunisolide (in a similar experimental rationale to Rh123 dose escalation; chapter 4) exhibited a comparable if opposite trend to that observed with Rh123. Increase of nominal flunisolide dose from 2 μg to 40 μg caused a significant ($p<0.05$) decrease in percentage deposited dose absorbed. A further increase in nominal dose to 80 μg did not bring about an additional decrease in percentage deposited dose transported, suggesting saturation of an active process.

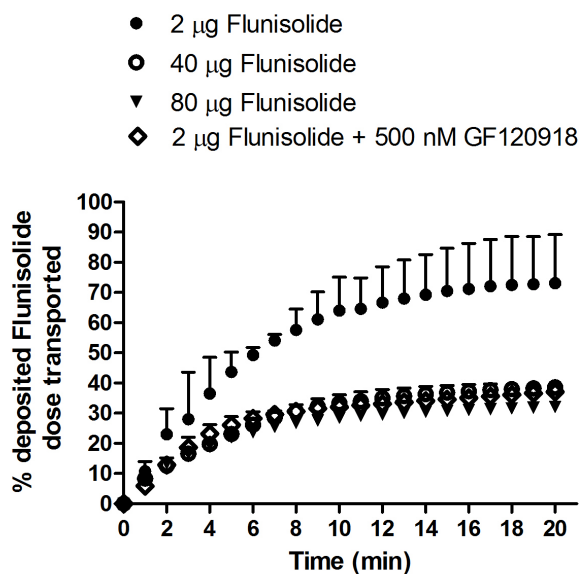


Figure 6.7 Effect of dose escalation and addition of GF120918 (500 nM), in perfusate and instillate, upon cumulative % of deposited flunisolide dose in the IPRL. Data shown are expressed as mean \pm S.D (n=4 for each treatment).

Table 6.3 illustrates that, increase of nominal flunisolide dose introduced to the single-pass IPRL resulted in a disproportionate increase in cumulative mass Flunisolide absorbed by 20 min. This disproportionate increase in cumulative mass absorbed translated to a disproportionate decrease in percentage deposited dose absorbed. An increase in nominal flunisolide dose from 2 μ g to 40 μ g resulted in a 1.89-fold decrease in percentage deposited dose absorbed. A comparable trend can also be observed for calculated $t_{1/2}$ in that nominal flunisolide dose increase resulted in a disproportionate increase in absorption half-life. A further doubling of nominal flunisolide dose, from 40 μ g to 80 μ g, did not result in a similar change recorded parameters, i.e. the percentage deposited dose absorbed at 20 min and the calculated $t_{1/2}$ relating to 80 μ g flunisolide dose are not statistically different ($p>0.05$) to those recorded for 40 μ g dose.

The inclusion of GF120918 with instilled flunisolide dose and IPRL perfusate produced analogous results to those achieved through dose escalation. As can be seen in table 6.3, the percentage of deposited flunisolide dose absorbed by 20 min or '40 μ g dose', '80 μ g dose' and '2 μ g + GF120918' are statistically indistinguishable ($p>0.05$) from each other and yet all remained statistically different ($p<0.05$) to '2 μ g dose' results. Further, the calculated $t_{1/2}$ for treatments '40 μ g dose', '80 μ g dose' and '2 μ g + GF120918' also displayed similarity to each other, however, '80 μ g dose' is not statistically comparable to '2 μ g + GF120918'. Again '2 μ g dose' calculated $t_{1/2}$ is statistically different ($p<0.05$) to all other treatments.

Treatment (Nominal Dose μg)	Cumulative mass of Flunisolide absorbed by 20 min(μg)	Percentage of deposited Flunisolide dose absorbed by 20 min(%)	$t_{1/2}$ (min.)
Flunisolide (2 μg)	0.33 ± 0.01	73.05 ± 16.12	5.17 ± 0.88
Flunisolide (40 μg)	6.60 ± 0.85	38.57 ± 1.69	16.39 ± 1.58
Flunisolide (80 μg)	26.50 ± 0.71	32.05 ± 1.20	18.96 ± 0.49
Flunisolide (2 μg) + 500 nM GF120918	0.15 ± 0.07	37.10 ± 1.48	14.32 ± 0.13

p>0.05

Table 6.3 Effect of dose escalation and addition of GF120918 upon the transport of flunisolide in the single-pass IPRL. The P-gp inhibitor was present at 500 nM in the perfusate and in the co-instilled airway doses of flunisolide. Data shown are expressed as mean \pm S.D (n=4 for each treatment).

6.3.4. Power Analysis

The data in table 6.4 documents the mean calculated AUC values for all Rh123 data obtained with the single-pass IPRL. A complete experimental data set was analysed in order to estimate required subject number to achieve adequate study power. Both 'dose transported' and 'dose remaining' are included within this table however, preliminary power curve calculations revealed 'dose remaining' data to produce the same results as 'dose transported' data and were therefore excluded from future analysis.

Rh123 dose to lung (nominal; μg)	AUC	Mean (n=4)	StDev
2 μg	Dose Transported AUC	52.2	44.6
40 μg	Dose Transported AUC	240.8	108
2 μg + GF120918	Dose Transported AUC	169.7	74.9
2 μg	Dose Remaining AUC	1947.8	44.6
40 μg	Dose Remaining AUC	1759.2	108
2 μg + GF120918	Dose Remaining AUC	1830.3	74.9

Table 6.4 Corresponding AUC data for all ‘single-pass Rh123’ data as calculated using the trapezium rule. AUC calculations were employed as a convenient way to summarise the data gathered over various time points. (n=4 for each treatment).

The plots in figure 6.8 depict power curves extrapolated from Rh123 data. Each power curve represents a comparison between two dose treatments. The dashed lines intersecting each power curve estimate the sample size needed in order to make comparisons between groups. For example, the power curve related to ‘Dose transported – Rh123 (2 μg) vs. Rh123 (40 μg) estimates that, in order to achieve 80 % power, approximately 5 subjects are required. The same is true for ‘Dose transported – Rh123 (2 μg) vs. Rh123 (2 μg) + GF120918.

Dose transported – Rh123 (2 µg) vs. Rh123 (40 µg)

Dose transported – Rh123 (2 µg) vs. Rh123 (2 µg) + GF120918

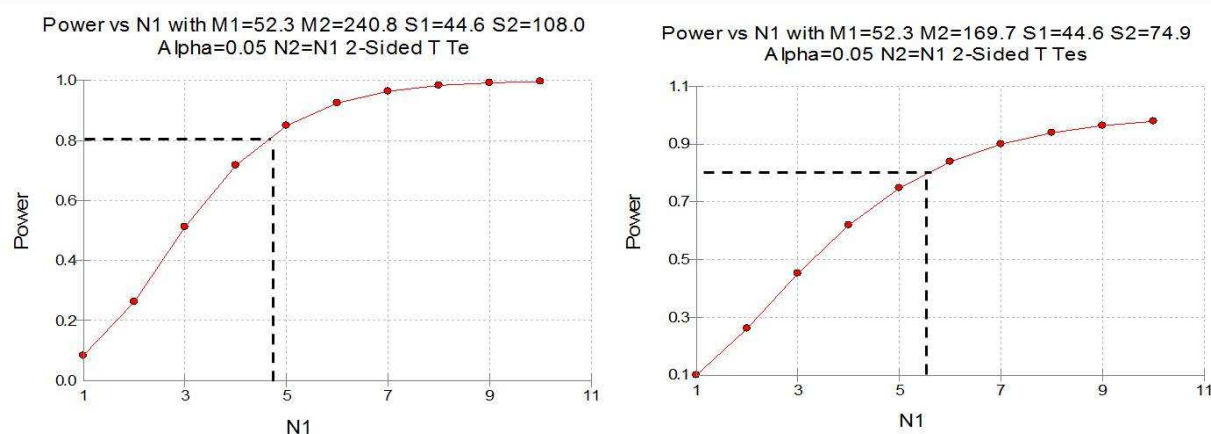


Figure 6.8 Power curves modelled from mean and S.D AUC data. N1 = number of subjects. Each power curve represents a comparison between two data sets to allow estimation of meaningfulness of comparison between each Rh123 treatment. (n=4 for each treatment)

The data in table 6.5 represents calculated AUC values for each Rh123 dose treatment within the dose ranging study conducted with the recirculating IPRL at Cardiff. Only data relating to 'dose transported' AUCs are reported as it was previously decided that this data set yields comparable data to 'dose remaining' values.

Treatment	Rh123 dose to lung (nominal; µg)	No. Obs	AUC Mean	AUC StDev
Rh123 (20 µg/mL)	2	12	424.02	423.81
Rh123 (50 µg/ml)	5	4	1040.67	158.69
Rh123 (400 µg/mL)	40	4	1762.39	371.26
Rh123 (800 µg/mL)	80	4	1685.36	295.30

Table 6.5 Calculated AUC values and summary statistics for individual Rh123 dose-ranging treatments (Cardiff data).

In a similar approach to that employed with 'GSK' data, power curves were generated allowing estimation of the number of subjects required to give adequate experimental power to individual treatment comparisons. Figure 6.9 represent the power curves modelled against mean AUC data relating to each Rh123 treatment. Again, dashed lines highlight the adequate number of subjects required to achieve 80 % experimental power.

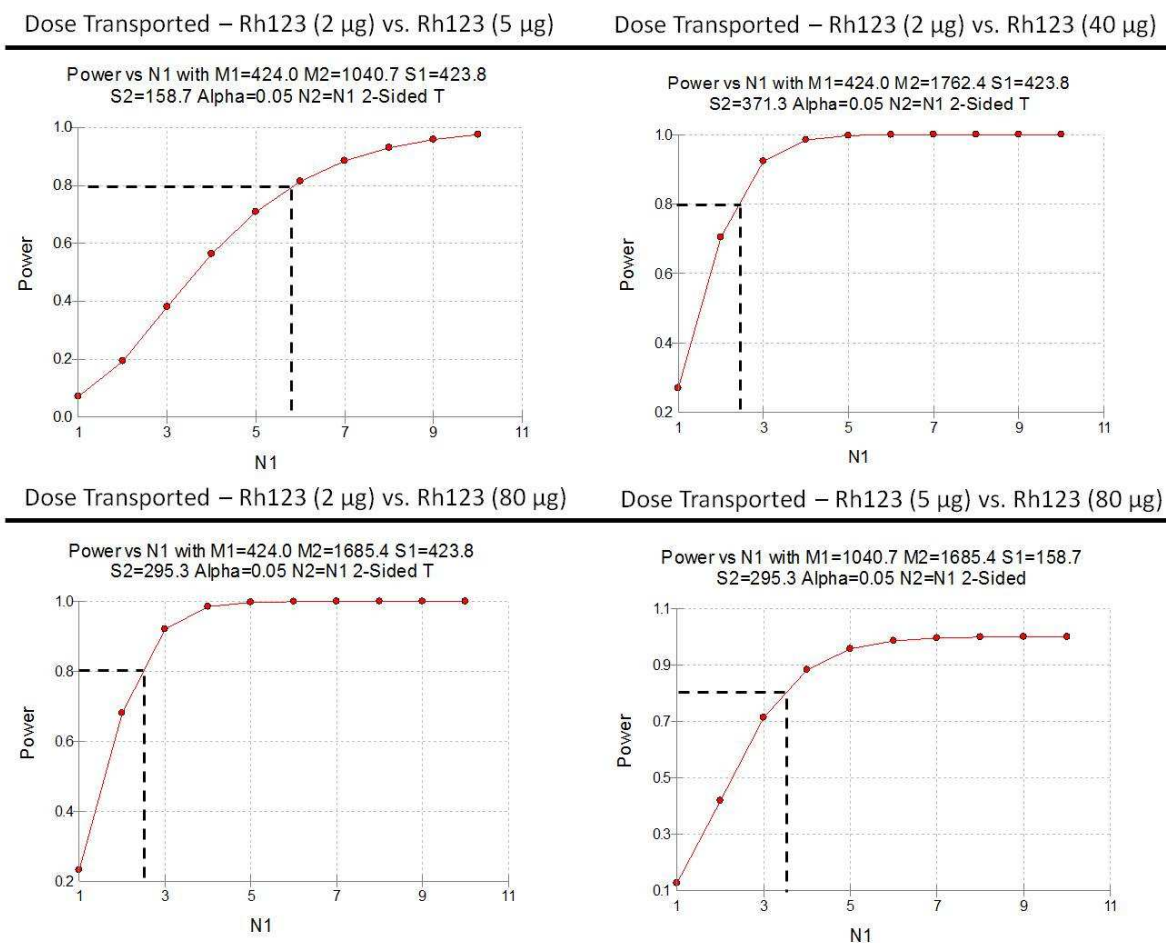


Figure 6.9 Generated power curves comparing individual dose treatments of the Cardiff dose-ranging study. N1 = number of subjects. Only those plots allowing meaningful comparison between treatments (i.e. comparison between non-saturable and saturable dose) were included within these results.

6.4. Discussion

Originating from the published discovery of P-glycoprotein by Juliano and Ling in 1976 [70], documented research into and around this significant active drug transporter has flourished. Today, the impact of drug transporters, and especially P-gp, upon pharmacokinetics, pharmacodynamics and drug safety are well recognized if not fully understood [354]. The *in vivo* roles of P-glycoprotein in drug disposition, therapeutic efficacy and drug-drug interactions has led much research to be focused upon functional impact in organs such as the intestine, liver, kidney and brain where the influence of P-gp upon drug absorption and disposition is now well characterised [68, 354].

As has been discussed in previous chapters, within the literature there exists an abundance of research concerning P-gp, with much focus upon reversal of drug resistance and foetal drug exposure, polymorphisms of the P-gp gene, transport substrates of P-gp and their interactions and the impact of the transporter upon diseases such as Alzheimer's disease and in particular disease treatments.

As this thesis has suggested, the existence and location of P-gp within the pulmonary system is now well accepted and table 6.6 summarises current understanding of P-gp localisation within the lung based upon knowledge obtained from contemporary literature reports [354].

Evidence of Immunohistochemical localisation of P-glycoprotein within cells of the lung	
Cell Type	Reference
Bronchial and Bronchiolar epithelium (Apical localisation)	Lechapt-Zalcman <i>et al.</i> , 1997 [112] Scheffer <i>et al.</i> , 2002 [43] Van der Valk <i>et al.</i> , 1990 [110] Cordon-Cardo <i>et al.</i> , 1990 [108]
Bronchial capillary endothelial cells (Apical localisation)	Schinkel <i>et al.</i> , 2003 [60]
Alveolar macrophage (Apical localisation)	Scheffer <i>et al.</i> , 2002 [43] Van der Valk <i>et al.</i> , 1990 [110]
Alveolar epithelial cells: (Apical localisation) Type I	Campbell <i>et al.</i> , 2003 [137] Endter <i>et al.</i> , 2007 [113]
Type II	Endter <i>et al.</i> , 2007 [113]

Table 6.6 Cellular localisation of P-gp within a variety of lung-specific cells. Localisation in all cases was determined by immunohistochemistry.

Together with a developing expression profile of 'pulmonary P-gp', distinct roles of P-gp within the lung are also emerging. Traditionally it is thought that 'pulmonary P-gp' acts to remove

environmental toxins from the lung and prevent accumulation of these within the lung lumen [43]. When regarding P-gp from a pharmacological viewpoint, it is the interaction of P-gp with drugs introduced to the lung that is important, again, with the aspects of drug-drug interactions, drug accumulation, toxicity and drug disposition being of relevance [445].

In a parallel manner to that employed at the Welsh School of Pharmacy (WSOP), this current work was undertaken using GSK's own in-house developed *in situ* isolated perfused rat lung model (IPRLu) with the airway instillation of test compounds to determine the potential of P-glycoprotein to modulate pulmonary absorption. Specifically, to consider the applicability and viability of such an isolated model within the pharmaceutical industry.

In a similar approach to that employed at WSOP, the P-gp substrates, Rh123 and flunisolide and inhibitor, GF120918, were introduced to the IPRLu and the influence of P-gp upon substrate examined. Within the literature there are many reports of Rh123 use as a P-gp substrate and the dye continues to be utilised in such a way. For example, there are recent published works of Rh123 being used as a P-gp substrate to illustrate multidrug resistance (MDR) reversal in mice with psoriatic arthritis and also to illustrate the novel applicability of ultrasound in altering P-gp gene expression in MDR cells [288, 446]. Similarly, there are many literature reports regarding the use of GF120918 as a P-gp inhibitor; ranging from its first published use by Letrent *et al.* to current use in examining the influence of P-gp upon drug substrates such as Tandutinib and Darunavir [372, 447, 448]. However, while there is significant evidence rationalising the use of such drugs within this chapters studies, Rh123 and GF120918 were primarily used to also allow comparison of results between the IPRL at WSOP and the IPRLu at GSK. Further, as has been discussed in a previous chapter (Chapter 4), while there is little literature evidence supporting the use of Flunisolide as a P-gp substrate, the steroid was previously used to highlight P-gp functionality in the WSOP IPRL and within the R&D facilities of GSK at Stevenage, flunisolide has also been identified as a substrate of P-gp via in-house GSK MDCK assays.

While the use of an isolated and perfused rat lung was employed both at WSOP and GSK, the main differences between the WSOP IPRL and the GSK IPRLu are obvious, i.e., *in situ* versus *ex vivo*, open-circuit (single pass) versus closed-circuit (recirculating). However, the variations employed at GSK have been used previously within the literature and highlight the diversity of such a model. Most obviously, each of the isolated lung preparations varies in the positioning of the lungs. As discussed in Chapter 3, the removal of the isolated lungs to a humidified glass chamber allows greater control over experimental parameters; however, use of an *in situ* isolated lung setup is also common. *In situ*

isolated lung setups allow for simpler experimental arrangement, provide accurate cell-cell interactions, *in vivo*-like lung positioning within the thorax and less tissue disruption whilst also providing isolation of the lung from surrounding tissue vasculature for lung specific investigations [449]. Within the literature, use of the *in situ* isolated perfused lung appears to be focussed towards innate physiological and biochemical studies while the *ex vivo* setup seems to be related more to studies examining the effects of external stressors or drugs delivered to the lung [444, 450, 451]. Similarly, use of an open-circuit perfusion method compared to that of a closed-circuit method appears also to be 'experimental-aim' dependent. There are many pros and cons regarding each perfusion method and the use of an open-circuit model would allow for easy acquisition of perfusate samples, a somewhat simpler setup in terms of perfusion circuit and the simpler determination of initial pharmacokinetic parameters. It is therefore apparent that despite the versatile nature of the IPRL, specific experimental parameters are linked to specific experimental aims hence the differences between WSOP and GSK models. By mirroring the P-gp studies performed at WSOP, this chapter aimed to allow comparison of data, to highlight variability and efficiencies of each IPRL model and ultimately to emphasize the importance of P-gp within drug discovery and drug delivery.

In order to assess the extent of dose distribution in the IPRLu, a solution of the azo-dye Evans blue was introduced to the isolated lung via the trachea by means of a Hamilton syringe. Despite a lack of direct corroborating evidence within the literature, techniques such as Evans blue dye distribution have been utilised previously by researchers as a simple means to visually illustrate adequate dose distribution, organ perfusion and intracellular damage within an isolated organ system [452, 453]. Although traditionally employed as a marker of extracellular leakage, the application of Evans blue for alternative purposes within isolated organ preparations is common. For example, Evans blue staining has recently been used to monitor myocardial contractility within the isolated rabbit heart and in the isolated lung has been employed as a means to measure permeability-surface area product [216, 454].

Within this chapter, the introduction of Evans blue was used as a simple and effective means to assess dose distribution. As can be seen in figure 6.5, the dye could be visualised throughout the isolated lung parenchyma, highlighting extensive dose distribution. In comparison to results obtained with the WSOP IPRL, (Figure 3.7), much more Evans blue could be seen in the trachea of the IPRLu following Hamilton syringe instillation than in the IPRL following forced solution instillation. This simple evaluation of results suggests that the application of a forced solution dosing method is more effective at immediately introducing dose to the deep lung. However, as can be

seen in figure 6.3, the isolated lung at GSK is elevated to a 45° angle in order to overcome the lack of initial dose propulsion to the deep lung.

The use of intra-tracheal instillation as a method of introducing particles to an experimental animal is widespread; further, there are many studies that document the similarity in drug plasma profile following intra-tracheal instillation or aerosol administration to the lung and pharmacokinetic analysis of data has also indicated overall similarity in absorption [455]. When comparing the WSOP IPRL to the GSK IPRLu studies, dosing method essentially vary only in the presence of a pMDI creating forced instillation in the WSOP model. Both dosing methods present a simple, rapid and reproducible means of introducing dose to the isolated lung and when considering the similarity in Evans blue distribution profile and literature evidence regarding resemblance between intra-tracheal instillation and aerosol administration (to which forced-solution instillation is loosely comparable), it is likely that this difference in dosing technique would impact minimally on data comparison and result interpretation [456].

To rationalise the development of an IPRLu at GSK it was important to functionally validate the setup in terms of its P-glycoprotein drug transporter activity and thus provide assurance of the value of such a setup in the determination of the impact of P-gp upon drug discovery. The functional activity of P-gp as an efflux transporter is unquestionable and its influence upon multi-drug resistance, drug-drug interactions and drug pharmacokinetics well recognised [73]. In a comparable experimental method employed at WSOP, the functional activity of P-gp in the IPRLu was assessed through substrate dose escalation and transporter modulation. As has been reasoned in Chapter 4, the use of the P-gp substrate, Rh123, and inhibitor, GF120918, were employed together with the IPRLu; experimental doses also mimicked those at WSOP [366, 367, 371, 372]. Although a number of techniques for transporter inhibition exist, (e.g. siRNA knockdown, genetic knockout animals, irradiation, transcriptional regulation), the use of chemical inhibitors remains the simplest within the experimental setting [358, 457, 458]. The use of flunisolide as a P-gp substrate was also duplicated with the IPRLu as, although previously only confirmed as a P-gp substrate by Florea and co-workers [398], the corticosteroid did display an altered IPRL absorption profile via the influence of GF120918 in the WSOP IPRL. As a consequence of the unexpected results documented with the IPRL, the replication of this experiment would provide further evidence as to the influence of P-gp upon flunisolide transport in the lung.

The dosing of Rh123 to the IPRLu yielded comparable results to those obtained with the WSOP IPRL. Increasing nominal Rh123 from 2 µg to 40 µg resulted in a disproportionate increase in the

percentage of deposited dose transported, deemed statistically significant by one way Analysis of Variance. Further, the addition of GF120918 (500 nM) produced a similar disproportionate increase in percentage of deposited dose transported, suggesting inhibition of P-gp as an active efflux transporter. Demonstration of active transporter functionality via dose escalation and eventual transporter saturation is standard and P-gp literature is strewn with examples of the involvement of P-gp upon drug substrate pharmacokinetics via interaction and efflux of transporter substrates [459, 460]. The results of this chapter concerning Rh123 dose escalation substantiate the hypothesis of P-gp functionality within the lung and mimic those results displayed in Chapter 4 and within the literature [355]. When comparing results obtained at WSOP to those documented at GSK, significant similarities can be noted. As can be seen in figure 6.10, when comparing the percentage deposited Rh123 dose transported over a 20 min period, no significant differences between isolated lung setups can be drawn. Essentially, the existence and functional influence of an active transporter within the isolated rat lung has been demonstrated via two individual setups by illustrating dose independent, non-linear transport of a transporter substrate.

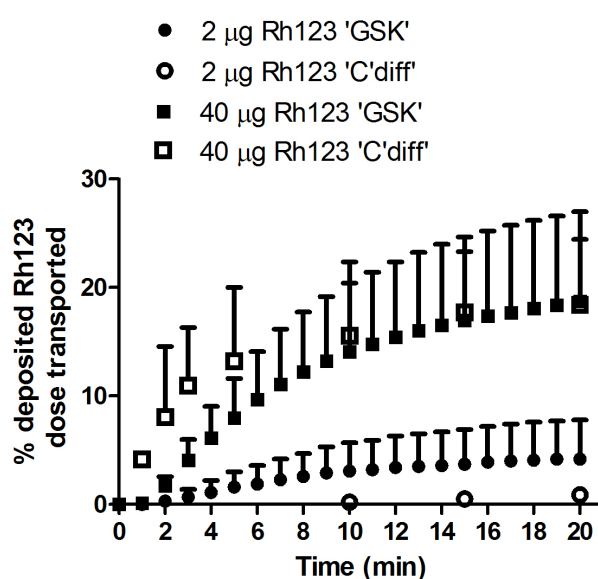


Figure 6.10 Comparison of initial transport profile of Rh123 delivered to the WSOP IPRL and the GSK IPRLu. Data are expressed as mean \pm S.D.

While initial Rh123 transport profiles are comparable, the overall percentage of deposited Rh123 dose transported over the lifetime of the experimental is also comparable, highlighting not only the analogous nature of Rh123 transport within an isolated rat lung but also the significant binding of Rh123 to lung tissue. The resulting transport profiles of Rh123 in the presence of GF120918 are also considerably similar, cementing the presence of a functional transporter, i.e. P-gp, within the

isolated rat lung and mimicking trends illustrated by Roerig *et al.*, [355], thus further emphasizing the authenticity of those results displayed in the IPRLu.

The transport of flunisolide across the IPRLu also replicates trends observed at WSOP. Escalation of nominal flunisolide dose from 2 µg ultimately to 80 µg resulted in a disproportionate *decrease* in the percentage of deposited dose transported through the IPRLu. Figure 6.7 illustrates that introduction of a 2 µg nominal dose to the IPRLu resulted in a very high percentage of flunisolide being transported to perfusate (73.05 ± 16.12 % by 20 min.) while introduction of a 40-fold higher nominal dose resulted in only 32.05 ± 1.20 % flunisolide dose transported within the same time period. Transporter saturation could be deemed to be reached between 40 µg and 80 µg nominal dose as there was no significant difference in percentage deposited dose transported within this dose escalation; both 40 µg and 80 µg nominal dose 'percentage of deposited dose transported' being significantly different from that of the 2 µg dose. Again, the addition of P-gp inhibitor GF120918 caused a significant alteration in the percentage of deposited dose transported, decreasing mean results from 73.05 ± 16.12 % of 2 µg nominal dose transported in the absence of inhibitor to 37.10 ± 1.48 % of 2 µg nominal dose transported in its presence.

However surprising the flunisolide results from both isolated lung preparations appear, they do illustrate the presence of an active process, capable of influencing the transport of flunisolide, within the rat lung. Within Chapter 4, the possibilities of the involvement of other active transporters were discussed, however, not only do the results obtained in the IPRLu diminish the likelihood of the observed trends being an artefact of the WSOP IPRL, the combination of substrate and inhibitor used does confirm the presence of at least one functionally active transporter within the rat lung.

To facilitate the understanding of the significance of pulmonary P-gp upon the mechanisms of drug absorption and distribution in the IPRLu, substrate transport data was subjected to analysis by PKtools pharmacokinetic modelling software. While the concept of pharmacokinetics is much more ancient than that of P-gp, the development of modern pharmacokinetics and pharmacokinetic modelling grew in parallel to P-gp knowledge in the 1960s and 70s [461] and throughout this period and beyond it has been of great importance to estimate and understand the contribution of drug transporters to the pharmacokinetic parameters of ADME [462]. Within the literature there are numerous accounts of active P-gp influence upon pharmacokinetics, however, to illustrate this same impact within an isolated lung model would be incredibly valuable to the field of pulmonary drug discovery [226, 462, 463]. By the use of PKtools, it could be determined that the results of this chapter mimic those in the literature where P-gp has been chemically modulated and the functional

activity of P-gp has been proved to influence pharmacokinetic parameters [464-466]. Within this chapter, it was demonstrated that the initial absorption half-life of both Rh123 and flunisolide was significantly affected by the non-linear increase in dose and the addition of P-gp inhibitor suggesting influence of P-gp upon the initial absorption of substrate drugs dosed to the lung. Again such findings mirror those reported in the WSOP IPRL and yet again verify the functional impact of P-gp upon drugs delivered to the lung through its function as an efflux transporter.

Through conducting substrate transport studies with the IPRLu, results have shown that the model is robust and sensitive enough to differentiate between substrate transport profiles in the presence and absence of a chemical modulator. Further, data obtained from this model have proven to be comparative to that obtained via the WSOP IPRL suggesting reproducibility between individual isolated lung preparations and substantiating credibility of findings from each model. Within the realm of a pharmaceutical company such as GSK, the IPRLu has proved to be a suitable model for lead optimisation programmes focussing upon pulmonary drug discovery and development and also as a tool for selecting drug analogues based upon lung retention following intra-tracheal instillation.

The existence of two parallel data sets, performed in isolated lung preparations with distinct experimental variations, presented an opportunity for model comparison. Highlighted in table 6.7 are key differences between the WSOP IPRL and the GSK IPRLu.

IPRL (WSOP model)	IPRLu (GSK model)
ONLY Pulmonary artery cannulated – Simpler surgery and avoids build-up of back pressure in pulmonary vein	Both Pulmonary artery and pulmonary vein cannulated - More complicated, prolonged surgery
Fast surgery time (≤ 10 min) - Aids in maintaining lung integrity through swift placement in AGT	Longer surgery time - Need for quick surgery as prep. can be maintained for only ~2-4 h i.e. prolonged surgery encroaches upon this
Perfused with 4 % BSA. No blood - Easier to monitor degree of lung perfusion. Fewer animals needed for prep.	Perfused with 3 % blood. No glucose - More realistic. Difficult to visually monitor degree of perfusion. More animals needed for prep.
Lungs removed and suspended in AGT - Allows greater control of expt. variables. Easy to visually monitor lung integrity	Lungs remain in cadaver - Less trauma. Difficult to visually monitor lung integrity. Does afford some tissue protection from external environment
Prep. maintained at 37 °C - More representative of <i>in vivo</i> state	Prep. maintained at room temperature - Simpler equipment setup
AGT humidified - Lung tissue shielded from laboratory environment e.g. Air conditioning	Lung tissue exposed to laboratory environment - Tissue damage as lungs dry out over experiment period
Heparin injected during surgery	Heparin injected before surgery - enhanced circulation of heparin prior to surgery; reduced likelihood of coagulation during expt.
Prep. ventilated with 2.5 mL tidal volume, 20 bpm	Prep. ventilated with 1.8 mL tidal volume, 40 bpm
15 mL min⁻¹ perfusate flow rate	10 mL min⁻¹ perfusate flow rate
Negative pressure ventilation - More representative of <i>in vivo</i> state	Positive pressure ventilation
95/5% O₂/CO₂ bubbled into perfusate – To maintain buffered pH of perfusate	No addition of O₂/CO₂ to perfusate
Recirculating perfusion - simpler to maintain prolonged experiment	Single pass perfusion - easier to calculate initial PK parameters
Dosing: Dosing rod & propellant only pMDI - Potential damage to lungs during forced inflation.	Dosing: Hamilton syringe - Deposition of proportion of dose in trachea
Observation sheet used - allows documentation of difficulties in surgery, lung appearance, dosing proficiency etc	No observation sheet - no accompanying evidence to offer explanation for anomalous results

Table 6.7 Key differences in experimental setup and procedure between two isolated perfused rat lung preparations.

As can be seen in the above table (Table 6.7), a number of distinct variations exist between each model, many of which can be linked to the experimental setup as a whole. Two main and obvious differences were noted to be the *in situ* versus *ex situ* placement of the isolated lungs and model perfusion circuit, i.e., single-pass versus recirculating. As has been discussed above and in Chapter 3,

isolated perfused lung experimental variations can be related to experimental purpose and individual variations between models justified according to experiment rationale and design. When comparing GSK IPRLu model to that of WSOP, a number of significant issues were identified;

- There exists a requirement for faster surgery - IPRLu was viable for up to 4 h once perfused, however, prolonged time taken to complete surgery may have impacted upon tissue viability, therefore overshadowing benefit of retaining lungs *in situ*.
- Use of an observation sheet - Recording factors such as; tissue touching (in WSOP lungs are transported to AGT via trachea), surgery time, difficulty in cannulating blood vessels (prolonged difficulty in cannulating pulmonary artery may compromise overall integrity of tissue) and lung appearance (glassy = poor perfusion, enlarged = oedema occurrence. Such observations would allow accurate data interpretation by study directors.
- Exposure of less pulmonary tissue during isolation surgery - Removal of a smaller proportion of rib cage would help prevent the lungs from 'drying out' due to exposure to air conditioning. *If lungs must be kept moist during experiment suggest light covering with spare perfusate rather than tissue dabbing. (WSOP believe that touching the lungs damages integrity).*

As a further comparison between isolated lung preparations, a power analysis study was performed upon data generated via use of each model. Such a study was undertaken to uncover the sample size needed to allow accurate statistical judgements of each data set. On examining figures 6.8-6.9, the graphical output of each study comparison, it was concluded that a larger sample size would be required to allow comparison of 'GSK data' that that of 'WSOP data' thus, a larger degree of variability was found to exist within and between GSK data sets. Table 6.8 highlights this.

Treatment	Estimated <i>n</i> value
IPRLu (GSK)	
Rh123 (2 µg) vs. Rh132 (40 µg)	5
Rh123 (2 µg) vs. Rh132 + GF120918	5
IPRL (WSOP)	
Rh123 (2 µg) vs. Rh132 (40 µg)	3
Rh123 (2 µg) vs. Rh132 (80 µg)	3
Rh123 (5 µg) vs. Rh132 (80 µg)	3

Table 6.8 Summary of a power analysis study, from which necessary experiment sample sizes to allow reliable statistical analysis were graphically determined.

While the power analysis study does seem to suggest a requirement for a higher treatment sample sizes when utilising the GSK IPRLu, the study does not include interpersonal variability. All power analysis data considered from WSOP IPRL was generated by a single study operator, while GSK IPRLu data considered was generated by 1+ researcher. Further, data yielded through use of the IPRLu was generated by one seasoned and one novice IPRLu operator, somewhat rationalizing the existence of a larger degree of variability within such 'GSK data sets'.

Overall, the replication of drug transport studies performed at WSOP through use of the IPRLu at GSK support data trends and conclusions drawn from 'WSOP data'. In summary, the hypothesis of functionally active drug transporter presence in the isolated rat lung, also assumed *in vivo*, was substantiated via drug substrate dose escalation and drug transporter inhibition studies in the IPRLu. The use of P-gp substrate drugs and a specific P-gp chemical inhibitor strongly suggests P-gp to be the transporter protein responsible for trends observed. All data generated via the IPRLu mimics that generated via the IPRL in terms of overall observations outlined providing an exceptional collection of data from which to further understand the influence of an active transporter upon drugs delivered to the lung. In addition, the merits of the isolated and perfused rat lung at GSK present this model as an excellent specific and relatively high throughput model for use in the fast paced field of pharmaceutical research.

Chapter 7

General Discussion

7.0. General Discussion

In 2006 alone, the global value of the 'inhaled drug' market was estimated at US \$ 18.5 billion with the respiratory market as a whole representing the 4th largest therapeutic area within pharmaceutical sales. With ~65 % of this market being occupied by drugs for asthma/COPD treatment, it was expected that such treatments would generate US \$ 21.9 billion in sales in 2010, highlighting the significant revenue pulmonary drug delivery can create [467]. Today there are at least 65 inhaled drugs available for the treatment of respiratory diseases. While most drugs are generated for local targeting of diseases such as asthma, COPD, influenza and TB, there are also a number of drugs (particularly biotechnology molecules) in development whose delivery to the systemic circulation via the lungs is being examined [468]. The delivery of drugs via the lung for diseases and conditions that do not involve the pulmonary system has been an increasing focus over the last 20+ years. The lung offers a number of beneficial physiological characteristics (i.e. expansive surface area, thin barrier at the alveolar epithelium, high vascularisation) that can be exploited to provide non-invasive access to the systemic circulation [469]. Already there have been a number of success stories, most famously inhaled insulin, Exubera, which reached the market in 2006 for the treatment of diabetes but due to its limited approved indications it was later withdrawn. Small molecule drugs have also been the subject of systemic delivery via the lungs, for example, both morphine and fentanyl have been reported and have been successfully delivered via the lung for pain relief and ergotamine has been delivered through the lung for the treatment of migraine. Such examples serve to highlight the opportunities manifested by pulmonary drug delivery. Further, encouraging research is progressing developments in this area and that will undoubtedly lead to more efficacious inhaled therapies for the treatment of a variety of diseases [468, 469].

The lungs are constantly exposed to xenobiotics notably from the environment. From this, the lungs possess a number of barriers and defence mechanism, including the airway geometry promoting particle deposition, mucus and mucociliary clearance, as well as immune defence and the physical cell barrier itself, all of which will limit inhaled drug delivery to submucosal sites [469]. The presence of active drug transporters within the many cells of the lung provides a further barrier to drug delivery. Drug transporter proteins are increasingly recognised as important determinants in drug disposition and response, with impact upon the pharmacokinetics of drugs [45].

There is a growing body of knowledge on the presence of drug transporters in the lung. Through exploitation of RT-PCR techniques a surprisingly large number of transporters, from a variety of families, have been localised to the cells of the lung. Less is known on the actual spatial expression

of drug transporter proteins in the lung and as a consequence predictions of how a given transporter may impact upon pulmonary drug absorption and disposition are highly speculative. Generally, literature reports constrain drug transporter localisation to the apical side of pulmonary-specific cells, suggesting a role in defence via extrusion of inhaled toxins and pathogens to the airspace for expulsion [104, 354].

The overall objective of this thesis was to explore the functional significance of P-glycoprotein upon pulmonary absorption using an isolated perfused lung preparation as a model system. An initial objective of this was to positively establish an accurate expression profile for a selection of relevant active drug transporters within the rodent lung. The rodent lung was chosen as it represents a commonly utilised and well recognised experimental species, and the isolated perfused lung preparation that was developed and used in this thesis was based around the rat [23, 417]. Initially, 'drug transporter experiments' mimicked those performed by others, such as Endter *et al.* and Bleasby *et al.* [69, 104] and sought to determine the presence of individual drug transporters at the mRNA level within different rat lung cell samples. Uniquely we investigated the expression, not only in whole rat lung tissue, but also in primary cultures of rat alveolar epithelial cells which retain many morphological and biochemical features of their in-vivo counterparts, i.e. the isolated cuboidal ATE cell able to undergo cell division, produce surfactant and display significant metabolic capacity, while the non-dividing squamous ATI-like cell displaying a more limited metabolic capacity. Perhaps not surprisingly we found variable patterns of expression between whole lung, freshly isolated ATE cells and day 8 AEI-like cells across the various transporters. Figure 7.1 is a graphical summary or profile of the findings. The generation of such an expression profile in rat lung and AE cells helped to provide a platform for further work, i.e., understanding the functional impact of drug transporters upon an airway-administered drug substrate.

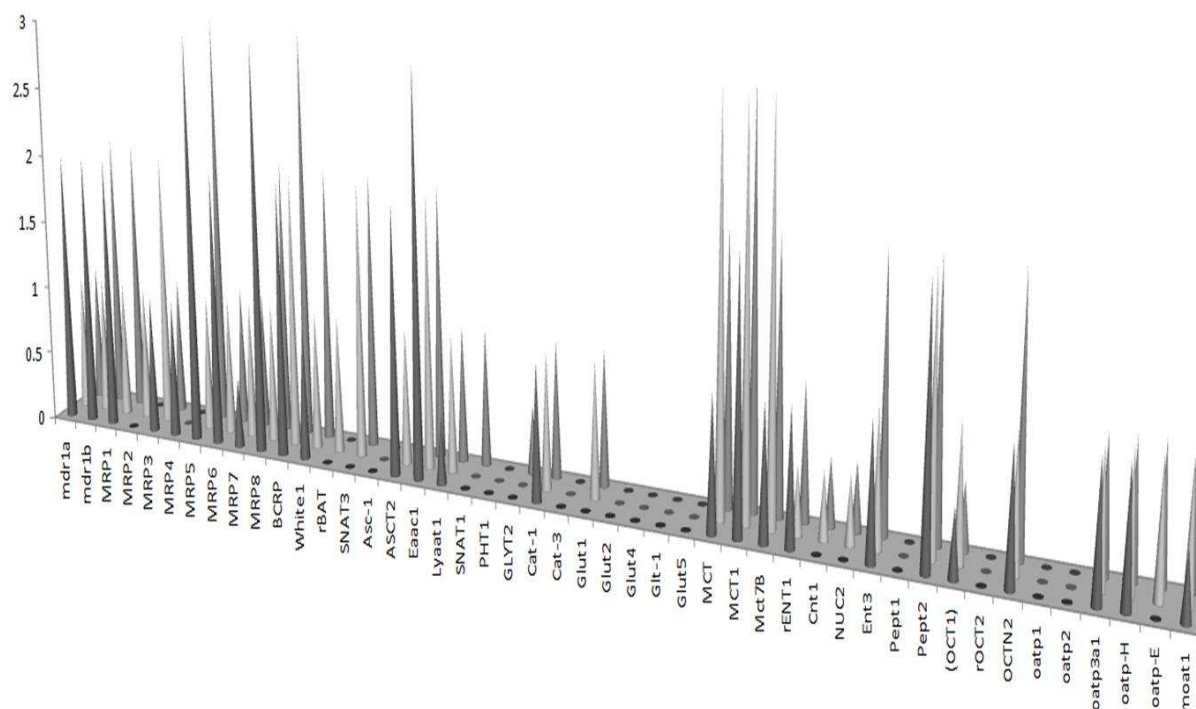


Figure 7.1 Graphical presentation of drug transporter expression in the rat lung. Black bars (front-most bars) represent perceived expression in whole rat lung samples. Light grey (middle bars) represent mRNA expression in freshly isolated AEII cells and dark grey (furthermost bars) represent expression in AEI-'like' cells at day 8 of culture. Data are expressed as mean, n=3 for each transporter)

As can be seen from figure 7.1, almost all ABC transporters studied could be detected via mRNA in whole rat lung samples, in many cases expression decreased from strong (+++/interpreted as '3' in order to generate the above figure) in whole lung samples to a lower level of expression in freshly isolated and 'day 8' AE II cells. This trend does not transfer to SLC transporters studied, where proportionately; fewer transporters were detected in rat lung cell samples. It is worthwhile to note that investigated drug transporters were chosen upon their relevance to drug discovery as a whole and not specifically for their theoretical expression within the lung. For example, when examining glucose transporters in the lung, only those with reported ubiquitous/broad expression patterns were detected. Further, of the five glucose transporters studied, three were recognised in the literature as transporters that display a more specific localisation pattern; i.e. Glut4 specific to brown and white adipose tissue and skeletal and cardiac muscle [209], Glut5 specific to the jejunal region of the small intestine [209, 221] and GLT-1 specific to the proximal tubule of nephrons [211]. Therefore, it is perhaps unsurprising that these individual transporters were found to be absent from the lung cell samples studied. In a contrary manner, however, the renal isoform of the proton-coupled oligopeptide transporter, PEPT2, (named as such due to expression in kidney tubular cells

and therefore supposed not to be expressed in pulmonary tissue), is well documented to be present in the lung [251].

Once a comprehensive expression profile of drug transporters in rodent lung had been established, it was then sought to examine the functional significance of a drug transporter protein in the intact lung.

Attention was focussed upon the P-glycoprotein drug transporter as this transporter alone is at the centre of a large proportion of drug transporter research. The positioning of P-gp within mucosal barriers and indeed within the BBB represents an important challenge to drug absorption and disposition. The role of P-gp in pharmacokinetics is now quite well established and there exists much evidence of the ability of this drug transporter to influence greatly drug discovery and delivery processes. For example, through interaction with a drug substrate, P-gp has the capacity to influence a drug's bioavailability, to bring about drug-drug interactions, to limit or enhance tissue penetration, to influence drug elimination, to create adverse side effects through unexpected drug retention and to generate issues of toxicity through unpredicted variability in whole-body or tissue specific drug concentrations [72].

In order to examine the influence of P-gp upon drugs delivered to the lung, an adequate model was required. In the literature, there exist a number of models applicable to the investigation of drug absorption in the lung. Within a review authored by Sakagami, such models are compared and contrasted and their relevance to specific experimental requirements and goals discussed [23]. The isolated perfused rat lung has emerged over time as an excellent model for examining drug absorption. This model has been promoted within biopharmaceutical research as one that surmounts negative aspects of other pulmonary models where the mechanisms of drug absorption and disposition are indistinguishable. The isolated perfused rat lung offers a well-designed resolution to the problems presented by other models in that it allows the partitioning of complex whole-body pharmacokinetic processes whilst maintaining accurately the architecture and innate functionality of the lung [23]. In a similar vein to P-gp, the isolated perfused rat lung is also featured in abundance in the literature. Initial uses for such a model include exploitation as a 'respirator' for an isolated heart preparation, while today use ranges from examination of distribution of a range of inhaled toxins to more physiological examinations such as the effect of altered end-expiratory pressure and tidal volume upon alveolar stability [36, 470].

Within the scope of this thesis, P-gp functionality was examined systematically through use of the isolated perfused rat lung, several known P-gp substrates and a specific P-gp inhibitor designed by GSK. Initially, presence of an active efflux process, (assumed to be mediated by P-gp via use of a P-gp substrate), was illustrated by dose independent transport of Rh123 and flunisolide. It was hypothesised that, if influenced by P-gp, such substrates would display nonlinear transport profiles as P-gp actively effluxed substrate to the airspace of the lung thus slowing appearance in perfusate. Figure 7.2 summarises the non-linear transport of these P-gp substrates, presence of an active transport process is assumed since the transport profile of each substrate does not resemble that of a substrate transported by passive diffusion alone.

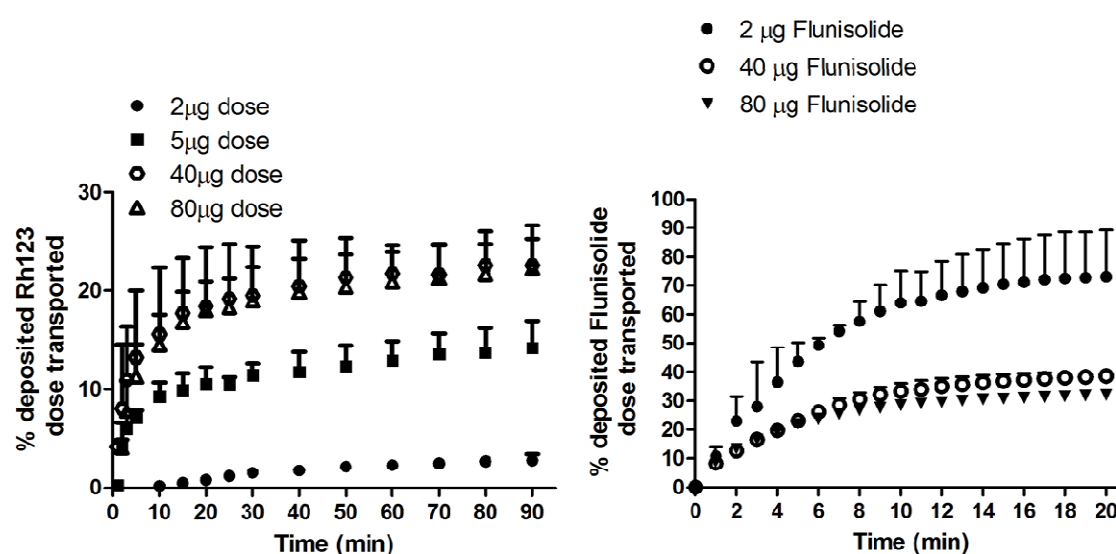


Figure 7.2 Transport profiles of two P-gp substrates, Rh123 and flunisolide, after dosing to the IPRL. Each profile illustrates non-linear substrate transport across the IPRL, as dose deposited to the lung increases; the percentage of deposited dose transported to perfusate does not alter linearly suggesting involvement of an active transport process. Data are expressed as mean \pm S.D, $n=4$ for each treatment.

In order to aid in confirmation of P-gp as responsible for the active efflux of substrates observed in the IPRL, the addition of a 3rd generation P-gp inhibitor was included with instilled dose and/or with recirculating perfusate. It was believed that, through modulation of P-gp via a chemical inhibitor, dose independent transport of P-gp substrates would be abolished thus rendering substrate transport to be influenced only by passive diffusional processes. Figure 7.3 reviews the effect of the P-gp inhibitor, GF120918, upon the transport of Rh123, flunisolide and digoxin.

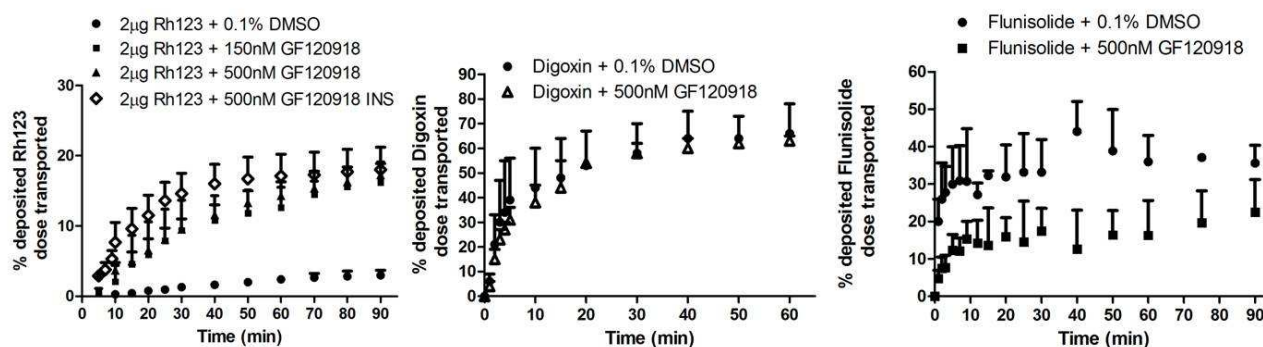


Figure 7.3 Transport profiles of three P-gp substrates across the IPRL in the presence of GF120918. Both Rh123 and flunisolide displayed altered transport profiles in the presence of the P-gp inhibitor suggesting influence of P-gp upon transport its absence. Data are expressed as mean \pm S.D, n=4 for each treatment, 'INS' represents presence of GF120918 in instilled dose only.

As can be seen from figure 7.3, in the presence of P-gp inhibitor, (in instillate and perfusate or instillate only), Rh123 and flunisolide displayed a transport profile similar to that of high substrate doses where P-gp saturation is presumed, thus confirming the presence of an active transporter in the absence of a chemical P-gp inhibitor. The transport of the P-gp substrate digoxin did not alter in the presence of P-gp inhibitor, however, rapid transport has been observed elsewhere and it is hypothesised that this substrate displays such a high rate of passive diffusion that it overcomes the efflux capacity of P-gp [361].

In order to confirm findings achieved with the Cardiff IPRL, complementary experiments were conducted at GSK utilising a single-pass IPRLu model. Results obtained from this isolated lung preparation enhanced the power of those obtained at Cardiff through their similar findings, figure 7.4 summarises these.

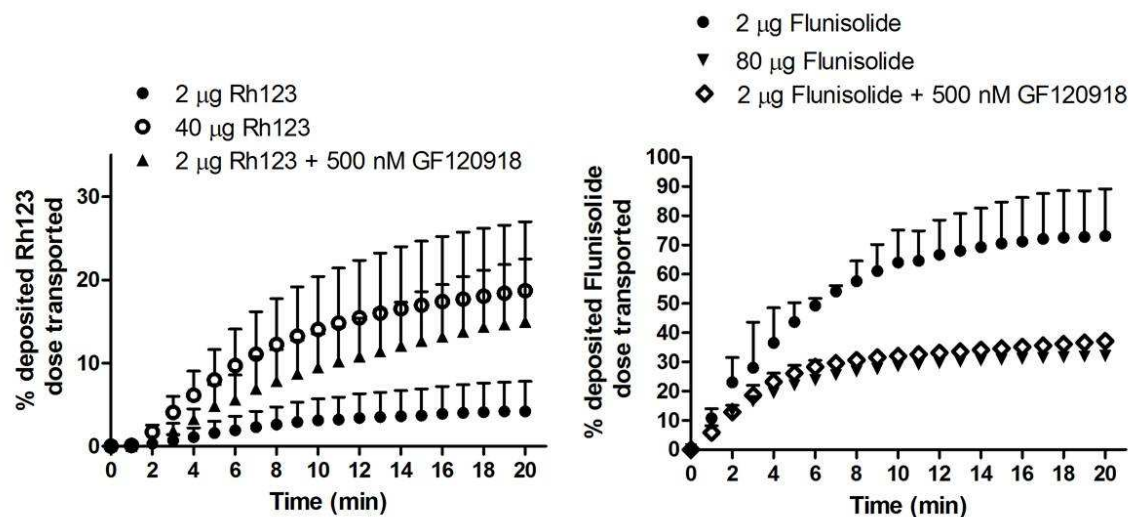


Figure 7.4 Mean transport profiles of Rh123 and flunisolide across the IPRLu. Substrate transport was monitored in the presence and absence of GF120918. The presence of this inhibitor caused an alteration in observed transport profile of each substrate. Data are expressed as mean \pm S.D, $n = 4$ for each treatment.

In addition to graphically analysing P-gp substrate transport across isolated and perfused rat lung models, pharmacokinetic data, generated by nonlinear modelling, was evaluated. The non-linear modelling of transport data was difficult and revealed complex processes involved in the active transport of substrates in the lung. While much pharmacokinetic modelling was lacking in its accuracy, highlighted was the presence of intricate and multifaceted transport processes involved in the absorption of substrates in the lung. My results and data interpretations ultimately indicate the presence of at least one active efflux transporter, deduced to be P-gp, to be present in the lung and to be significant in the transport of Rh123 and flunisolide. Such findings add to the reliability of literature data, where P-gp is suggested to be present and functionally active within the lung.

Although the potential of P-gp to influence drug discovery and development is realised, function and localisation within the lung is poorly investigated and knowledge of the impact upon drug absorption and disposition is limited. In a recent review by Gumbleton *et al.*, current literature regarding the spatial expression of P-gp was reviewed and the potential impact of P-gp, as well as several other drug transporters, was considered.

Within the literature, P-gp has been localised at protein and mRNA level within the lung, suggesting presence to be conclusive [43, 108, 110, 112, 113, 137]. Further, the potential for P-gp to impact upon drug absorption, retention within the lung, activity, and a number of other ADME aspects is recognised. To confirm the influence of P-gp upon the transport profile of substrates examined

within these chapters, another, more specific inhibitor could have been implemented. Further, there is potential for an alternative drug transporter to be responsible for the observed alterations in transport profile. There is evidence within the literature to support the presence of other drug transporters within the lung. Transporters such as BCRP, PEPT1, MRP1 and OCT have all localised to lung tissue [39, 43, 115, 119]. Additionally, it is understood that BCRP can act as a transporter of Rh123 and can be inhibited by GF120918. In order to exclude the influence of BCRP upon Rh123 transport, the BCRP selective inhibitor fumitremorgin C could have been introduced to the IPRL together with Rh123, thus inhibiting BCRP action and allowing comparison of Rh123 transport profiles to those where GF120918 was present. It could also be argued that BCRP was not responsible for the alterations in Rh123 transport observed as, within the studies of this thesis, GF120918 was only present at concentrations capable of inhibiting P-gp and not BCRP action.

Overall, the findings of this thesis have underlined the presence of at least one active efflux transporter within the rodent lung. However, the findings of many experiments have proposed new questions and have thus created the need for future works. There is a great need to achieve consensus in the presence and extent of drug transporters within pulmonary tissue. Expanding from the RT-PCR profile generated within chapter 2, both a quantitative analysis of the abundance of individual transporters and their specific spatial localisation is needed in order to aid in data interpretation and in determining the potential impact of specific transporters upon drugs delivered to the lung. While the literature suggests predominant apical localisation within pulmonary specific cells, the results regarding Flunisolide transport across the IPRL and IPRLu are interesting and accurate localisation of P-gp within the alveolar region of the lung would enhance interpretation of this data. Further, there is scope to expand studies examining the influence of P-gp upon substrates delivered to the lung. Firstly, the involvement of P-gp alone should be confirmed and a range of other drugs should be examined to evaluate the extent of this influence. From this, it would also be of interest to examine the presence and functional significance of active influx transporters in the IPRL and to determine the relative influence of such transporters upon the absorption and disposition of inhaled drugs.

Ultimately, the findings of this thesis have acknowledged the presence of an active efflux transporter within the rodent lung and have enhanced the need for accurate and comprehensive knowledge of the impact of such transporters upon drug delivery and development. Complete understanding of drug transporters within the lung is vital for many reasons; to allow assessment of the impact of an active transporter upon the absorption and disposition of a drug candidate, to integrate knowledge of species-specific variations for data extrapolation, to approximate impact upon any drug delivered

to the lung, to allow for inter-individual patient variation, drug-drug interactions and to compensate for altered drug transporter profile within specific disease states. Only once such a level of knowledge is achieved can the potential for drug transporters to transform drug discovery and development be fully exploited.

References

1. Empey, D.W., *Diseases of the respiratory system. Introduction: structure and function of the lungs*. Br Med J, 1978. **1**(6113): p. 631-3.
2. Twigg, H.L., 3rd, *Pulmonary host defenses*. J Thorac Imaging, 1998. **13**(4): p. 221-33.
3. Somers, G.I., et al., *A comparison of the expression and metabolizing activities of phase I and II enzymes in freshly isolated human lung parenchymal cells and cryopreserved human hepatocytes*. Drug Metab Dispos, 2007. **35**(10): p. 1797-805.
4. Gray, H., *Anatomy of the Human Body*. 20th ed. 1918, Philadelphia: LEA & FEBIGER.
5. TeachPC.com.
http://images.google.com/imgres?imgurl=http://www.teachpe.com/images/alveoli.jpg&imgrefurl=http://www.teachpe.com/qcse_anatomy/respiratory.php&usq=aZMCni13zK9XLYDGF7tO0BjSQg0=&h=430&w=454&sz=45&hl=en&start=15&um=1&tbnid=E6QREfg49PJOM:&tbnh=121&tbnw=128&prev=/images%3Fq%3Dlung%2Balvioli%26hl%3Den%26client%3Dfirefox-a%26channel%3Ds%26rls%3Dorg.mozilla:en-US:official%26sa%3DG%26um%3D1. 2009 [cited].
6. Weibel, E.R., *Morphometry of the Human Lung* 1963, Heidelberg: Springer Verlag.
7. Patton, J.S., *Mechanisms of macromolecule absorption by the lungs*. Advanced Drug Delivery Reviews, 1996. **19**(1).
8. Patton, J.S., C.S. Fishburn, and J.G. Weers, *The lungs as a portal of entry for systemic drug delivery*. Proc Am Thorac Soc, 2004. **1**(4): p. 338-44.
9. Rose, M.C., *Mucins: structure, function, and role in pulmonary diseases*. Am J Physiol, 1992. **263**(4 Pt 1): p. L413-29.
10. Wanner, A., M. Salathe, and T.G. O'Riordan, *Mucociliary clearance in the airways*. Am J Respir Crit Care Med, 1996. **154**(6 Pt 1): p. 1868-902.
11. Veldhuizen, R., et al., *The role of lipids in pulmonary surfactant*. Biochim Biophys Acta, 1998. **1408**(2-3): p. 90-108.
12. Haagsman, H.P. and R.V. Diemel, *Surfactant-associated proteins: functions and structural variation*. Comp Biochem Physiol A Mol Integr Physiol, 2001. **129**(1): p. 91-108.
13. Gehr, P., et al., *Airway surfactant, a primary defense barrier: mechanical and immunological aspects*. J Aerosol Med, 1996. **9**(2): p. 163-81.
14. Crapo, J.D., et al., *Cell number and cell characteristics of the normal human lung*. Am Rev Respir Dis, 1982. **126**(2): p. 332-7.
15. Schneeberger-Keeley, E.E. and M.J. Karnovsky, *The ultrastructural basis of alveolar-capillary membrane permeability to peroxidase used as a tracer*. J Cell Biol, 1968. **37**(3): p. 781-93.
16. Gansslen, M., *Über Inhalation von Insulin*. Klin.Wochenschr, 1925. **4**.
17. Whitehead, K., N. Karr, and S. Mitragotri, *Safe and effective permeation enhancers for oral drug delivery*. Pharm Res, 2008. **25**(8): p. 1782-8.
18. Laube, B.L., *The expanding role of aerosols in systemic drug delivery, gene therapy, and vaccination*. Respir Care, 2005. **50**(9): p. 1161-76.
19. Lipworth, B.J., *Pharmacokinetics of inhaled drugs*. Br J Clin Pharmacol, 1996. **42**(6): p. 697-705.
20. Patton, J.S.a.B., M.J., *Drug delivery strategies for proteins and peptides from discovery and development to life cycle management*. Drug Deliv. Technol., 2004. **4**: p. 73-77.
21. von Wichert, P. and C. Seifart, *The lung, an organ for absorption?* Respiration, 2005. **72**(5): p. 552-8.
22. Patton, J.S. and P.R. Byron, *Inhaling medicines: delivering drugs to the body through the lungs*. Nat Rev Drug Discov, 2007. **6**(1): p. 67-74.

23. Sakagami, M., *In vivo, in vitro and ex vivo models to assess pulmonary absorption and disposition of inhaled therapeutics for systemic delivery*. Adv Drug Deliv Rev, 2006. **58**(9-10): p. 1030-60.
24. MIMS. 2011 [cited; Available from: www.mims.co.uk/tables/882435/Asthma-COPD-Preparations-Compatible-Devices].
25. Byron, P.R., *Drug delivery devices: issues in drug development*. Proc Am Thorac Soc, 2004. **1**(4): p. 321-8.
26. Programme, U.N.E., *Montreal Protocol on Substances That Deplete the Ozone Layer: UNEP Technology and Economic Assessment Panel, 1998 Report*. 1999: United Nations Environment Programme (1 Aug 1999) 200.
27. Bell, J.H., P.S. Hartley, and J.S. Cox, *Dry powder aerosols. I. A new powder inhalation device*. J Pharm Sci, 1971. **60**(10): p. 1559-64.
28. Agu, R.U., et al., *The lung as a route for systemic delivery of therapeutic proteins and peptides*. Respir Res, 2001. **2**(4): p. 198-209.
29. Skyler, J.S., et al., *Efficacy of inhaled human insulin in type 1 diabetes mellitus: a randomised proof-of-concept study*. Lancet, 2001. **357**(9253): p. 331-5.
30. Dershwitz, M., et al., *Pharmacokinetics and pharmacodynamics of inhaled versus intravenous morphine in healthy volunteers*. Anesthesiology, 2000. **93**(3): p. 619-28.
31. Chipman, J., Lucas, R., Jackson, B., Blizzard, C., Mant, T., Cleverly, A., Spoaldin, V., and C. Johnston, & Cutler, G., *Pharmacokinetic and safety results of a human single dose comparison of somatropin inhalation powder vs subcutaneous injection of somatropin.*, in *87th Annual Meeting of The Endocrine Society*. 2005: San Diego.
32. Walvoord, E.C., et al., *Inhaled growth hormone (GH) compared with subcutaneous GH in children with GH deficiency: pharmacokinetics, pharmacodynamics, and safety*. J Clin Endocrinol Metab, 2009. **94**(6): p. 2052-9.
33. Tronde, A., *Pulmonary Drug Absorption: In Vitro and In Vivo Investigations of Drug Absorption Across the Lung Barrier and Its Relation to Drug Physicochemical Properties.*, in *Faculty of Pharmacy*. 2002, Uppsala University: Uppsala. p. 86.
34. Schanker, L.S. and J.A. Hemberger, *Relation between molecular weight and pulmonary absorption rate of lipid-insoluble compounds in neonatal and adult rats*. Biochem Pharmacol, 1983. **32**(17): p. 2599-601.
35. Schanker, L.S., E.W. Mitchell, and R.A. Brown, Jr., *Species comparison of drug absorption from the lung after aerosol inhalation or intratracheal injection*. Drug Metab Dispos, 1986. **14**(1): p. 79-88.
36. Effros, R.M. and G.R. Mason, *Measurements of pulmonary epithelial permeability in vivo*. Am Rev Respir Dis, 1983. **127**(5 Pt 2): p. S59-65.
37. Crandall, E.D. and M.A. Matthay, *Alveolar epithelial transport. Basic science to clinical medicine*. Am J Respir Crit Care Med, 2001. **163**(4): p. 1021-9.
38. Gumbleton, M., *Caveolae as potential macromolecule trafficking compartments within alveolar epithelium*. Adv Drug Deliv Rev, 2001. **49**(3): p. 281-300.
39. Groneberg, D.A., et al., *Distribution and function of the peptide transporter PEPT2 in normal and cystic fibrosis human lung*. Thorax, 2002. **57**(1): p. 55-60.
40. Langmann, T., et al., *Real-time reverse transcription-PCR expression profiling of the complete human ATP-binding cassette transporter superfamily in various tissues*. Clin Chem, 2003. **49**(2): p. 230-8.
41. Schanker, L.S., *Drug absorption from the lung*. Biochem Pharmacol, 1978. **27**(4): p. 381-5.
42. Gumbleton, M., Morris, C.J., Francombe, D., Sakagami, M., *Drug transport processes of the air-blood barrier*, in *Pulmonary Drug Delivery: Basics, Applications and Opportunities for small molecules and biopharmaceuticals*, K.B.-P.a.H. Luessen, Editor. 2006. p. 332-353.

43. Scheffer, G.L., et al., *Multidrug resistance related molecules in human and murine lung*. J Clin Pathol, 2002. **55**(5): p. 332-9.
44. Hediger, M.A., et al., *The ABCs of solute carriers: physiological, pathological and therapeutic implications of human membrane transport proteins* Introduction. Pflugers Arch, 2004. **447**(5): p. 465-8.
45. Kim, R.B., *Transporters and drug discovery: why, when, and how*. Mol Pharm, 2006. **3**(1): p. 26-32.
46. Hagenbuch, B. and P.J. Meier, *Organic anion transporting polypeptides of the OATP/ SLC21 family: phylogenetic classification as OATP/ SLCO superfamily, new nomenclature and molecular/functional properties*. Pflugers Arch, 2004. **447**(5): p. 653-65.
47. Shayakul, C. and M.A. Hediger, *The SLC14 gene family of urea transporters*. Pflugers Arch, 2004. **447**(5): p. 603-9.
48. Hebert, S.C., D.B. Mount, and G. Gamba, *Molecular physiology of cation-coupled Cl-cotransport: the SLC12 family*. Pflugers Arch, 2004. **447**(5): p. 580-93.
49. Orłowski, J. and S. Grinstein, *Diversity of the mammalian sodium/proton exchanger SLC9 gene family*. Pflugers Arch, 2004. **447**(5): p. 549-65.
50. Stahl, A., *A current review of fatty acid transport proteins (SLC27)*. Pflugers Arch, 2004. **447**(5): p. 722-7.
51. Saurin, W., M. Hofnung, and E. Dassa, *Getting in or out: early segregation between importers and exporters in the evolution of ATP-binding cassette (ABC) transporters*. J Mol Evol, 1999. **48**(1): p. 22-41.
52. Sheps, J.A., et al., *The ABC transporter gene family of Caenorhabditis elegans has implications for the evolutionary dynamics of multidrug resistance in eukaryotes*. Genome Biol, 2004. **5**(3): p. R15.
53. Hollenstein, K., R.J. Dawson, and K.P. Locher, *Structure and mechanism of ABC transporter proteins*. Curr Opin Struct Biol, 2007. **17**(4): p. 412-8.
54. Ambudkar, S.V., et al., *The A-loop, a novel conserved aromatic acid subdomain upstream of the Walker A motif in ABC transporters, is critical for ATP binding*. FEBS Lett, 2006. **580**(4): p. 1049-55.
55. Davidson, A.L. and J. Chen, *ATP-binding cassette transporters in bacteria*. Annu Rev Biochem, 2004. **73**: p. 241-68.
56. Zaitseva, J., et al., *H662 is the linchpin of ATP hydrolysis in the nucleotide-binding domain of the ABC transporter HlyB*. EMBO J, 2005. **24**(11): p. 1901-10.
57. Dawson, R.J. and K.P. Locher, *Structure of a bacterial multidrug ABC transporter*. Nature, 2006. **443**(7108): p. 180-5.
58. Stenham, D.R., et al., *An atomic detail model for the human ATP binding cassette transporter P-glycoprotein derived from disulfide cross-linking and homology modeling*. FASEB J, 2003. **17**(15): p. 2287-9.
59. Higgins, C.F., *Multiple molecular mechanisms for multidrug resistance transporters*. Nature, 2007. **446**(7137): p. 749-57.
60. Schinkel, A.H. and J.W. Jonker, *Mammalian drug efflux transporters of the ATP binding cassette (ABC) family: an overview*. Adv Drug Deliv Rev, 2003. **55**(1): p. 3-29.
61. Rosenberg, M.F., et al., *Structure of the multidrug resistance P-glycoprotein to 2.5 nm resolution determined by electron microscopy and image analysis*. J Biol Chem, 1997. **272**(16): p. 10685-94.
62. Rosenberg, M.F., et al., *Repacking of the transmembrane domains of P-glycoprotein during the transport ATPase cycle*. EMBO J, 2001. **20**(20): p. 5615-25.
63. Rosenberg, M.F., et al., *Three-dimensional structures of the mammalian multidrug resistance P-glycoprotein demonstrate major conformational changes in the transmembrane domains upon nucleotide binding*. J Biol Chem, 2003. **278**(10): p. 8294-9.

64. Rosenberg, M.F., et al., *Three-dimensional structure of P-glycoprotein: the transmembrane regions adopt an asymmetric configuration in the nucleotide-bound state*. J Biol Chem, 2005. **280**(4): p. 2857-62.
65. Loo, T.W. and D.M. Clarke, *The packing of the transmembrane segments of human multidrug resistance P-glycoprotein is revealed by disulfide cross-linking analysis*. J Biol Chem, 2000. **275**(8): p. 5253-6.
66. Higgins, C.F. and M.M. Gottesman, *Is the multidrug transporter a flippase?* Trends Biochem Sci, 1992. **17**(1): p. 18-21.
67. Bolhuis, H., et al., *Multidrug resistance in Lactococcus lactis: evidence for ATP-dependent drug extrusion from the inner leaflet of the cytoplasmic membrane*. EMBO J, 1996. **15**(16): p. 4239-45.
68. Giacomini, K.M., et al., *Membrane transporters in drug development*. Nat Rev Drug Discov, 2010. **9**(3): p. 215-36.
69. Bleasby, K., et al., *Expression profiles of 50 xenobiotic transporter genes in humans and pre-clinical species: a resource for investigations into drug disposition*. Xenobiotica, 2006. **36**(10-11): p. 963-88.
70. Juliano, R.L. and V. Ling, *A surface glycoprotein modulating drug permeability in Chinese hamster ovary cell mutants*. Biochim Biophys Acta, 1976. **455**(1): p. 152-62.
71. Dean, M., Y. Hamon, and G. Chimini, *The human ATP-binding cassette (ABC) transporter superfamily*. J Lipid Res, 2001. **42**(7): p. 1007-17.
72. Fromm, M.F., *Importance of P-glycoprotein for drug disposition in humans*. Eur J Clin Invest, 2003. **33 Suppl 2**: p. 6-9.
73. Dean, M., *ABC transporters, drug resistance, and cancer stem cells*. J Mammary Gland Biol Neoplasia, 2009. **14**(1): p. 3-9.
74. Loscher, W. and H. Potschka, *Role of drug efflux transporters in the brain for drug disposition and treatment of brain diseases*. Prog Neurobiol, 2005. **76**(1): p. 22-76.
75. Steimer, A., E. Haltner, and C.M. Lehr, *Cell culture models of the respiratory tract relevant to pulmonary drug delivery*. J Aerosol Med, 2005. **18**(2): p. 137-82.
76. Forbes, B. and C. Ehrhardt, *Human respiratory epithelial cell culture for drug delivery applications*. Eur J Pharm Biopharm, 2005. **60**(2): p. 193-205.
77. Ehrhardt, C., Kim, K-J., and Lehr, C-M., *Isolation and Culture of Human Alveolar Epithelial Cells*, in *Human Cell Culture Protocols*, J. Picot, Editor. 2004. p. 207-216.
78. Skillrud, D.M. and W.J. Martin, 2nd, *The isolation of rat alveolar type II cells: a simplified approach using Percoll density centrifugation*. Lung, 1984. **162**(4): p. 245-52.
79. Blickwede, M. and J. Borlak, *Isolation and characterization of metabolically competent pulmonary epithelial cells from pig lung tissue*. Xenobiotica, 2005. **35**(10-11): p. 927-41.
80. Madlova, M., et al., *In-vitro respiratory drug absorption models possess nominal functional P-glycoprotein activity*. J Pharm Pharmacol, 2009. **61**(3): p. 293-301.
81. Hofmann, W., L. Koblinger, and T.B. Martonen, *Structural differences between human and rat lungs: implications for Monte Carlo modeling of aerosol deposition*. Health Phys, 1989. **57 Suppl 1**: p. 41-6; discussion 46-7.
82. Bernard, C., *Sur le mecanisme de la formation du sucre dans la foie*. CR Seances Acad Sci, 1855. **41**: p. 461.
83. Fisher, A.B., *The Isolated Perfused Lung*, in *Handbook of experimental pharmacology*, H.B. Witschi, J., Editor. 1985, Springer-Verlag: Heidelberg. p. 149-179.
84. Mehendale, H.M., L.S. Angevine, and Y. Ohmiya, *The isolated perfused lung--a critical evaluation*. Toxicology, 1981. **21**(1): p. 1-36.
85. Allison, P.R., deBurgh, D.I., Waaler, B.A., *Bronchial circulation and pulmonary vasomotor nerve responses in isolated perfused lungs*. J. Physiol, 1961. **157**: p. 462-474.

86. Hauge, A., *Conditions concerning the pressor response to ventilation hypoxia in isolated perfused rat lungs*. Acta Physiol Scand, 1968. **72**: p. 33-44.
87. Levey, S.G., R., *Isolated perfused rat lung preparation*. J Appl Physiol, 1966. **21**: p. 313-316.
88. Lloyd, T.C., *Effect of alveolar hypoxia on pulmonary vascular resistance*. J. Appl. Physiol., 1964. **19**: p. 1086-1094.
89. Rosenberg, E.F., R.E., *Changes in diffusing capacity of isolated cat lungs with blood pressure and flow*. J Appl Physiol, 1960. **15**: p. 883-892.
90. Rosenbloom, P.M.B., A.D., *A lung perfusion preparation for the study of drug metabolism*. J Appl Physiol, 1970. **29**: p. 138-144.
91. West, J.B., Dollery, C.T., Naimark, A., *Distribution of blood flow in isolated lung: relation to vascular and alveolar pressures*. J. Appl. Physiol., 1964. **19**: p. 713-724.
92. Bassett, D.J.P.R., R.A., *The isolated perfused lung preparation*, in *In Vitro methods of toxicology*, R.R. Watson, Editor. 1992, CRC Press: London. p. 144-155.
93. Young, S.L., *An isolated perfused rat lung preparation*. Environ Health Perspect, 1976. **16**: p. 61-6.
94. Niemeier, R.W., *The isolated perfused lung*. Environ Health Perspect, 1984. **56**: p. 35-41.
95. Byron, P.R., N.S. Roberts, and A.R. Clark, *An isolated perfused rat lung preparation for the study of aerosolized drug deposition and absorption*. J Pharm Sci, 1986. **75**(2): p. 168-71.
96. Byron, P.R. and R.W. Niven, *A novel dosing method for drug administration to the airways of the isolated perfused rat lung*. J Pharm Sci, 1988. **77**(8): p. 693-5.
97. Audi, S.H., et al., *Pulmonary disposition of lipophilic amine compounds in the isolated perfused rabbit lung*. J Appl Physiol, 1998. **84**(2): p. 516-30.
98. Dollery, C.T. and A.F. Junod, *Concentration of (+/-)-propranolol in isolated, perfused lungs of rat*. Br J Pharmacol, 1976. **57**(1): p. 67-71.
99. Gillespie, M.N., et al., *Pulmonary metabolism of exogenous enkephalins in isolated perfused rat lungs*. J Pharmacol Exp Ther, 1985. **232**(3): p. 675-81.
100. Ryrfeldt, A., G. Persson, and E. Nilsson, *Pulmonary disposition of the potent glucocorticoid budesonide, evaluated in an isolated perfused rat lung model*. Biochem Pharmacol, 1989. **38**(1): p. 17-22.
101. Sakagami, M., P.R. Byron, and F. Rypacek, *Biochemical evidence for transcytotic absorption of polyaspartamide from the rat lung: effects of temperature and metabolic inhibitors*. J Pharm Sci, 2002. **91**(9): p. 1958-68.
102. Tronde, A., et al., *High airway-to-blood transport of an opioid tetrapeptide in the isolated rat lung after aerosol delivery*. Peptides, 2002. **23**(3): p. 469-78.
103. Sai, Y. and A. Tsuji, *Transporter-mediated drug delivery: recent progress and experimental approaches*. Drug Discov Today, 2004. **9**(16): p. 712-20.
104. Endter, S., et al., *RT-PCR analysis of ABC, SLC and SLCO drug transporters in human lung epithelial cell models*. J Pharm Pharmacol, 2009. **61**(5): p. 583-91.
105. Polgar, O. and S.E. Bates, *ABC transporters in the balance: is there a role in multidrug resistance?* Biochem Soc Trans, 2005. **33**(Pt 1): p. 241-5.
106. Kalliokoski, A. and M. Niemi, *Impact of OATP transporters on pharmacokinetics*. Br J Pharmacol, 2009. **158**(3): p. 693-705.
107. Bremer, S., et al., *Quantitative expression patterns of multidrug-resistance P-glycoprotein (MDR1) and differentially spliced cystic-fibrosis transmembrane-conductance regulator mRNA transcripts in human epithelia*. Eur J Biochem, 1992. **206**(1): p. 137-49.
108. Cordon-Cardo, C., et al., *Expression of the multidrug resistance gene product (P-glycoprotein) in human normal and tumor tissues*. J Histochem Cytochem, 1990. **38**(9): p. 1277-87.
109. Wioland, M.A., et al., *CFTR, MDR1, and MRP1 immunolocalization in normal human nasal respiratory mucosa*. J Histochem Cytochem, 2000. **48**(9): p. 1215-22.

110. van der Valk, P., et al., *Distribution of multi-drug resistance-associated P-glycoprotein in normal and neoplastic human tissues. Analysis with 3 monoclonal antibodies recognizing different epitopes of the P-glycoprotein molecule.* Ann Oncol, 1990. **1**(1): p. 56-64.
111. Lehmann, T., et al., *Expression of MRP1 and related transporters in human lung cells in culture.* Toxicology, 2001. **167**(1): p. 59-72.
112. Lechapt-Zalcman, E., et al., *MDR1-Pgp 170 expression in human bronchus.* Eur Respir J, 1997. **10**(8): p. 1837-43.
113. Endter, S., et al., *P-glycoprotein (MDR1) functional activity in human alveolar epithelial cell monolayers.* Cell Tissue Res, 2007. **328**(1): p. 77-84.
114. Torky, A.R., et al., *Immuno-histochemical detection of MRPs in human lung cells in culture.* Toxicology, 2005. **207**(3): p. 437-50.
115. Brechot, J.M., et al., *Different pattern of MRP localization in ciliated and basal cells from human bronchial epithelium.* J Histochem Cytochem, 1998. **46**(4): p. 513-7.
116. Summer, R., et al., *Side population cells and Bcrp1 expression in lung.* Am J Physiol Lung Cell Mol Physiol, 2003. **285**(1): p. L97-104.
117. Gumbleton, M., et al., *Spatial expression and functionality of drug transporters in the intact lung: Objectives for further research.* Adv Drug Deliv Rev, 2011.
118. Li, S. and D. Li, *DNA microarray technology and data analysis in cancer research.* 2008: World Scientific.
119. Lips, K.S., et al., *Polyspecific cation transporters mediate luminal release of acetylcholine from bronchial epithelium.* Am J Respir Cell Mol Biol, 2005. **33**(1): p. 79-88.
120. Liu, Q.R., et al., *Cloning and expression of a spinal cord- and brain-specific glycine transporter with novel structural features.* J Biol Chem, 1993. **268**(30): p. 22802-8.
121. Liu, W., et al., *Molecular cloning of PEPT 2, a new member of the H⁺/peptide cotransporter family, from human kidney.* Biochim Biophys Acta, 1995. **1235**(2): p. 461-6.
122. Mackenzie, B. and J.D. Erickson, *Sodium-coupled neutral amino acid (System N/A) transporters of the SLC38 gene family.* Pflugers Arch, 2004. **447**(5): p. 784-95.
123. McAleer, M.A., et al., *pABC11 (also known as MOAT-C and MRP5), a member of the ABC family of proteins, has anion transporter activity but does not confer multidrug resistance when overexpressed in human embryonic kidney 293 cells.* J Biol Chem, 1999. **274**(33): p. 23541-8.
124. Martz, E. 2000 [cited 2010 16/02/2010]; Available from: <http://bio.umass.edu/micro/immunology/facs542/facsprin.htm>.
125. Carsten Ehrhardt, K.-j.K., *Drug Absorption Studies: In Situ, In Vitro and In Silico Models*, ed. K.-j.K. Carsten Ehrhardt. 2008: Springer. 696.
126. Doherty, M.M., et al., *Phenotype and differentiation potential of a novel rat tracheal epithelial cell line.* Am J Respir Cell Mol Biol, 1995. **12**(4): p. 385-95.
127. Sambrook J, R.D., *Molecular Cloning: A Laboratory Manual.* 3rd Ed. ed. 2001, New York: Cold Spring Harbor Laboratory Press.
128. Gatlik-Landwojtowicz, E., P. Aanismaa, and A. Seelig, *Quantification and characterization of P-glycoprotein-substrate interactions.* Biochemistry, 2006. **45**(9): p. 3020-32.
129. Huisman, M.T., et al., *Assessing safety and efficacy of directed P-glycoprotein inhibition to improve the pharmacokinetic properties of saquinavir coadministered with ritonavir.* J Pharmacol Exp Ther, 2003. **304**(2): p. 596-602.
130. Loo, T.W. and D.M. Clarke, *Recent progress in understanding the mechanism of P-glycoprotein-mediated drug efflux.* J Membr Biol, 2005. **206**(3): p. 173-85.
131. Sugawara, I., et al., *Lung resistance protein (LRP) expression in human normal tissues in comparison with that of MDR1 and MRP.* Cancer Lett, 1997. **112**(1): p. 23-31.
132. Moscow, J.A., et al., *Expression of anionic glutathione-S-transferase and P-glycoprotein genes in human tissues and tumors.* Cancer Res, 1989. **49**(6): p. 1422-8.

133. Scheffer, G.L., et al., *Tissue distribution and induction of human multidrug resistant protein 3*. Lab Invest, 2002. **82**(2): p. 193-201.
134. Demeule, M., et al., *Dexamethasone modulation of multidrug transporters in normal tissues*. FEBS Lett, 1999. **442**(2-3): p. 208-14.
135. Scheffer, G.L., et al., *MRP6 (ABCC6) detection in normal human tissues and tumors*. Lab Invest, 2002. **82**(4): p. 515-8.
136. Shultz, M.A., et al., *Gene expression analysis in response to lung toxicants: I. Sequencing and microarray development*. Am J Respir Cell Mol Biol, 2004. **30**(3): p. 296-310.
137. Campbell, L., et al., *Constitutive expression of p-glycoprotein in normal lung alveolar epithelium and functionality in primary alveolar epithelial cultures*. J Pharmacol Exp Ther, 2003. **304**(1): p. 441-52.
138. Brady, J.M., et al., *Tissue distribution and chemical induction of multiple drug resistance genes in rats*. Drug Metab Dispos, 2002. **30**(7): p. 838-44.
139. Haimeur, A., et al., *The MRP-related and BCRP/ABCG2 multidrug resistance proteins: biology, substrate specificity and regulation*. Curr Drug Metab, 2004. **5**(1): p. 21-53.
140. Schaub, T.P., et al., *Expression of the MRP2 gene-encoded conjugate export pump in human kidney proximal tubules and in renal cell carcinoma*. J Am Soc Nephrol, 1999. **10**(6): p. 1159-69.
141. van der Deen, M., et al., *ATP-binding cassette (ABC) transporters in normal and pathological lung*. Respir Res, 2005. **6**: p. 59.
142. Belinsky, M.G., et al., *Analysis of the in vivo functions of Mrp3*. Mol Pharmacol, 2005. **68**(1): p. 160-8.
143. Kool, M., et al., *Analysis of expression of cMOAT (MRP2), MRP3, MRP4, and MRP5, homologues of the multidrug resistance-associated protein gene (MRP1), in human cancer cell lines*. Cancer Res, 1997. **57**(16): p. 3537-47.
144. Oguri, T., et al., *Association between expression of the MRP3 gene and exposure to platinum drugs in lung cancer*. Int J Cancer, 2001. **93**(4): p. 584-9.
145. Young, L.C., et al., *Multidrug resistance proteins MRP3, MRP1, and MRP2 in lung cancer: correlation of protein levels with drug response and messenger RNA levels*. Clin Cancer Res, 2001. **7**(6): p. 1798-804.
146. Lee, K., et al., *Isolation of MOAT-B, a widely expressed multidrug resistance-associated protein/canalicular multispecific organic anion transporter-related transporter*. Cancer Res, 1998. **58**(13): p. 2741-7.
147. Rius, M., et al., *Prostanoid transport by multidrug resistance protein 4 (MRP4/ABCC4) localized in tissues of the human urogenital tract*. J Urol, 2005. **174**(6): p. 2409-14.
148. Chen, C. and C.D. Klaassen, *Rat multidrug resistance protein 4 (Mrp4, Abcc4): molecular cloning, organ distribution, postnatal renal expression, and chemical inducibility*. Biochem Biophys Res Commun, 2004. **317**(1): p. 46-53.
149. Campbell, L. and M. Gumbleton, *Aberrant caveolin-1 expression in psoriasis: a signalling hypothesis*. IUBMB Life, 2000. **50**(6): p. 361-4.
150. Denning, G.M., L.S. Ostedgaard, and M.J. Welsh, *Abnormal localization of cystic fibrosis transmembrane conductance regulator in primary cultures of cystic fibrosis airway epithelia*. J Cell Biol, 1992. **118**(3): p. 551-9.
151. Engelhardt, J.F., et al., *Expression of the cystic fibrosis gene in adult human lung*. J Clin Invest, 1994. **93**(2): p. 737-49.
152. Fang, X., et al., *Contribution of CFTR to apical-basolateral fluid transport in cultured human alveolar epithelial type II cells*. Am J Physiol Lung Cell Mol Physiol, 2006. **290**(2): p. L242-9.
153. Kalin, N., et al., *DeltaF508 CFTR protein expression in tissues from patients with cystic fibrosis*. J Clin Invest, 1999. **103**(10): p. 1379-89.

154. Puchelle, E., et al., *Differential localization of the cystic fibrosis transmembrane conductance regulator in normal and cystic fibrosis airway epithelium*. Am J Respir Cell Mol Biol, 1992. **7**(5): p. 485-91.
155. Croop, J.M., et al., *Isolation and characterization of a mammalian homolog of the Drosophila white gene*. Gene, 1997. **185**(1): p. 77-85.
156. Klucken, J., et al., *ABCG1 (ABC8), the human homolog of the Drosophila white gene, is a regulator of macrophage cholesterol and phospholipid transport*. Proc Natl Acad Sci U S A, 2000. **97**(2): p. 817-22.
157. Thomassen, M.J., et al., *ABCG1 is deficient in alveolar macrophages of GM-CSF knockout mice and patients with pulmonary alveolar proteinosis*. J Lipid Res, 2007. **48**(12): p. 2762-8.
158. Beck, K., et al., *Analysis of ABCC6 (MRP6) in normal human tissues*. Histochem Cell Biol, 2005. **123**(4-5): p. 517-28.
159. Hopper, E., et al., *Analysis of the structure and expression pattern of MRP7 (ABCC10), a new member of the MRP subfamily*. Cancer Lett, 2001. **162**(2): p. 181-91.
160. Tammur, J., et al., *Two new genes from the human ATP-binding cassette transporter superfamily, ABCC11 and ABCC12, tandemly duplicated on chromosome 16q12*. Gene, 2001. **273**(1): p. 89-96.
161. Aszalos, A., *Drug-drug interactions affected by the transporter protein, P-glycoprotein (ABCB1, MDR1) II. Clinical aspects*. Drug Discov Today, 2007. **12**(19-20): p. 838-43.
162. Kerb, R., *Implications of genetic polymorphisms in drug transporters for pharmacotherapy*. Cancer Lett, 2006. **234**(1): p. 4-33.
163. Kanai, Y. and M.A. Hediger, *The glutamate/neutral amino acid transporter family SLC1: molecular, physiological and pharmacological aspects*. Pflugers Arch, 2004. **447**(5): p. 469-79.
164. Kanai, Y. and M.A. Hediger, *Primary structure and functional characterization of a high-affinity glutamate transporter*. Nature, 1992. **360**(6403): p. 467-71.
165. Berger, U.V. and M.A. Hediger, *Comparative analysis of glutamate transporter expression in rat brain using differential double in situ hybridization*. Anat Embryol (Berl), 1998. **198**(1): p. 13-30.
166. Kanai, Y., et al., *Neuronal high-affinity glutamate transport in the rat central nervous system*. Neuroreport, 1995. **6**(17): p. 2357-62.
167. Rothstein, J.D., et al., *Localization of neuronal and glial glutamate transporters*. Neuron, 1994. **13**(3): p. 713-25.
168. Shayakul, C., et al., *Localization of the high-affinity glutamate transporter EAAC1 in rat kidney*. Am J Physiol, 1997. **273**(6 Pt 2): p. F1023-9.
169. Nakayama, T., et al., *Expression of three glutamate transporter subtype mRNAs in human brain regions and peripheral tissues*. Brain Res Mol Brain Res, 1996. **36**(1): p. 189-92.
170. Velaz-Faircloth, M., et al., *Characterization and distribution of the neuronal glutamate transporter EAAC1 in rat brain*. Am J Physiol, 1996. **270**(1 Pt 1): p. C67-75.
171. Avissar, N.E., et al., *Na(+)-dependent neutral amino acid transporter ATB(0) is a rabbit epithelial cell brush-border protein*. Am J Physiol Cell Physiol, 2001. **281**(3): p. C963-71.
172. Utsunomiya-Tate, N., H. Endou, and Y. Kanai, *Cloning and functional characterization of a system ASC-like Na+-dependent neutral amino acid transporter*. J Biol Chem, 1996. **271**(25): p. 14883-90.
173. Dun, Y., et al., *Functional and molecular analysis of D-serine transport in retinal Muller cells*. Exp Eye Res, 2007. **84**(1): p. 191-9.
174. Fuchs, B.C. and B.P. Bode, *Amino acid transporters ASCT2 and LAT1 in cancer: partners in crime?* Semin Cancer Biol, 2005. **15**(4): p. 254-66.
175. Palacin, M. and Y. Kanai, *The ancillary proteins of HATs: SLC3 family of amino acid transporters*. Pflugers Arch, 2004. **447**(5): p. 490-4.

176. Bertran, J., et al., *Expression cloning of a human renal cDNA that induces high affinity transport of L-cystine shared with dibasic amino acids in Xenopus oocytes*. J Biol Chem, 1993. **268**(20): p. 14842-9.
177. Furriols, M., et al., *rBAT, related to L-cysteine transport, is localized to the microvilli of proximal straight tubules, and its expression is regulated in kidney by development*. J Biol Chem, 1993. **268**(36): p. 27060-8.
178. Bertran, J., et al., *Expression cloning of a cDNA from rabbit kidney cortex that induces a single transport system for cystine and dibasic and neutral amino acids*. Proc Natl Acad Sci U S A, 1992. **89**(12): p. 5601-5.
179. Lee, W.S., et al., *Cloning and chromosomal localization of a human kidney cDNA involved in cystine, dibasic, and neutral amino acid transport*. J Clin Invest, 1993. **91**(5): p. 1959-63.
180. Pickel, V.M., et al., *Ultrastructural localization of a neutral and basic amino acid transporter in rat kidney and intestine*. Proc Natl Acad Sci U S A, 1993. **90**(16): p. 7779-83.
181. Kim, C.M., J.L. Goldstein, and M.S. Brown, *cDNA cloning of MEV, a mutant protein that facilitates cellular uptake of mevalonate, and identification of the point mutation responsible for its gain of function*. J Biol Chem, 1992. **267**(32): p. 23113-21.
182. Wells, R.G. and M.A. Hediger, *Cloning of a rat kidney cDNA that stimulates dibasic and neutral amino acid transport and has sequence similarity to glucosidases*. Proc Natl Acad Sci U S A, 1992. **89**(12): p. 5596-600.
183. Fernandez, E., et al., *rBAT-b(0,+)-AT heterodimer is the main apical reabsorption system for cystine in the kidney*. Am J Physiol Renal Physiol, 2002. **283**(3): p. F540-8.
184. Parvari, R., et al., *The 2p21 deletion syndrome: characterization of the transcription content*. Genomics, 2005. **86**(2): p. 195-211.
185. Knickelbein, R.G., et al., *Characterization of multiple cysteine and cystine transporters in rat alveolar type II cells*. Am J Physiol, 1997. **273**(6 Pt 1): p. L1147-55.
186. Bannai, S. and N. Tateishi, *Role of membrane transport in metabolism and function of glutathione in mammals*. Journal of Membrane Biology, 1986. **89**(1): p. 1-8.
187. Deneke, S.M. and B.L. Fanburg, *Regulation of cellular glutathione*. Am J Physiol, 1989. **257**(4 Pt 1): p. L163-73.
188. Verrey, F., et al., *CATs and HATs: the SLC7 family of amino acid transporters*. Pflugers Arch, 2004. **447**(5): p. 532-42.
189. Fukasawa, Y., et al., *Identification and characterization of a Na(+)-independent neutral amino acid transporter that associates with the 4F2 heavy chain and exhibits substrate selectivity for small neutral D- and L-amino acids*. J Biol Chem, 2000. **275**(13): p. 9690-8.
190. Nishimura, M. and S. Naito, *Tissue-specific mRNA expression profiles of human ATP-binding cassette and solute carrier transporter superfamilies*. Drug Metab Pharmacokinet, 2005. **20**(6): p. 452-77.
191. Fornes, A., et al., *Trafficking properties and activity regulation of the neuronal glycine transporter GLYT2 by protein kinase C*. Biochem J, 2008. **412**(3): p. 495-506.
192. Closs, E.I., et al., *Plasma membrane transporters for arginine*. J Nutr, 2004. **134**(10 Suppl): p. 2752S-2759S; discussion 2765S-2767S.
193. Wang, Y., et al., *DNA microarray reveals novel genes induced by mechanical forces in fetal lung type II epithelial cells*. Pediatr Res, 2006. **60**(2): p. 118-24.
194. Bermingham, J.R., Jr. and J. Pennington, *Organization and expression of the SLC36 cluster of amino acid transporter genes*. Mamm Genome, 2004. **15**(2): p. 114-25.
195. Herrera-Ruiz, D., et al., *Spatial expression patterns of peptide transporters in the human and rat gastrointestinal tracts, Caco-2 in vitro cell culture model, and multiple human tissues*. AAPS PharmSci, 2001. **3**(1): p. E9.
196. Yamashita, T., et al., *Cloning and functional expression of a brain peptide/histidine transporter*. J Biol Chem, 1997. **272**(15): p. 10205-11.

197. Ito, K. and M. Groudine, *A new member of the cationic amino acid transporter family is preferentially expressed in adult mouse brain*. J Biol Chem, 1997. **272**(42): p. 26780-6.
198. Nagasawa, K., et al., *Monocarboxylate transporter mediates uptake of lovastatin acid in rat cultured mesangial cells*. J Pharm Sci, 2002. **91**(12): p. 2605-13.
199. Scumpia, P.O., et al., *Hypothermia attenuates iNOS, CAT-1, CAT-2, and nitric oxide expression in lungs of endotoxemic rats*. Am J Physiol Lung Cell Mol Physiol, 2002. **283**(6): p. L1231-8.
200. Rotoli, B.M., et al., *Alveolar macrophages from normal subjects lack the NOS-related system y+ for arginine transport*. Am J Respir Cell Mol Biol, 2007. **37**(1): p. 105-12.
201. Armano, S., et al., *Localization and functional relevance of system a neutral amino acid transporters in cultured hippocampal neurons*. J Biol Chem, 2002. **277**(12): p. 10467-73.
202. Bain, P.J., et al., *The mechanism for transcriptional activation of the human ATA2 transporter gene by amino acid deprivation is different than that for asparagine synthetase*. J Nutr, 2002. **132**(10): p. 3023-9.
203. Gu, S., et al., *Identification and characterization of an amino acid transporter expressed differentially in liver*. Proc Natl Acad Sci U S A, 2000. **97**(7): p. 3230-5.
204. Chen, Z., et al., *Structure, function and immunolocalization of a proton-coupled amino acid transporter (hPAT1) in the human intestinal cell line Caco-2*. J Physiol, 2003. **546**(Pt 2): p. 349-61.
205. Tsai, G., et al., *D-serine added to antipsychotics for the treatment of schizophrenia*. Biol Psychiatry, 1998. **44**(11): p. 1081-9.
206. Boll, M., H. Daniel, and B. Gasnier, *The SLC36 family: proton-coupled transporters for the absorption of selected amino acids from extracellular and intracellular proteolysis*. Pflugers Arch, 2004. **447**(5): p. 776-9.
207. Lieb, W.R. and W.D. Stein, *New theory for glucose transport across membranes*. Nat New Biol, 1971. **230**(12): p. 108-9.
208. Mueckler, M., et al., *Sequence and structure of a human glucose transporter*. Science, 1985. **229**(4717): p. 941-5.
209. Uldry, M. and B. Thorens, *The SLC2 family of facilitated hexose and polyol transporters*. Pflugers Arch, 2004. **447**(5): p. 480-9.
210. Maher, F., S.J. Vannucci, and I.A. Simpson, *Glucose transporter proteins in brain*. FASEB J, 1994. **8**(13): p. 1003-11.
211. Wright, E.M., B.A. Hirayama, and D.F. Loo, *Active sugar transport in health and disease*. J Intern Med, 2007. **261**(1): p. 32-43.
212. Birnbaum, M.J., H.C. Haspel, and O.M. Rosen, *Cloning and characterization of a cDNA encoding the rat brain glucose-transporter protein*. Proc Natl Acad Sci U S A, 1986. **83**(16): p. 5784-8.
213. Kasanicki, M.A., et al., *Identification and characterization of the glucose-transport protein of the bovine blood/brain barrier*. Biochem J, 1987. **247**(1): p. 101-8.
214. Kalsi, K.K., et al., *Apical and basolateral localisation of GLUT2 transporters in human lung epithelial cells*. Pflugers Arch, 2008. **456**(5): p. 991-1003.
215. Devaskar, S.U. and D.E. deMello, *Cell-specific localization of glucose transporter proteins in mammalian lung*. J Clin Endocrinol Metab, 1996. **81**(12): p. 4373-8.
216. Dong Zhao, T.I., Li Quan, Tomomi Michiue, Chiemi Yoshida, Ayumi Komatu, and Q.W. Jian-Hua Chen, Bao-Li Zhu, Hitoshi Maeda *Evaluation of pulmonary GLUT1 and VEGF mRNA levels in relation to lung weight in medicolegal autopsy cases*. Legal Medicine, 2009. **11**: p. S290–S293.
217. Wood D, B.D., Woollhead AM, Philips BJ, Baker EH, *Functional and molecular evidence for glucose transporters in human airway epithelium*. Am J Respir Crit Care Med, 2004. **169**.
218. Mamchaoui, K., Y. Makhoulfi, and G. Saumon, *Glucose transporter gene expression in freshly isolated and cultured rat pneumocytes*. Acta Physiol Scand, 2002. **175**(1): p. 19-24.

219. Thorens, B., et al., *Liver glucose transporter: a basolateral protein in hepatocytes and intestine and kidney cells*. Am J Physiol, 1990. **259**(6 Pt 1): p. C279-85.
220. Michalski, J.-C.C., C, *Glycoproteins Methods and Protocols*. Methods in molecular biology, ed. A.P. Corfield. Vol. 125, Totowa, NJ: Humana press Inc.
221. Mantych, G.J., D.E. James, and S.U. Devaskar, *Jejunal/kidney glucose transporter isoform (Glut-5) is expressed in the human blood-brain barrier*. Endocrinology, 1993. **132**(1): p. 35-40.
222. Bergersen, L., et al., *Cellular and subcellular expression of monocarboxylate transporters in the pigment epithelium and retina of the rat*. Neuroscience, 1999. **90**(1): p. 319-31.
223. Halestrap, A.P. and N.T. Price, *The proton-linked monocarboxylate transporter (MCT) family: structure, function and regulation*. Biochem J, 1999. **343 Pt 2**: p. 281-99.
224. Halestrap, A.P. and D. Meredith, *The SLC16 gene family-from monocarboxylate transporters (MCTs) to aromatic amino acid transporters and beyond*. Pflugers Arch, 2004. **447**(5): p. 619-28.
225. Philp, N.J., H. Yoon, and E.F. Grollman, *Monocarboxylate transporter MCT1 is located in the apical membrane and MCT3 in the basal membrane of rat RPE*. Am J Physiol, 1998. **274**(6 Pt 2): p. R1824-8.
226. Garcia, C.K., et al., *cDNA cloning of MCT2, a second monocarboxylate transporter expressed in different cells than MCT1*. J Biol Chem, 1995. **270**(4): p. 1843-9.
227. Garcia, C.K., et al., *Molecular characterization of a membrane transporter for lactate, pyruvate, and other monocarboxylates: implications for the Cori cycle*. Cell, 1994. **76**(5): p. 865-73.
228. Nakai, M., L. Chen, and R.A. Nowak, *Tissue distribution of basigin and monocarboxylate transporter 1 in the adult male mouse: a study using the wild-type and basigin gene knockout mice*. Anat Rec A Discov Mol Cell Evol Biol, 2006. **288**(5): p. 527-35.
229. Price, N.T., V.N. Jackson, and A.P. Halestrap, *Cloning and sequencing of four new mammalian monocarboxylate transporter (MCT) homologues confirms the existence of a transporter family with an ancient past*. Biochem J, 1998. **329 (Pt 2)**: p. 321-8.
230. Koehler-Stec, E.M., et al., *Monocarboxylate transporter expression in mouse brain*. Am J Physiol, 1998. **275**(3 Pt 1): p. E516-24.
231. Morris, M.E. and M.A. Felmler, *Overview of the proton-coupled MCT (SLC16A) family of transporters: characterization, function and role in the transport of the drug of abuse gamma-hydroxybutyric acid*. AAPS J, 2008. **10**(2): p. 311-21.
232. Hosoya, K., et al., *MCT1-mediated transport of L-lactic acid at the inner blood-retinal barrier: a possible route for delivery of monocarboxylic acid drugs to the retina*. Pharm Res, 2001. **18**(12): p. 1669-76.
233. Balimane, P.V. and P.J. Sinko, *Involvement of multiple transporters in the oral absorption of nucleoside analogues*. Adv Drug Deliv Rev, 1999. **39**(1-3): p. 183-209.
234. Baldwin, S.A., et al., *The equilibrative nucleoside transporter family, SLC29*. Pflugers Arch, 2004. **447**(5): p. 735-43.
235. Gray, J.H., R.P. Owen, and K.M. Giacomini, *The concentrative nucleoside transporter family, SLC28*. Pflugers Arch, 2004. **447**(5): p. 728-34.
236. Anderson, C.M., et al., *Demonstration of the existence of mRNAs encoding N1/cif and N2/cit sodium/nucleoside cotransporters in rat brain*. Brain Res Mol Brain Res, 1996. **42**(2): p. 358-61.
237. Wang, J., et al., *Functional and molecular characteristics of Na(+)-dependent nucleoside transporters*. Pharm Res, 1997. **14**(11): p. 1524-32.
238. Fedan, J.S., *Nucleosides and nucleotides in the lung: role in asthma*. Am J Respir Cell Mol Biol, 1999. **21**(1): p. 7-9.

239. Crawford, C.R., et al., *Cloning of the human equilibrative, nitrobenzylmercaptapurine riboside (NBMPR)-insensitive nucleoside transporter ei by functional expression in a transport-deficient cell line*. J Biol Chem, 1998. **273**(9): p. 5288-93.
240. Griffiths, M., et al., *Cloning of a human nucleoside transporter implicated in the cellular uptake of adenosine and chemotherapeutic drugs*. Nat Med, 1997. **3**(1): p. 89-93.
241. Griffiths, M., et al., *Molecular cloning and characterization of a nitrobenzylthioinosine-insensitive (ei) equilibrative nucleoside transporter from human placenta*. Biochem J, 1997. **328 (Pt 3)**: p. 739-43.
242. Hamilton, K.O., et al., *Multidrug resistance-associated protein-1 functional activity in Calu-3 cells*. J Pharmacol Exp Ther, 2001. **298**(3): p. 1199-205.
243. Handa, M., et al., *Cloning of a novel isoform of the mouse NBMPR-sensitive equilibrative nucleoside transporter (ENT1) lacking a putative phosphorylation site*. Gene, 2001. **262**(1-2): p. 301-7.
244. Huang, M., et al., *Inhibition of nucleoside transport by protein kinase inhibitors*. J Pharmacol Exp Ther, 2003. **304**(2): p. 753-60.
245. Shi, M.M. and J.D. Young, *[3H]dipyridamole binding to nucleoside transporters from guinea-pig and rat lung*. Biochem J, 1986. **240**(3): p. 879-83.
246. Chen, Z., et al., *Identification of rat lung--prominent genes by a parallel DNA microarray hybridization*. BMC Genomics, 2006. **7**: p. 47.
247. Oguri, T., et al., *The absence of human equilibrative nucleoside transporter 1 expression predicts nonresponse to gemcitabine-containing chemotherapy in non-small cell lung cancer*. Cancer Lett, 2007. **256**(1): p. 112-9.
248. Shi, M.M., et al., *Nucleoside transport. Photoaffinity labelling of high-affinity nitrobenzylthioinosine binding sites in rat and guinea pig lung*. Biochem Biophys Res Commun, 1984. **118**(2): p. 594-600.
249. King, A.E., et al., *Nucleoside transporters: from scavengers to novel therapeutic targets*. Trends Pharmacol Sci, 2006. **27**(8): p. 416-25.
250. Feoktistov, I. and I. Biaggioni, *Role of adenosine in asthma*. Drug Dev Res, 1996. **39**: p. 333-6.
251. Daniel, H. and G. Kottra, *The proton oligopeptide cotransporter family SLC15 in physiology and pharmacology*. Pflugers Arch, 2004. **447**(5): p. 610-8.
252. Kamal, M.A., R.F. Keep, and D.E. Smith, *Role and relevance of PEPT2 in drug disposition, dynamics, and toxicity*. Drug Metab Pharmacokinet, 2008. **23**(4): p. 236-42.
253. Daniel, H. and I. Rubio-Aliaga, *An update on renal peptide transporters*. Am J Physiol Renal Physiol, 2003. **284**(5): p. F885-92.
254. Ogihara, H., et al., *Immuno-localization of H⁺/peptide cotransporter in rat digestive tract*. Biochem Biophys Res Commun, 1996. **220**(3): p. 848-52.
255. Fei, Y.J., et al., *Expression cloning of a mammalian proton-coupled oligopeptide transporter*. Nature, 1994. **368**(6471): p. 563-6.
256. Gonzalez, D.E., et al., *An oligopeptide transporter is expressed at high levels in the pancreatic carcinoma cell lines AsPc-1 and Capan-2*. Cancer Res, 1998. **58**(3): p. 519-25.
257. Herrera-Ruiz, D. and G.T. Knipp, *Current perspectives on established and putative mammalian oligopeptide transporters*. J Pharm Sci, 2003. **92**(4): p. 691-714.
258. Groneberg, D.A., et al., *Peptide transport in the mammary gland: expression and distribution of PEPT2 mRNA and protein*. Am J Physiol Endocrinol Metab, 2002. **282**(5): p. E1172-9.
259. Groneberg, D.A., et al., *Localization of the peptide transporter PEPT2 in the lung: implications for pulmonary oligopeptide uptake*. Am J Pathol, 2001. **158**(2): p. 707-14.
260. Saito, H., et al., *Cloning and characterization of a rat H⁺/peptide cotransporter mediating absorption of beta-lactam antibiotics in the intestine and kidney*. J Pharmacol Exp Ther, 1995. **275**(3): p. 1631-7.

261. Saito, H., et al., *Molecular cloning and tissue distribution of rat peptide transporter PEPT2*. Biochim Biophys Acta, 1996. **1280**(2): p. 173-7.
262. Bahadduri, P.M., et al., *Functional characterization of the peptide transporter PEPT2 in primary cultures of human upper airway epithelium*. Am J Respir Cell Mol Biol, 2005. **32**(4): p. 319-25.
263. Smith, D.E., C.E. Johanson, and R.F. Keep, *Peptide and peptide analog transport systems at the blood-CSF barrier*. Adv Drug Deliv Rev, 2004. **56**(12): p. 1765-91.
264. Zhang, L., et al., *Antimicrobial peptide therapeutics for cystic fibrosis*. Antimicrob Agents Chemother, 2005. **49**(7): p. 2921-7.
265. Harlfinger, S., et al., *Are organic cation transporters capable of transporting prostaglandins?* Naunyn Schmiedebergs Arch Pharmacol, 2005. **372**(2): p. 125-30.
266. Keller, T., et al., *Purification and functional reconstitution of the rat organic cation transporter OCT1*. Biochemistry, 2005. **44**(36): p. 12253-63.
267. Koepsell, H. and H. Endou, *The SLC22 drug transporter family*. Pflugers Arch, 2004. **447**(5): p. 666-76.
268. Grundemann, D., et al., *Drug excretion mediated by a new prototype of polyspecific transporter*. Nature, 1994. **372**(6506): p. 549-52.
269. Gorboulev, V., et al., *Cloning and characterization of two human polyspecific organic cation transporters*. DNA Cell Biol, 1997. **16**(7): p. 871-81.
270. Koepsell, H., B.M. Schmitt, and V. Gorboulev, *Organic cation transporters*. Rev Physiol Biochem Pharmacol, 2003. **150**: p. 36-90.
271. Zhang, L., et al., *Cloning and functional expression of a human liver organic cation transporter*. Mol Pharmacol, 1997. **51**(6): p. 913-21.
272. Okuda, M., et al., *cDNA cloning and functional expression of a novel rat kidney organic cation transporter, OCT2*. Biochem Biophys Res Commun, 1996. **224**(2): p. 500-7.
273. Tamai, I., et al., *Molecular and functional identification of sodium ion-dependent, high affinity human carnitine transporter OCTN2*. J Biol Chem, 1998. **273**(32): p. 20378-82.
274. Ohashi, R., et al., *Na(+)-dependent carnitine transport by organic cation transporter (OCTN2): its pharmacological and toxicological relevance*. J Pharmacol Exp Ther, 1999. **291**(2): p. 778-84.
275. Wagner, C.A., et al., *Functional and pharmacological characterization of human Na(+)-carnitine cotransporter hOCTN2*. Am J Physiol Renal Physiol, 2000. **279**(3): p. F584-91.
276. Chen, J.J., et al., *Maintenance of serotonin in the intestinal mucosa and ganglia of mice that lack the high-affinity serotonin transporter: Abnormal intestinal motility and the expression of cation transporters*. J Neurosci, 2001. **21**(16): p. 6348-61.
277. Karbach, U., et al., *Localization of organic cation transporters OCT1 and OCT2 in rat kidney*. Am J Physiol Renal Physiol, 2000. **279**(4): p. F679-87.
278. Jigorel, E., et al., *Functional expression of sinusoidal drug transporters in primary human and rat hepatocytes*. Drug Metab Dispos, 2005. **33**(10): p. 1418-22.
279. Pavlova, A., et al., *Developmentally regulated expression of organic ion transporters NKT (OAT1), OCT1, NLT (OAT2), and Roct*. Am J Physiol Renal Physiol, 2000. **278**(4): p. F635-43.
280. Koepsell, H., K. Lips, and C. Volk, *Polyspecific organic cation transporters: structure, function, physiological roles, and biopharmaceutical implications*. Pharm Res, 2007. **24**(7): p. 1227-51.
281. Lips, K.S., et al., *Down-regulation of the non-neuronal acetylcholine synthesis and release machinery in acute allergic airway inflammation of rat and mouse*. Life Sci, 2007. **80**(24-25): p. 2263-9.
282. Kummer, W., et al., *Role of acetylcholine and polyspecific cation transporters in serotonin-induced bronchoconstriction in the mouse*. Respir Res, 2006. **7**: p. 65.
283. Slitt, A.L., et al., *Tissue distribution and renal developmental changes in rat organic cation transporter mRNA levels*. Drug Metab Dispos, 2002. **30**(2): p. 212-9.

284. Busch, A.E., et al., *Human neurons express the polyspecific cation transporter hOCT2, which translocates monoamine neurotransmitters, amantadine, and memantine*. *Mol Pharmacol*, 1998. **54**(2): p. 342-52.
285. Nezu, J., et al., *Primary systemic carnitine deficiency is caused by mutations in a gene encoding sodium ion-dependent carnitine transporter*. *Nat Genet*, 1999. **21**(1): p. 91-4.
286. Sekine, T., et al., *Molecular cloning and characterization of high-affinity carnitine transporter from rat intestine*. *Biochem Biophys Res Commun*, 1998. **251**(2): p. 586-91.
287. Tamai, I., et al., *Na(+)-coupled transport of L-carnitine via high-affinity carnitine transporter OCTN2 and its subcellular localization in kidney*. *Biochim Biophys Acta*, 2001. **1512**(2): p. 273-84.
288. Wu, X., et al., *cDNA sequence, transport function, and genomic organization of human OCTN2, a new member of the organic cation transporter family*. *Biochem Biophys Res Commun*, 1998. **246**(3): p. 589-95.
289. Horvath, G., et al., *Epithelial organic cation transporters ensure pH-dependent drug absorption in the airway*. *Am J Respir Cell Mol Biol*, 2007. **36**(1): p. 53-60.
290. Wright, S.H., *Role of organic cation transporters in the renal handling of therapeutic agents and xenobiotics*. *Toxicol Appl Pharmacol*, 2005. **204**(3): p. 309-19.
291. Filipski, K.K., et al., *Contribution of Organic Cation Transporter 2 (OCT2) to Cisplatin-Induced Nephrotoxicity*. *Clin Pharmacol Ther*, 2009.
292. Shikata, E., et al., *Human organic cation transporter (OCT1 and OCT2) gene polymorphisms and therapeutic effects of metformin*. *J Hum Genet*, 2007. **52**(2): p. 117-22.
293. Anzai, N., Y. Kanai, and H. Endou, *Organic anion transporter family: current knowledge*. *J Pharmacol Sci*, 2006. **100**(5): p. 411-26.
294. Konig, J., et al., *Pharmacogenomics of human OATP transporters*. *Naunyn Schmiedeberg Arch Pharmacol*, 2006. **372**(6): p. 432-43.
295. Hagenbuch, B. and P.J. Meier, *The superfamily of organic anion transporting polypeptides*. *Biochim Biophys Acta*, 2003. **1609**(1): p. 1-18.
296. Tamai, I., et al., *Molecular identification and characterization of novel members of the human organic anion transporter (OATP) family*. *Biochem Biophys Res Commun*, 2000. **273**(1): p. 251-60.
297. Sweet, D.H., K.T. Bush, and S.K. Nigam, *The organic anion transporter family: from physiology to ontogeny and the clinic*. *Am J Physiol Renal Physiol*, 2001. **281**(2): p. F197-205.
298. Kullak-Ublick, G.A., et al., *Organic anion-transporting polypeptide B (OATP-B) and its functional comparison with three other OATPs of human liver*. *Gastroenterology*, 2001. **120**(2): p. 525-33.
299. Pritchard, J.B., et al., *Mechanism of organic anion transport across the apical membrane of choroid plexus*. *J Biol Chem*, 1999. **274**(47): p. 33382-7.
300. Sweet, D.H., N.A. Wolff, and J.B. Pritchard, *Expression cloning and characterization of ROAT1. The basolateral organic anion transporter in rat kidney*. *J Biol Chem*, 1997. **272**(48): p. 30088-95.
301. Abe, T., et al., *Identification of a novel gene family encoding human liver-specific organic anion transporter LST-1*. *J Biol Chem*, 1999. **274**(24): p. 17159-63.
302. Hsiang, B., et al., *A novel human hepatic organic anion transporting polypeptide (OATP2). Identification of a liver-specific human organic anion transporting polypeptide and identification of rat and human hydroxymethylglutaryl-CoA reductase inhibitor transporters*. *J Biol Chem*, 1999. **274**(52): p. 37161-8.
303. Konig, J., et al., *A novel human organic anion transporting polypeptide localized to the basolateral hepatocyte membrane*. *Am J Physiol Gastrointest Liver Physiol*, 2000. **278**(1): p. G156-64.

304. Fujiwara, K., et al., *Identification of thyroid hormone transporters in humans: different molecules are involved in a tissue-specific manner*. Endocrinology, 2001. **142**(5): p. 2005-12.
305. Hitchcock, K.R., J. Harney, and S. Reichlin, *Hormones and the lung. III. Thyroid hormone uptake kinetics of perinatal rat lung*. Endocrinology, 1980. **107**(1): p. 294-9.
306. St-Pierre, M.V., et al., *Characterization of an organic anion-transporting polypeptide (OATP-B) in human placenta*. J Clin Endocrinol Metab, 2002. **87**(4): p. 1856-63.
307. Leake, C.D., *An Historical Account of Pharmacology to the Twentieth Century*. 1975, Springfield, IL: Charles C. Thomas.
308. Scheindlin, S. *A Brief History of Pharmacology*. 2001 [cited 2010 04/05/2010]; Available from: <http://pubs.acs.org/subscribe/journals/mdd/v04/i05/html/05timeline.html>.
309. Holmes, F.L. *Claude Bernard*. 2010 09/05/2010 [cited 2010 11/05/2010]; Available from: http://en.wikipedia.org/wiki/Claude_Bernard.
310. Bernard, C., *An Introduction to the Study of Experimental Medicine*. Reprint ed. 1865: Dover publication. 272.
311. Knowlton, F.P. and E.H. Starling, *The influence of variations in temperature and blood-pressure on the performance of the isolated mammalian heart*. J Physiol, 1912. **44**(3): p. 206-19.
312. Newell Martin, H., *The Direct Influence of Gradual Variations of Temperature upon the Rate of Beat of the Dog's Heart*. Philosophical Transactions of the Royal Society of London, 1883. **174**.
313. Delaunois, A.L. and T.O. King, *Improvements in an isolated perfused lung technique*. Arch Int Pharmacodyn Ther, 1956. **107**(1): p. 90-2.
314. Davis, J.H. and S. Levy, *Removal of bacteria from the blood stream by an isolated perfused rat lung*. Surg Forum, 1965. **16**: p. 77-8.
315. Leary, W.P. and U. Smith, *In situ perfusion of isolated rat lung*. Life Sci I, 1970. **9**(23): p. 1321-6.
316. Leary, W.P. and J.G. Ledingham, *Removal of angiotensin by isolated perfused organs of the rat*. Nature, 1969. **222**(5197): p. 959-60.
317. Hems, R., et al., *Gluconeogenesis in the perfused rat liver*. Biochem J, 1966. **101**(2): p. 284-92.
318. Krebs, H.A.a.H., K., *Urea formation in the animal body*. Hoppe-Seyl. Z. , 1932. **210**.
319. Ryan, J.W., et al., *Metabolism of angiotensin I in the pulmonary circulation*. Biochem J, 1970. **120**(1): p. 221-3.
320. Baker, D.G., et al., *Establishment and validation of an isolated rat lung model for pulmonary metabolism studies*. J Appl Toxicol, 1999. **19**(2): p. 83-91.
321. Ewing, P., et al., *Vasoconstriction after inhalation of budesonide: a study in the isolated and perfused rat lung*. Pulm Pharmacol Ther. **23**(1): p. 9-14.
322. Forbes, B., et al., *Challenges in inhaled product development and opportunities for open innovation*. Adv Drug Deliv Rev.
323. Ewing, P., et al., *Increasing exposure levels cause an abrupt change in the absorption and metabolism of acutely inhaled benzo(a)pyrene in the isolated, ventilated, and perfused lung of the rat*. Toxicol Sci, 2006. **91**(2): p. 332-40.
324. Niven, R.W. and P.R. Byron, *Solute absorption from the airways of the isolated rat lung. I. The use of absorption data to quantify drug dissolution or release in the respiratory tract*. Pharm Res, 1988. **5**(9): p. 574-9.
325. Byron, P.R., et al., *Solute absorption from the airways of the isolated rat lung. IV. Mechanisms of absorption of fluorophore-labeled poly-alpha,beta-[N(2-hydroxyethyl)-DL-aspartamide]*. Pharm Res, 1994. **11**(2): p. 221-5.
326. Niven, R.W. and P.R. Byron, *Solute absorption from the airways of the isolated rat lung. II. Effect of surfactants on absorption of fluorescein*. Pharm Res, 1990. **7**(1): p. 8-13.

327. Niven, R.W., F. Rypacek, and P.R. Byron, *Solute absorption from the airways of the isolated rat lung. III. Absorption of several peptidase-resistant, synthetic polypeptides: poly-(2-hydroxyethyl)-aspartamides*. Pharm Res, 1990. **7**(10): p. 990-4.
328. Pang, Y., M. Sakagami, and P.R. Byron, *The pharmacokinetics of pulmonary insulin in the in vitro isolated perfused rat lung: implications of metabolism and regional deposition*. Eur J Pharm Sci, 2005. **25**(4-5): p. 369-78.
329. Manford, F., et al., *Drug permeability in 16HBE14o- airway cell layers correlates with absorption from the isolated perfused rat lung*. Eur J Pharm Sci, 2005. **26**(5): p. 414-20.
330. Tronde, A., et al., *Pulmonary absorption rate and bioavailability of drugs in vivo in rats: structure-absorption relationships and physicochemical profiling of inhaled drugs*. J Pharm Sci, 2003. **92**(6): p. 1216-33.
331. Biotechnology, P.L., *Gel Filtration - Principles and Methods*, in (Technical Manual). 1991: Uppsala, Sweden.
332. Fisher, A.B., C. Dodia, and J. Linask, *Perfusate composition and edema formation in isolated rat lungs*. Exp Lung Res, 1980. **1**(1): p. 13-21.
333. Czartolomna, J., N.F. Voelkel, and S.W. Chang, *Permeability characteristics of isolated perfused rat lungs*. J Appl Physiol, 1991. **70**(4): p. 1854-60.
334. Pang, Y., M. Sakagami, and P.R. Byron, *Insulin self-association: effects on lung disposition kinetics in the airways of the isolated perfused rat lung (IPRL)*. Pharm Res, 2007. **24**(9): p. 1636-44.
335. Byron, P.R. and J.S. Patton, *Drug delivery via the respiratory tract*. J Aerosol Med, 1994. **7**(1): p. 49-75.
336. Sun, J.Z., P.R. Byron, and F. Rypacek, *Solute absorption from the airways of the isolated rat lung. V. Charge effects on the absorption of copolymers of N(2-hydroxyethyl)-DL-aspartamide with DL-aspartic acid or dimethylaminopropyl-DL-aspartamide*. Pharm Res, 1999. **16**(7): p. 1104-8.
337. Aulton, M., *Pulmonary Drug Delivery*, in *Aulton's Pharmaceutics The Design and Manufacture of Medicines*, K. Taylor, Editor. 2007, Churchill Livingstone.
338. Ingbar, M.A.M.a.D.H., *Measurement of Lung Water*, in *Pulmonary Edema (Lung Biology in Health and Disease)*. 1998, Informa Healthcare. p. 638 pages
339. Reinoso, R.F., B.A. Telfer, and M. Rowland, *Tissue water content in rats measured by desiccation*. J Pharmacol Toxicol Methods, 1997. **38**(2): p. 87-92.
340. Altman, P.L. and D.S. Dittmer, *Biology Data Book*. Amrl-Tr-64-100. AMRL TR, 1964: p. 1-631.
341. Wang, X.D., et al., *Antioxidant and calcium channel blockers counteract endothelial barrier injury induced by acute pancreatitis in rats*. Scand J Gastroenterol, 1995. **30**(11): p. 1129-36.
342. Yoshikawa, T., et al., *Effect of pregnancy on tissue distribution of salicylate in rats*. Drug Metab Dispos, 1984. **12**(4): p. 500-5.
343. Takada, K., Yamamoto, M., Asada, S., *Evidence for the pulmonary absorption of fluorescent-labeled macromolecular compounds*. J. Pharm. Dyn., 1978. **1**: p. 281-287.
344. Sakagami, M., et al., *Solute disposition in the rat lung in vivo and in vitro: determining regional absorption kinetics in the presence of mucociliary escalator*. J Pharm Sci, 2002. **91**(2): p. 594-604.
345. Enna, S.J.S., L.S., *Absorption of drugs from the rat lung*. Am. J. Physiol., 1972. **223**: p. 1227 - 1231.
346. Mathia, N.R., et al., *Permeability characteristics of calu-3 human bronchial epithelial cells: in vitro-in vivo correlation to predict lung absorption in rats*. J Drug Target, 2002. **10**(1): p. 31-40.
347. Matsukawa, Y., et al., *Size-dependent dextran transport across rat alveolar epithelial cell monolayers*. J Pharm Sci, 1997. **86**(3): p. 305-9.

348. Kurmi, B.D., et al., *Micro- and nanocarrier-mediated lung targeting*. Expert Opin Drug Deliv. **7**(7): p. 781-94.
349. Mansour, H.M., Y.S. Rhee, and X. Wu, *Nanomedicine in pulmonary delivery*. Int J Nanomedicine, 2009. **4**: p. 299-319.
350. Winkler, J., G. Hochhaus, and H. Derendorf, *How the lung handles drugs: pharmacokinetics and pharmacodynamics of inhaled corticosteroids*. Proc Am Thorac Soc, 2004. **1**(4): p. 356-63.
351. Bosquillon, C., *Drug transporters in the lung--do they play a role in the biopharmaceutics of inhaled drugs?* J Pharm Sci. **99**(5): p. 2240-55.
352. Dumont, J.A., et al., *Delivery of an erythropoietin-Fc fusion protein by inhalation in humans through an immunoglobulin transport pathway*. J Aerosol Med, 2005. **18**(3): p. 294-303.
353. Bitonti, A.J. and J.A. Dumont, *Pulmonary administration of therapeutic proteins using an immunoglobulin transport pathway*. Adv Drug Deliv Rev, 2006. **58**(9-10): p. 1106-18.
354. Bosquillon, C., *Drug transporters in the lung--do they play a role in the biopharmaceutics of inhaled drugs?* J Pharm Sci, 2010. **99**(5): p. 2240-55.
355. Roerig, D.L., S.H. Audi, and S.B. Ahlf, *Kinetic characterization of P-glycoprotein-mediated efflux of rhodamine 6G in the intact rabbit lung*. Drug Metab Dispos, 2004. **32**(9): p. 953-8.
356. Eytan, G.D., et al., *The role of passive transbilayer drug movement in multidrug resistance and its modulation*. J Biol Chem, 1996. **271**(22): p. 12897-902.
357. Varma, M.V., et al., *P-glycoprotein inhibitors and their screening: a perspective from bioavailability enhancement*. Pharmacol Res, 2003. **48**(4): p. 347-59.
358. Wu, C.P., A.M. Calcagno, and S.V. Ambudkar, *Reversal of ABC drug transporter-mediated multidrug resistance in cancer cells: evaluation of current strategies*. Curr Mol Pharmacol, 2008. **1**(2): p. 93-105.
359. Ponte-Sucre, A., *Availability and applications of ATP-binding cassette (ABC) transporter blockers*. Appl Microbiol Biotechnol, 2007. **76**(2): p. 279-86.
360. Fromm, M.F., et al., *Inhibition of P-glycoprotein-mediated drug transport: A unifying mechanism to explain the interaction between digoxin and quinidine [seecomments]*. Circulation, 1999. **99**(4): p. 552-7.
361. Manford, F., et al., *Lack of difference in pulmonary absorption of digoxin, a P-glycoprotein substrate, in mdr1a-deficient and mdr1a-competent mice*. J Pharm Pharmacol, 2008. **60**(10): p. 1305-10.
362. Schinkel, A.H., et al., *Absence of the mdr1a P-Glycoprotein in mice affects tissue distribution and pharmacokinetics of dexamethasone, digoxin, and cyclosporin A*. J Clin Invest, 1995. **96**(4): p. 1698-705.
363. Iqbal, T., M. Kinjo, and T.C. Dowling, *Determination of Rhodamine 123 in cell lysate by HPLC with visible wavelength detection*. J Chromatogr B Analyt Technol Biomed Life Sci, 2005. **814**(2): p. 259-62.
364. Research, F.a.D.A.C.f.D.E.a., *Guidance for Industry: Bioanalytical Method Validation*. 2001, Drug Information Branch: Rockville, MD. p. 25.
365. Lampidis, T.J., Castello, C., del Giglio, A., Pressman, B.D., Viallet, P., Trevorow, K.W., Valet, G.K., Tapiero, H., and Savaraj, N., *RELEVANCE OF THE CHEMICAL CHARGE OF RHODAMINE DYES TO MULTIPLE DRUG RESISTANCE*. Biochemical pharmacology, 1989. **38**(23): p. 4267-4271.
366. Annaert, P.P., et al., *P-glycoprotein-mediated in vitro biliary excretion in sandwich-cultured rat hepatocytes*. Drug Metab Dispos, 2001. **29**(10): p. 1277-83.
367. Loetchutinat, C., et al., *New insights into the P-glycoprotein-mediated effluxes of rhodamines*. Eur J Biochem, 2003. **270**(3): p. 476-85.
368. Shapiro, A.B. and V. Ling, *Positively cooperative sites for drug transport by P-glycoprotein with distinct drug specificities*. Eur J Biochem, 1997. **250**(1): p. 130-7.

369. Ardrey, R.E.A., Robert, *Liquid chromatography-mass spectrometry: an introduction*, ed. J. Wiley. 2003, London.
370. Yergey, A.L., *Liquid chromatography/mass spectrometry: techniques and applications*. 1990, New York: Plenum Press.
371. Wang, Y., et al., *A kinetic study of Rhodamine123 pumping by P-glycoprotein*. Biochim Biophys Acta, 2006. **1758**(10): p. 1671-6.
372. Letrent, S.P., et al., *Effects of a potent and specific P-glycoprotein inhibitor on the blood-brain barrier distribution and antinociceptive effect of morphine in the rat*. Drug Metab Dispos, 1999. **27**(7): p. 827-34.
373. Hyafil, F., et al., *In vitro and in vivo reversal of multidrug resistance by GF120918, an acridonecarboxamide derivative*. Cancer Res, 1993. **53**(19): p. 4595-602.
374. Ozben, T., *Mechanisms and strategies to overcome multiple drug resistance in cancer*. FEBS Lett, 2006. **580**(12): p. 2903-9.
375. Kajikawa, T., et al., *Role of P-glycoprotein in distribution of rhodamine 123 into aqueous humor in rabbits*. Curr Eye Res, 1999. **18**(3): p. 240-6.
376. Mistry, P., et al., *In vitro and in vivo reversal of P-glycoprotein-mediated multidrug resistance by a novel potent modulator, XR9576*. Cancer Res, 2001. **61**(2): p. 749-58.
377. Pichler, A., J.L. Prior, and D. Piwnica-Worms, *Imaging reversal of multidrug resistance in living mice with bioluminescence: MDR1 P-glycoprotein transports coelenterazine*. Proc Natl Acad Sci U S A, 2004. **101**(6): p. 1702-7.
378. Rao, V.V., et al., *Choroid plexus epithelial expression of MDR1 P glycoprotein and multidrug resistance-associated protein contribute to the blood-cerebrospinal-fluid drug-permeability barrier*. Proc Natl Acad Sci U S A, 1999. **96**(7): p. 3900-5.
379. Cisternino, S., et al., *Nonlinear accumulation in the brain of the new taxoid TXD258 following saturation of P-glycoprotein at the blood-brain barrier in mice and rats*. Br J Pharmacol, 2003. **138**(7): p. 1367-75.
380. Schinkel, A.H., et al., *Disruption of the mouse mdr1a P-glycoprotein gene leads to a deficiency in the blood-brain barrier and to increased sensitivity to drugs*. Cell, 1994. **77**(4): p. 491-502.
381. van Asperen, J., et al., *Altered pharmacokinetics of vinblastine in Mdr1a P-glycoprotein-deficient Mice*. J Natl Cancer Inst, 1996. **88**(14): p. 994-9.
382. Schinkel, A.H., et al., *Normal viability and altered pharmacokinetics in mice lacking mdr1-type (drug-transporting) P-glycoproteins*. Proc Natl Acad Sci U S A, 1997. **94**(8): p. 4028-33.
383. van Asperen, J., et al., *Comparative pharmacokinetics of vinblastine after a 96-hour continuous infusion in wild-type mice and mice lacking mdr1a P-glycoprotein*. J Pharmacol Exp Ther, 1999. **289**(1): p. 329-33.
384. Shrewsbury, S.B., et al., *Safety and pharmacokinetics of dihydroergotamine mesylate administered via a Novel (Tempo) inhaler*. Headache, 2008. **48**(3): p. 355-67.
385. van der Sandt, I.C., et al., *P-glycoprotein inhibition leads to enhanced disruptive effects by anti-microtubule cytostatics at the in vitro blood-brain barrier*. Pharm Res, 2001. **18**(5): p. 587-92.
386. Cavet, M.E., M. West, and N.L. Simmons, *Transport and epithelial secretion of the cardiac glycoside, digoxin, by human intestinal epithelial (Caco-2) cells*. Br J Pharmacol, 1996. **118**(6): p. 1389-96.
387. Djuv, A. and O.G. Nilsen, *Caco-2 cell methodology and inhibition of the P-glycoprotein transport of digoxin by Aloe vera juice*. Phytother Res, 2008. **22**(12): p. 1623-8.
388. Taub, M.E., et al., *Functional assessment of multiple P-glycoprotein (P-gp) probe substrates: influence of cell line and modulator concentration on P-gp activity*. Drug Metab Dispos, 2005. **33**(11): p. 1679-87.

389. Teeter, L.D., et al., *Activation of distinct multidrug-resistance (P-glycoprotein) genes during rat liver regeneration and hepatocarcinogenesis*. Mol Carcinog, 1993. **8**(2): p. 67-73.
390. Zhou, G., R. Song, and M.T. Kuo, *A novel cis-acting element is involved in the promoter activity of the rat mdr1b gene*. Cell Growth Differ, 1996. **7**(10): p. 1369-81.
391. Lanman, R.C., R.M. Gillilan, and L.S. Schanker, *Absorption of cardiac glycosides from the rat respiratory tract*. J Pharmacol Exp Ther, 1973. **187**(1): p. 105-11.
392. Ferte, J., *Analysis of the tangled relationships between P-glycoprotein-mediated multidrug resistance and the lipid phase of the cell membrane*. Eur J Biochem, 2000. **267**(2): p. 277-94.
393. Lentz, K.A., et al., *Influence of passive permeability on apparent P-glycoprotein kinetics*. Pharm Res, 2000. **17**(12): p. 1456-60.
394. Campbell, J.W. and P.A. Chyka, *Physicochemical characteristics of drugs and response to repeat-dose activated charcoal*. Am J Emerg Med, 1992. **10**(3): p. 208-10.
395. Bruce C. McGorum, N.E.R., Padraic M. Dixon, Jim Schumacher, ed. *Equine respiratory medicine and surgery*. 2006, Saunders Ltd.
396. Casale, T.B., Nelson, H.S., Corren. J., and Newman, K., *Long-Term Safety of Flunisolide Hydrofluoroalkane Metered-Dose Inhaler in Adults and Adolescents with Asthma*. Clinical Drug Investigation, 2001. **21**(11).
397. Meijer, D.K.F., Smit, J.W., and Müller, M., *Hepatobiliary elimination of cationic drugs: the role of P-glycoproteins and other ATP-dependent transporters* Advanced Drug Delivery Reviews, 1997. **25**(2-3): p. 159-200.
398. Florea, B.I., et al., *Evidence of P-glycoprotein mediated apical to basolateral transport of flunisolide in human broncho-tracheal epithelial cells (Calu-3)*. Br J Pharmacol, 2001. **134**(7): p. 1555-63.
399. Gottesman, M.M. and I. Pastan, *Biochemistry of multidrug resistance mediated by the multidrug transporter*. Annu Rev Biochem, 1993. **62**: p. 385-427.
400. Luker, G.D., et al., *Multidrug resistance (MDR1) P-glycoprotein enhances esterification of plasma membrane cholesterol*. J Biol Chem, 1999. **274**(11): p. 6979-91.
401. Cordon-Cardo, C., et al., *Multidrug-resistance gene (P-glycoprotein) is expressed by endothelial cells at blood-brain barrier sites*. Proc Natl Acad Sci U S A, 1989. **86**(2): p. 695-8.
402. Thiebaut, F., et al., *Cellular localization of the multidrug-resistance gene product P-glycoprotein in normal human tissues*. Proc Natl Acad Sci U S A, 1987. **84**(21): p. 7735-8.
403. Hamilton, K.O., et al., *P-glycoprotein efflux pump expression and activity in Calu-3 cells*. J Pharm Sci, 2001. **90**(5): p. 647-58.
404. Kandimalla, K.K. and M.D. Donovan, *Localization and differential activity of P-glycoprotein in the bovine olfactory and nasal respiratory mucosae*. Pharm Res, 2005. **22**(7): p. 1121-8.
405. Uematsu, T., et al., *P-glycoprotein expression in human major and minor salivary glands*. Arch Oral Biol, 2001. **46**(6): p. 521-7.
406. Petriz, J., et al., *Is rhodamine 123 an appropriate fluorescent probe to assess P-glycoprotein mediated multidrug resistance in vinblastine-resistant CHO cells?* Anal Cell Pathol, 1997. **14**(3): p. 129-40.
407. Altenberg, G.A., et al., *Unidirectional fluxes of rhodamine 123 in multidrug-resistant cells: evidence against direct drug extrusion from the plasma membrane*. Proc Natl Acad Sci U S A, 1994. **91**(11): p. 4654-7.
408. Yumoto, R., et al., *Transport of rhodamine 123, a P-glycoprotein substrate, across rat intestine and Caco-2 cell monolayers in the presence of cytochrome P-450 3A-related compounds*. J Pharmacol Exp Ther, 1999. **289**(1): p. 149-55.
409. Kuhnke, D., et al., *MDR1-P-Glycoprotein (ABCB1) Mediates Transport of Alzheimer's amyloid-beta peptides--implications for the mechanisms of Abeta clearance at the blood-brain barrier*. Brain Pathol, 2007. **17**(4): p. 347-53.

410. Petriz, J. and J. Garcia-Lopez, *Flow cytometric analysis of P-glycoprotein function using rhodamine 123*. *Leukemia*, 1997. **11**(7): p. 1124-30.
411. Masereeuw, R., M.M. Moons, and F.G. Russel, *Rhodamine 123 accumulates extensively in the isolated perfused rat kidney and is secreted by the organic cation system*. *Eur J Pharmacol*, 1997. **321**(3): p. 315-23.
412. Duvvuri, M., et al., *Weak base permeability characteristics influence the intracellular sequestration site in the multidrug-resistant human leukemic cell line HL-60*. *J Biol Chem*, 2004. **279**(31): p. 32367-72.
413. SRC. 2010 [cited; Available from: <http://esc.syrres.com/interkow/webprop.exe?CAS=136470-78-5>.
414. Bebok, Z., et al., *Reactive oxygen nitrogen species decrease cystic fibrosis transmembrane conductance regulator expression and cAMP-mediated Cl⁻ secretion in airway epithelia*. *J Biol Chem*, 2002. **277**(45): p. 43041-9.
415. Shen, B.Q., et al., *Calu-3: a human airway epithelial cell line that shows cAMP-dependent Cl⁻ secretion*. *Am J Physiol*, 1994. **266**(5 Pt 1): p. L493-501.
416. Janvilisri, T., et al., *Sterol transport by the human breast cancer resistance protein (ABCG2) expressed in Lactococcus lactis*. *J Biol Chem*, 2003. **278**(23): p. 20645-51.
417. Krinkle, G., *The laboratory rat; history, models and strains*, in *Handbook of Experimental Animals*, Bullock, Editor. 2000, Academic Press. p. 3-16.
418. Wanner, A., *Circulation of the airway mucosa*. *J Appl Physiol*, 1989. **67**(3): p. 917-25.
419. *Biology Corner*. 2010 [cited 2010 15/09/10]; Available from: http://www.biologycorner.com/resources/rat_circ_artery.gif&imgrefurl=http://www.biologycorner.com/worksheets/rat_circulatory.html&usq=_jpBQhmVxNQxzVdv6gGCLe0zPpZk=&h=473&w=400&sz=17&hl=en&start=1&zoom=1&um=1&itbs=1&tbnid=-8keCVk7u3IGiM:&tbnh=129&tbnw=109&prev=/images%3Fq%3Drat%2Bcirculation%26um%3D1%26hl%3Den%26sa%3DN%26tbs%3Disch:1.
420. Ferreira, P.G., Silva, A.C., Águas, A.P., Pereira, A.S. and Grande, N.R. , *Detailed arrangement of the bronchial arteries in the Wistar rat: A study using vascular injection and scanning electron microscopy*. *Eur. J. Anat*, 2001. **5**(2): p. 67-76.
421. Hyytinen, T.A., K.J. Kairemo, and S.P. Mattila, *The role of pulmonary and systemic circulation in the tracheal blood supply in rats*. *Scand Cardiovasc J*, 1999. **33**(5): p. 274-7.
422. Chediak, A.D.a.W., A., *The circulation of the airways: anatomy, physiology and potential role in drug delivery to the respiratory tract*. *Advanced Drug Delivery Reviews*, 1990. **5**: p. 11-18.
423. Fromm, M.F., *Importance of P-glycoprotein at blood-tissue barriers*. *Trends Pharmacol Sci*, 2004. **25**(8): p. 423-9.
424. Schinkel, A.H., *P-Glycoprotein, a gatekeeper in the blood-brain barrier*. *Adv Drug Deliv Rev*, 1999. **36**(2-3): p. 179-194.
425. Tai, L.M., et al., *Polarized P-glycoprotein expression by the immortalised human brain endothelial cell line, hCMEC/D3, restricts apical-to-basolateral permeability to rhodamine 123*. *Brain Res*, 2009. **1292**: p. 14-24.
426. Miller, D.S., Bauer, B. and Hartz, A.M.S., *Modulation of P-Glycoprotein at the Blood-Brain Barrier: Opportunities to Improve Central Nervous System Pharmacotherapy*. *Pharmacological Reviews*, 2008. **60**: p. 196-209.
427. Kaddoumi, A., Choi, S-U., Kinman, L., Whittington, D., Tsai, C-C., Ho, R.J., Anderson, B.D., and Unadkat, J.D., *Inhibition of P-gp activity at the primate blood-brain barrier increases the distribution of nelfinavir into the brain but not into the CSF*. *Drug Metab Dispos*, 2007. **35**(9): p. 1459-62.
428. SYVANEN, S., HOOKER, A., RAHMAN, O., WILKING, H., BLOMQUIST, G., LANGSTROM, B., BERGSTROM, M. and HAMMARLUND-UDENAES, M., *Pharmacokinetics of P-Glycoprotein*

- Inhibition in the Rat Blood-Brain Barrier*. JOURNAL OF PHARMACEUTICAL SCIENCES, 2008. **97**(12): p. 5386-5400.
429. Demeule, M., et al., *Isolation of endothelial cells from brain, lung, and kidney: expression of the multidrug resistance P-glycoprotein isoforms*. Biochem Biophys Res Commun, 2001. **281**(3): p. 827-34.
 430. Chishty, M., et al., *Affinity for the P-glycoprotein efflux pump at the blood-brain barrier may explain the lack of CNS side-effects of modern antihistamines*. J Drug Target, 2001. **9**(3): p. 223-8.
 431. Jedlitschky, G., S. Vogelgesang, and H.K. Kroemer, *MDR1-P-glycoprotein (ABCB1)-mediated disposition of amyloid-beta peptides: implications for the pathogenesis and therapy of Alzheimer's disease*. Clin Pharmacol Ther. **88**(4): p. 441-3.
 432. Karszen, A.M., et al., *The role of the efflux transporter P-glycoprotein in brain penetration of prednisolone*. J Endocrinol, 2002. **175**(1): p. 251-60.
 433. Tsuji, A., et al., *P-glycoprotein as the drug efflux pump in primary cultured bovine brain capillary endothelial cells*. Life Sci, 1992. **51**(18): p. 1427-37.
 434. Yu, C., et al., *TNF activates P-glycoprotein in cerebral microvascular endothelial cells*. Cell Physiol Biochem, 2007. **20**(6): p. 853-8.
 435. Cornwell, M.M., I. Pastan, and M.M. Gottesman, *Certain calcium channel blockers bind specifically to multidrug-resistant human KB carcinoma membrane vesicles and inhibit drug binding to P-glycoprotein*. J Biol Chem, 1987. **262**(5): p. 2166-70.
 436. Ling, V., et al., *Multidrug-resistance phenotype in Chinese hamster ovary cells*. Cancer Treat Rep, 1983. **67**(10): p. 869-74.
 437. Fling, M.E., et al., *Analysis of a Candida albicans gene that encodes a novel mechanism for resistance to benomyl and methotrexate*. Mol Gen Genet, 1991. **227**(2): p. 318-29.
 438. Polli, J.W., et al., *Role of P-glycoprotein on the CNS disposition of amprenavir (141W94), an HIV protease inhibitor*. Pharm Res, 1999. **16**(8): p. 1206-12.
 439. Joseph Polli: Director, *In Vitro Drug Metabolism at GlaxoSmithKline*. 2010 [cited 2010 11/11/10]; Available from: <http://www.linkedin.com/in/josephwpolli>.
 440. GSK: *Prescription Drugs*. 2001 28/10/2010 [cited 2010 11/11/2010]; Available from: <http://www.gsk.com/products/prescription-medicines/index.htm>.
 441. Sherrieff, E.B., Edwards, C.D., John-Baptiste, P., Potter, J. and Ranshaw, L., *Investigating the effect of solubility in the isolated perfused and respiring rat lung model*, in *Respiratory CEDD DMPK*. 2010: GlaxoSmithKline R&D, Stevenage.
 442. Tschumperlin, D.J. and S.S. Margulies, *Alveolar epithelial surface area-volume relationship in isolated rat lungs*. J Appl Physiol, 1999. **86**(6): p. 2026-33.
 443. Kao, S.J., et al., *Static inflation attenuates ischemia/reperfusion injury in an isolated rat lung in situ*. Chest, 2004. **126**(2): p. 552-8.
 444. Williams, E.A., et al., *Lung injury following pulmonary resection in the isolated, blood-perfused rat lung*. Eur Respir J, 1999. **14**(4): p. 745-50.
 445. Brillault, J., et al., *P-glycoprotein-mediated transport of moxifloxacin in a Calu-3 lung epithelial cell model*. Antimicrob Agents Chemother, 2009. **53**(4): p. 1457-62.
 446. Diamanti, A.P., et al., *Reversion of resistance to immunosuppressive agents in three patients with psoriatic arthritis by cyclosporine A: Modulation of P-glycoprotein function*. Clin Immunol.
 447. Holmstock, N., et al., *In situ intestinal perfusion in knockout mice demonstrates inhibition of intestinal p-glycoprotein by ritonavir causing increased darunavir absorption*. Drug Metab Dispos. **38**(9): p. 1407-10.
 448. Yang, J.J., et al., *P-glycoprotein and Breast Cancer Resistance Protein Affect Disposition of Tandutinib, A Tyrosine Kinase Inhibitor*. Drug Metab Lett.

449. Rhoades, R.A., *Isolated perfused lung preparation for studying altered gaseous environments*. Environ Health Perspect, 1984. **56**: p. 43-50.
450. Uhlig, S. and L. Wollin, *An improved setup for the isolated perfused rat lung*. J Pharmacol Toxicol Methods, 1994. **31**(2): p. 85-94.
451. Watkins, C.A. and D.E. Rannels, *Measurement of protein synthesis in rat lungs perfused in situ*. Biochem J, 1980. **188**(1): p. 269-78.
452. Kendler, J., et al., *Effect of chlorpromazine on the function of the perfused isolated liver*. Biochem Pharmacol, 1971. **20**(9): p. 2439-45.
453. Van Huis, G.A. and M.F. Kramer, *Vascular perfusion of the isolated rat stomach with a fluorocarbon emulsion*. Gut, 1981. **22**(9): p. 713-9.
454. Dallal, M.M. and S.W. Chang, *Evans blue dye in the assessment of permeability-surface area product in perfused rat lungs*. J Appl Physiol, 1994. **77**(2): p. 1030-5.
455. Bennett, D.B., et al., *Pulmonary delivery of detirelix by intratracheal instillation and aerosol inhalation in the briefly anesthetized dog*. Pharm Res, 1994. **11**(7): p. 1048-55.
456. Tronde, A., Bosquillon, C., & Forbes, B., *The Isolated Perfused Lung for Drug Absorption Studies*, in *Drug Absorption Studies: In Situ, In Vitro and In Silico Models*, C. Ehrhardt, & Kim, K-J, Editor. 2008, Springer US. p. 135-163.
457. Bart, J., et al., *Irradiation of rat brain reduces P-glycoprotein expression and function*. Br J Cancer, 2007. **97**(3): p. 322-6.
458. Rumpold, H., et al., *Knockdown of Pgp resensitizes leukemic cells to proteasome inhibitors*. Biochem Biophys Res Commun, 2007. **361**(2): p. 549-54.
459. Malingre, M.M., et al., *Metabolism and excretion of paclitaxel after oral administration in combination with cyclosporin A and after i.v. administration*. Anticancer Drugs, 2000. **11**(10): p. 813-20.
460. Tubic, M., et al., *In silico modeling of non-linear drug absorption for the P-gp substrate talinolol and of consequences for the resulting pharmacodynamic effect*. Pharm Res, 2006. **23**(8): p. 1712-20.
461. Wagner, J.G., *History of pharmacokinetics*. Pharmacol Ther, 1981. **12**(3): p. 537-62.
462. Petzinger, E. and J. Geyer, *Drug transporters in pharmacokinetics*. Naunyn Schmiedeberg Arch Pharmacol, 2006. **372**(6): p. 465-75.
463. Hindenburg, A.A., et al., *Intracellular distribution and pharmacokinetics of daunorubicin in anthracycline-sensitive and -resistant HL-60 cells*. Cancer Res, 1989. **49**(16): p. 4607-14.
464. Castro, A.F. and G.A. Altenberg, *Inhibition of drug transport by genistein in multidrug-resistant cells expressing P-glycoprotein*. Biochem Pharmacol, 1997. **53**(1): p. 89-93.
465. Perloff, M.D., et al., *Rapid assessment of P-glycoprotein inhibition and induction in vitro*. Pharm Res, 2003. **20**(8): p. 1177-83.
466. Zhou, J., et al., *Reversal of P-glycoprotein-mediated multidrug resistance in cancer cells by the c-Jun NH2-terminal kinase*. Cancer Res, 2006. **66**(1): p. 445-52.
467. Hunter, E.C., Wiener, M.A. and Hebrank, J. *Pulmonary Drug Delivery*. 2010 [cited 2010 15/12/2010]; Available from: <http://www.nextsafety.com/pulmonary-drug-delivery/>.
468. Labiris, N.R. and M.B. Dolovich, *Pulmonary drug delivery. Part I: physiological factors affecting therapeutic effectiveness of aerosolized medications*. Br J Clin Pharmacol, 2003. **56**(6): p. 588-99.
469. Fernandes, C.A. and R. Vanbever, *Preclinical models for pulmonary drug delivery*. Expert Opin Drug Deliv, 2009. **6**(11): p. 1231-45.
470. Maertens, L.A., et al., *Formation and distribution of NNK metabolites in an isolated perfused rat lung*. Drug Metab Dispos. **38**(5): p. 752-60.

Appendices**Appendix i****Transporter expression intensities - raw data**

	Whole Lung			SPOC-1			AEII – Freshly Isolated			AEII – Day 2 of Culture			AEI-‘like’ Day 8 of Culture		
mdr1a	++	+	++	±	+	+	+	+	+	+	+	+	+	+	±
mdr1b	++	+	++	+	+	+	+	+	±	+	+	±	++	+	++
mrp1	+++	+	+++	++	++	++	+	+	+	+++	+++	+++	+++	++	++
mrp2	±	±	±	±	±	±	+	±	+	++	+	+	±	±	±
mrp3	+	++	+	++	+++	++	++	+	++	++	++	++	±	+	+
mrp4	±	++	+	±	±	±	±	±	±	±	±	±	±	±	±
mrp5	+++	++	+++	+	+	±	+	+	+	++	+++	++	+++	++	+++
mrp6	++	++	+	±	±	+	+	+	+	+	±	±	±	+	+
CFTR	+	±	±	+	+	+	±	+	+	+	+	+	+	+	+
mrp8	+++	+++	+++	+	++	+	+	+	+	±	±	±	+++	+	++
White1	++	++	++	++	+	++	++	++	++	+++	+++	++	++	+++	+++
BCRP	+	+	+	±	±	±	+	+	+	+	++	+	+++	++	++
β-actin	+++	+++	+++	+	+	+	+	++	++	++	++	++	++	+++	+++

Table A.2.1 Individual expression intensity results for 12 ABC drug transporters in 5 rat lung cell samples. n=3 for each drug transporter

	Whole Lung			SPOC-1			AEII – Freshly Isolated			AEII – Day 2 of Culture			AEI-‘like’ Day 8 of Culture		
rBAT	±	±	±	+	±	±	+	+	+	+	±	±	±	±	±
SNAT3	±	±	±	++	++	++	++	++	++	++	++	+	++	++	++
Asc-1	±	±	±	±	±	±	±	±	±	±	±	±	±	±	±
ASCT2	++	+++	++	+	+	+	+	+	+	±	++	+	++	++	+
Eaac1	+++	+++	++	±	±	±	±	+++	++	+++	+++	++	+++	+++	+
Lyaat1	+	±	±	±	±	±	±	+	+	+++	++	++	+	++	+
SNAT1	±	±	±	±	±	±	±	±	±	++	++	+	+	++	+
PHT1	±	±	±	±	±	±	±	±	±	±	+	±	±	±	±
GLYT2	±	±	±	±	±	±	±	±	±	+	+	±	±	±	+
Cat-1	+	+	+	++	++	+	++	+	+	++	++	+	+	++	+
Cat-3	±	±	±	±	±	±	±	±	±	+	±	±	±	±	±
β-actin	++	++	+++	++	++	++	++	++	++	++	+++	++	+++	+++	++

Table A.2.2 Individual expression intensity results for 11 amino acid drug transporters in 5 rat lung cell samples. n=3 for each drug transporter

	Whole Lung			SPOC-1			AEII – Freshly Isolated			AEII – Day 2 of Culture			AEI-‘like’ Day 8 of Culture		
Glut1	±	±	±	+	+	+	+	++	+	+	+	+	+	+	+
Glut2	±	±	±	++	++	+	±	±	±	±	±	±	±	±	±
Glut4	±	±	±	±	±	+	±	±	±	±	±	±	±	±	±
Glt-1	±	±	±	±	±	+	±	±	±	±	±	±	±	±	±
Glut5	±	±	±	±	+	±	±	±	±	±	±	±	±	±	±
β-actin	+	++	++	+++	+++	++	++	++	++	+++	++	+++	++	+++	+++

Table A.2.3 Individual expression intensity results for 5 glucose drug transporters in 5 rat lung cell samples. n=3 for each drug transporter

	Whole Lung			SPOC-1			AEII – Freshly Isolated			AEII – Day 2 of Culture			AEI-‘like’ Day 8 of Culture		
MCT	+	+	+	++	++	++	+++	+++	++	+	++	++	+	++	++
MCT1	+++	++	++	++	++	+++	+++	+++	+++	+++	+++	+++	+++	++	+++
Mct7B	++	+	+	+	+	+	++	+++	+++	+	++	++	++	++	++
β-actin	+	+	++	++	+++	+++	+++	+++	+++	++	++	+++	+++	++	+++

Table A.2.4 Individual expression intensity results for 3 monocarboxylate drug transporters in 5 rat lung cell samples. n=3 for each drug transporter

	Whole Lung			SPOC-1			AEII – Freshly Isolated			AEII – Day 2 of Culture			AEI-‘like’ Day 8 of Culture		
rENT1	+	+	++	+	+	+	±	±	+	+	++	+	+	+	+
Cnt1	±	±	±	±	±	±	±	±	+	±	±	+	±	+	±
NUC2	±	±	±	±	±	±	±	±	+	+	+	±	±	±	+
Ent3	+	±	+	±	±	+	+	+	+	++	++	++	++	++	++
β-actin	+++	++	+++	++	+++	+++	+++	+++	+++	+++	+++	++	+++	+++	++

Table A.2.5 Individual expression intensity results for 4 nucleoside drug transporters in 5 rat lung cell samples. n=3 for each drug transporter

	Whole Lung			SPOC-1			AEII – Freshly Isolated			AEII – Day 2 of Culture			AEI-‘like’ Day 8 of Culture		
Pept1	±	±	±	±	±	±	±	±	±	±	±	±	±	±	±
Pept2	++	++	++	++	+++	++	+	++	++	++	++	+++	+	++	++
β-actin	+++	+++	++	+++	+++	++	++	+++	+++	+++	++	+++	+	+++	++

Table A.2.6 Individual expression intensity results for 2 peptide drug transporters in 5 rat lung cell samples. n=3 for each drug transporter

	Whole Lung			SPOC-1			AEII – Freshly Isolated			AEII – Day 2 of Culture			AEI-‘like’ Day 8 of Culture		
Oct1	±	+	±	±	±	±	+	±	+	+	+	+	±	+	±
rOCT2	±	±	±	±	±	±	±	±	±	±	±	±	±	±	±
OCTN2	+	+	+	++	++	+	+	++	+	++	++	++	++	++	++
β-actin	++	+++	++	+++	+++	++	++	+++	+++	+++	+++	+++	+++	+++	+++

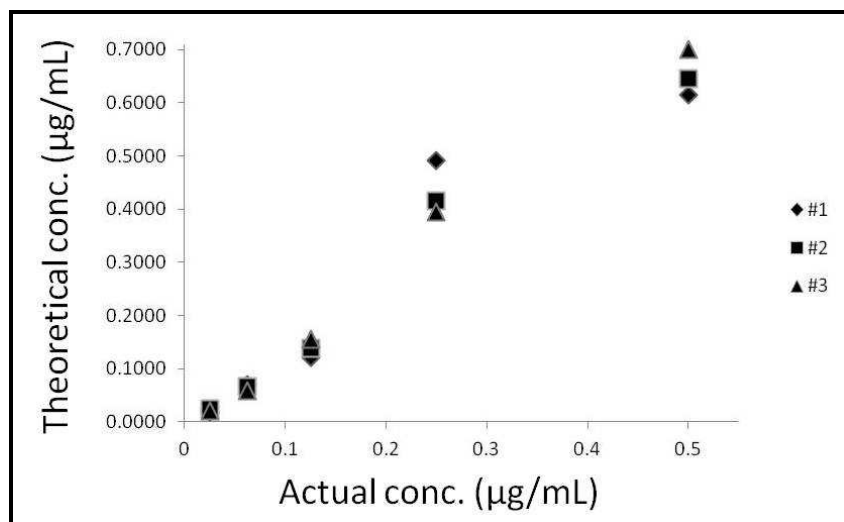
Table A.2.7 Individual expression intensity results for 3 organic cation drug transporters in 5 rat lung cell samples. n=3 for each drug transporter

	Whole Lung			SPOC-1			AEII – Freshly Isolated			AEII – Day 2 of Culture			AEI-‘like’ Day 8 of Culture		
oatp1	±	±	±	±	±	±	±	±	±	±	±	±	±	±	±
oatp2	±	±	±	±	±	±	±	±	±	±	±	±	±	±	±
oatp3a1	+	+	±	±	±	+	+	+	+	+	+	+	+	+	++
oatp-H	+	+	+	±	±	±	+	+	+	+	+	+	+	++	++
oatp-E	±	±	±	++	++	++	+	+	+	+	+	+	+	+	++
moat1	±	+	±	+	±	+	+	+	±	+	±	±	+	+	+
β-actin	++	++	++	+++	+++	+++	+++	++	+++	++	++	+++	+++	+++	+++

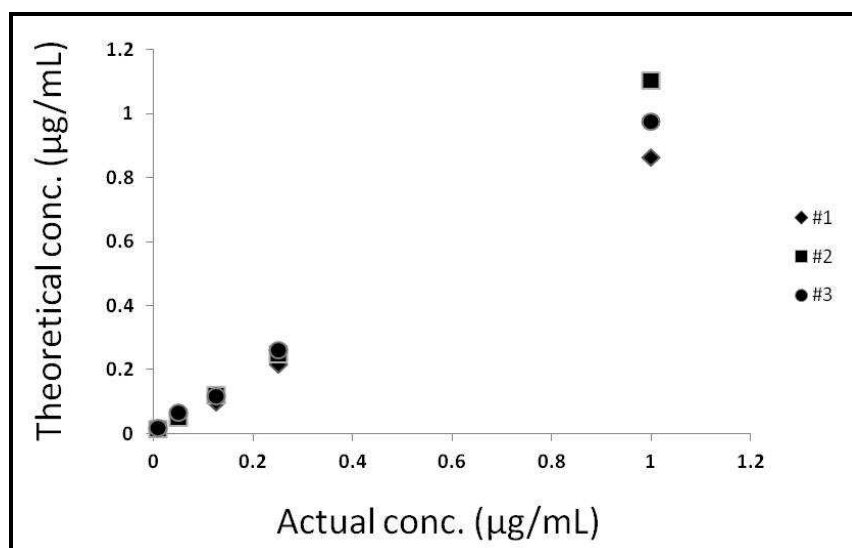
Table A.2.8 Individual expression intensity results for 6 organic anion drug transporters in 5 rat lung cell samples. n=3 for each drug transporter

Appendix ii**Chapter 4: Rh123 analytical validation: Precision and accuracy****Precision and accuracy calibration curves**

Individual calibration plots used to assess Rh123 HPLC assay precision

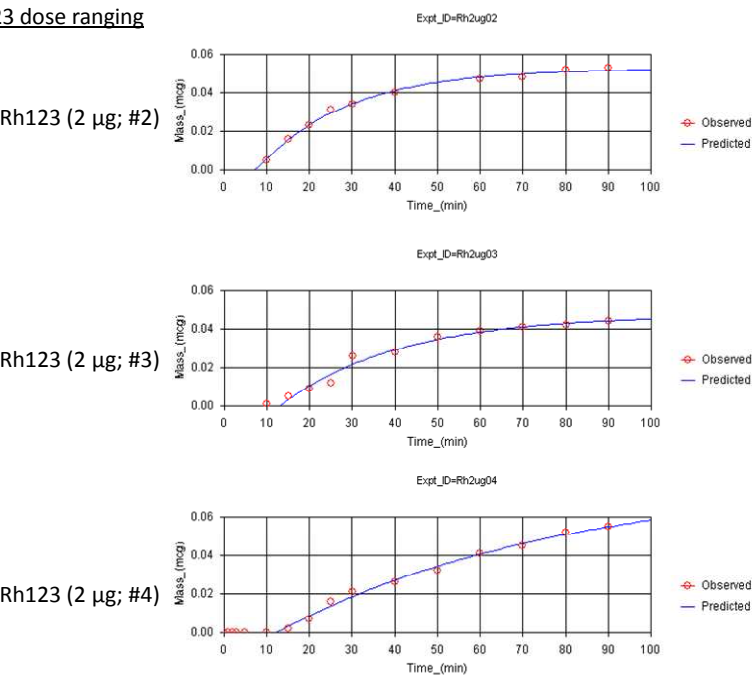


Individual calibration plots used to assess F-Na HPLC assay precision

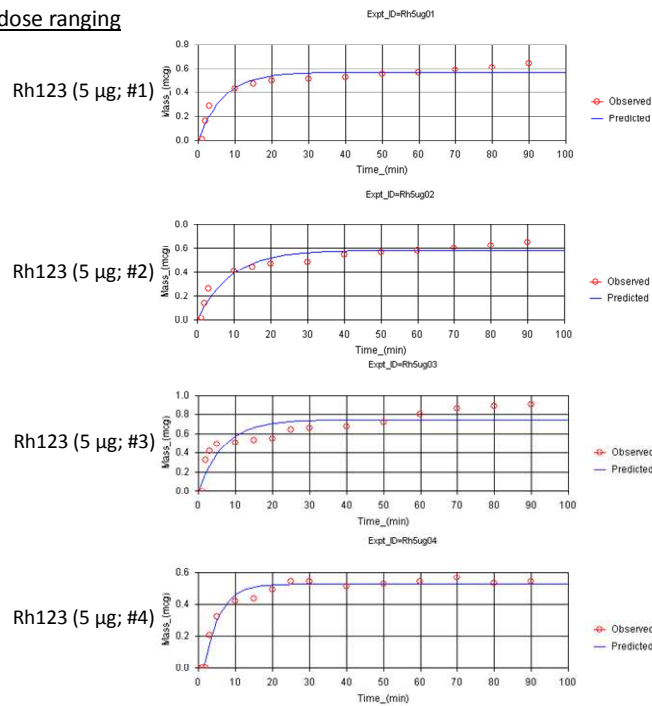
**Chapter 4: Functional significance of a drug transporter on instilled substrates to the IPRL**

Individual nonlinear regression plots for IPRL substrate transport data

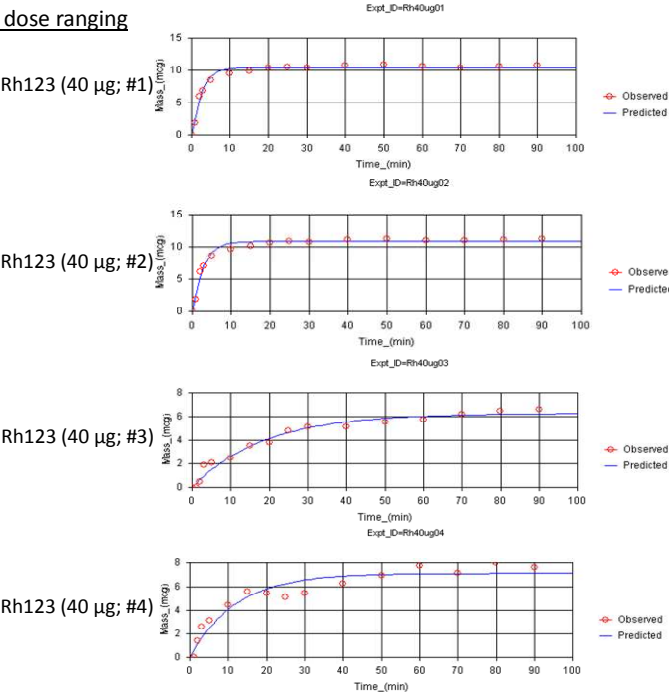
Rh123 dose ranging



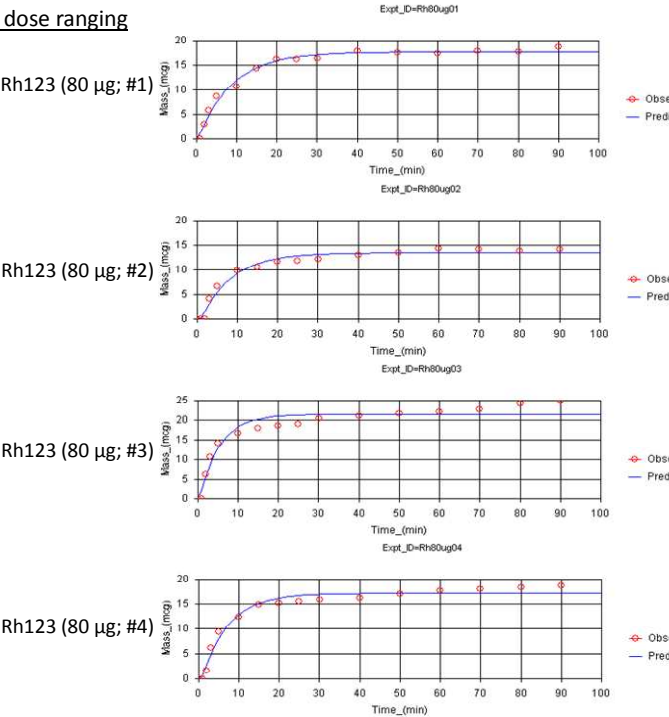
Rh123 dose ranging



Rh123 dose ranging

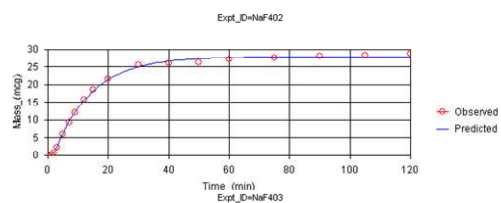


Rh123 dose ranging

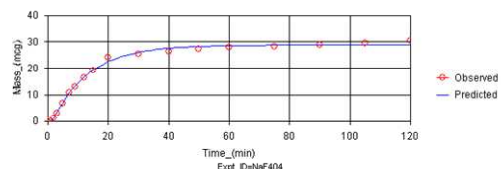


F-Na dose ranging

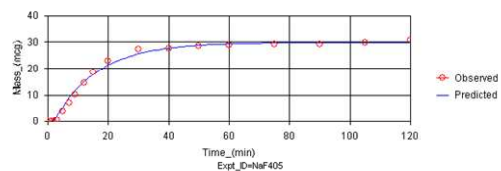
F-Na (40 µg; #2)



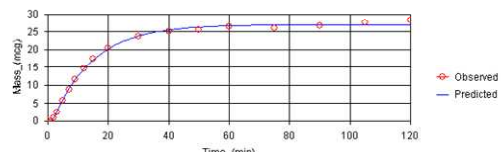
F-Na (40 µg; #3)



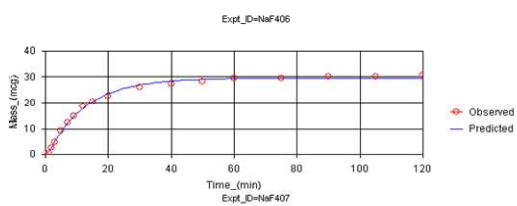
F-Na (40 µg; #4)



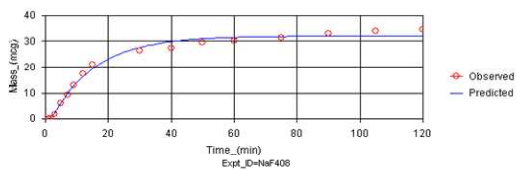
F-Na (40 µg; #5)

F-Na dose ranging

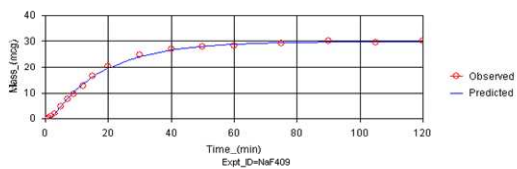
F-Na (40 µg; #6)



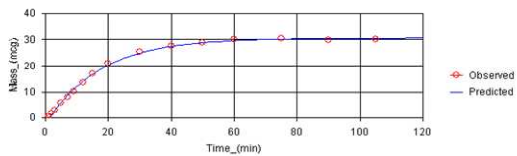
F-Na (40 µg; #7)

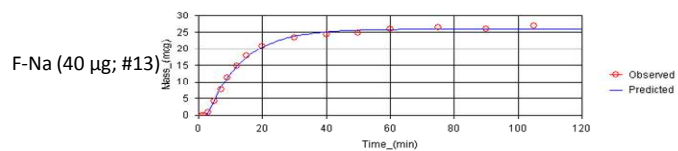
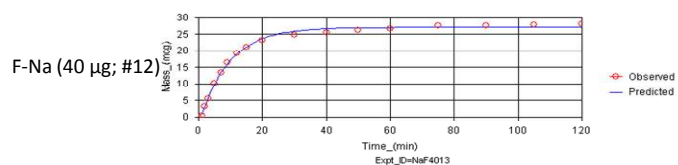
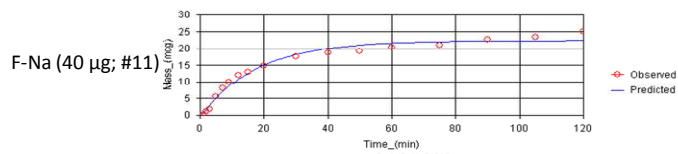
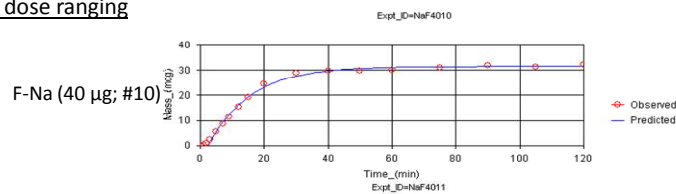
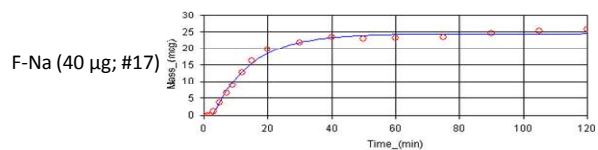
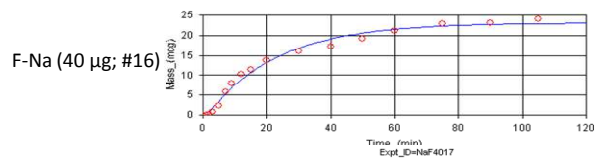
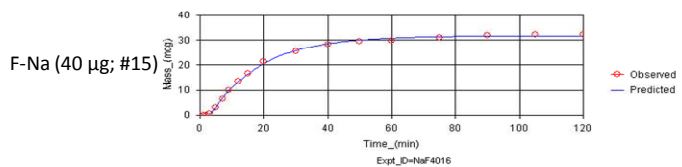
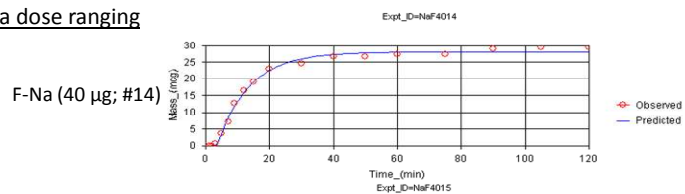


F-Na (40 µg; #8)



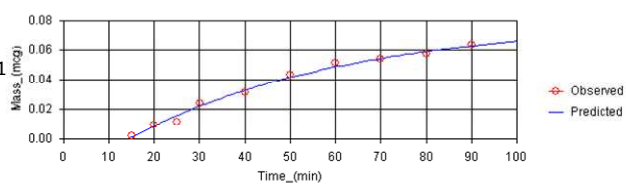
F-Na (40 µg; #9)



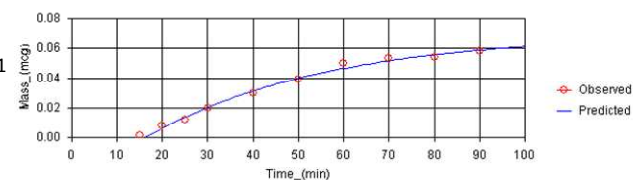
F-Na dose rangingF-Na dose ranging

Rh123 +/- GF120918 co-instilled and in perfusate

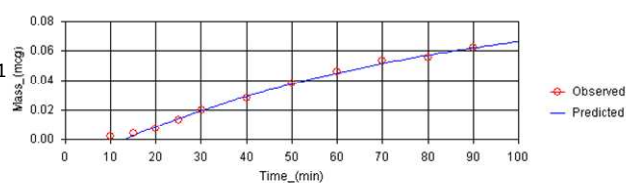
Expt_ID=Rh+DMSO2

Rh123 (2 μ g + 0.1
% DMSO; #2)

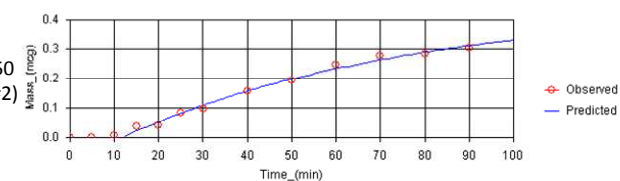
Expt_ID=Rh+DMSO3

Rh123 (2 μ g + 0.1
% DMSO; #3)

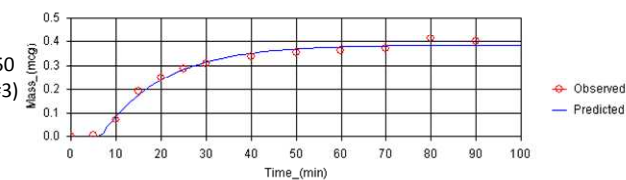
Expt_ID=Rh+DMSO4

Rh123 (2 μ g + 0.1
% DMSO; #4)Rh123 +/- GF120918 co-instilled and in perfusate

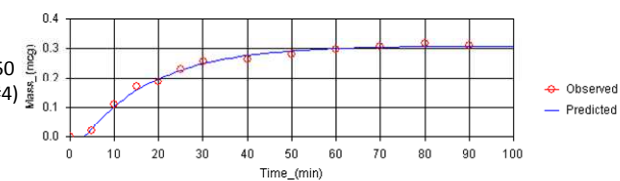
Expt_ID=RhG1502

Rh123 (2 μ g + 150
nM GF120918; #2)

Expt_ID=RhG1503

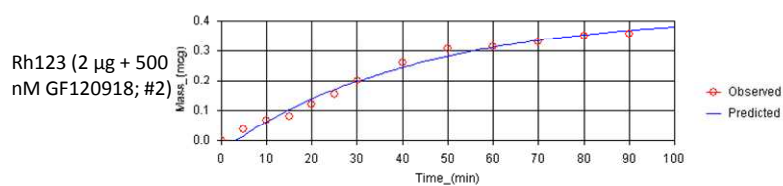
Rh123 (2 μ g + 150
nM GF120918; #3)

Expt_ID=RhG1504

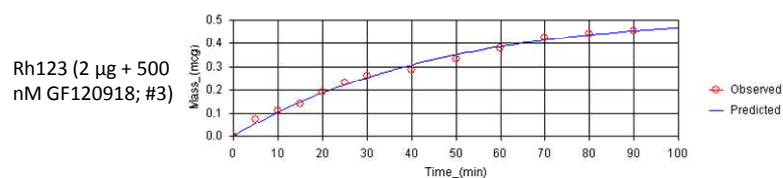
Rh123 (2 μ g + 150
nM GF120918; #4)

Rh123 +/- GF120918 co-instilled and in perfusate

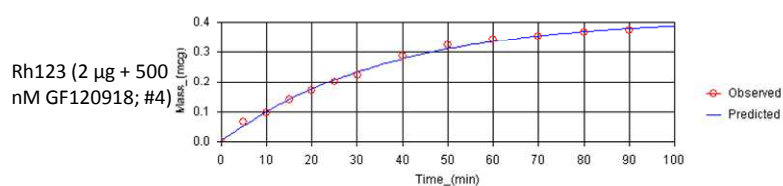
Expt_ID=RhGS002



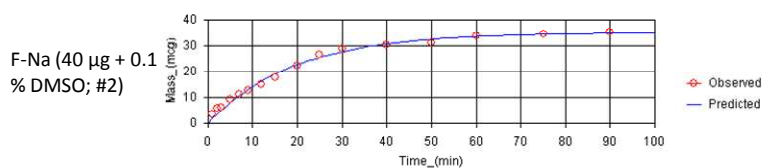
Expt_ID=RhGS003



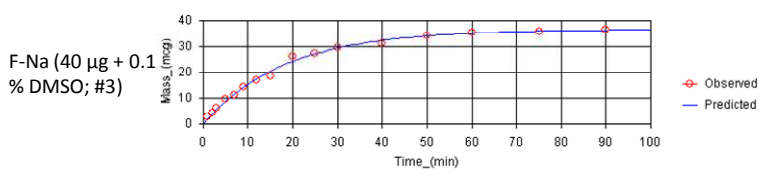
Expt_ID=RhGS004

F-Na +/- GF120918 co-instilled and in perfusate

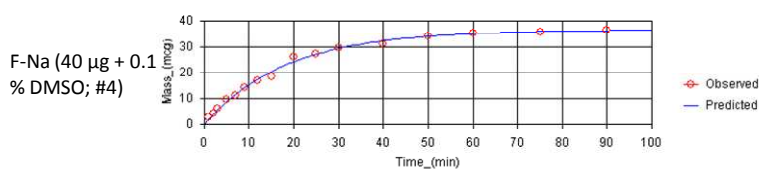
Expt_ID=FNadMSO2



Expt_ID=FNadMSO3

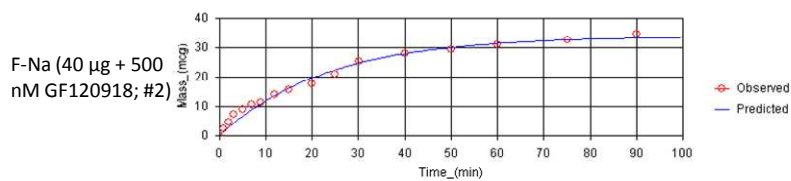


Expt_ID=FNadMSO4

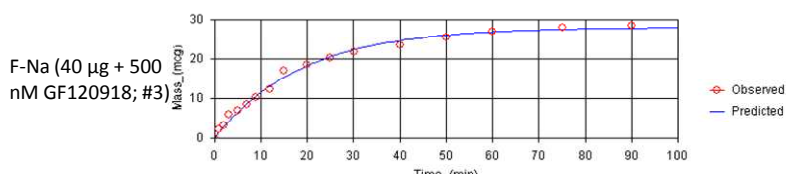


F-Na +/- GF120918 co-instilled and in perfusate

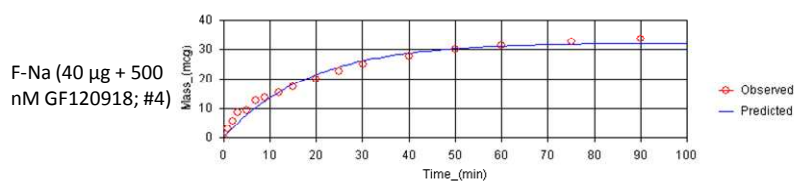
Expt_ID=FNaGF2



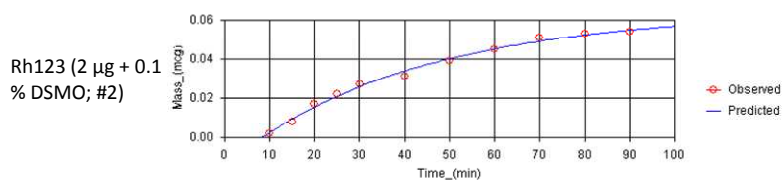
Expt_ID=FNaGF3



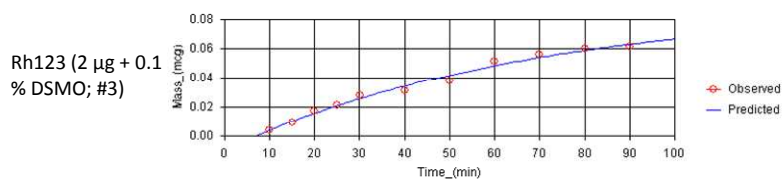
Expt_ID=FNaGF4

Rh123 +/- GF120918 co-instilled only

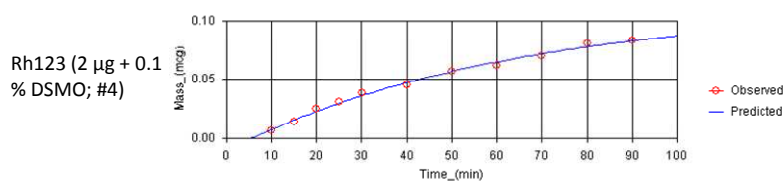
Expt_ID=Rh+DMSO2



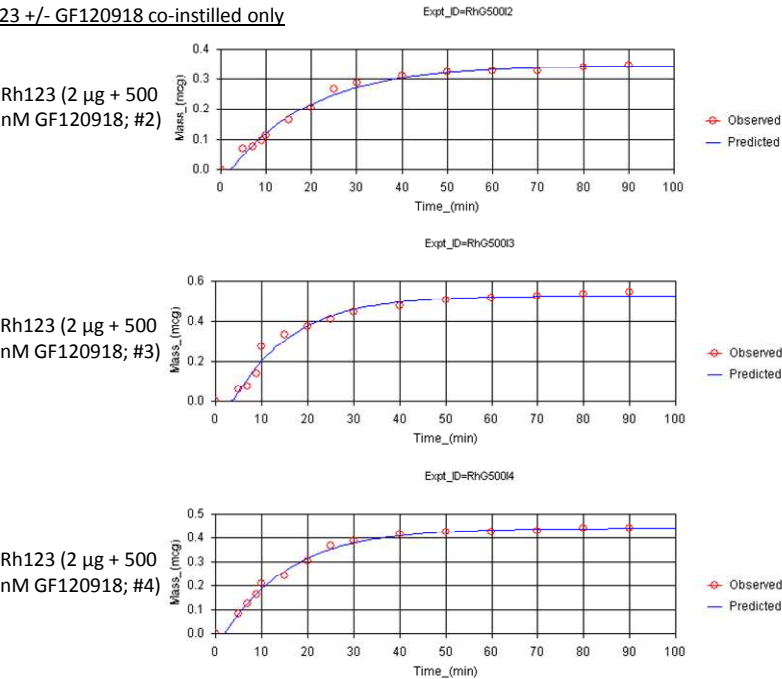
Expt_ID=Rh+DMSO3



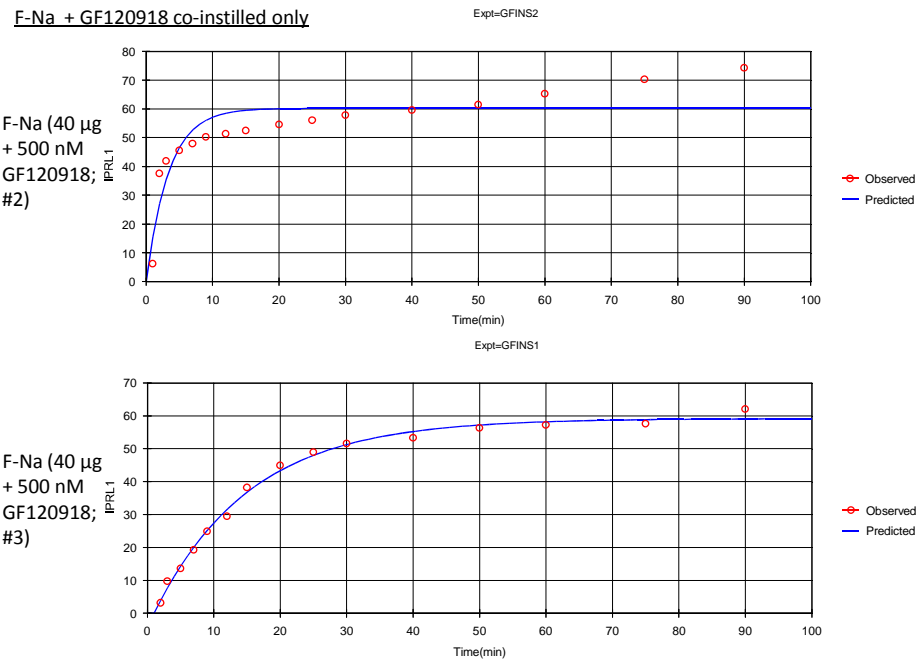
Expt_ID=Rh+DMSO4



Rh123 +/- GF120918 co-instilled only

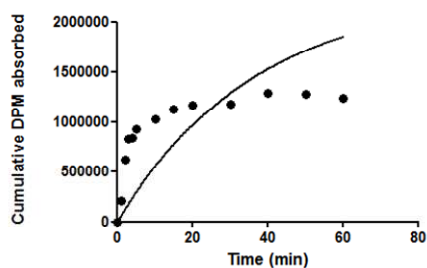


F-Na + GF120918 co-instilled only

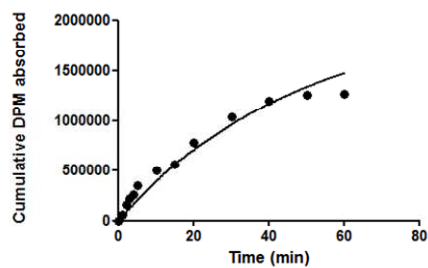


Digoxin +/- GF120918 co-instilled
and in IPRL perfusate

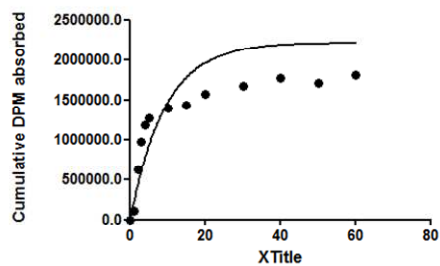
Digoxin + 0.1
% DMSO; #2



Digoxin + 0.1 %
DMSO; #3

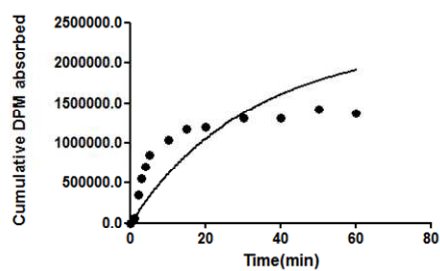


Digoxin + 0.1 %
DMSO; #4

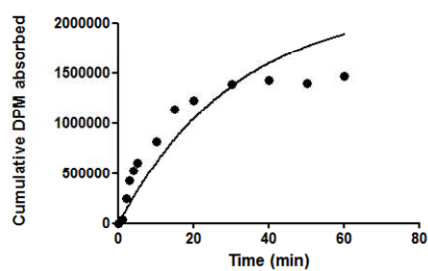


Digoxin +/- GF120918 co-
instilled and in IPRL perfusate

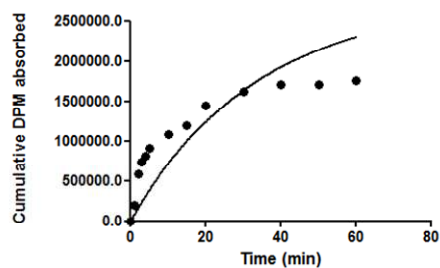
Digoxin + 500 nM
GF120918; #2



Digoxin + 500 nM
GF120918; #3

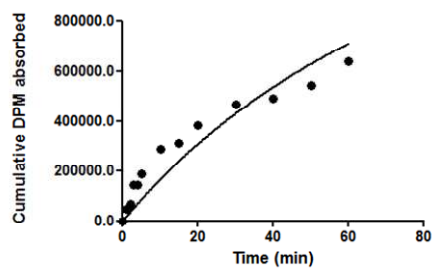


Digoxin + 500 nM
GF120918; #4

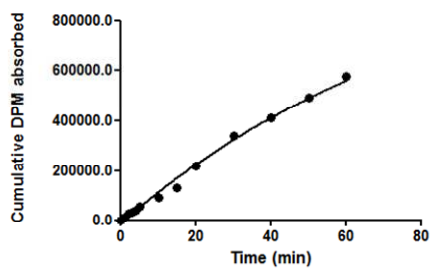


Mannitol +/- GF120918 co-
instilled and in IPRL perfusate

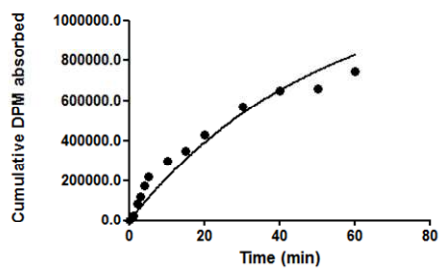
Mannitol + 0.1
% DMSO; #2



Mannitol + 0.1
% DMSO; #3

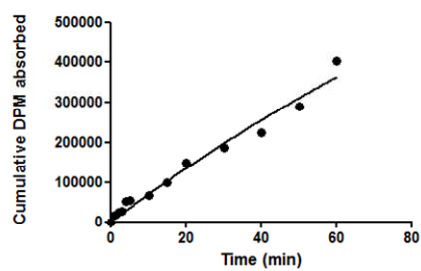


Mannitol + 0.1
% DMSO; #4

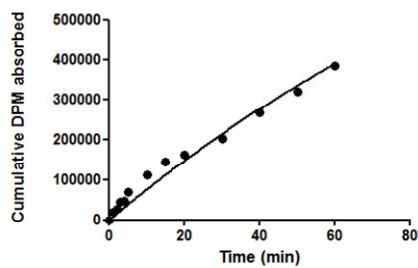


Mannitol +/- GF120918 co-
instilled and in IPRL perfusate

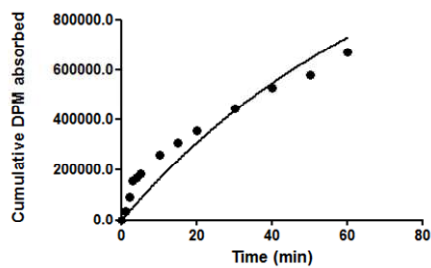
Mannitol +
500 nM
GF120918; #2



Mannitol +
500 nM
GF120918; #3

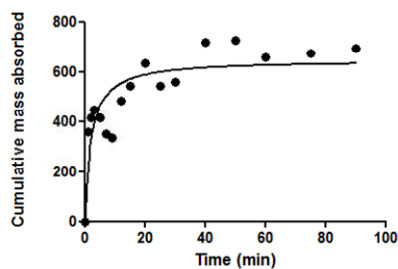


Mannitol +
500 nM
GF120918; #4

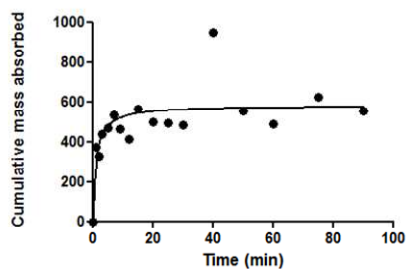


Flunisolide +/- GF120918 co-
instilled and in IPRL perfusate

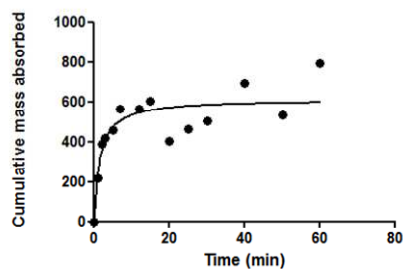
Flunisolide +
0.1 % DMSO;
#2



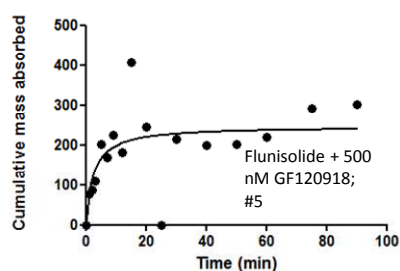
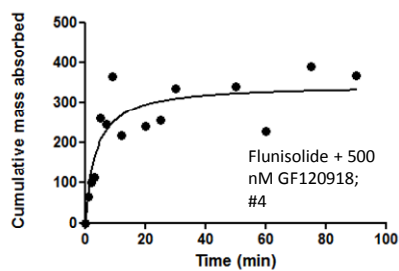
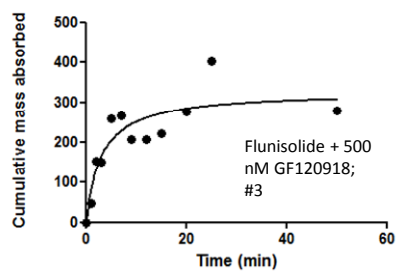
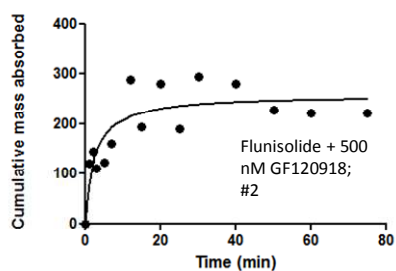
Flunisolide +
0.1 % DMSO;
#3



Flunisolide +
0.1 % DMSO;
#4



Flunisolide +/- GF120918 co-instilled and in IPRL perfusate

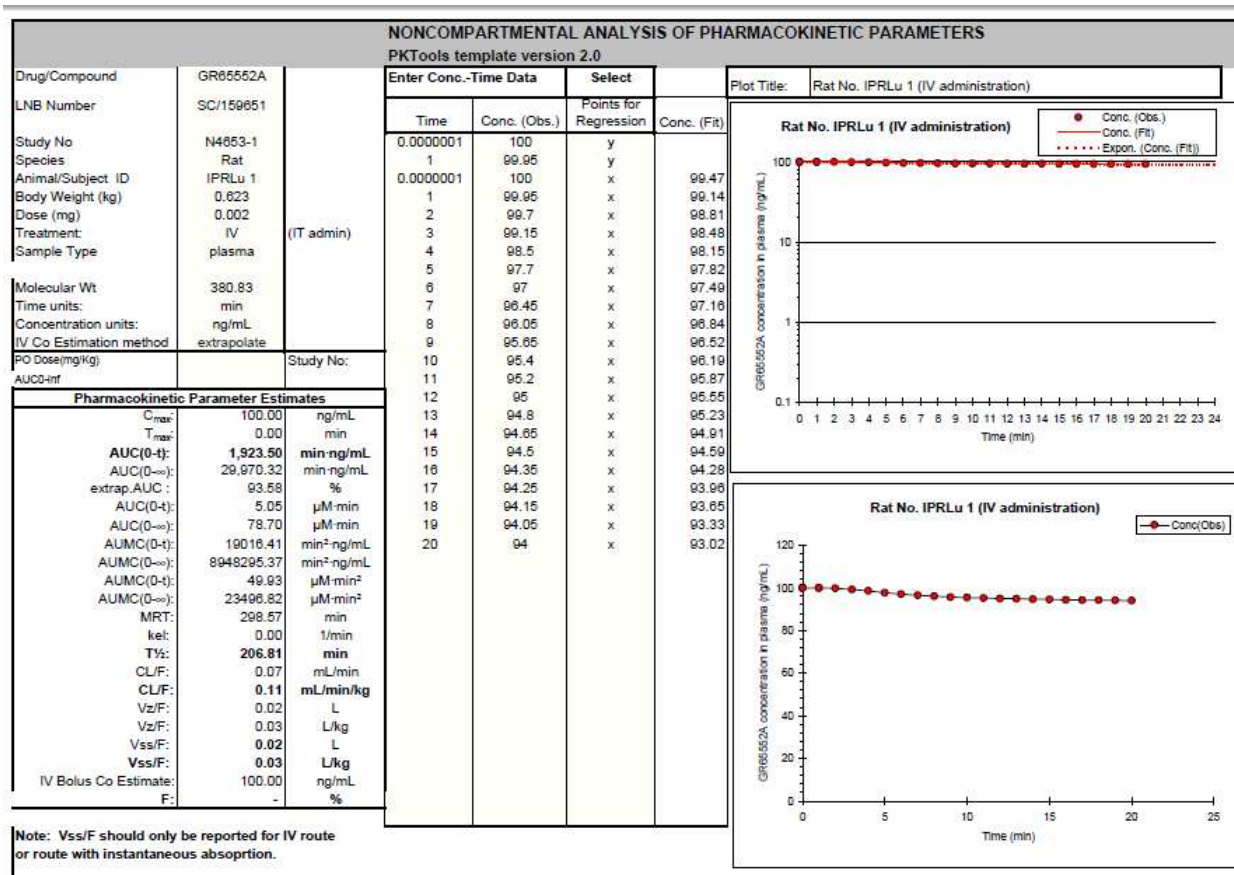


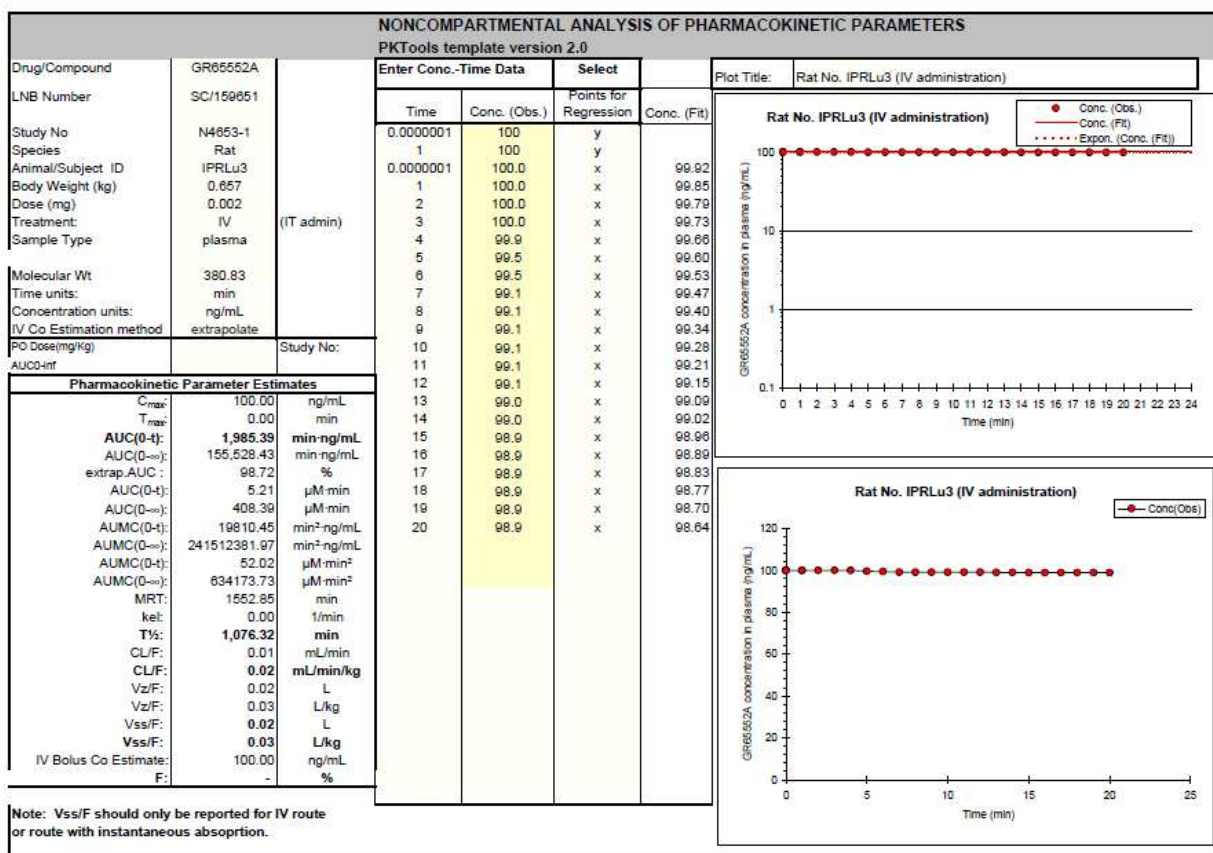
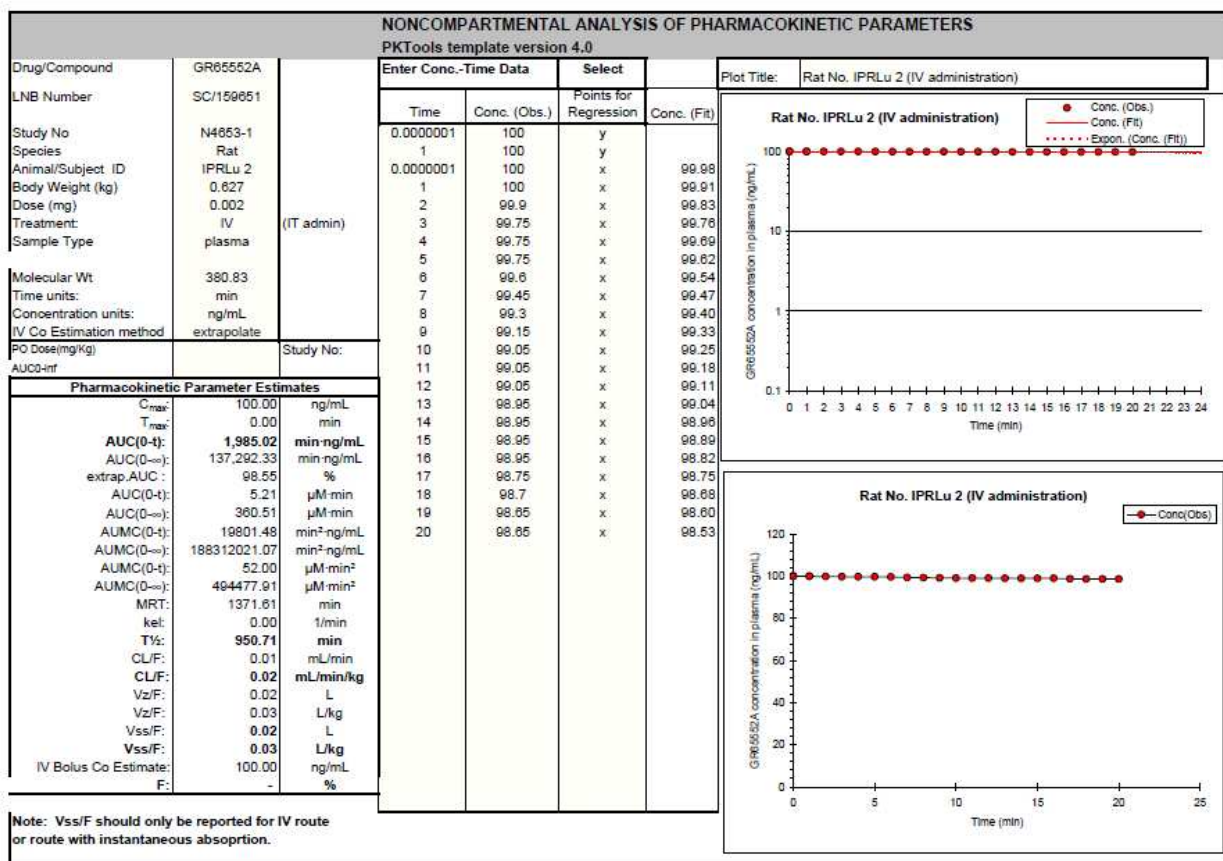
Appendix iii

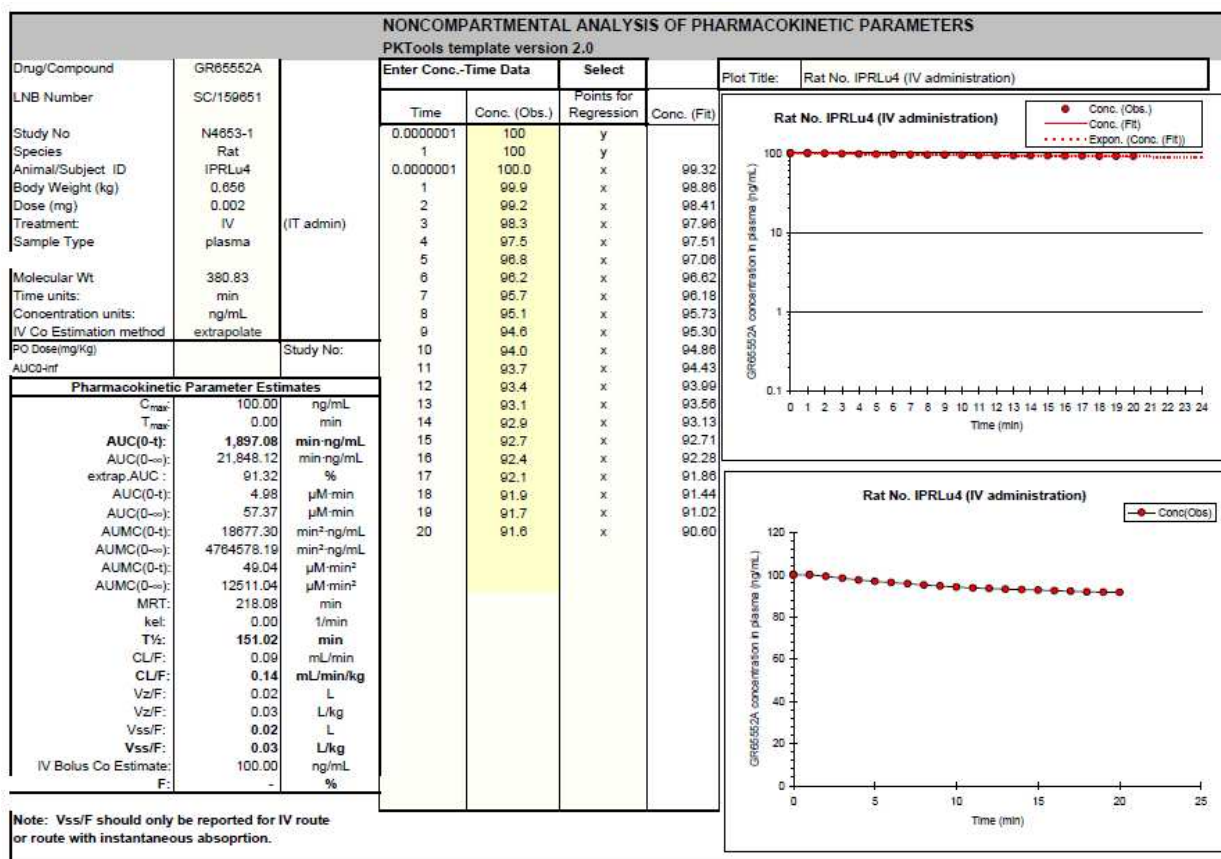
Chapter 6: Functional significance of drug transporters in a first-pass IPRL

Individual PKTools output for data generated using the first-pass IPRL

Noncompartmental analysis of experiment: Rh123 (2 µg dose) n=4

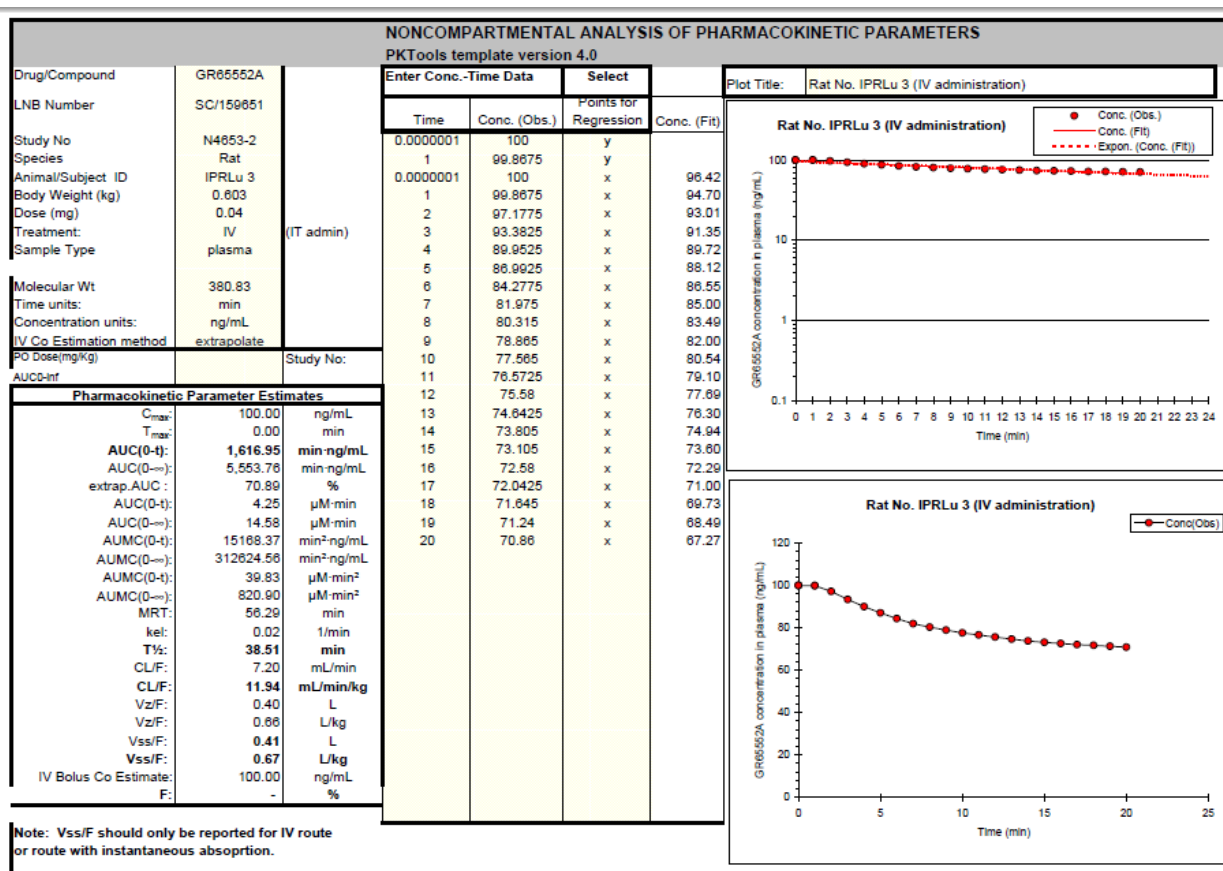
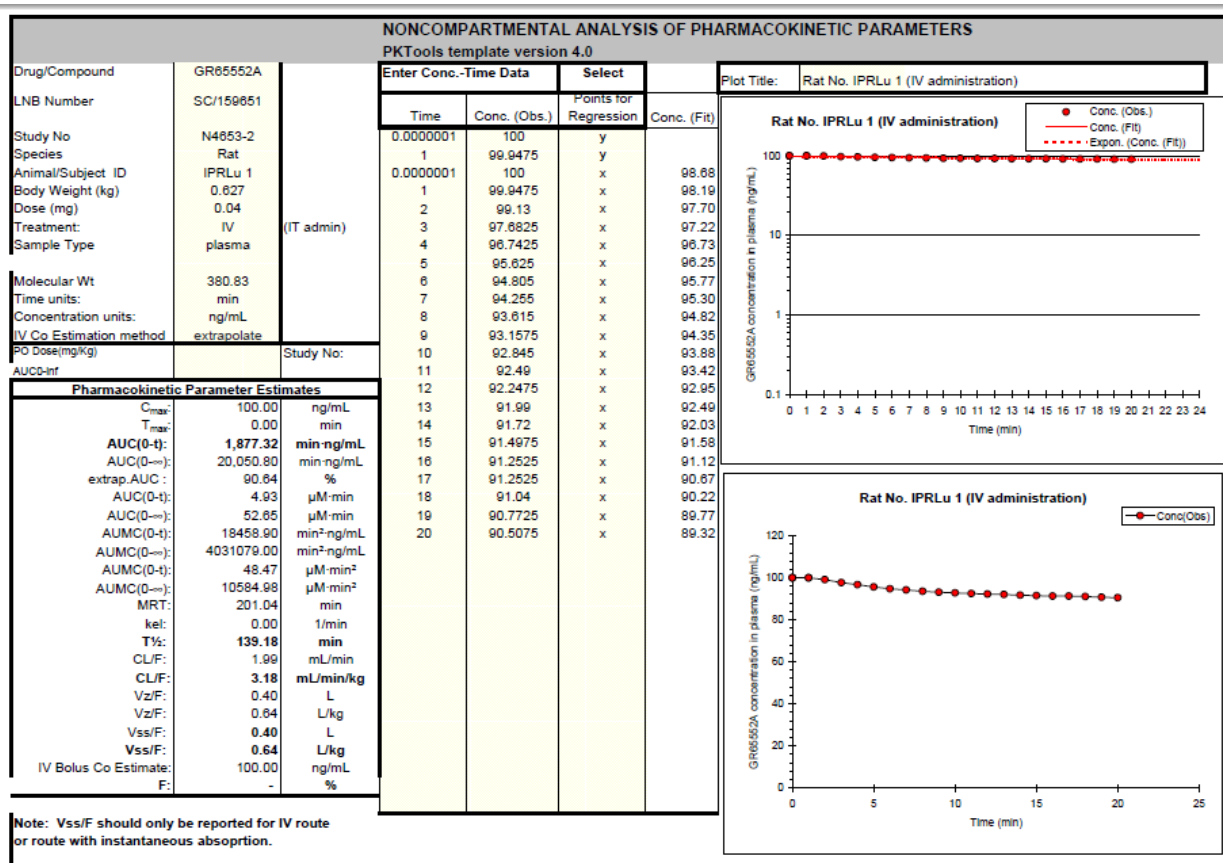


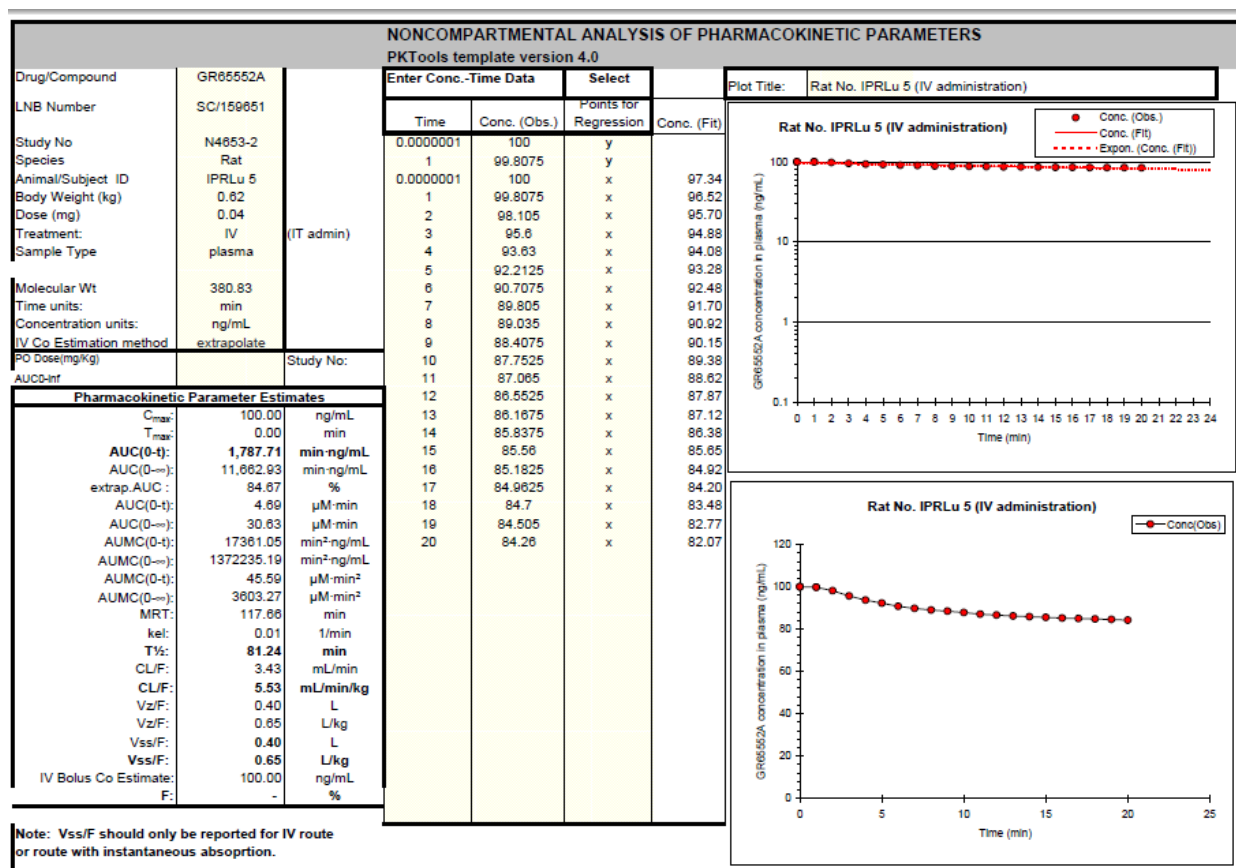
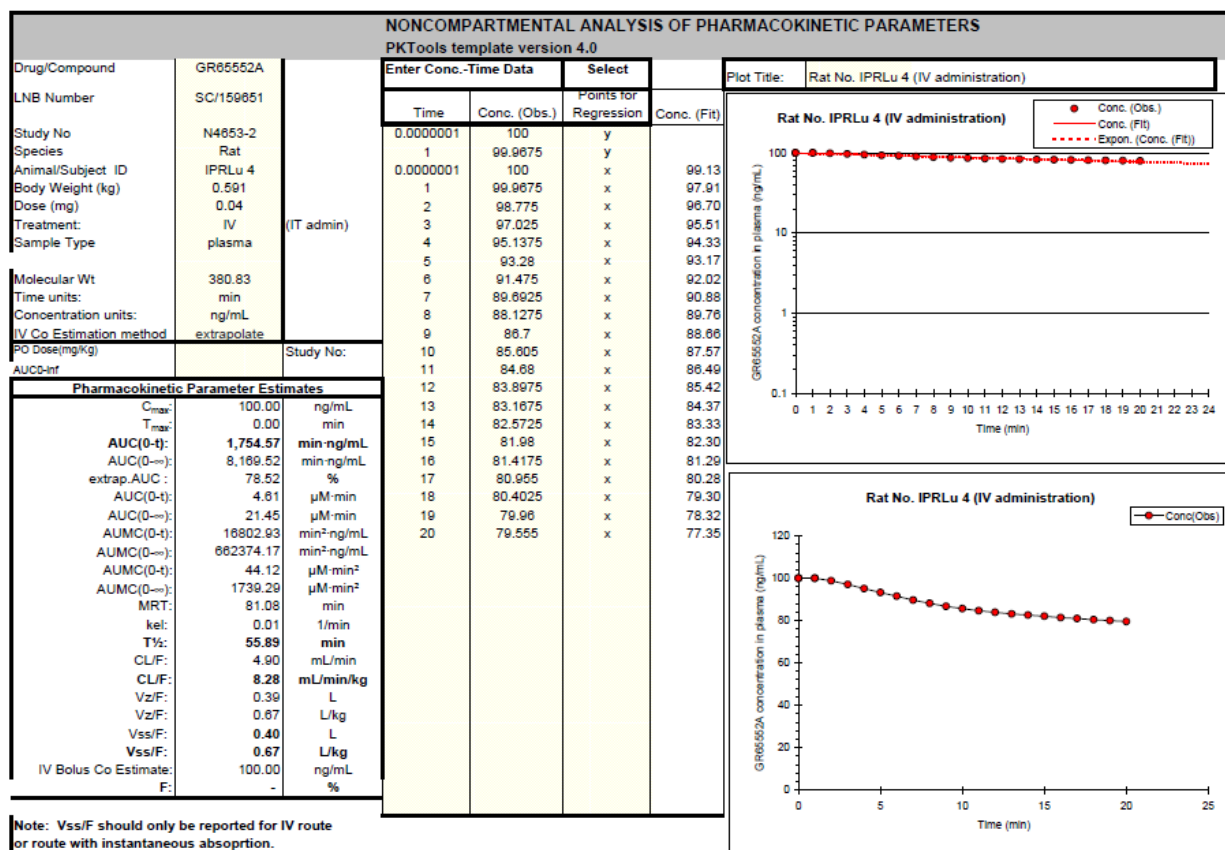




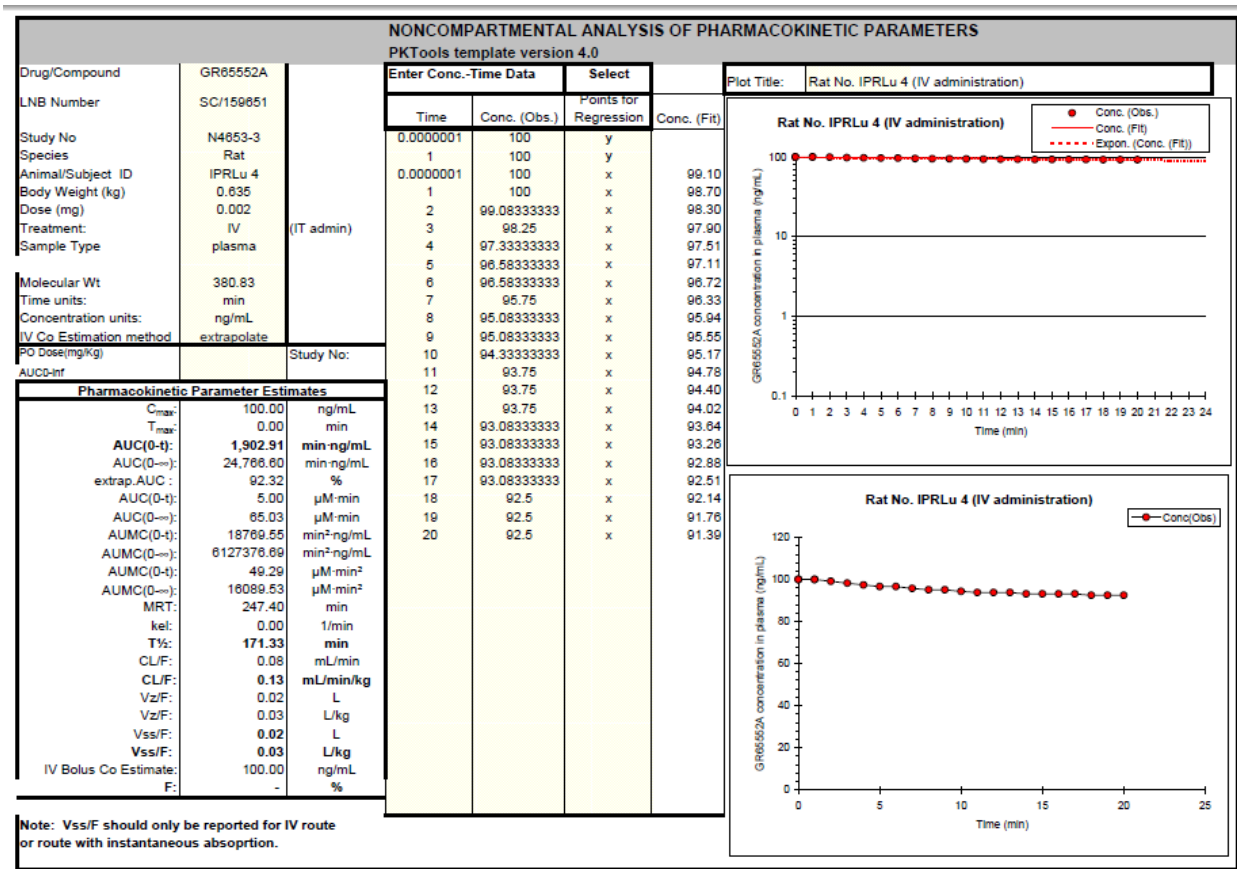
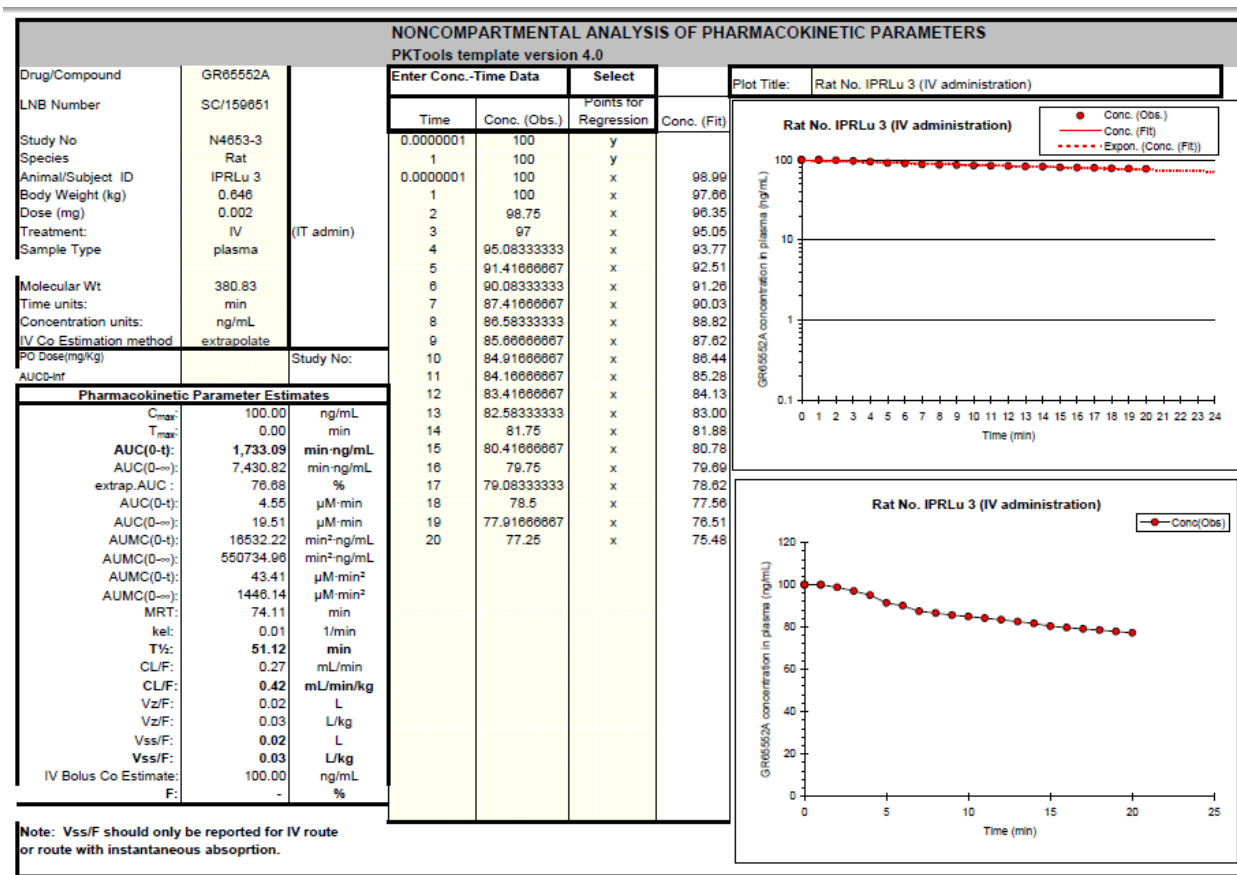
Noncompartmental analysis of experiment: Rh123 (40 μg dose)

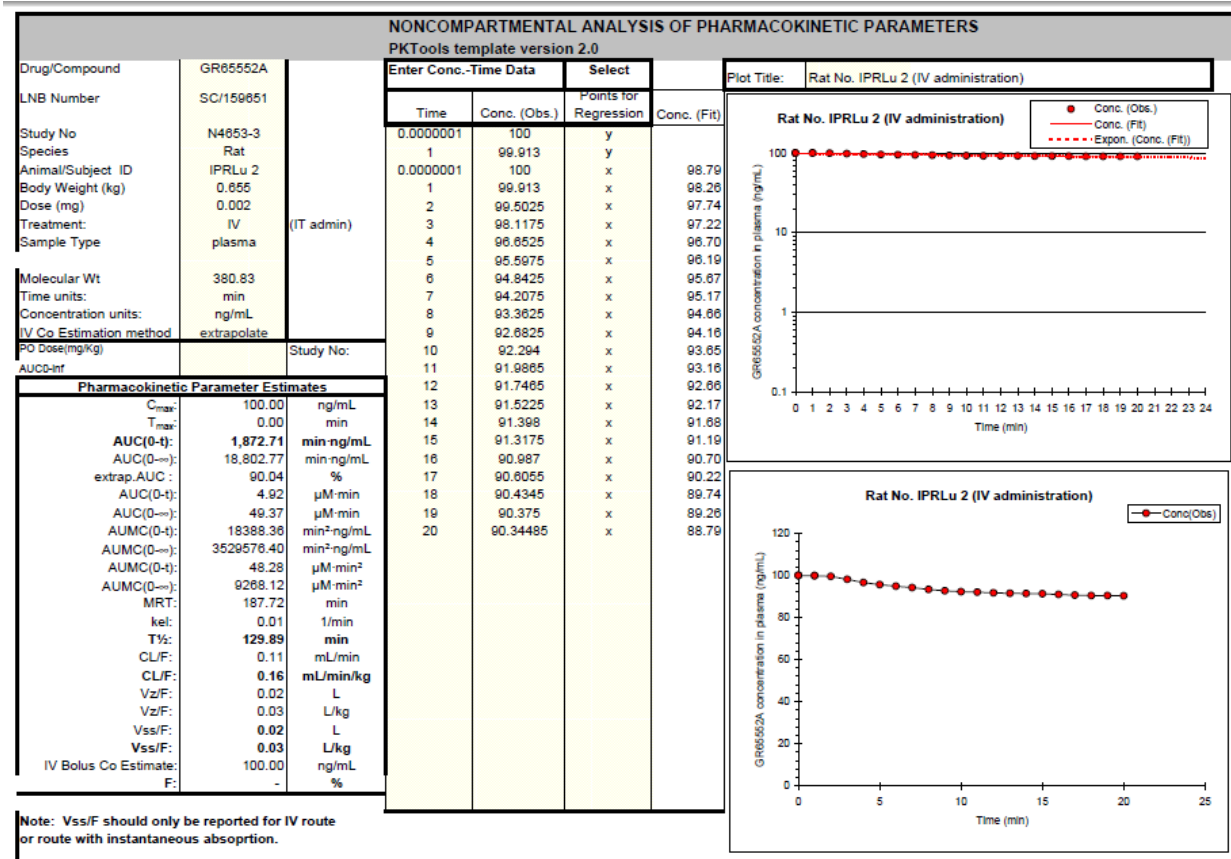
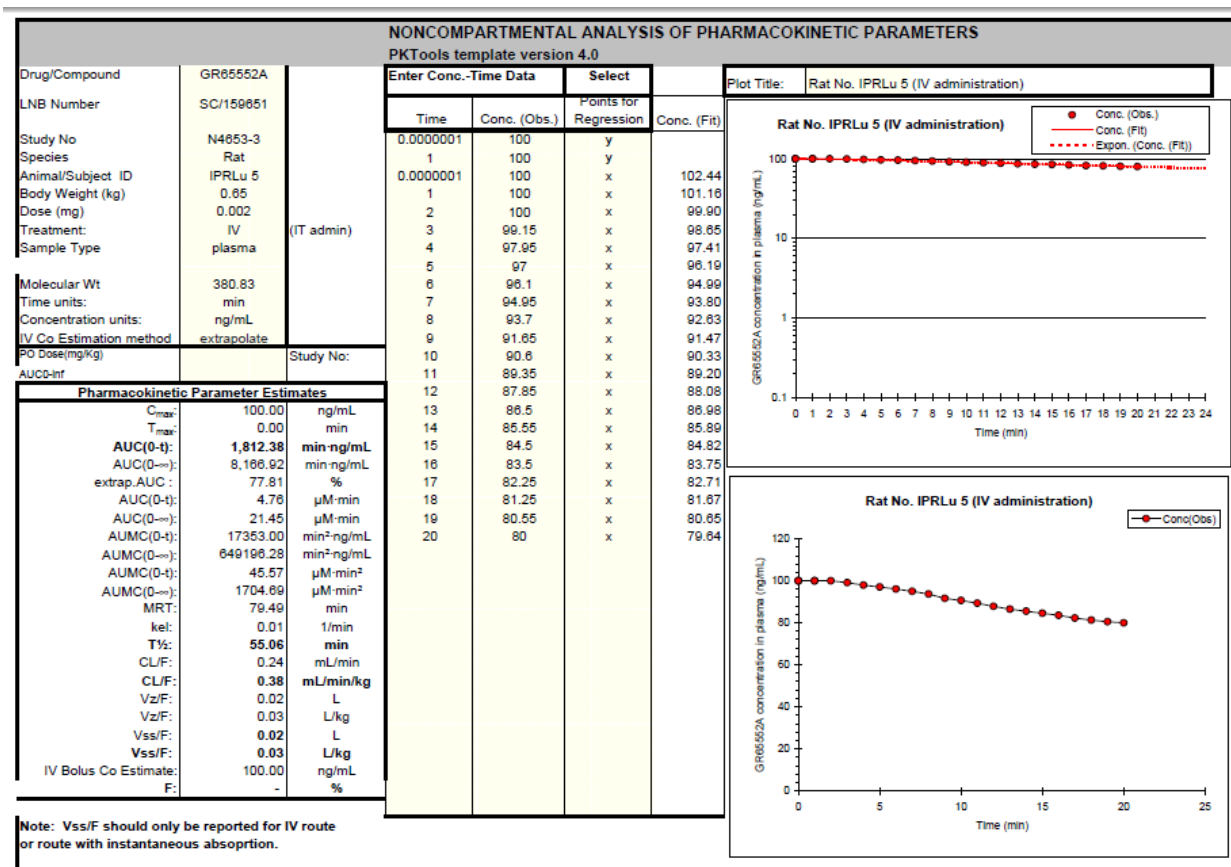
n=4





Noncompartmental analysis of experiment: Rh123 (2 μg dose)+ GF120918 n=4





Noncompartmental analysis of experiment: Flunisolide (2 µg dose) n=2

NONCOMPARTMENTAL ANALYSIS OF PHARMACOKINETIC PARAMETERS			
PKTools template version 2.0			
Drug/Compound	CCI18772		
LNB Number	SC/180270		
Study No	N5065-1		
Species	Rat		
Animal/Subject ID	IPRLu1		
Body Weight (kg)	0.72		
Dose (mg)	0.002		
Treatment:	IV	(IT admin)	
Sample Type	plasma		
Molecular Wt	434.509		
Time units:	min		
Concentration units:	ng/mL		
IV Co Estimation method	extrapolate		
PO Dose(mg/kg)			
AUC0-inf			
Pharmacokinetic Parameter Estimates			
C _{max} :	100.00	ng/mL	
T _{max} :	0.00	min	
AUC(0-t):	850.57	min-ng/mL	
AUC(0-∞):	1,477.11	min-ng/mL	
extrap.AUC:	42.42	%	
AUC(0-t):	1.96	μM-min	
AUC(0-∞):	3.40	μM-min	
AUMC(0-t):	8674.58	min ² -ng/mL	
AUMC(0-∞):	32233.61	min ² -ng/mL	
AUMC(0-t):	16.05	μM-min ²	
AUMC(0-∞):	74.18	μM-min ²	
MRT:	21.82	min	
k _{el} :	0.05	1/min	
T _{1/2} :	14.08	min	
CL/F:	1.35	mL/min	
CL/F:	1.88	mL/min/kg	
Vz/F:	0.03	L	
Vz/F:	0.04	L/kg	
Vss/F:	0.03	L	
Vss/F:	0.04	L/kg	
IV Bolus Co Estimate:	100.00	ng/mL	
F:	-	%	

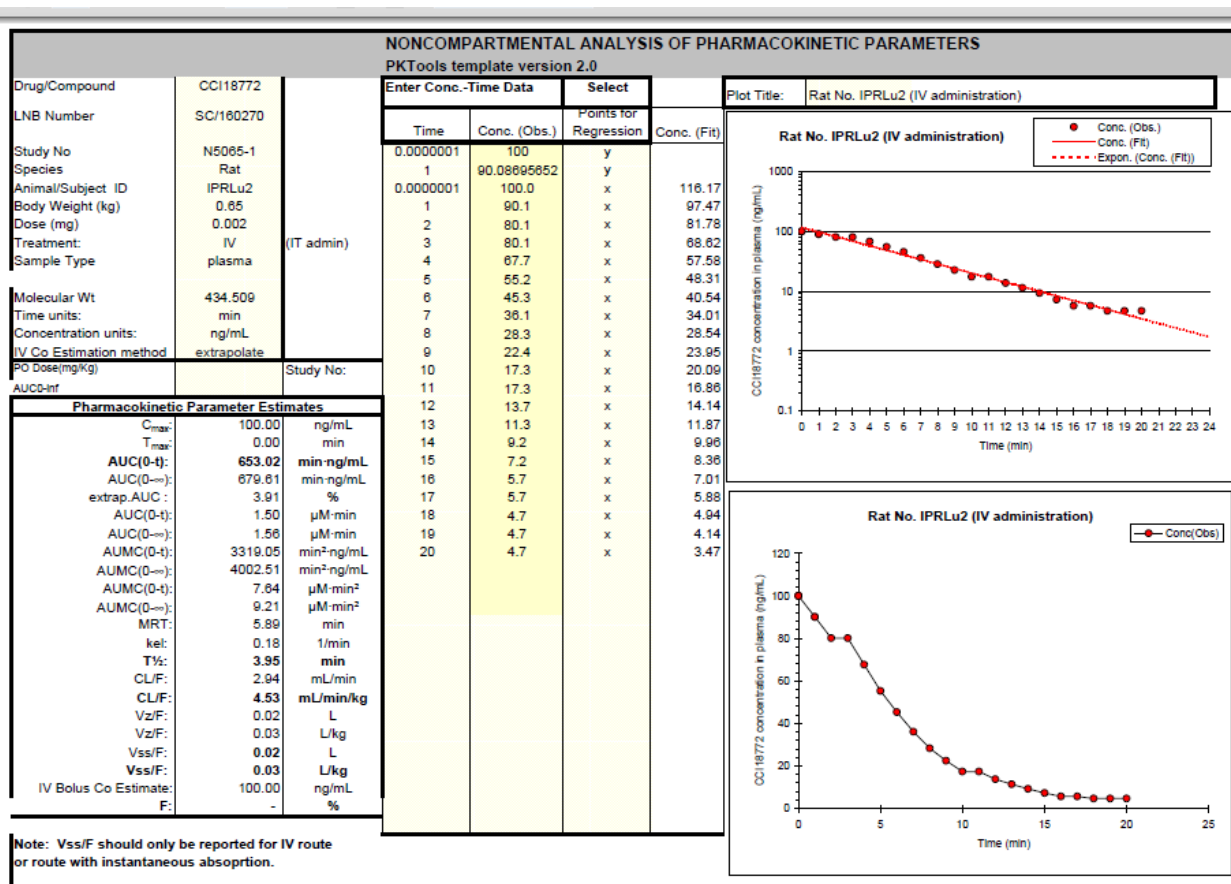
Enter Conc.-Time Data	Select	
Time	Conc. (Obs.)	Points for Regression
0.0000001	100	y
1	85.44827538	y
0.0000001	100.0	x
1	85.4	x
2	87.2	x
3	55.8	x
4	48.9	x
5	45.0	x
6	42.0	x
7	40.0	x
8	40.0	x
9	37.8	x
10	36.1	x
11	34.6	x
12	33.4	x
13	32.4	x
14	31.6	x
15	31.6	x
16	31.6	x
17	30.8	x
18	30.8	x
19	30.8	x
20	30.8	x

Conc. (Fit)	
66.89	
63.67	
60.62	
57.70	
54.93	
52.29	
49.78	
47.39	
45.12	
42.95	
40.89	
38.92	
37.05	
35.27	
33.58	
31.97	
30.43	
28.97	
27.58	
26.25	
24.99	

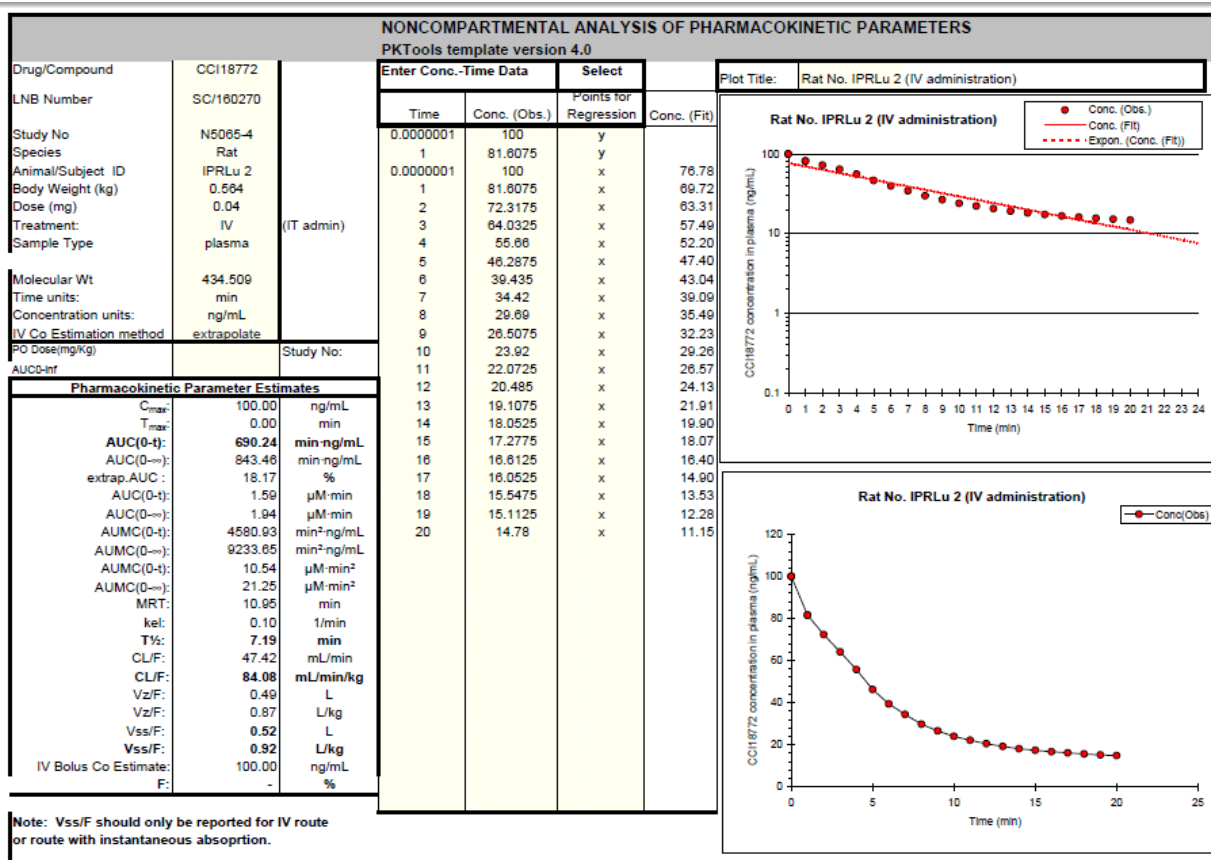
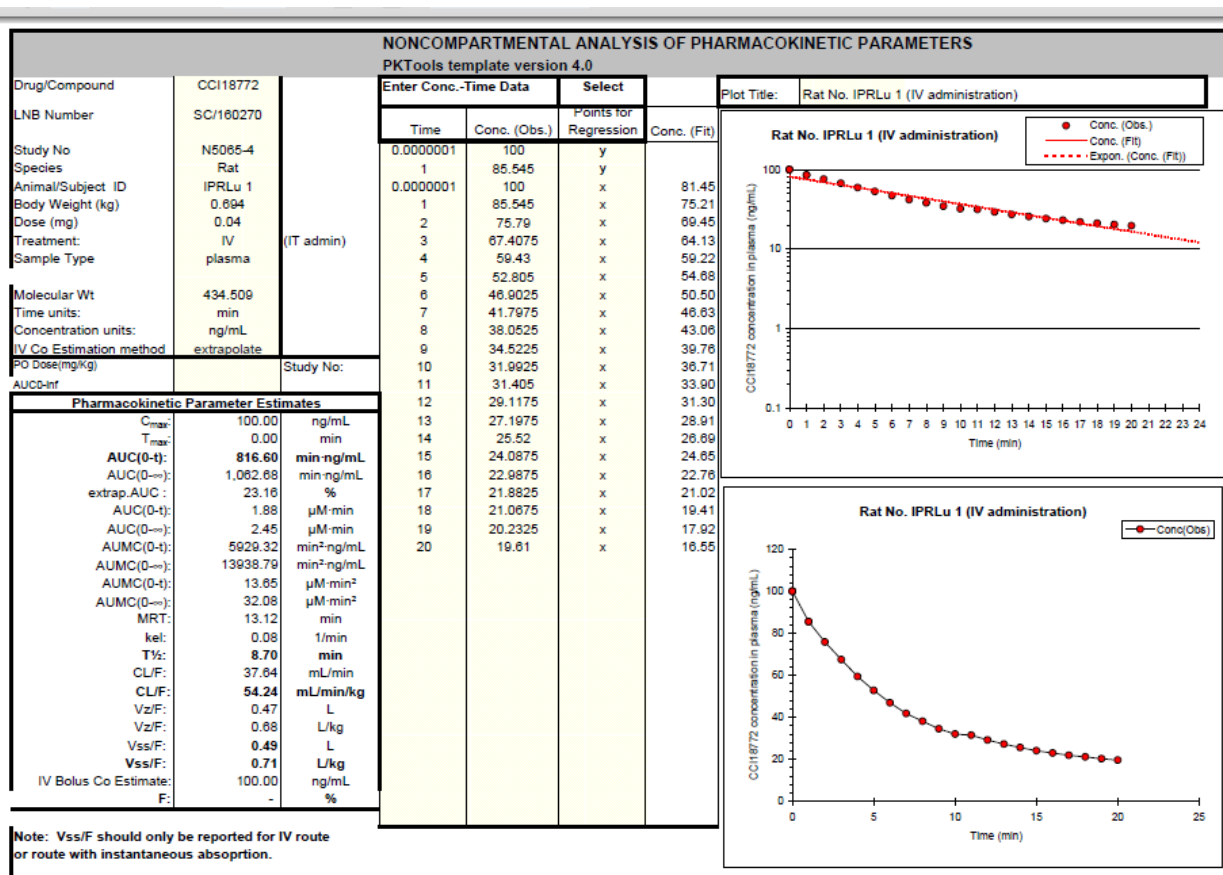
Plot Title:
Rat No. IPRLu1 (IV administration)

Plot Title:
Rat No. IPRLu1 (IV administration)

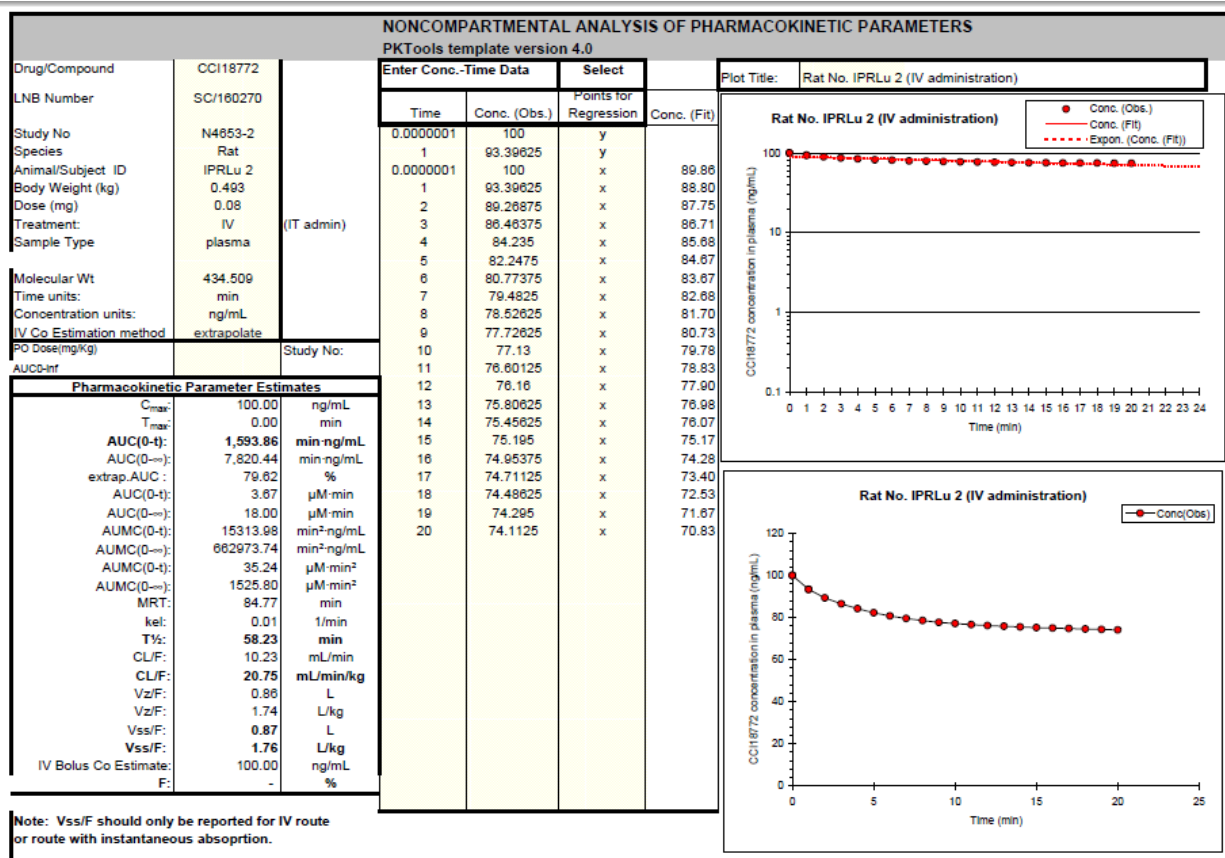
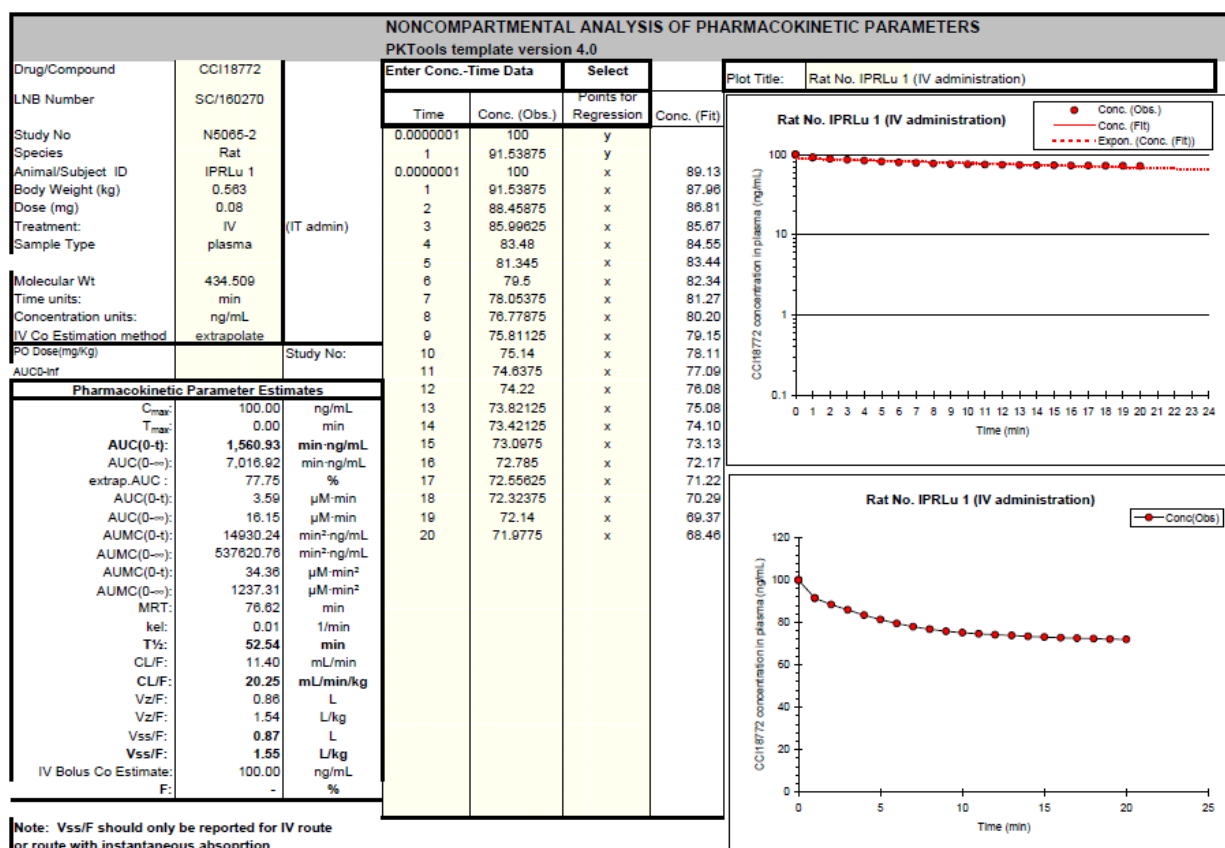
Note: Vss/F should only be reported for IV route or route with instantaneous absorption.



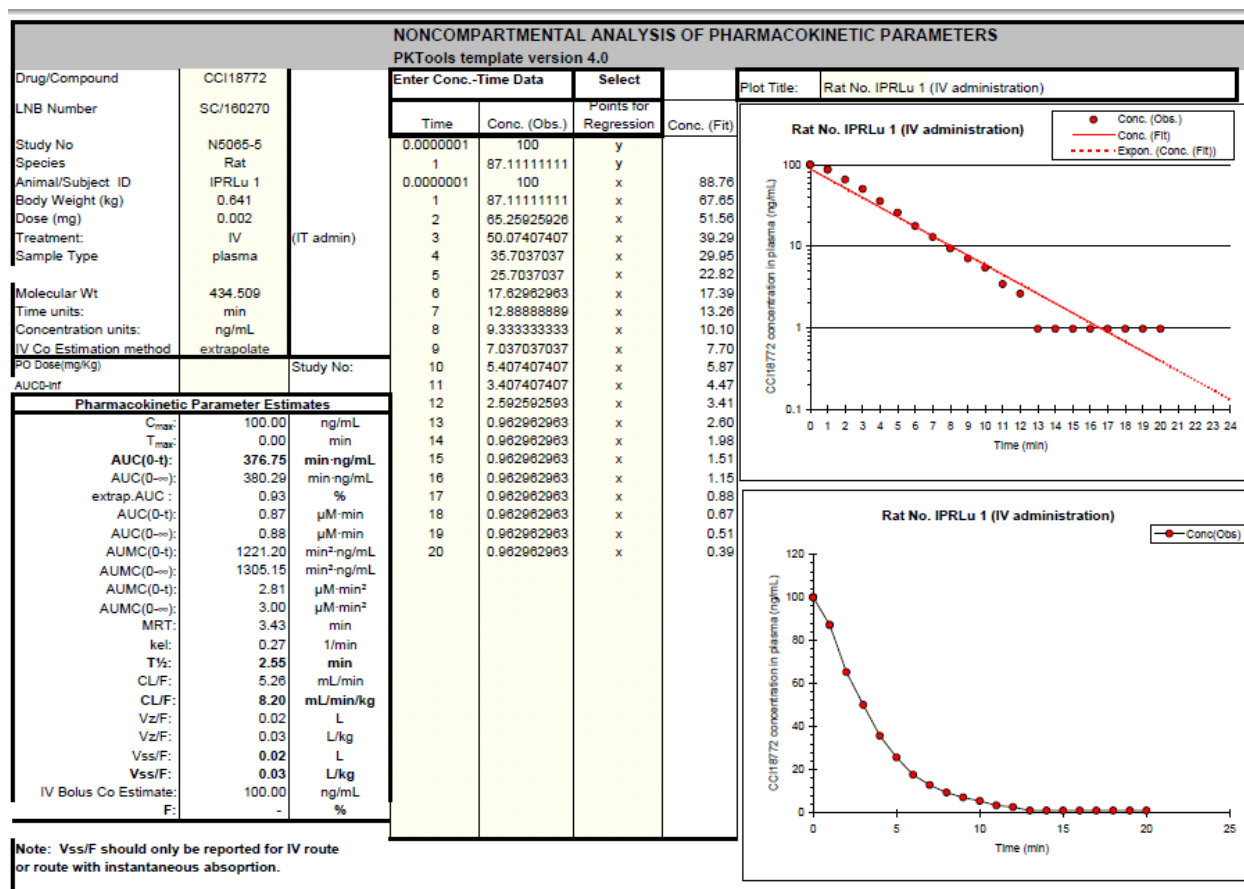
Noncompartmental analysis of experiment: Flunisolide (40 μg dose) n=2

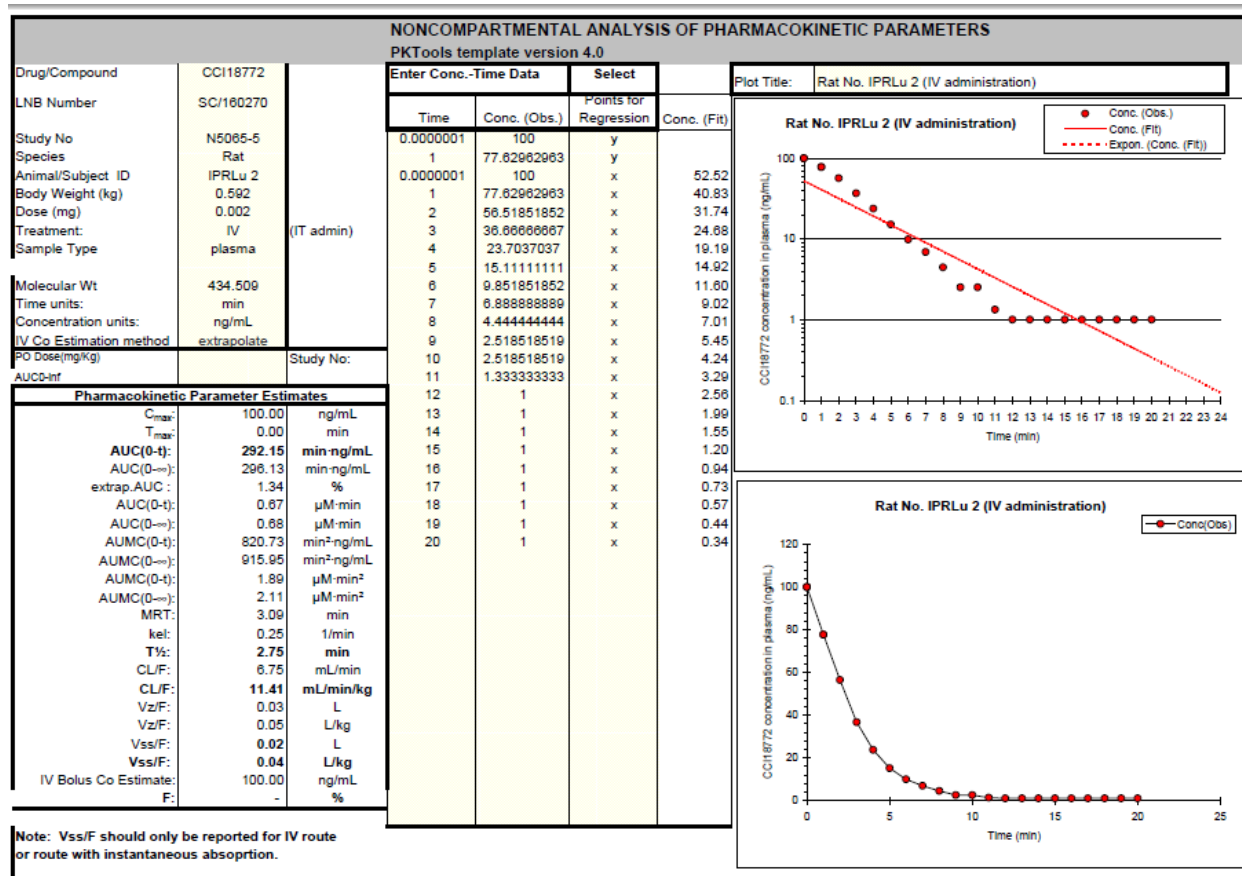


Noncompartmental analysis of experiment: Flunisolide (80 µg dose) n=2



Noncompartmental analysis of experiment: Flunisolide (2 µg dose) + GF120918 n=2





Complete Power analysis output – conducted at GSK

Power analysis of GSK Rh123 data

Conducted at GSK by L. Wallis



Aims and Objectives

To calculate the appropriate number of subjects required for the study to have adequate power. This will be done using AUC calculations as this is a convenient way to summarise data over various time points.

AUC data

The calculated AUC's are in the table below. I have excluded two sets of the data, the run on 21/9 pm, and also 12/10 am due to problems with the test and inconsistent results being produced. Including these would skew the results and make them unreliable.

Date	am/pm	surgeon	dose conc (µg/mL)	dose lung(µg)	dose transported AUC	dose remaining AUC
20/09/2007	am	PJB	20	2	76.5	1923.5
20/09/2007	pm	DF	20	2	14.9	1985
02/11/2007	am	DF	20	2	14.6	1985.4
02/11/2007	am	DF	20	2	102.9	1897.1
21/09/2007	am	DF	400	40	122.7	1877.3
26/10/2007	am	PJB	400	40	382.9	1617
26/10/2007	am	PJB	400	40	245.4	1754.6
07/11/2007	am	DF	400	40	212.3	1787.7
12/10/2007	pm	DF	20 + 500nM GF120918 inhibitor	2	127.3	1872.7
06/11/2007	am	DF	20 + 500nM GF120918 inhibitor	2	266.9	1733.1
06/11/2007	am	PJB	20 + 500nM GF120918 inhibitor	2	97.1	1902.9
07/11/2007	am	PJB	20 + 500nM GF120918 inhibitor	2	187.6	1812.4

For ease from here onwards I have referred to the dose groups by category, which I have named 'dose_conc' rather than specifying dose concentration and dose to lung every time.

dose conc (µg/mL)	dose lung(µg)	Dose_conc
20	2	1
400	40	2
20 + 500nM GF120918 inhibitor	2	3

For each of the dosage categories the mean and standard deviation was calculated and then used to produce power curves.

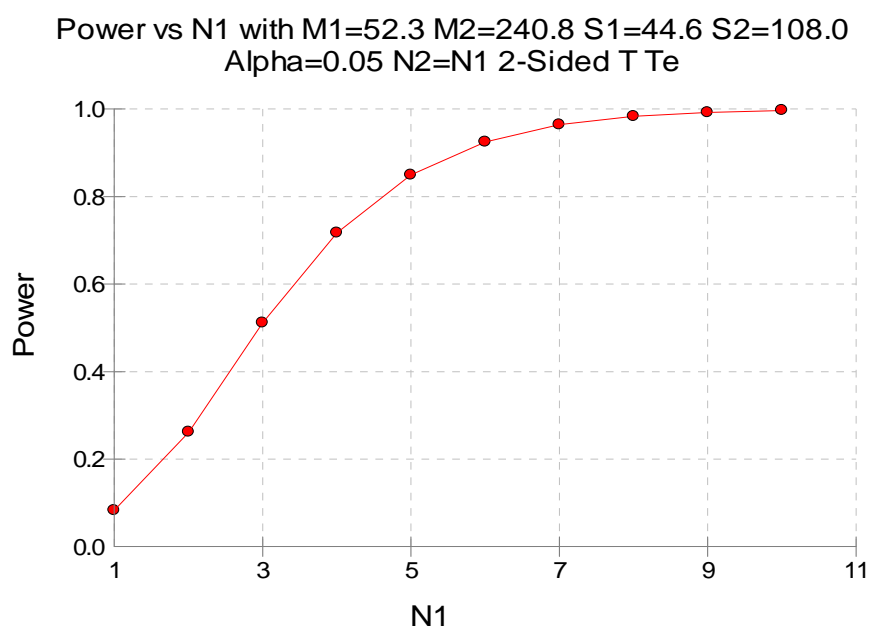
dose_conc	AUC	Mean	StdDev
1	dose transported AUC	52.2	44.6
2	dose transported AUC	240.8	108
3	dose transported AUC	169.7	74.9
1	dose remaining AUC	1947.8	44.6
2	dose remaining AUC	1759.2	108
3	dose remaining AUC	1830.3	74.9

Power Curves

Power curves are used to estimate how large the sample needs to be in order to make comparisons between groups. I have looked at the comparisons between dose groups 1 and 2, and also groups 1 and 3. The other possible comparison was to look at groups 2 and 3 but this isn't very useful and a direct comparison cannot be made.

Dose Transported

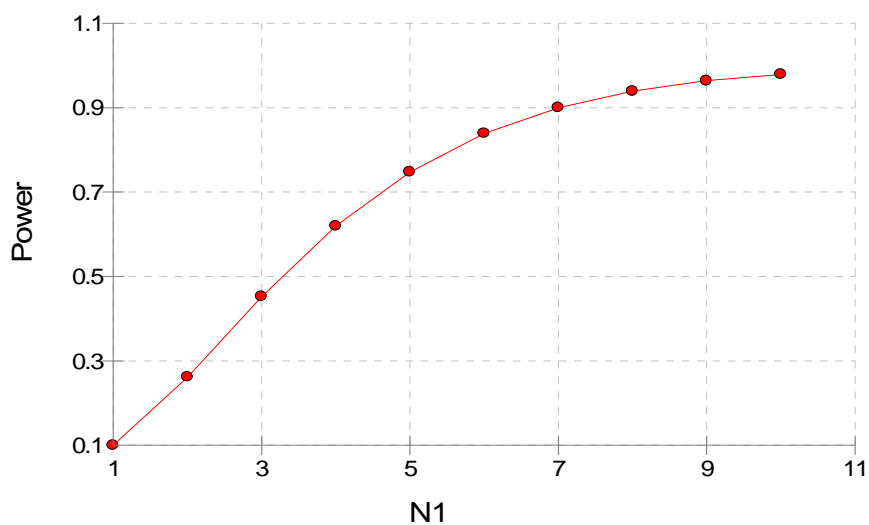
1v2



In order to compare dose categories 1 and 2 at 80% power you will need 5 animals, the same is true with comparing 1 and 3 for the dose transported data.

1v3

Power vs N1 with M1=52.3 M2=169.7 S1=44.6 S2=74.9
Alpha=0.05 N2=N1 2-Sided T Tes

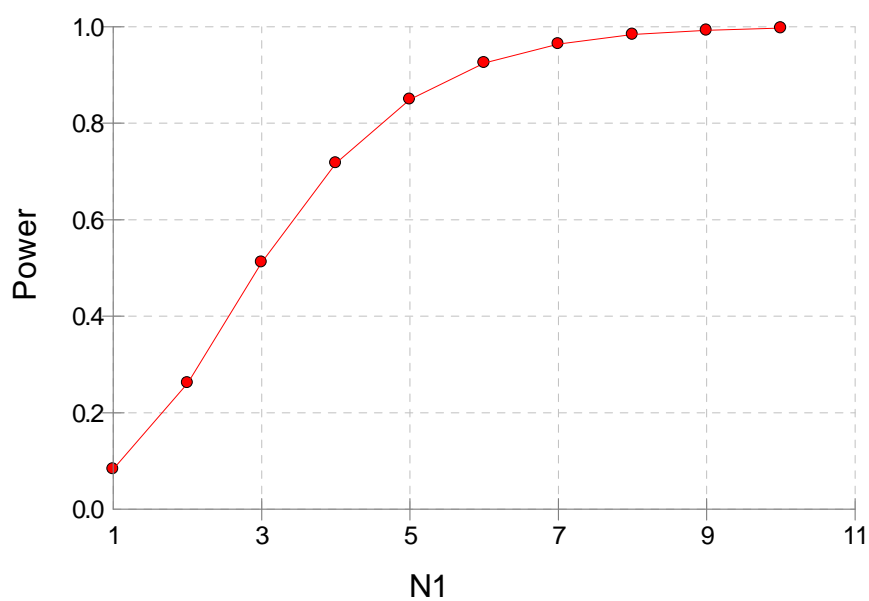


The same findings are true for the dose remaining data as well. There appears to be a high correlation in the data, and so is producing the same results. I do not feel it is necessary in future in analyse both data sets.

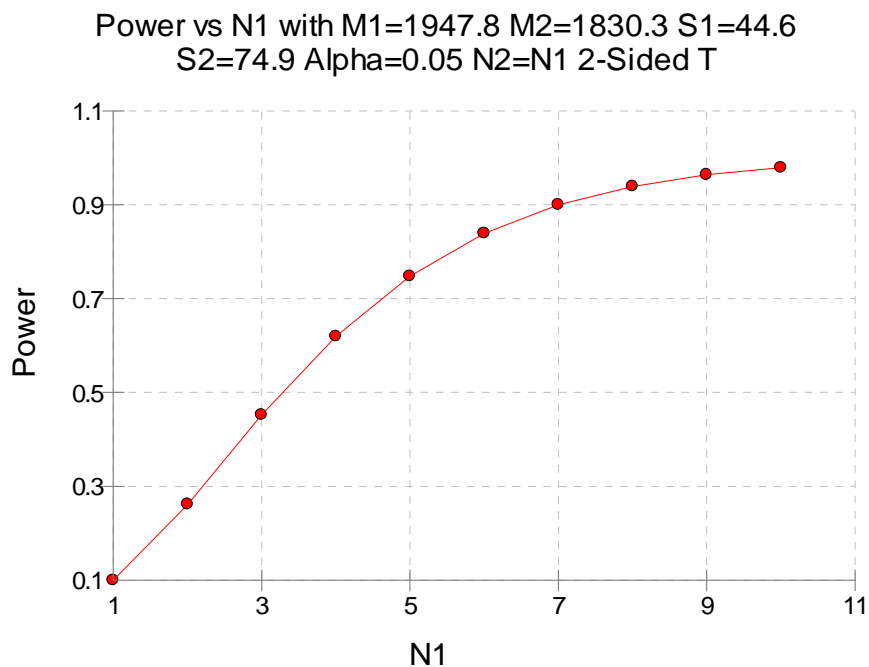
Dose Remaining

1v2

Power vs N1 with M1=1947.8 M2=1759.2 S1=44.6
S2=108.0 Alpha=0.05 N2=N1 2-Sided T



1v3



Conclusion

It is advisable to use a minimum sample size of 5 for the study. This will produce power of around 80% so will achieve reliable results.

Power analysis of Cardiff Rh123 dose-ranging data



Conducted at GSK by L. Wallis

Analysis Outline

To calculate the appropriate number of subjects required for the study to have adequate power. This will be done using AUC calculations as this is a convenient way to summarise data over various time points.

I am only looking at dose transported as we found previously that the two measurements yielded the same results.

AUC calculations

AUC is an estimate of the area under the curve. It is calculated using the trapezium rule. This splits up the curve into trapeziums and approximates the area by calculating the area of these.

For ease I have referred to the various treatments for the rest of the report by number.

Rh123 Dose Conc. (µg/mL)	Rh123 Dose to lung (µg)	Treatment
20	2	1
50	5	2
400	40	3
800	80	4

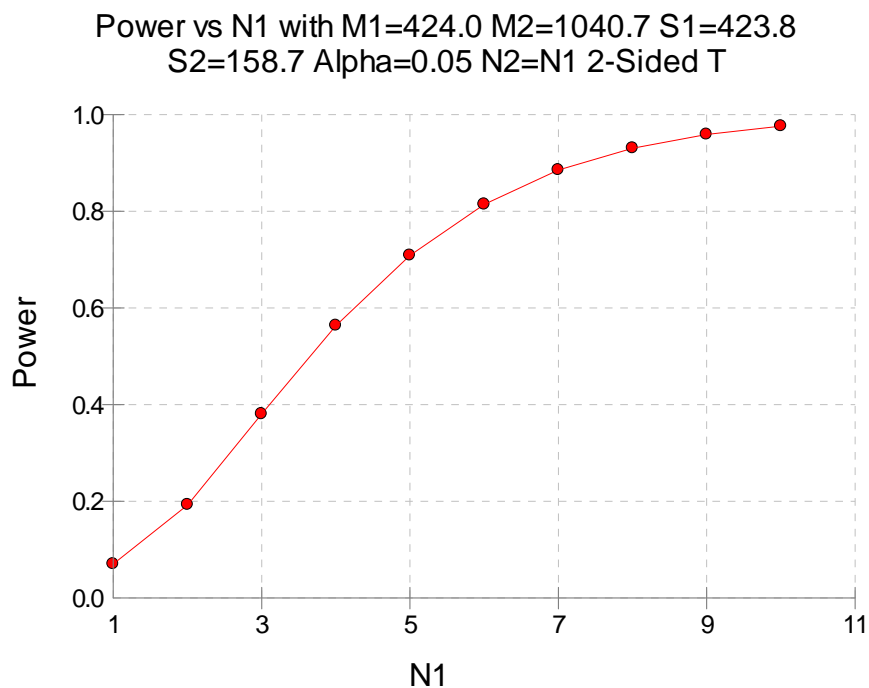
Then AUC has been calculated for each data set then summary statistics have been obtained for each treatment group.

Treatment	No. obs	AUC mean	AUC std dev	AUC min	AUC max
1	12	424.02	423.81	104.43	1148.37
2	4	1040.67	158.69	902.78	1267.36
3	4	1762.39	371.26	1415.96	2132.29
4	4	1685.36	295.30	1331.12	2052.96

Power curves

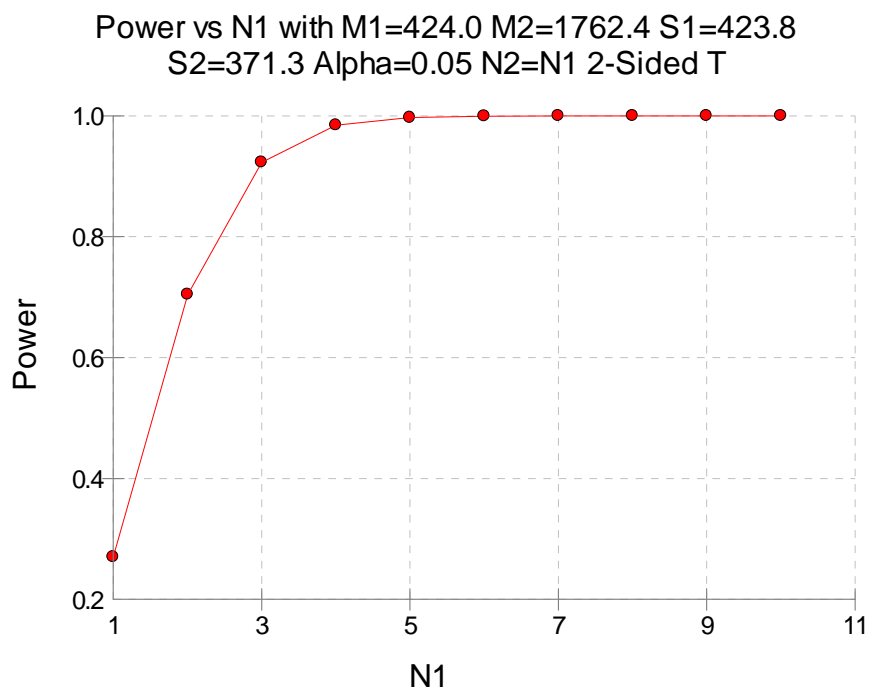
To assess the number of animals that are required to give the experiment adequate power I have created power curves. Ideally we would like to have around 80% power.

Treatment 1 vs. 2



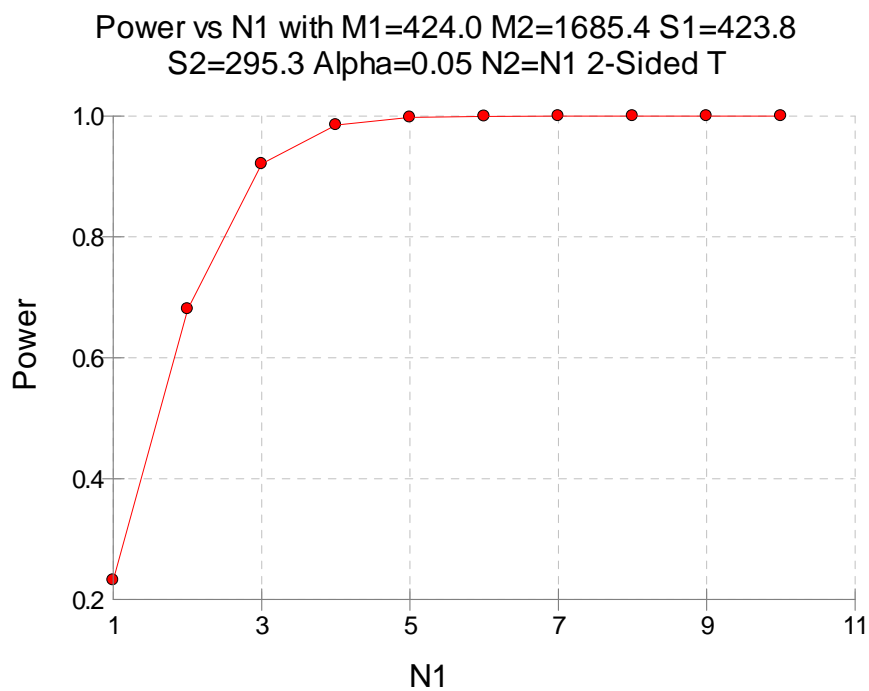
So to be able to compare treatments 1 and 2 you would need approximately 6 animals in each group to have 80% power.

Treatment 1 vs. 3



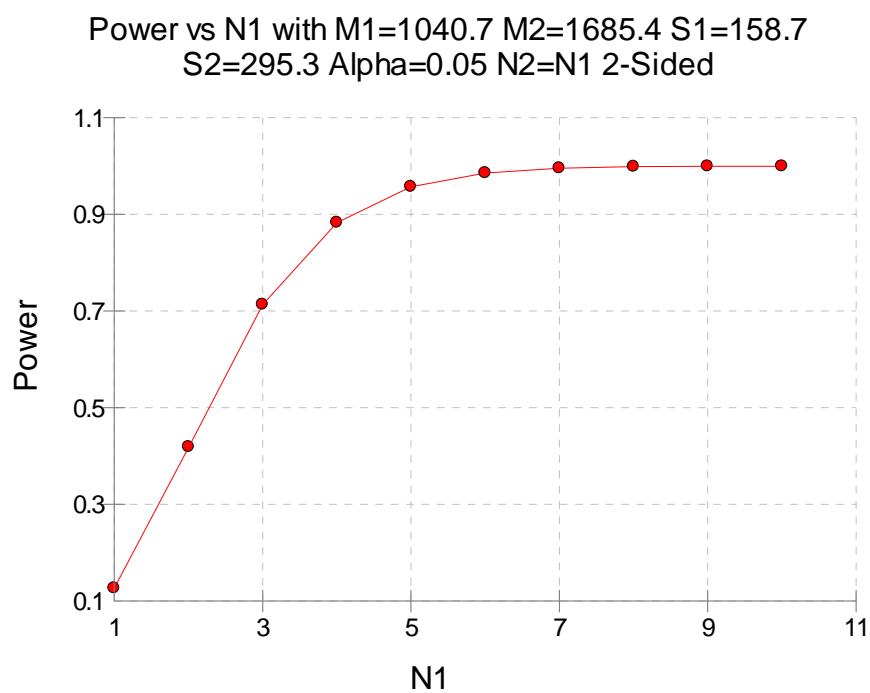
Treatments 1 and 3 are very powerful, it is only necessary to have 3 animals in each group for adequate power.

Treatment 1 vs. 4



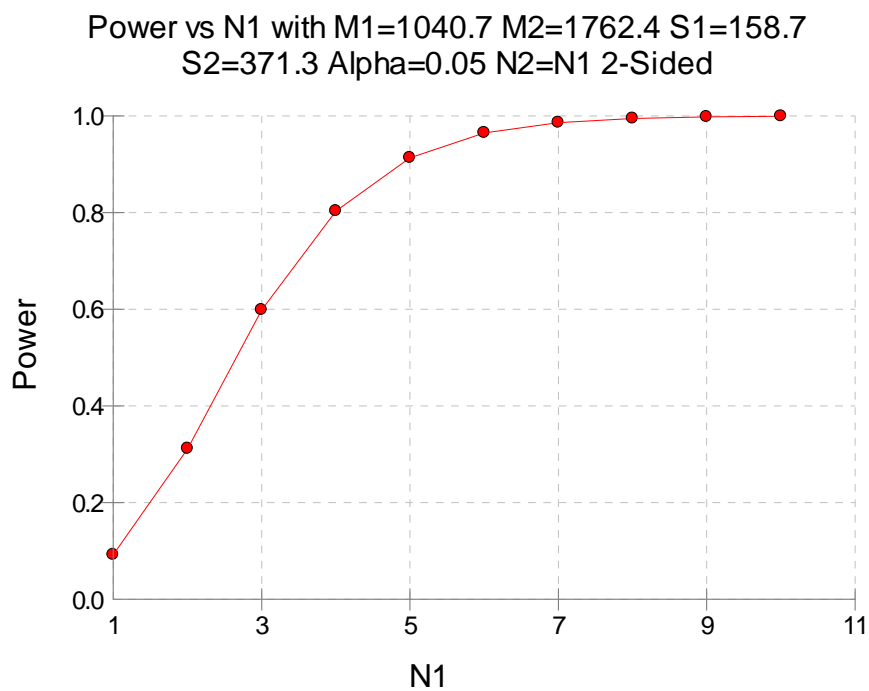
This is also a very powerful comparison, only 3 animals are needed for almost 90% power.

Treatment 2 vs. 4



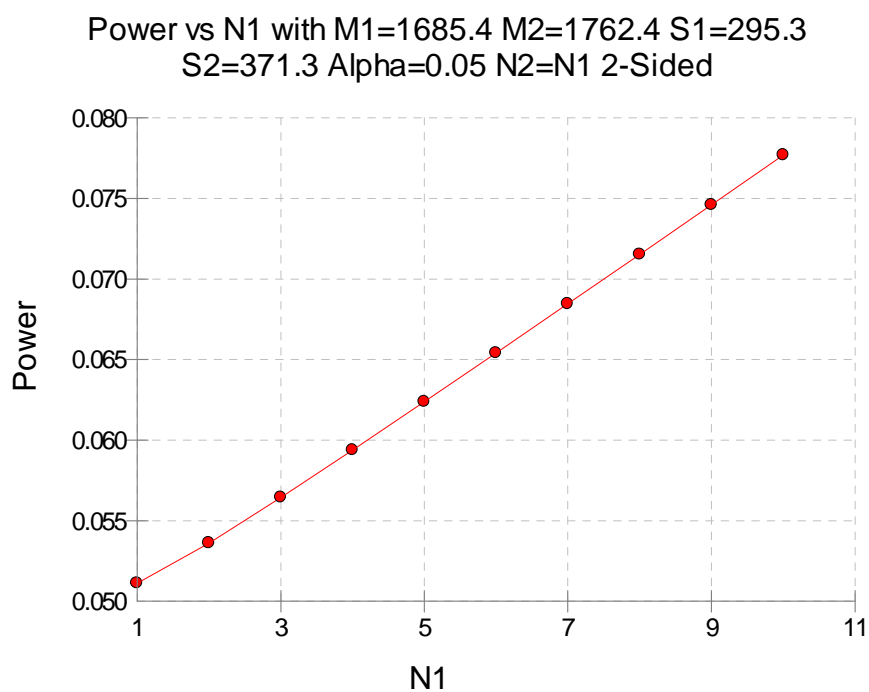
For comparing treatments 2 and 4 we need 3-4 animals for 80% power.

Treatment 2 vs. 3



4 animals are required to compare treatments 2 and 3.

Treatment 3 vs. 4



To compare treatments 3 and 4 there is very low power. This comparison isn't really possible without using 12+ animals.

Conclusions

Using 3-4 animals across the groups is generally acceptable and produces power of approx 80%. Though to be confidently able to compare treatment groups 1 and 2 you would need a minimum of 6 animals per group. Also the comparison between treatment groups 3 and 4 is not possible without using 12+ animals, and even here using 12 only produces power of 8% so it is not an advisable comparison to make.